

**HANDBOOK OF**

**INFRARED RADIATION**

**FROM COMBUSTION GASES**

CASE FILE  
COPY



**NATIONAL AERONAUTICS AND SPACE ADMINISTRATION**

# HANDBOOK OF

# INFRARED RADIATION

# FROM COMBUSTION GASES

By C. B. Ludwig, W. Malkmus, J. E. Reardon,  
and J. A. L. Thomson

*Marshall Space Flight Center*

*Editors*

R. Goulard and J. A. L. Thomson

*Prepared by Marshall Space Flight Center*



*Scientific and Technical Information Office*  
NATIONAL AERONAUTICS AND SPACE ADMINISTRATION  
Washington, D.C.

1973

## ACKNOWLEDGMENT

The authors wish to acknowledge the great contribution of Dr. Carmine C. Ferriso, who conceived the overall experimental program upon which much of this handbook is based and guided it during the initial phases. Before his untimely death in 1966 at the age of 35, he was recognized as a leading scientist in the field of high temperature gas spectroscopy. He developed techniques for measuring the emissivities of exhaust gases produced by specially designed research rockets and for determining curves of growth of gases behind reflected shock waves. For the experimental program sponsored by NASA/MSFC, Carmine Ferriso conceived the idea of the "long burner" which was utilized in the determination of spectroscopic parameters for hot water vapor. His dedication and determination in the pursuit of scientific knowledge contributed greatly to the successful completion of the program.

## PREFACE

When the development of the Saturn rocket vehicles began in the late 1950's, the various base heating mishaps of the midfifties were a recent and painful memory. The chance of a repetition with the large and expensive Saturns was unacceptable. Radiative transfer is one of the two base heating mechanisms, and in contrast to its counterpart, the convective transfer, it cannot be assessed by scale model tests because there are no appropriate modeling laws. On the other hand, data then available for estimating the radiative output from the inhomogeneous rocket jets were insufficient for confident predictions.

To break this impasse, an industry-university-government team was assembled to plan and execute an effort to collect the available data, to fill the existing gaps by analytical and experimental research, and to develop the tools for a sufficiently accurate analytical prediction of the thermal radiation from given, inhomogeneous masses of hot gases and flames. Besides the authors and editors of this book, the team included the late Carmine C. Ferriso of General Dynamics; Richard H. Tourin, Burt Krakow, and Harold J. Babrov of Warner and Swasey; William Herget, A. G. DeBell, and James Muirhead of Rocketdyne; and Robert Yossa of Brown Engineering. The team's task was successfully completed by about 1968.

However, realizing that the results of their work were applicable to many engineering problems, the nucleus of the team stayed together to compile this material in a form useful to the engineering community. The result is this handbook. The editors and authors realize that the book has some shortcomings of style and form, forced by a shortage of time and funds. Rather than accepting further delays and jeopardizing publication, they ask the reader to bear with these flaws.

The handbook is intended primarily for use by the working design engineer. In most college engineering courses at the undergraduate or first-year graduate level, radiative heat transfer is treated in terms of various limiting cases, such as the transparent gas, the highly opaque gas, or in terms of a gas whose absorption coefficient is independent of frequency, i. e., the so-called "grey" gas. It is assumed that the readers have such a background. While some background in molecular and atomic structure and spectral line emission is desirable, the handbook can be profitably used by engineers without such experience. The mathematical background required is equivalent to that required for a bachelor's degree in engineering.

The handbook is primarily addressed to the treatment of radiant emission and absorption by combustion gases. Typical applications include rocket combustion chambers and exhausts, turbojet engines and exhausts, and industrial furnaces. Some mention is made of radiant heat transfer problems in planetary atmospheres, in stellar atmospheres, and in reentry plasmas; however, the handbook is not intended as a definitive source book for such applications. Particular consideration is given to the temperature range from 500K to 3000K and the pressure range from 0.001 atmosphere to 30 atmospheres. Strong emphasis is given to the combustion products of hydrocarbon fuels with oxygen, specifically to carbon dioxide, water vapor, and carbon monoxide. In addition, species such as HF, HCl, CN, OH, and NO are treated.

Chapter 1 introduces the book with a qualitative discussion of molecular radiators, molecular spectra, and radiative heat transfer in nongrey gases. A description of the logical procedure which should be followed in evaluating heat transfer from a given flow system is outlined and guidelines for practical application of the handbook are given. Subsequent chapters present detailed discussions of the properties of gaseous radiators and theoretical models for spectral emission from homogeneous and nonhomogeneous gases. Properties of most commonly occurring molecules are tabulated and specific computational models for these molecules are discussed. Emission from particle clouds is included, and scattering effects in such clouds are briefly reviewed; however, no attempt is made to present detailed computational techniques for strongly scattering media since methods of sufficient generality are lacking. A source bank of data completes the handbook.

Special mention should be made of the key role played by R.M. Huffaker, MSFC, in the conception and execution of this program. Without his vision and patient determination, this handbook would not exist. Both research and handbook writing were conducted under the guidance of the Marshall Space Flight Center, with Office of Advanced Research and Technology sponsorship.

Werner K. Dahm  
Chief, Aerophysics Division  
Marshall Space Flight Center

## TABLE OF CONTENTS

	Page
CHAPTER 1 INTRODUCTION .....	1
1.1 PROPERTIES OF GASEOUS RADIATORS .....	1
1.1.1 INTRODUCTION .....	1
1.1.2 THE QUANTUM THEORY DESCRIPTION OF MATTER...	3
1.1.2.1 Energy Quantization and the Uncertainty Principle .....	4
1.1.2.2 Energy States in a Harmonic Oscillator .....	4
1.1.3 INTENSITY AND SPECTRA .....	8
1.1.3.1 Types of Spectra .....	12
1.2 STRUCTURE OF A SINGLE SPECTRAL LINE .....	14
1.2.1 DOPPLER LINE BROADENING .....	14
1.2.2 NATURAL LIFETIME LINE BROADENING .....	15
1.2.3 COLLISIONAL LINE BROADENING .....	15
CHAPTER 2 BASIC PRINCIPLES .....	17
2.1 RADIATIVE TRANSFER .....	18
2.1.1 NOMENCLATURE .....	18
2.1.2 BLACKBODY .....	18
2.1.3 RADIANT EMITTANCE .....	22
2.1.4 RADIANCE .....	23
2.1.4.1 Spectral Radiance .....	23
2.1.4.1.1 Maximum Blackbody Spectral Radiance .....	24
2.1.4.2 Spectral Emissivity .....	25
2.1.4.3 Spectral Absorptivity .....	25
2.1.4.4 Spectral Reflectivity .....	25
2.1.4.5 Spectral Transmissivity .....	25
2.1.5 ABSORPTION COEFFICIENT .....	26
2.1.6 EQUATION OF TRANSFER IN NONSCATTERING MEDIA (IN LOCAL THERMODYNAMIC EQUILIBRIUM) .....	26
2.1.7 SPECTRAL RADIANCE OF AN EXTENDED MEDIUM .....	26
2.1.8 TRANSMISSIVITY .....	27
2.2 LINE RADIATION .....	29
2.2.1 HOMOGENEOUS MEDIA .....	29
2.2.1.1 Line Strength .....	29
2.2.1.2 Line Width .....	29
2.2.1.3 Equivalent Width .....	29
2.2.1.3.1 Equivalent Width for Collision Broadened Lines .....	30

## TABLE OF CONTENTS (Continued)

	Page
2.2.1.3.2 Equivalent Width for Doppler Broadened Lines . . . . .	31
2.2.1.3.3 Equivalent Width for Combined Doppler-Lorentz (Voigt) Lines . . .	32
2.2.2 INHOMOGENEOUS MEDIA . . . . .	34
2.2.2.1 A Two-Parameter Approximation of Low Resolution Curves of Growth . . . . .	35
2.3 MOLECULAR EMISSION . . . . .	37
2.3.1 MOLECULAR STRUCTURE . . . . .	38
2.3.1.1 Diatomic Molecules . . . . .	38
2.3.1.2 Triatomic Molecules . . . . .	41
2.3.2 TRANSITION PROBABILITIES . . . . .	43
2.3.3 STRENGTHS OF VIBRATION-ROTATION TRANSITIONS . . . . .	46
2.3.3.1 Diatomic Molecules: Line Strength . . . . .	47
2.3.3.2 Diatomic Molecules: Band Intensities . . . . .	48
2.3.3.3 Triatomic Molecules: Line and Band Strengths . . . . .	50
2.3.4 NONEQUILIBRIUM EFFECTS: SCATTERING VS. ABSORPTION . . . . .	51
2.4 COLLISION LINE WIDTH DEPENDENCE ON THERMO- DYNAMIC PROPERTIES . . . . .	53
2.4.1 LINE BROADENING THEORIES . . . . .	53
2.4.2 PRESSURE DEPENDENCE OF COLLISION BROADENING . . . . .	54
2.4.3 TEMPERATURE DEPENDENCE OF COLLISION BROADENING . . . . .	55
2.5 PARTICULATE EMISSION AND SCATTERING . . . . .	58
2.5.1 THE EQUATIONS OF TRANSFER . . . . .	58
2.5.2 SOLUTIONS TO COMMON SCATTERING PROBLEMS . . .	62
APPENDIX 2-A COLLISION BROADENING — THE LADENBURG- REICHE FUNCTION $f(x)$ . . . . .	64
APPENDIX 2-B DOPPLER BROADENING . . . . .	68
REFERENCES . . . . .	70

TABLE OF CONTENTS (Continued)

	Page
CHAPTER 3 CALCULATIONAL TECHNIQUES FOR HOMOGENEOUS GASES .....	73
3.1 LIMITING CASES AND "FIRST GUESS" PROCEDURES .....	74
3.1.1 THIN GAS .....	74
3.1.2 GREY GAS .....	75
3.1.3 NONOVERLAPPING LINES .....	76
3.1.4 INTEGRATED EMISSIVITIES .....	77
3.1.5 TOTAL EMISSIVITY .....	78
3.1.6 BOX MODEL .....	78
3.1.7 OTHER EMPIRICAL FORMS .....	79
3.1.8 MEAN BEAM LENGTH .....	81
3.2 BAND MODELS .....	81
3.2.1 REGULAR BAND MODELS .....	81
3.2.1.1 Regular Model for Collision-Broadened Lines Having Lorentz Constants (Elsasser) .....	81
3.2.1.2 Regular Model for Doppler Broadened Lines (Golden) .....	82
3.2.1.3 Regular Model for Mixed Doppler-Lorentz Lines .....	84
3.2.2 RANDOM BAND MODELS .....	84
3.2.2.1 Lines of Equal Strength .....	85
3.2.2.2 Exponential Line Strength Distribution .....	87
3.2.2.3 Inverse Line Strength ( $S^{-1}$ ) Distributions .....	89
3.2.2.4 Exponential-Tailed $S^{-1}$ Distribution .....	91
3.2.2.5 The Choice of a Random Band Model .....	91
3.2.3 RANDOM DOPPLER MODELS .....	94
3.2.3.1 Lines of the Same Intensity .....	94
3.2.3.2 Lines Having Exponential Distribution .....	95
3.2.3.3 Lines with $S^{-1}$ Distribution .....	98
3.2.3.4 Random Band Models: Mixed Lorentz- Doppler .....	98
3.2.4 HYBRID MODELS .....	101
3.2.4.1 Random Regular Model .....	101
3.2.4.2 Quasi-Random Model .....	103
3.2.5 APPROXIMATION FORMULAS .....	103
APPENDIX 3-A REGULAR BAND MODELS .....	107
3-A.1 COLLISION BROADENING .....	107
3-A.2 DOPPLER BROADENING .....	108

TABLE OF CONTENTS (Continued)

	Page
APPENDIX 3-B SELECTION OF BAND MODEL TO DESCRIBE EXPERIMENTAL DATA . . . . .	114
3-B.1 RANDOMNESS OF LINE LOCATIONS . . . . .	118
3-B.2 LORENTZ LINE SHAPE . . . . .	120
3-B.3 LINE STRENGTH DISTRIBUTION . . . . .	120
APPENDIX 3-C CRITERIA FOR ACCURACY OF MEASUREMENT OF LINE STRENGTHS AND MEAN ABSORPTION COEFFICIENTS . . . . .	125
REFERENCES . . . . .	132
 CHAPTER 4 CALCULATIONAL TECHNIQUES FOR INHOMOGENEOUS GASES . . . . .	 135
4.1 EXACT CALCULATIONS . . . . .	136
4.1.1 GENERAL CONSIDERATIONS . . . . .	136
4.1.2 THE N-PARAMETER APPROXIMATION METHODS . . . . .	136
4.2 THE CURTIS-GODSON APPROXIMATION FOR BAND MODELS . . . . .	138
4.3 SENSITIVITY ANALYSIS . . . . .	142
4.3.1 ERRORS CAUSED BY THE CURTIS-GODSON APPROXIMATION . . . . .	142
4.3.2 ERRORS RESULTING FROM THE USE OF THE RANDOM MODEL AND SIMPLIFIED CURVES OF GROWTH . . . . .	143
4.3.3 CHOICE OF THE CURVE OF GROWTH . . . . .	146
4.4 SUMMARY . . . . .	152
REFERENCES . . . . .	153
 CHAPTER 5 REPRESENTATIONS FOR SPECIFIC MOLECULES . . . . .	 155
5.1 DIATOMIC MOLECULES . . . . .	156
5.1.1 MEAN ABSORPTION COEFFICIENTS AND LINE SPACING (THEORY) . . . . .	156
5.1.2 RANDOM REGULAR (ELSASSER) MODEL . . . . .	157
5.1.3 RANDOM MODEL . . . . .	158
5.1.4 LIMITING FORMS FOR THE MEAN SPECTRAL TRANSMISSIVITY . . . . .	159
5.1.4.1 Collision-Broadened Lines . . . . .	160
5.1.4.2 Doppler-Broadened Lines . . . . .	161
5.1.4.3 Regions of Validity . . . . .	161

## TABLE OF CONTENTS (Continued)

	Page
5.1.5 DATA FOR DIATOMIC MOLECULES .....	163
5.1.5.1 CO Data .....	163
5.1.5.2 NO Data .....	169
5.1.5.3 CN Data .....	174
5.1.5.4 OH Data .....	178
5.1.5.5 HCl Data .....	181
5.1.5.6 HF Data .....	185
5.2 POLYATOMIC MOLECULES .....	188
5.2.1 CARBON DIOXIDE (CO <sub>2</sub> ) .....	188
5.2.2 WATER VAPOR (H <sub>2</sub> O) .....	201
5.2.2.1 Curves of Growth and Absorption Coefficients .....	201
5.2.2.2 Water Vapor Line Widths .....	202
5.2.2.3 Fine Structure Parameter (1/d) .....	209
5.2.2.4 Detailed Line-by-Line Calculations for H <sub>2</sub> O .....	210
5.3 SUMMARY OF TWO RECOMMENDED BAND MODELS .....	214
5.4 CALCULATION PROCEDURE FOR CARBON PARTICLES .....	224
APPENDIX 5-A CALCULATION OF DIATOMIC SPECTRA — THEORY .....	230
APPENDIX 5-B MOLECULAR CONSTANTS .....	233
REFERENCES .....	236
 CHAPTER 6 COMPUTED RADIATION DATA .....	 239
6.1 SPECTRAL CHARACTERISTICS OF GASEOUS RADIATORS .....	240
6.1.1 WATER VAPOR .....	240
6.1.2 CARBON DIOXIDE .....	243
6.1.3 CARBON MONOXIDE .....	243
6.1.4 CARBON PARTICLES .....	256
6.2 INTEGRATED ABSORPTANCES FOR DIATOMIC GASES .....	255
6.3 INTEGRATED ABSORPTANCE FOR CARBON DIOXIDE .....	277
6.4 TOTAL EMISSIVITY FOR WATER VAPOR .....	280
6.5 TOTAL EMISSIVITY FOR MIXTURES OF GASES .....	286
REFERENCES .....	287

TABLE OF CONTENTS (Continued)

	Page
CHAPTER 7 ACCURACY OF CALCULATIONAL MODELS . . . . .	289
7.1 EXPERIMENT PROCEDURES . . . . .	291
7.1.1 EQUIPMENT FOR HIGH-TEMPERATURE GAS SPECTROSCOPY . . . . .	291
7.1.2 OPTICAL DETERMINATION OF THE GAS TEMPERATURE . . . . .	301
7.1.2.1 Homogeneous Gases . . . . .	301
7.1.2.2 Inhomogeneous Gases . . . . .	303
7.2 DIATOMIC MOLECULES . . . . .	304
7.3 CARBON DIOXIDE . . . . .	308
7.3.1 HOMOGENEOUS . . . . .	308
7.3.1.1 The 2.7- $\mu$ Band . . . . .	308
7.3.1.2 The 4.3- $\mu$ Band . . . . .	309
7.3.2 INHOMOGENEOUS GAS . . . . .	310
7.4 WATER VAPOR . . . . .	313
7.4.1 HOMOGENEOUS GAS . . . . .	313
7.4.1.1 Absorption Coefficient Data . . . . .	313
7.4.1.2 Spectral Emissivities . . . . .	313
7.4.2 INHOMOGENEOUS GAS . . . . .	329
7.4.3 BAND ABSORPTION . . . . .	333
7.5 MIXTURE OF CARBON DIOXIDE AND WATER VAPOR . . . . .	335
REFERENCES . . . . .	336
 CHAPTER 8 PREDICTIVE TECHNIQUES . . . . .	 341
8.1 INTEGRATION INTERVAL CONSIDERATIONS . . . . .	344
8.1.1 LINE OF SIGHT INTERVAL - $\Delta l$ . . . . .	344
8.1.2 SPECTRAL INTERVAL - $\Delta\omega$ . . . . .	344
8.2 COMPARISON OF VARIOUS BAND MODELS IN ROCKET EXHAUST CALCULATIONS . . . . .	347
8.3 COMPARISON OF PREDICTIONS WITH MEASUREMENTS FOR ROCKET EXHAUSTS . . . . .	362
8.3.1 MODEL F-1 MEASUREMENT . . . . .	362
8.3.2 J-2 LEVEL MEASUREMENT . . . . .	367
8.4 EFFECT OF SCALE ON GASEOUS RADIATION . . . . .	370
REFERENCES . . . . .	375

## TABLE OF CONTENTS (Concluded)

	Page
GENERAL APPENDIX .....	377
A1 INTRODUCTION TO THE USE OF THE TABLES .....	377
A1.1 Typical Calculation .....	377
A1.1.1 Calculation Procedure .....	377
A1.1.2 Example Calculation .....	380
A2 RADIATION DATA TABLES .....	384
A2.1 Blackbody Radiation Functions .....	384
A2.2 Diatomic Molecules .....	384
A2.3 CO <sub>2</sub> .....	384
A2.4 Water Vapor .....	385
A2.5 Carbon .....	385

## CHAPTER 1

## INTRODUCTION

1.1 PROPERTIES OF GASEOUS RADIATORS

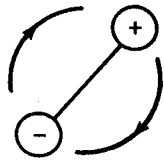
## 1.1.1 INTRODUCTION

All matter when viewed at the microscopic level consists of atoms or molecules packed closely together (as in a solid or liquid) or rather sparsely distributed (as in a gas). Heat can be transferred from one region to another by one of three processes: convection, conduction, or radiation. In the first process, the energy transfer simply results from a transfer of heated or energy-containing matter from one point to another. In conduction, molecular kinetic energy in the form of vibration, rotation, or simply random translational motion is transferred from atom to atom or molecule to molecule by exchanges occurring during direct collisions. The third mechanism, radiative transfer, is the topic of this handbook. Radiative transfer occurs when a molecule emits (or absorbs) a train of electromagnetic waves (in the fashion of a radio transmitter). These waves transport energy at the speed of light; when they impinge on some other body, they are either deflected or absorbed, or both. This interaction is the subject of radiative transfer studies.

This handbook includes detailed methods and techniques for calculating the radiative transfer from gases that are representative of common combustion systems. To provide a general background for the detailed analyses presented in the main part of the handbook, a brief summary of the basic physics of radiative emission and absorption from molecular gases is given in this chapter.

In order to understand the basic features of molecular radiative transfer, it is important to remember two facts. First, radiation is the emission and transfer of energy by electromagnetic waves. Such waves can be generated only when electrical charges are accelerated (Fig. 1-1) and the processes can be thought of an equivalent to the broadcast or reception of radiation by a radio antenna. Most molecules tend to be electrically polarized with positive charges separated to various extents from the negative charges. As the molecules rotate or vibrate, these charges are accelerated in a periodic fashion and a sinusoidal oscillating train of electromagnetic waves is emitted. The second feature characterizing molecular radiative transfer is that molecules or atoms may be thought of as complex, highly resonant harmonic systems. Their internal structure can be interpreted as having a large number of resonant frequencies. Consequently the frequency distribution or spectrum of the emitted radiation often consists of a large number of distinct spectral "lines." It is

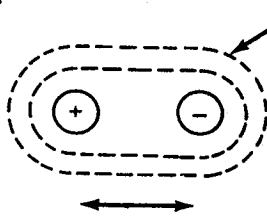
MOLECULAR ROTATION



$$\frac{d\vec{u}}{dt} = r\omega^2$$

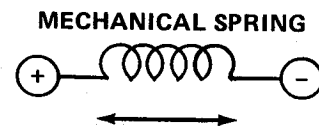
$$\frac{d\vec{u}}{dt} \neq 0 \therefore \text{RADIATES (IF CHARGED)}$$

VIBRATION



ELECTRONIC ORBITS

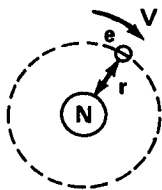
EQUIVALENT TO:



MECHANICAL SPRING

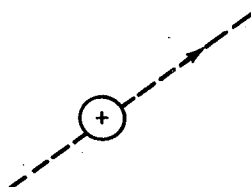
$$\frac{d\vec{u}}{dt} = -\frac{k}{m}(x - x_0) = -\omega_0^2(x - x_0) \neq 0 \therefore \text{RADIATES (IF CHARGED)}$$

ELECTRONIC



$$\frac{d\vec{u}}{dt} = \frac{v^2}{r} \text{ (RADIAL)} \neq 0 \therefore \text{RADIATES}$$

FREE TRANSLATION



$\vec{u} = \text{CONSTANT (IF NO COLLISIONS)}$

$$\frac{d\vec{u}}{dt} = 0 \therefore \text{DOES NOT RADIATE}$$

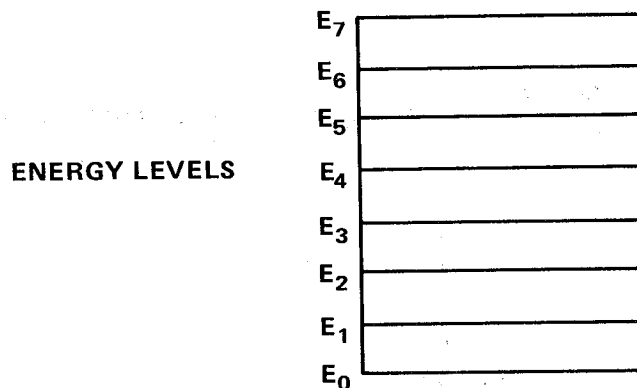
Figure 1-1. Illustration of accelerations giving rise to electromagnetic radiation.

this line character of the spectrum of common combustion gases that makes radiation from molecules much more complex and difficult to treat than that from solid bodies. Much of this handbook is devoted to techniques for obtaining useful engineering representations of the average radiative properties of such spectra.

The next several sections contain a brief summary of the properties of molecules and molecular radiation that underly the mathematical and numerical formalism that forms the basis of the bulk of the handbook.

### 1.1.2 THE QUANTUM THEORY DESCRIPTION OF MATTER

All matter is "quantized": That is, an atom or molecule can exist in only one of a number of unique, discrete energy states. Any molecule can be described by an "energy level" diagram — one for each degree of freedom:



In the quantum theory description, a molecule exists in one or the other of these states (actually, one can only say that a molecule has a certain probability of being in any given state).

The fact that molecules or atoms exist only in discrete energy states and that the electromagnetic radiation emitted by an excited molecule appears only in discrete "chunks" is the basis for the quantum theory of matter. The chunks of radiation are called "photons" and are simply wave packets of finite length. The basic observation law of quantum mechanics is that the wave packets (photons) of electromagnetic energy are "quantized" and that the energy of a photon is proportional to its frequency ( $\nu$ ):

$$E (\text{photon}) = h \nu \quad (1-1)$$

where  $h$  is a constant known as Planck's constant ( $h = 6.625 \times 10^{-34}$  joule seconds).

When applied to macroscopic systems, quantum theory usually leads to results very close to the normal theory of mechanics (Newton's laws). Only when applied to small systems having low energy are quantum effects important. There are a few notable exceptions: Superfluidity and superconductivity are examples of quantum effects on a large scale. The other major area where quantum effects are important on a macroscopic scale is radiant transfer.

#### 1.1.2.1 Energy Quantization and the Uncertainty Principle

It can be shown that a single wave packet of finite length can be resolved into a superposition of a number of single frequency plane waves whose frequencies are spread over a frequency interval between  $\omega_0 + \gamma/2$  to  $\omega_0 - \gamma/2$ . Here  $\gamma$  is inversely proportional to the effective length ("coherence" length) of the packet and  $\omega_0$  is the mean or center frequency.<sup>1</sup>

According to quantum theory the energy of a photon is proportional to its frequency, and if the frequency of a wave packet does not have a precise value, but is spread over an interval of width  $\gamma$ , then neither does the photon energy have a precise value.

This imprecision of a quantity such as energy is a basic feature of quantum mechanics and may be stated in the following fashion. If a photon is known to occur in (or last for) a certain time interval  $\Delta t$ , then its energy cannot be known precisely but only within an uncertainty  $\Delta E$ , whose value obeys:

$$\Delta E \Delta t \geq h/2\pi \tag{1-2}$$

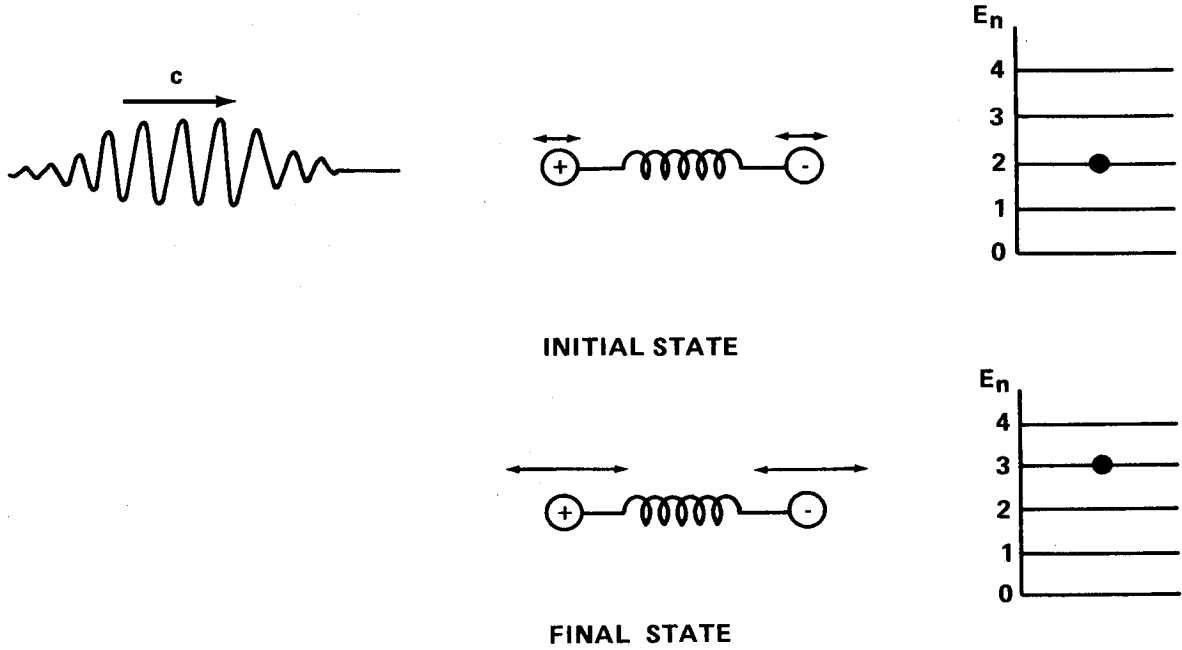
where  $h$  is Planck's constant. For such a photon,  $\Delta E = h\gamma/2\pi$ . Hence, the line width  $\gamma$  must correspond to a lifetime according to  $\gamma \sim \Delta t^{-1}$ .

#### 1.1.2.2 Energy States in a Harmonic Oscillator

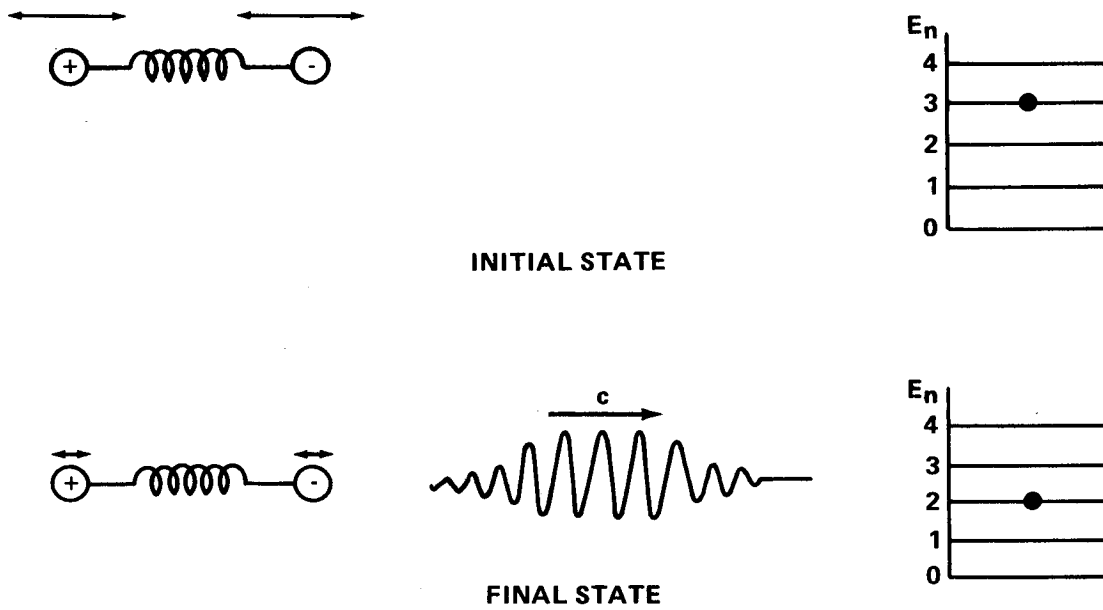
Most molecules vibrate as if the various nuclei were interconnected by springs (Fig. 1-2). For small amplitude vibrations, the equation of motion for a simple molecule has the form

---

1. In this chapter  $\omega$  refers to frequency in radians per sec and  $\gamma$  has units of  $\text{sec}^{-1}$ . Later in the book wavenumber units are used.



a. Absorption of a photon by a harmonic oscillator.



b. Emission of a photon by a harmonic oscillator.

Figure 1-2. Representations of absorption and emission by a harmonic oscillator.

CHAPTER 1 – INTRODUCTION

$$m \frac{d^2x}{dt^2} + k (x - x_0) = 0 \quad (1-3)$$

or

$$\ddot{x} + \omega_0^2 (x - x_0) = 0 \quad (1-4)$$

Here  $x_0$  is the equilibrium separation of the nuclei. The total energy of this oscillator is

$$E = \frac{1}{2} m (d\xi/dt)^2 + k\xi^2/2 \quad (1-5)$$

or, in terms of the mean square displacement  $\overline{\xi^2}$  :

$$E = m\omega_0^2 \overline{\xi^2} \quad (1-6)$$

where

$$\xi = x - x_0 \quad .$$

A quantum mechanical analysis of this vibrator shows that the allowed discrete energy states are equally spaced. In other words, the  $n$ th state above the lowest energy state has an energy (writing  $h/2\pi$  as  $\hbar$ )

$$E_n - E_0 = \hbar n \omega_0 \quad (1-7)$$

This equal spacing of energy levels is pretty much what one should expect since this oscillator, when it radiates, must radiate a wave packet having a frequency essentially equal to  $\omega_0$ . The energy of the emitted photon is  $\hbar\omega_0$  and this must be the energy difference between the initial state and the final state of the molecule.

$$E_{\text{final}} = E_{\text{initial}} \pm \hbar\omega_0 \quad (1-8)$$

Therefore, for the transition from a state  $E_{n+1}$  to a state  $E_n$ ,

$$\hbar\omega_0 = E_{n+1} - E_n \quad (1-9)$$

Thus, one must have

$$E_n = E_0 + n\hbar\omega_0 \quad (1-10)$$

if the radiating transitions correspond to adjacent energy states.

If transitions can occur between nonadjacent states, "harmonics" are emitted:

$$\hbar\omega_{\text{photon}} = E_m - E_n = (m - n)\hbar\omega_0 \quad (1-11)$$

or

$$\omega_{\text{photon}} = (m - n)\omega_0 \quad (1-12)$$

These harmonics are exactly analogous to harmonics in mechanical systems and result from nonlinearities in the spring constants (they can result also from electrical nonlinearities).

However, for small amplitudes and linear spring constants, the harmonic distortion is negligible, and radiation is emitted only as a result of a transition from one energy state to one immediately adjacent. Thus, there is a "selection rule" that in a "radiative" transition the "quantum" number  $n$  can change by only one unit:

$$\Delta n = \pm 1 \quad (1-13)$$

CHAPTER 1 – INTRODUCTION

If  $n$  decreases, the molecular energy is reduced and a photon is emitted. If  $n$  increases, the molecule gains energy by absorption of a photon from the radiation field ( Fig. 1-2) .

1.1.3 INTENSITY AND SPECTRA

Consider a plane electromagnetic wave packet traveling in the  $x$  direction. One wants to calculate the flux of power passing through a unit area in a plane perpendicular to the  $x$  axis. The power flux  $\vec{S}$  (watts/cm<sup>2</sup>) is given by the well known expression<sup>2</sup>

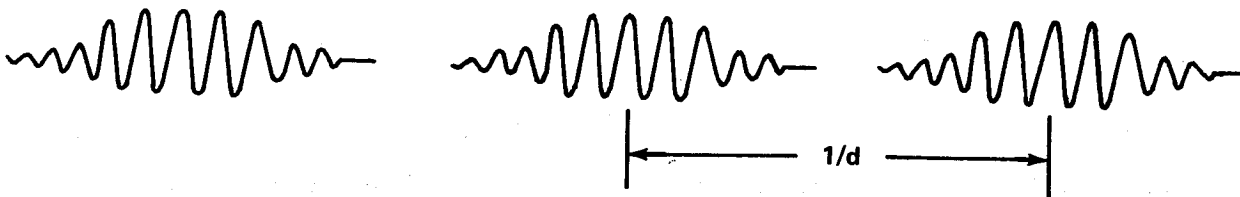
$$\vec{S} = \vec{E} \times \vec{B}/\mu = (|\vec{E}|^2/\mu c) \frac{\vec{k}}{k} \quad (1-14)$$

$$|\vec{S}| = \frac{|\vec{E}|^2}{\mu c} = c\epsilon |\vec{E}|^2 \quad (1-15)$$

Here  $\vec{S}$  is the so-called Poynting vector,  $\vec{E}$  and  $\vec{B}$  are the electric and magnetic fields,  $\epsilon$  and  $\mu$  the electric permittivity and magnetic permeability of the medium,  $c$  the velocity of light ( $c = 1/\sqrt{\mu\epsilon}$ ) and  $\vec{k}$  the wave vector ( $|\vec{k}| = 2\pi/\lambda$ ). The mean (time-averaged) magnitude of  $S$  is called the intensity of the wave:

$$I = c\epsilon |\vec{E}|^2 \quad (1-16)$$

Suppose the wavetrain is really a sequence of a number of individual packets as shown below:



2. See any text book on electromagnetic theory, for example, J. A. Stratton, Electromagnetic Theory, McGraw-Hill, 1941.

The intensity is the time-averaged value of the power flux  $|\vec{S}|$  :

$$I = \frac{1}{T} \int_{-T/2}^{T/2} c\epsilon |\vec{E}|^2 dt \quad . \quad (1-17)$$

Since the electric field is a function of the difference  $(x - ct)$ , one can average over either  $x$  or  $t$  :

$$I = \frac{1}{cT} \int_{-cT/2}^{cT/2} c\epsilon |\vec{E}|^2 dx \quad . \quad (1-18)$$

For the averaging distance  $cT$  much longer than the length of a packet and larger than the average space between packets ( $\bar{d}$ ), the intensity is given by

$$I = \frac{1}{cT} \left( \frac{cT}{\bar{d}} \right) \int_{-\infty}^{\infty} c\epsilon |\vec{E}|^2 dx = n \int_{-\infty}^{\infty} c\epsilon |\vec{E}|^2 dx \quad (1-19)$$

one packet

where  $n$  is the number of packets per meter.

In order to describe the spectral distribution of the radiation, one needs to evaluate the power in the spectral interval  $\omega$  to  $\omega + d\omega$ , i. e., the spectral intensity  $I_\omega$  (watts/m<sup>2</sup>-sec<sup>-1</sup>) multiplied by  $d\omega$ . Clearly,

$$I = \int_{-\infty}^{\infty} I_\omega d\omega \quad . \quad (1-20)$$

It is common to consider frequency only as positive. One can write this equation as

CHAPTER 1 – INTRODUCTION

$$I = \int_0^{\infty} (I_{\omega} + I_{-\omega}) d\omega \quad (1-21)$$

and call  $I'_{\omega} = I_{\omega} + I_{-\omega}$  the net spectral intensity.

It is appropriate now to write  $E(t)$  in terms of its Fourier components  $e(\omega)$ :

$$E(t) = \int_{-\infty}^{\infty} \frac{e(\omega)}{\sqrt{2\pi}} e^{i\omega t} d\omega \quad (1-22)$$

To relate the spectral intensity  $I_{\omega}$  to the Fourier components  $e(\omega)$ , one proceeds as follows. After substituting for  $|E(t)|^2$  in the expression for the total intensity  $I$ , one obtains

$$\begin{aligned} I &= nc\epsilon \int_{-\infty}^{\infty} \left\{ \int_{-\infty}^{\infty} \frac{e(\omega)}{\sqrt{2\pi}} e^{-\omega u/c} d\omega \int_{-\infty}^{\infty} \frac{e^*(\omega')}{\sqrt{2\pi}} e^{i\omega' u/c} d\omega' \right\} du \\ &= \frac{nc\epsilon}{2\pi} \int_{-\infty}^{\infty} \int_{-\infty}^{\infty} e(\omega) e^*(\omega') \left[ \int_{-\infty}^{\infty} e^{iu(\omega' - \omega)/c} du \right] d\omega' d\omega \quad (1-23) \end{aligned}$$

Since the term in square brackets is simply the delta function  $\delta\left(\frac{\omega' - \omega}{c}\right)$ , one may write

$$I = \frac{nc^2\epsilon}{2\pi} \int_{-\infty}^{\infty} |e(\omega)|^2 d\omega \quad (1-24)$$

Thus, one can write an expression for a spectral intensity,  $I_{\omega}$ :

$$I_{\omega} = \frac{nc^2\epsilon}{2\pi} |e(\omega)|^2 \quad (1-25)$$

For example, for an exponentially decaying oscillator,

$$E = E_0 e^{-\gamma t/2} \cos \omega_0 t \quad (1-26)$$

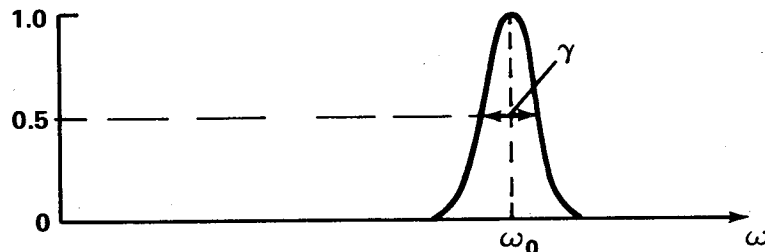
$$e(\omega) \propto \frac{1}{2\sqrt{2\pi}} \left[ \frac{1}{\frac{\gamma}{2} + i(\omega - \omega_0)} + \frac{1}{\frac{\gamma}{2} + i(\omega + \omega_0)} \right] \quad (1-27)$$

Now in almost all cases of interest in practical heat transfer applications, the damping rate  $\gamma$  is very much smaller than the characteristic frequency  $\omega_0$ . Thus  $e(\omega)$  is small except for  $\omega$  relatively near  $\omega_0$ . The term with  $\omega + \omega_0$  is then small compared to that with  $\omega - \omega_0$  and, approximately,

$$e(\omega) \propto \frac{1}{2\sqrt{2\pi}} \frac{1}{\frac{\gamma}{2} + i(\omega - \omega_0)} \quad (1-28)$$

The frequency variation of the spectral intensity  $I_{\omega}$ , then, has a simple bell-shaped form

$$I_{\omega} \approx \frac{nc^2\epsilon}{2\pi} \left( \frac{1}{8\pi} \right) \frac{1}{\frac{\gamma^2}{4} + (\omega - \omega_0)^2} \quad (1-29)$$



Here  $\gamma$  measures the width of the spectral interval around  $\omega_0$  that contains appreciable power. If a material has many different characteristic frequencies ( $\omega_{0_i}$ ), the intensity of the emitted radiation may have the form illustrated in Figure 1-3.

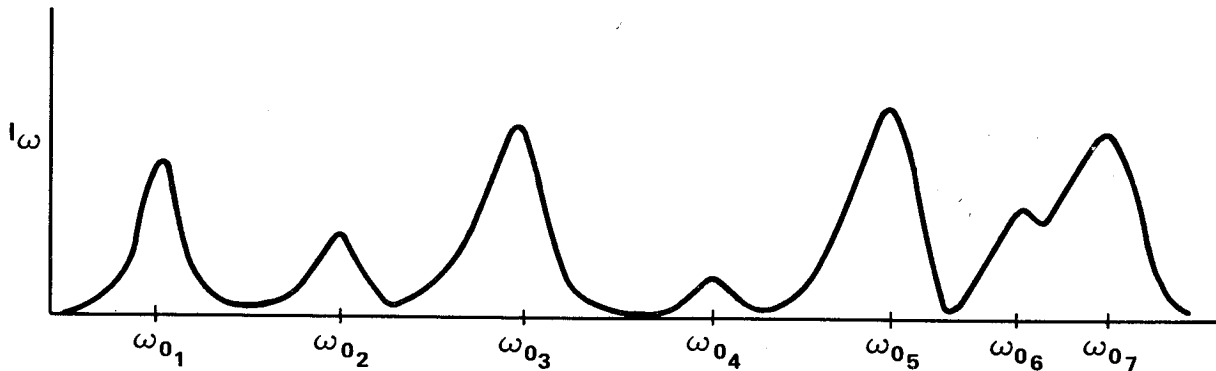


Figure 1-3. Spectrum of emitted radiation.

1.1.3.1 Types of Spectra

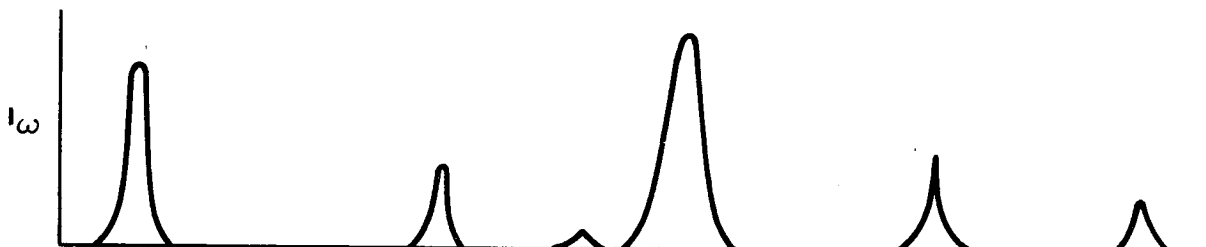
The basic phenomena determining the spectrum of the radiation emitted from a volume of gas are the following.

By random molecular motions, some natural modes (oscillatory or rotary) of the material are excited. These excitations occur at random times. As soon as this degree of freedom is excited, it begins to lose energy by radiative loss and the amplitude decays exponentially.

In some cases the excitation of an oscillatory mode can be stimulated by the electromagnetic field radiated from some other region of space — this is absorption of radiation.

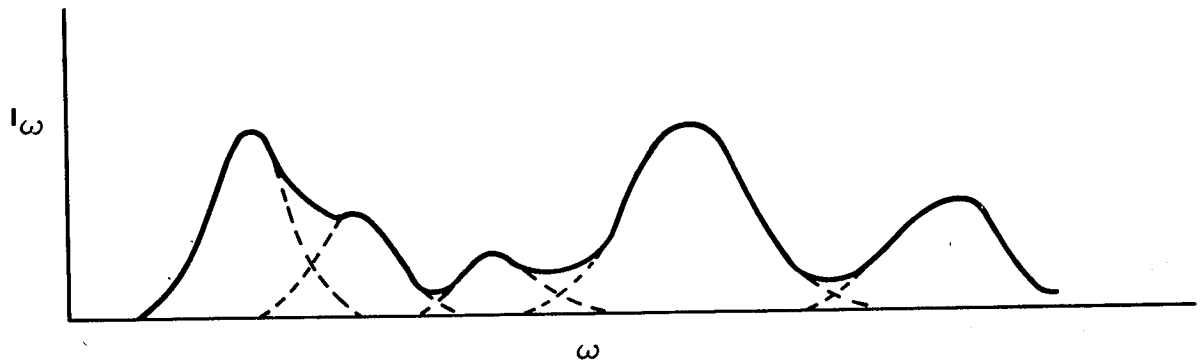
The properties of the emission and absorption are very much determined by the shape of the spectrum. Three general types of spectra occur:

a. Separated Spectral Lines:



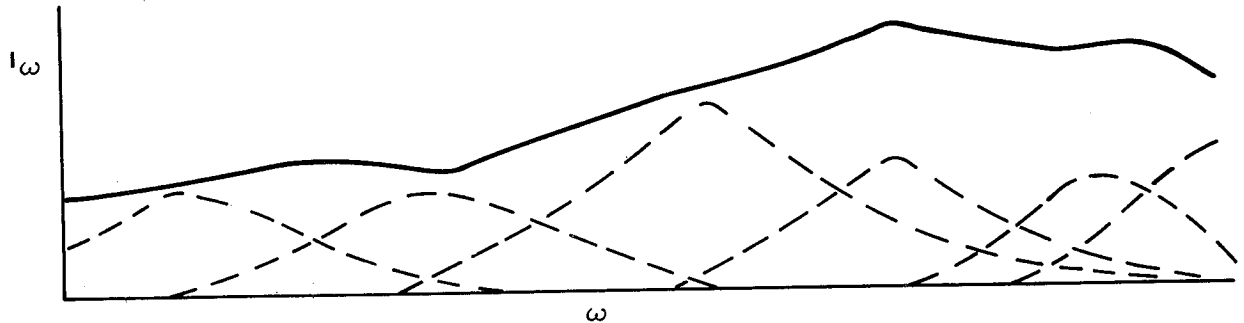
Such spectra are characteristic of low pressure flames, planetary atmospheres, stars, electric arcs, discharges, and high temperature plasmas.

b. Partially Overlapping Spectral Lines:



These spectra are characteristic of flames, combustion zones, planetary atmospheres, and moderate-to-high pressure gases.

c. Strongly Overlapping Lines:



These spectra exhibit no strong spectral feature or colors. They are characteristic of the emission from solids, liquids, and very high pressure gases.

1.2 STRUCTURE OF A SINGLE SPECTRAL LINE

An individual spectral line may be characterized by a width, height, or area, and a shape. Three effects are commonly important for determining the width and shape of a spectral line: (a) the translational motion of the molecule, (b) collisions with other molecules, and (c) the finite radiative lifetime.

## 1.2.1 DOPPLER LINE BROADENING

The random motion of a molecule in a gas gives rise to positive or negative Doppler frequency shifts. When the emission is observed from a gas containing many molecules, the molecules moving toward the observer will appear to have slightly increased frequency of emission and those moving away from the observer will seem to have a lower frequency. The probable number of molecules having a velocity between  $v$  and  $v + dv$  is given by the expression

$$N(v) dv = \sqrt{\frac{kT}{m\pi}} e^{-mv^2/kT} dv, \quad (1-30)$$

where  $k$  is the Boltzmann constant and  $T$  is the kinetic temperature of the gas. The Doppler shift caused by the motion of the molecule toward the observer, with velocity  $v$ , is given by

$$\frac{\Delta\omega}{\omega} = \frac{\Delta f}{f} = \frac{v}{c} \quad (1-31)$$

where  $\omega$  is the average frequency of the transition and  $c$  is the velocity of light. Thus the probability that the emission will occur in a spectral interval between wave number  $\omega$  and  $\omega + d\omega$  is given by the expression

$$e^{-\frac{(\omega - \omega_0)^2 \ln 2}{\gamma_D^2}}$$

where the Doppler half-width (displacement from  $\omega_0$  at half-height) is given by

$$\gamma_D = \frac{\omega_0}{c} \sqrt{kT \ln 2/m} \quad (1-32)$$

## 1.2.2 NATURAL LIFETIME LINE BROADENING

The second effect that gives rise to a finite width for the line is the so-called "natural lifetime" broadening. This effect is most easily understood by considering the problem of a free classical oscillator which radiates and whose oscillation amplitude decreases as a result of the energy radiated. If one supposes that the time for the amplitude of the oscillation to fall by a factor  $e^{-1} = 0.368$  is  $\tau$ , then one may write an expression for the amplitude for the radiative wave:

$$e^{-t/2\tau} \sin(\omega_0 t) \quad (1-33)$$

In the last section, it was shown that the absolute square of the Fourier transform of this amplitude is proportional to the power radiated per unit frequency interval. This power spectrum provides a fundamental limit to the possible sharpness of a spectral line and has the form:

$$\frac{\text{constant}}{(\omega - \omega_0)^2 + \tau^{-2}}$$

## 1.2.3 COLLISIONAL LINE BROADENING

The third mechanism that gives finite width to a spectral line is that caused by random collisions between molecules. Suppose that there are a number of molecules in a gas volume which are radiating at a finite rate. For the purpose of this example, assume that their natural radiative lifetime is very long. During the time the molecule radiates, it undergoes random collisions with other molecules. As a result of these collisions, the wavetrain that is being emitted tends to be disrupted. As a rough approximation, a collision can be conveniently described as producing a discontinuous change in the phase of the oscillator at the time of the collision. Because of the occasional disruption of the wavetrain at each collision, this wavetrain cannot be characterized by a single frequency but must be represented in terms of a collection of frequencies which are centered about the characteristic oscillation frequency. Fourier analysis of such a spectrum yields a power spectrum of the following form

$$\frac{\text{constant}}{(\omega - \omega_0)^2 + \tau_c^{-2}}$$

## CHAPTER 1 – INTRODUCTION

where  $\tau_c$  is the mean time between phase-disrupting collisions. It is interesting to note that the line shape resulting from collision broadening is of identical form to that for natural line broadening, although the mechanisms involved are quite different. The time between effective collisions  $\tau_c$  is usually related to the time between collisions that are sufficiently strong to change the direction and momentum of the two colliding molecules. However, this relation is only qualitative and, in general, it is necessary to measure the spectral line width directly. Two facts about the widths of collision broadened lines should be remembered. First, the widths at pressures and temperatures of interest for combustion problems tend to be very small compared to the width of the entire spectrum. This latter width is conveniently represented as the half-width of the Planck function (see Chapter 2) which at a temperature of 2000K is of the order of  $3000 \text{ cm}^{-1}$ . Indeed, the widths of the lines are so small that it is often difficult to get a direct measurement of the line width, even with very good high-resolution infrared instruments, so indirect techniques are usually required. It is primarily the fact that these line widths are very much smaller than the spectral interval that leads to the great computational difficulties in computing the radiative transfer.

A precise numerical evaluation of the emission would require evaluating the emission at wavelength intervals separated by a small fraction of a spectral line width. In a typical case (e.g., water vapor), it would be necessary to carry out the computation of the emission at between 4000 and 400 000 different frequencies. Since each evaluation of a particular frequency requires a separate integration over the line of sight, such a direct calculation technique is warranted only under most extreme circumstances and for most heat transfer problems cannot be tolerated. Much of the effort in the past several years in the field of radiative heat transfer has been devoted to developing approximate techniques for eliminating the necessity of carrying out this detailed frequency evaluation and integration. The result of this effort has been the development of the so-called "band model" techniques and these form the base for the prediction procedures to be described in the following chapters.

## CHAPTER 2

## BASIC PRINCIPLES

A survey of the basic concepts and expressions that are required for the proper understanding of the procedures and techniques which are developed later is given here.

Section 2.1 is a review of the basic principles of radiant transfer: radiation from black and nonblack bodies, and the equations for radiant heat transfer.

Section 2.2 is a study of the types and properties of isolated spectral lines, a necessary background for the later study of band models.

Section 2.3 is a descriptive review of the spectra of molecular gases: their spectral structure and strength of the bands and individual lines.

Section 2.4 summarizes the dependence of line width on pressure and temperature and presents the methods used for adjusting the line width for these effects.

Section 2.5 considers the spectral properties of particulate matter — both absorption and scattering.

2.1 RADIATIVE TRANSFER

## 2.1.1 NOMENCLATURE

The system of symbols and nomenclature for radiometric quantities adopted by the Working Group on Infrared Backgrounds [2-1] is used in this discussion. Reference 2-1 may be consulted for a comparison of this system with other systems of nomenclature. A nomenclature for some of the quantities which will be discussed in this section is given as Table 2-1. The following abbreviations for units of measure will be used in this discussion:

cm	centimeters
cm <sup>-1</sup>	wavenumbers
K	degrees Kelvin

The values of several physical constants of basic interest to infrared radiation are listed in Table 2-2.

## 2.1.2 BLACKBODY

A blackbody is defined as a body whose surface absorbs all incident radiation. The absorption and emission characteristics of such a body depend on the temperature  $T$  of the surface and not on its chemical and physical states. The spectral distribution of radiant power emitted by the surface of a blackbody at temperature  $T$  into a solid angle of  $2\pi$  steradians (the "blackbody spectral radiant emittance") is given by the Planck function [2-1] (values are given in Table A2-1)

$$W_{\omega}^0(\omega, T) = \frac{C_1 \omega^3}{\exp(C_2 \omega/T) - 1} \text{ watts/cm}^2 \text{ cm}^{-1} \quad (2-1)$$

or

$$W_{\lambda}^0(\lambda, T) = \frac{C_1 \lambda^{-5}}{\exp(C_2/\lambda T) - 1} \text{ watts/cm}^2\text{-cm} \quad , \quad (2-2)$$

where  $C_1$  and  $C_2$  are the first and second radiation constants (Table 2-2).

TABLE 2-1. NOMENCLATURE OF INFRARED RADIOMETRIC QUANTITIES

Property	Symbol	Equation No.	Description
Spectrometer Slit Function	$g(\omega', \omega)$		Instrument response to radiation of wavenumber $\omega'$ when set at wavenumber $\omega$ , normalized so that $\int g(\omega', \omega) d\omega' = 1.$
Absorption Coefficient	$k(\omega, T)$	2-14	Coefficient of proportionality between the decay of spectral radiance and its optical path (Beer's Law).
Mean Absorption Coefficient	$\bar{k}(\omega, T)^a$		An average value of the absorption coefficient $k(\omega, T)$ taken over an interval centered at $\omega$ such as to smooth out the fine structure in $k(\omega, T)$ .
Radiance	$N(T)$	2-5	Power radiated per unit solid angle per unit projected area.
Spectral Radiance	$N_{\omega}(\omega, T)$		Spectral distribution of radiance (q.v.) with respect to wavenumber (also referred to as "intensity" in the radiation transfer literature).
Line Strength	S	2-23	Wavenumber integral of absorption coefficient of a spectral line.

TABLE 2-1. (Continued)

Property	Symbol	Equation No.	Description
Equivalent Width	$W$	2-24	Wavenumber integral of absorptivity of a spectral line.
Radiant Emittance	$W(T)$	2-3	Power radiated into a solid angle of $2\pi$ radians per unit area of a surface at temperature $T$ .
Spectral Radiant Emittance	$W_{\omega}(\omega, T)$ $[W_{\lambda}(\lambda, T)]$		Spectral distribution of radiant emittance (q.v.) per unit wavenumber [wavelength] interval.
Blackbody Spectral Radiant Emittance	$W_{\omega}^0(\omega, T)$ $[W_{\lambda}^0(\lambda, T)]$	2-1 [2-2]	Spectral distribution of radiant emittance of a blackbody per unit wavenumber [wavelength] interval.
Spectral Absorptivity	$\alpha(\omega, T)$	2-12	The fraction of the radiant energy of wavenumber $\omega$ incident upon a body which is absorbed by it.
Half-width	$\gamma$		Wavenumber interval between the wavenumber of the line center and the wavenumber at which the absorption coefficient is one-half of its value at the line center.

TABLE 2-1. (Concluded)

Property	Symbol	Equation No.	Description
Spectral Emissivity	$\epsilon(\omega, T)$	2-11	The ratio of spectral radiance of a body to the spectral radiance of a blackbody at the same temperature.
Mean Emissivity [ Mean Absorptivity ] [ Mean Transmissivity ]	$\bar{\epsilon}(\omega, T)^a$ $[\bar{\alpha}(\omega, T)]^a$ $[\bar{\tau}(\omega, T)]^a$		An average value of emissivity [ absorptivity, transmissivity ] taken over an interval centered at $\omega$ such as to smooth out the fine structure in $\epsilon[\omega, \tau]$ .
Total Emissivity	$\epsilon_T(T)$	3-12	Ratio of the radiance of a body at temperature $T$ to that of a blackbody at the same temperature.
Transmissivity	$\tau(\omega, T)$	2-13	The fraction of the radiant energy of wavenumber $\omega$ incident upon a body which is transmitted by it.
Wavenumber of Maximum Blackbody Spectral Radiance	$\omega_m$	2-9	Value of $\omega$ for which $W_\omega^0(\omega, T)$ is a maximum.

- a. The bar to indicate averaging over a spectral interval is often omitted in the discussion of band models and experimental data when it is not required for clarity.

TABLE 2-2. VALUES OF SELECTED PHYSICAL CONSTANTS

Name	Symbol	Value <sup>a</sup>
Planck Constant	h	$6.6256 \times 10^{-27}$ erg-sec
Speed of Light in Vacuum	c	$2.997925 \times 10^{10}$ cm sec <sup>-1</sup>
Boltzmann Constant	k	$1.38054 \times 10^{-16}$ ergK <sup>-1</sup>
First Radiation Constant	C <sub>1</sub>	$2\pi hc^2 = 3.7405 \times 10^{-12}$ watts cm <sup>2</sup>
Second Radiation Constant	C <sub>2</sub>	$hc/k = 1.43879$ cmK
Stefan-Boltzmann Constant	$\sigma$	$\frac{2k^4\pi^5}{15h^3c^2} = 5.6697 \times 10^{-12}$ watts cm <sup>-2</sup> K <sup>-4</sup>

a. Values recommended by NAS-NRC Committee on Fundamental Constants. See NBS Technical News Bulletin, October 1963.

### 2.1.3 RADIANT EMITTANCE

The power emitted per unit area into a solid angle of  $2\pi$  steradians and per unit wavenumber interval at a wavenumber  $\omega$  is the "spectral radiant emittance"  $W_{\omega}(\omega, T)$ . The total power emitted per unit area into a solid angle of  $2\pi$  steradians is called the "radiant emittance," and is found by integration of equation (2-1) over all  $\omega$  to be

$$W(T) \equiv \int_0^{\infty} W_{\omega}(\omega, T) d\omega \quad (2-3)$$

If the emitting surface is a blackbody, the radiant emittance  $W(T)$  becomes

$$W^0(T) \equiv \int_0^{\infty} W_{\omega}^0(\omega, T) d\omega = \sigma T^4 \quad , \quad (2-4)$$

where  $\sigma$  is the Stefan-Boltzmann constant (Table 2-2). Functions for evaluating the integral in equation (2-4) are given in Table A2-1.

#### 2.1.4 RADIANCE

Radiance  $N$  is defined as the power radiated from a surface in a given direction per unit solid angle  $\Omega$  per unit projected area; symbolically,

$$N = \frac{1}{\cos \theta} \frac{\partial}{\partial \Omega} W \quad (2-5)$$

where  $\theta$  is the angle between the normal to the surface and the direction under consideration. Equation (2-5) is expressed more properly as

$$\int_{2\pi} N \cos \theta d\Omega \equiv W \quad . \quad (2-6)$$

For an isotropic emitter ( $N$  independent of angle) such as a blackbody, the integral  $\int_{2\pi} \cos \theta d\Omega$  leads to

$$N = \frac{1}{\pi} W \quad . \quad (2-7)$$

##### 2.1.4.1 Spectral Radiance

The spectral radiance  $N_{\omega}$  and the spectral radiant emittance  $W_{\omega}$  are related by equations identical to equations (2-5), (2-6), and (2-7) in which  $N$  and  $W$  are replaced by  $N_{\omega}$  and  $W_{\omega}$ , respectively.

2.1.4.1.1 Maximum Blackbody Spectral Radiance

The maximum value of the blackbody spectral emittance  $W_{\omega}^0$ , at a given temperature, is obtained from equation (2-1) by setting  $(\partial W_{\omega}^0 / \partial \omega) = 0$ . The corresponding wavenumber is

$$\omega_m = 1.961 T \quad (2-8)$$

Similarly, the wavelength  $\lambda_m$  (cm) corresponding to maximum emittance  $W_{\lambda}^0$  is obtained from equation (2-9):

$$\lambda_m = \frac{1}{3.451 T} \quad (2-9)$$

Note that the spectral radiance per unit wavenumber  $W_{\omega}^0$  has a maximum at a different wavelength than the spectral radiance per unit wavelength  $W_{\lambda}^0$ . Thus for  $T = 300K$ ,  $W_{\omega}^0$  is a maximum at  $\omega = 588 \text{ cm}^{-1}$ , while  $W_{\lambda}^0$  is a maximum at  $\lambda = 9.66 \times 10^{-4} \text{ cm} = 9.66 \mu$ , or  $\omega = 1035 \text{ cm}^{-1}$ .

Expressions for the maximum blackbody spectral radiance are obtained by substituting the values for the spectral location of the maximum in the Planck function. The results are

$$W_{\omega_m} = 1.785 \times 10^{-12} T^3 \text{ watts/cm}^2\text{-cm}^{-1} \quad (2-10)$$

from equations (2-1) and (2-8), and

$$W_{\lambda_m} = 12.86 \times 10^{-16} T^5 \text{ watts/cm}^2\text{-}\mu \quad (2-10a)$$

from equations (2-2) and (2-9).

2.1.4.2 Spectral Emissivity

The ratio of the spectral radiance of any real body to the spectral radiance of a blackbody at the same temperature is defined as the spectral emissivity:

$$\epsilon(\omega) = N_{\omega}(\omega, T) / N_{\omega}^0(\omega, T) \quad . \quad (2-11)$$

2.1.4.3 Spectral Absorptivity

The spectral absorptivity  $\alpha(\omega)$  is defined as the fraction of the radiant energy of wavenumber  $\omega$  incident upon the body which is absorbed by it. Kirchhoff's law states that under conditions of thermal equilibrium, the emissivity and the absorptivity are equal:

$$\alpha(\omega) = \epsilon(\omega) \quad . \quad (2-12)$$

2.1.4.4 Spectral Reflectivity

The spectral reflectivity  $r(\omega)$  is defined as the fraction of the radiant energy of wavenumber  $\omega$  incident upon a body which is reflected at its surface.

2.1.4.5 Spectral Transmissivity

When the surface is not totally opaque, its absorption and reflection do not account for all the energy received, as a fraction of this energy crosses the surface and penetrates into the second medium. The spectral transmissivity  $\tau(\omega)$  is denoted by the fraction:

$$\tau(\omega) \equiv 1 - \alpha(\omega) - r(\omega) \quad . \quad (2-13)$$

Note that, in general,  $\epsilon$ ,  $\alpha$ ,  $r$ , and  $\tau$  depend on the angle between the light path and the normal to the surface.

2.1.5 ABSORPTION COEFFICIENT

Consider a straight-line path in the direction  $\vec{L}$  through the radiating medium from an arbitrary origin. Let  $s$  denote the position of a point  $M$  on this path and  $\rho(s)$  the local density at  $M$ . At a given wavenumber  $\omega$ , an absorption coefficient  $k$  is defined such that the spectral radiance absorbed by the small segment  $\Delta s$  around  $M$  is given by

$$\Delta N_{\omega}(\omega, s) = -k(\omega, s)\rho(s)N_{\omega}(\omega, s)\Delta s \quad . \quad (2-14)$$

Equation (2-14) is a statement of the fundamental law of radiation transfer, variously credited to Bouguer, Lambert, or Beer. It is a phenomenological statement of proportionality and serves, therefore, as a definition for the absorption coefficient  $k$ , given in units reciprocal to those of  $\rho(s)\Delta s$ .

2.1.6 EQUATION OF TRANSFER IN NONSCATTERING MEDIA  
(IN LOCAL THERMODYNAMIC EQUILIBRIUM)

The differential equation for the spectral radiance as a function of  $s$  is

$$\frac{\partial N_{\omega}(\omega, s)}{\partial s} = -k(\omega, s)\rho(s)N_{\omega}(\omega, s) + k(\omega, s)\rho(s)N_{\omega}^0(\omega, s) \quad , \quad (2-15)$$

where  $N_{\omega}(\omega, s)$ , and  $k(\omega, s)$  mean  $N_{\omega}[\omega, T(s)]$  and  $k[\omega, T(s)]$ .

2.1.7 SPECTRAL RADIANCE OF AN EXTENDED MEDIUM

The solution of this equation of transfer is given by

$$N_{\omega}(\omega, s) = \int_{-\infty}^s N_{\omega}^0(\omega, s') \exp \left[ - \int_{s'}^s k(\omega, s'')\rho(s'') ds'' \right] k(\omega, s')\rho(s') ds' \quad (2-16)$$

when the medium extends to infinity in the direction opposite to  $\vec{L}$ . If the radiating medium does not extend to  $-\infty$  but, say, to a point  $a$ , this lower limit may be replaced with the appropriate value  $s = a$ . If the medium is bounded by walls,

$$N_{\omega}(\omega, s) = N_{\omega}(\omega, a) \exp \left[ - \int_a^s k(\omega, s') \rho(s') ds' \right] + \int_a^s N_{\omega}^0(\omega, s') \exp \left[ - \int_{s'}^s k(\omega, s'') \rho(s'') ds'' \right] k(\omega, s') \rho(s') ds' \quad (2-17)$$

where  $N_{\omega}(\omega, a)$  is the wall radiance.

#### 2.1.8 TRANSMISSIVITY

The transmissivity of the volume between  $s$  and  $s'$  is defined as

$$\tau(\omega; s', s) = \exp \left[ - \int_{s'}^s k(\omega, s'') \rho(s'') ds'' \right] \quad , \quad (2-18)$$

while its absorptivity in the absence of any reflective interface [equation (2-13)] is

$$\alpha(\omega; s', s) = 1 - \exp \left[ - \int_{s'}^s k(\omega, s'') \rho(s'') ds'' \right] \quad . \quad (2-19)$$

The transmissivity  $\tau$  [equation(2-18)] can be introduced into equation (2-17):

CHAPTER 2 – BASIC PRINCIPLES

$$N_{\omega}(\omega, s) = N_{\omega}(\omega, a)\tau(\omega; a, s) + \int_a^s N_{\omega}^0(\omega, s')\tau(\omega; s', s)k(\omega, s')\rho(s')ds' , \quad (2-20)$$

or

$$N_{\omega}(\omega, s) = N_{\omega}(\omega, a)\tau(\omega; a, s) + \int_a^s N_{\omega}^0(\omega, s') \frac{\partial}{\partial s'} \tau(\omega; s', s) ds' , \quad (2-21)$$

or

$$N_{\omega}(\omega, s) = \int_{-\infty}^s N_{\omega}^0(\omega, s') \frac{\partial}{\partial s'} \tau(\omega; s', s) ds' , \quad (2-22)$$

if the radiating medium extends to infinity in the negative direction.

## 2.2 LINE RADIATION

### 2.2.1 HOMOGENEOUS MEDIA

Radiation which is emitted by molecular gases in the infrared region characteristically has a line structure, resulting from transitions which take place between discrete energy levels in the molecules.

This section is concerned with emission from gases whose physical properties (temperature, composition, pressure) are uniform throughout.

#### 2.2.1.1 Line Strength

The spectral contour of a particular line is defined by an absorption coefficient  $k(\omega)$ . The line strength  $S$  is defined as:

$$S \equiv \int k(\omega) d\omega \quad . \quad (2-23)$$

#### 2.2.1.2 Line Width

In Section 1.2 the structure of a single line was discussed. Once the line strength is known, as well as its kind of broadening (Doppler or collision), Section 1.1.3 shows that the additional knowledge of the parameter  $\gamma$  (the line half-width) specifies the line contour completely. A combined Doppler-collision broadening can be similarly calculated through existing tables on the basis of the knowledge of  $\gamma_D$  and  $\gamma_C$  (Section 2.2.1.3.3).

#### 2.2.1.3 Equivalent Width

The equivalent width of a line is defined as the wavenumber integral of the spectral absorptivity

$$W = \int \alpha(\omega) d\omega = \int \{1 - \exp[-k(\omega)u]\} d\omega \quad (2-24)$$

The symbol  $W$  is a standard one for denoting equivalent width (units of  $\text{cm}^{-1}$ ) and should not be confused with the symbol  $W(T)$  denoting radiant emittance (units of  $\text{watts cm}^{-2}$ ). Equation (2-24) illustrates the fact that  $W$  is the frequency interval which one would have to make totally absorbing (black) to produce the same absorption as  $\alpha(\omega)$  over the whole spectrum, hence the name "equivalent width." The curve defined by  $W$  as a function of pathlength is known as the "curve of growth."

### 2.2.1.3.1 Equivalent Width for Collision Broadened Lines

Many theories have been advanced to describe the shape of a collision broadened line; the simplest of these yields the so-called Lorentz shape for the line contour (which, in general, is quite well verified experimentally):

$$k(\omega) = \frac{S\gamma}{\pi} \frac{1}{(\omega - \omega_0)^2 + \gamma^2} \quad (2-25)$$

In this expression,  $S$  represents the line strength [equation (2-23)] and  $\gamma$  represents the half-width at half-height. The half-width depends on the partial pressure of the gas mixture:

$$\gamma = \sum_i \gamma_{0_i} p_i \quad (2-26)$$

where  $p_i$  is the partial pressure of the components of the gas and  $\gamma_{0_i}$  is the corresponding line half-width parameter. It will be seen in Section 2.2.1.6 that  $\gamma_{0_i}$  depends on temperature as well.

The equivalent width  $W$  of a Lorentz line, which was defined by equation (2-24) to be the integral of the absorptivity of this line (and of this line only) over the whole frequency interval, is given by References 2-2 and 2-3:

$$W = 2\pi\gamma f(x) \quad , \quad (2-27)$$

where

$$x = Su/2\pi\gamma$$

and  $f(x)$  is the Ladenburg-Reiche function shown in Chapter 3 (Fig. 3-2):

$$f(x) \equiv x \exp(-x)[I_0(x) + I_1(x)] \quad , \quad (2-28)$$

in which  $I_0$  and  $I_1$  are modified Bessel functions. (See Appendix 2-A for table of  $f(x)$ , series representations, and approximation formulas.)

#### 2.2.1.3.2 Equivalent Width for Doppler Broadened Lines

The contour of a Doppler line of intensity  $S$  centered at  $\omega_0$  is given by References 2-2 and 2-3:

$$k(\omega) = k_0 \exp \left[ - (\omega - \omega_0)^2 (\ln 2) / \gamma_D^2 \right] \quad , \quad (2-29)$$

where

$$k_0 = k(\omega_0) = (S/\gamma_D) [(\ln 2)/\pi]^{1/2}$$

and where  $\gamma_D$  is the Doppler half-width (i.e., the half-width at half-height):

$$\gamma_D = [2kT (\ln 2) / mc^2]^{1/2} \omega_0 \quad , \quad (2-30)$$

where  $m$  is the molecular mass, or, numerically,

$$\gamma_D = 0.3581 \times 10^{-6} \omega (T/M)^{1/2} \quad , \quad (2-31)$$

where M is the molecular weight in unified atomic mass units, T is in K, and  $\gamma_D$  and  $\omega$  are in the same units.

The equivalent width is

$$W = \frac{S}{k_0} D(k_0 u) \quad , \quad (2-32)$$

where

$$D(y) = \pi^{-1/2} \int_{-\infty}^{\infty} \{1 - \exp[-y \exp(-\xi^2)]\} d\xi \quad . \quad (2-33)$$

The integration cannot be performed directly. Various series forms have been developed, and tabulated values are available. A graph of  $D(y)$  is given in Chapter 3 (Fig. 3-7) and series expansions are given in Appendix 2-B.

For long pathlengths it is usually necessary to consider the effect of the Lorentz component of the line shape. (See Section 2.2.1.3.3.)

Several approximate forms for  $W$ , and their error limits, are presented in Appendix 2-B.

### 2.2.1.3.3 Equivalent Width for Combined Doppler-Lorentz (Voigt) Lines

In the intermediate range in which both the Doppler and the Lorentz components are important, the line shape is usually defined as a convolution of the Doppler and Lorentz components (Fig. 2-1):

$$k(\omega) = \frac{S a}{\pi \gamma_D} \left( \frac{\ln 2}{\pi} \right)^{1/2} \int_{-\infty}^{\infty} \frac{\exp(-y^2)}{a^2 + (\xi - y)^2} dy \quad , \quad (2-34)$$

where

$$a = (\ln 2)^{1/2} \gamma / \gamma_D$$

$$\xi = (\ln 2)^{1/2} (\omega - \omega_0) / \gamma_D$$

and  $y$  is a dummy variable. Numerous series expansions for equation (2-34) have been developed. For example, see pp. 45-54 of Reference 2-4.

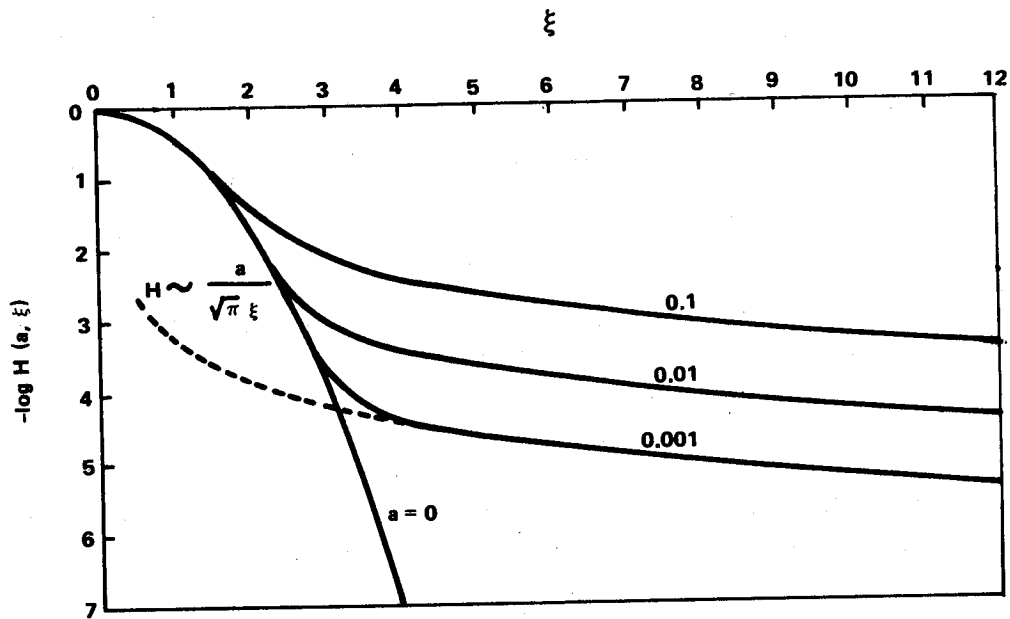


Figure 2-1. The function

$$H(a, \xi) \equiv \frac{a}{\pi} \int_{-\infty}^{+\infty} \frac{\exp(-y^2)}{a^2 + (\xi - y)^2} dy$$

for various values of the collision-Doppler ratio  $a$  [equation (2-34)].

No convenient algebraic forms are available for the equivalent width of a combined Doppler-Lorentz line. Tables and graphs are available (see pp. 55-59 of Reference 2-4).

2.2.2 INHOMOGENEOUS MEDIA

In the general case where the temperature, pressure, and absorber concentration vary along the line of sight, the expression for line spectral radiance obtained from the integration of the spectral radiance  $N_{\omega}$  [equation (2-20)] over the line spectral interval  $\Delta\omega$  is:

$$\begin{aligned}
 N(s) &\equiv \int_{\Delta\omega} N_{\omega}(\omega, s) d\omega \\
 &= \int_{\Delta\omega} \int_{-\infty}^s N_{\omega}^0(\omega, s') \exp \left[ - \int_{s'}^s k(\omega, s'') \rho(s'') ds'' \right] k(\omega, s') \rho(s') ds' d\omega,
 \end{aligned}
 \tag{2-35}$$

or, equivalently,

$$N(s) = \int_{\Delta\omega} \int_{-\infty}^s N_{\omega}^0(\omega, s') \frac{\partial}{\partial s'} \tau(\omega; s', s) ds' d\omega, \tag{2-36}$$

where  $\Delta\omega$  refers to the spectral interval over which the line radiates.

If the line is thin, i.e.,  $\tau(\omega; s', s) \approx 1$  for all  $\omega$  and  $s'$ , then

$$N(s) \approx \int_{\Delta\omega} \int_{-\infty}^s N_{\omega}^0(\omega, s') k(\omega, s') \rho(s') ds' d\omega, \tag{2-37}$$

or,

$$N(s) \approx \int_{-\infty}^s N_{\omega}^0(\omega_0, s') S(s') \rho(s') ds', \tag{2-38}$$

where  $\omega_0$  is the wavenumber at the line center.

If the temperature is approximately constant along the line of sight (although the pressure and concentration may vary),

$$\begin{aligned}
 N(s) &\approx \int_{\Delta\omega} N_{\omega}^0(\omega, T_0) \int_{-\infty}^s \exp \left[ - \int_{s'}^s k(\omega, s'') \rho(s'') ds'' \right] \\
 &\quad \times k(\omega, s') \rho(s') ds' d\omega \approx \int_{\Delta\omega} N_{\omega}^0(\omega, T_0) [1 - \tau(\omega, s)] d\omega \\
 &\approx N_{\omega}^0(\omega_0, T_0) W(s) \quad , \quad (2-39)
 \end{aligned}$$

where  $W(s)$  is the equivalent width of the line [equation (2-27)]:

$$W(s) = \int_{\Delta\omega} \left\{ 1 - \exp \left[ - \int_{-\infty}^s k(\omega, s') \rho(s') ds' \right] \right\} d\omega .$$

#### 2.2.2.1 A Two-Parameter Approximation for Low Resolution Curves of Growth

The Curtis-Godson approximation in its basic form represents the equivalent width of a single line along an inhomogeneous path (along which the line strength  $S$  and half-width  $\gamma$  may vary) in terms of the equivalent width of a single line for a homogeneous path using an appropriately defined effective strength  $S_e$  and half-width  $\gamma_e$ .

The effective strength and half-width are defined by the condition of a simultaneous matching of the equivalent widths for large and small values of the optical path. Consider the case of a path through several isothermal slabs. For a single Lorentz line described by  $S_i$  and  $\gamma_i$  in region  $i$  of thickness  $u_i$ , the equivalent  $S_e$  and  $\gamma_e$  are defined by

$$S_e \equiv \frac{\sum_i S_i u_i}{\sum_i u_i} \quad (2-40)$$

and

$$\gamma_e \equiv \frac{\sum_i S_i \gamma_i u_i}{\sum_i S_i u_i} \quad , \quad (2-41)$$

and the approximate equivalent width is given by the Curtis-Godson approximation:

$$W = 2\pi\gamma_e f(S_e u / 2\pi\gamma_e) \quad , \quad (2-42)$$

where  $u = \sum_i u_i$ . This prescription is exact in certain limiting cases (when absorption at the line center is either very weak or very strong). In other cases, some error results. The Curtis-Godson approximation is also applied to band models, in addition to single lines, and is discussed in detail in Chapter 4.

2.3 MOLECULAR EMISSION

Vibrational band systems appear in the infrared region as a result of a change in electric dipole moment between two vibrational states. In general, a diatomic molecule with a center of symmetry (e.g.,  $N_2$ ,  $O_2$ ) has a zero dipole moment in all vibrational states, and hence has a zero band strength. (The weak  $O_2$  band system in the near infrared results from an electronic transition.) In the case of centrally symmetric polyatomic molecules (e.g.,  $CO_2$ ), some transitions are excluded by symmetry considerations, while others are not. A brief review of molecular structure is given in Section 2.3.1.

An idealized representation of a diatomic molecule as a harmonic oscillator (i.e., a linear spring-point mass model with a dipole moment also linear in the nuclear displacement) predicts the existence of vibrational transitions in which the vibrational quantum number changes by unity (the "fundamental" system). Consideration of various nonlinearities explains the observed existence of generally much weaker higher-order ("overtone") transitions in which the change in vibrational quantum number is an integer greater than unity.

The strength of these bands can be expressed in various equivalent ways. Quantum-mechanically, the dipole moment matrix element,

$\int \psi M \psi' dx$ , is a logical parameter. An experimentalist might prefer to define a band strength as an integral of the absorption coefficient over the spectral region in which absorption occurs. An alternative scheme is to describe the strength of absorption in terms of the absorption of a free electron oscillating at the vibrational frequency (the "f-number"). The interrelationships of these quantities are summarized in Section 2.3.2.

It is frequently necessary to subscript or otherwise identify the particular transitions to which these parameters refer. The term "band" is used here to refer to a particular vibrational transition  $v \rightarrow v'$ ; whereas, the term "band system" refers to the set of all vibrational transitions in which the quantum numbers change by the same amount. This distinction, which may be unimportant at low temperatures, becomes quite significant at high temperatures. Line and band strengths for various molecules are discussed in Section 2.3.3.

## 2.3.1 MOLECULAR STRUCTURE

2.3.1.1 Diatomic Molecules

A diatomic molecule can be rather well represented in a semiclassical picture as a rotating pair of masses joined by a spring. There is some degree of interaction between the vibrational and rotational motion. This interaction will be discussed later; these motions will first be considered separately.

The molecule may rotate around an axis perpendicular to the molecular axis (i. e., the axis through the two nuclei). The kinetic energy of rotation is expressed in wavenumber units by

$$T_r = E_r/hc = BJ(J + 1) \quad , \quad (2-43)$$

where  $B$  is the rotational constant ( $=h/8\pi^2 cI$ , where  $I$  is the moment of inertia), and the rotational quantum number  $J$  may assume the values 0, 1, 2, ... .

To the extent to which the molecule rotates as a rigid body,  $B$  is constant. However, effects of nonrigidity, such as centrifugal stretching and vibrational motion, cause deviations from equation (2-43). These effects are usually accounted for by replacing the constant  $B$  by a multiple power series expansion in  $J(J+1)$  and  $\left(v + \frac{1}{2}\right)$ , where  $v$  is the vibrational quantum number. [See equation (2-45).]

If the vibrational motion is analyzed by representing the molecule as a harmonic oscillator (i. e., a linear spring and point mass model), the vibrational energy levels in units of  $\text{cm}^{-1}$  are given by

$$T_v = E_v/hc = \omega_0 \left( v + \frac{1}{2} \right) \quad , \quad (2-44)$$

where  $\omega_0$  is the oscillator frequency (in  $\text{cm}^{-1}$ ).

The assumption of a quadratic potential well is usually quite good near the minimum. However, with increasing vibrational quantum number, it becomes progressively poorer (Fig. 2-2). The energy levels are usually represented by a power series in  $\left( v + \frac{1}{2} \right)$ .

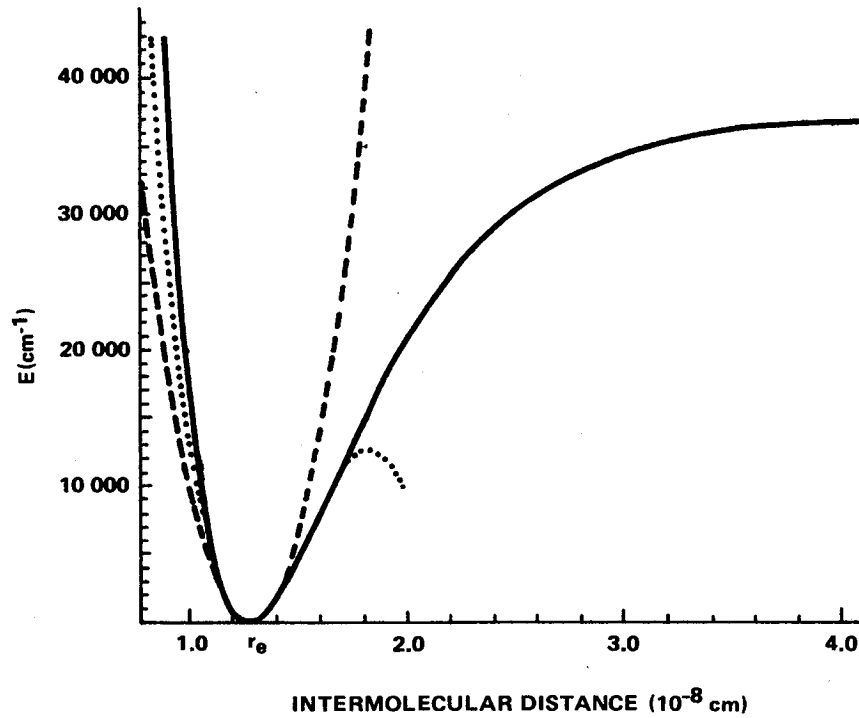


Figure 2-2. Potential curve of the molecule (anharmonic oscillator). (The full curve is drawn for the ground state of HCl. The broken-line and the dotted curves are the ordinary and the cubic parabola, respectively, that form the best approximation to the full curve at the minimum.)

A general expression for the vibrational-rotational energy levels of a real diatomic molecule is

$$\begin{aligned}
 T(v, J) = E(v, J)/hc = & \omega_e \left( v + \frac{1}{2} \right) - \omega_e x_e \left( v + \frac{1}{2} \right)^2 + \omega_e y_e \left( v + \frac{1}{2} \right)^3 \\
 & + \omega_e z_e \left( v + \frac{1}{2} \right)^4 + B_e J(J+1) - \alpha_e \left( v + \frac{1}{2} \right) J(J+1) \\
 & - D_e J^2(J+1)^2 + \dots \quad (2-45)
 \end{aligned}$$

## CHAPTER 2 – BASIC PRINCIPLES

The coefficients of higher-order terms in the power series expansion usually decrease rapidly. For example, for CO, Herzberg [2-5] lists

$$\omega_e = 2170.21 \text{ cm}^{-1}$$

$$B_e = 1.9314 \text{ cm}^{-1}$$

$$\omega_e x_e = 13.461 \text{ cm}^{-1}$$

$$\alpha_e = 0.01749 \text{ cm}^{-1}$$

$$\omega_e y_e = 0.0308 \text{ cm}^{-1}$$

$$D_e = 0.000006 \text{ cm}^{-1}$$

Transitions may take place between two vibration-rotation levels when the electric dipole moment changes between these levels and certain "selection rules" are met. In particular, the rotational quantum number must change by unity:  $\Delta J = \pm 1$ . A selection rule for the vibrational quantum number is obeyed, at least approximately:  $\Delta v = \pm 1$ . Transitions may also occur with  $|\Delta v| = 2, 3, \dots$ , although usually with rapidly decreasing intensity. Transitions for which  $|\Delta v| = 1$  are called fundamental transitions, and those for which  $|\Delta v| > 1$  are called overtones. Quantitative expressions for the intensities will be discussed in Section 2.3.3.

If the molecule has a permanent dipole moment, pure rotational transitions may occur with  $\Delta v = 0$ . Such transitions take place at quite low frequencies, typically of the order of  $10$  to  $10^2 \text{ cm}^{-1}$ . The tail of the rotational band of molecules having small moments of inertia (e.g., of  $\text{H}_2\text{O}$ ,  $\text{HF}$ , or  $\text{HCl}$ ) may be significant up to about  $10^3 \text{ cm}^{-1}$ .

Qualitatively, a vibration-rotation band of a diatomic molecule at low temperatures consists of two sequences of nearly equally spaced lines heading toward lower and higher frequencies from the band center (the "P" and "R" branches, respectively). The intensities of the lines increase initially outward from the band center, reach maxima, then decrease. At higher temperatures, the appearance of band system changes. With increasing temperature, the maxima move outward from the band center, as more lines in each band become of significant intensity (Fig. 2-3).

As the temperature is further increased, other bands with the same value of  $\Delta v$  appear superposed on the fundamental band. The lines in each band are nearly equally spaced, but there is no regular relationship between the locations of the lines in one band and those in another.

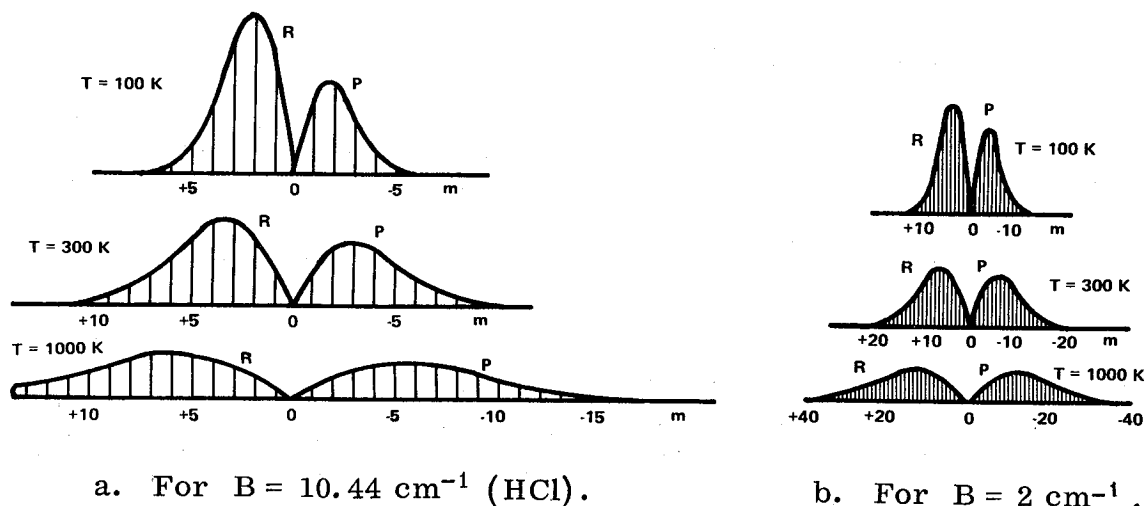


Figure 2-3. Intensity distribution in rotation-vibration bands in absorption at 100K, 300K, and 1000K ( $m = J + 1$  in the R branch and  $m = -J$  in the P branch).

Because of anharmonicities in the molecule, these higher-order vibrational transitions have progressively lower frequencies. Since the line spacing tends to increase toward lower frequencies and decrease toward higher frequencies, the band tends to spread more toward the direction of lower frequencies (Fig. 2-4).

The preceding remarks apply in general to diatomic molecules with an even number of electrons. Some molecules (e.g., NO, OH) have an odd number of electrons; this adds somewhat to the complexity of the spectrum. The odd electron produces a nonzero orbital angular momentum as well as a nonzero spin. Both cause a splitting of the energy levels; the spin splitting, however, is generally of much greater magnitude.

In general, each line in the spectrum is split into four strong components. The magnitude of the splitting is typically smaller than the average separation between adjacent rotational lines.

### 2.3.1.2 Triatomic Molecules

The spectrum of a linear molecule, such as CO<sub>2</sub>, has many strong similarities to that of a diatomic molecule because of its linearity, which results in a negligible moment of inertia about the axis through the nuclei.

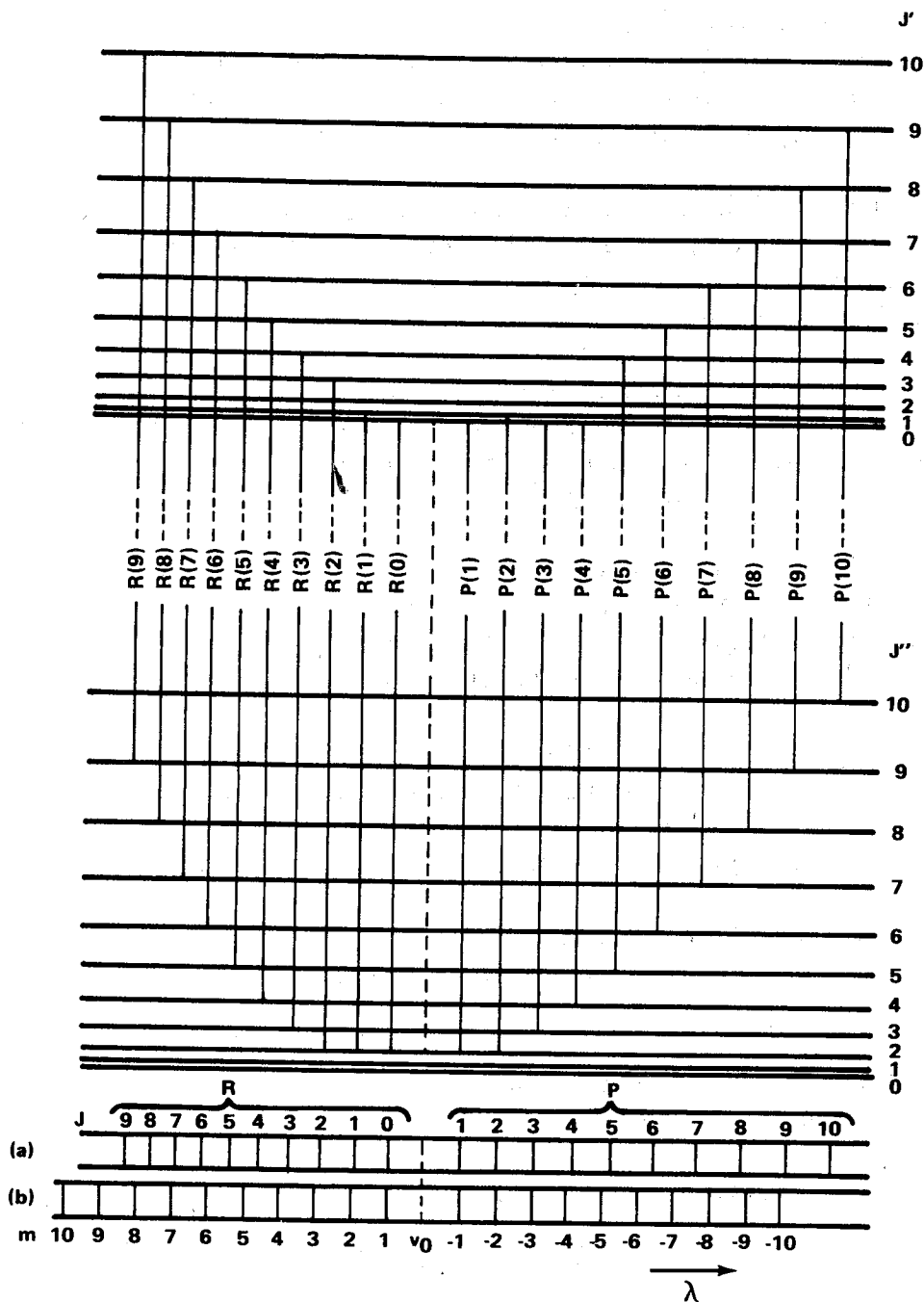


Figure 2-4. Energy level diagram explaining the fine structure of a rotation-vibration band. [In general, the separation of the two vibrational levels is considerably larger compared to the spacing of the rotational levels than shown in the figure (indicated by the broken parts of the vertical lines representing the transitions). The schematic spectrograms (a) and (b) give the resulting spectrum with and without allowance for the interaction between rotation and vibration. In these spectrograms, unlike most of the others, short wave lengths are at the left.]

The linear triatomic molecule has four vibrational degrees of freedom. A symmetric stretching vibration is described by the quantum number  $\nu_1$ . A doubly degenerate bending vibration is described by quantum numbers  $\nu_2$  and  $\ell$ , and an unsymmetric stretching vibration by  $\nu_3$ .

As a result of the presence of the bending vibration, the molecule may have a net angular momentum about the axis of the equilibrium position of the nuclei. This results in a splitting of the energy levels, as in the case of the diatomic molecule with nonzero orbital angular momentum.

The symmetry properties of the  $\text{CO}_2$  molecule result in a vanishing of alternate rotational levels (except for the molecules containing a rare isotopic O nucleus, occurring in a concentration of about 0.002, which do not possess a center of symmetry).

The  $\text{H}_2\text{O}$  molecule provides a classic example of the asymmetric top molecule. Even for the ideal case of a rigid asymmetric top, expressions for the rotational energy levels do not exist in closed form, since these levels are representable as roots of high-order algebraic equations.

Because of the presence of the light H nuclei, the molecule has a relatively small moment of inertia and, consequently, fairly widely spaced rotational levels. Also, because of its small moment of inertia, rotational distortion effects are quite significant.

Tabulations of  $\text{H}_2\text{O}$  rotational energy levels are available [2-6, 2-7] and are useful primarily for analysis of low-temperature ( $\lesssim 300\text{K}$ ) spectra. At higher temperatures ( $\gtrsim 1000\text{K}$ ), high rotational levels become of major importance and reference to experimental spectral and band model representations is required.

### 2.3.2 TRANSITION PROBABILITIES

The Einstein coefficient  $A_{u \rightarrow \ell}$  is defined as a spontaneous transition rate of a quantum-mechanical system from an upper state to a lower state so that the number of spontaneous transitions per unit time is given by

$$n_u A_{u \rightarrow \ell} \quad (2-46)$$

CHAPTER 2 – BASIC PRINCIPLES

where  $n_u$  is the number density of particles in the upper state. The coefficient  $B_{l \rightarrow u}$  is defined such that, in a radiation field of spectral density  $\rho_\omega = (4/c)W_\omega^0$ , the number rate of upward transitions is given by

$$n_l \rho_\omega B_{l \rightarrow u} \quad . \quad (2-47)$$

Similarly, the radiation field induces downward transitions at the rate

$$n_u \rho_\omega B_{u \rightarrow l} \quad . \quad (2-48)$$

The units of  $A_{u \rightarrow l}$  are  $\text{sec}^{-1}$ , and those of  $B_{l \rightarrow u}$  and  $B_{u \rightarrow l}$  are  $\text{cm}^2 \text{erg}^{-1} \text{sec}^{-1}$ , if  $\rho_\omega$  is in  $\text{erg cm}^{-2}$ .

The condition  $n_l B_{l \rightarrow u} \rho_\omega = n_u B_{u \rightarrow l} \rho_\omega + n_u A_{u \rightarrow l}$  holds at thermal equilibrium, and by identification with the Planck blackbody function, it is found that

$$A_{u \rightarrow l} = 8\pi c \omega^3 B_{u \rightarrow l} \quad (2-49)$$

and

$$g_l B_{l \rightarrow u} = g_u B_{u \rightarrow l} \quad , \quad (2-50)$$

where  $g_u$  and  $g_l$  are the statistical weights of the upper and lower states.

The strength of the transition  $S_{lu}$  is defined in terms of the Einstein coefficient  $B_{l \rightarrow u}$ :

$$S_{\ell u} = \left( \frac{n_{\ell}}{P} \right) B_{\ell \rightarrow u} \frac{h\omega}{c} \left[ 1 - \exp \left( \frac{-hc\omega}{kT} \right) \right] \quad (2-51)$$

where  $P$  is the pressure.

The Einstein coefficient  $B_{\ell \rightarrow u}$  is related to the electric dipole moment matrix element as follows:

$$B_{\ell \rightarrow u} = \frac{8\pi^2}{3h^2c} |R_{\ell u}|^2 \quad (2-52)$$

Thus  $S_{\ell u}$  is given by

$$S_{\ell u} = \frac{8\pi^3}{3hc^2} \omega \frac{n_{\ell}}{P} |R_{\ell u}|^2 \left[ 1 - \exp \left( \frac{-hc\omega}{kT} \right) \right] \quad (2-53)$$

The relationship between the strength and the absorption f-number is given by

$$S_{\ell u} = \frac{\pi e^2}{mc^2} \frac{n_{\ell}}{P} f \left[ 1 - \exp \left( \frac{-hc\omega}{kT} \right) \right] \quad (2-54)$$

where  $e$  and  $m$  are the electronic charge and mass, respectively.

The quantities  $f$ ,  $|R_{\ell u}|^2$ ,  $A_{u \rightarrow \ell}$ , and  $B_{\ell \rightarrow u}$  are thus related as follows:

$$f = \frac{8\pi^2 mc}{3e^2 h} \omega |R_{\ell u}|^2 \quad (2-55)$$

$$B_{\ell \rightarrow u} = \frac{8\pi^3}{3h^2c} |R_{\ell u}|^2 \quad (2-56)$$

$$A_{u \rightarrow l} = 8\pi hc \omega^3 \left( g_l / g_u \right) B_{l \rightarrow u} \quad , \quad (2-57)$$

and

$$f = \frac{mc^2 h}{\pi e^2} \omega B_{l \rightarrow u} \quad , \quad (2-58)$$

or, numerically,

$$f = 1.0848 \times 10^{11} \text{ cm}^{-1} \omega |R_{lu}/e|^2 \quad , \quad (2-59)$$

$$B_{l \rightarrow u} = 1.4493 \times 10^{25} \text{ erg}^{-1} \text{ sec}^{-1} |R_{lu}/e|^2 \quad , \quad (2-60)$$

$$A_{u \rightarrow l} = 4.9921 \times 10^{-15} \text{ erg-cm} \omega^3 \left( g_l / g_u \right) B_{l \rightarrow u} \quad (2-61)$$

$$= 7.2351 \times 10^{10} \text{ cm sec}^{-1} \omega^3 \left( g_l / g_u \right) |R_{lu}/e|^2 \quad , \quad (2-62)$$

and

$$f = 7.4846 \times 10^{-15} \text{ erg-sec-cm}^{-1} \omega B_{l \rightarrow u} \quad . \quad (2-63)$$

### 2.3.3 STRENGTHS OF VIBRATION-ROTATION TRANSITIONS

Strengths of vibration-rotation transitions for diatomic molecules are discussed first in some detail. Then, more briefly, strengths of linear and nonlinear triatomic molecules are discussed.

2.3.3.1 Diatomic Molecules: Line Strength

The electric dipole moment of the molecule can be represented as a power series in the displacement of the nuclei from their equilibrium positions:

$$M = M_0 + M_1(r-r_e) + M_2(r-r_e)^2 + \dots \quad , \quad (2-64)$$

where  $r$  is the internuclear separation and  $r_e$  the equilibrium value of  $r$ . It is found that the quadratic and higher terms in  $M$  result in the appearance of overtone bands but have only a relatively minor effect on the fundamental bands.

By taking the electric dipole moment to be a linear function of  $r$  and assuming separability of the rotational and vibrational parts of the wave function, an expression for line strength is obtained:

$$S_{vJ}^{v'J'} = \frac{8\pi^3}{3hc} \frac{n}{P} \frac{\exp[-E(v,J)/kT]}{Q} \omega \times M_1^2 \langle v|r-r_e|v' \rangle^2 \left[ J\delta_{J-1,J'} + (J+1)\delta_{J+1,J'} \right] \left[ 1 - \exp(-hc\omega/kT) \right] \quad , \quad (2-65)$$

where  $\langle v|r-r_e|v' \rangle$  is the matrix element of  $r-r_e$  between the two vibrational states  $v$  and  $v'$ , and  $Q$  is the partition function.

The effect of the interaction of vibration and rotation on the line intensities has been studied by numerous investigators [2-8, 2-9]. The anharmonicity of the molecule and the nonlinearity of the electric dipole moment enter into a correction factor which may be applied to equation (2-65). A first-order correction is provided by the Herman-Wallis F-factor [2-7] given by

$$F(m) = 1 - 4\theta \gamma m \quad , \quad (2-66)$$

where

$$\gamma = 2B_e / \omega_e$$

(typically of the order of  $10^{-2}$  to  $10^{-3}$ ), and

$$\theta = \frac{M_0}{M_1 r_e} ,$$

where  $r_e$  is the equilibrium internuclear distance. The rotational quantum number  $m$  is defined by

$$m = \begin{cases} J+1 & \text{(R branch)} \\ -J & \text{(P branch)} \end{cases} .$$

More precise expressions are available in the literature [2-8, 2-9], in terms of higher-order corrections to the potential and electric dipole moment functions, or for particular assumed potential functions.

If the parameter  $\theta$  is positive (i.e., if a stretching of the molecule increases the magnitude of the electric dipole moment), the total intensity of the P branch is increased and that of the R branch is diminished.

### 2.3.3.2 Diatomic Molecules: Band Intensities

The band intensity is the sum of the intensities of all the lines in the band:

$$\alpha_v^{v'} = \sum_{J, J'} S_{vJ}^{v'J'} \quad (2-67)$$

The factor  $\omega[1 - \exp(-hc\omega/kT)]$  in equation (2-65) may be taken outside the summation and evaluated at a mean value of  $\omega$ , which, because of the approximate symmetry of the band, will be approximately  $\omega_0$ :

$$\alpha_{\nu}^{\nu'} \approx \frac{8\pi^3}{3hc} \frac{n}{P} \omega_0 \left[ 1 - \exp\left(\frac{hc\omega_0}{kT}\right) \right] M_1^2 \left\langle \nu | r - r_e | \nu+1 \right\rangle^2$$

$$\times \exp(-E_{\nu}/kT) Q_{\nu}^{-1} Q_R^{-1} \sum_m (1-4\theta\gamma m) |m| \exp\left[\frac{-hcBm(m-1)}{kT}\right]$$

(2-68)

A direct summation yields (to a good approximation)

$$\alpha_{\nu}^{\nu'} \approx \frac{8\pi^2}{3hc} \frac{n}{P} \omega_0 \left[ 1 - \exp\left(\frac{-hc\omega_0}{kT}\right) \right] M_1^2 \left\langle \nu | r - r_e | \nu' \right\rangle^2 \exp\left(-\frac{E_{\nu}}{kT}\right) Q_{\nu}^{-1}$$

(2-69)

To the extent to which the molecule can be represented as a harmonic oscillator (a good approximation near the equilibrium point and, hence, good for at least the lowest vibrational states), the square of the matrix element  $\left\langle \nu | r - r_e | \nu+1 \right\rangle$  can be written in algebraic form:

$$\left\langle \nu | r - r_e | \nu+1 \right\rangle^2 = \left( \frac{h}{8\pi^2 m_r c \omega_0} \right) (\nu+1),$$

(2-70)

where  $m_r$  is the reduced mass of the molecule.

Using this expression and the corresponding expression for the vibrational energy levels of a harmonic oscillator, the following result is obtained:

$$\sum_{\nu} \alpha_{\nu}^{\nu+1} = \frac{\pi}{3m_r c^2} \frac{n}{P} M_1^2$$

(2-71)

A customary procedure, which is followed in this Handbook, is to refer to the density in units of density of a standard atmosphere (STP); that is, density at standard temperature (273.16K) and standard pressure (1 atm). In the system of units used here, band strengths are given in ( $\text{cm}^{-2}$ ) (STP). A corresponding adjustment is given in optical depth. Thus a pathlength of 1 cm through a pure gas at 3000K and 1 atm has an optical depth of 0.091 cm (STP).

The independence of total band strength with respect to temperature can be explicitly expressed by rewriting equation (2-71):

$$\frac{\sum \alpha_v^{v+1}(T)}{\sum \alpha_v^{v+1}(T_0)} = 1 \quad (2-72)$$

A similar expression has been developed for the overtone intensities of a diatomic molecule [2-10, 2-11]:

$$\frac{\sum \alpha_v^{v+n}(T)}{\sum \alpha_v^{v+n}(T_0)} = \left[ 1 - \exp\left(\frac{-hc\omega_0}{kT}\right) \right]^{-n} \left[ 1 - \exp\left(\frac{-nhc\omega_0}{kT}\right) \right] \quad (2-73)$$

### 2.3.3.3 Triatomic Molecules: Line and Band Strengths

A general expression for the line strengths of polyatomic molecules cannot be written in closed form. Line strengths may be obtained from quantum-mechanical calculations [2-12, 2-13] or by interpolation from existing tables. Such an approach is not contemplated, however, for the user of this handbook.

In the special case of linear molecules (such as  $\text{CO}_2$ ), the negligible moment of inertia about the molecular axis results in a great simplification of the line strength expressions. Vibrations which take place along the molecular axis (e.g., the  $4.3\text{-}\mu$  system of  $\text{CO}_2$ ) have expressions for line strength similar to those for diatomic molecules. However, as a result of the additional vibrational degrees of freedom, there will be many more vibrational transitions to consider, which may impede calculations at higher temperatures.

Bending vibrations of linear molecules also have simplified analytic forms for the line strengths, although the band structure is different from that of a diatomic molecule in that approximately half of the band strength appears in a Q-branch (e.g., the CO<sub>2</sub> 15- $\mu$  band).

The expressions for the band strengths are similar to those for diatomic molecules. A transition in a fundamental band system in which  $v_i$  changes by unity is assumed to have a matrix element squared proportional to  $(v_i+1)$  for a  $v_i \rightarrow (v_i+1)$  transition. Combination bands (e.g., the CO<sub>2</sub> 2.7- $\mu$  band) become somewhat more complicated (see References 2-10 and 2-11).

#### 2.3.4 NONEQUILIBRIUM EFFECTS: SCATTERING VS. ABSORPTION

In a classical paper written in 1928 [2-14], Milne recast the radiation energy transfer equation (following Milne's notation)

$$dN_\omega = \epsilon_\omega - \alpha_\omega N_\omega \quad (2-74)$$

in terms of the three Einstein coefficients  $A_{u \rightarrow l}$ ,  $B_{u \rightarrow l}$ ,  $B_{l \rightarrow u}$ .

The interesting part of this treatment is that it brought out the physical meaning of the equilibrium assumption ( $\epsilon_\omega = \alpha_\omega N_\omega^0$ ) at the microscopic level.

The energy exchanged through these three types of transitions is proportional to the populations of either upper or lower states  $l$  and  $u$ . These populations are also controlled by collision processes of cross sections  $b_{u \rightarrow l}$  and  $b_{l \rightarrow u}$ .

In general, a solution to an actual problem is extremely complex and rarely available in closed form (see Jeffries [2-15]). However, in the case of a steady "two-level" atom, Milne finds a relatively simple solution to the function

$$\frac{\epsilon_\omega}{\alpha_\omega} = \frac{\int N_\omega \frac{d\Omega}{4\pi} + \eta N_\omega^0}{1 + \eta} \quad (2-75)$$

where

$$\eta = \frac{b_{l \rightarrow u}}{B_{l \rightarrow u}} \frac{e^{h\nu/kT} - 1}{\frac{2h\nu^3}{c^2}}$$

The term  $\eta$  is a collision-radiation rate ratio. If the collisions dominate (at atmospheric densities for instance),  $\eta$  is large and  $\epsilon_{\omega}$  takes the value  $\alpha_{\omega} N_{\omega}^0$ , the equilibrium value assumed so far in this handbook (i.e., the local thermodynamic equilibrium assumption: LTE).

On the contrary, if the collision exchanges are less active than the radiation transitions (upper atmosphere, for instance),  $\eta$  tends to zero and  $\epsilon_{\omega}$ , the source function, takes the form of a scattering term.

Thus, Milne has shown that Kirchoff's law ( $\epsilon_{\omega} = \alpha_{\omega} N_{\omega}^0$ ) can be numerically tested in terms of atomic or molecular constants and he gave an exact meaning to the concept of scattering as well.

## 2.4

COLLISION LINE WIDTH DEPENDENCE ON THERMODYNAMIC PROPERTIES

It has been known for a long time that the presence of a gas which is transparent in a certain spectral region can have a significant effect on the absorptivity of a species which does absorb radiation in that region. This phenomenon results from the pressure broadening of the spectral lines of the absorbing gas by the transparent species.

## 2.4.1 LINE BROADENING THEORIES

Very elaborate theories of line broadening have been developed [2-16, 2-17]. The data presented here are based, as far as possible, on experimental measurements, with the simplest relevant theory used to extend their ranges of application.

Broadening is determined by the forces between molecules. When two molecules approach each other sufficiently close that strong forces between them come into play, they are said to "collide." The collision process may be viewed as an interruption to the process of emission or absorption of radiation. The net effect of many such random interruptions is a spreading of frequencies associated with a particular transition. This spread of frequencies is defined by a line shape, which is determined by the nature of the forces between the molecules at the time of collision. The Lorentz line shape (Section 2.2.1.3.1) results from an assumption of rigid particles ("billiard-ball" collisions). The Lorentz line shape is generally applied to all collision-broadened lines, as it is extremely difficult to observe any deviations from the Lorentz shape. Any such deviations are first observed in the distant wings of the line and are, normally, important only when the spectrum of one region is dominated by the wings of distant, very intense lines (such as in the region beyond a band head).

Another important class of interactions consists of "resonant-dipole" collisions. Two molecules having large permanent electric dipole moments may interact strongly if they are in neighboring rotational states. Such effects must be considered for highly polar molecules such as H<sub>2</sub>O or hydrogen halides, but they do not exist for a symmetric molecule such as CO<sub>2</sub>.

Other multipole moments contribute to line broadening, but the two factors above provide a sufficiently good description for most purposes.

## 2.4.2 PRESSURE DEPENDENCE OF COLLISION BROADENING

A linear dependence of the line width  $\gamma$  on pressure has been well established both experimentally and theoretically. However, it is necessary to ascribe different broadening powers to each component of a mixture.

The general expression [equation (2-26)] for the half-width,  $\gamma$ , of a spectral line can be written as

$$\gamma = \sum_i \gamma_{0_i} p_i = \left( \sum_i \gamma_{0_i} c_i \right) p \quad , \quad (2-76)$$

where  $p$  is the total pressure,  $p_i$  and  $c_i$  are the partial pressure and mole fraction, respectively, of component  $i$  of the gas mixture, and  $\gamma_{0_i}$  is the line half-width resulting from a unit pressure of component  $i$ . For self-broadening in a single gas

$$\gamma = \gamma_0 p \quad .$$

The quantities  $\gamma_{0_i}$  are usually determined by experiment, although it is possible to calculate  $\gamma_{0_i}$  with some accuracy.

The half-widths of individual lines in a spectrum are different, in general. The variation from line to line may be quite small, and an average value may be quite serviceable. In some cases (in particular, for highly polar molecules with few intense lines in the spectrum, e.g., HF at low temperatures), the range of line widths may be rather large (perhaps by a factor of 10), and the use of an average value of half-width may be misleading. However, for most heat transfer calculations, the use of an average half-width is generally quite reasonable.

Burch, et al. [2-18] have defined a "self-broadening coefficient"  $B$ , which is frequently seen in the literature. This  $B$  is the ratio of the self-broadened half-width to the nitrogen-broadened half-width. For a

two-component system, equation (2-76) becomes

$$\begin{aligned}
 \gamma &= \gamma_{0_x} p_x + \gamma_{0_N} p_N \\
 &= \gamma_{0_N} \left[ c_N + \left( \gamma_{0_x} / \gamma_{0_N} \right) c_x \right] p \\
 &= \gamma_{0_N} \left[ 1 + (B-1) c_x \right] p \quad , \quad (2-77)
 \end{aligned}$$

where the "self-broadening coefficient"  $B$  is defined by

$$B = \gamma_{0_x} / \gamma_{0_N} \quad . \quad (2-78)$$

An "equivalent pressure"  $P_e$  is defined as

$$P_e = \left[ 1 + (B-1) c_x \right] p \quad , \quad (2-79)$$

so that equation (2-77) can be rewritten as

$$\gamma = \gamma_{0_N} P_e \quad . \quad (2-80)$$

### 2.4.3 TEMPERATURE DEPENDENCE OF COLLISION BROADENING

Quite apart from Doppler broadening, the ambient temperature  $T$  plays an important part in the collision process. Under simplest assumptions of kinetic theory, at least for foreign gas broadening, an inverse square root dependence on temperature is predicted:

$$\gamma_{0,i} \propto T^{-1/2} \quad (2-81)$$

It is worth noting that this temperature dependence is based on a half-width at constant pressure (not constant density). The factor  $T^{-1/2}$  is the product of two factors:  $T^{+1/2}$ , resulting from the increase of speed of the molecules with temperature, and  $T^{-1}$ , resulting from the decrease in density with temperature at constant pressure.

Despite the oversimplifications of the theory, the  $T^{-1/2}$  dependence is rather well verified by experiment. A better fit to experimental data may sometimes be made, however, by using an empirical relationship

$$\gamma_{0,i} \propto T^{-n} \quad (2-82)$$

where  $n$  may differ from a value of 0.5.

The situation for self-broadening is somewhat more complicated, at least for highly polar molecules, such as  $H_2O$  or  $HF$ . The collisions between like molecules may be divided into two categories: resonant and nonresonant. Nonresonant collisions are analogous to inert-gas broadening and can be so treated. Resonant collisions, on the other hand, are more effective in broadening the spectral lines. The mechanism involved is more complex, and the temperature dependence is different. Generally, it is assumed that, for resonant collisions, the contribution to the line width  $\gamma_{0,x}^*$  is given by [2-19]

$$\gamma_{0,x}^* \propto T^{-n^*} \quad (2-83)$$

where  $n^* \approx 1.0$ . Thus, the temperature dependence for self-broadening can be expressed by

$$\gamma_{0x}(T) = \gamma_{0x}'(T_0)(T_0/T)^{n'_x} + \gamma_{0x}''(T_0)(T_0/T)^{n^*} \quad , \quad (2-84)$$

where  $n'_x \approx 0.5$  , and  $n^* \approx 1.0$  .

More sophisticated expressions could be derived, but those which have been examined have not been of sufficient value to justify their adoption in the radiance calculations described in Chapter 5.

2.5 PARTICULATE EMISSION AND SCATTERING

The properties of a system composed of spherical particles of a given index of refraction suspended in a medium of different properties have been studied over a long period of time [2-20] and are of considerable importance to a study of radiant transfer. Conceptually, the problem is simple, merely requiring the matching of boundary conditions for the electromagnetic field on the surface of the sphere, to determine its scattering and absorption cross sections.

In practice, various difficulties are encountered and, while evaluation of the series solutions for the cross sections is somewhat involved, a more basic problem is that real systems may be composed of particles which are not uniform in size and may not even be spherical. Also, it may not be known whether the particles are liquid or solid, and accurate values for the complex index of refraction may not be available.

## 2.5.1 THE EQUATIONS OF TRANSFER

Consider a pencil of radiation propagating in a direction defined by the polar coordinate angles  $\theta$  and  $\varphi$ . The radiated power (in a wavenumber interval  $d\omega$ ) passing through an elemental area  $dA$  and contained within the solid angle  $d\Omega$  is

$$N_{\omega}(s, \theta, \varphi) dA d\Omega d\omega ,$$

where  $N_{\omega}$  is the spectral intensity in units of watts/cm<sup>2</sup>-cm<sup>-1</sup>-sr. If there are  $n$  scattering centers per unit volume, each having a total scattering cross section  $\sigma_{sc}$ , the power scattered out of the beam in traversing a distance  $ds$  is

$$dN_{\omega} = N_{\omega} n \sigma_{sc} dA d\Omega d\omega ds \quad (2-86)$$

Radiation propagating in other directions may be scattered into the cone  $d\Omega$ . This scattering is most easily expressed in terms of a differential scattering cross section  $d\sigma/d\Omega$ , defined as follows. Consider a plane wave of radiance

$N_\omega$  propagating in the positive  $z$  direction and incident on a single scattering particle. The radiance of the scattered light at a distance  $r$  from the particle may be expressed in the form

$$\frac{dN_\omega(\theta, \varphi)}{d\Omega} = \frac{N_\omega}{r^2} \frac{d\sigma(\theta, \varphi)}{d\Omega} \quad (2-87)$$

The total scattered power is

$$\int_{4\pi} \frac{dN_\omega}{d\Omega} r^2 d\Omega = N_\omega \int_{4\pi} \frac{d\sigma}{d\Omega} d\Omega = \sigma_{sc} N_\omega \quad (2-88)$$

It is usually convenient to introduce a dimensionless angular scattering function  $\gamma(\theta, \varphi)$ , defined by

$$\gamma(\theta, \varphi) \equiv \frac{1}{\sigma_{sc}} \frac{d\sigma}{d\Omega}(\theta, \varphi) \quad (2-89)$$

In terms of this function, the increase in the radiance  $N_\omega(\theta, \varphi)$  in the direction  $(\theta, \varphi)$  due to scattering of radiation propagating in a cone  $d\Omega'$  centered at  $\theta', \varphi'$  is

$$dN_\omega = N_\omega(\theta', \varphi') n \sigma_{sc}(s) \gamma(\theta - \theta', \varphi - \varphi') d\Omega' ds \quad (2-90)$$

and the total increment in  $N_\omega$  due to scattering from all other directions is

$$\frac{dN_\omega}{ds} = n \sigma_{sc} \int N_\omega(\theta', \varphi') \gamma(\theta - \theta', \varphi - \varphi') d\Omega' \quad (2-91)$$

CHAPTER 2 – BASIC PRINCIPLES

In writing the angular scattering function as dependent only on the scattered angles  $\theta-\theta'$ , and  $\varphi-\varphi'$ , we have implicitly assumed that the particles have no preferred orientation. In the general case, for the nonspherical particles, the scattering from the direction  $\theta'$ ,  $\varphi'$  to  $\theta$ ,  $\varphi$  will depend on the particle orientation and cannot be expressed simply in terms of a function of the difference between these angles.

Thus in the case of an atmosphere containing spherical or randomly oriented scatterers, the change of the intensity  $N_\omega(\theta, \varphi, s)$  along a ray path is governed by the relation

$$\frac{dN_\omega}{ds}(\theta, \varphi) = n \sigma_{sc} \left[ -N_\omega(\theta, \varphi) + \int \gamma(\theta-\theta', \varphi-\varphi') N_\omega(\theta', \varphi') d\Omega' \right] \quad (2-92)$$

This is the equation of transfer for a purely scattering medium and is appropriate for nonabsorbing scatterers. In general, particles will both scatter and absorb. In this case  $N_\omega$  decreases by absorption:

$$\left( \frac{dN_\omega}{ds} \right)_{\text{absorption}} = -n\sigma_a N_\omega, \quad (2-93)$$

where  $\sigma_a$  is the absorption cross section.  $N_\omega$  also increases because of thermal emission. When the particles are in local thermodynamic equilibrium, the increase in  $N_\omega$  due to emission is given by

$$\left( \frac{dN_\omega}{ds} \right)_{\text{emission}} = n\sigma_a N_\omega^0, \quad (2-94)$$

where  $N_\omega^0$  is the Planck function (divided by  $\pi$ ) in units of watts/cm<sup>2</sup>-cm<sup>-1</sup>-sr. Thus for absorbing and scattering media in thermal equilibrium the equation of transfer assumes the form

$$\begin{aligned} \frac{dN_{\omega}}{ds}(\vec{\Omega}) = & -n(\sigma_{sc} + \sigma_a)N_{\omega}(\vec{\Omega}) + n\sigma_a N_{\omega}^0 \\ & + n\sigma_{sc} \int_{4\pi} \gamma(\vec{\Omega}-\vec{\Omega}')N_{\omega}(\vec{\Omega}') d\Omega' \quad , \end{aligned} \quad (2-95)$$

where the notation  $\vec{\Omega}$  has been introduced to represent the direction  $\theta, \varphi$ .

Many authors introduce the concept of a particle albedo  $\beta$  and an optical depth parameter  $\xi$  at this point to simplify the notation. The particle albedo is defined as the ratio of the scattered power to the total power (scattering + absorption):

$$\beta = \frac{\sigma_{sc}}{\sigma_{sc} + \sigma_a} \quad . \quad (2-96)$$

The optical depth in a direction  $\vec{\Omega}$  is a dimensionless distance parameter defined by the relation

$$d\xi = n(\sigma_{sc} + \sigma_a) ds \quad . \quad (2-97)$$

In terms of  $\beta(s)$  and  $\xi(s)$ , the equation of transfer assumes the form

$$\frac{dN_{\omega}(\vec{\Omega})}{d\xi(\vec{\Omega})} = -N_{\omega}(\vec{\Omega}) + \beta \int_{4\pi} \gamma(\vec{\Omega}-\vec{\Omega}')N_{\omega}(\vec{\Omega}') d\Omega' + (1-\beta)N_{\omega}^0 \quad . \quad (2-98)$$

In the general case of a three-dimensional inhomogeneous scattering medium, the introduction of the optical depth parameter is not particularly useful since its value is a function of  $\theta$  and  $\varphi$ . However, in plane-stratified media, where the density and scattering properties vary only in one direction (say the  $z$  direction), the optical depths in different directions are simply related in terms of the cosine of the polar angle  $\mu (= \cos \theta)$

$$d\xi(\theta) = d\xi(\mu = 1)/\mu \quad . \quad (2-99)$$

In this case, the independent variable in the equation of transfer can be taken to be the optical depth in the  $z$  direction,  $\xi(\mu = 1)$ , which will now be denoted simply as  $\xi$ . Thus the equation of transfer for a plane-stratified scattering and absorbing medium may be written

$$\begin{aligned} \mu \frac{dN_{\omega}}{d\xi}(\vec{\Omega}, \xi) = & -N_{\omega}(\vec{\Omega}, \xi) + \beta \int \gamma(\vec{\Omega}-\vec{\Omega}') N_{\omega}(\vec{\Omega}', \xi) d\Omega' \\ & + (1 - \beta) N_{\omega}^0(\xi) \quad . \end{aligned} \quad (2-100)$$

### 2.5.2 SOLUTIONS TO COMMON SCATTERING PROBLEMS

The solution to the equation of transfer in the general case is exceedingly difficult analytically. Most of the available calculations of the radiance of inhomogeneous scattering media have been restricted to planar, one-dimensional approximations. In general, stratified media can be treated by dividing the region into a number of thin parallel uniform slabs, evaluating the emittance and transmittance of each, and solving the resulting set of equations numerically.

The exact treatment of the scattering problem, even for homogeneous media, is very difficult. If the scattering mean free path is comparable to the slab thickness or if the absorption cross section is comparable to or greater than the scattering cross section, an iterative approach which starts with a single scattering approximation and includes one higher scattering order at each iteration may converge rapidly enough to be practical. However, the particle densities in typical combustion gases at moderate pressures can be high enough that high order scattering can be quite important.

When the geometry of the cloud has simple symmetry characteristics (planar or axisymmetric) and only a small number of cases and wavelengths are to be treated, a Monte Carlo approach can be useful [2-21]. However, since several hundred photon tracings need to be carried out for each significant emitting volume element in the flow and for each wavelength in order to

get good statistics, this approach is expected to be more beneficial for checking the validity of various approximate procedures rather than direct calculation.

The major problems in developing accurate analytic procedures, even for the evaluation of the monochromatic radiance of a uniform slab, arise in the treatment of the angular scattering function. Exact solutions have been obtained for limiting cases such as isotropic scattering, Rayleigh scattering, and "infinitely" anisotropic or one-dimensional scattering (i.e., scattering only directly forward or directly backward). Mie scattering cross sections for typical clouds in which the particles are condensed droplets have a strong forward scattering component and a less strong but still pronounced back scattering component (Fig. 2-5). Thus, the one-dimensional approximation is expected to be a useful first approximation when the ratio of scattering mean free path to plume thickness is greater than the square of the sine of the mean scattering angle. For more arbitrary phase functions, other methods (6-flux method, Legendre polynomial expansion) give reasonable results [2-22].

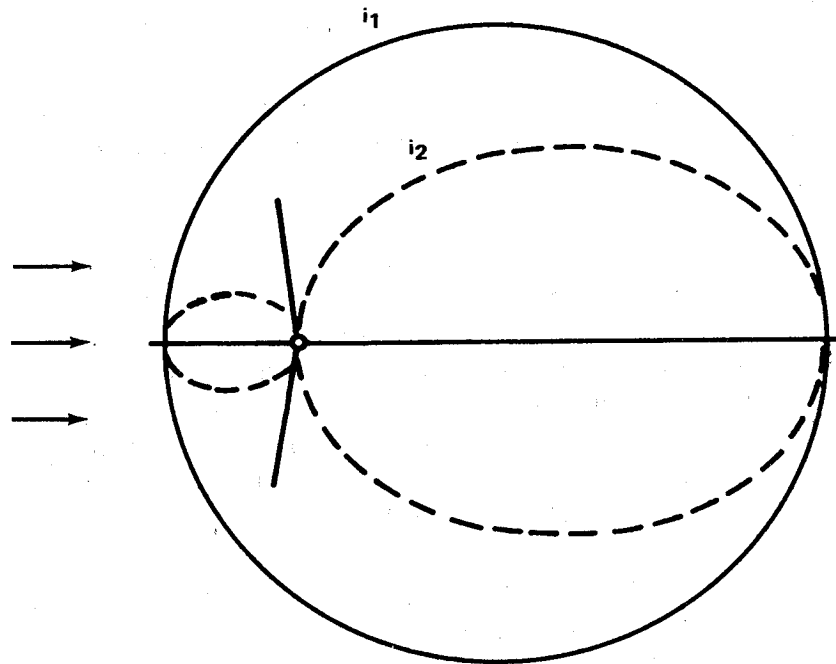


Figure 2-5. Scattering diagram for spheres with  $m = 2$ ,  $x = 1$ , showing characteristic preponderance of forward scattering. (The two polarization components  $I_1$  and  $I_2$  have been plotted separately.)

APPENDIX 2-A

COLLISION BROADENING – THE LADENBURG-REICHE FUNCTION  $f(x)$

The Ladenburg-Reiche function  $f(x)$  is defined by the relation:

$$f(x) = x \exp(-x)[I_0(x) + I_1(x)] \quad , \quad (2-A-1)$$

in which  $I_0$  and  $I_1$  are modified Bessel functions (see Table 2-A-1). Series expressions exist for large and small values of  $x$ . The first six terms of the power series expansion

$$f(x) = x - \frac{1}{2}x^2 + \frac{1}{4}x^3 - \frac{5}{48}x^4 + \frac{7}{192}x^5 - \frac{7}{640}x^6 + \dots \quad (2-A-2)$$

yield two-place accuracy for  $x < 1$  and four-place accuracy for  $x < 0.5$ .

A semiconvergent asymptotic expansion is useful for large values of  $x$ :

$$f(x) = \left(\frac{2}{\pi}\right)^{1/2} x^{1/2} \left( 1 - \frac{1}{8x} - \frac{3}{128x^2} - \frac{15}{1024x^3} - \frac{525}{32768x^4} - \dots \right) \quad (2-A-3)$$

This, as well as other semiconvergent series, must be handled with caution. Specifically, they must be truncated while the terms are still decreasing in magnitude; thus, their accuracy is limited. For example, for  $x = 10$ , equation (2-A-3) yields

$$f(10) = \left(\frac{2}{\pi}\right)^{1/2} (10)^{1/2} \begin{bmatrix} 1. \\ -0.0125 \\ -0.000234 \\ -0.000015 \\ -0.000002 \\ \dots \end{bmatrix} = 2.49096 \quad , \quad (2-A-4)$$

which should be accurate to six significant figures. [The tabulated value is  $f(10) = 2.4910$ .] However, for  $x = 1$ ,

$$f(1) = \left(\frac{2}{\pi}\right)^{1/2} (1)^{1/2} \begin{bmatrix} 1 \\ -0.125 \\ -0.023438 \\ -0.014648 \\ -0.016022 \\ \dots \end{bmatrix} \quad (2-A-5)$$

In this case, the series should be truncated after the fourth term and rounded to two significant figures, thus yielding

$$f(1) = \left(\frac{2}{\pi}\right)^{1/2} (1)^{1/2} [0.84] = 0.67 \quad (2-A-6)$$

A glance at a table of  $f(x)$  shows that  $f(1) = 0.6737$ . Equation (2-A-3) will yield two-place accuracy for  $x > 1$  and three-place accuracy for  $x > 2$ .

For computational purposes, it may be convenient to approximate  $f(x)$  by some closed-form algebraic expression which has the proper asymptotic behavior [ $f(x) \sim x$  for small  $x$ ;  $f(x) \sim (2/\pi)^{1/2} x^{1/2}$  for large  $x$ ] and which fits  $f(x)$  to within a predetermined accuracy in the transition region. Several such approximate forms and their error limits are presented in Table 2-A-2 (see References 2-23 and 2-24).

TABLE 2-A-1.  $f(x) = x \exp(-x)[I_0(x) + I_1(x)]$  (Reference 2-25)

x	0	1	2	3	4	5	6	7	8	9
0.0	0.0000	0.0099	0.0198	0.0295	0.0392	0.0488	0.0583	0.0676	0.0769	0.0861
0.1	0.0952	0.1042	0.1132	0.1220	0.1308	0.1395	0.1482	0.1567	0.1652	0.1735
0.2	0.1818	0.1900	0.1982	0.2063	0.2143	0.2223	0.2302	0.2380	0.2457	0.2534
0.3	0.2610	0.2685	0.2760	0.2834	0.2908	0.2981	0.3055	0.3125	0.3196	0.3267
0.4	0.3337	0.3406	0.3475	0.3543	0.3611	0.3678	0.3745	0.3811	0.3877	0.3942
0.5	0.4007	0.4071	0.4135	0.4198	0.4261	0.4324	0.4386	0.4447	0.4508	0.4569
0.6	0.4629	0.4689	0.4748	0.4807	0.4865	0.4923	0.4981	0.5038	0.5095	0.5152
0.7	0.5208	0.5264	0.5319	0.5374	0.5429	0.5483	0.5537	0.5591	0.5644	0.5697
0.8	0.5749	0.5801	0.5853	0.5905	0.5956	0.6007	0.6058	0.6108	0.6158	0.6208
0.9	0.6258	0.6307	0.6356	0.6404	0.6452	0.6500	0.6548	0.6596	0.6643	0.6690
1.0	0.6737	0.6783	0.6829	0.6875	0.6921	0.6966	0.7012	0.7057	0.7101	0.7146
1.1	0.7190	0.7234	0.7278	0.7322	0.7365	0.7408	0.7451	0.7494	0.7536	0.7578
1.2	0.7620	0.7662	0.7704	0.7746	0.7787	0.7828	0.7869	0.7910	0.7950	0.7990
1.3	0.8030	0.8070	0.8110	0.8150	0.8189	0.8228	0.8267	0.8306	0.8345	0.8384
1.4	0.8422	0.8460	0.8498	0.8536	0.8574	0.8612	0.8649	0.8686	0.8723	0.8760
1.5	0.8797	0.8834	0.8870	0.8907	0.8943	0.8979	0.9015	0.9051	0.9086	0.9122
1.6	0.9157	0.9193	0.9228	0.9263	0.9298	0.9333	0.9367	0.9402	0.9436	0.9470
1.7	0.9504	0.9538	0.9572	0.9606	0.9639	0.9673	0.9706	0.9740	0.9773	0.9806
1.8	0.9839	0.9872	0.9904	0.9937	0.9969	1.0002	1.0034	1.0066	1.0098	1.0130
1.9	1.0162	1.0194	1.0226	1.0257	1.0289	1.0320	1.0351	1.0383	1.0414	1.0445
2.0	1.0476	1.0506	1.0537	1.0568	1.0598	1.0629	1.0659	1.0689	1.0719	1.0750
2.1	1.0780	1.0809	1.0839	1.0869	1.0899	1.0928	1.0958	1.0987	1.1016	1.1046
2.2	1.1075	1.1104	1.1133	1.1162	1.1191	1.1220	1.1248	1.1277	1.1305	1.1334
2.3	1.1362	1.1391	1.1419	1.1447	1.1475	1.1503	1.1531	1.1559	1.1587	1.1615
2.4	1.1642	1.1670	1.1698	1.1725	1.1753	1.1780	1.1807	1.1835	1.1862	1.1889
2.5	1.1916	1.1943	1.1970	1.1997	1.2023	1.2050	1.2077	1.2103	1.2130	1.2156
2.6	1.2183	1.2209	1.2235	1.2262	1.2288	1.2314	1.2340	1.2366	1.2392	1.2418
2.7	1.2444	1.2470	1.2495	1.2521	1.2547	1.2572	1.2598	1.2623	1.2649	1.2674
2.8	1.2699	1.2725	1.2750	1.2775	1.2800	1.2825	1.2850	1.2875	1.2900	1.2925
2.9	1.2949	1.2974	1.2999	1.3024	1.3048	1.3073	1.3097	1.3122	1.3146	1.3171
3.0	1.3195	1.3219	1.3243	1.3268	1.3292	1.3316	1.3340	1.3364	1.3388	1.3412
3.1	1.3436	1.3459	1.3483	1.3507	1.3531	1.3554	1.3578	1.3601	1.3625	1.3649
3.2	1.3672	1.3695	1.3719	1.3742	1.3765	1.3789	1.3812	1.3835	1.3858	1.3881
3.3	1.3904	1.3927	1.3950	1.3973	1.3996	1.4019	1.4042	1.4064	1.4087	1.4110
3.4	1.4132	1.4155	1.4178	1.4200	1.4223	1.4245	1.4268	1.4290	1.4312	1.4335
3.5	1.4357	1.4379	1.4402	1.4424	1.4446	1.4468	1.4490	1.4512	1.4534	1.4556
3.6	1.4578	1.4600	1.4622	1.4644	1.4666	1.4687	1.4709	1.4731	1.4753	1.4774
3.7	1.4796	1.4817	1.4839	1.4861	1.4882	1.4903	1.4925	1.4946	1.4968	1.4989
3.8	1.5010	1.5032	1.5053	1.5074	1.5095	1.5116	1.5137	1.5159	1.5180	1.5201
3.9	1.5222	1.5243	1.5264	1.5285	1.5305	1.5326	1.5347	1.5368	1.5389	1.5409
4.0	1.5430	1.5451	1.5471	1.5492	1.5513	1.5533	1.5554	1.5574	1.5595	1.5615
4.1	1.5636	1.5656	1.5677	1.5697	1.5717	1.5738	1.5758	1.5778	1.5798	1.5818
4.2	1.5839	1.5859	1.5879	1.5899	1.5919	1.5939	1.5959	1.5979	1.5999	1.6019
4.3	1.6039	1.6059	1.6079	1.6099	1.6118	1.6138	1.6158	1.6178	1.6197	1.6217
4.4	1.6237	1.6256	1.6276	1.6296	1.6315	1.6335	1.6354	1.6374	1.6393	1.6413
4.5	1.6432	1.6452	1.6471	1.6490	1.6510	1.6529	1.6548	1.6567	1.6587	1.6606
4.6	1.6625	1.6644	1.6663	1.6683	1.6702	1.6721	1.6740	1.6759	1.6778	1.6797
4.7	1.6816	1.6835	1.6853	1.6872	1.6891	1.6910	1.6929	1.6948	1.6967	1.6986
4.8	1.7005	1.7023	1.7042	1.7061	1.7079	1.7098	1.7117	1.7135	1.7154	1.7173
4.9	1.7191	1.7210	1.7228	1.7247	1.7265	1.7284	1.7302	1.7321	1.7339	1.7357
5	1.7376	1.7558	1.7739	1.7918	1.8095	1.8270	1.8444	1.8616	1.8786	1.8955
6	1.9123	1.9288	1.9453	1.9616	1.9778	1.9938	2.0097	2.0255	2.0412	2.0568
7	2.0722	2.0875	2.1027	2.1178	2.1328	2.1477	2.1625	2.1771	2.1917	2.2062
8	2.2206	2.2349	2.2491	2.2632	2.2772	2.2912	2.3050	2.3188	2.3325	2.3461
9	2.3597	2.3731	2.3865	2.3998	2.4130	2.4262	2.4393	2.4523	2.4653	2.4781
10	2.4910	2.5037	2.5164	2.5290	2.5416	2.5541	2.5665	2.5789	2.5912	2.6035
11	2.6157	2.6278	2.6399	2.6519	2.6639	2.6758	2.6877	2.6995	2.7113	2.7230
12	2.7347	2.7463	2.7579	2.7694	2.7809	2.7923	2.8037	2.8150	2.8263	2.8375
13	2.8487	2.8599	2.8710	2.8821	2.8931	2.9041	2.9150	2.9259	2.9368	2.9476
14	2.9584	2.9691	2.9798	2.9905	3.0011	3.0117	3.0223	3.0328	3.0433	3.0537
15	3.0641	3.0745	3.0848	3.0951	3.1054	3.1156	3.1258	3.1360	3.1461	3.1562
16	3.1663	3.1763	3.1863	3.1963	3.2063	3.2162	3.2261	3.2359	3.2457	3.2555
17	3.2653	3.2750	3.2847	3.2944	3.3041	3.3137	3.3233	3.3328	3.3424	3.3519
18	3.3614	3.3708	3.3803	3.3897	3.3990	3.4084	3.4177	3.4270	3.4363	3.4456
19	3.4548	3.4640	3.4732	3.4823	3.4914	3.5006	3.5096	3.5187	3.5277	3.5367
20	3.5457	3.6344	3.7210	3.8055	3.8883	3.9693	4.0487	4.1266	4.2030	4.2781
30	4.3519	4.4244	4.4958	4.5660	4.6352	4.7034	4.7706	4.8369	4.9022	4.9667
40	5.0304	5.0933	5.1554	5.2163	5.2775	5.3374	5.3968	5.4554	5.5135	5.5709
50	5.6277									

TABLE 2-A-2. USEFUL APPROXIMATIONS FOR THE EQUIVALENT WIDTH OF AN ISOLATED LORENTZ LINE

$W = 2\pi\gamma f(Su/2\pi\gamma)$ where $f(x) = x \exp(-x) [I_0(x) + I_1(x)]$	
Representations for $f(x)$	Accuracy
$f(x) = x \exp(-x) [I_0(x) + I_1(x)]$	Exact
$f(x) \approx x - 0.5x^2 + 0.25x^3 - 0.1042x^4 + 0.0365x^5 - 0.0109x^6$	$< \frac{1}{2}\%$ for $x \leq 1$
$f(x) \approx 0.7979x^{1/2} (1 - 0.125x^{-1} - 0.0234x^{-2} - 0.0146x^{-3})$	$< 1\%$ for $x \geq 1$
$f(x) \approx x[1 + 1.57x]^{-1/2}$	$< 10\%$ for all $x$
$f(x) \approx x[1 + 1.57x]^{-1/2} + 0.07x^{3/2} (1 + 0.5x^2)^{-1}$	$< \frac{1}{2}\%$ for all $x$
$f(x) \approx x(1 + 1.76 x^{1.25})^{-0.4}$	$< \frac{1}{2}\%$ for all $x$
$f(x) \approx 0.798 x^{1/2} [1 - \exp(-1.57x)]^{1/2}$	$< 6\%$ for all $x$
$f(x) \approx 0.798 x^{1/2} [1 - \exp(-1.25 x^{1/2})]$	$< 18\%$ for all $x$

## APPENDIX 2-B

## DOPPLER BROADENING

The following series form for the equivalent width of a Doppler broadened line [equation (2-32)] is absolutely convergent for all values of  $k_0u$  but becomes unwieldy for values above about 10:

$$W = \left( \frac{S}{k_0} \right) \sum_{n=0}^{\infty} \frac{(-1)^n (k_0u)^{n+1}}{(n+1)! (n+1)^{1/2}} \quad (2-B-1)$$

A semiconvergent asymptotic expansion is given by

$$W = \left( \frac{S}{k_0} \right) 2\pi^{-1/2} [\ln(k_0u)]^{1/2} \left\{ 1 + 0.2886 [\ln(k_0u)]^{-1} \right. \\ \left. - 0.2473 [\ln(k_0u)]^{-2} \right. \\ \left. + 0.3403 [\ln(k_0u)]^{-3} \dots \right\} \quad (2-B-2)$$

This expression gives three-place accuracy for  $k_0u > 20$ .

Various approximate forms for the equivalent width  $W$  are listed in Table 2-B-1.

TABLE 2-B-1. USEFUL APPROXIMATIONS FOR THE EQUIVALENT WIDTH OF AN ISOLATED DOPPLER LINE

$W = \int_{-\infty}^{\infty} \left\{ 1 - \exp \left[ -k_0 u \exp \left[ -(\omega - \omega_0)^2 \ln 2 / \gamma_D^2 \right] \right] \right\} d\omega$	
Expression	Accuracy
$W \approx (Su) \left[ 1 - 0.3536k_0u + 0.0962(k_0u)^2 - 0.02083(k_0u)^3 + 0.003727(k_0u)^4 - 0.000567(k_0u)^5 \right]$	$\left\{ \begin{array}{l} < 1\% \text{ for } k_0u \leq 2, \\ < 10\% \text{ for } k_0u \leq 3 \end{array} \right.$
$W \approx 1.128(S/k_0) [\ln(k_0u)]^{1/2} \left\{ 1 + 0.2886 [\ln(k_0u)]^{-1} - 0.2473 [\ln(k_0u)]^{-2} \right\}$	$\left\{ \begin{array}{l} < 3\% \text{ for } k_0u \geq 5, \\ < 10\% \text{ for } k_0u \geq 3 \end{array} \right.$
$W \approx 1.70\gamma_D \left\{ \ln \left[ 1 + (0.589Su/\gamma_D)^2 \right] \right\}^{1/2}$	$< 10\% \text{ for all } u$

Note:  $k_0 = k(\omega_0) = 0.470S/\gamma_D$

## REFERENCES

- 2-1. Report of the Working Group on Infrared Backgrounds, Part II: Concepts and Units for the Presentation of Infrared Background Information. Report No. 2389-3-S, University of Michigan, Institute of Science and Technology, Ann Arbor, Mich., 1956.
- 2-2. Plass, G. N.: J. Opt. Soc. Am., no. 48, 1958, p. 690.
- 2-3. Plass, G. N.: J. Opt. Soc. Am., no. 50, 1960, p. 868.
- 2-4. Penner, S. S.: Qualitative Molecular Spectroscopy and Gas Emissivities. Addison-Wesley Publishing Company, Inc., Reading, Mass., 1959.
- 2-5. Herzberg, G.: Molecular Spectra and Molecular Structure, I. Spectra of Diatomic Molecules. D. Von Nostrand Company, Inc., Princeton, N. J., 1950.
- 2-6. Gates, D. M.; Calfee, R. F.; Hansen, D. W.; and Benedict, W. S.: Line Parameters and Computed Spectra for Water Vapor Bands at 2.7 $\mu$ . NBS Monograph 71, 1964.
- 2-7. Benedict, W. S. and Calfee, R. F.: Line Parameters for the 1.9 and 6.3 Micron Water Vapor Bands. ESSA Professional Paper 2, 1967.
- 2-8. Herman, R. and Wallis, R. F.: J. Chem. Phys., no. 23, 1955, p. 637.
- 2-9. Herman, R.; Rothery, R. W.; and Rubin, R. J.: J. Mol. Spectry., no. 2, 1958, p. 369.
- 2-10. Breeze, J. C.; Ferriso, C. C.; Ludwig, C. B.; and Malkmus, W.: J. Chem. Phys., no. 42, 1965, p. 402.
- 2-11. Malkmus, W.; Ludwig, C. B.; and Ferriso, C. C.: J. Chem. Phys., no. 45, 1966, p. 3953.
- 2-12. King, G. W.; Hainer, R. M.; and Cross, P. C.: J. Chem. Phys., no. 11, 1943, p. 27.
- 2-13. Cross, P. C.; Hainer, R. M.; and King, G. W.: J. Chem. Phys., no. 12, 1944, p. 210.

## REFERENCES (Concluded)

- 2-14. Milne, E. A.: The Effect of Collisions on Monochromatic Radiative Equilibrium. Monthly Notices of the Royal Astronomical Society, vol. 88, 1928, p. 493.
- 2-15. Jeffries, J. T.: Spectral Line Formation. Blaisdell Publishing Co., 1968.
- 2-16. Breene, R. G.: The Shift and Shape of Spectral Lines. Pergamon Press, N. Y., 1961.
- 2-17. Chén, S. Y. and Takeo, M.: Rev. Modern Phys., no. 29, 1957, p. 20.
- 2-18. Burch, D. E.; Gryvnak, D.; Singleton, E. B.; France, W. L.; and Williams, D.: Infrared Absorption by Carbon Dioxide, Water Vapor, and Minor Atmospheric Constituents. AFCRL-62-698, July 1962.
- 2-19. Benedict, W. S.; Herman, R.; Moore, G. E.; and Silverman, S.: Can. J. Phys., no. 34, 1956, p. 850.
- 2-20. van de Hulst, H. C.: Light Scattering by Small Particles. John Wiley & Sons, Inc., N. Y., 1957.
- 2-21. Plass, G. N., and Kattawar, G. W.: Applied Optics, no. 7, 1968, p. 361.
- 2-22. Dave, J. V.: Applied Optics, no. 9, 1970, p. 1888.
- 2-23. Goldman, A.: J. Quant. Spectry. Radiative Transfer, no. 8, 1968, p. 829.
- 2-24. Tien, C.L.: J. Quant. Spectry. Radiative Transfer, no. 6, 1966, p. 893.
- 2-25. Kaplan, L. D. and Eggers, D. F.: J. Chem. Phys., no. 25, 1956. p. 879.



CHAPTER 3

CALCULATIONAL TECHNIQUES FOR HOMOGENEOUS GASES

The transfer equation [equation (2-22)] can be rewritten as:

$$N_{\omega}(\omega, u) = \int_{-\infty}^u N_{\omega}^0(\omega, u') \frac{\partial}{\partial u'} \tau(\omega; u', u) du' \quad , \quad (3-1)$$

where  $du = \rho ds$ . For a gas which is at a uniform temperature throughout, it reduces to the form

$$N_{\omega}(\omega, u) = N_{\omega}^0(\omega, T)[1 - \tau(\omega, u)] \quad , \quad (3-2)$$

where the transmissivity  $\tau$  is simply

$$\tau(\omega, u) = \exp[-k(\omega)u] \quad . \quad (3-3)$$

In general,  $k(\omega)$  may be a very rapidly varying function of wavenumber, so that a precise determination of  $\int N_{\omega}(\omega, u)d\omega$  may require evaluation of equation (3-1) at a very large number of frequencies. Such detailed calculations may be impractical or undesirable. The band model concept, developed for this purpose, is discussed in Section 3.2.

In certain special cases, such as that of a weakly absorbing gas, the direct evaluation of  $\int N_{\omega}(\omega, u)d\omega$  is greatly simplified. These special cases are discussed in Section 3.1.

### 3.1 LIMITING CASES AND "FIRST GUESS" PROCEDURES

These special cases often provide a useful method for obtaining rough estimates of the radiance.

#### 3.1.1 THIN GAS

If the absorptivity is small at every frequency, i.e.,  $ku \ll 1$  at all  $\omega$ 's, then

$$N_{\omega}(\omega, u) \approx N_{\omega}^0(\omega, T) k(\omega)u \quad , \quad (3-4)$$

and, over wavenumber intervals that are small compared to  $kT/hc$ ,

$$\int_{\Delta\omega} N_{\omega}(\omega, u) d\omega \approx N_{\omega}^0(\omega_0, T) \alpha u \quad , \quad (3-5)$$

where

$$\alpha = \int_{\Delta\omega} k(\omega) d\omega$$

and  $\omega_0$  is an appropriate mean frequency. Clearly, this approximation is an upper limit to the actual value of  $N_{\omega}$ .

#### 3.1.2 GREY GAS

If the monochromatic absorption coefficient remains constant ( $k = \bar{k}$ ) over a wide spectral interval, the gas is said to be grey. In this event, the quantity  $\int_{\Delta\omega} N_{\omega}(\omega, u) d\omega$  over an interval  $\Delta\omega$  is given by

$$\int_{\Delta\omega} N_{\omega}(\omega, u) d\omega = [1 - \exp(-\bar{k}u)] \int_{\Delta\omega} N_{\omega}^0(\omega, u) d\omega \quad . \quad (3-6)$$

When the absorption coefficient is not constant, but when it is convenient to make that approximation, equation (3-6) defines the value of  $\bar{k}$  which will define the grey model.

Because of the inequality

$$\int_{\Delta\omega} \{1 - \exp[-k(\omega)u]\} d\omega \leq [1 - \exp(-\bar{k}u)] \Delta\omega \quad ,$$

where

$$\bar{k} = \int k(\omega) d\omega / \Delta\omega \quad ,$$

equation (3-6) always provides an upper limit for the spectral radiance of any isothermal gas.

Because of the notoriously nongrey features of molecular spectra, better models are usually needed and some will be introduced in Section 3.2.

### 3.1.3 NONOVERLAPPING LINES

When the spectrum consists of a number of very narrow lines separated by regions of low emissivity, the radiance integrated over a spectral interval  $\Delta\omega$  may be reduced to a summation of equivalent widths. In other words, the quantity  $\int_{\Delta\omega} N_{\omega}(\omega, u) d\omega$  over an interval  $\Delta\omega$  is given by

$$\begin{aligned} \int_{\Delta\omega} N_{\omega}(\omega, u) d\omega &\simeq \sum_i N_{\omega}(\omega_i, u) \int_{\Delta\omega} \{1 - \exp[-k(\omega)u]\} d\omega \\ &\simeq \sum_i N_{\omega}(\omega_i, u) W_i(u) \end{aligned} \quad (3-7)$$

where  $W_i(u)$  is the equivalent width of the  $i$ th line whose center lies in the

interval  $\Delta\omega$  (see Section 2.2). Equation (3-7) provides a useful approximation so long as two conditions are satisfied: (a) The gas should be essentially transparent between adjacent lines (i. e.,  $k(\omega)u \ll 1$  at some point between each two neighboring lines), and (b) the equivalent widths of the lines should be small enough that the Planck function does not vary by a large amount across a single line.

Because of the inequality

$$\int_{\Delta\omega} \left\{ 1 - \exp \left[ - \sum_i k_i(\omega)u \right] \right\} d\omega \leq \sum_i \int_{\Delta\omega} \{ 1 - \exp[-k_i(\omega)u] \} d\omega$$

the nonoverlapping line approximation always provides an upper limit for the spectral radiance of any isothermal gas.

The two upper limits specified by the grey gas approximation [equation (3-6)] and the nonoverlapping line approximation [equation (3-7)] provide useful bounds to the radiance over a wide range of pressures and optical depths.

### 3.1.4 INTEGRATED EMISSIVITIES

The equation of transfer for a gas at a uniform temperature [equation (3-2)] may be integrated over a band of width  $\Delta\omega$  to determine the radiance emitted in that spectral region:

$$\int_{\Delta\omega} N_{\omega}(\omega, s) d\omega = \int_{\Delta\omega} N_{\omega}^0(\omega, T) \epsilon(\omega, s) d\omega \quad (3-8)$$

If the spectral radiance  $N_{\omega}^0$  is evaluated at an appropriate average wave-number  $\bar{\omega}$  (e. g., the center of the band), equation (3-8) becomes

$$\int_{\Delta\omega} N_{\omega}(\omega, s) d\omega = N_{\omega}^0(\bar{\omega}, T) \int_{\Delta\omega} \epsilon(\omega, s) d\omega \quad (3-8a)$$

If the integral  $\int_{\Delta\omega} \epsilon d\omega$  (the "integrated emissivity") can be evaluated

theoretically or empirically, the total band radiance is then determinable by equation (3-8a).

Directly from the definition of emissivity, one obtains

$$\int_{\Delta\omega} \epsilon(\omega) d\omega = \int_{\Delta\omega} \{1 - \exp[-k(\omega)u]\} d\omega \leq u \int_{\Delta\omega} k(\omega)d\omega = \alpha u \quad , \quad (3-9)$$

where  $\alpha$  is the band strength. The approximate equality holds when  $k(\omega)u$  is small ( $\ll 1$ ) throughout the band, i. e., for "sufficiently" small path-lengths. Generally, this relation is not of particular value in heat transfer calculations [since the condition  $k(\omega)u \ll 1$  may not be met], except insofar as an upper limit of  $\int_{\Delta\omega} \epsilon d\omega$ , however poor, may be of use in evaluating the importance of some particular band.

### 3.1.5 TOTAL EMISSIVITY

The rate of emission of radiant energy from a unit area of the surface of a body at temperature  $T$  and emissivity  $\epsilon(\omega, T)$  is given by

$$\int_0^{\infty} W_{\omega}(\omega, T) d\omega = \int_0^{\infty} \epsilon(\omega, T) W_{\omega}^0(\omega, T) d\omega \quad . \quad (3-10)$$

The comparable rate of emission from a blackbody at the same temperature is given by

$$\int_0^{\infty} W_{\omega}^0(\omega, T) d\omega = \sigma T^4 \quad . \quad (3-11)$$

The total emissivity is defined as the ratio of those two quantities:

$$\epsilon_T = \int_0^{\infty} \epsilon(\omega, T) W_{\omega}^0(\omega, T) d\omega / \sigma T^4 \quad . \quad (3-12)$$

### 3.1.6 BOX MODEL

The box model is a much simplified description of an entire band in which a uniform absorption coefficient is prescribed within an effective bandwidth  $\Delta\omega$  and zero absorption is assumed outside the interval  $\Delta\omega$ .

The integrated emissivity of the band is represented as

$$\int_{\Delta\omega} \epsilon d\omega = \Delta\omega [1 - \exp(-\alpha u/\Delta\omega)] \quad , \quad (3-13)$$

where  $\Delta\omega$  is an effective bandwidth. For diatomic molecules, a prescription for  $\Delta\omega$  which yields useful results for rough calculations is [3-1]

$$\Delta\omega = 9.9 (B_e T)^{1/2} \quad (3-14)$$

where  $B_e$  is the equilibrium rotational constant of equation (2-45). The coefficient (9.9) in equation (3-14) is based on a somewhat arbitrary criterion of smallness of the mean absorption coefficient at the edges of the band; however, the value of  $\Delta\omega$  is not particularly sensitive to the value prescribed for the cutoff absorption coefficient.

### 3.1.7 OTHER EMPIRICAL FORMS

As a result of extensive measurements on numerous gaseous absorbers, Burch, et al. [3-2] have represented their values of integrated absorptivity for particular molecular bands with an equation of the form

$$\int \alpha(\omega) d\omega = c u^m P_e^n \quad , \quad (3-15)$$

in which  $c$ ,  $m$ , and  $n$  are experimentally determined for each molecule and band, over a specified range of pathlengths. For larger pathlengths an equation of the form

$$\int \alpha(\omega) d\omega = C + D \log u + K \log P_e \quad (3-16)$$

has been used.

### 3.1.8 MEAN BEAM LENGTH

The radiant heat flux from an arbitrarily shaped volume of gas to a selected surface element is given by

$$\int_{2\pi} \int_0^{\infty} N_{\omega}^0(\omega, T) \epsilon(\omega, \ell) d\omega \cos\theta d\Omega \quad (3-17)$$

where  $d\Omega$  is the element of solid angle in direction  $(\theta, \phi)$ ;  $\theta$  is the angle between the line of sight and the normal to the surface element, and  $\ell$  is the pathlength through the gas in that direction. From the definition of total emissivity, equation (3-17) becomes

$$\int_{2\pi} \frac{1}{\pi} \sigma T^4 \epsilon_T(\ell) \cos\theta d\Omega \quad (3-18)$$

The "mean beam length" is defined as the radius of a hemispherical gas volume having, at the center of the hemisphere base, the same radiant flux as the gas volume under consideration. Thus, the mean beam length  $L$  is defined by the relation

$$\epsilon_T(L) = \int_{2\pi} \epsilon_T(\ell) \cos\theta d\Omega \quad (3-19)$$

In the optically thin limit,  $L$  is equal to the "geometric mean beam length"  $L_0$ :

$$L = L_0 = \frac{1}{\pi} \int_{2\pi} \ell \cos\theta d\Omega \quad (3-20)$$

**CHAPTER 3 - CALCULATIONAL  
TECHNIQUES FOR HOMOGENEOUS GASES**

When the gas is not optically thin, the mean beam length  $L$  is somewhat smaller than the geometric mean beam length  $L_0$  for volumes other than hemispheres. Tien [3-3] states that for "common gas-body geometries of practical interest,"  $L_0$  differs from  $L$  by at most 20 percent.

### 3.2 BAND MODELS

Band models are hypothetical models of simplified mathematical structure which are introduced to provide fair representations of the properties of real spectra at reasonable computing cost. In general, a model consists of a set of lines in a spectral interval with specified properties regarding the intensities, shape, number, and distribution of the lines.

#### 3.2.1 REGULAR BAND MODELS

At moderately low temperatures, the spectrum of a diatomic or linear molecule (aside from the Q-branch region) is usually composed of lines of slowly varying intensity and spacing. A mathematically simple model which may provide a good representation is an infinite sequence of equally spaced spectral lines of identical intensity and shape. When the line is collision-broadened, this model is known variously as the Elsasser model, the regular-collision model, or the regular-Lorentz model. Tabulations of the absorption coefficient and mean transmissivity are available (Appendix 3-A). When the lines are Doppler broadened, a different representation must be used, for which tabular data are also available (Appendix 3-A). Such models would not be expected to provide a good representation in the region of a band head, near a Q-branch peak, or in a far wing of a band where the absorption in a given spectral interval has significant contributions from lines of widely differing strengths.

##### 3.2.1.1 Regular Model for Collision-Broadened Lines Having Lorentz Constants (Elsasser)

The absorption coefficient of the regular-Lorentz model [3-4] follows from equation (2-25) and from the definition of the model:

$$k(\omega) = \sum_{n=-\infty}^{\infty} \frac{S\gamma/\pi}{\gamma^2 + (\omega - nd)^2} \quad , \quad (3-21)$$

in which  $S$  and  $\gamma$  are the line strength and half-width, and  $d$  is the line spacing. Equation (3-21) can be transformed as follows:

$$k(\omega) = \frac{S}{d} \frac{\sinh(2\pi\gamma/d)}{\cosh(2\pi\gamma/d) - \cos(2\pi\omega/d)} \quad . \quad (3-21a)$$

The mean absorptivity is found by averaging  $\alpha(\omega)$  over an interval of  $d$ :

$$\bar{\alpha} = 1 - (2\pi)^{-1} \int_{-\pi}^{\pi} \exp\left(\frac{-\beta x \sinh \beta}{\cosh \beta - \cos z}\right) dz, \quad (3-22)$$

where  $\beta = 2\pi\gamma/d$ , and  $x = Su/2\pi\gamma$ . There are no closed form solutions. Tables and approximations are given in Appendix 3-A.

### 3.2.1.2 Regular Model for Doppler Broadened Lines (Golden)

The analogous problem of a band of equally intense, equally spaced, and equally wide lines of Doppler shape has been studied by Golden [3-5, 3-6]. Tabulated values of mean absorptivity are available and are extensive enough to permit accurate interpolation for any desired conditions. As purely Doppler-broadened lines indicate relatively low pressure or high temperature, the application of this model to molecular gases is not likely to be as common as that of the collision-broadened model.

This model, like the regular-Lorentz model, should give a reasonable representation of a real spectrum when the lines are varying slowly in intensity and spacing. As distinct from the case of Lorentz lines, the widths of Doppler lines vary in proportion to the frequency. However, since this variability is quite gradual, its effect is insignificant.

Since any real line is affected by collision broadening, however small, sufficiently far out in its wings, it should be remembered that the Doppler model will always provide a lower limit to the absorptivity.

For such a model, it follows from equation (2-29) that the absorption coefficient is given by

$$k(\omega) = k_0 \sum_{n=-\infty}^{\infty} \exp[-(\omega - \omega_0 - nd)^2 \ln 2/\gamma_D^2], \quad (3-23)$$

or, alternatively,

$$k(\omega) = \frac{S}{d} \theta_3 \left[ \pi(\omega - \omega_0)/d, \exp(-\pi^2 \gamma_D^2/d^2 \ln 2) \right], \quad (3-24)$$

where  $\theta_3$ , the third Jacobi theta function, is defined by

$$\theta_3(x, y) = 1 + 2 \sum_{n=1}^{\infty} (y)^{n^2} \cos(2nx) \quad .$$

The mean absorptivity is given by

$$\bar{\alpha} = 2 \int_0^{1/2} \left\{ 1 - \exp \left[ - \frac{Su}{d} \theta_3 \left( \pi v, \exp(-\pi^2 \gamma_D^2/d^2 \ln 2) \right) \right] \right\} dv \quad . \quad (3-25)$$

A graph of  $\bar{\alpha}$  versus  $Su/d$  is shown (Fig. 3-1) for various values of  $\gamma_D/d$ .

Extensive tabulations are presented by Golden in References 3-5 and 3-6. Two approximate forms with their regions of applicability are reproduced in Table 3-A-3.

Frequently it may be found that the line width is small enough relative to the line spacing that the effect of overlapping of the lines is negligible. In this event, the mean absorptivity is simply

$$\bar{\alpha} = W/d \quad , \quad (3-26)$$

where  $W$  is the equivalent width of an isolated Doppler line (as given in Section 2.2.1.3.2). As was pointed out in Section 3.1.3, the assumption of no line overlapping used in obtaining equation (3-26) will always provide an upper limit to the mean absorptivity.

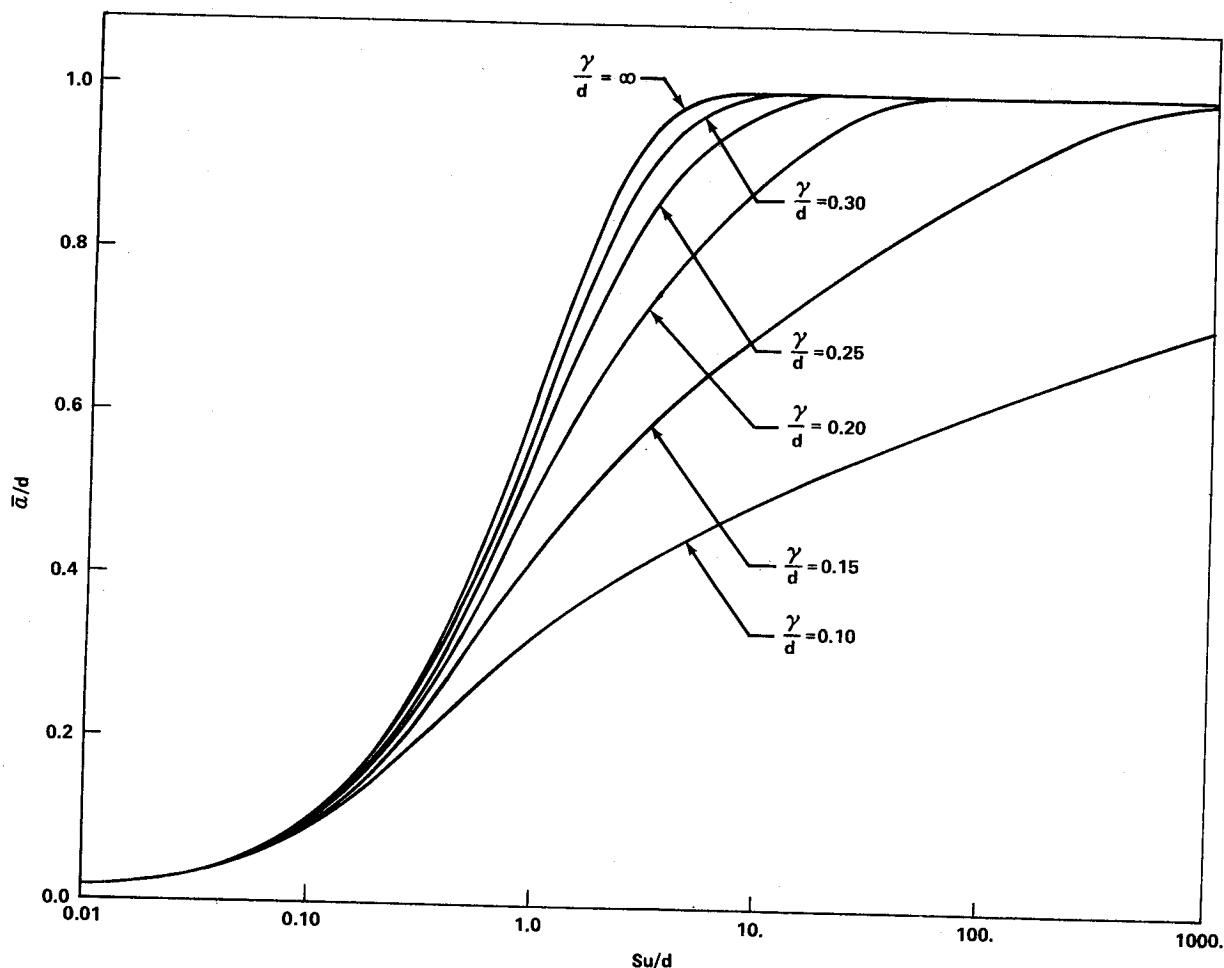


Figure 3-1. The mean absorptivity of the regular Doppler band.

### 3.2.1.3 Regular Model for Mixed Doppler-Lorentz Lines

The general case of a regular model composed of mixed Doppler-Lorentz (Voigt) lines has been studied by Golden [3-7]. Various series expansions for the absorption coefficient are presented, but no convenient analytic forms for the absorption coefficient or the mean absorptivity have been developed. Much of Reference 3-7 is devoted to a study of conditions under which the limiting cases (regular Lorentz, regular Doppler, isolated Voigt line) are applicable. It is useful to note that all three limiting cases provide lower limits to the mean absorptivity of the regular Voigt model.

### 3.2.2 RANDOM BAND MODELS

One striking characteristic of many high-resolution molecular spectra, especially of asymmetric top molecules, and particularly at high temperatures,

is the seemingly irregular line spacing or intensity. A regular model such as Elsasser's would be clearly inapplicable to such a spectrum. To treat such spectra, "random" band models, in which the location of any line is assumed to be statistically unrelated to the locations of other lines, have been developed. Generally, in these models, the line strengths are also described by a probability distribution, and it is assumed that all lines have an identical shape, differing only in strength.

The assumption of lack of statistical correlation permits considerable mathematical simplification in the form of separation of integrals over frequency, strength, and path.

### 3.2.2.1 Lines of Equal Strength

The simplest random band model is one in which all lines are assumed to have the same strength. The mean line spacing is denoted by  $d$ , meaning that a large spectral interval  $D$  will contain  $D/d$  lines, on the average. Such a model is unreasonable in that any real spectrum in which the lines are randomly distributed in spectral location would not have all lines of equal strength. However, the results are so simple that this model is worth considering first.

It is found that the mean absorptivity [equation (2-19)] of a spectrum composed of lines of strength  $S$ , of arbitrary but identical shape, and randomly located at a mean spacing  $d$  is given simply by [3-8, 3-9]

$$\bar{\alpha} \equiv \int_{\text{band}} \alpha(\omega) d\omega = 1 - \exp[-W(S)/d] \quad , \quad (3-27)$$

where  $W(S)$  is the equivalent width of a single such isolated line. The properties of the band model are, thus, expressed in terms of the properties of a single line. The mean absorptivities are shown in Table 3-1 (Model A) and in Figure 3-2.

If the real spectrum is dominated by a number of intense lines, the "equal strength" model may give a good representation of the spectrum if  $S$  is replaced by the average strength of these lines.

TABLE 3-1. CURVES OF GROWTH FOR VARIOUS RANDOM LORENTZ MODELS

Model	$P(S)$	$\bar{S}$	$S_E$	$-\ln \tau$ in terms of $\bar{k}$ and $a$	$-\ln \tau$ in terms of $S_E$ , $d_E$ , and $\gamma$	$-\ln \tau$ in terms of $\beta$ and $x$
A	$= \delta(S - S_0)$	$S_0$	$S_0$	$2\pi a f\left(\frac{\bar{k}u}{2\pi a}\right)$	$\frac{2\pi\gamma}{d_E} f\left(\frac{S_0 u}{2\pi\gamma}\right)$	$\beta f(x_0)$
B	$= S_0^{-1} \exp(-S/S_0)$	$S_0$	$\frac{4}{\pi} S_0$	$\bar{k}u \left(1 + \frac{\bar{k}u}{4a}\right)^{-1/2}$	$\frac{S_E}{d_E} u \left(1 + \frac{S_E u}{4\gamma}\right)^{-1/2}$	$\beta_E x_E \left(1 + \frac{\pi}{2} x_E\right)^{-1/2}$
C	$\propto S^{-1}$ (for $S \leq S_M$ ) $= 0$ (for $S > S_M$ )	$\rightarrow 0$	$\frac{1}{4} S_M$	$2\pi a g\left(\frac{\bar{k}u}{2\pi a}\right)$	$\frac{2\pi\gamma}{d_E} \left[g\left(\frac{S_E u}{2\pi\gamma}\right)\right]$	$\beta_E g(x_E)$
D	$\propto S^{-1} \exp(-S/S_M)$	$\rightarrow 0$	$\frac{1}{\pi} S_M$	$2a \left[\left(1 + \frac{\bar{k}u}{a}\right)^{1/2} - 1\right]$	$\frac{2\gamma}{d_E} \left[\left(1 + \frac{S_E u}{\gamma}\right)^{1/2} - 1\right]$	$\frac{1}{\pi} \beta_E \left[\left(1 + 2\pi x_E\right)^{1/2} - 1\right]$

Notes:  $f(x) = x \exp(-x) [I_0(x) + I_1(x)]$

$$g(x) = \frac{1}{2} f(4x) + \frac{1}{4} \exp(-4x) I_0(4x) - \frac{1}{4}$$

$$\bar{k} = \text{mean absorption coefficient} = S_E/d_E$$

$$a = \text{fine-structure parameter} = \gamma/d_E$$

$$x_E = S_E u / 2\pi\gamma$$

$$\beta_E = 2\pi\gamma/d_E$$

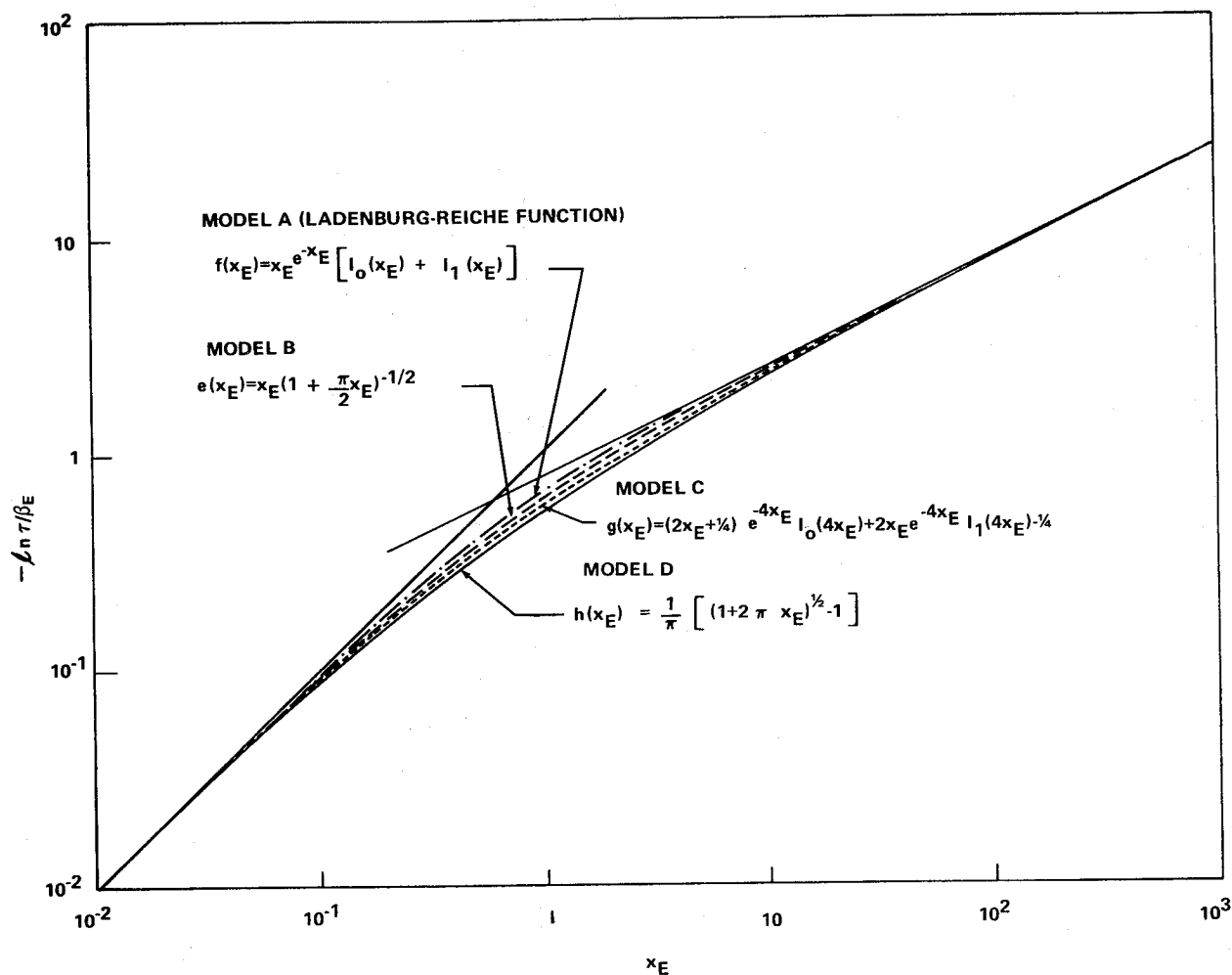


Figure 3-2. Curves of growth for random band models composed of Lorentz lines for the four different intensity distribution functions (A through D) given on Table 3-1.

However, it is frequently found (especially at higher temperatures) that the presence of numerous low-strength lines has a significant effect on the mean absorptivity. Thus, one is led to the introduction of a line strength probability distribution.

### 3.2.2.2 Exponential Line Strength Distribution

A commonly used probability distribution of line strength is the exponential distribution:

$$P(S) = \frac{4}{\pi S_E} \exp\left(-\frac{4S}{\pi S_E}\right) \quad (3-28)$$

This strength distribution in a random spectrum of Lorentz lines of equal widths defines the so-called "Goody" model. The widespread use of this model results not so much from any rational physical basis for the particular  $P(S)$  as from the fact that the expression for the curve of growth is found to have a simple algebraic form. In particular, it is found [3-10] that the mean absorptivity  $\bar{\alpha}$  [equation (2-21)] is:

$$\bar{\alpha} \equiv \int_{\text{band}} \alpha(\omega) d\omega = 1 - \exp\left[-\frac{S_E u}{d_E} \left(1 + \frac{S_E u}{4\gamma}\right)^{-1/2}\right], \quad (3-29)$$

or, alternatively,

$$-\ln \tau = \frac{S_E u}{d_E} \left(1 + \frac{S_E u}{4\gamma}\right)^{-1/2} \quad (3-30)$$

The function representing  $-\ln \tau$  is called the curve of growth for the particular model.

It is desirable to relate the parameters  $S_E$ ,  $\gamma$ , and  $d_E$  to observable parameters. In this particular case,  $S_E$  is related to the mean strength  $\left(\int_0^\infty SP(S)dS = \frac{\pi S_E}{4}\right)$ ; however, this is not a readily determined quantity and, in fact, for some models such as those having an infinite number of lines, an average line strength (or spacing) may not be meaningful.

However, if a curve of growth has two asymptotic regions in which the logarithm of the transmissivity varies as a power of the gas thickness, the band model parameters are determinable (at least in principle) by making observations with sufficiently short and sufficiently long pathlengths. In terms of the quantities  $S_E$ ,  $\gamma$ , and  $d_E$ , the curve of growth for the exponential line strength model has a linear asymptotic region

$$-\ln \tau \rightarrow S_E u / d_E \quad \text{as} \quad u \rightarrow 0, \quad (3-31)$$

and a square root asymptotic region

$$-\ln \tau \rightarrow 2(S_E \gamma u)^{1/2} / d_E \quad \text{as} \quad \gamma u \rightarrow \infty. \quad (3-32)$$

These are shown on Table 3-1 (Model B) and in Figure 3-2.

### 3.2.2.3 Inverse Line Strength ( $S^{-1}$ ) Distributions.

There are both theoretical and experimental justifications for assuming a line strength probability distribution,  $P(S)$ , whose behavior is dominated at small  $S$  by a dependence on  $S^{-1}$ . Such models have a very large number of very weak lines, and it is necessary to relinquish any simple concepts of mean line strength and mean line spacing as these quantities may approach zero in limiting cases. However, the previous definitions of equivalent line strength ( $S_E$ ) and equivalent line spacing ( $d_E$ ) remain useful.

Figure 3-3 shows an actual histogram of the number of lines in each of six intensity decades, based on a count of lines tabulated by Gates, et al. [3-11, 3-12] for the 3750 to 3800  $\text{cm}^{-1}$  region of the  $\text{H}_2\text{O}$  spectrum. An approximate  $S^{-1}$  relationship is observed over this range of line strengths.

A maximum strength is often imposed on the line strength by introducing a "truncated"  $S^{-1}$  distribution:

$$\begin{aligned} P(S) &\propto S^{-1} && \text{for} && S \leq 4S_E \\ P(S) &= 0 && \text{for} && S > 4S_E \end{aligned} \quad (3-33)$$

Table 3-1 gives the corresponding curve of growth (Model C), and Figure 3-2 shows it graphically.

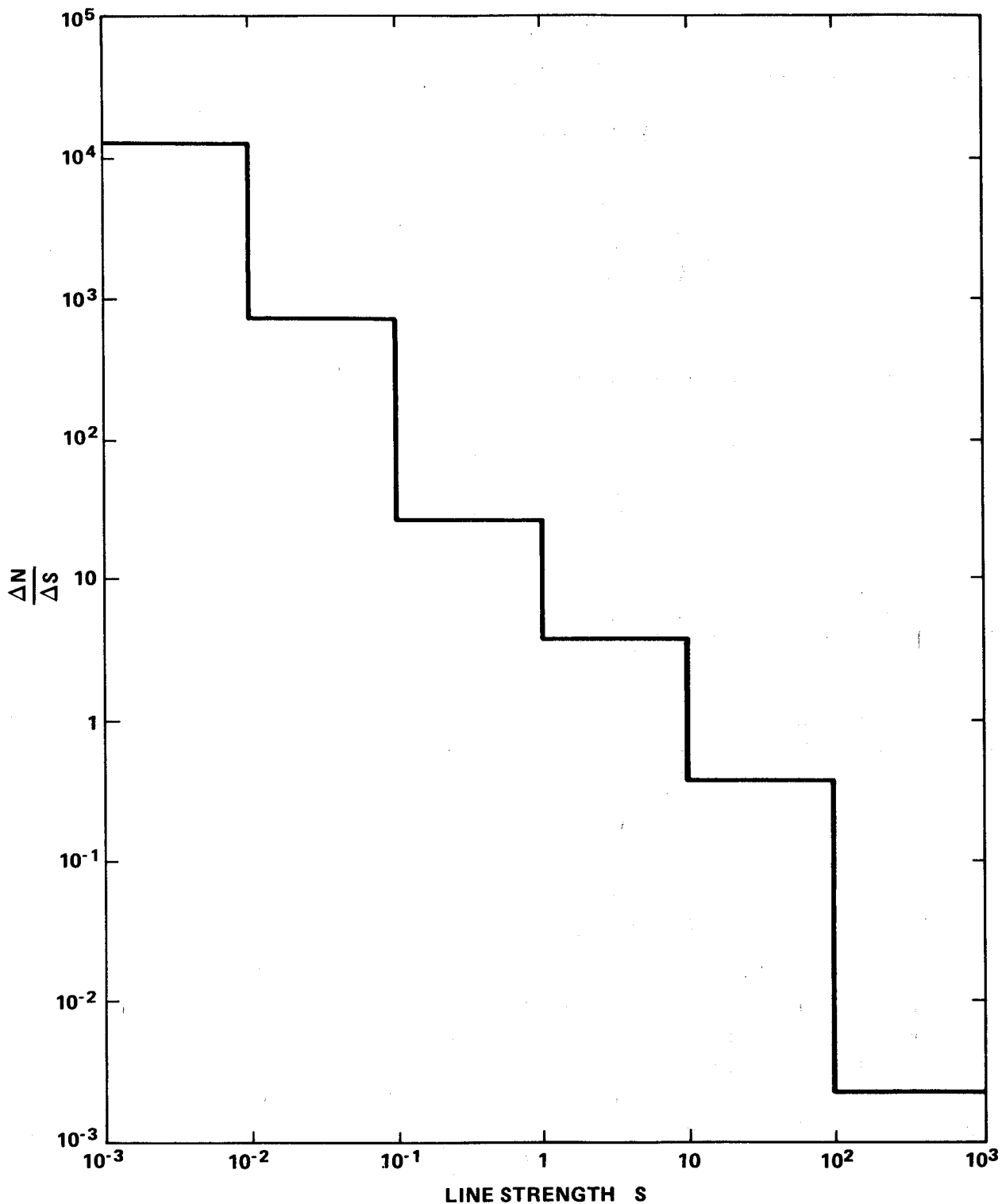


Figure 3-3.  $\Delta N / \Delta S$  [proportional to  $P(S)$ ] for  $H_2O$  lines in spectral region  $3750$  to  $3800 \text{ cm}^{-1}$ , obtained by actual count of lines in each strength decade as tabulated in References 3-11 and 3-12. [Corrections were made for the deletion of weak lines occurring in the immediate vicinity of strong lines (see References 3-11 and 3-12)].

### 3.2.2.4 Exponential-Tailed $S^{-1}$ Distribution

A line strength probability distribution defined by

$$P(S) \propto S^{-1} \exp\left(-\frac{S}{\pi S_E}\right) \quad (3-34)$$

results in a curve of growth having the simple form [3-13]:

$$-\ln \tau = \frac{2\gamma}{d_E} \left[ \left(1 + \frac{S_E u}{\gamma}\right)^{1/2} - 1 \right] \quad (3-35)$$

This equation and its alternative formulations are summarized in Table 3-1 (Model D), and the curve of growth is shown as  $h(x_E)$  in Figure 3-2.

This model has the broadest distribution of line strengths and consequently has the widest transition region between the linear and square root regions. The quantities  $S_E$  and  $d_E$  are defined so that the curve of growth has the same asymptotes as the curves of growth for the other models (Fig. 3-2).

### 3.2.2.5 The Choice of a Random Band Model

Figure 3-2 illustrates how the adoption of models displaying an increasing number of weak lines (from A to D) leads to a broader interval between the two asymptotic regimes. The multiplication of weak lines is itself related to the complexity of the molecule and to its temperature. Therefore, it is interesting to introduce here a synthetic model where the effect of weak lines can be controlled by a simple parameter  $r$ . Consider a model consisting of  $n + 1$  lines of intensities

$$S_M, rS_M, r^2S_M, \dots, r^n S_M \quad (r < 1), \quad (3-36)$$

randomly located in a spectral interval. This model is described by the following probability distribution function:

$$P(S) = \frac{1}{n+1} \sum_{m=0}^n \delta(S - r^m S_M) \quad . \quad (3-37)$$

One finds in the limit of  $n \rightarrow \infty$

$$\beta_E = \frac{1+r^{1/2}}{1-r^{1/2}} \beta_M \quad (3-38)$$

and

$$x_E = \frac{1}{(1+r^{1/2})^2} x_M \quad . \quad (3-39)$$

Thus one has, explicitly,

$$F(x_E, r) = \frac{1-r^{1/2}}{1+r^{1/2}} \sum_{m=0}^{\infty} f \left[ r^m (1+r^{1/2})^2 x_E \right] \quad . \quad (3-40)$$

The mean absorptivity of a band consisting of randomly located lines of intensities  $S_M$ ,  $rS_M$ ,  $r^2S_M$ , . . . , is thus given by

$$\bar{\epsilon} = 1 - \exp \left[ -\beta_E F(x_E, r) \right] \quad . \quad (3-41)$$

The definition of  $F(x_E, r)$  as an infinite series of Ladenburg-Reiche functions is not particularly convenient for general use. However, for certain values of  $r$ ,  $F(x_E, r)$  is readily evaluated from existing tabulations of  $f(x)$  [3-14].

The function  $F(x_E, r)$  is shown in Figure 3-4 for values of  $r$  of 0.01, 0.1, 0.5, and 1.0. Also shown is  $f(x)$ , which is the limit of  $F(x_E, r)$  as  $r \rightarrow 0$ .

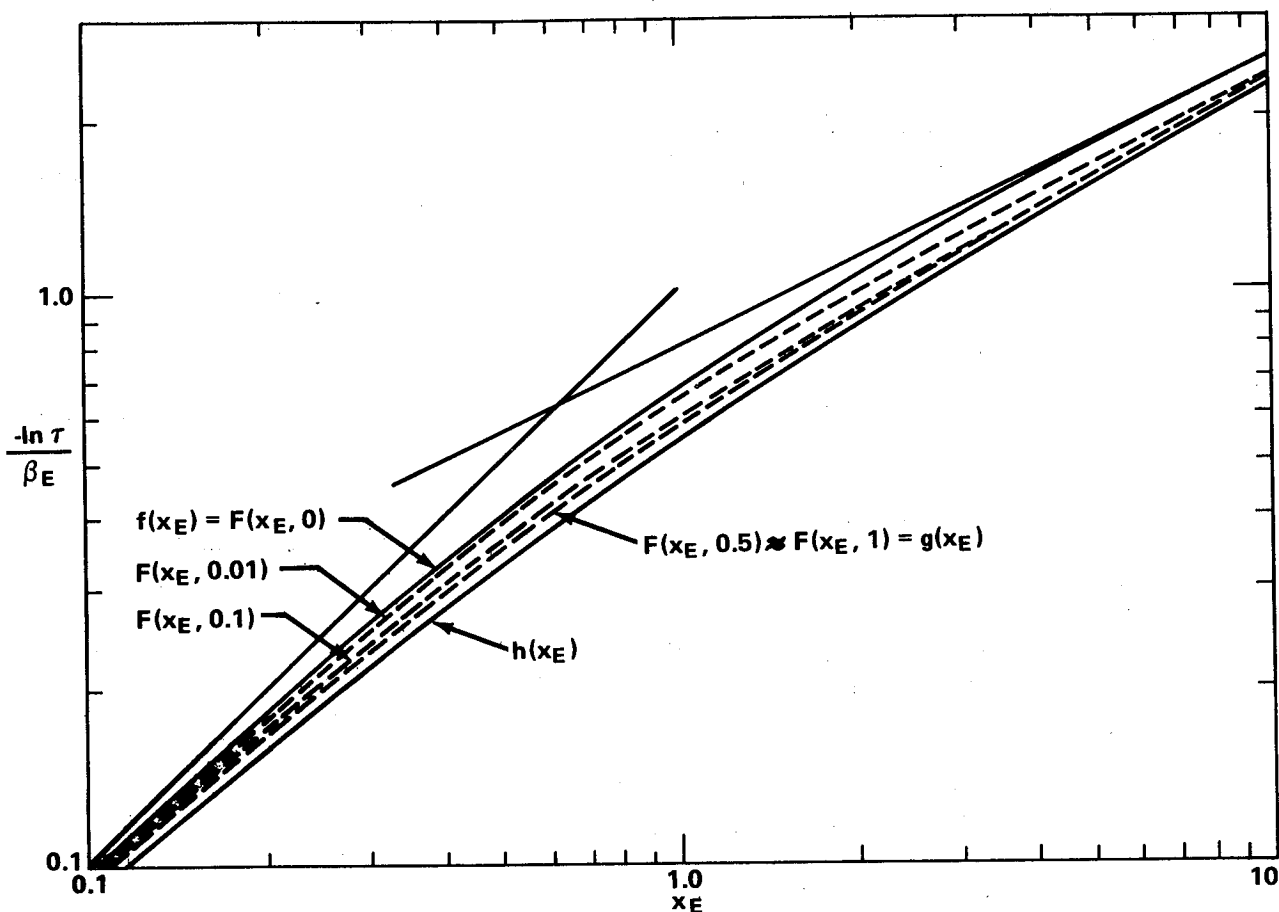


Figure 3-4. Transition regions of curves of growth for random band models composed of Lorentz lines for various intensity distribution functions.

From Figure 3-4 it is seen that even for  $r$  as low as 0.01 the curve of growth defined by equation (3-40) deviates significantly from the Ladenburg-Reiche curve for a single line. It is also seen that, on the average, the curve for  $r = 0.1$  is closer to the  $S^{-1}$  curve of growth  $g(x)$  (and, in fact, to the curve of growth for the exponential-tailed  $S^{-1}$  distribution  $[h(x)]$ ) than to the Ladenburg-Reiche curve  $f(x)$ . This suggests that at temperatures such that

$$\exp(-hc\omega_0/kT) > 0.1 \quad , \quad (3-42)$$

or, equivalently,

$$T(K) > 0.6 \omega_0 (\text{cm}^{-1}) \quad , \quad (3-43)$$

(where  $\omega_0$  is the lowest vibrational energy level in  $\text{cm}^{-1}$ ), the  $S^{-1}$  curves of growth [ $g(x)$  and  $h(x)$ ] are better approximations to the true curve of growth than the single intensity curve  $f(x)$ .

As an example, consider the interpretation of experimental measurements of the  $\text{CO}_2$  4.3- $\mu$  band system at 1200K. Note first that for  $\text{CO}_2$ , equation (3-43) yields a value of about 400K above which temperature the use of  $h(x)$  rather than  $f(x)$  is preferable. Figure 3-5 (which is taken partly from Figure 8 of Reference 3-15) shows experimentally measured points along the curve of growth at  $2273 \text{ cm}^{-1}$  with a Ladenburg-Reiche curve [ $f(x)$ ] and its asymptotes fitted to these points by Oppenheim and Ben-Aryeh. It also shows the same experimental points to which the curve of growth  $h(x)$  has now been fitted. It is noted that both curves provide an apparently good fit to the experimental points, and that neither curve could be selected or rejected on the basis of its fit. It can be seen however, that the extrapolation to the asymptotic regions (primarily the square root region) is affected considerably.

Figure 3-6 (which is taken from Figure 20 of Reference 3-16) shows a comparison of a calculated square root region parameter with the experimentally determined values of Oppenheim and Ben-Aryeh. It was commented previously [3-16] that the apparent disagreement in the 2200 to 2300  $\text{cm}^{-1}$  range, in which the square root region was least well determined experimentally, would be lessened by the use of any band model containing a non-constant intensity distribution. The arrow and dot show the change (of about 30 percent) at  $2273 \text{ cm}^{-1}$  resulting from the different choice of curve of growth represented by equation (3-35).

### 3.2.3 RANDOM DOPPLER MODELS

The four line distribution models used in the previous sections for collision broadened profiles can be used also when the dominant broadening is due to Doppler effects [3-17]. They shall be described and compared briefly in this section.

#### 3.2.3.1 Lines of the Same Strength

If all the lines are of the same strength  $S_0$ ,

$$\bar{W}/d = (\bar{k}/k_{00}) D(y_0) \quad , \quad (3-44)$$

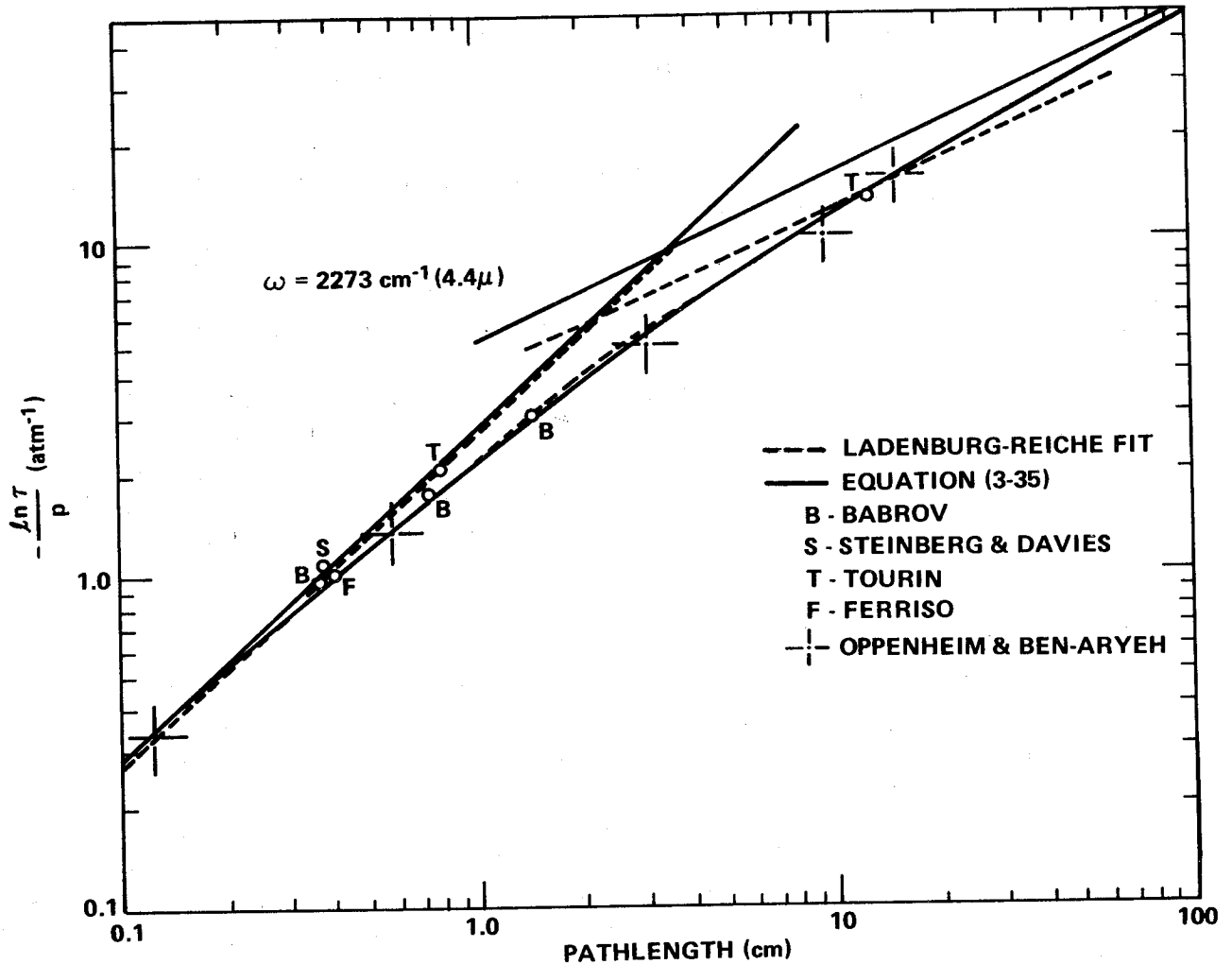


Figure 3-5. Measured values of  $-(\ln \tau)/p$  for  $\text{CO}_2$  at  $\omega = 2273 \text{ cm}^{-1}$  and  $T = 1200\text{K}$  with Ladenburg-Reiche curve fitted by Oppenheim and Ben-Aryeh [3-16] compared with an exponential-tailed curve of growth [equation (3-35)].

where  $y_0 (= k_{00} u)$  is the optical depth at the line center,  $k_{00}$  is the absorption coefficient at the line center, and  $D$  is the curve of growth for an isolated Doppler line [equation (2-33)].

### 3.2.3.2 Lines Having Exponential Distribution

If the lines have an exponential distribution with respect to a mean intensity  $S_0$ , as given by

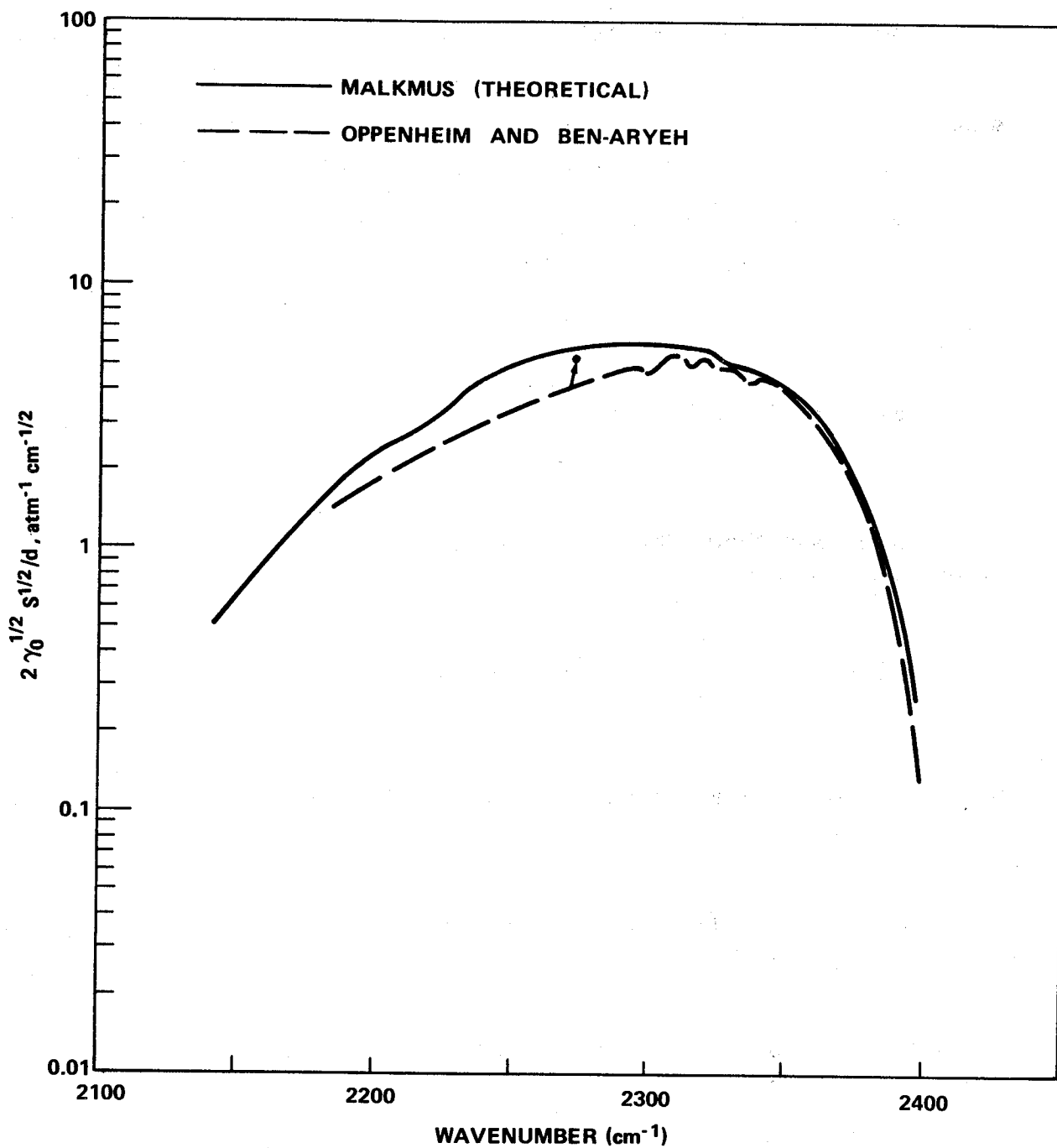


Figure 3-6. Comparison of theoretical and experimental values of  $2\gamma_0^{1/2} S^{1/2}/d$  (Reference 3-16).

$$P(S) = S_0^{-1} \exp(-S/S_0) \quad , \quad (3-45)$$

then

$$\bar{W}/d = (\bar{k}/k_{00}) E(y_0) \quad , \quad (3-46)$$

where

$$E(y) = \int_0^{\infty} \exp(-v) D(vy) dv \quad . \quad (3-47)$$

If one substitutes the integral form of  $D$  [equation (2-33)], the following is obtained:

$$E(y) = \pi^{-1/2} \int_{-\infty}^{\infty} \{y \exp(-\xi^2) / [y \exp(-\xi^2) + 1]\} d\xi \quad . \quad (3-48)$$

If  $y \leq 1$ , a power series expansion can be written:

$$E(y) = \sum_{n=0}^{\infty} (-1)^n y^{n+1} / (n+1)^{1/2} \quad . \quad (3-49)$$

The following expansion valid for any  $y$  ( $0 \leq y < \infty$ ) can also be obtained:

$$E(y) = \sum_{n=0}^{\infty} a_n [y/(y+1)]^{n+1} \quad , \quad (3-50)$$

where

$$a_n = \sum_{m=0}^n n! (-1)^m / m! (n-m)! (m+1)^{1/2} \quad .$$

The convergence of this equation is very slow for large  $y$ , in which case an asymptotic expansion is convenient:

$$E(y) = 2\pi^{-1/2} (\ln y)^{1/2} [1 - (\pi^2/24) (\ln y)^{-2} - (7\pi^4/192) (\ln y)^{-4} - \dots] \quad (3-51)$$

This series (as is the corresponding expression for an isolated line) is semi-convergent and must be handled with some caution (see Appendix 2-A).

The two curves of growth,  $D(y)$  and  $E(y)$ , are compared in Figure 3-7. It is seen that the curve of growth for the exponential intensity distribution  $E(y)$  also has the familiar  $(\log)^{1/2}$  asymptotic behavior characteristic of an isolated Doppler line.

### 3.2.3.3 Lines with $S^{-1}$ Distribution

If an  $S^{-1}$  distribution is adopted, two curves of growth can be derived:  $G(y)$  if the distribution function is truncated at a maximum  $S$  [ $P(S) = 0$  for  $S > S_E$ ] or  $H(y)$  if an exponential tail is fitted to the distribution

$$\left[ P(S) \propto S^{-1} \exp\left(-\frac{S}{S_E}\right) \right] \quad .$$

The curves  $G(y)$  and  $H(y)$  are also shown on Figure 3-7. Both curves of growth demonstrate the same asymptotic behavior for large  $y$ 's. The curve  $H(y)$  has a somewhat more gradual transition region, since the corresponding intensity distribution is broader.

One notes that (in distinction from the case of the Lorentz line shape) the change to strength distribution function with an  $S^{-1}$  dependence markedly changes the asymptotic behavior of the curve of growth. Since the  $S^{-1}$  models are expected to provide a reasonable representation of the behavior of high-temperature gases, and since the Doppler line shape provides a lower limit to the mean emissivity, the  $(\log)^{3/2}$  dependence may be quite significant in extrapolating mean emissivity data to long pathlengths.

### 3.2.3.4 Random Band Models: Mixed Lorentz-Doppler

For the case of collision broadening, the statistical band model representation of the optical depth is approximated by

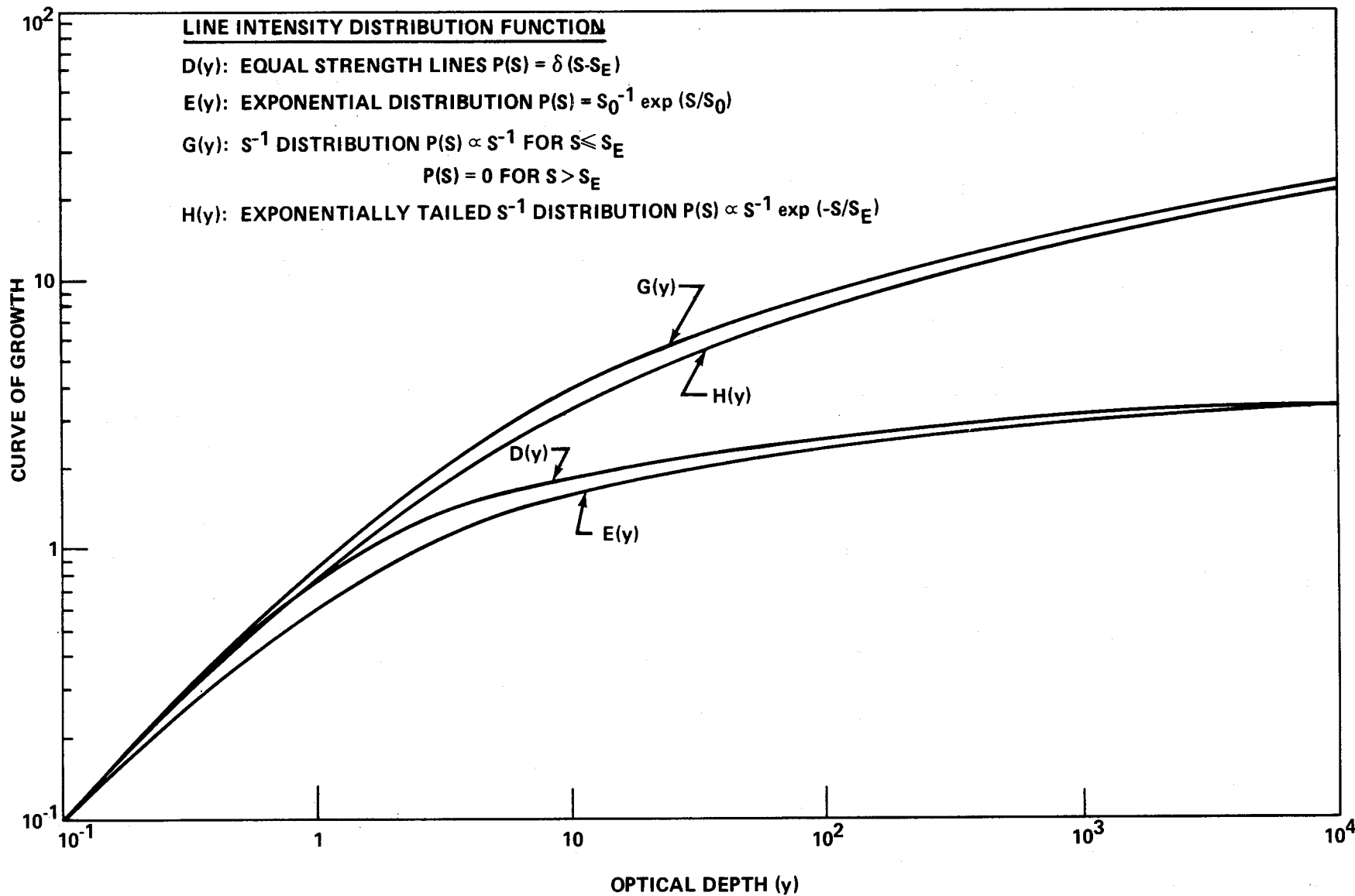


Figure 3-7. Pure Doppler curves of growth for various intensity distribution functions (Random Model).

$$X_C = ku / (1 + ku/4a_C)^{1/2} \quad (3-52)$$

where  $a_C$  is the collision-broadened fine structure parameter ( $\gamma_C/d$ ). This expression provides a transition from the linear region (where  $ku \ll a_C$  and  $X_C$  approximates  $ku$ ) to the square root region (where  $ku \gg a_C$  and  $X_C$  approximates  $(4a_C ku)^{1/2}$ ). Figure 3-8 presents an example of the behavior of this function for water vapor with varying total pressures.

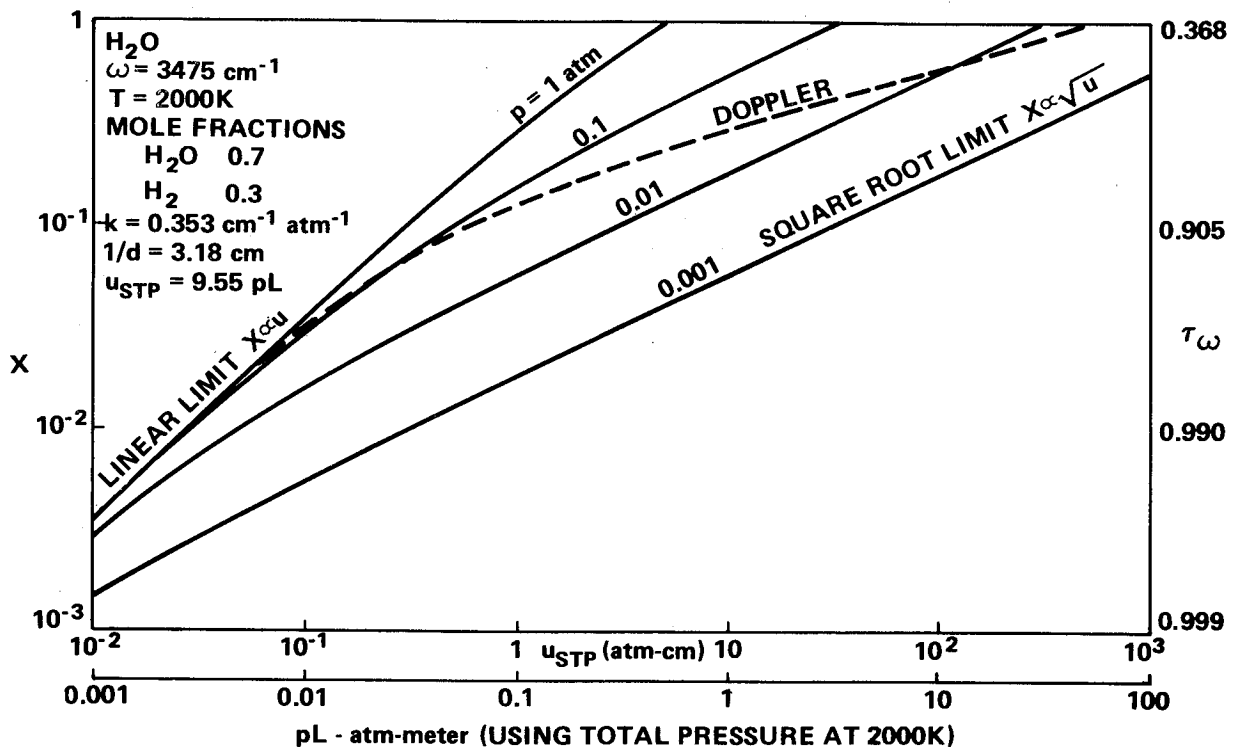


Figure 3-8. Example of optical depth variations with pressure and pathlength.

As the collision-broadened optical depth decreases with decreasing pressure, Doppler broadening becomes significant. An approximate representation for the Doppler broadened optical depth (see Section 3.2.5) is

$$X_D = 1.7a_D \left\{ \ln \left[ 1 + \left( \frac{ku}{1.7a_D} \right)^2 \right] \right\}^{1/2}, \quad (3-53)$$

where  $a_D$  is the Doppler-broadened fine structure parameter ( $\gamma_D/d$ ). As with collision broadening, this expression reduces to  $X_D \approx k u$  when  $k u \ll a_D$ , but since the Doppler half-width,  $\gamma_D$ , is not a function of pressure, there is a single curve for Doppler broadening for a given temperature and wavenumber.

The relative behavior of the collision and Doppler curves of growth are shown in Figure 3-8. Although this representation is for a particular temperature and spectral position, it illustrates the general condition that Doppler broadening is most significant at low pressures. The method of combining the Doppler and collision broadened optical depths into an overall optical depth is described in Section 5.3, but an approximate method is to neglect the smaller of the two depths as long as they differ by a factor of 3 or more.

### 3.2.4 HYBRID MODELS

At times, neither a simple regular model nor a random model appears to provide the optimum representation for a particular spectrum. As an example, the moderate-temperature spectrum of a linear molecule may locally be closely represented by a set of several superposed regular bands of different intensities.

#### 3.2.4.1 Random Regular Model

A model combining features of both regular and random band models is developed by assuming that a spectrum can be represented by a random superposition of a number of regular bands. The properties of each band — line spacing, strength, and half-width — may be different. Such a model would be expected to provide a good representation of the spectrum of a linear molecule at moderate temperatures when the higher-order bands become of significant strength.

For a random superposition of  $n$  bands, the transmissivities combine multiplicatively,

$$\tau = \prod_{i=1}^n \tau_i \quad , \quad (3-54)$$

so that the mean absorptivity is given by

CHAPTER 3 – CALCULATIONAL  
TECHNIQUES FOR HOMOGENEOUS GASES

$$\alpha = 1 - \prod_{i=1}^n (1 - \alpha_i) \quad , \quad (3-55)$$

in which  $\alpha_i$  is calculated for  $n$  regular bands by equation (3-22).

The major difference between the regular and random Lorentz models arises when the line width to line spacing ratio ( $\beta = 2\pi\gamma/d$ ) is small and the optical depth ( $x = Su/2\pi\gamma$ ) is large (the "error-function" and "square-root" regions, respectively). Plots of the mean absorptivity versus optical depth for these two models are shown in Figure 3-9 as the uppermost and lowest curves, respectively. The second and third curves are for random-regular models composed of the random superposition of two and five regular bands of equal intensity, respectively. The rapid approach to the totally random band model curve can be seen.

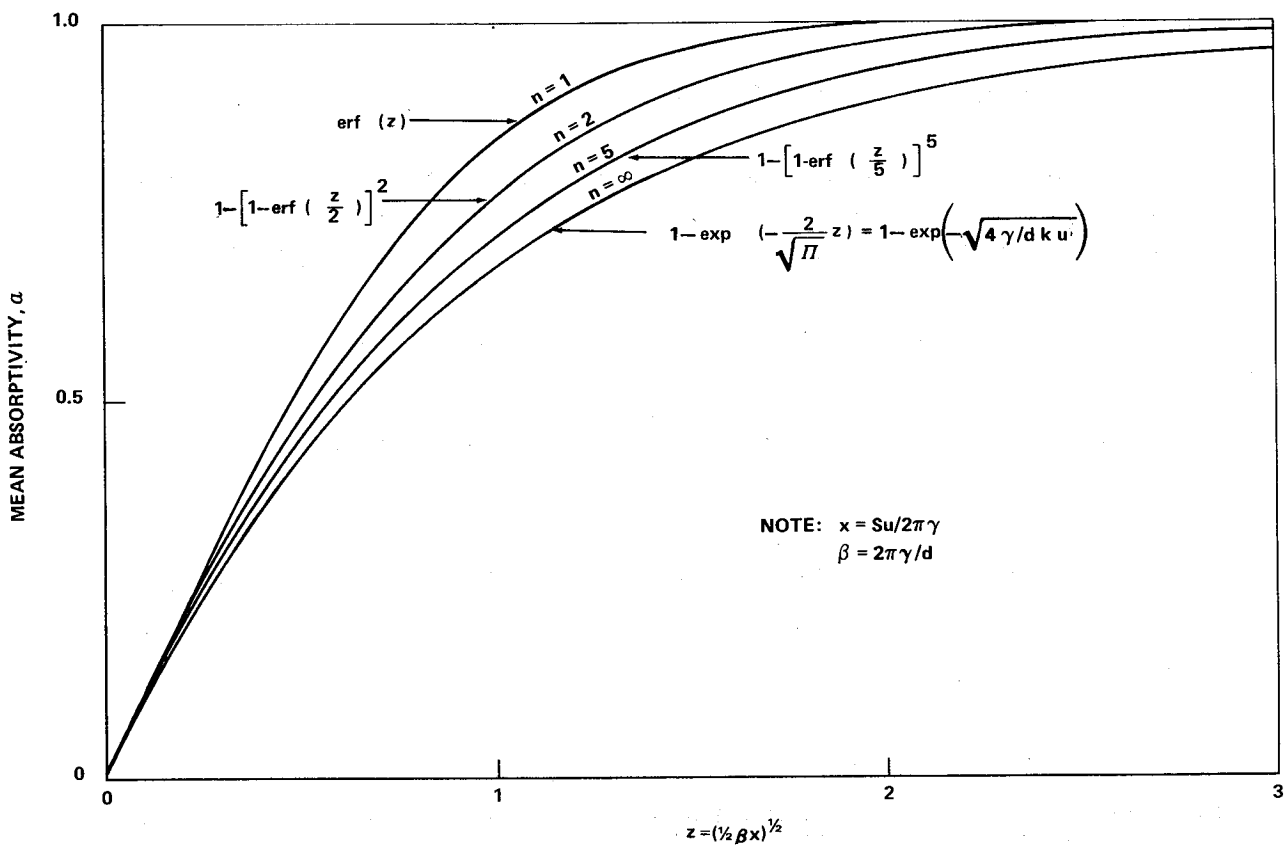


Figure 3-9. Mean absorptivity for the regular Lorentz [equation (3-A1)], random regular [equation (3-55)], and random Lorentz (Goody) [equation (3-32)] models in the square root limit showing the variations between these models.

### 3.2.4.2 Quasi-Random Model

A different approach, representing an effort to bridge the gap between the simplicity of the random band model and the extensive labor and detailed spectral information required for the precise calculation of monochromatic emissivities, is taken by the so-called "quasi-random" band model [3-18]. The quasi-random model requires explicit knowledge of the locations of the spectral lines. In this model the spectrum is divided into an arbitrary number of subintervals. The number, strengths, and widths of the lines falling in each subinterval are first tabulated. The model is developed by assuming that within each interval the lines belonging to that interval are randomly located. The curve of growth for each interval results from contributions from the lines whose centers fall in the interval and from tails of lines whose centers are located in neighboring intervals. For very broad intervals (much greater than the line equivalent widths), the model reduces to the ordinary statistical model and, for very narrow intervals (small compared to a line width), the calculation becomes equivalent to the exact monochromatic calculation.

### 3.2.5 APPROXIMATION FORMULAS

In numerical calculations of radiant heat transfer, the computation time may often be considerably reduced if simple analytic expressions for the curves of growth can be used. The following expressions can be useful:

#### a. Equally Intense, Randomly Spaced Lorentz Lines

$$\ln \tau \approx -ku/\sqrt{1 + ku/4a_C} \quad : \quad \text{within 8 percent}$$

Here  $ku$  is the mean opacity in the weak line approximation and  $a_C$  is the value of the ratio of the (intensity weighted) mean line width to the mean line spacing ( $\gamma_C/d$ ).

#### b. Superposition of Equally Intense Groups of Randomly Spaced Lorentz Lines of Geometrically Decaying Line Strength [ $k_n = (1-r)r^n k$ ]:

$$\ln \tau \approx -\frac{ku(1-r)}{\sqrt{1 + ku(1-r)/4a'_C}} - \frac{8a_C}{1-r} \left\{ \sqrt{1 + \left[ r(1-r)ku/4a'_C \right]} - 1 \right\} .$$

CHAPTER 3 – CALCULATIONAL  
TECHNIQUES FOR HOMOGENEOUS GASES

For  $r$  close to unity (slowly decaying intensities), this expression reduces to that for the intensity probability distribution function  $S^{-1} e^{-S/S_M}$ :

$$\ln \tau = \left\{ - 2a_C \left( \sqrt{1 + ku/a_C} - 1 \right) \right\} .$$

where  $a_C = 4a_C'/(1 - r)$ , and  $a_C'$  is the value of the width to spacing ratio for a single group of lines.

c. Equally Intense, Randomly Spaced Doppler Lines:

$$\ln \tau \approx - \sqrt{2/\ln 2} a_D \sqrt{\ln \left[ 1 + \frac{\ln 2}{2} (ku/a_D)^2 \right]} : \text{ within 9 percent}$$

d. Superposition of Equally Intense Groups of Randomly Spaced Doppler Lines of Geometrically Decaying Strengths:

$$\begin{aligned} \ln \tau \approx & - \sqrt{2/\ln 2} a_D' \sqrt{\ln \left\{ 1 + \frac{\ln 2}{2} \left[ ku(1-r)/a_D' \right]^2 \right\}} \\ & - \sqrt{\frac{6}{\ln 2}} \frac{a_D'}{1-r} \left\{ \ln \left[ 1 + \left( \sqrt{\frac{\ln 2}{6}} \frac{ku(1-r)}{a_D'} \right)^{2/3} \right] \right\}^{3/2} . \end{aligned}$$

where  $a_D'$  is the width to spacing ratio for a single group of lines. For  $r$  close to unity, this reduces to an approximate expression for the  $S^{-1} e^{-S/S_M}$  intensity distribution:

$$\ln \tau \approx - \sqrt{\frac{3}{2\ln 2}} a_D \left\{ \ln \left[ 1 + \left( \sqrt{\frac{2\ln 2}{3}} ku/a_D \right)^{2/3} \right] \right\}^{3/2}$$

where  $a_D = 2a_D'/(1 - r)$  .

e. Random Band Model Composed of Lines of Doppler-Lorentz Shape  
with  $P(S) = \delta(S-S_0)$  or  $P(S) = S_0^{-1} \exp(-S/S_0)$ :

$$\ln \tau = -ku (1 - y_2^{-1/2})^{1/2},$$

where

$$y_2 = \left[ 1 - \left( \frac{X_{C1}}{\bar{k}u} \right)^2 \right]^{-2} + \left[ 1 - \left( \frac{X_{D1}}{\bar{k}u} \right)^2 \right]^{-2} - 1$$

with

$$X_{C1} = ku (1 + ku/4a_C)^{-1/2}$$

and

$$X_{D1} = 1.70a_D \{ \ln [1 + (0.589 ku/a_D)^2] \}^{1/2} .$$

f. Random Band Model Composed of Lines of Doppler-Lorentz Shape  
with  $P(S) \propto S^{-1}$  (for  $S \leq S_M$ ) or  $P(S) \propto S^{-1} \exp(-S/S_M)$ :

$$\ln \tau = -ku (1 - y_3^{-1/2})^{1/2}$$

where

$$y_3 = \left[ 1 - \left( \frac{X_{C2}}{\bar{k}u} \right)^2 \right]^{-2} + \left[ 1 - \left( \frac{X_{D2}}{\bar{k}u} \right)^2 \right]^{-2} - 1$$

CHAPTER 3 – CALCULATIONAL  
TECHNIQUES FOR HOMOGENEOUS GASES

with

$$X_{C_2} = 2 a_C \left[ \left( 1 + \frac{ku}{a_C} \right)^{1/2} - 1 \right]$$

and

$$X_{D_2} = 0.937 a_D \left\{ \ln \left[ 1 + \left( 1.07 \frac{ku}{a_D} \right)^{2/3} \right] \right\}^{3/2}$$

APPENDIX 3-A

REGULAR BAND MODELS

3-A.1 COLLISION BROADENING

Closed-form expressions for the mean absorptivity are not available; however, various approximations have been developed [3-4]. The following expression, which in any event provides an upper limit for  $\alpha$ , is a good approximation for  $\beta$  small and  $x$  large<sup>1</sup>

$$\alpha \leq \operatorname{erf} \left[ \left( \frac{1}{2} \beta^2 x \right)^{1/2} \right] \quad , \quad (3-A-1)$$

where the error function is defined by

$$\operatorname{erf}(z) = 2\pi^{-1/2} \int_0^z \exp(-y^2) dy \quad . \quad (3-A-2)$$

The error function is tabulated on pages 310-311 of Reference 3-19, and various expansions are presented on pages 297-298 of the same reference. The power series expansion for  $\operatorname{erf}(z)$  is obtained by expansion of the exponential in the integral in equation (3-A-2):

$$\operatorname{erf}(z) = 2\pi^{-1/2} \sum_{n=0}^{\infty} \frac{(-1)^n z^{2n+1}}{n! (2n+1)} \quad . \quad (3-A-3)$$

This expansion is absolutely convergent for all values of  $z$  but is inconvenient for large values. A useful expansion for large  $z$  is

$$\operatorname{erf}(z) = 1 - \pi^{-1/2} z^{-1} \exp(-z^2) \left[ 1 + \sum_{m=1}^{\infty} (-1)^m \frac{1 \cdot 3 \cdot \dots \cdot (2m-1)}{(2z^2)^m} \right] \quad . \quad (3-A-4)$$

1. Recall that  $x = Su/2\pi\gamma$  ,  $\beta = 2\pi\gamma/d$  .

This expression is semiconvergent and must be handled cautiously (see Appendix 2-A).

For large values of  $\beta$ , Elsasser gives the following approximation:

$$\alpha \approx 1 - \exp [-(Su/d)\tanh \beta] \quad (3-A-5)$$

This approximation is fairly good even for values of  $\beta$  which are not large. Note that equation (3-A-5) does not provide an upper or lower limit to  $\alpha$ , but for any  $\beta$ ,

$$1 - \exp [-(Su/d)\tanh \beta] \leq 1 - \exp (-Su/d) \quad (3-A-6)$$

(the equality holding as  $\beta \rightarrow \infty$ ); and also, under any conditions,

$$\alpha \leq 1 - \exp (-Su/d) \quad (3-A-7)$$

where equality holds as  $\beta \rightarrow \infty$  or  $\beta x \rightarrow 0$ .

If the equivalent width of a single line is given by  $W$ , an upper limit to the mean absorptivity of a regular-Lorentz (Elsasser) band is given by

$$\alpha \leq W/d = (2\pi\gamma/d) f(Su/2\pi\gamma) \quad (3-A-8)$$

If the effect of overlapping is negligible (i. e., if the monochromatic absorptivity is small in the troughs between the lines), the equality in equation (3-A-8) holds.

These limiting forms are summarized in Table 3-A-1. Numerical values for the mean absorptivity of a regular-Lorentz band are tabulated in Table 3-A-2.

### 3-A-2. DOPPLER BROADENING

Approximations to the regular Doppler model are given in Table 3-A-3.

TABLE 3-A-1. APPROXIMATIONS FOR THE REGULAR-LORENTZ (ELSASSER) MODEL

Approximation providing lower limit to $\alpha$	Approximation providing no limit to $\alpha$	Approximation providing upper limits to $\alpha$
$1 - \exp [-\beta f(x)]$ ( $\beta$ small)	$1 - \exp (-\beta x \tanh \beta)$ ( $\beta$ large)	$1 - \exp (-\beta x)$ $\beta$ large or $x$ small $\operatorname{erf} \left[ \left( \frac{1}{2} \beta^2 x \right)^{1/2} \right]$ $\beta$ small and $x$ large $\beta f(x)$ $x$ small or $\beta^2 x$ small

NOTES:  $\beta = 2\pi\gamma/d$

$x = Su/2\pi\gamma$

**[ This page left blank intentionally]**



TABLE 3-A-3. APPROXIMATIONS FOR THE REGULAR DOPPLER MODEL

Approximations for $\alpha$	Accuracy
(lower limit) $\alpha = 1 - I_0\left(\frac{Su}{d} \alpha'\right) \exp\left(-\frac{Su}{d}\right)$ (large $\gamma_D/d$ )	$< 1/2\%$ for $\gamma_D/d \geq 0.27$ $< 2\%$ for $\gamma_D/d \geq 0.24$ (any $Su/d$ )
(upper limit) $\alpha = \frac{S}{k_0 d} D(k_0 u)$ (small $\gamma_D/d$ )  or 1, whichever is smaller	$< 3\%$ for $\gamma_D/d \leq 0.16$ $< 6\%$ for $\gamma_D/d \leq 0.24$ (any $Su/d$ )

NOTES:  $\alpha' = \frac{1}{2} \left[ \theta_3\left(0, e^{-\beta^2}\right) - \theta_3\left(\frac{\pi}{2}, e^{-\beta^2}\right) \right], \beta = \frac{\pi^2}{\ln 2} \left(\frac{\gamma}{d}\right)^2$

$\theta_3(x, y) =$  third Jacobi theta function  $= 1 + 2 \sum_{n=1}^{\infty} (y)^{n^2} \cos(2nx)$

$k_0 = 0.470 S/\gamma_D = k(\omega_0)$  for isolated Doppler line

APPENDIX 3-B

SELECTION OF BAND MODEL TO DESCRIBE  
EXPERIMENTAL DATA

In an ideal situation, laboratory measurements of the mean spectral absorptivity of any molecule of interest should be sufficiently extensive and accurate to determine the form of the curve of growth for all conditions (pressure, pathlength, etc.) which may be of possible future concern.

However, before such an ideal state is reached, it is frequently necessary to make use of more fragmentary experimental data. The state of available data may range from a set of very extensive and accurate measurements to a single measurement of possibly low accuracy.

As a first step in analyzing the data, the pressure and temperature ranges should be examined to determine the dominant form of line shape. For example, if the laboratory data are all at atmospheric pressure, the effect of Doppler broadening can be immediately ignored. In general, if the Lorentz half-width is greater than the Doppler half-width, the effect of Doppler broadening is negligible (less than 10 percent - see Figure 3-B-1).

As an example, for CO<sub>2</sub> at 300K, the mean Lorentz half-width is given by  $\gamma_C$  (cm<sup>-1</sup>)  $\approx$  0.06 p, where p is the pressure in atmospheres. The Doppler half-width is dependent upon the frequency, but at  $\omega = 2000$  cm<sup>-1</sup>, it is equal to [see equation (2-31)]  $\gamma_D \approx 0.002$  cm<sup>-1</sup>. Thus at 300K  $\gamma_C/\gamma_D \approx 30$  p results, indicating that Doppler broadening should not be significant at pressures above  $\sim 1/30$  atm. Note that a pressure below 1/30 atm is a necessary condition for Doppler broadening to be significant but is not sufficient since the Doppler effect is noticeable only in the transition region of the curve of growth (see Fig. 3-B-2).

At other temperatures, since  $\gamma_D \propto T^{1/2}$  and  $\gamma_C \propto T^{-1/2}$  (approximately), one finds  $\gamma_C/\gamma_D \approx 30$  p (300/T). Thus  $\gamma_C/\gamma_D \gtrsim 1$  when  $p \gtrsim (1/30) (T/300)$ ; e.g.,  $p \gtrsim 1/3$  atm for  $T = 3000$ K. Again  $p \lesssim 1/3$  atm is a necessary condition for Doppler broadening to be significant. It has been shown elsewhere [3-15] that at this temperature the overlapping of the large number of lines in the CO<sub>2</sub> spectrum is so extensive that the curve of

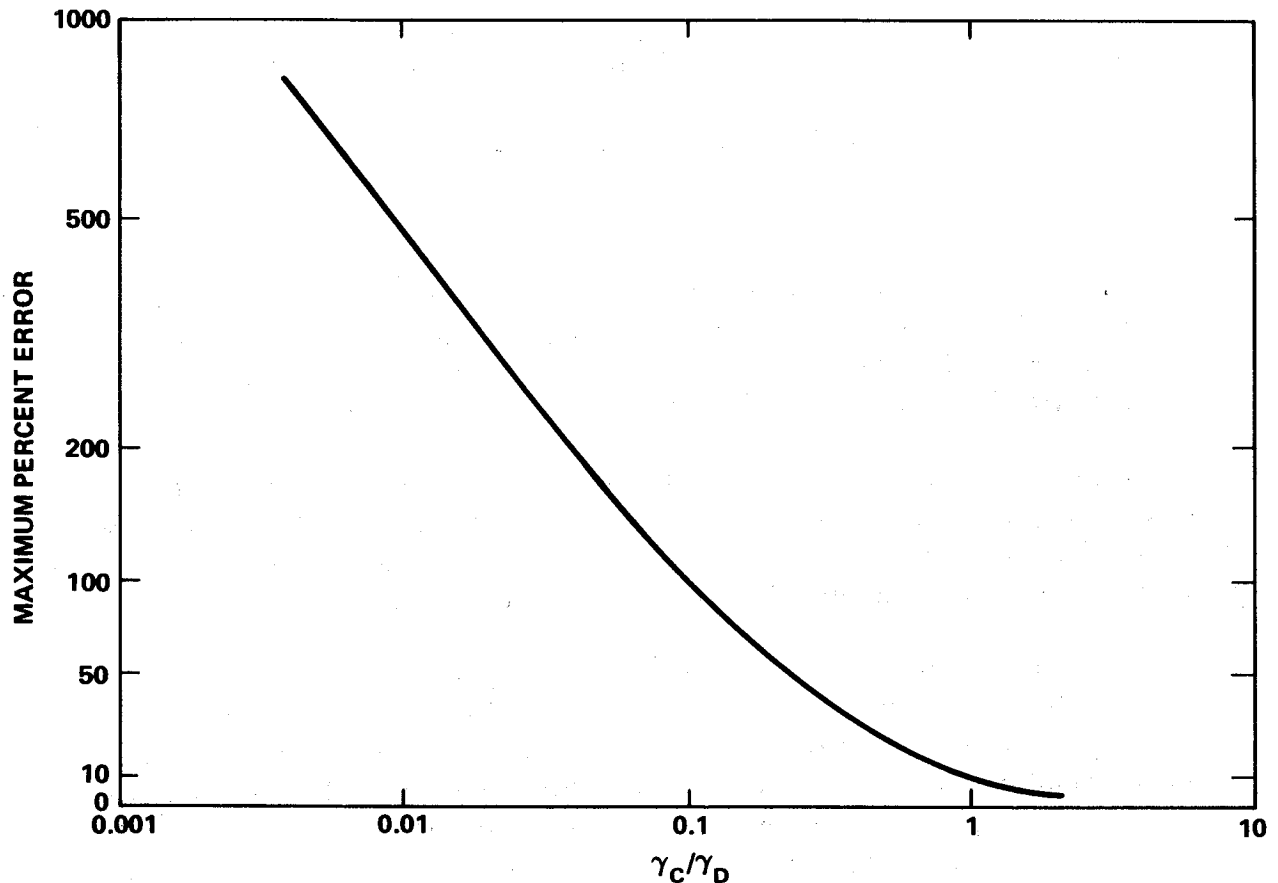


Figure 3-B-1. Maximum error in curve of growth for Doppler-Lorentz line resulting from neglect of Doppler component.

growth is virtually insensitive to any change in line shape. Thus, the absorptivity is described adequately by Beer's law in this case.

Assuming then that collision broadening is the dominating factor for the conditions of the experimental data, what is the proper choice of Lorentz band model? It will be shown in Section 3-B.3 that the form of the curve of growth of random Lorentz models is relatively insensitive to large variations in the line intensity distribution function. The question of randomness is possibly a more critical one than that of the line intensity distribution.

If the molecule is linear, the spectrum (at least at low temperatures) will show an obvious regularity of spectral lines of almost equal intensity with nearly equal spacing. In such a case, the regular or Elsasser model is the plausible choice, or, if the presence of "hot" bands is significant, the random-regular model.

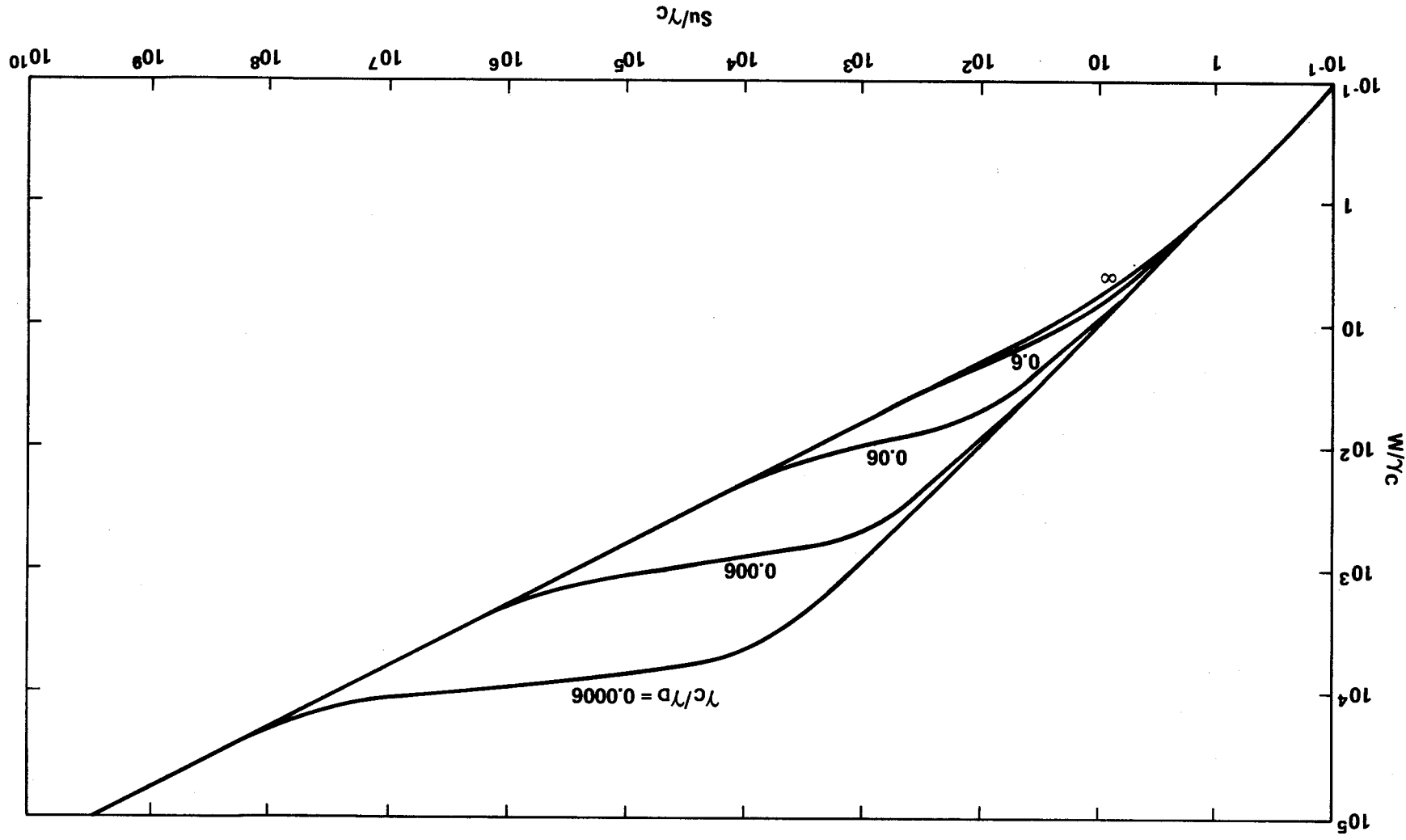


Figure 3-B-2. Curves of growth for combined Doppler-Lorentz lines.

In other cases, a totally random model may be more reasonable. To see if such a model will provide a proper fit, consider the random exponential Lorentz band model. Its curve of growth [equation (3-30)] is given by

$$\ln \tau = -ku \left(1 + \frac{ku}{4a}\right)^{-1/2}, \quad (3-B-1)$$

or

$$\ln \tau = -ku \left(1 + \frac{klc_i}{4a_0}\right)^{-1/2}, \quad (3-B-2)$$

where  $u = p_i^\ell = c_i p_T^\ell$ ,  $a = a_0 p_T$ ,  $c_i$  is the mole fraction of the absorbing species, and  $p_i$  and  $p_T$  are the partial and total pressures. A convenient transformation can be made as follows:

$$\left(-u/\ln \tau\right)^2 = k^{-2} + (4a_0k)^{-1} c_i^\ell. \quad (3-B-3)$$

Thus, if measurements are available for a spectral region described by such a band, a graph of  $(-u/\ln \tau)^2$  versus  $c_i^\ell$  will form a straight line with the intercept (at  $c_i^\ell = 0$ ) determining  $k$  and the slope determining the product  $a_0k$  (see, for example, Figures 3-B-3 and 3-B-4).

The accuracy to which these parameters are determinable depends on the accuracy and the extent of the experimental data. Clearly, if none of the data fall near the square-root region of the curve of growth, it will not come as a surprise that the graph of equation (3-B-3) may determine the intercept (i. e.,  $k$ ) with considerable accuracy but fail to determine any slope (i. e.,  $a_0$  is indeterminate).

If the points can be fit with a straight line within experimental error, this indicates that the chosen model adequately represents the experimental data. A poor fit with apparently random scatter in the data (if the data

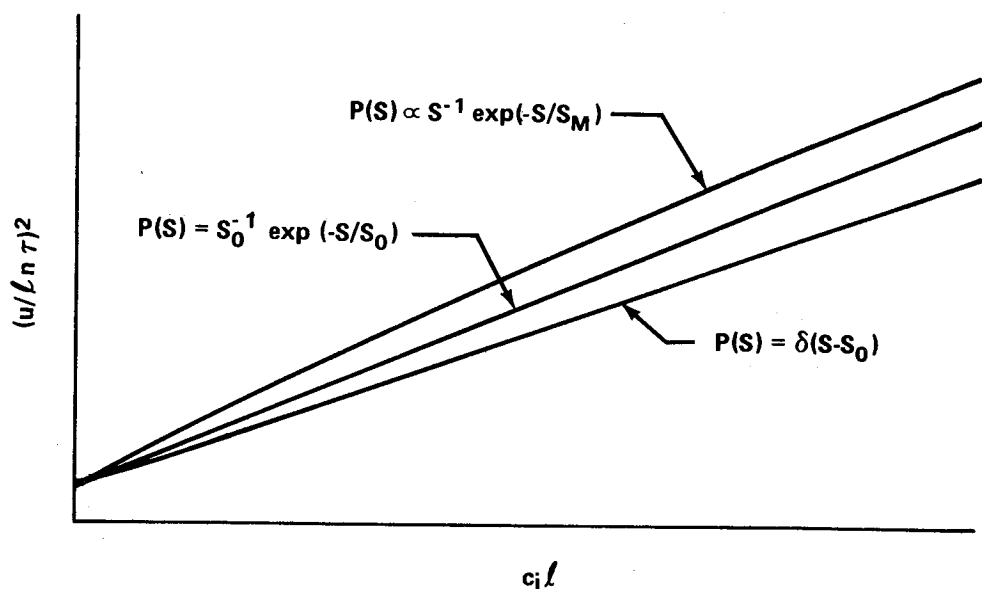


Figure 3-B-3. The function  $(u/\ln \tau)^2$  for various random Lorentz band models.

cannot be fit by any reasonably smooth curve) indicates uncertainty about the specified experimental accuracy. If the data can be fit by a smooth (but nonlinear) curve, the validity of the model is dubious. Three major assumptions should be examined: randomness of line locations, Lorentz line shape, and line intensity distribution. Consider the effect that the violation of any of these assumptions would have on the shape of the curve.

### 3-B.1. RANDOMNESS OF LINE LOCATIONS

It is this assumption which leads to the prediction of asymptotic square root behavior of the curve of growth at long pathlengths. As a consequence of this assumption, a nonzero probability is assigned to any arbitrarily small absorption coefficient. Since over any real spectral interval an actual nonzero minimum absorption coefficient exists, this assumption is necessarily violated, and a deviation from a square root to a linear behavior will appear at sufficiently long pathlengths.

Except for the case of spectra composed of widely separated lines, this deviation may appear at values of absorptivity so close to unity that experimental error in  $\ln \tau$  becomes extremely large. Conversely, a very large error in the predicted curve of growth may make only a small error in the predicted absorptivity.

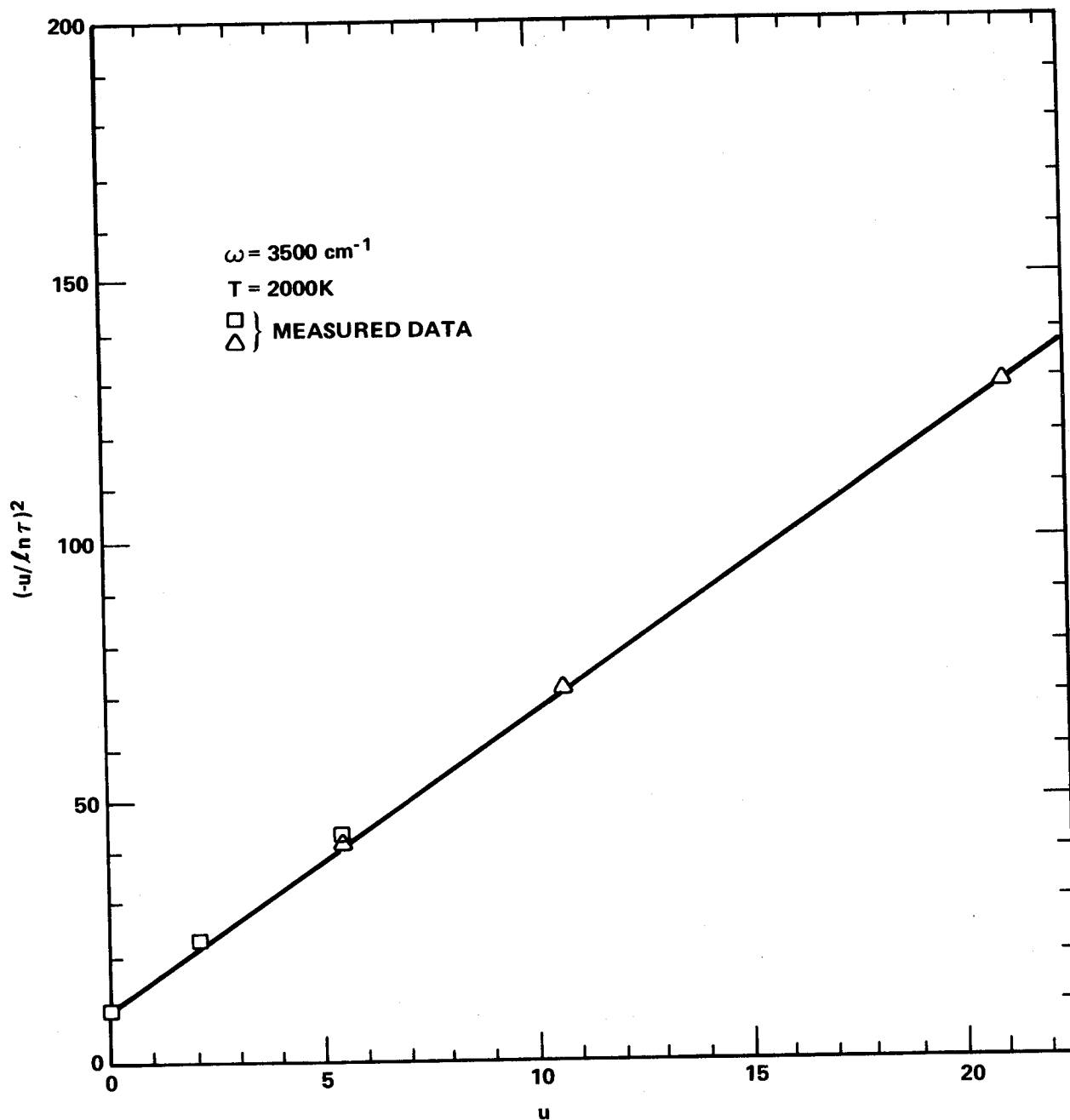


Figure 3-B-4. Example of transformed curve of growth for  $\text{H}_2\text{O}$  at 2000K for  $\omega = 3500 \text{ cm}^{-1}$  in terms of  $(-u/\ln \tau)^2$  versus  $u$ .

If the transmissivity (rather than absorptivity) is of primary concern, the situation is much more critical at long pathlengths, since what is a small relative error in the absorptivity may correspond to a large relative error in transmissivity.

3-B.2. LORENTZ LINE SHAPE

Consider separately (1) non-Lorentzian shape of pressure-broadened line wings and (2) presence of a significant Doppler component. The effect of (1) will appear in the long pathlength region. A dependence proportional to  $(\omega - \omega_0)^{-n}$  in the far wings of the line leads to an asymptotic  $(c_i \ell)^{1/n}$  behavior of the curve of growth ( $n = 2$  for a Lorentz line). A dependence such as  $(\omega - \omega_0)^{-1.8}$  as observed in the far wings of HF lines leads to a predicted asymptotic  $(c_i \ell)^{0.55}$  behavior of the curve of growth [and  $(c_i \ell)^{0.9}$  for  $(u/\ln \tau)^2$ ]. More complex line shapes are more difficult to analyze; however, the effect of the exponential-type dropoff observed in the far line wings of CO<sub>2</sub> is probably more than overshadowed by the effect of nonrandomness described in paragraph 3-B.1.

The effect, (2), of a significant Doppler component appears in the intermediate (transition) region of the curve of growth. Its effect on the function  $(-u/\ln \tau)^2$  is to lower the curve in the small  $c_i \ell$  region but to leave the intercept (at  $c_i \ell = 0$ ) and the linear portion at large  $c_i \ell$  values unchanged, (see Figure 3-B-5). An upper limit to the effect of Doppler broadening on the curve of growth may be obtained from Figure 3-B-1.

3-B.3 LINE STRENGTH DISTRIBUTION

The exponential line strength distribution function has been selected on a quite arbitrary basis, largely because of the simplicity of the mathematical form of the resulting curve of growth. It has been remarked previously that the curve of growth is not particularly sensitive to wide variations in the line strength distribution function. Consider the corresponding effect on the function  $(-u/\ln \tau)^2$ .

At one extreme is certainly the delta-function distribution  $P(S) = \delta(S - S_0)$ , which assigns identical strengths to all lines. The curve of growth is given by the Ladenburg-Reiche function:

$$-\ln \tau = 2\pi a f\left(\frac{ku}{2\pi a}\right) \quad , \quad (3-B-4)$$

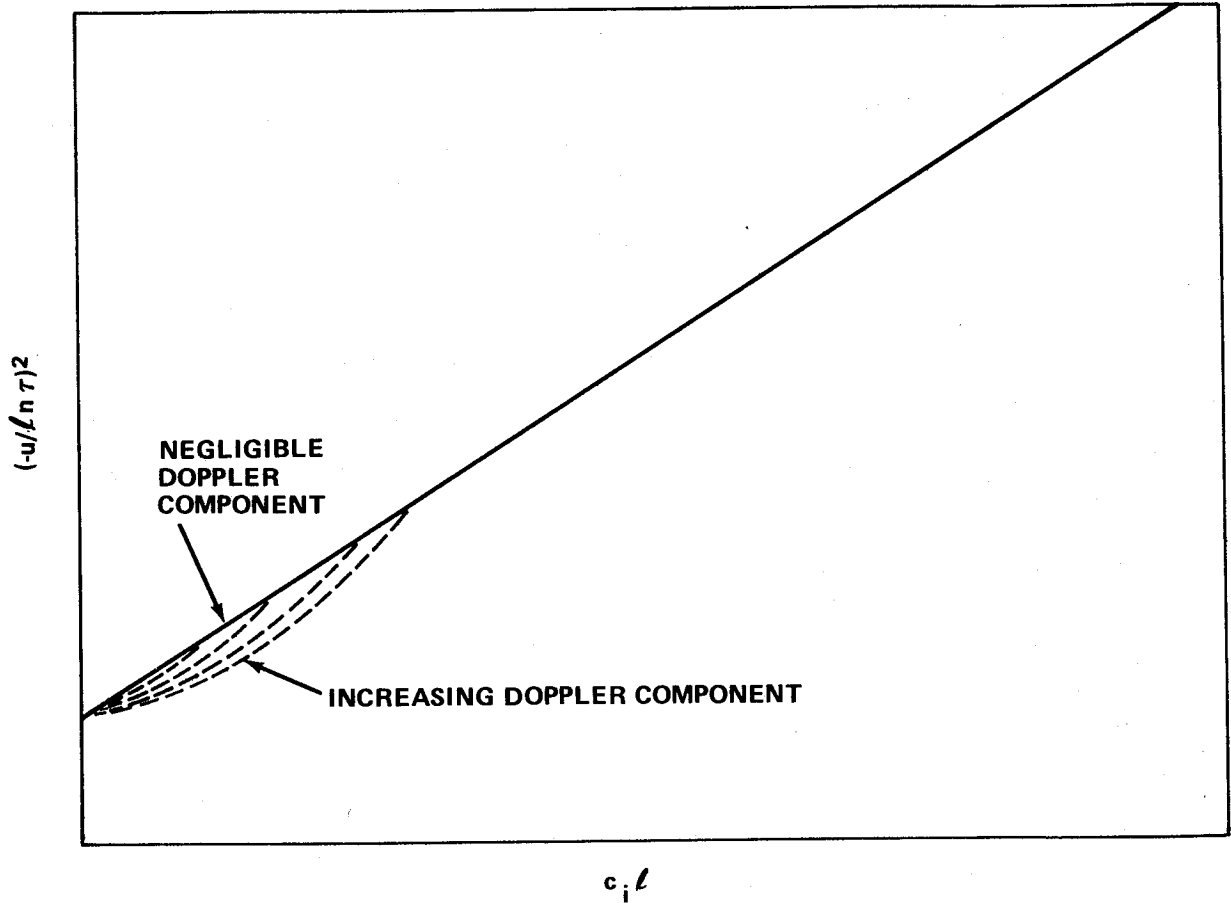


Figure 3-B-5. Qualitative effect of Doppler component on the function  $(-u/\ln \tau)^2$ . For  $\gamma_C/\gamma_D \approx 1$ , the maximum lowering of the curve is  $\approx 20$  percent.

where

$$f(x) = x \exp(-x) [I_0(x) + I_1(x)]$$

$$a = \gamma/d = (\gamma_0/d) p_T ,$$

and

$$x = ku/2\pi a = kc_i l / 2\pi a_0 .$$

For this curve of growth, direct evaluation yields

$$(-u/\ln \tau)^2 = k^{-2} \exp(2x) [I_0(x) + I_1(x)]^{-2} \quad (3-B-5)$$

This function is slightly concave upward (see Figure 3-B-3). It is asymptotic to the straight line

$$(\pi/8) k^{-2} + (4 a_0 k)^{-1} c_i \ell \quad (3-B-6)$$

Thus, if only the asymptotic (large  $c_i \ell$ ) region is plotted, the slope will give the correct value of the product  $a_0 k$ . The intercept gives  $(\pi/8)k^{-2}$  rather than  $k^{-2}$ , so the deduced "k" is  $(8/\pi)^{1/2} k = 1.60 k$ , i.e., a value of  $k$  which is 60 percent higher than the correct value. On the other hand, the curve at  $c_i \ell = 0$  is tangent to the straight line

$$k^{-2} + (2\pi a_0 k)^{-1} c_i \ell \quad (3-B-7)$$

Thus, if only data at small  $c_i \ell$  are used, the correct value of  $k$  is obtained from the intercept, but the deduced "a<sub>0</sub>" is  $(\pi/2)a_0 = 1.57 a_0$ , i.e., a value of  $a_0$  57 percent higher than the correct value.

These two cases represent the worst possible extremes. If the data are in the transition region, say around  $x = 1$ , where the tangent to the curve is given by

$$0.84 k^{-2} + (4.62 a_0 k)^{-1} c_i \ell \quad (3-B-8)$$

the deduced "k" is  $k/\sqrt{0.84}$ , i.e., only 8 percent too high. The deduced "a<sub>0</sub>k" is  $(4.62/4)a_0 k$ , i.e., 15 percent too high, so that the deduced "a<sub>0</sub>" is 7 percent too high. Thus a fit to the random exponential band model in this region will lead to errors in the curve of growth of no more than 8 percent on extrapolation all the way into the linear or square root regions.

As the second case of a different line intensity distribution, consider the function  $P(S) \propto S^{-1} \exp(-S/S_0)$ . As previously discussed, this is an extremely broad distribution of line intensities, probably realistic at quite high temperatures. For the exponential-tailed  $1/S$  distribution, one has [equation (3-35)]

$$\ln \tau = -2a \left[ (1 + ku/a)^{1/2} - 1 \right] \quad , \quad (3-B-9)$$

or

$$(-u/\ln \tau)^2 = \left\{ 8a_0^2 \left[ 1 + \frac{1}{2} \frac{kc_i \ell}{a_0} - \left( 1 + \frac{kc_i \ell}{a_0} \right)^{1/2} \right] \right\}^{-1} \ell^2 \quad , \quad (3-B-10)$$

(see Figure 3-B-3). This curve is tangent, at  $c_i \ell = 0$ , to the line

$$k^{-2} + (2 a_0 k)^{-1} c_i \ell \quad .$$

Thus data near  $c_i \ell = 0$  determine the correct value of  $k$ , but the deduced value of "a<sub>0</sub>" is  $\frac{1}{2} a_0$ , 50 percent too low. The predicted curve of growth in the square root region [dependent on  $(a_0 k)^{1/2}$ ] will be 29 percent too low.

The curve only slowly approaches a straight line at large values of  $c_i \ell$ . However, consider an intermediate portion of the curve, say around  $kl/a_0 = 8$ , at which point the curve is tangent to the line

$$\frac{4}{3} k^{-2} + (3 a_0 k)^{-1} c_i \ell \quad .$$

Reliance on data in this region would produce an indicated value of "k,"  $\sqrt{3/4} k$ , or 13 percent too low. Similarly, the indicated value of "a<sub>0</sub>k" is  $(3/4) a_0 k$ , so that "a<sub>0</sub>" is also 13 percent too low. Therefore, extrapolations of the curve of growth to the linear or square root regions would involve errors of not more than 13 percent.

**CHAPTER 3 – CALCULATIONAL  
TECHNIQUES FOR HOMOGENEOUS GASES**

Without very extensive and accurate measurements extending into both regions of the curve of growth, it would probably be quite difficult to discriminate between the various line intensity distributions. If measurements are available in the transition region of the curve of growth, band model parameters can be obtained which will probably represent the curve of growth with sufficient accuracy for many purposes. In any event, it must be recognized that measurements restricted to either of the linear or square root regions cannot accurately determine the parameter describing the other regions.

APPENDIX 3-C

CRITERIA FOR ACCURACY OF MEASUREMENT OF LINE  
STRENGTHS AND MEAN ABSORPTION COEFFICIENTS

In this appendix, the errors involved in deducing the value of mean absorption coefficients and individual line intensities from real spectral data measured for finite gas samples and recorded with instruments having finite spectral resolving power are discussed. All spectrometric instruments will distort the shape of a spectrum to some extent. To a good approximation, the response of a spectrometer to a spectral input of the form  $I(\omega)$  can usually be represented in terms of the spectrometer slit function  $g(\omega - \omega')$ , such that the signal recorded has the form  $I_s(\omega)$ :

$$I_s(\omega') = \int_0^{\infty} I(\omega)g(\omega' - \omega)d\omega \quad (3-C-1)$$

where  $\omega'$  is the value of the wavenumber setting on the instrument wavenumber scale. Thus, the spectrometer tends to smear out or average the fine scale spectral features of  $I(\omega)$  over wavenumber intervals determined by the spectral width of the slit function  $g(\omega' - \omega)$ . This slit function distortion usually makes it very difficult to obtain accurate determination of the profile of an individual spectral line unless instruments having very high spectral resolving powers are used. However, because the slit function can usually be represented to a good approximation as a function of the difference between the actual wavenumber  $\omega$  and the instrumental setting  $\omega'$ , the area under the recorded line profile is equal to the area under the actual profile even when the slit function width exceeds the characteristic line width:

$$\int_0^{\infty} I_s(\omega')d\omega = \int_0^{\infty} I(\omega)d\omega \quad (3-C-2)$$

Thus, accurate values for equivalent line widths can be obtained using instruments of moderate resolving power and it is usually this quantity ( $W$ ) that is available from experiments.

In a transparent gas, the equivalent width is directly proportional to the line intensity. However, since all experimental measurements require gas samples having finite depths, the deduction of the line strength from experimental data requires some knowledge of the effects of self-absorption. Criteria for the accuracy of the determination of line strength from measurements of equivalent widths have been explicitly presented by Plass [3-8] for lines of Doppler or Lorentz shape. For lines of different or undetermined shape (such as a Q-branch in which the individual lines are completely overlapped), similar criteria would be desirable. In the related problem of a spectrum in which lines are overlapped but the true absorption coefficient fluctuates about a mean value, a criterion for the accuracy of determination of this mean value from a measurement of mean absorptivity would also be desirable.

First, consider a single isolated spectral line of arbitrary shape defined by an absorption coefficient  $k(\omega)$ , and use the customary definitions:

Line Strength:

$$S = \int k(\omega) d\omega \quad , \quad (3-C-3)$$

Equivalent Width:

$$W = \int \{1 - \exp[-k(\omega)u]\} d\omega \quad , \quad (3-C-4)$$

where  $u$  is the optical path in units inverse to those of  $k(\omega)$ , and the integrals, for an isolated line are taken from  $-\infty$  to  $+\infty$ . The integrand in equation (3-C-4) is the (monochromatic) absorptivity  $\alpha(\omega)$ , and the usefulness of equation (3-C-4) (hence, that at the curve-of-growth concept) lies in the well-known fact [3-21] that

$$W = \int \alpha(\omega) d\omega = \int \alpha^*(\omega) d\omega \quad (3-C-5)$$

is an invariant, where  $\alpha^*(\omega)$  is the absorptivity indicated by a spectrometer of imperfect, and possibly undetermined, resolution. Another experimentally determinable quantity is defined:

$$S^* = u^{-1} \int \ln [1 - \alpha^*(\omega)]^{-1} d\omega \quad . \quad (3-C-6)$$

The quantity  $S^*$  is dependent on the resolution of the particular spectrometer, but the inequality

$$W/u \leq S^* \leq S \quad (3-C-7)$$

is always valid. The quantity  $S^*$  approaches its upper (lower) limit as the instrumental resolving power increases (decreases).

The fractional error in approximating  $S$  by  $S^*$  is given by  $e^*$ :

$$e^* = (S - S^*)/S \leq (S - W/u)/S = e_0 \quad . \quad (3-C-8)$$

For a Lorentz line [using the inequality  $f(x) \geq x - \frac{1}{2} x^2$  for the Ladenburg-Reiche function], Plass [3-8] obtained (rewriting in terms of the maximum absorption coefficient)

$$(S - W/u)/S \leq \frac{1}{4} k_{\max} u \quad , \quad (3-C-9)$$

that is,

$$e_0 \leq q\% \quad \text{if} \quad k_{\max} u \leq 0.04 q \quad . \quad (3-C-10)$$

A similar criterion has been developed for the Doppler shape [3-8]. This criterion is listed in Table 3-C-1, along with criteria for lines of other shapes, viz., rectangular, triangular, and exponential shapes (the latter has been shown to provide a good approximation for the shape of the Q-branches of certain molecules [3-22]).

CHAPTER 3 – CALCULATIONAL  
TECHNIQUES FOR HOMOGENEOUS GASES

All the criteria are similar, and the coefficient of  $q$  increases slightly as the line becomes more sharply peaked. The rectangular line shape certainly provides an upper limit for a line of any shape whatsoever; however, the criterion for a Doppler line should be sufficiently conservative to apply to any real line of unknown shape.

Next, consider a spectrum defined by an absorption coefficient which fluctuates with period  $\delta\omega$  about an average value  $\bar{k}$ :

$$k(\omega) = \bar{k} [1 + f(\omega)] \quad , \quad (3-C-11)$$

where  $\int_{\delta\omega} f(\omega) d\omega = 0$ . Mean absorptivity is defined as:

$$\bar{\alpha} = (\delta\omega)^{-1} \int_{\delta\omega} \{ 1 - \exp [-k(\omega)u] \} d\omega \quad . \quad (3-C-12)$$

If the average value of the absorptivity measured by an instrument of finite resolving power is taken, it is found to be  $\bar{\alpha}$ , independent of the instrumental resolution; hence  $\bar{\alpha}$  is a convenient observable. Next, define

$$k^* = u^{-1}(\delta\omega)^{-1} \int_{\delta\omega} \ln [1 - \alpha^*(\omega)]^{-1} d\omega \quad , \quad (3-C-13)$$

where  $\alpha^*(\omega)$  is the indicated absorptivity as measured by the spectrometer ( $\alpha^*$  is dependent on the resolving power). Also, define

$$k_0 = u^{-1} \ln [1 - \bar{\alpha}]^{-1} \quad . \quad (3-C-14)$$

One finds that the inequality

$$k_0 \leq k^* \leq \bar{k} \quad (3-C-15)$$

is valid, where  $k^*$  approaches the upper (lower) limit as the instrumental resolving power increases (decreases).

The fractional error in approximating  $\bar{k}$  by  $k^*$  is given by  $e^*$ :

$$e^* = (\bar{k} - k^*)/\bar{k} \leq (\bar{k} - k_0)/\bar{k} = e_0 \quad (3-C-16)$$

If the spectrum is composed of lines which overlap considerably, so that the fluctuation from the average is not large, a good approximation may be provided by a sinusoidal curve:

$$k(\omega) = \bar{k} (1 + b \sin \omega) \quad , \quad (|b| < 1) \quad (3-C-17)$$

In this case, the integration in equation (3-C-10) can be performed yielding the result [3-23]

$$\bar{\alpha} = 1 - \exp(-\bar{k}u) I_0(b\bar{k}u) \quad , \quad (3-C-18)$$

where  $I_0$  is a modified Bessel function. Thus, one finds

$$(\bar{k} - k_0)/\bar{k} = \ln I_0(b\bar{k}u)/\bar{k}u \quad (3-C-19)$$

Using the inequality  $\ln I_0(y) \leq \frac{1}{4}y^2$ , one finds

$$e_0 \leq \frac{1}{4} b^2 \bar{k}u \quad , \quad (3-C-20)$$

that is,

$$e_0 \leq q\% \quad \text{if} \quad \bar{k}u \leq 0.04 b^{-2} q \quad (3-C-21)$$

CHAPTER 3 - CALCULATIONAL  
TECHNIQUES FOR HOMOGENEOUS GASES

For example, for a  $\pm 50$  percent fluctuation in  $k(\omega)$ , one has  $e_0 \leq 10$  percent if  $\bar{k}u \leq 1.6$  (or, in terms of the measured quantities,  $e_0 \leq 10$  percent if either  $k_0u$  or  $k^*u \leq 1.44$ ).

If one considers square wave forms, saw-tooth forms [in each case  $k_{\max} = \bar{k}(1+b)$ ,  $k_{\min} = \bar{k}(1-b)$ ,  $0 \leq b \leq 1$ ], and unsymmetric rectangular wave forms [in which  $k_{\max} = \bar{k}(1+b)$ ,  $k_{\min} = \bar{k}(1-b')$  where  $b \geq 0$ ,  $0 \leq b' \leq 1$ ], one obtains the criteria listed in Table 3-C-2.

These expansions are, of course, useful only if it is possible to estimate in some manner the maximum variations of the monochromatic absorption coefficient from its mean value [3-23]. However, if this is possible, a suitable model can then be chosen to give an upper limit on the error (e.g., the rectangular wave form can always be used to provide a conservative upper limit).

TABLE 3-C-1. MAXIMUM ERROR IN DETERMINING LINE INTENSITY  
WITH INSTRUMENT OF FINITE RESOLVING POWER [3-8, 3-23]

Line Shape	$e_0 \leq q\%$ if $k_{\max} u \leq$
Rectangular	0.02 q
Doppler <sup>a</sup>	0.028 q
Triangular <sup>b</sup>	0.03 q
Exponential <sup>b</sup>	0.04 q
Lorentz	0.04 q

a. Factor  $0.028 = 2(2)^{1/2}/100$ .

b. May be one- or two-sided; not necessarily symmetrical.

TABLE 3-C-2. MAXIMUM ERROR IN DETERMINING MEAN ABSORPTION  
COEFFICIENT WITH INSTRUMENT OF FINITE RESOLVING POWER [3-23]

Form <sup>a</sup> of $k(\omega)$	$e_0 \leq q\%$ if $\bar{k}u \leq$
Square Wave	$0.02 q b^{-2}$
Rectangular (unsymmetric) Wave	$0.02 q (bb')^{-1}$
Sinusoidal	$0.04 q b^{-2}$
Sawtooth <sup>b</sup>	$0.06 q b^{-2}$

a. See text for definitions of  $b, b'$ .

b. Not necessarily symmetrical.

REFERENCES

- 3-1. Penner, S.S.: Quantitative Molecular Spectroscopy and Gas Emissivities. Addison-Wesley Publishing Co., Inc., Reading, Mass., 1959, p. 266.
- 3-2. Burch, D.E.; Gryvnak, D.; France, W.L.; and Williams, D.: Infrared Absorption by Carbon Dioxide, Water Vapor, and Minor Atmospheric Constituents. AFCRL-62-698, July 1962.
- 3-3. Tien, C.L.: Advances in Heat Transfer, no. 5, 1968, p. 253.
- 3-4. Elsasser, W.M.: Phys. Rev., no. 54, 1938, p. 126.
- 3-5. Golden, S.A.: J. Quant. Spectry. Radiative Transfer, no. 7, 1967, p. 483.
- 3-6. Golden, S.A.: J. Quant. Spectry. Radiative Transfer, no. 8, 1968, p. 877.
- 3-7. Golden, S.A.: J. Quant. Spectry. Radiative Transfer, no. 9, 1969, p. 1067.
- 3-8. Plass, G.N.: J. Opt. Soc. Am., no. 48, 1958, p. 690.
- 3-9. Plass, G.N.: J. Opt. Soc. Am., no. 50, 1960, p. 868.
- 3-10. Goody, R.M.: Quant. J. Roy. Meteor. Soc., no. 78, 1952, p. 165.
- 3-11. Gates, D.M.; Calfee, R.F.; Hansen, D.W.; and Benedict, W.S.: Line Parameters and Computed Spectra for Water Vapor Bands at  $2.7\mu$ . NBS Monograph 71, 1964.
- 3-12. Benedict, W.S. and Calfee, R.F.: Line Parameters for the 1.9 and 6.3 Micron Water Vapor Bands. ESSA Professional Paper 2, 1967.
- 3-13. Malkmus, W.: J. Opt. Soc. Am., no. 57, 1967, p. 323.
- 3-14. Kaplan, L.D. and Eggers, D.F.: J. Chem. Phys., no. 25, 1956, p. 879.

REFERENCES (Concluded)

- 3-15. Oppenheim, U.P. and Ben-Aryeh, Y.: J. Opt. Soc. Am., no. 53, 1963, p. 344.
- 3-16. Malkmus, W.: J. Opt. Soc. Am., no. 53, 1963, p. 951.
- 3-17. Malkmus, W.: J. Opt. Soc. Am., no. 58, 1968, p. 1214.
- 3-18. Wyatt, P.J.; Stull, V.R.; and Plass, G.N.: J. Opt. Soc. Am., no. 52, 1962, p. 1209.
- 3-19. Abramowitz, M. and Stegun, I.A.: Handbook of Mathematical Functions with Formulas, Graphs, and Mathematical Tables. NBS Applied Mathematics Series 55, 1964.
- 3-20. Zachor, A.S.: J. Quant. Spectry. Radiative Transfer, no. 7, 1967, p. 857.
- 3-21. Babrov, H.J.: J. Opt. Soc. Am., no. 51, 1961, p. 171.
- 3-22. Ludwig, C.B.; Ferriso, C.C.; and Acton, L.: J. Opt. Soc. Am., no. 56, 1966, p. 1685.
- 3-23. Malkmus, W.: Applied Optics, no. 6, 1967, p. 349.



CHAPTER 4

CALCULATIONAL TECHNIQUES FOR INHOMOGENEOUS GASES

A physical situation in which pressure, temperature, and species concentration vary spatially provides a far more complex computational problem than one in which these parameters are constant. Unfortunately, the constant-parameter situation is usually encountered only under elaborate laboratory conditions, so procedures for calculating radiation from inhomogeneous bodies are essential.

Conceptually, the calculation can be performed directly by multiple integration of the equation of radiative transfer over space and frequency. In practice, sufficiently detailed spectral information is generally not known; even if it were known (or assumed) the computing time and cost might well be prohibitive when the spectrum exhibits considerable fine scale structure.

Hence, a strong need for approximate calculational techniques which can provide results of acceptable accuracy. Such techniques and rough tests of their accuracy are presented in this section.

## 4.1 EXACT CALCULATIONS

### 4.1.1 GENERAL CONSIDERATIONS

In principle, exact radiance calculations may be made for any gas in thermodynamic equilibrium and whose optical properties are known. When the distributions of pressure, temperature, and concentration are given explicitly as functions of the path distance  $u$ , the equation of transfer reads:

$$N_{\omega}(\omega, u) = \int_{-\infty}^u N_{\omega}^0(\omega, u') \frac{\partial}{\partial u'} \tau(\omega, u', u) du' \quad (4-1)$$

Precise calculations of this expression are frequently not feasible in engineering applications since the amount of computer time required to evaluate equation (4-1) over the entire spectral region of interest is quite often prohibitive.

In certain special cases, the evaluation of equation (4-1) may be greatly simplified, e. g., if the absorption coefficient is approximately constant over a large spectral interval or if the gas is optically thin (i. e., the absorptivity is  $\ll 1$  at all frequencies). These cases were discussed in Chapter 3.

Quite frequently, however, it is necessary to resort to the use of additional approximations to make equation (4-1) manageable. The methods discussed in this chapter may be categorized under the general heading of N-parameter techniques and involve approximations which allow the spatial integrations and frequency integrations to be carried out separately.

### 4.1.2 THE N-PARAMETER APPROXIMATION METHODS

The basic difficulty in the numerical evaluation of radiant heat transfer according to equation (4-1) is associated with the fact that, for each line of sight, the radiance must be computed at a large number of frequencies, each frequency involving an integration along the line of sight. After performing these spatial integrations, the radiance must then be integrated over frequency to obtain the total heat transfer. To reduce this computational problem to one of manageable proportions, an approximation procedure is often introduced to separate the spatial and frequency integrations.

Here it is assumed that the spectral transmissivity integrated or averaged over a small set of relatively broad spectral intervals ( $\Delta\omega$ ) can be approximated by the form:

$$\bar{\tau}_{\omega} \left( = \frac{1}{\Delta\omega} \int_{\Delta\omega} \tau_{\omega} d\omega \right) = f(s_1, s_2, s_3 \dots s_n) \quad , \quad (4-2)$$

where the parameters  $s_1, \dots, s_n$  are various integrals or moments of the gas properties over the line of sight. The functional form  $f(s_1, \dots, s_n)$  is generally chosen so that the expression for the mean transmissivity  $\bar{\tau}_{\omega}$  when calculated for a homogeneous volume agrees with one of the band model prescriptions described in Chapter 3.

Most applications of these multiple parameter methods have been restricted to one or two parameters ( $N \leq 2$ ). The most commonly used is a two-parameter method commonly called the Curtis-Godson approximation. This is described in the following section.

4.2 THE CURTIS-GODSON APPROXIMATION FOR BAND MODELS

For a homogeneous gas, a useful approximation for the mean transmissivity for the statistical Lorentz line band model was given in Section 3.2.5 (a):

$$\tau = \exp \left( -ku / \sqrt{1 + \frac{ku}{4a}} \right) \quad , \quad (4-3)$$

where  $a$  is the line width to line spacing ratio.

To obtain a two-parameter representation for the mean transmissivity of a nonhomogeneous volume, it is required that  $\tau$  be expressed in the form

$$\tau = f(s_1, s_2) \quad (4-4)$$

where  $s_1$  and  $s_2$  are integrals of the gas properties over the line of sight. It is also required that  $f(s_1, s_2)$  reduce to equation (4-3) for the special case of a homogeneous gas and that it yield an accurate representation of the mean transmissivity in the limiting case of very thin and very thick gas volumes.

For an inhomogeneous gas in the weak line limit  $\left( \int_0^u k \, du \ll 1 \right)$ ,

the mean transmission is given by

$$\tau \approx \exp \left( - \int_0^u k \, du \right) \quad (4-5)$$

and in the collisional strong line limit  $\left[ \int_0^u (k/4a) \, du \gg 1 \right]$  by

$$\tau \approx \exp \left( - \sqrt{4 \int_0^u ka \, du} \right) \quad . \quad (4-6)$$

The requirement that a two-parameter model reduce to these exact forms in the appropriate limits and that it reduce to the exact expression for the case of a homogeneous gas essentially specifies  $s_1, s_2$  and the functional form of  $f(s_1, s_2)$  :

$$s_1 \sim \int_0^u k \, du \quad , \quad (4-7)$$

$$s_2 \sim \int_0^u ka \, du \quad , \quad (4-8)$$

and

$$f(s_1, s_2) = \exp \left( - \frac{s_1}{\sqrt{1 + s_1^2/4s_2}} \right) \quad . \quad (4-9)$$

This representation is known as the Curtis-Godson approximation for inhomogeneous gases and is exact in the limiting cases when all lines are in the weak line regime or all lines are in the strong line regime. In other regimes, the approximation introduces an error.

This model is useful when the temperature variation across the slab is moderate. When large variations in temperature exist along the line of sight and the relative strength of different spectral lines within the spectral band of interest change drastically with spatial position, the requirement that the approximation reduce to the exact expression in the weak line and strong line limits may not be strict enough to yield accurate results in the intermediate regime. This will commonly be the case when there are large differences in individual line strengths within the spectral band. Polyatomic molecules such as H<sub>2</sub>O and CO<sub>2</sub> typically exhibit such characteristics at moderately high temperatures.

To improve the accuracy of calculation for those molecules, a more detailed model in which the spectral lines are divided into groups so that all lines in a particular group will have similar strengths and temperature dependencies may be necessary. The reasonable assumption is also made that line locations in one group are uncorrelated with those in the others. The Curtis-Godson approximation is then applied to each line group in turn, and the net transmission is taken to be the product of the transmissions calculated for each of the line groups.

This grouping is best done on the basis of the value of the energy of the lower state of the transition so that all the lines belonging to one group have a similar dependence on temperature. With these approximations, the mean transmission may be determined from the relation

$$-\ln [\tau(\omega, s)] = \sum_n \left( \frac{W_n}{d_n} \right) \quad , \quad (4-10)$$

where the summed term is the ratio of the equivalent width to mean line spacing for the  $n$ th group. In general it will be found that, when the lines are divided into a relatively small number of groups, the temperature dependence of all the lines will not be exactly the same and the effective spectral density of lines of one group will vary somewhat with temperature (and thus with position).

Using the Curtis-Godson approximation<sup>1</sup> for each line group separately, one may express the value of  $(W/d)_n$  for the inhomogeneous path in terms of the curve of growth for equivalent homogeneous paths:

$$\frac{W}{d}_n = F\left(X_n^*, \bar{a}_{C,n}, \bar{a}_{D,n}\right) \quad , \quad (4-11)$$

where  $X_n^*$  is the optical depth for the  $n$ th group in the just-overlapping line approximation:

$$X_n^* = \int_0^S k_n ds \quad , \quad (4-12)$$

and  $\bar{a}_{C,n}$  and  $\bar{a}_{D,n}$  are mean values for the fine structure parameters:

$$\bar{a}_{C,n} = \frac{1}{X_n^*} \int_0^S \frac{\gamma_{C,n}}{d_n} k_n ds \quad , \quad (4-13)$$

$$\bar{a}_{D,n} = \frac{1}{X_n^*} \int_0^S \frac{\gamma_D}{d_n} k_n ds \quad . \quad (4-14)$$

Here  $\gamma_{C,n}$  and  $\gamma_D$  are values for the collision-broadened and Doppler-broadened half-widths, respectively, and  $d_n$  is the mean line spacing for the  $n$ th group.

---

1. In the radiant transfer literature, the Curtis-Godson approximation is usually developed for isolated spectral lines and involves approximations for average values of individual line strengths and line widths. The development in this text differs from the usual treatment in that it is applied to groups of lines and expresses the results in terms of average values for the ratios of line strength to line spacing ( $S/d = k$ ) and line width to line spacing ( $\gamma/d = a$ ).

When the line groups are to be chosen on the basis of their having similar temperature dependencies, it is often convenient to divide the energy scale into equal increments  $\Delta E$  and represent the mean absorption coefficients for each group in the form:

$$k_n = \bar{k}(\omega, T) f_n e^{-n\Delta E/kT} / \left( \sum_{n=0}^{\infty} f_n e^{-n\Delta E/kT} \right), \quad (4-15)$$

and the line density from

$$\frac{1}{d_n} = g_n / d_0(\omega, T) \quad (4-16)$$

Here  $\bar{k}(\omega, T)$  is the mean absorption coefficient in the interval

$$\Delta\omega \left[ \bar{k}(\omega, T) = \sum_i S_i / \Delta\omega \right], \text{ where the summation extends over all lines in}$$

the interval  $\Delta\omega$ ],  $f_n$  and  $g_n$  are only weakly dependent on temperature and can usually be taken to be constants, and  $\Delta E$  is the line grouping parameter. When the energy spacing  $\Delta E$  and the parameters  $f_n$  and  $g_n$  are carefully chosen, the parameter  $d_0(\omega, T)$  will show only a weak dependence on temperature and often can be approximated by a constant. However, in general, it is better to select  $\Delta E$ ,  $f_n$ , and  $g_n$  on the basis of the known spectral properties of the molecules in question and then to derive the value of  $d_0(\omega, T)$  [and of  $\bar{k}(\omega, T)$ ] by fitting detailed theoretical calculations or measurements of the weak and strong line limits.

For approximate calculations, a considerable savings in computation time can be achieved by utilizing simple analytic representations of the appropriate curves of growth  $F(X^*, \bar{a}_C, \bar{a}_D)$ . Some useful formulas are tabulated in Section 3.2.4.

### 4.3                    SENSITIVITY ANALYSIS

In many cases, particularly for water vapor, it has been necessary to derive the appropriate band model parameters directly from experimental data. Generally, it has not been possible to take high temperature data with sufficiently high resolution to separate individual lines to measure their strengths and widths. Even if this were possible, the cost of the experiment would be high. More commonly, curves of growth are measured at fairly low spectral resolution. From these latter data, absorption coefficients and fine structure parameters may be deduced. However, since such fine structure parameters really have no direct physical meaning and represent some sort of effective or "average" quantities, it can be dangerous to use these data to extrapolate to applications which may be considerably different in terms of pressure, relative concentrations, and degree of inhomogeneity. This is especially true when the model formalism being used is not obviously reliable or is clearly oversimplified. Nevertheless, this is essentially what has to be done in practice. Thus, it is important to establish, for a given formalism, what sort of errors may be involved. A number of parametric sensitivity analyses have been carried out to determine the type of errors that might be expected under various conditions using the simple formalism described in the previous section. These have included "numerical" tests of the statistical approximation, the Curtis-Godson approximation, the assumptions involved in the choice of the line widths, the effects of including or not including "hot" lines<sup>2</sup> (i.e., line groups for which  $n > 1$ ), and the effects of choosing different curve-of-growth functions.

#### 4.3.1                ERRORS CAUSED BY THE CURTIS-GODSON APPROXIMATION

To obtain an estimate of the error associated with the modified Curtis-Godson approximation, a simple two-slab distribution is treated. First, consider a difference in the line density in the two slabs. Here the front layer, which is assumed to have a low temperature, is assumed to have only one spectral line in the interval under consideration; whereas, in the rear high temperature section of the gas, the oscillator strength of this line is presumed to be divided among  $n$  equally intense lines, one of which coincides with the original line. The remaining ones are new and displaced hot lines. Since the primary interest is in the effect of the variable line spacing term, one assumes the line width to be the same in both sections.

---

2. "Hot" lines are those showing a very rapid increase in strength with increasing temperature and thus contribute to emission from the high temperature regions of the gas but do not appreciably absorb in the low temperature regions.

In Figures 4-1a and 4-1b, the Curtis-Godson estimate is compared to the exact value of the emission from the rear layer as a function of both the depth of the rear layer and the thickness of the front layer. By referring to these figures, one can see that the line density variations are reasonably accounted for by the Curtis-Godson approximation so long as the mass in the rear layer is not too small. The error does not appear to be strongly dependent on how many new lines appear as long as there is at least one. The fact that the errors become large when the mass of the emitting layer becomes small compared to that of the absorbing layer is characteristic of the Curtis-Godson approximation and is associated with the fact that the line width and line spacing ratios are mass-averaged.

The effects of varying line widths are shown in Figures 4-2 and 4-3. In Figure 4-2 the Curtis-Godson approximations for the total equivalent width of a two-slab volume are shown for Lorentz and Doppler lines. It is apparent that the Curtis-Godson approximation yields reasonably accurate estimates so long as the variation in line width is not excessive (<500 percent for a Lorentz line and <50 percent for a Doppler line). The emission from a hot region located behind a cool absorbing layer is more sensitive to differences between the line widths in the two slabs (Fig. 4-3). The worst case occurs when the emission width is small and the absorption path is large. In this case, for Lorentz lines, errors greater than a factor of two can occur. Again, however, the errors are relatively small when the thickness of absorber is not too large compared to that of the emitter.

#### 4.3.2 ERRORS RESULTING FROM THE USE OF THE RANDOM MODEL AND SIMPLIFIED CURVES OF GROWTH

The validity of the random band model is fairly easily tested experimentally. It is well known that, for Lorentz lines, the random model predicts that the logarithm of the low resolution transmission of a cell of absorber should be exactly linear in the pressure so long as the cell length, temperature, and mole fractions of the various species are held constant. This is not true of other models. For example, an Elsasser model predicts a linear dependence at high transmission, changing over to a quadratic dependence at low transmission. Examination of data taken by Burch [4-1, 4-2] and by Simmons [4-3] indicates that, for temperatures above 600K, the random model is consistent with the data within experimental scatter. However, since the measurements used in these data cover a limited range of pathlengths and pressures, it is desirable to obtain additional confirmation. To accomplish this and also to test the data reduction procedure used for interpreting laboratory data to derive appropriate band model parameters for inhomogeneous radiance calculations, the following numerical "experiment" has been carried out. The

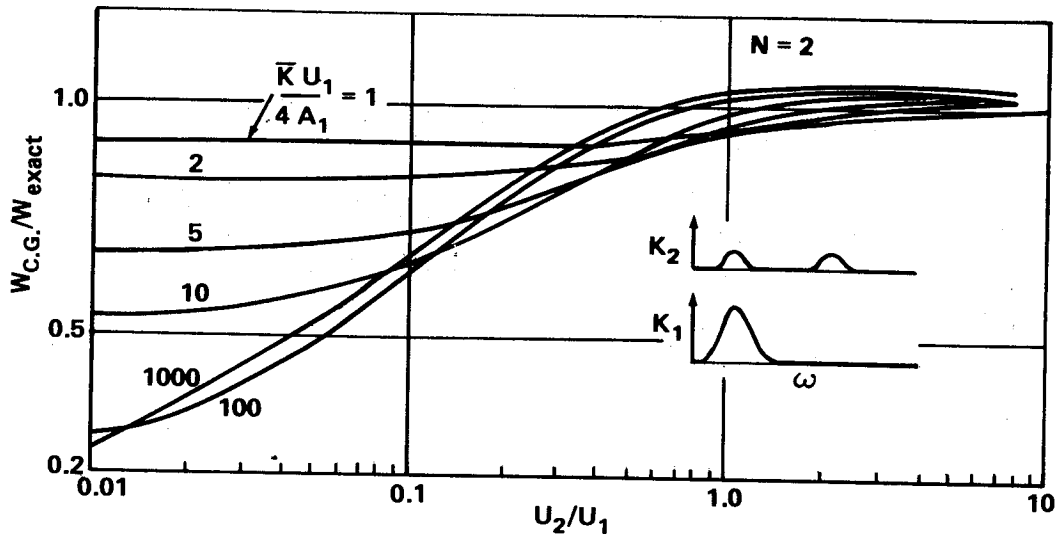


Figure 4-1a. Effect of hot lines on the emission from a high temperature gas viewed through a cool absorbing layer. (The ordinate is the ratio of the radiance of two temperature slabs computed in the Curtis-Godson approximation to the exact value. The abscissa is the ratio of the mass of the high temperature rear slab to that of the low temperature front slab. In the rear slab two equally intense lines are excited; whereas, in the front slab, all the line strength is concentrated in only one of the lines.)

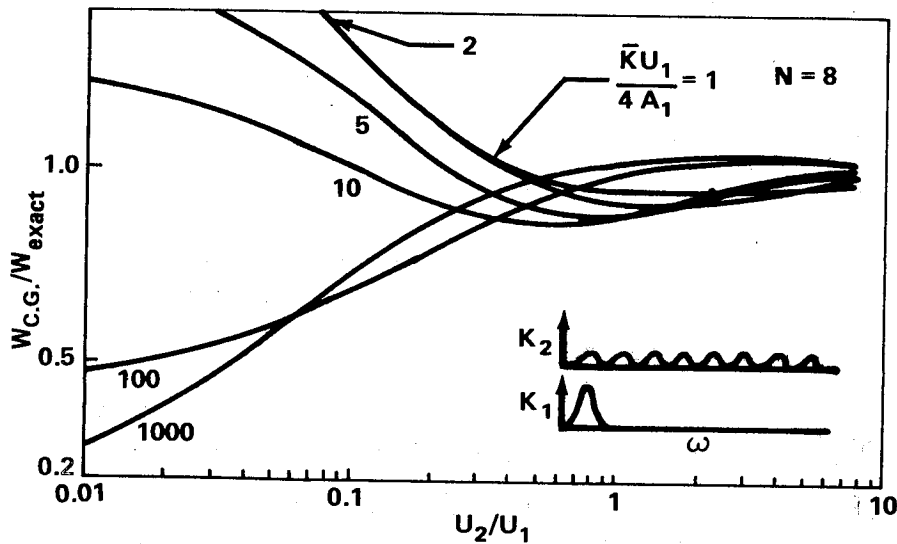


Figure 4-1b. Effect of hot lines on the emission from a high temperature gas viewed through a cool absorbing layer. (This figure is the same as Figure 4-1a except that the single line in the cool section is divided into eight equally intense lines in the hot section, one of which is the original line.)

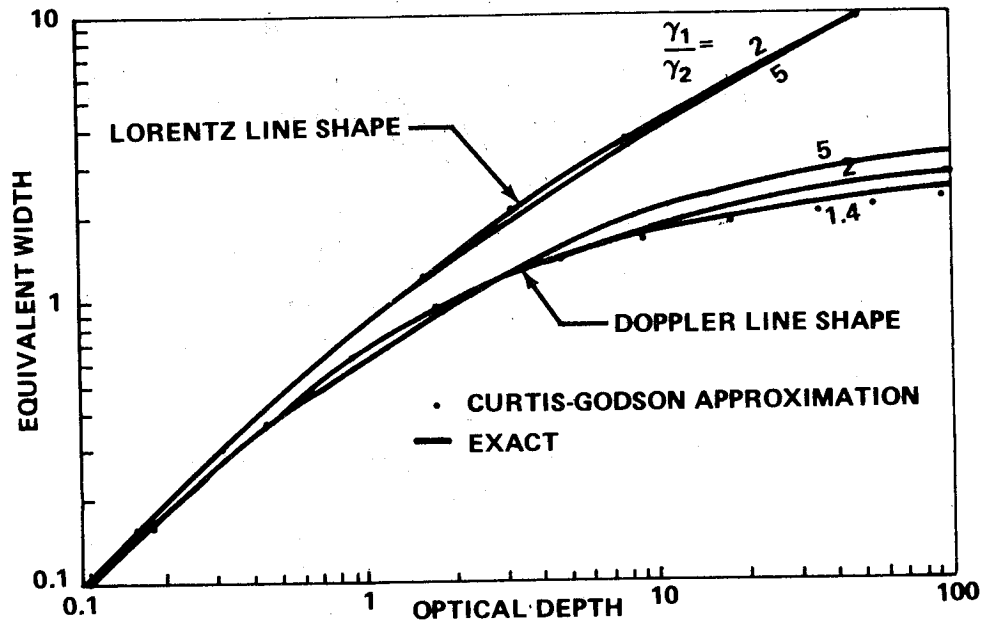


Figure 4-2. Accuracy of the Curtis-Godson approximation for evaluating total equivalent absorption widths for a two-slab gas. (The solid lines represent the exact values and the points represent the values given by the Curtis-Godson approximation. The two slabs have the same masses but different line half-widths.)

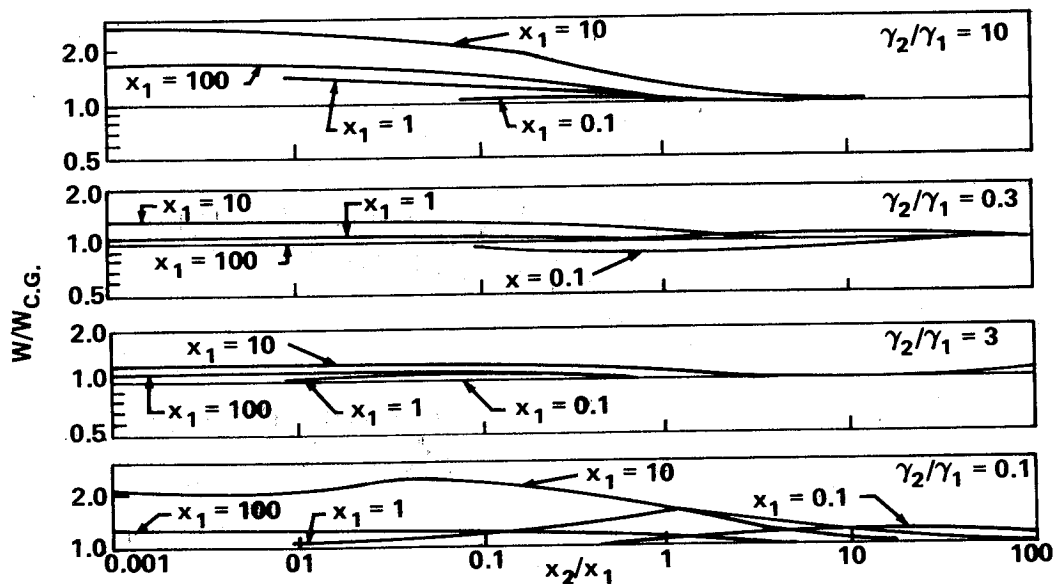


Figure 4-3. Accuracy of the Curtis-Godson approximation for evaluating the equivalent emission width of a Lorentz line for a two-slab gas when only the rear slab radiates. (The abscissa is the ratio at the line center of the optical depth of the rear slab to that of the front slab.)

quasi-random band model procedure (see Section 3.2.4.2) with a  $1 \text{ cm}^{-1}$  cell size was used to calculate the transmission of various pathlengths between 0 and 10 meters of water vapor at one atmosphere pressure and at various temperatures. These data were then degraded spectrally with a triangular slit function of  $25 \text{ cm}^{-1}$  half-width. These resulting low resolution data were then reduced by experimental data analysis procedures to obtain values for the mean absorption coefficient and the fine structure parameter ( $a = \gamma/d$ ), that is, by fitting the experimental curves of growth with a Ladenburg-Reiche function.

To test the inhomogeneous formalism, two sets of calculations were carried out. The radiances of various two-slab volumes were calculated with the low resolution (MLG) model described in Section 5.3 using these "experimentally" derived band model parameters. In Figures 4-4 and 4-5, these data are compared to the values obtained from a direct quasi-random band model calculation of the inhomogeneous path (using the normal Curtis-Godson approximation to evaluate the effective half-widths). The calculations were carried out for a range of slab thickness between 0 and 10 meters and pressures between 0.1 and 1 atmosphere. Figure 4-4 shows that, when the temperature varies by less than a factor of two, the two calculations agree quite well — even when all the lines are assigned a uniform average intensity ( $\Delta E = \infty$ ). The data in Figure 4-5 indicate, however, that when the front layer is at a very low temperature, sizeable errors may be incurred when the cold layer is appreciably absorbing if hot lines are not considered.

#### 4.3.3 CHOICE OF THE CURVE OF GROWTH

It is well known that, for a homogeneous volume of gas, the curves of growth for collision-broadened lines are not very sensitive to the distribution of line intensities. This is demonstrated in Figure 3-2.

To study the effect of hot lines in a more reasonable inhomogeneous flow field, some calculations were carried out for a temperature and concentration distribution characteristic of a constant pressure turbulent flame. Here the temperature distribution was assumed to be bell-shaped and the water vapor mole fraction to be either similarly bell-shaped or to be uniform (Fig. 4-6). In Figure 4-7, the calculated radiances for three models are compared. In the first ( $f_1 = g_1 = 1$  and all other  $f_n$  and  $g_n = 0$ ), all the lines are assigned a uniform average intensity (SLG model described in Section 5.3), the second ( $g_n = f_n = 1$  for all  $n$ ) roughly corresponds to an  $S^{-1}$  distribution (MLG model described in Section 5.3), and the third ( $f_n, g_n$  variable) is

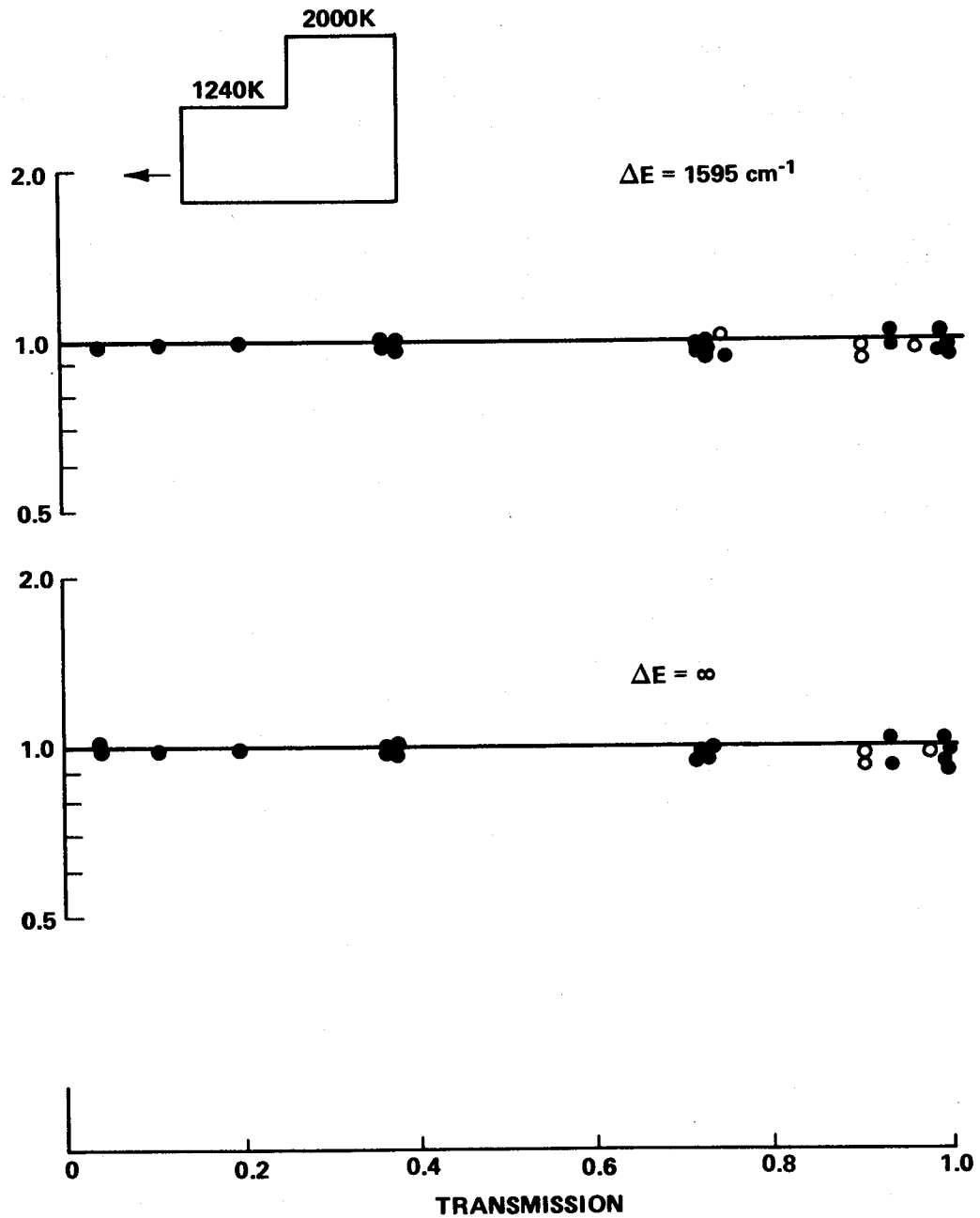


Figure 4-4. Effect of the choice of the line grouping parameter  $\Delta E$  on the calculated emission of a two-slab gas when the temperature variations are moderate. (The points represent the ratios of the predicted low resolution radiance to the "exact" values for various combinations of pressures and slab thicknesses. The pressures varied from 0.1 to 1 atmosphere and the slab thicknesses from 0 to 10 meters. The abscissa is the transmission of the front slab for grey radiation.)

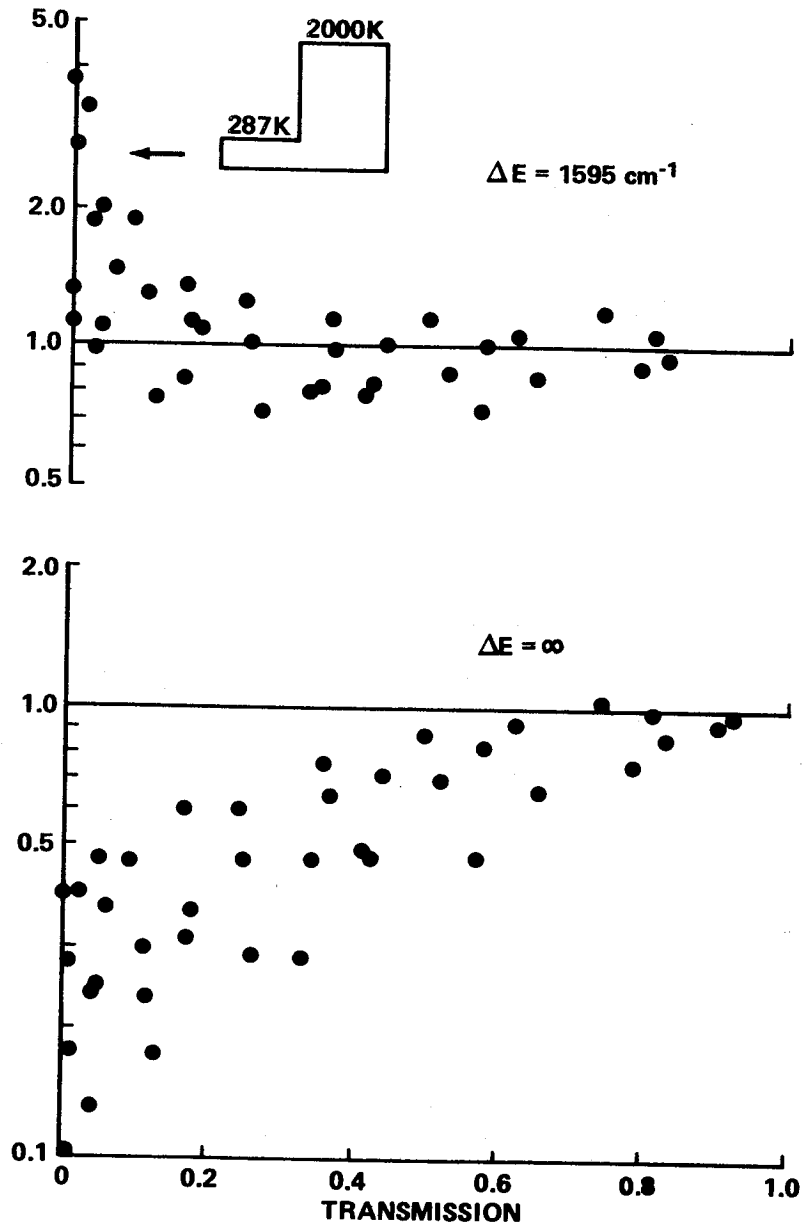


Figure 4-5. Effect of the choice of the line grouping parameter on the calculated emission of a two-slab gas when the front slab has a low temperature. (Here the abscissa is the transmission of the front slab for the radiation emitted by the rear slab.)

deduced from detailed line strength calculations by fitting the MLG model described in Section 5.3 to the calculations.<sup>3</sup> In all cases the line density and the mean absorption coefficients were normalized so that each model gave the same answer for a homogeneous path in the optically thin limit and in the square root limit.

The characteristic widths of the temperature profile varied from 1 to 10 meters at 1 atmosphere pressure to 10 to 100 meters at 0.01 atmosphere. Two peak temperatures were considered: 1900K and 1000K. Figure 4-7 shows that the computed radiances for the second and third cases do not differ by more than 30 percent except at the lowest pressure (where Doppler broadening is important) or when the gas is highly opaque. However, considerable error can occur when the first (and simplest) model is used ( $f_1 = g_1 = 1$  and all other  $f_n$  and  $g_n$  are 0).

There is little information available for individual collision line widths at high temperature. However, the calculations do not appear very sensitive to variations in the widths of the hot lines so long as the low resolution curves of growth can be measured for homogeneous paths. A decrease of a factor of two in the width of the hot lines caused the computed radiances for these particular inhomogeneous paths to change by less than 11 percent.

---

3. Malkmus, W., Private communication.

CHAPTER 4 - CALCULATIONAL  
TECHNIQUES FOR INHOMOGENEOUS GASES

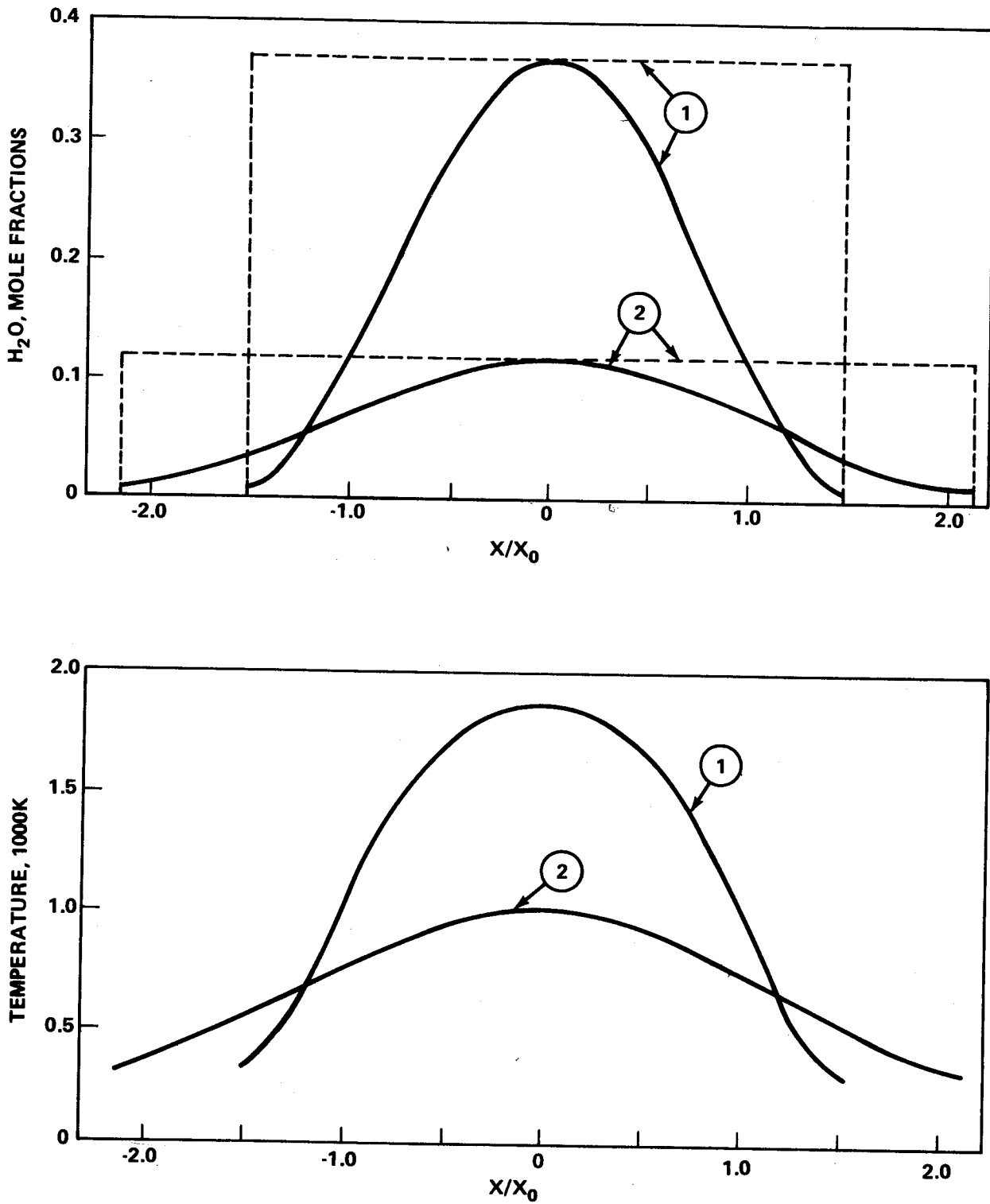


Figure 4-6. Temperature and concentration profiles used to compare various radiance models (see Fig. 4-7).

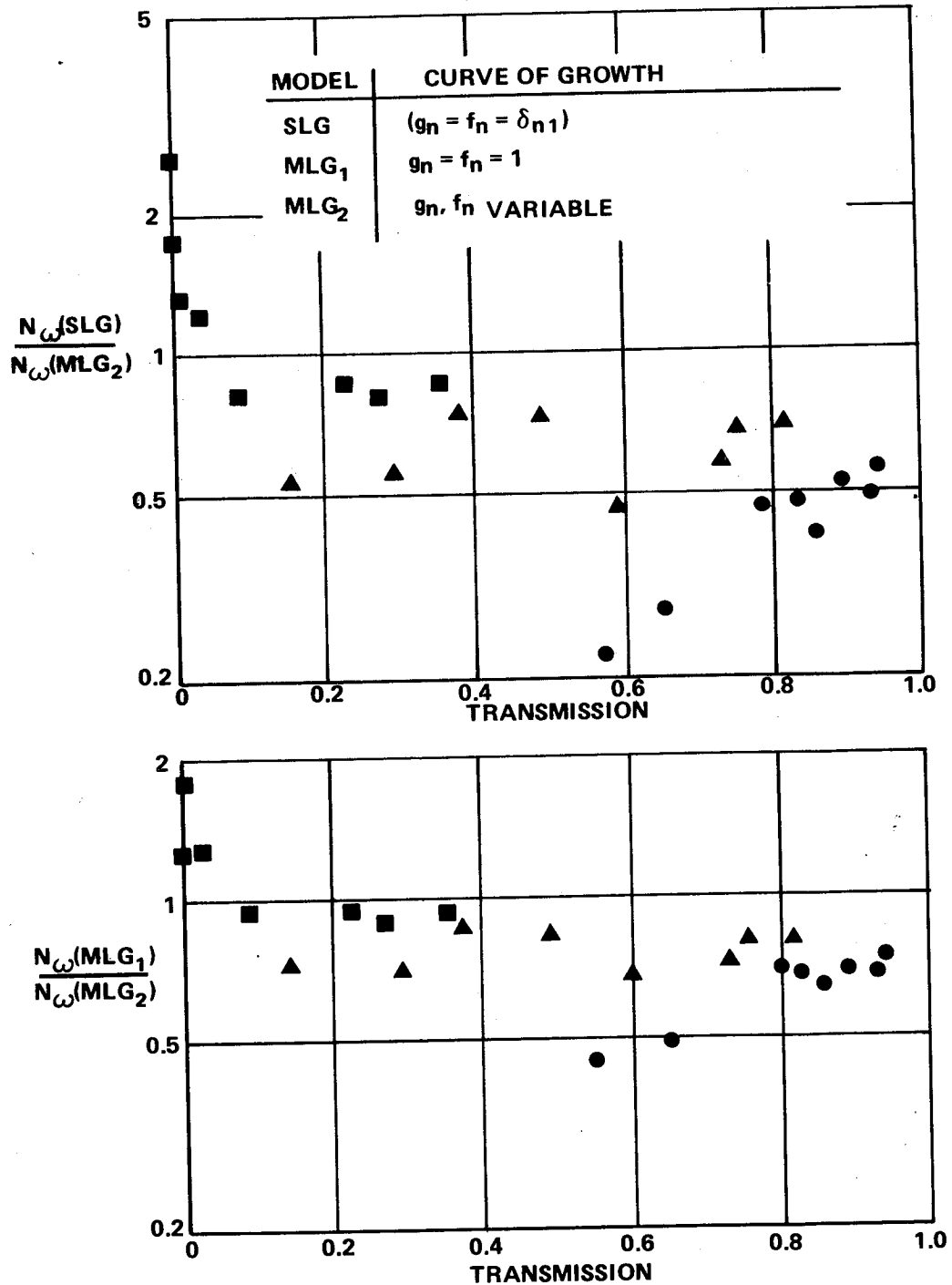


Figure 4-7. Effect of model complexity on the computer radiance for the gas profiles shown in Figure 4-6. (The squares, triangles and circles correspond to pressures of 1, 0.1, and 0.01 atmosphere, respectively. The abscissa is the transmission of the entire volume for grey radiation.)

4.4            SUMMARY

These sensitivity analyses give some indication of the absolute accuracy that may be expected in numerical band model calculations of the infrared radiant heat transfer from typical combustion gases. Although it was found that the use of different models for the curves of growth and the use of the Curtis-Godson approximation can result in errors of a factor of two or more in some cases, these large errors occur only in rather unique situations, such as a short hot path being viewed through a long cool absorber. The larger errors for inhomogeneous paths tend to occur at very low pressures and/or when the total transmission along the line of sight is small. For more moderate conditions, the errors tend to be less than about 30 percent. This is comparable to our present uncertainty in the absolute value of typical absorption coefficients (e. g., for water vapor).

In practical numerical computations it is recommended that the radiance computations include or be preceded by spot checks of the net transmission, or the mean pressure, and of the temperature variation along representative lines of sight. These numbers and the data presented in this chapter can be used for rough estimates of the expected accuracy of the calculation. Also, it is recommended that before extensive numerical computations are carried out with a given model, preliminary calculations be carried out for representative lines of sight to select the simplest band model representation and the minimum spectral (and spatial) resolution required to achieve the desired accuracy.

REFERENCES

- 4-1. Burch, D. E. and Gryvnak, D. A.: Report U-1929, Ford Motor Company, 1962.
- 4-2. Burch, D. E.; France, W. L.; and Williams, D.: Appl. Optics, vol. 2, 1963, p. 585.
- 4-3. Simmons, F. S.; Arnold, C. B.; and Smith, D. H.: Studies of Infrared Radiative Transfer in Hot Gases, I: Spectral Absorptance Measurements in the  $2.7 \mu$  H<sub>2</sub>O Bands. BAMIRAC Report 4613-91-T, Infrared Physics Laboratory, Willow Run Laboratories, University of Michigan, August 1965.



CHAPTER 5

REPRESENTATIONS FOR SPECIFIC MOLECULES

In this section, the data available for various molecules are discussed individually. The theoretical treatments for calculating the absorption properties are briefly reviewed in each case, and the data needed for constructing band model representations are summarized in graphical form. (Tabular data are presented in the General Appendix for all species.)

At the end of the section, a detailed series of reference tables and charts summarizes the recommended band model procedures for each molecule: curves of growth, absorption coefficient models, and line width and line spacing models.

An explanation of the format and nature of the data presented in this section is in order. In much of the theoretical literature on infrared characteristics of molecules, it has been common practice to present the results of the calculations in two limiting cases: the weak-line limit, and the strong-line limit for collision-broadened lines. These two regimes are of particular value for data presentation since the dependence on pathlength, concentration, and total pressure are factors in the expressions for the logarithm of the transmissivity. In other regimes, such as the low-pressure (Doppler) limit, such scaling is not possible and data are commonly presented for specific pathlengths, temperatures, and pressures.

An attempt has been made to present the available data in two formats: (1) the data specifically required for constructing band model representations of the smoothed spectra (mean absorption coefficients, curves of growth, spectral line densities, and line widths), and (2) where appropriate and where the data are available, extensive graphical presentations of computed spectral emissivities and integrated absorptivities for various combinations of pathlength, concentration, temperature, and pressure have been included (Chapter 6). These latter data are useful for obtaining quick rough estimates of the emissivity or absorptivity in special cases. These curves can often also be used as a guide for determining the level of sophistication required in the band model representation for specific numerical calculations.

## 5.1 DIATOMIC MOLECULES

### 5.1.1 MEAN ABSORPTION COEFFICIENTS AND LINE SPACING (THEORY)

A first approximation to the infrared spectral emissivity of a diatomic gas can be made by assuming a harmonic oscillator model [5-1] for the molecule. This has the advantage of simplicity, but the very nearly symmetric intensity distribution which it yields about the band center does not closely match the asymmetric shape which is found experimentally or calculated by a line-by-line method.

To improve the approximation, a model of an anharmonic oscillator with the first approximation to the vibration-rotation interaction can be used. This will improve the approximation to the actual spectral emissivity without resorting to the more detailed approach of considering the emission from each individual spectral line.

The procedure used in this text to evaluate the mean emissivity and transmissivity functions for diatomic molecules may be briefly summarized as follows. (For a more detailed description, see Appendix 5-A and Reference 5-2.) For a specific vibrational transition ( $v \rightarrow v + 1$ ), the frequency of emitted radiation is expressed as a quadratic function of the rotational quantum number  $m$ , which is solved to express  $m$  as a function of  $\omega$ . This expression is substituted for  $m$  in the equations used for computing the average line intensity  $S(\omega)$  and average line spacing  $d(\omega)$  so that  $S(\omega)$  and  $d(\omega)$  become explicit functions of  $\omega$ . The line spacing for the  $v \rightarrow v + 1$  band in the neighborhood of the frequency  $\omega$  is given formally by [5-2]

$$d_v = \left| \frac{dm(\omega)}{d\omega} \right|^{-1}$$

$$\approx 2\{ [ (B_e - \alpha_e (v + 1))^2 - \alpha_e (\omega - \omega_v) ] \}^{1/2} \quad (5-1)$$

Here  $B_e$  and  $\alpha_e$  are the usual spectroscopic constants (see Chapter 2),  $\omega_v$  is the wavenumber of the band origin, and  $v$  is the vibrational quantum number of the lower vibrational state of the transition.

For some sufficiently large value of  $\omega$ ,  $d \rightarrow 0$ , and a "band head" is formed in the R-branch. Note that two sequences of lines extend down from the band head: the main sequence (the P-branch and main portion of the R-branch) and the returning portion of the R-branch. This latter sequence is usually only of importance at the highest temperatures.

The line strengths in the main sequence are denoted by  $S_V^{v+1(-)}(\omega)$  and those in the returning R-branch by  $S_V^{v+1(+)}(\omega)$  [5-2]. Expressions  $S_V^{v+1(-)}(\omega)$  and  $S_V^{v+1(+)}(\omega)$  are given in Appendix 5-A. The line spacings in the two sequences are identical at any value of  $\omega$ .

### 5.1.2 RANDOM REGULAR (ELSASSER) MODEL

If the mean spectral properties of each sequence of each band are represented by the Elsasser model (Section 3.2.1.1), the composite effect of both sequences of all bands can be well represented [5-3, 5-4] by the random Elsasser model [equation (3-54)]:

$$\bar{\tau}(\omega) = \prod_V \bar{\tau}_V^{(-)}(\omega) \bar{\tau}_V^{(+)}(\omega) ,$$

where  $\bar{\tau}_V^{(\pm)}(\omega)$  represents the mean transmissivity of an Elsasser band with lines of strength  $S_V^{v+1(\pm)}(\omega)$ , spacing  $d_V(\omega)$ , and half-width  $\gamma$ , from equation (3-22) in which

$$k_V^{(\pm)} = S_V^{v+1(\pm)}(\omega)/d_V(\omega) \quad (5-2)$$

and

$$\beta_V = 2\pi\gamma/d_V(\omega) .$$

5.1.3 RANDOM MODEL

In the event that the effects of overlapping of lines in the same sequence can be ignored, the mean transmissivity may be determined from the equivalent width of a single line, i. e.,

$$\bar{\tau}_v^{(+)}(\omega) = 1 - \frac{W_v^{(+)}(\omega)}{d_v(\omega)}, \quad (5-3)$$

in which, from Section 2.2.1.3.1,

$$W_v^{(+)}(\omega) = 2\pi\gamma f(S_v^{(+)}u/2\pi\gamma), \quad (5-4)$$

where

$$f(x) = xe^{-x}[I_0(x) + I_1(x)] .$$

Thus, the mean transmissivity of the band system is given by

$$\bar{\tau}(\omega) = \prod_v \left[ 1 - \frac{W_v^{(-)}(\omega)}{d_v(\omega)} \right] \left[ 1 - \frac{W_v^{(+)}(\omega)}{d_v(\omega)} \right], \quad (5-5)$$

which in the limit of large  $v$  becomes

$$\bar{\tau}(\omega) = \exp \left[ - \sum_v \frac{W_v^{(-)}(\omega) + W_v^{(+)}(\omega)}{d_v(\omega)} \right] . \quad (5-6)$$

This equation is the same as for a random model, in which all line positions are only statistically defined.

In the event that partial overlapping between adjacent lines in the same sequence occurs, the Elsasser or Golden functions (Appendix 3-A) should be used to compute  $\tau_v^{(\pm)}(\omega)$  when high accuracy is required. However, for many cases, particularly those involving heat transfer, sufficient accuracy (< 10 percent error, see Appendix 3-B) can be obtained by using the totally random model [equation (5-6)]. When suitable simplified forms for the line equivalent widths ( $W_v^{(\pm)}$ ) are available, this procedure yields fairly accurate values for the mean transmissivity [ $\bar{\tau}(\omega)$ ] for a low computational cost.

In the remainder of this section, the prescriptions and data needed for carrying out rapid calculations of the emission and transmission of homogeneous and inhomogeneous volumes of gas are presented. In general, these procedures are band model techniques which utilize tabular data for the mean absorption coefficient  $\bar{k}(\omega)$  and the line density  $1/d(\omega)$ . For diatomic molecules at moderate temperatures, the spectra are sufficiently simple that direct computation with the explicit formulas for  $S_v^{v+1(\pm)}$  and  $1/d_v(\omega)$  may be preferable to using table look-up procedures, both because of the simpler numerical procedures involved and because of the greater accuracy obtainable. For polyatomic molecules, however, the spectra are much more complex and the use of tabular data is often more efficient.

The procedures using the direct formulas for  $S_v^{v+1(\pm)}(\omega)$  and  $d_v(\omega)$  for diatomic molecules are summarized in Appendix 5-A.

#### 5.1.4 LIMITING FORMS FOR THE MEAN SPECTRAL TRANSMISSIVITY

In the weak-line approximation, the transmissivity has the form

$$\bar{\tau}(\omega) = \exp \left\{ - \left[ \sum_v \frac{S_v^{v+1(-)}(\omega) + S_v^{v+1(+)}(\omega)}{d_v(\omega)} \right] u \right\}, \quad (5-7)$$

where the quantity  $u$  factors out of the summation over  $v$  to yield

$$\bar{\tau}(\omega) = \exp[-\bar{k}(\omega)u] \quad , \quad (5-8)$$

where the local mean absorption coefficient

$$\bar{k}(\omega) = \sum_v \left[ \frac{S_v^{v+1(-)}(\omega) + S_v^{v+1(+)}(\omega)}{d_v(\omega)} \right]$$

is a function of  $\omega$ , independent of  $u$ .

#### 5.1.4.1 Collision-Broadened Lines

In the strong-line limit for collision-broadened lines, the mean transmissivity is given by

$$\bar{\tau}(\omega) = \exp \left\{ -2(\gamma u)^{1/2} \sum_v \frac{\left[ \left( S_v^{v+1(-)}(\omega) \right)^{1/2} + \left( S_v^{v+1(+)}(\omega) \right)^{1/2} \right]}{d_v} \right\} \quad (5-9)$$

where a uniform line width  $\gamma$  is assumed for all lines in the band. Again, the quantity  $u$  factors out of the summation over  $v$ .

Results of theoretical calculations have commonly been given in the infrared literature in terms of a mean absorption coefficient  $\bar{k}$ , defined by

$$\bar{k} = \overline{(S/d)} = \sum_v \left[ \frac{S_v^{v+1(-)}(\omega) + S_v^{v+1(+)}(\omega)}{d_v} \right] \quad (5-10)$$

and a mean strong-line parameter  $\overline{(S^{1/2}/d)}$  defined by

$$\overline{S^{1/2}/d} = \sum_v \left\{ \frac{\left[ S_v^{v+1(-)}(\omega) \right]^{1/2} + \left[ S_v^{v+1(+)}(\omega) \right]^{1/2}}{d_v} \right\} \quad (5-11)$$

Graphical or tabulated values of these quantities can be used to construct band model representations for collision-broadened lines.

An equivalent strong-line parameter  $\overline{(1/d)}$  may be defined:

$$\overline{(1/d)} = \left( \overline{(S^{1/2}/d)} \right)^2 / \overline{(S/d)} \quad . \quad (5-12)$$

The parameters  $\overline{(S/d)}$  (or  $\overline{k}$ ) and  $\overline{(1/d)}$  for various molecules are presented in graphical form in this chapter and in tabular form in the General Appendix.

#### 5.1.4.2 Doppler-Broadened Lines

The equivalent width of an isolated line of integrated intensity  $S$  with Doppler shape is given [equation (2-B-1) and following] by:

$$W = Su \sum_{n=0}^{\infty} \frac{(-k_0 u)^n}{(n+1)! \sqrt{n+1}} \quad . \quad (5-13)$$

Results of calculations for Doppler-broadened lines have generally been presented directly in terms of the spectral emissivity or transmissivity. The simplified band model representations such as those given at the end of this section are generally based on fits to the weak line and strong collision-broadened line calculations (or measurements) and do not usually rely on the pure Doppler calculations. For applications involving very low pressure, it is often advisable to check the accuracy of such simplified band model prescriptions against the detailed numerical calculations for pure Doppler lines.

#### 5.1.4.3 Regions of Validity

A detailed discussion of the range of validity of the various approximations is given by Plass [5-3, 5-4]. An example from this work illustrated in Figure 5-1 indicates regions of validity for a statistical band model. When the ranges in Figure 5-1 are applied to pure CO with  $\epsilon_{\omega} = 0.6$ , the results indicate that the weak line approximation is accurate within 10 percent when  $\beta (=2\pi\gamma/d) > 3$ . [This requires the pressure to be above some minimum value

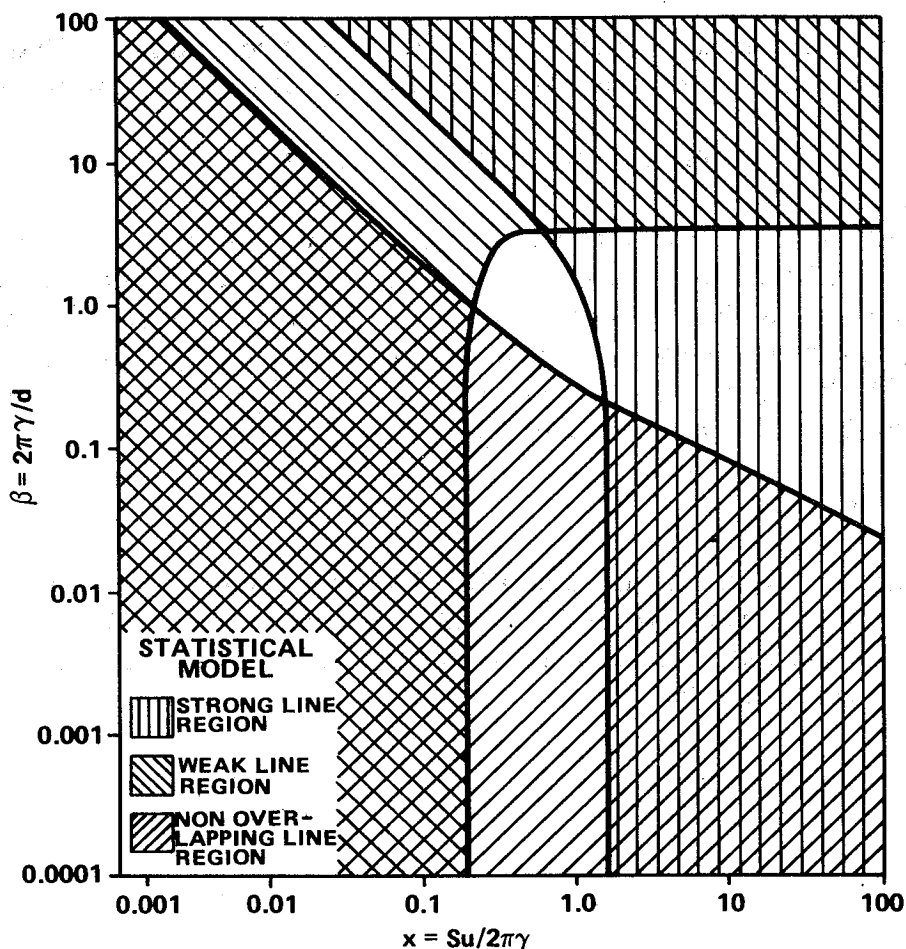


Figure 5-1. Regions of validity for three different approximations of absorption as a function of  $\beta$  and  $x$ . (The statistical model with all lines of equal intensity was assumed. Within the indicated regions, the given approximation is accurate within 10 percent.)

which is largest ( $p \approx 50$  atm) when  $T \approx 1200\text{K}$ .] The strong approximation for this example is accurate within 10 percent when  $\beta < 1$ . (For  $T \approx 1200\text{K}$ , this implies a maximum  $p \approx 17$  atm.) A lower limit to the validity of the collisional strong line approximation is imposed by the presence of Doppler broadening. The Doppler and Lorentz widths are comparable for  $p \approx 1/2$  atm at  $T \approx 1200\text{K}$ . If the Doppler width is less than the Lorentz width, the maximum effect of Doppler broadening on the equivalent width is less than 10 percent.

For pure HF, the collisional strong-line approximation may be used for pressures up to a certain value (a maximum  $p \approx 35$  atm for  $T \approx 3000\text{K}$ )

and above a minimum determined by the Doppler broadening. (The Doppler and Lorentz widths are comparable for  $p \approx 0.4$  atm and  $T \approx 3000$ K.)

#### 5.1.5 DATA FOR DIATOMIC MOLECULES

In this section the basic data required for constructing band models are summarized for six diatomic molecules (CO, NO, CN, OH, HCl, and HF). These data include tables of band strengths and line half-widths, and graphical presentations of mean absorption coefficients ( $k$ ) and mean line densities ( $1/d$ ). The absorption coefficients and line densities are given in tabular form in the General Appendix.

##### 5.1.5.1 CO Data

Measured band strengths and line half-widths for CO are tabulated in Tables 5-1 and 5-2 respectively. Calculated values for the mean absorption coefficient  $k$  and for the line density parameter ( $1/d$ ) are shown in Figures 5-2 and 5-3, respectively.

TABLE 5-1. CO BAND STRENGTHS ( $\text{cm}^{-2}\text{atm}^{-1}$  at STP)

Fundamental ( $2143 \text{ cm}^{-1}$ )	First Overtone ( $4260 \text{ cm}^{-1}$ )	Second Overtone ( $6350 \text{ cm}^{-1}$ )	Source
258 ± 4	1.78		Armstrong and Welsh (1965) <sup>a</sup>
236	1.66 ± 0.33		Benedict et al. (1962) <sup>b</sup>
289 ± 30	2.3 ± 0.3		Breeze and Ferriso (1965) <sup>c</sup>
260			Burch and Williams (1962) <sup>d</sup>
238			Coulon et al. (1954) <sup>e</sup>
419 ± 82	2.3 ± 0.5		Dinsmore and Crawford (1949) <sup>f</sup>
	2.51 ± 0.50	0.008 ± 0.008	Dinsmore (1949) <sup>g</sup>
280			Havens (1938) <sup>h</sup>
	1.95 ± 0.10		Kostkowski and Bass (1961) <sup>i</sup>
259			Locke and Herzberg (1953) <sup>j</sup>
394	5.13		Matheson (1932) <sup>k</sup>
	1.66		Oppenheim and Goldring (1962) <sup>l</sup>
260 ± 13	1.83 ± 0.09		Penner and Weber (1951) <sup>m</sup>
		0.0104 ± 0.001	Plyler et al. (1952) <sup>n</sup>
	2.15 ± 0.10	0.0127 ± 0.0013	Schurin and Ellis (1966) <sup>o</sup>
262	1.83		Vincent-Geisse (1954) <sup>p</sup>
	1.73 ± 0.17		Vu et al. <sup>q</sup>
260	2.2	0.011	Recommended Values

a. R. L. Armstrong and H. L. Welsh, *Can. J. Phys.*, no. 43, 1965, p. 547.

b. W. S. Benedict, R. Herman, G. E. Moore, and S. Silverman, *Astrophys. J.*, no. 135, 1962, p. 277.

- c. J. C. Breeze and C. C. Ferriso, *J. Chem. Phys.*, no. 43, 1965, p. 3253.
- d. D. E. Burch and D. Williams, *Applied Optics*, no. 1, 1962, p. 587.
- e. R. Coulon, L. Galatry, B. Oksengorn, S. Robin, and B. Vodar, *J. Phys. Radium*, no. 15, 1954, p. 641.
- f. H. L. Dinsmore and B. L. Crawford, Report NR-109-104, University of Minnesota, October 1949.
- g. H. L. Dinsmore, dissertation, University of Minnesota, 1949.
- h. R. J. Havens, dissertation, University of Wisconsin, 1938.
- i. H. J. Kostkowski and A. M. Bass, *J. Quant. Spectry. Radiative Transfer*, no. 1, 1961, p. 177.
- j. J. L. Locke and L. Herzberg, *Can. J. Phys.*, no. 31, 1953, p. 504.
- k. L. A. Matheson, *Phys. Rev.*, no. 40, 1932, p. 813.
- l. V. P. Oppenheim and H. Goldring, *J. Quant. Spectry. Radiative Transfer*, no. 2, 1962, p. 293.
- m. S. S. Penner and D. Weber, *J. Chem. Phys.*, no. 19, 1951, p. 807.
- n. E. K. Plyler, W. S. Benedict, and S. Silverman, *J. Chem. Phys.*, no. 20, 1952, p. 175.
- o. B. Schurin and R. E. Ellis, *J. Chem. Phys.*, no. 43, 1966, p. 2528.
- p. J. Vincent-Geisse, *Compt. Rend.*, no. 239, 1954, p. 251.
- q. H. Vu, M. R. Atwood, and B. Vodar, *J. Chem. Phys.*, no. 38, 1963, p. 2671.

CHAPTER 5 – REPRESENTATIONS  
FOR SPECIFIC MOLECULES

TABLE 5-2. CO MEAN LINE HALF-WIDTHS ( $\text{cm}^{-1}\text{atm}^{-1}$  at 300K)<sup>a</sup>

Broadener						Source
CO	N <sub>2</sub>	O <sub>2</sub>	H <sub>2</sub>	CO <sub>2</sub>	H <sub>2</sub> O	
1.02x	x		0.85x			Burch et al. <sup>b,c</sup>
	y	0.87y	1.25y			Cross and Daniels <sup>b,d</sup>
0.042			0.043			Penner and Weber <sup>e</sup>
0.105						Locke and Herzberg (1953) <sup>f</sup>
0.061			0.064			Weber and Penner (1952) <sup>g</sup>
0.064						Vincent-Geisse (1954) <sup>h</sup>
0.055	0.054	0.045	0.057	0.068		Eaton and Thomson (1959) <sup>i</sup>
0.069						Kostowski and Bass (1961) <sup>j</sup>
0.058						Benedict et al. (1962) <sup>k</sup>
0.072						Hoover and Williams (1969) <sup>l</sup>
0.06	0.06	0.05	0.06	0.07	(0.06)	Recommended Values (Estimates in parentheses)

- a. These data represent mean values averaged over the entire band. For measurements of individual line half-widths, see Eaton and Thomson<sup>(i)</sup>, Benedict et al.<sup>(k)</sup>, and Hoover and Williams<sup>(l)</sup>.
- b. Only the ratio of the line width to the pure nitrogen broadened line width was measured. The quantities x and y refer to the undetermined N<sub>2</sub>-broadened line half-widths.
- c. D. E. Burch, D. Gryvnak, E. B. Singleton, W. L. France, and D. Williams, AFCRL-62-698, 1962.
- d. P. C. Cross and F. Daniels, J. Chem. Phys, no. 2, 1934, p. 6.
- e. S. S. Penner and D. Weber, J. Chem. Phys., no. 19, 1951, p. 807.

- f. J. L. Locke and L. Herzberg, *Can. J. Phys.*, no. 31, 1953, p. 504.
- g. D. Weber and S. S. Penner, *J. Chem. Phys.*, no. 21, 1953, p. 1503.
- h. J. Vincent-Geisse, *Compt. Rend.*, no. 239, 1954, p. 251.
- i. D. R. Eaton and H. W. Thompson, *Proc. Roy. Soc. A.*, no. 251, 1959, pp. 458 and 475.
- j. H. J. Kostkowski and A. M. Bass, *J. Quant. Spectry. Radiative Transfer*, no. 1, 1961, p. 117.
- k. W. S. Benedict, R. Herman, G. E. Moore, and S. Silverman, *Astrophys. J.*, no. 135, 1962, p. 277.
- l. G. M. Hoover and D. Williams, *J. Opt. Soc. Am.*, no. 59, 1969, p. 28.

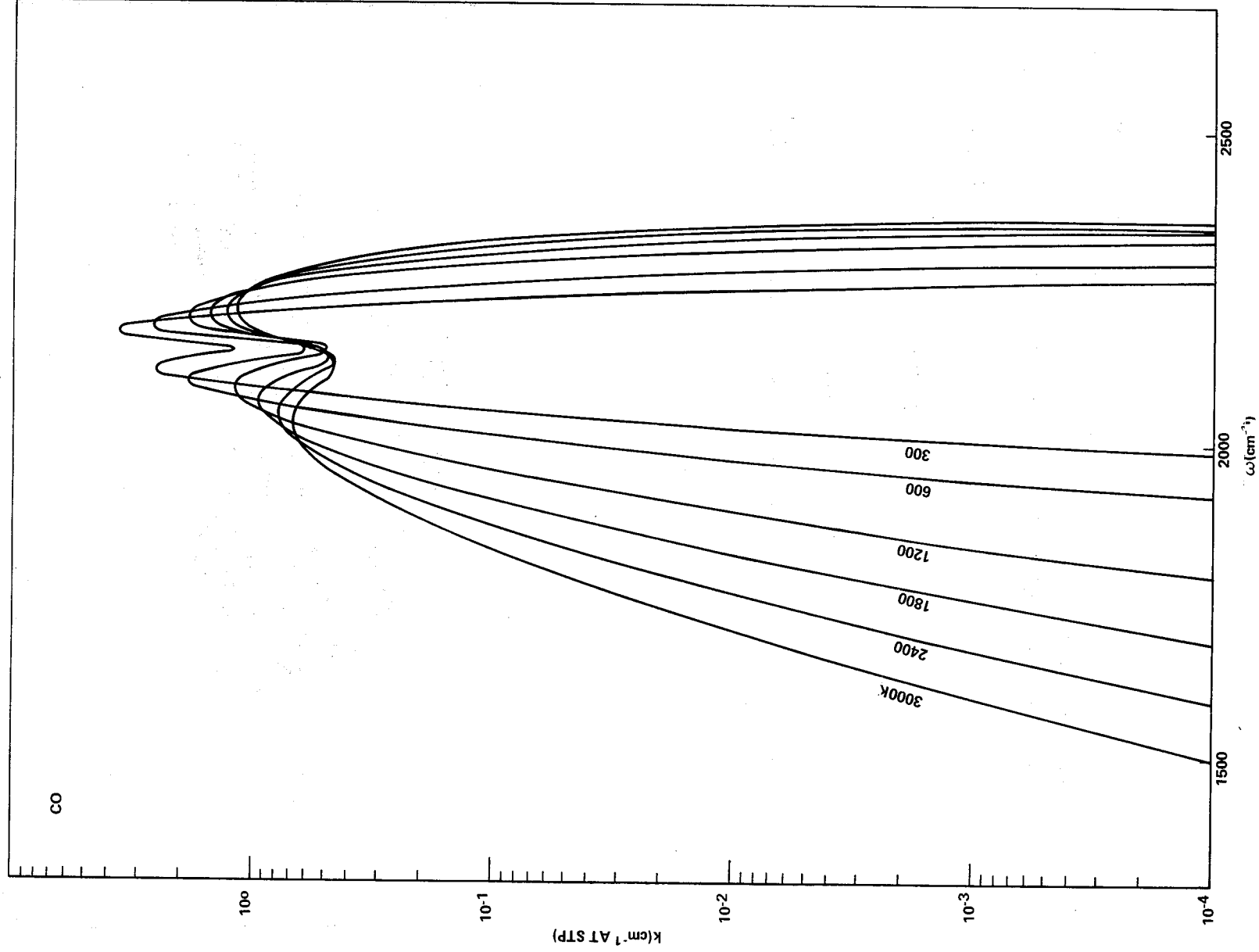


Figure 5-2. Absorption coefficient for CO at standard temperature and pressure.

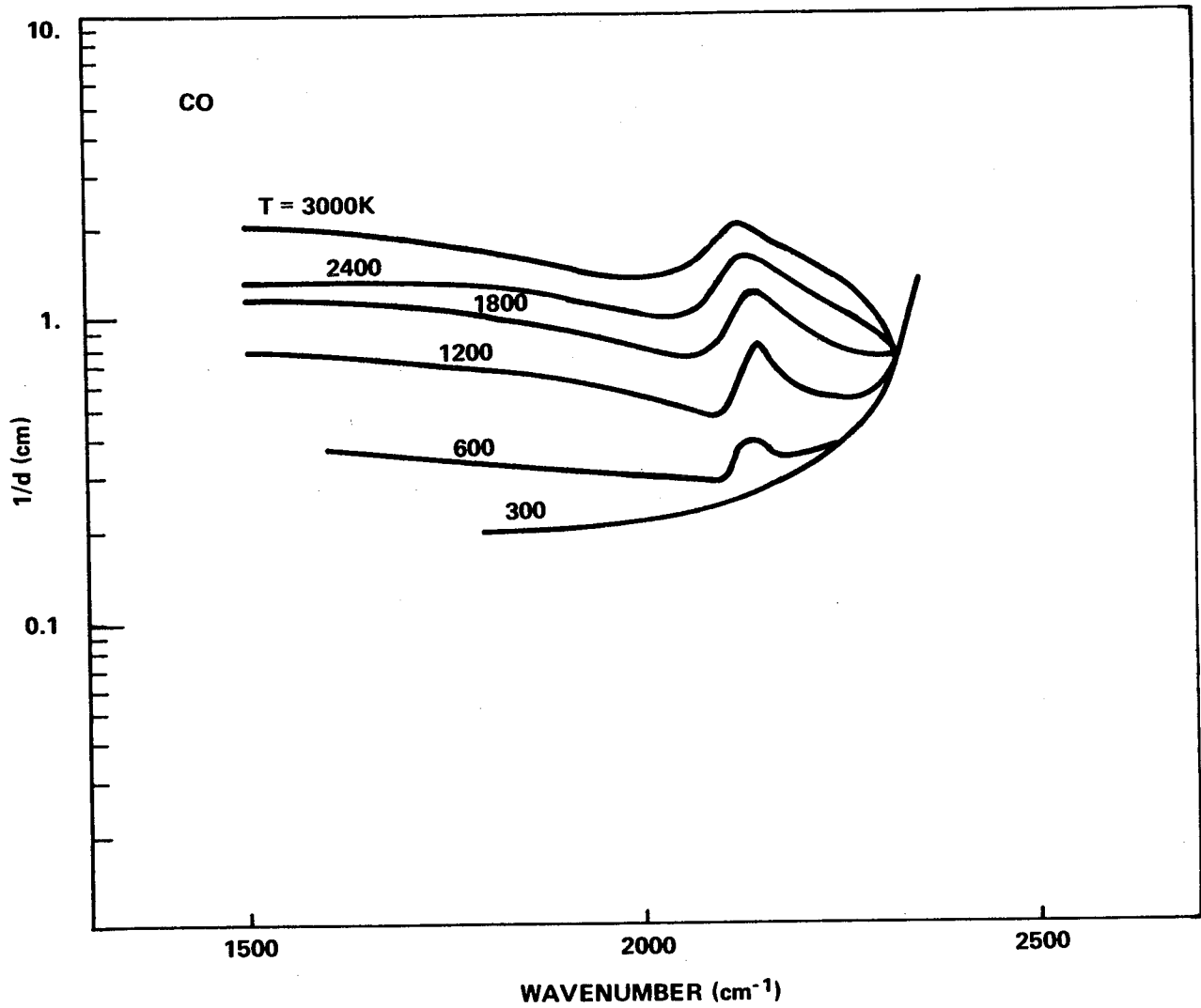


Figure 5-3. Line density for CO.

5.1.5.2 NO Data

Measured band strengths and line half-widths for NO are tabulated in Tables 5-3 and 5-4, respectively. Calculated values for the mean absorption coefficient  $k$  and for the line density ( $1/d$ ) are shown in Figures 5-4 and 5-5, respectively.

TABLE 5-3. NO BAND STRENGTHS ( $\text{cm}^{-2}\text{atm}^{-1}$  at STP)

Fundamental ( $1876 \text{ cm}^{-1}$ )	First Overtone ( $3724 \text{ cm}^{-1}$ )	Second Overtone ( $5544 \text{ cm}^{-1}$ )	Source
122 ± 6			Abels and Shaw (1966) <sup>a</sup>
76 ± 7	2.8 ± 0.5		Breeze and Ferriso (1964) <sup>b</sup>
145 ± 29	2.57 ± 0.51	0.015 ± 0.015	Dinsmore (1949) <sup>c</sup>
124 ± 22			Feinberg and Camac (1967) <sup>d</sup>
115 ± 9			Ford and Shaw (1965) <sup>e</sup>
70 to 77			Fukuda (1965) <sup>f</sup>
121			Havens (1938) <sup>g</sup>
138 ± 6			James (1964) <sup>h</sup>
	1.66	0.035	Meyer et al. (1965) <sup>i</sup>
70 ± 7	2.3 ± 0.6		Penner and Weber (1953) <sup>j</sup>
111 ± 7			Schurin and Clough (1963) <sup>k</sup>
	2.11 ± 0.10	0.0458 ± 0.0046	Schurin and Ellis (1966) <sup>l</sup>
128 ± 10			Varanasi and Penner (1966) <sup>m</sup>
82			Vincent-Geisse (1954) <sup>n</sup>
132	2.2	0.044	Recommended Values

- a. L. L. Abels and J. H. Shaw, *J. Molecular Spectroscopy*, no. 20, 1966, p. 11.
- b. J. C. Breeze and C. C. Ferriso, *J. Chem. Phys.*, no. 41, 1964, p. 3420.
- c. H. L. Dinsmore, dissertation, University of Minnesota, 1949.
- d. R. M. Feinberg and M. Camac, *J. Quant. Spectry. Radiative Transfer*, no. 7, 1967, p. 581.
- e. D. Ford and J. H. Shaw, *Bull. Am. Phys. Soc.*, no. 10, 1965, p. 636.

- f. K. Fukuda, J. Chem. Phys., no. 42, 1965, p. 521.
- g. R. J. Havens, dissertation, University of Wisconsin, 1938.
- h. T. C. James, J. Chem. Phys., no. 40, 1964, p. 762.
- i. C. Meyer, C. Haeusler, and P. Barchewitz, J. Phys. (Paris), no. 26, 1965, p. 305.
- j. S. S. Penner and D. Weber, J. Chem. Phys., no. 21, 1953, p. 649.
- k. B. Schurin and S. A. Clough, J. Chem. Phys., no. 38, 1963, p. 1855.
- l. B. Schurin and R. E. Ellis, J. Chem. Phys., no. 45, 1966, p. 2528.
- m. P. Varanasi and S. S. Penner, J. Quant. Spectry. Radiative Transfer, no. 7, 1967, p. 279.
- n. J. Vincent-Geisse, Compt. Rend., no. 239, 1954, p. 251.

TABLE 5-4. NO MEAN LINE HALF-WIDTHS ( $\text{cm}^{-1}\text{atm}^{-1}$  at 300K)

Broadener							Source
NO	N <sub>2</sub>	O <sub>2</sub>	H <sub>2</sub>	CO	CO <sub>2</sub>	H <sub>2</sub> O	
0.055							Abels and Shaw <sup>a</sup>
0.043							Penner <sup>b</sup>
0.05	(0.05)	(0.04)	(0.05)	(0.05)	(0.05)	(0.05)	Recommended Values (Estimates in Parentheses)

- a. L. L. Abels and J. H. Shaw, *J. Molecular Spectroscopy*, no. 20, 1966, p. 11.
- b. S. S. Penner, *Quantitative Molecular Spectroscopy and Gas Emissivities*, Addison-Wesley Co., Reading, Mass., 1959.

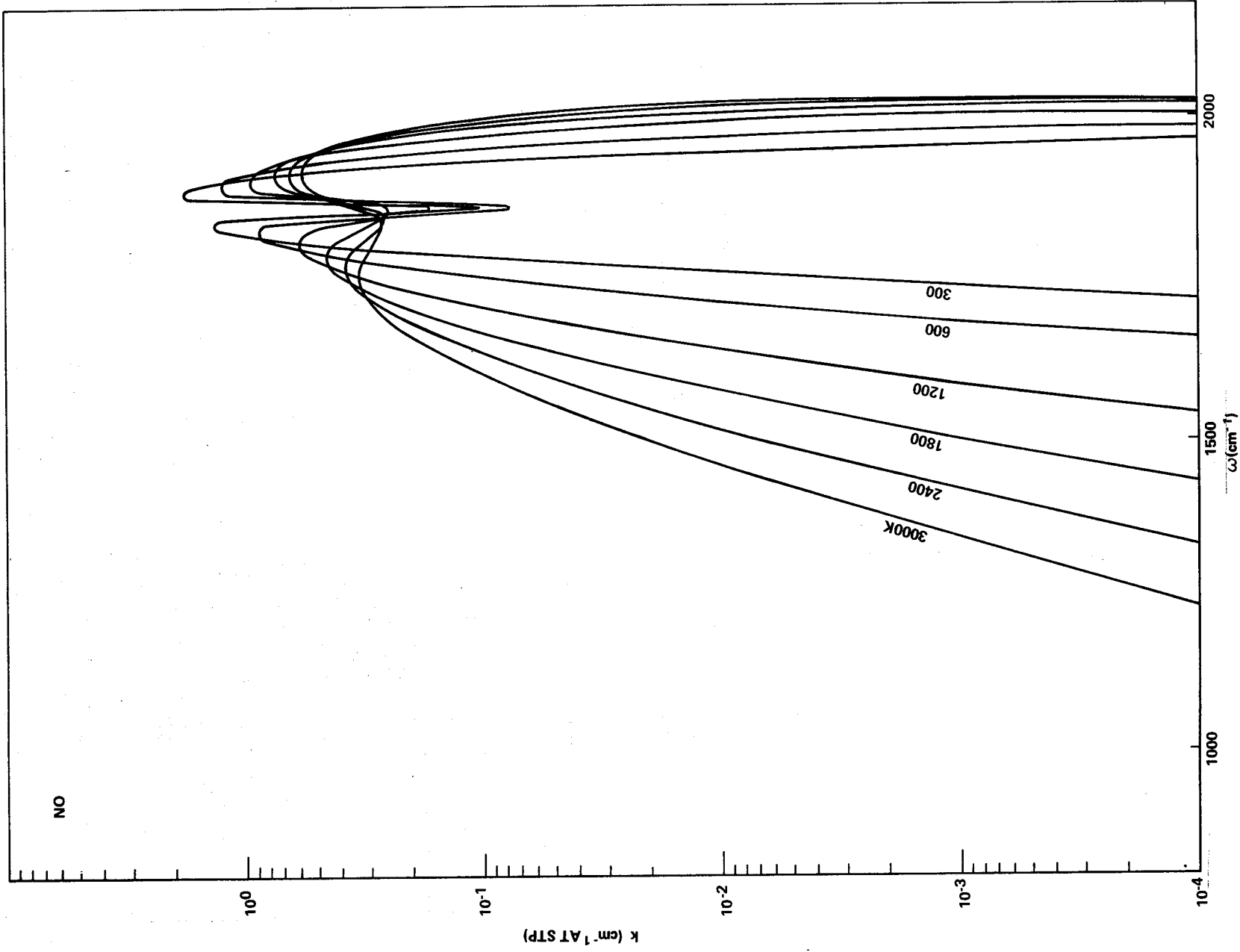


Figure 5-4. Absorption coefficient for NO at standard temperature and pressure.

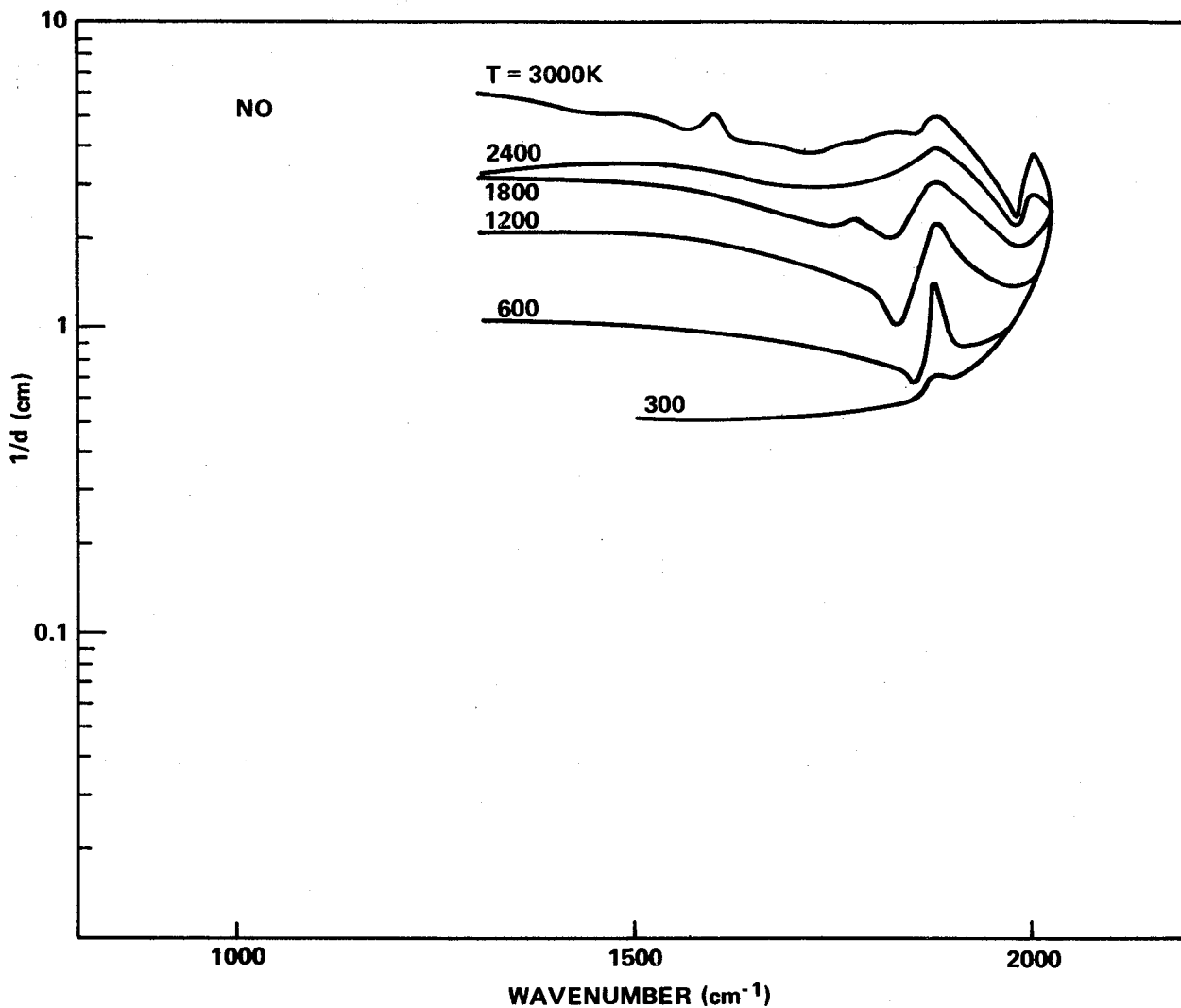


Figure 5-5. Line density for NO.

### 5.1.5.3 CN Data

Measured band strengths and line half-widths for CN are tabulated in Tables 5-5 and 5-6, respectively. Calculated values for the mean absorption coefficient  $k$  and for the line density ( $1/d$ ) are shown in Figures 5-6 and 5-7, respectively.

TABLE 5-5. CN BAND STRENGTHS ( $\text{cm}^{-2}\text{atm}^{-1}$  at STP)

Fundamental ( $2042 \text{ cm}^{-1}$ )	First Overtone ( $4058 \text{ cm}^{-1}$ )	Second Overtone ( $6048 \text{ cm}^{-1}$ )	Source
(110)	(2.3)	(0.044)	Recommended Values (Estimates in Parentheses)

TABLE 5-6. CN MEAN LINE HALF-WIDTHS ( $\text{cm}^{-1}\text{atm}^{-1}$  at STP)

Broadener		Source
CN	Other	
(0.05)	(0.05)	Recommended Values (Estimates in parentheses)

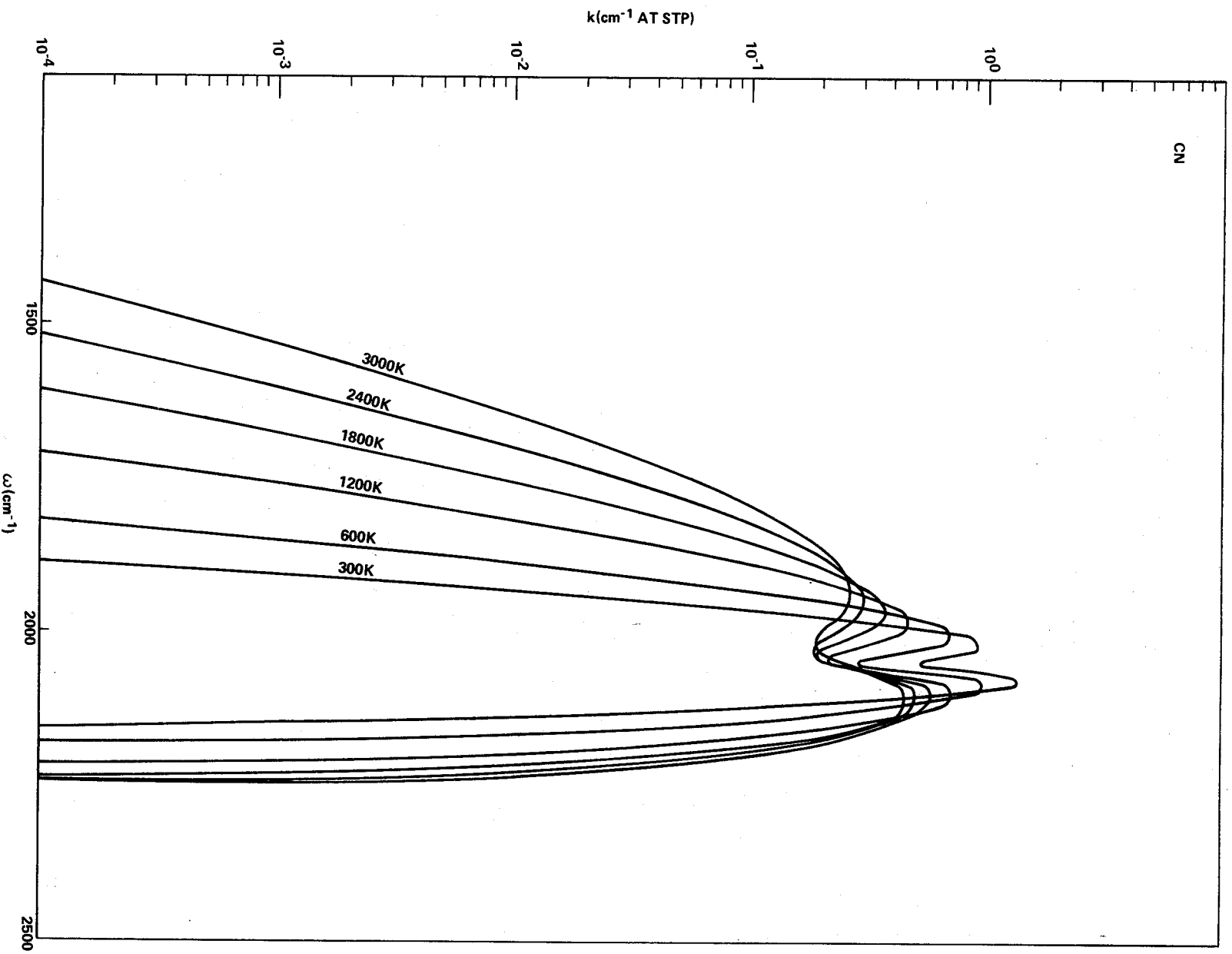


Figure 5-6. Absorption coefficient for CN at standard temperature and pressure.

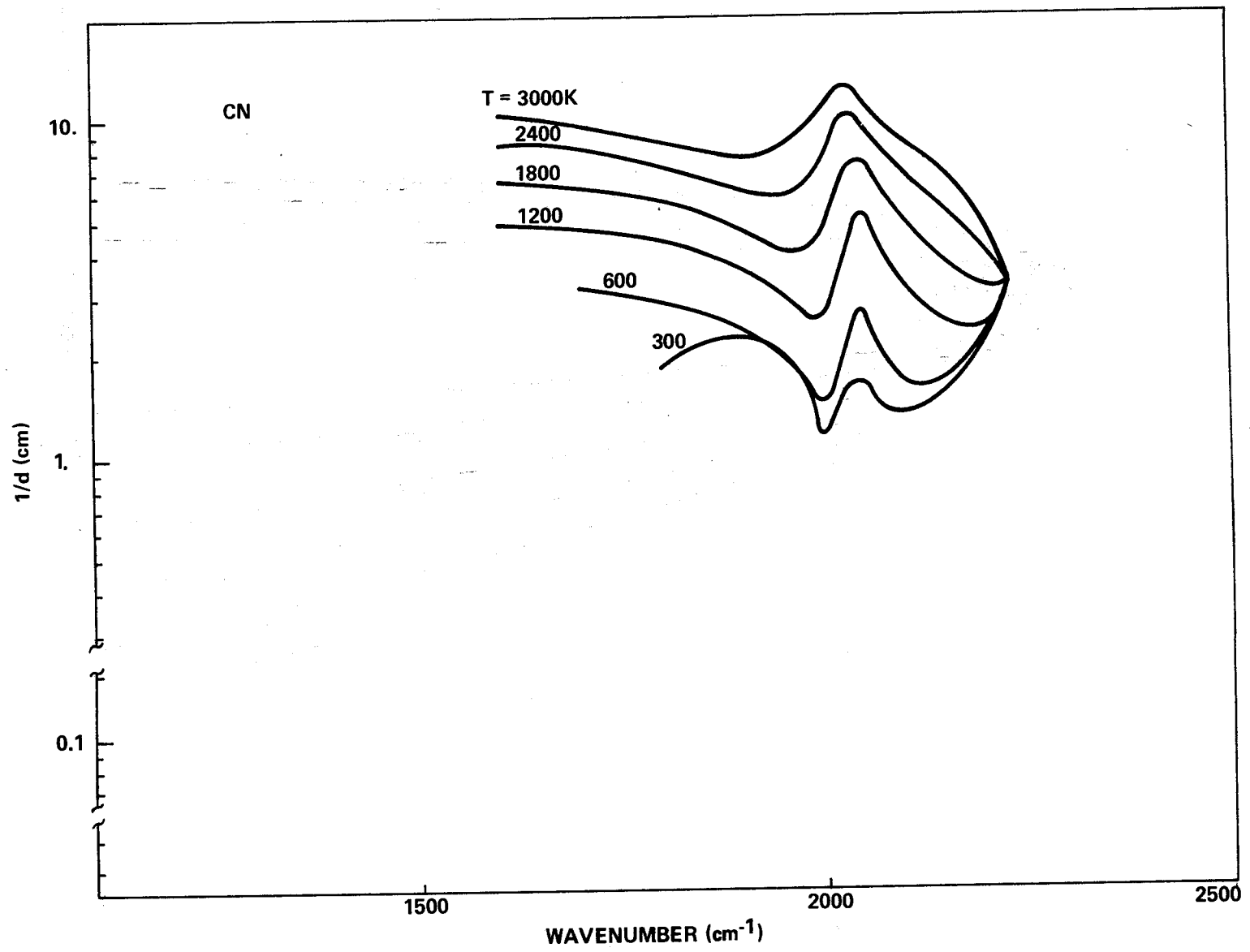


Figure 5-7. Line density for CN.

5.1.5.4 OH Data

Measured band strengths and line half-widths for OH are tabulated in Tables 5-7 and 5-8, respectively. Calculated values for the mean absorption coefficient  $k$  and for the line density ( $1/d$ ) are shown in Figures 5-8 and 5-9, respectively.

TABLE 5-7. OH BAND STRENGTHS ( $\text{cm}^{-2}\text{atm}^{-1}$  at STP)

Fundamental ( $3570 \text{ cm}^{-1}$ )	First Overtone ( $6974 \text{ cm}^{-1}$ )	Source
(110)	(4.4)	Recommended Values (Estimates in parentheses)

TABLE 5-8. OH MEAN LINE HALF-WIDTHS ( $\text{cm}^{-1}\text{atm}^{-1}$  at STP)

Broadener		Source
OH	Other	
(0.5)	(0.05)	Recommended Values (Estimates in parentheses)

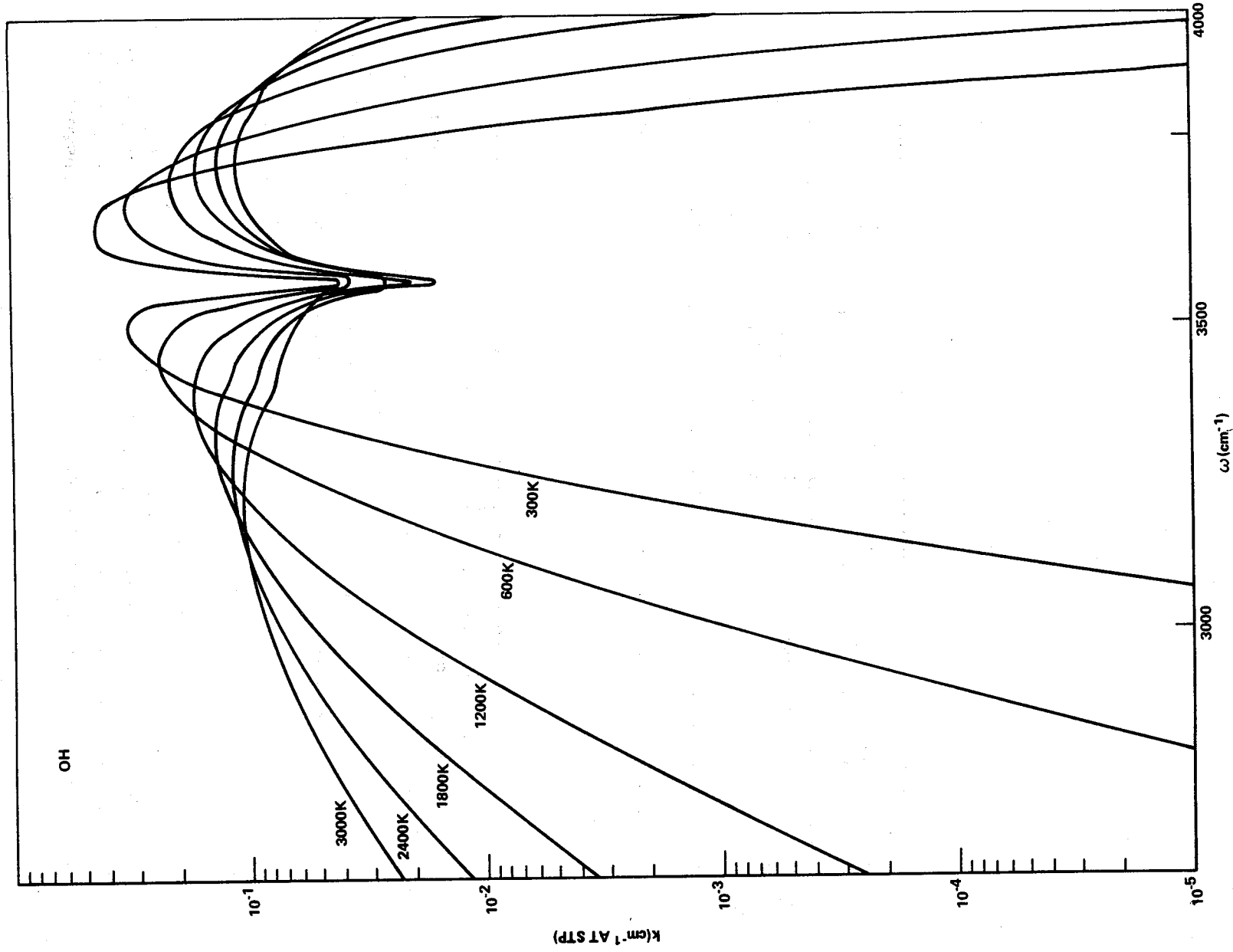


Figure 5-8. Absorption coefficient for OH at standard temperature and pressure.

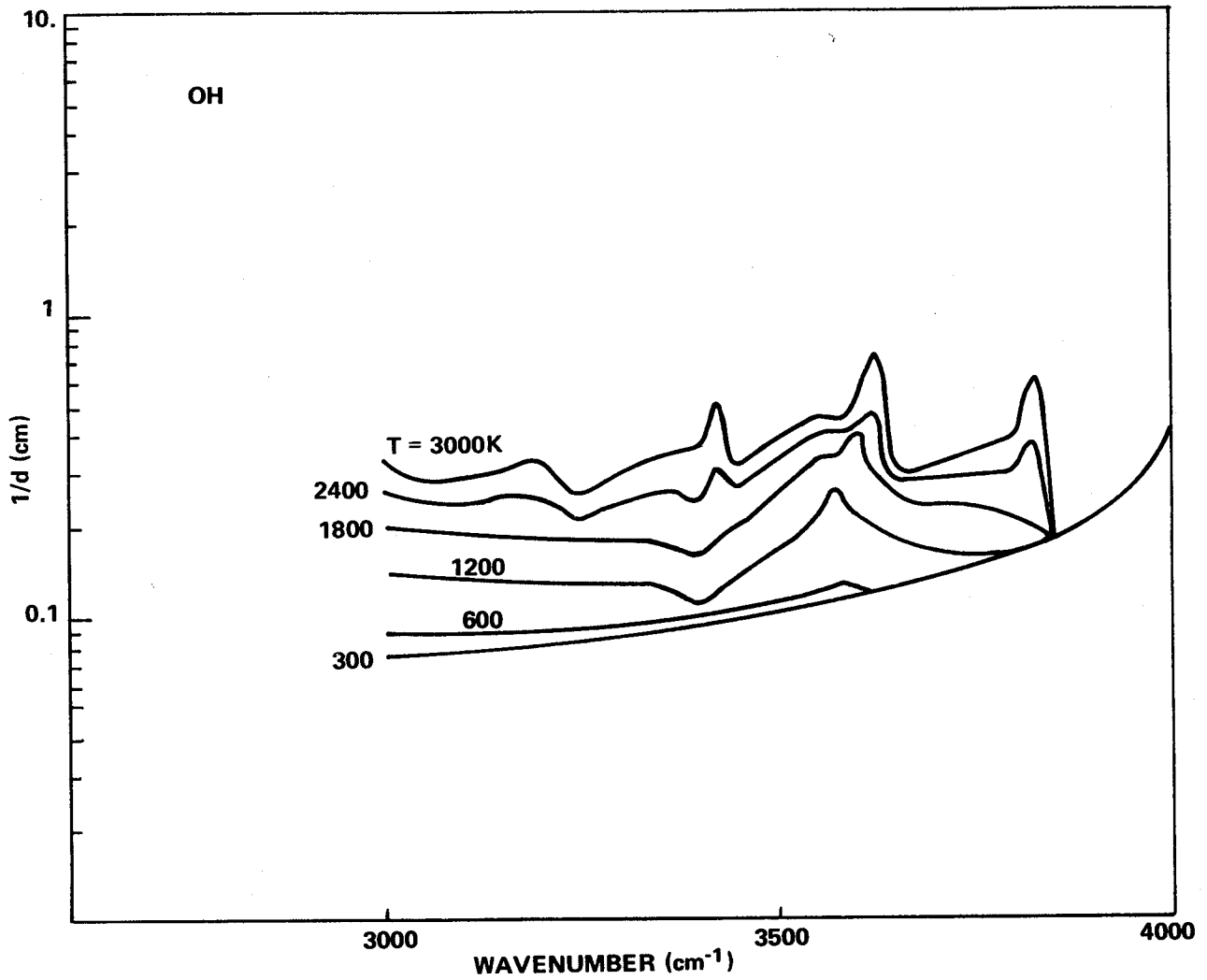


Figure 5-9. Line density for OH.

5.1.5.5 HCl Data

Measured band strengths and line half-widths for HCl are tabulated in Tables 5-9 and 5-10, respectively. Calculated values for the mean absorption coefficient  $k$  and for the line density ( $1/d$ ) are shown in Figures 5-10 and 5-11, respectively.

TABLE 5-9. HCl BAND STRENGTHS ( $\text{cm}^{-2}\text{atm}^{-1}$  at STP)

Fundamental ( $2886 \text{ cm}^{-1}$ )	First Overtone ( $5668 \text{ cm}^{-1}$ )	Source
$157 \pm 6$		Babrov et al. (1959) <sup>a</sup>
$143 \pm 8$	3.15	Benedict et al. (1956) <sup>b</sup>
$174 \pm 33$	$4.00 \pm 0.33$	Penner and Weber (1953) <sup>c</sup>
155	3.8	Recommended Values

- a. H. Babrov, G. Ameer, and W. Benesch, *J. Mol. Spectry.*, no. 3, 1959, p. 185.
- b. W. S. Benedict, R. Herman, G. E. Moore, and S. Silverman, *Can. J. Phys.*, no. 34, 1956, p. 850.
- c. S. S. Penner and D. Weber, *J. Chem. Phys.*, no. 21, 1953, p. 649.

TABLE 5-10. HCl MEAN LINE HALF-WIDTH ( $\text{cm}^{-1}\text{atm}^{-1}$  at STP)

Broadener							Source
HCl	N <sub>2</sub>	He	Ne	Ar	Kr	Xe	
0.13- 0.25	0.028- 0.11	0.025	0.02	0.01- 0.05	0.02- 0.07	0.07- 0.025	Babrov et al. (1959) <sup>a</sup>  Tipping and Herman (1970) <sup>b</sup>
0.2	(0.05)						Recommended Values (Estimates in Parentheses)

a. H. Babrov, G. Ameer, and W. Benesch, *J. Mol. Spectry.*, no. 3, 1959, p. 185.

b. R. H. Tipping and R. M. Herman, *J. Quant. Spectry. Radiative Transfer*, no. 10, 1970, p. 881.

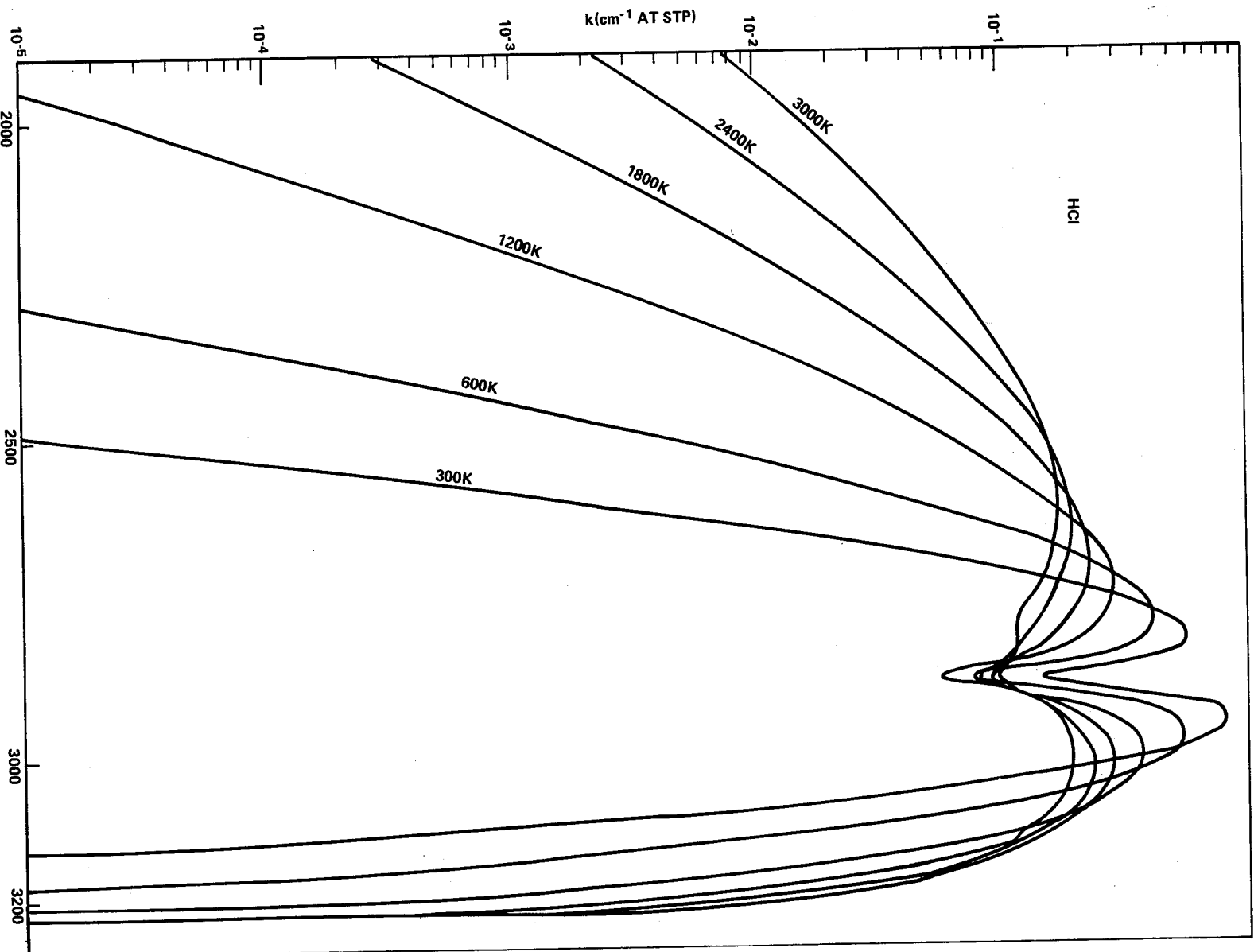


Figure 5-10. Absorption coefficient for HCl at standard temperature and pressure.

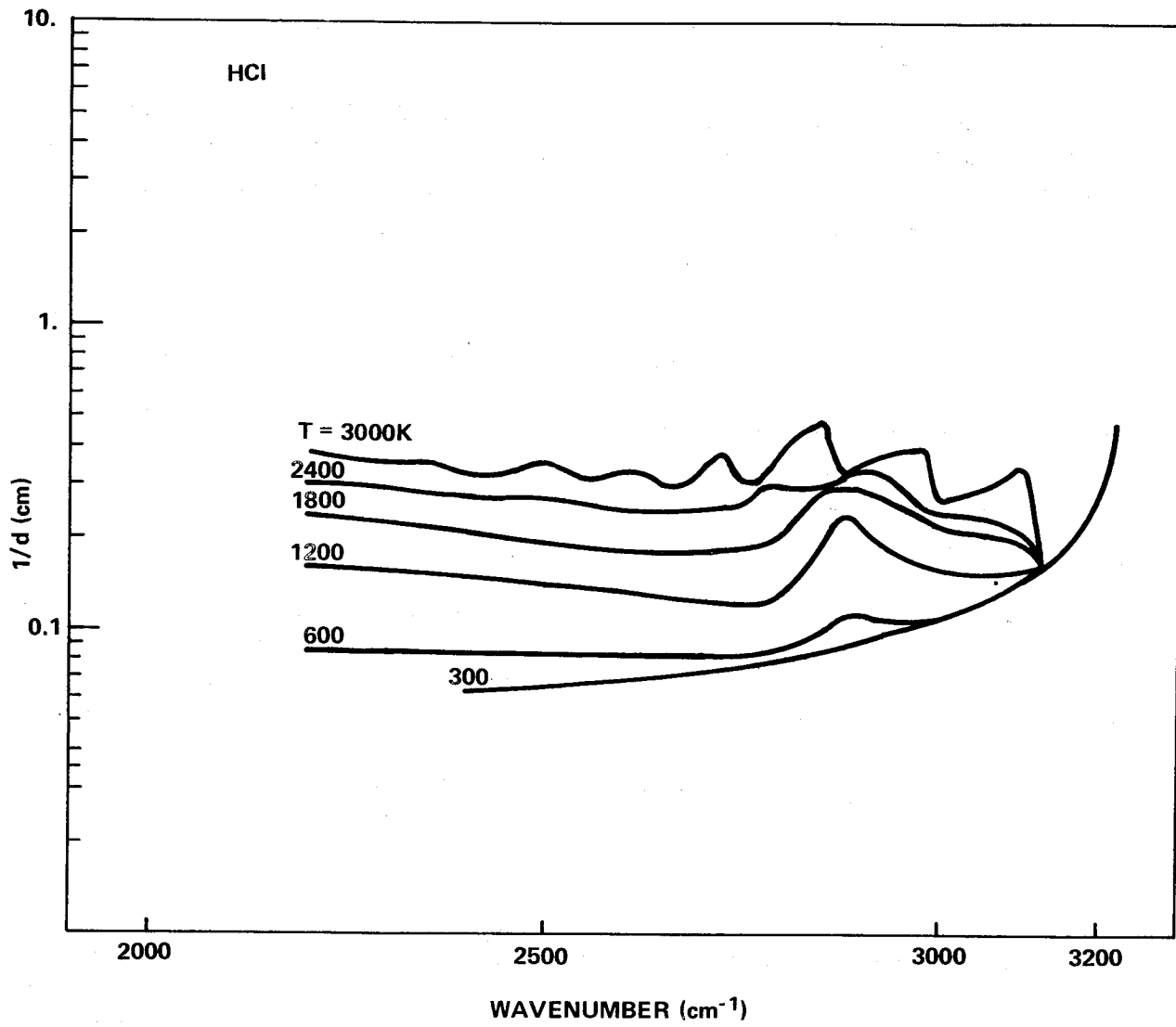


Figure 5-11. Line density for HCl.

5.1.5.6 HF Data

Measured band strengths and line half-widths for HF are tabulated in Tables 5-11 and 5-12, respectively. Calculated values for the mean absorption coefficient  $k$  and for the line density  $(1/d)$  are shown in Figures 5-12 and 5-13, respectively.

TABLE 5-11. HF BAND STRENGTHS ( $\text{cm}^{-2}\text{atm}^{-1}$  at STP)

Fundamental ( $3962 \text{ cm}^{-1}$ )	First Overtone ( $7751 \text{ cm}^{-1}$ )	Source
453		Kuipers (1958) <sup>a</sup>
450	(11)	Recommended Values (Estimates in Parentheses)

a. G. A. Kuipers, J. Mol. Spectry., no. 2, 1958, p. 75.

TABLE 5-12. HF MEAN LINE HALF-WIDTHS ( $\text{cm}^{-1}\text{atm}^{-1}$  at STP)

Broadener		Source
HF	Other	
0.07-0.51 (at 390K)		Kuipers (1958) <sup>a</sup>
0.05	(0.05)	Recommended Values (Estimates in Parentheses)

a. G. A. Kuipers, J. Mol. Spectry., no. 2, 1958, p. 75.

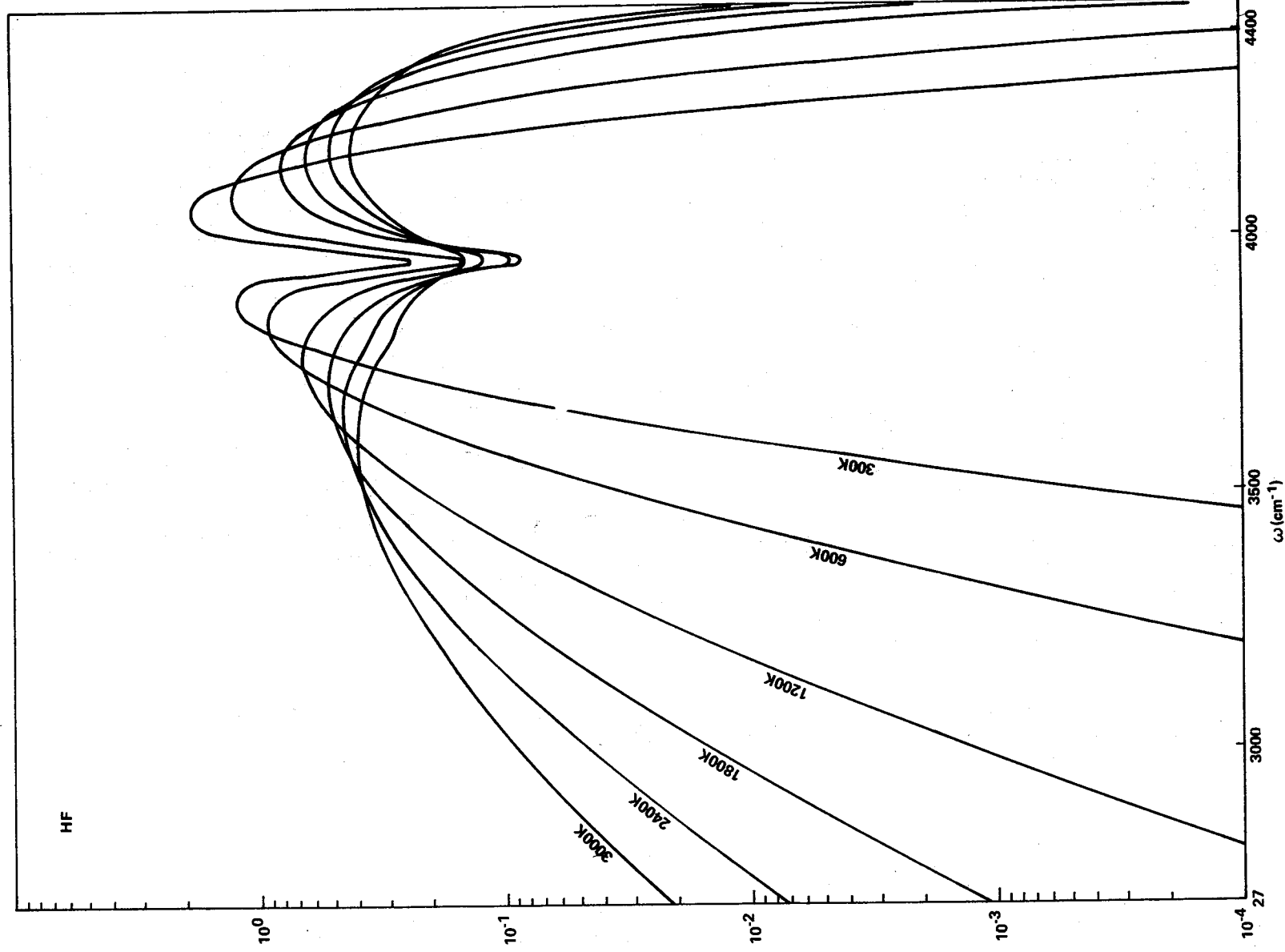


Figure 5-12. Absorption coefficient for HF at standard temperature and pressure.

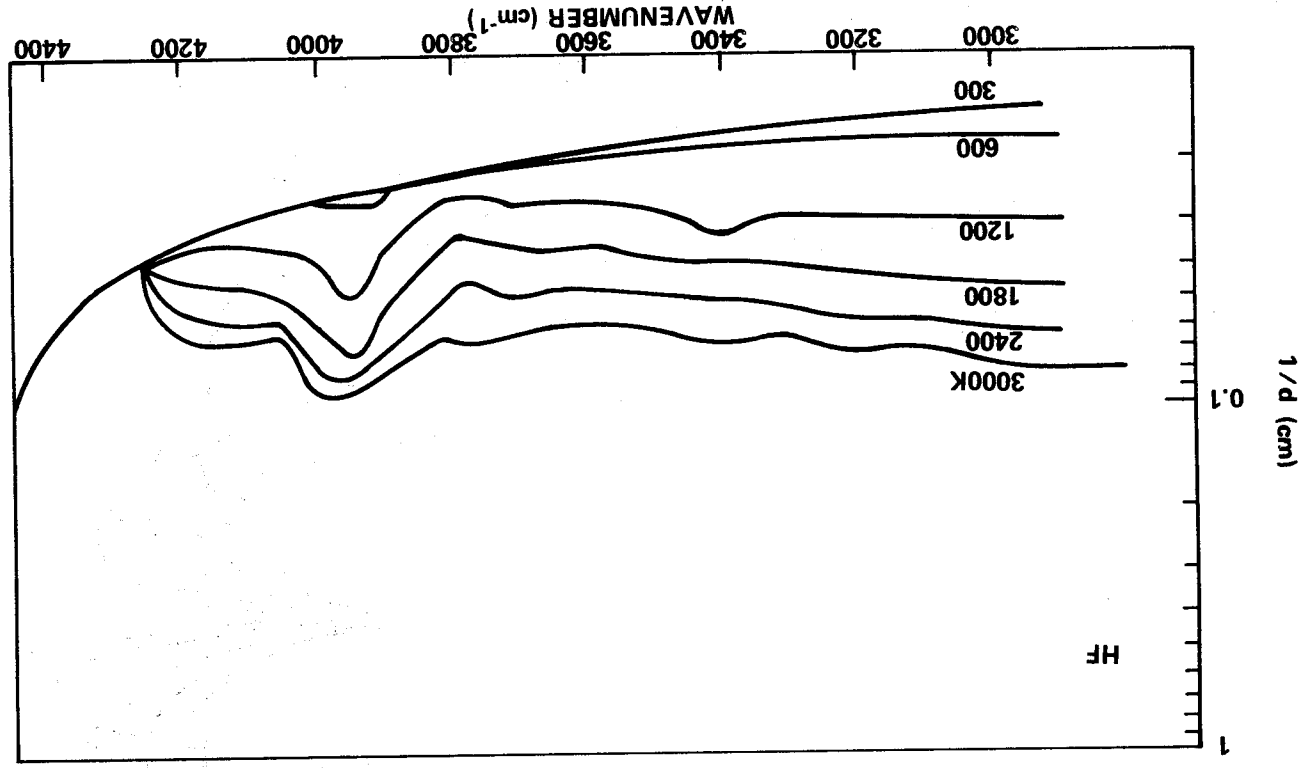


Figure 5-13. Line density for HF.

## 5.2 POLYATOMIC MOLECULES

### 5.2.1 CARBON DIOXIDE (CO<sub>2</sub>)

The linear symmetric molecule CO<sub>2</sub> has three degrees of freedom associated with vibration. The first, a symmetric vibration in which there is no change in electric dipole moment, is infrared inactive. The second is a doubly degenerate vibration described by the quantum number  $v_2$ . The level determined by  $v_2$  has a degeneracy of  $v_2 + 1$ . A second quantum number,  $l$ , which represents the angular momentum associated with vibration and which can assume values of  $v_2, v_2 - 2, \dots, 1$  or  $0$ , partially resolves the degeneracy; a level described by  $v_2$  and  $l$  is either singly or doubly degenerate, depending on whether  $l = 0$  or  $l > 0$ . Transitions for which  $v_2$  and  $l$  change by unity and  $v_1$  and  $v_3$  do not change are responsible for the 15- $\mu$  band of CO<sub>2</sub>. The third is an unsymmetric vibration described by the quantum number  $v_3$ . The transitions for which  $v_3$  changes by unity but the other quantum numbers do not change give rise to the 4.3- $\mu$  band.

The gross structure of a CO<sub>2</sub> vibration-rotation band for which  $\Delta l = 0$ , such as the 4.3- $\mu$  band, is quite similar to that of a diatomic molecule, so the equations previously developed for diatomic molecules can be used, with only slight modifications, for CO<sub>2</sub>. Thus, in the weak-line approximation, the equations previously developed for diatomic molecules can be used directly by replacing the single summation over  $v$  by a double summation over  $v$  and  $v_3$ . Specifically, in the weak-line approximation, the emissivity is given by

$$\epsilon_{\omega} = 1 - \exp \left[ -u \overline{S(\omega)/d(\omega)} \right] \quad (5-14)$$

where

$$\overline{S(\omega)/d(\omega)} = \sum_{v=0}^{\infty} \sum_{v_3=0}^{\infty} \left[ S_{vv_3}^{(-)}(\omega) + S_{vv_3}^{(+)}(\omega) \right] / d_{vv_3}(\omega) .$$

Hence, using the random Elsasser model and approximating the error function by the exponential function (Section 5.1.3), or, equivalently, assuming the statistical model, one obtains

$$\epsilon_{\omega} = 1 - \exp \left[ - 2 (\gamma u)^{1/2} \overline{S^{1/2}(\omega)/d(\omega)} \right] \quad , \quad (5-15)$$

where

$$\overline{S^{1/2}(\omega)/d(\omega)} = \sum_{v=0}^{\infty} \sum_{v_3=0}^{\infty} \left( \frac{1}{2} g^v \right)^{1/2} \left\{ \left[ S_{vv_3}^{(-)}(\omega) \right]^{1/2} + \left[ S_{vv_3}^{(+)}(\omega) \right]^{1/2} \right\} / d_{vv_3}(\omega) .$$

For temperatures less than several hundred degrees Kelvin, it is feasible to perform line-by-line calculations for CO<sub>2</sub>. Measured values for the absolute band intensity, theoretical values for the relative rotational intensity in individual bands, and the spectral locations and widths of the spectral lines can be used to synthesize a high-resolution spectrum.

This approach is useful when only a few temperature and pressure profiles are required, and it has been used, for example, to obtain rather precise representations of the spectral transmission of the planetary atmospheres. However, the rapid increase in line density with temperature usually leads to the use of band model procedures at intermediate temperatures (see Section 6.1.2).

Theoretical calculations of band model parameters have been performed for CO<sub>2</sub> for temperatures up to 3000K. Many of these results have been verified by experiment (see Section 7). These calculated values are therefore believed to provide an adequate representation of the spectral properties of CO<sub>2</sub>.

The quantities  $\overline{(S/d)}_{\text{STP}}$  and  $1/d = \left[ \overline{(S^{1/2}/d)^2} / \overline{(S/d)} \right]_{\text{STP}}$  have been tabulated for the 4.3- $\mu$  fundamental band and the 2.7- $\mu$  overtone band (see General Appendix). These bands are the only ones which contribute appreciably to the total emission at moderate optical depths and high temperatures, since the 1.9- $\mu$  and shorter wavelengths are weak.

Measured values for the CO<sub>2</sub> band strengths and the line widths are tabulated in Tables 5-13 and 5-14, respectively. The 2.7- $\mu$  transition is a combination band for which the lower state is not the ground state. Consequently, the band strength is temperature dependent (see Section 2.3.3.2); this dependence is shown in Figure 5-14. Theoretical values for the mean absorption coefficient  $k$  and the line structure parameter  $1/d_0$  are plotted in Figures 5-15 through 5-21.

CHAPTER 5 – REPRESENTATIONS  
FOR SPECIFIC MOLECULES

TABLE 5-13. MEASURED CO<sub>2</sub> INTEGRATED BAND STRENGTHS  
AT 300K (cm<sup>-2</sup>atm<sup>-1</sup> at STP)

2- $\mu$ <sup>a</sup>	2.7- $\mu$ <sup>b</sup>	4.3- $\mu$	4.9- $\mu$ <sup>c</sup>	15- $\mu$	Footnote
1.57					d
1.61					e
1.88					f
	66.4	2693	0.14 <sup>g</sup>	161 $\pm$ 20	h
	91	2500		330 $\pm$ 90	i
	80	2640		161	j
		2500		220	j
	77.8	2943	0.161 <sup>k</sup>		l
			0.38 <sup>m</sup>		n
				240	o
				179	p
				220	q
				187	r
		2970 $\pm$ 60		240 $\pm$ 5	s
				172	t
				255	u
				240	v
				240	w
				220 $\pm$ 10	x
				246	y
				240 $\pm$ 20	z
1.6	67	2700	0.6	240	Recommended Values

[Footnotes on following pages]

- a. Includes  $2\nu_1 + \nu_3$ ,  $\nu_1 + 2\nu_2 + \nu_3$ , and  $4\nu_2 + \nu_3$ .
- b. Includes  $2\nu_2 + \nu_3$  and  $\nu_1 + \nu_3$ .
- c. Includes  $\nu_1 + \nu_2$ ,  $3\nu_2$  and two transitions from excited states:  $01^10 - 20^00$  and  $01^10 - 12^20$ .
- d. R. F. Calfee and W. S. Benedict, NBS Tech. Note 332, Washington, D. C., 1966.
- e. D. E. Burch, D. A. Gryvnak, and R. R. Patty, Absorption by  $\text{CO}_2$  Between 4500 and 5400  $\text{cm}^{-1}$ , Sci. Rept. No. U-2955, Aeronutronic Div. of Philco, Newport Beach, Calif., 1964.
- f. S. S. Penner, Quantitative Molecular Spectroscopy and Gas Emissivities, Addison-Wesley, Reading, Mass., 1959.
- g.  $00^00 - 11^10$  transition only.
- h. D. F. Eggers, Jr. and B. L. Crawford, Jr., J. Chem. Phys., no. 19, 1951, p. 1554.
- i. D. E. Burch, D. Gryvnak, E. B. Singleton, W. L. France, and D. Williams, Infrared Absorption by Carbon Dioxide, Water Vapor and Minor Atmospheric Constituents, AFCRL Res. Rept. AFCRL-62-698, Air Force Cambridge Res. Lab., Bedford, Mass., 1962.
- j. J. Fahrenfort, in Infrared Spectroscopy and Molecular Structure (M. Davies, ed.), Elsevier, Amsterdam, 1963, p. 377 et seq.
- k.  $\left. \begin{array}{l} 01^10 - 20^00 \\ 01^10 - 12^20 \\ 00^00 - 11^10 \end{array} \right\}$  transition only.
- l. E. K. Plyler, E. D. Tidwell, and W. S. Benedict, J. Opt. Soc. Am., no. 52, 1962, p. 1017.
- m.  $00^00 - 03^10$  transition only.
- n. W. S. Benedict, Theoretical Studies of Infrared Spectra of Atmospheric Gases, Final Rept., AF19(604)-1001, Johns Hopkins Appl. Phys. Lab., Baltimore, Md., 1956.

CHAPTER 5 – REPRESENTATIONS  
FOR SPECIFIC MOLECULES

- o. L. D. Kaplan and D. F. Eggers, Jr., *J. Chem. Phys.*, no. 25, 1956, p. 876.
- p. O. Fues, *Z. Physik*, no. 46, 1927, p. 519.
- q. P. E. Martin and E. F. Barker, *Phys. Rev.*, no. 41, 1932, p. 291.
- r. A. M. Thorndike, *J. Chem. Phys.*, no. 15, 1947, p. 868.
- s. B. Schurin, *J. Chem. Phys.*, no. 33, 1960, p. 1878.
- t. D. Weber, R. J. Holm, and S. S. Penner, *J. Chem. Phys.*, no. 20, 1952, p. 1820.
- u. R. P. Madden, *J. Chem. Phys.*, no. 35, 1961, p. 2083.
- v. J. Overend, M. J. Youngquist, E. C. Curtis, and B. Crawford, Jr., *J. Chem. Phys.*, no. 30, 1959, p. 532.
- w. C. B. Ludwig, C. C. Ferriso, and L. Acton, *J. Opt. Soc. Am.*, no. 56, 1966, p. 1685.
- x. P. Varanasi and J. L. Lauer, *J. Quant. Spectry. Radiative Transfer*, no. 6, 1966, p. 127.
- y. M. Wolk, *J. Quant. Spectry. Radiative Transfer*, no. 7, 1967, p. 1.
- z. C. N. Harward and R. R. Patty, *J. Opt. Soc. Am.*, no. 58, 1968, p. 188.

TABLE 5-14. COLLISION-BROADENED LINE HALF-WIDTHS AT  
 HALF-HEIGHT FOR CO<sub>2</sub> AT STP (in cm<sup>-1</sup>)

Broadener						Source
CO <sub>2</sub>	N <sub>2</sub>	O <sub>2</sub>	H <sub>2</sub>	A	He	
0.1						Madden <sup>a</sup>
<0.12						Adel <sup>b</sup>
0.079						Benedict, Silverman <sup>c</sup>
0.088	0.06					Kostkowski <sup>d</sup>
	0.067					Kaplan, Eggers <sup>e</sup>
1.3x	x	0.81x	1.17x	0.78x	0.59x	Burch, et al. <sup>f, g</sup>
0.10	0.07	0.055	0.08	0.05	0.04	Recommended Values

- a. R. P. Madden, J. Chem. Phys., no. 35, 1961, p. 2083.
- b. A. Adel, Phys. Rev., no. 52, 1953, p. 53.
- c. W. S. Benedict and S. Silverman, Phys. Rev., no. 94, 1954, p. 752 (A).
- d. H. J. Kostowski, dissertation, The Johns Hopkins University, 1955.
- e. L. D. Kaplan and D. F. Eggers, J. Chem. Phys., no. 25, 1956, p. 876.
- f. D. E. Burch, D. Gryvnak, E. B. Singleton, W. L. France, and D. Williams, AFCRL-62-698, 1962.
- g. Only the ratios of the line width to the line width in pure N<sub>2</sub> were measured. The quantity x refers to the undetermined N<sub>2</sub>-broadened line half-width.

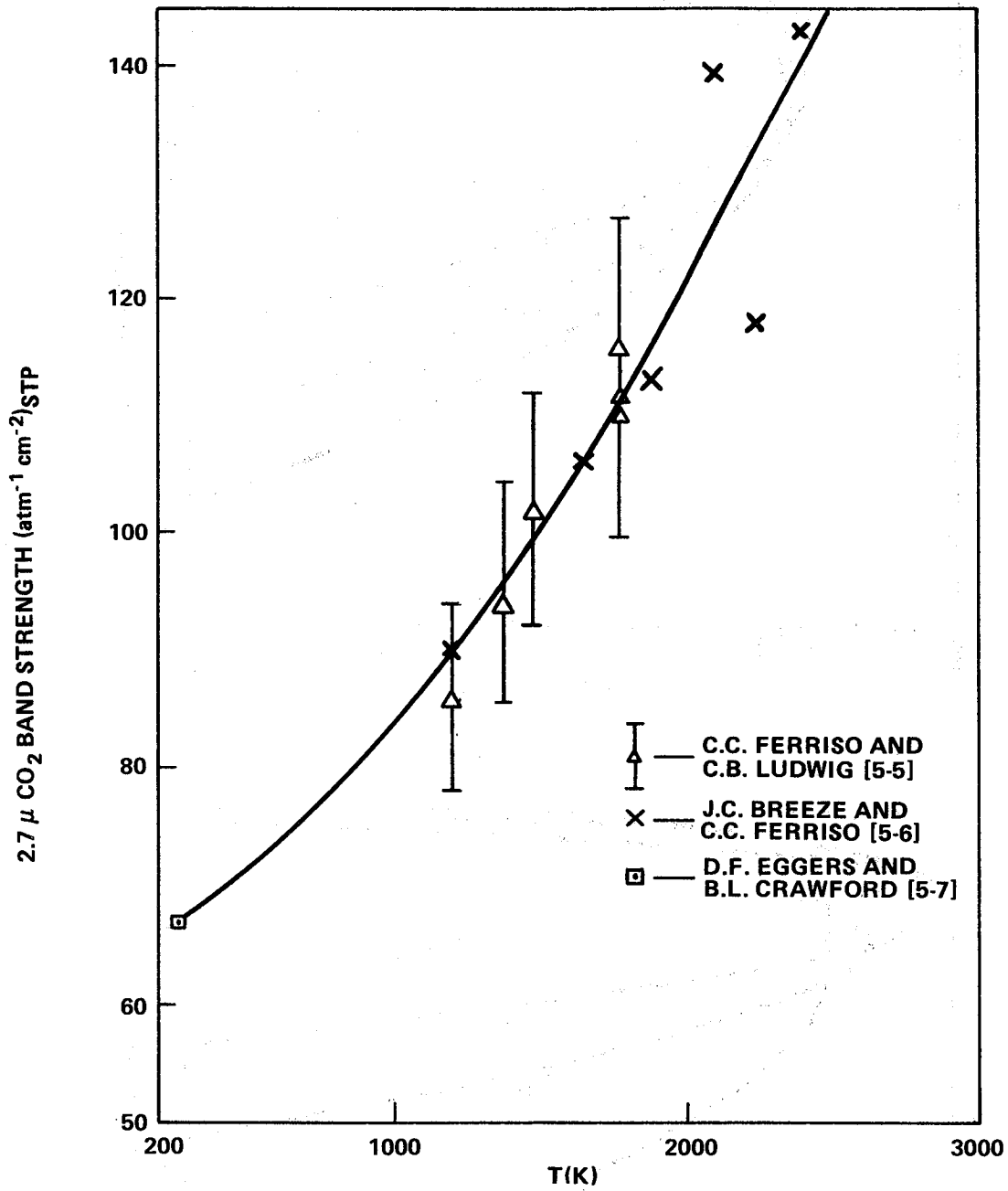


Figure 5-14. The total band strength of the 2.7-μ band of CO<sub>2</sub> as a function of temperature.

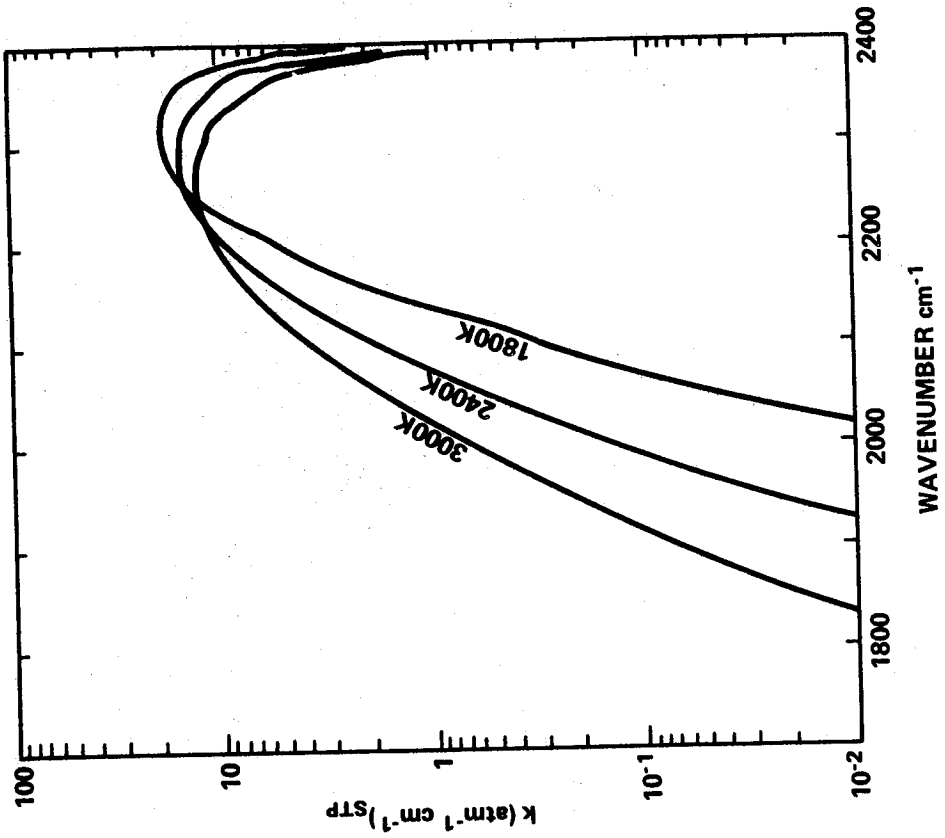


Figure 5-16.  $\bar{k} = \overline{S/d}$  of  $C^{12}O_2$  versus wavenumber for  $T = 1800, 2400, \text{ and } 3000\text{K}$ .

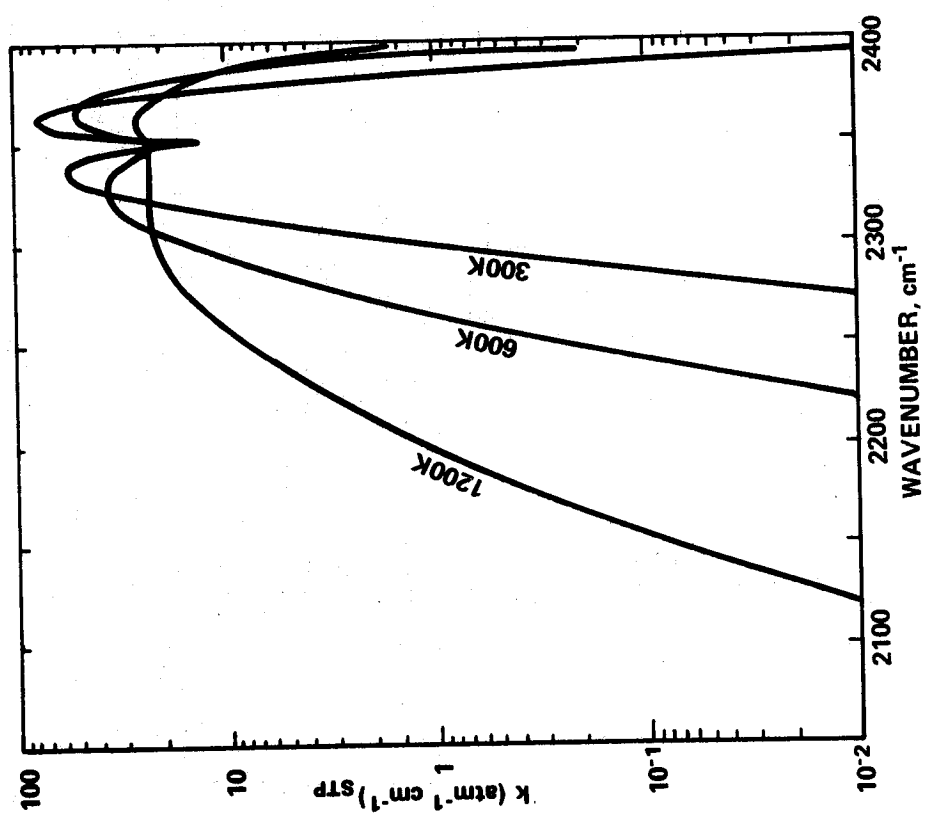


Figure 5-15.  $\bar{k} = \overline{S/d}$  of  $C^{12}O_2$  versus wavenumber for  $T = 300, 600, \text{ and } 1200\text{K}$ .

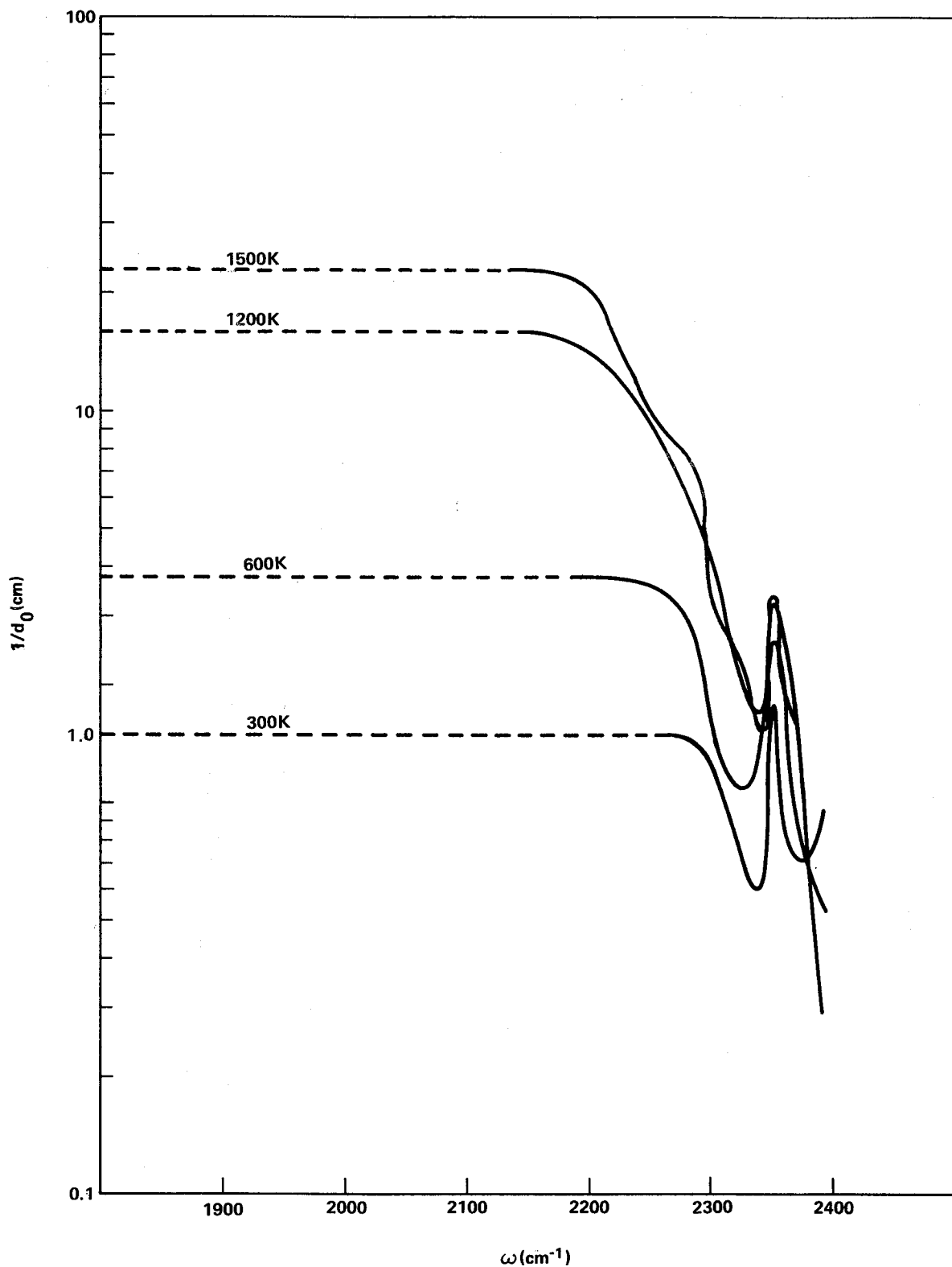


Figure 5-17. Values of the line density parameter  $1/d_0$  for the 4.3- $\mu$  band for  $C^{12}O_2$ . (The dashed portions of the curves are extrapolated values. These data are tabulated in the General Appendix.)

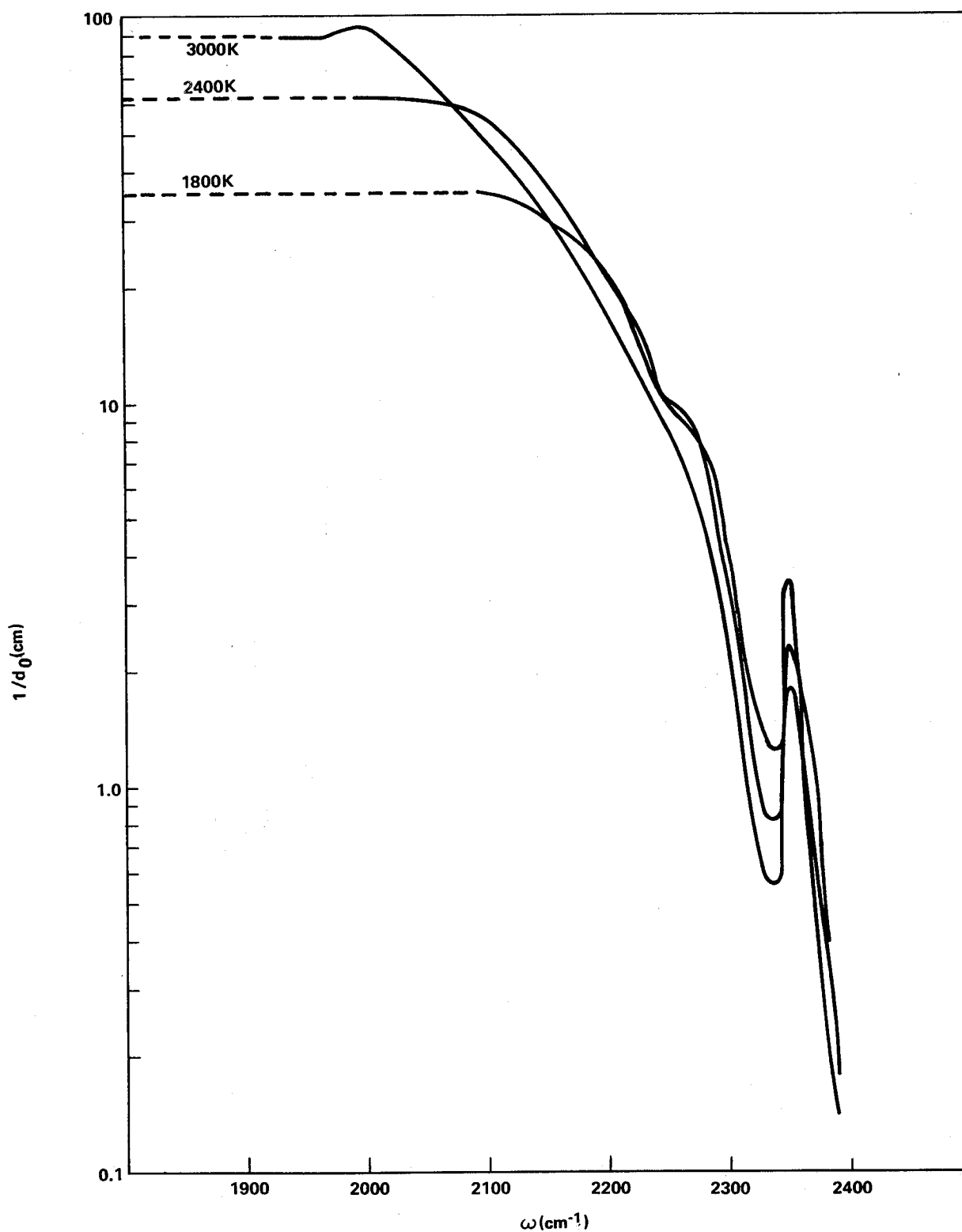


Figure 5-18. Values of the line density parameter  $1/d_0$  for the 4.3- $\mu$  band of  $C^{12}O_2$ . (The dashed portions of the curves are extrapolated values. These data are tabulated in the General Appendix.)

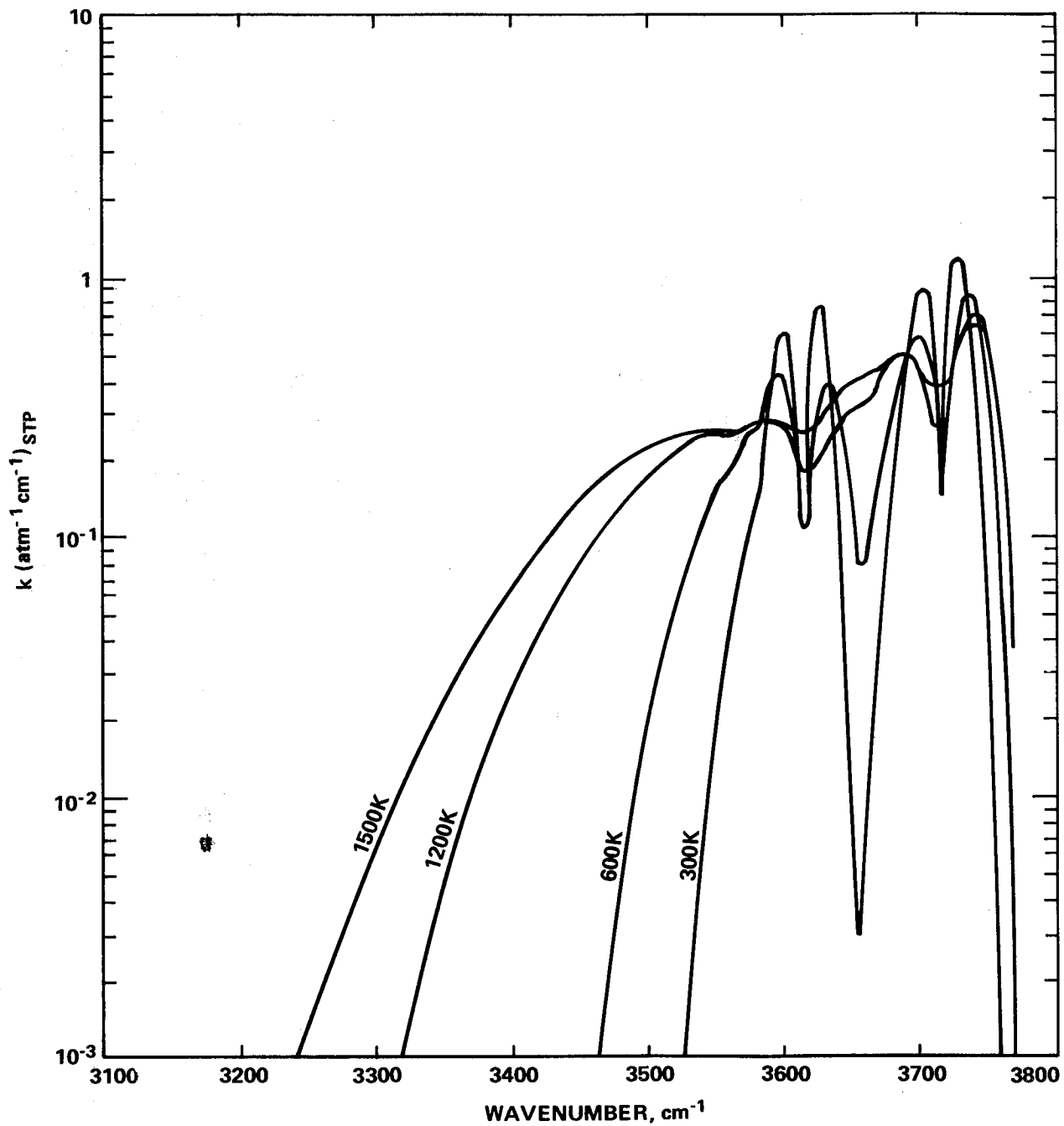


Figure 5-19.  $k = \overline{S/d}$  of  $\text{C}^{12}\text{O}_2$  versus wavenumber  
for  $T = 300, 600, 1200,$  and  $1500\text{K}$ .

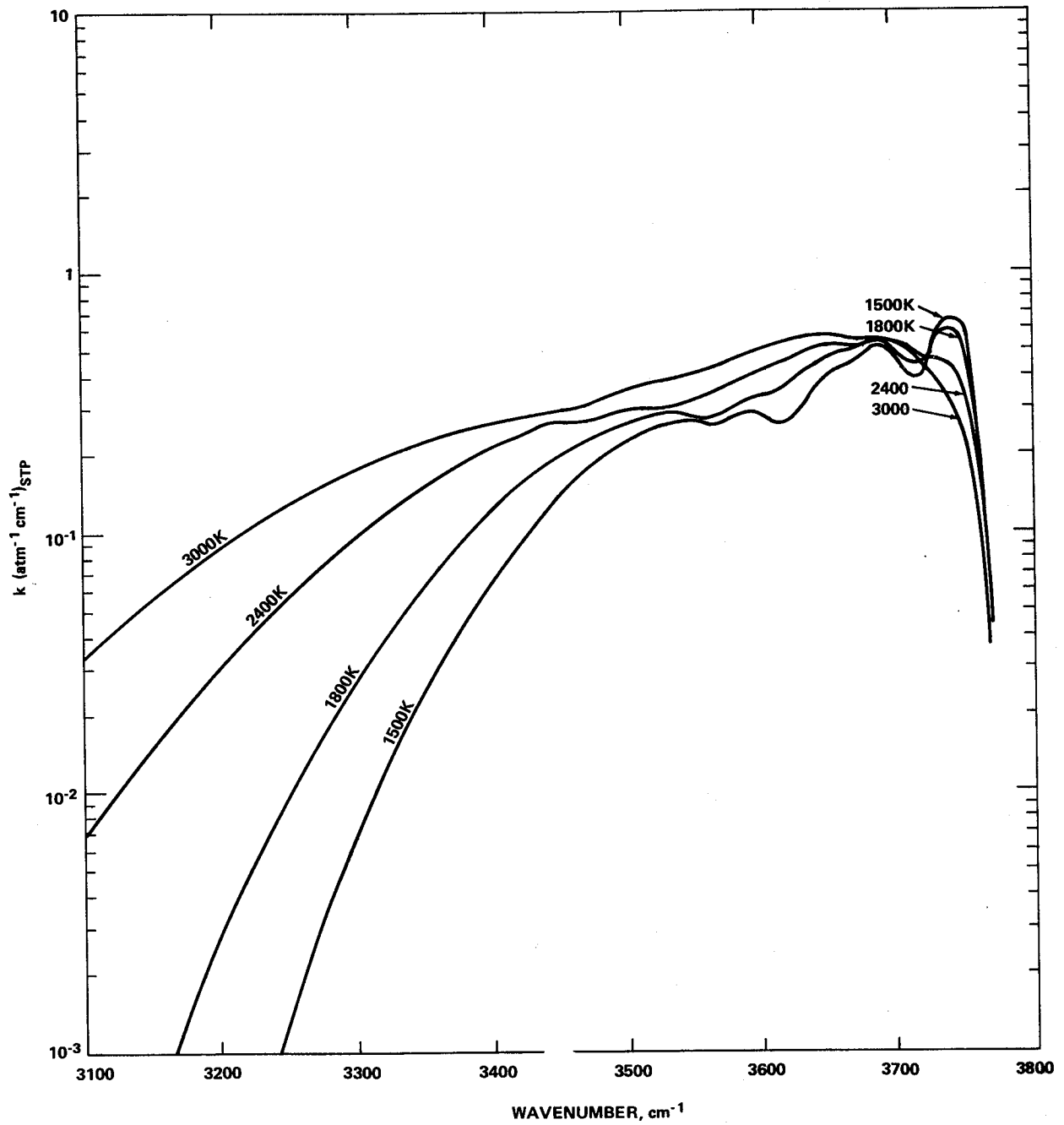


Figure 5-20.  $k = \overline{S/d}$  of  $\text{C}^{12}\text{O}_2$  versus wavenumber  
for  $T = 1500, 1800, 2400,$  and  $3000\text{K}$ .

CHAPTER 5 – REPRESENTATIONS  
FOR SPECIFIC MOLECULES

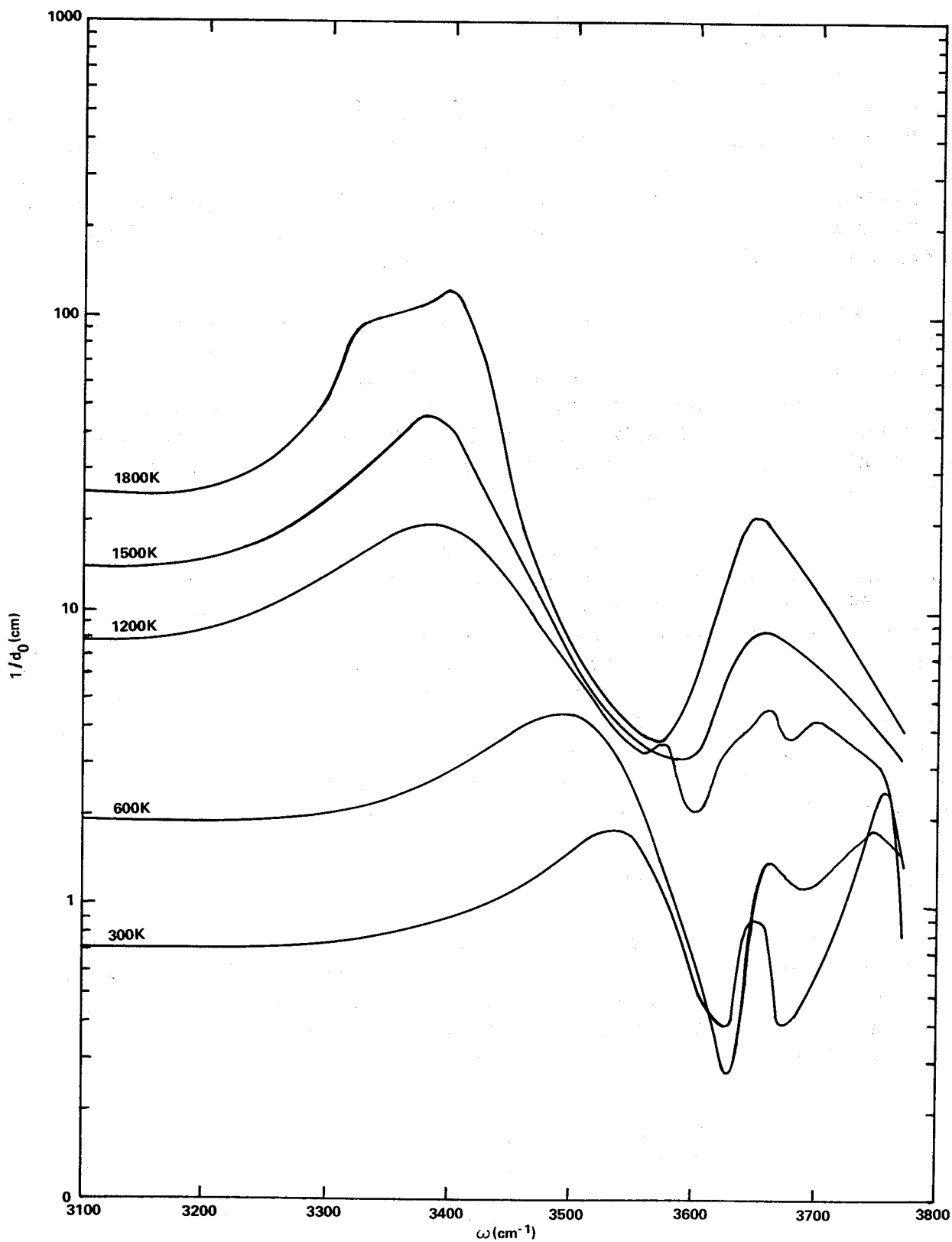


Figure 5-21. Values of the line density parameter  $1/d_0$  for the  $2.7\text{-}\mu$  band of  $\text{C}^{12}\text{O}_2$ .

5.2.2 WATER VAPOR (H<sub>2</sub>O)

The approximate theoretical methods for predicting spectral emissivities of diatomic and linear polyatomic molecules are not directly applicable to the H<sub>2</sub>O molecule. In general, a bent triatomic molecule, such as H<sub>2</sub>O, possesses three different values of moment of inertia about its principal axes. This simple fact causes great complexity in describing the energy level structure, transition frequencies, intensities, etc., for which simple explicit expressions exist for symmetric top molecules.

Line-by-line calculations have been made for H<sub>2</sub>O at low temperatures (~300K), but accurate extension of these calculations to higher temperatures (several thousand degrees) would require far more knowledge of the structure of the H<sub>2</sub>O molecule than is presently available. At the present time, no reliable theoretical calculations are available for band model parameters for H<sub>2</sub>O at high temperatures and the existing model data are derived entirely from experiment.

During recent years, much data for experimental spectra of high temperature water vapor in wavelength region between 1 and 22 microns have been published. These spectra have been measured by different techniques and cover the temperature range from 300 to 2700K (see Chapter 6, Figure 6-1). The optical depths range between about 0.2 and 800 atm-cm(STP) and total pressures range between 0.07 and 10 atm, but the range of parameters covered at any one temperature is rather limited, especially at higher temperatures. These measurements show that the spectral emissivity depends on the following independent variables: wavelength, temperature, partial pressure, line broadening ability of the various species, and pathlength.

5.2.2.1 Curves of Growth and Absorption Coefficients

The curve of growth given by the statistical band model has generally been used to evaluate the mean spectral absorption coefficients from nonthin water spectra. The parameters presented in this handbook were deduced from the experimental data using a curve of growth corresponding to an exponential distribution of line intensities:

$$- \ln \bar{\tau}(\omega) = \frac{\bar{W}(\omega)}{d(\omega)} = \frac{\bar{k}(\omega)u}{\sqrt{1 + \frac{\bar{k}(\omega)u}{4a(\omega)}}} \quad (5-16)$$

where  $\bar{k}(\omega)$  is the mean absorption coefficient (at STP),  $u$  the optical depth (at STP), and  $a(\omega)$  a fine structure parameter equal to the local mean value of the ratio of the collision half-width to the line spacing,  $\gamma/d$ .

The average absorption coefficients obtained by fitting equation (5-16) to experimental data are shown in Figure 5-22. In general, the mean deviation of the experimentally determined absorption coefficients from the plotted curves is within  $\pm 20$  percent. In some portions of the spectra, where the absorption coefficient changes rapidly, a much greater spread in the individual absorption coefficients is observed. The large spread here is probably introduced by small errors in the wavenumber calibration of the different measuring instruments.

#### 5.2.2.2 Water Vapor Line Widths

For water vapor the approximation of optical collision diameters which vary as a power of the temperature leads to an expression for the line width of the form

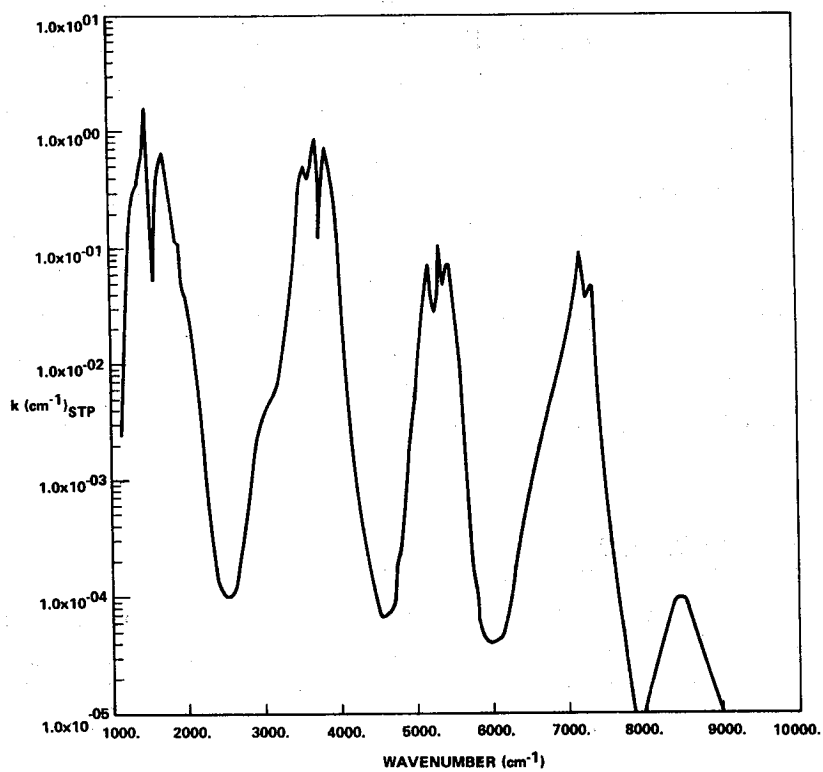
$$\gamma_C = \sum_j (\gamma_j)_{273} P_j \left(\frac{273}{T}\right)^{n_j} + (\gamma_{H_2O}^*)_{273} P_{H_2O} \left(\frac{273}{T}\right)^{n^*} \quad (5-17)$$

Here  $P_j$  is the partial pressure (atm) of the  $j$ th broadener and  $(\gamma_j)_{273}$  is the line width per unit pressure at  $T = 273K$  ( $cm^{-1}/atm$ ) due to collision with this species (including the nonresonant self broadening collisions).  $\gamma_{H_2O}^*$  is the corresponding contribution of resonant collisions. For high temperature gases, the available data do not warrant a sophisticated representation. Thus, the data have been correlated based on the constant collision diameter temperature exponents  $n_j = 0.5$  and  $n^* = 1.0$ .<sup>1</sup>

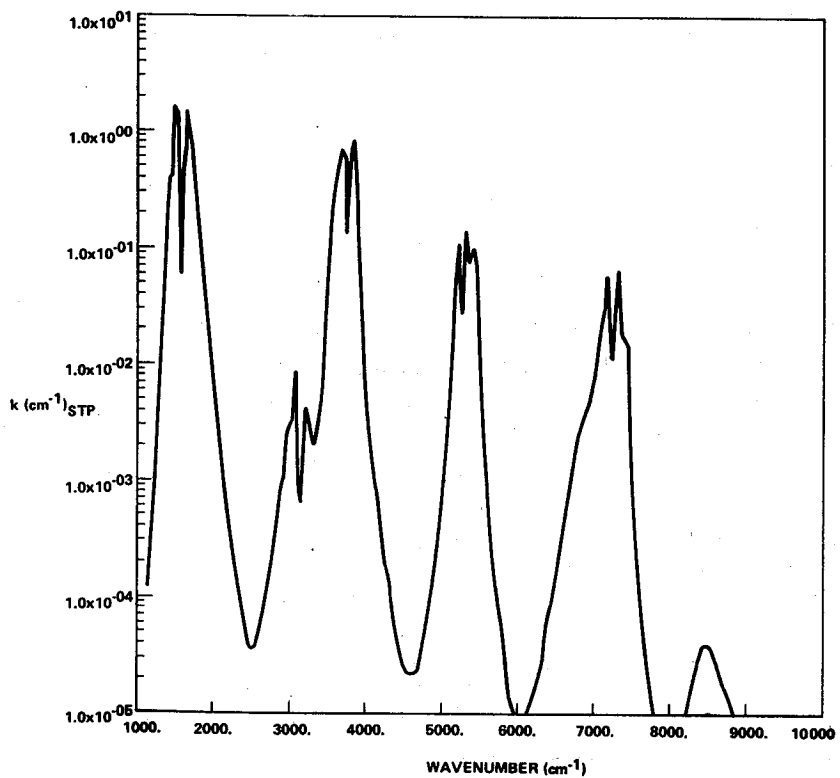
Measured water vapor band strengths are presented in Table 5-15, and values of half-widths for both self- and foreign-gas broadening are listed in Table 5-16. Recommended values of the individual line half-widths

---

1. The calculations of Benedict and Kaplan [5-8, 5-9] indicate that a somewhat improved representation for  $H_2O-N_2$  collisions can be obtained with  $n_j = 0.6$  to  $0.7$  instead of  $0.5$ .



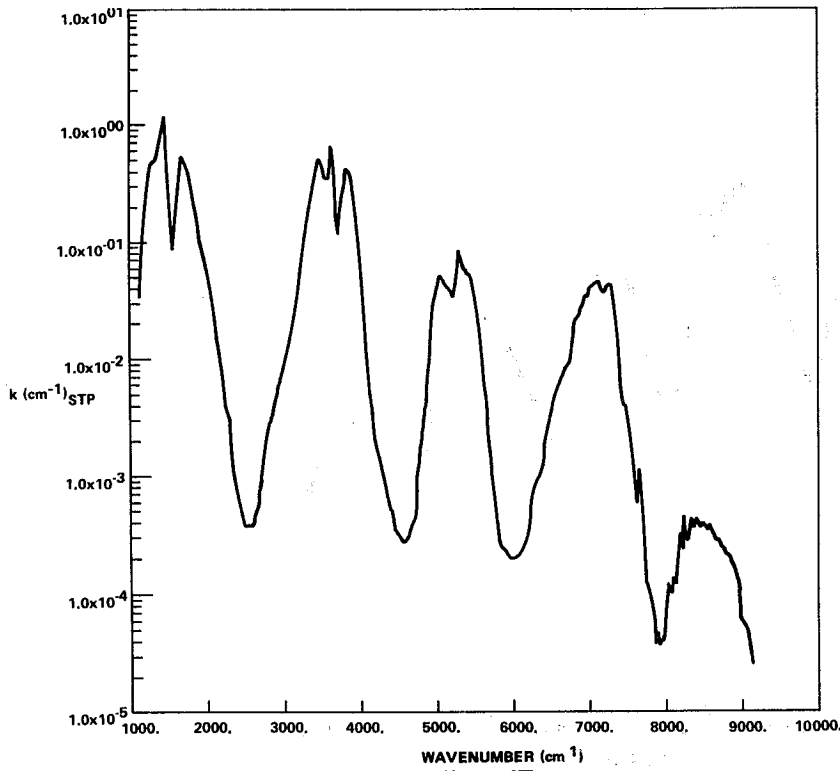
a. 300K.



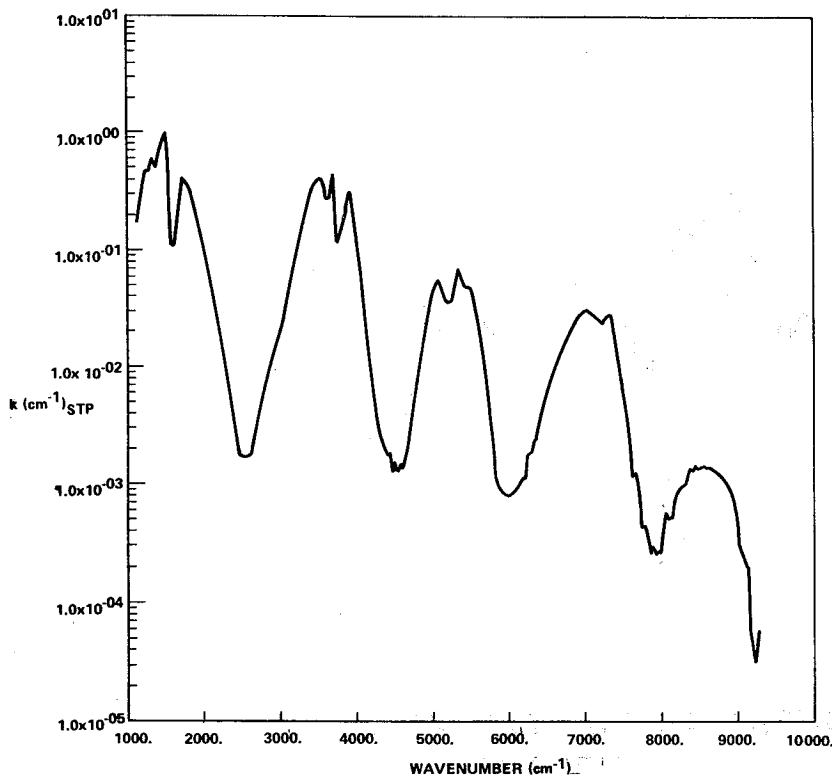
b. 600K.

Figure 5-22. Mean absorption coefficient for water vapor at various temperatures.

CHAPTER 5 – REPRESENTATIONS  
FOR SPECIFIC MOLECULES

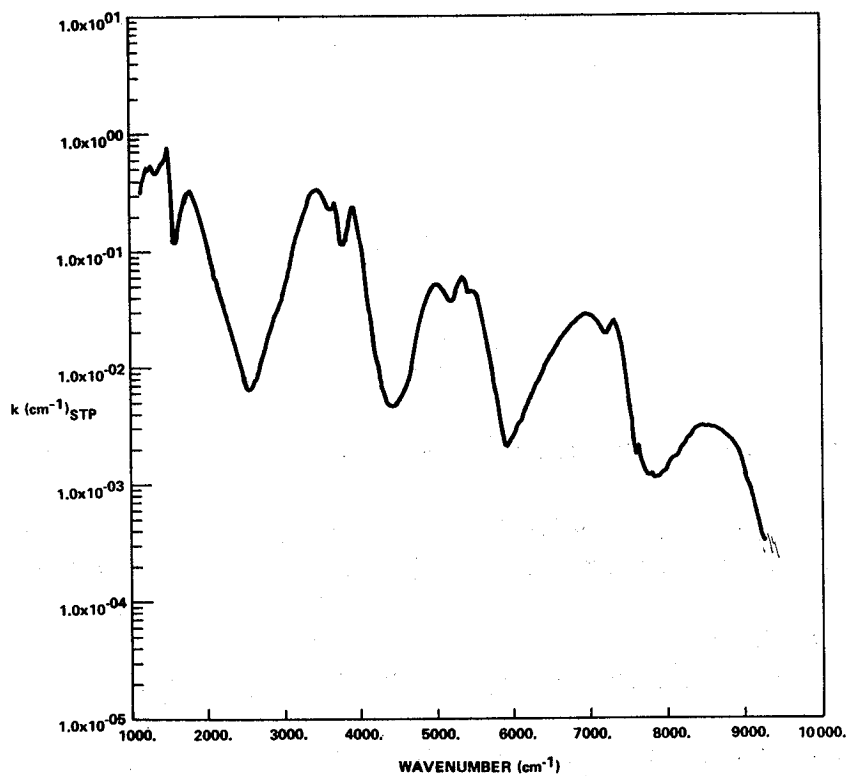


c. 1000K.

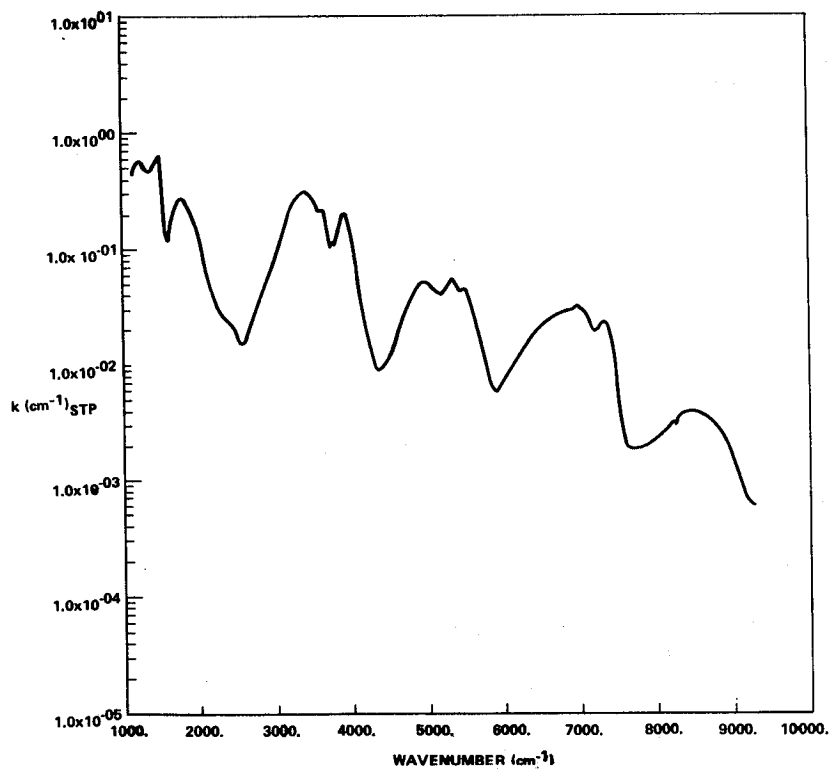


d. 1500K.

Figure 5-22. (Continued).



e. 2000K.



f. 2500K.

Figure 5-22. (Continued).

CHAPTER 5 – REPRESENTATIONS  
FOR SPECIFIC MOLECULES

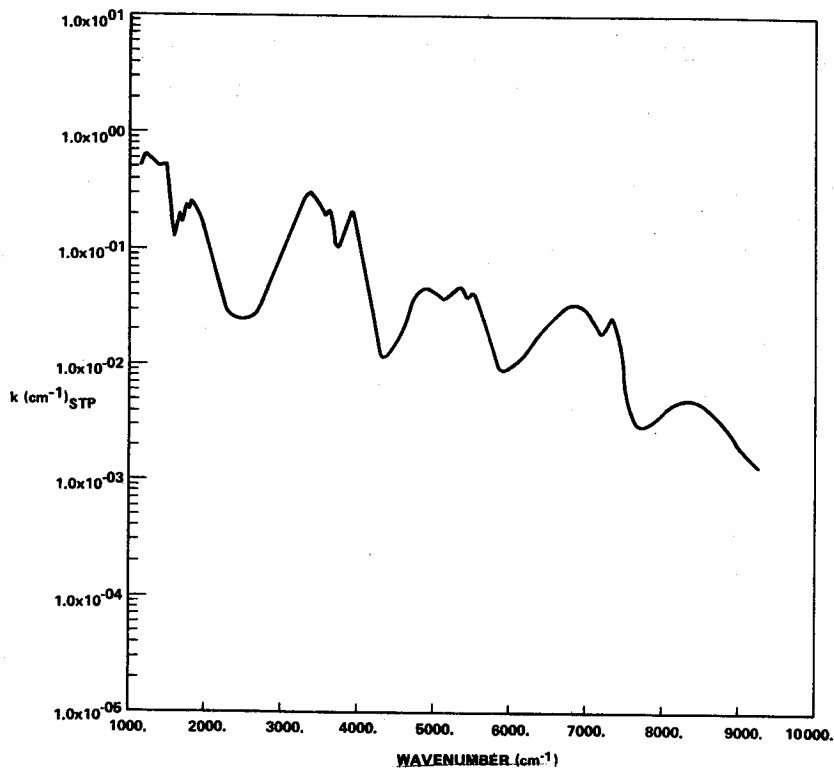


Figure 5-22. (Concluded).

for different broadeners for use in equation (5-17) are included in Table 5-19. For example, for a binary mixture of water vapor and nitrogen, equation (5-17) reduces to

$$\gamma_C^{\text{H}_2\text{O}} = p_T \left\{ c \left[ 0.44 \left( \frac{273}{T} \right) + 0.09 \left( \frac{273}{T} \right)^{1/2} \right] + (1 - c) \left( \frac{273}{T} \right)^{1/2} 0.09 \right\} \quad (5-18)$$

where  $c$  is the water vapor mole fraction.

TABLE 5-15. MEASURED WATER VAPOR INTEGRATED BAND  
STRENGTHS AT 300K ( $\text{cm}^{-2}\text{atm}^{-1}$  at STP)

6.3- $\mu$	2.7- $\mu$ <sup>a</sup>	1.87- $\mu$	1.38- $\mu$	1.14- $\mu$	Source
247 $\pm$ 10%	226 $\pm$ 21	24.2	17.8		Goldstein <sup>b</sup>
317		24.7			Benedict, Calfee <sup>c</sup>
220 $\pm$ 10%					Goldman, Oppenheim <sup>d</sup>
300 $\pm$ 20%					Ludwig, Ferriso, Abeyta <sup>e</sup>
338 $\pm$ $\begin{matrix} 17.3\% \\ 6.7\% \end{matrix}$					Rosenberg, Pratt, Bray <sup>f</sup>
	200 $\pm$ 15%	26 $\pm$ 7%	21.2 $\pm$ 10%	1.96 $\pm$ 50%	Ferriso, Ludwig <sup>g</sup>
	180 ( $\nu_3$ only)	21.2	17.9		Lowder <sup>h</sup>
	235				Gates et al. <sup>i</sup>
				0.4	Burch et al. <sup>j</sup>
	220 $\pm$ 20	19.8 + 2.7			Goldman et al. <sup>k</sup>
300	220	24	18	1	Recommended Values

- a. This band system includes the transitions  $\nu_3$ ,  $\nu_1$ , and  $2\nu_2$ , if not noted otherwise.
- b. R. Goldstein, JQSRT, no. 4, 1964, p. 343.
- c. W. S. Benedict and R. F. Calfee, ESSA Professional Paper 2, June 1967.
- d. A. Goldman and U.P. Oppenheim, Appl. Optics, no. 5, 1966, p. 1073.
- e. C.B. Ludwig, C.C. Ferriso, and C.N. Abeyta, JQSRT, no. 5, 1965, p. 281.
- f. C.W. Rosenberg, Jr., N.H. Pratt, and K.N.C. Bray, JQSRT, no. 10, 1970, p. 1155.

CHAPTER 5 – REPRESENTATIONS  
FOR SPECIFIC MOLECULES

- g. C. C. Ferriso and C. B. Ludwig, JCP, no. 41, 1964, p. 1668.
- h. J.E. Lowder, JQSRT, no. 11, 1971, p. 153.
- i. D. M. Gates, R. F. Calfee, D. W. Hansen, and W. S. Benedict, NBS Monograph 71, 1964.
- j. D. E. Burch, D. A. Gryvnak, and R. R. Patty, J. Opt. Soc. Am., no. 57, 1967, p. 885; Aeronutronic Report V-3704, July 31, 1966.
- k. A. Goldman and U.P. Oppenheim, JOSA, no. 55, 1965, p. 794.

TABLE 5-16. MEASURED VALUES OF COLLISION-BROADENED LINE  
HALF-WIDTHS AT HALF-HEIGHT FOR H<sub>2</sub>O AT STP (in cm<sup>-1</sup>)<sup>a</sup>

Broadener					Source
H <sub>2</sub> O	N <sub>2</sub>	O <sub>2</sub>	CO <sub>2</sub>	Ar	
0.53	0.092	0.044			Benedict, Kaplan <sup>b</sup>
5.2x	x				Burch et al. <sup>c</sup>
0.54	0.087		0.12	0.065	Vasilevsky, Neporent <sup>d</sup>
0.53	0.09	0.04	0.12	0.06	Recommended Values

- a. Values for foreign gas broadeners have been scaled to 273K according to  $\gamma \sim T^{-1/2}$ . For self broadening,  $\gamma \sim T^{-1}$  was used.
- b. W. S. Benedict and L. D. Kaplan, J. Chem. Phys., no. 30, 1959, p. 388.
- c. D. E. Burch, D. Gryvnak, E. B. Singleton, W. L. France, and D. Williams, Infrared Absorption by Carbon Dioxide, Water Vapor, and Minor Atmospheric Constituents, AFCRL-62-698, July 1962.
- d. K. P. Vasilevsky and B. S. Neporent, Opt. Spectry., no. 7, 1959, p. 353.

#### 5.2.2.3 Fine Structure Parameter (1/d)

In a simplified treatment, the line spacing,  $d(\omega)$ , may be averaged over the vibration-rotation bands to yield a  $d$  for which the temperature dependency may be represented by  $d(T) = \exp(-0.00106 T + 1.21)$ . A more accurate wavenumber-dependent representation of  $d(\omega, T)$  is given in Figure 5-23. The ordinate is chosen to be  $1/d(\omega, T)$  because the fine-structure parameter  $a(\omega, T)$  has the form  $\gamma/d$ , where  $\gamma$  is the mean H<sub>2</sub>O line half-width as discussed in Section 5.2.2.2. The data given in Figure 5-23

were obtained experimentally in the temperature range from 1200 to 2750K over the spectral region in which water vapor absorbs significantly.

In all cases, the deduced values of  $1/d$  increase toward the wings of the bands and become indeterminate in the center of the troughs, and the values of  $1/d$  were extrapolated into the trough regions. Since the plots of the experimentally determined values of  $1/d$  versus temperatures were smooth curves, over the observed range of 1200 to 2750K they were extrapolated to 600 and to 3000K.

The set of  $1/d$  versus  $\omega$  for  $T = 600, 1000, 1500, 2000, 2500,$  and  $3000\text{K}$  is shown in Figure 5-23, where all regions which were extrapolated are given as dashed lines.

#### 5.2.2.4 Detailed Line-by-Line Calculations for H<sub>2</sub>O

Precise monochromatic emissivity calculations for H<sub>2</sub>O were made over the spectral region  $3895$  to  $3905\text{ cm}^{-1}$  based on the tabulation of Gates et al. [5-10]. These are compared with band model calculations using parameters derived (for consistency) from the tabulated values of line intensity and half-width.

Values of the monochromatic absorption coefficient were computed at increments of  $0.001\text{ cm}^{-1}$ , assuming a Lorentz shape for all lines and considering the contributions of all lines within the  $5\text{ cm}^{-1}$  spectral interval as well as all lines located within  $5\text{ cm}^{-1}$  of either end of the interval.

The parameters  $\sum_i S_i/d$  and  $\sum_i (S_i \gamma_{0i})^{1/2}/d$  were evaluated for each  $5\text{ cm}^{-1}$  interval, and the band model parameters  $\bar{k}$  and  $a_0$  were determined as follows:

$$\bar{k} = \sum_i S_i/d \quad (5-19)$$

and

$$a_0 = \frac{\left[ \sum_i (S_i \gamma_{0i})^{1/2}/d \right]^2}{\left[ \sum_i S_i/d \right]} \quad (5-20)$$

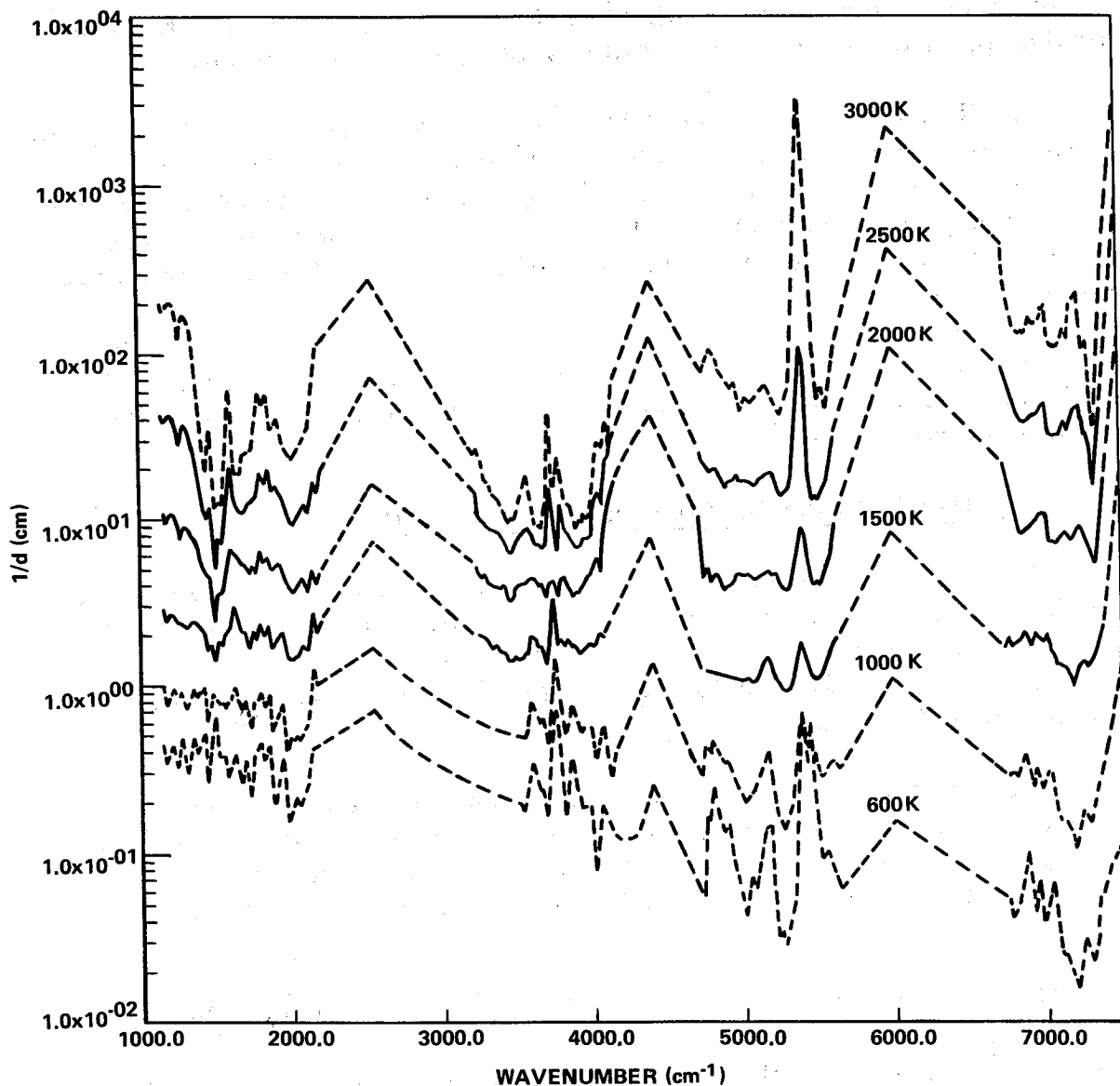


Figure 5-23. Plot of  $(1/d)$  for  $H_2O$  versus  $\omega$  between  $1150\text{ cm}^{-1}$  and  $7500\text{ cm}^{-1}$  for  $T = 600, 1000, 1500, 2000, 2500,$  and  $3000\text{K}$ .

The values of  $\int k d\omega/d$  and  $\sum_i S_i/d$  over the intervals agreed to better than three significant figures. This would be expected unless a strong line happened to be centered very near one end of the interval.

Graphs of the monochromatic spectral emissivity are shown in Figure 5-24. Table 5-17 shows a comparison of the mean emissivity determined for the spectrum ( $\bar{\epsilon} = \int \epsilon d\omega/d$ ) with the mean emissivities predicted by two different band models using the calculated parameters  $k$  and  $a_0$ . These comparisons show only the error in representing a particular calculated spectrum by a band model and do not reflect any error in calculating the properties of a real spectrum from tables of line intensities and half-widths.

TABLE 5-17. COMPARISON OF CALCULATED EMISSIVITIES

		3895 - 3900 ( $\text{cm}^{-1}$ )	3900 - 3905 ( $\text{cm}^{-1}$ )	3895 - 3905 ( $\text{cm}^{-1}$ )
	Exact	0.0909	0.0859	0.0884
Emissivity Calculation	Random Exponential Model	0.0962 (5.9% high)	0.0898 (4.6% high)	0.0931 (5.3% high)
	Random Exponential- $S^{-1}$ Model	0.0889 (2.2% low)	0.0851 (0.9% low)	0.0874 (1.1% low)
Band Model Parameters	$k$ ( $\text{cm}^2/\text{gm}$ )	367.4	554.9	461.2
	$a_0$ ( $\text{atm}^{-1}$ )	0.04414	0.02466	0.03234

### 5.3 SUMMARY OF TWO RECOMMENDED BAND MODELS

The two recommended models differ in the approximation used to account for inhomogeneous effects. The reasoning used in constructing the two approximations is presented in Section 4.2. In the single line group (SLG) model all lines in a spectral interval are treated as though there are no large differences in individual line strengths and the Curtis-Godson approximation is applied as though the parameters represented a single line. More detail is added in the multiple line group (MLG) model where the lines in the spectral interval are divided into groups so that all the lines in a particular group will have similar strengths. In this model the Curtis-Godson approximation is applied to each line group in turn and the transmission is taken to be the product of the transmissions for each of the line groups.

The curves of growth are the same for each line group with differences in the line spacing to account for division into line groups. Both models are based on random band models. The curve of growth used for the collision broadening is exact for an exponential distribution of Lorentz lines (Section 3.2.2.2), but it is also a reasonable approximation for lines of equal strength (Sections 3.2.2.1 and 3.2.5(a)). Doppler lines are modeled using an approximate expression for a random distribution of equal strength lines (Section 3.2.3.1 and Table 2-B-1). A functional relation has been selected for combining collision and Doppler broadened optical depths which essentially selects the larger of the two if they differ by a factor of 3 or more.

The spectral radiance is calculated along a line of sight through a gas from the point on which the radiation is incident. If  $l$  is the distance along the path and  $L$  is the total pathlength, then

$$N_{\omega} = - \int_0^L N_{\omega}^0 (d\bar{\tau}(l, \omega)/dl) dl \quad . \quad (5-21)$$

The transmissivity is indicated as an average since the band model calculations define radiation over some wavenumber interval (usually  $25 \text{ cm}^{-1}$ ) centered about  $\omega$ . The functional dependency of transmissivity on  $l$  includes not only the physical length but also the gas properties (temperature, pressure, and mole fraction) which are functions of  $l$ . Transmissivity is defined as

$$\bar{\tau}(l, \omega) = \exp[-X(l, \omega)] \quad , \quad (5-22)$$

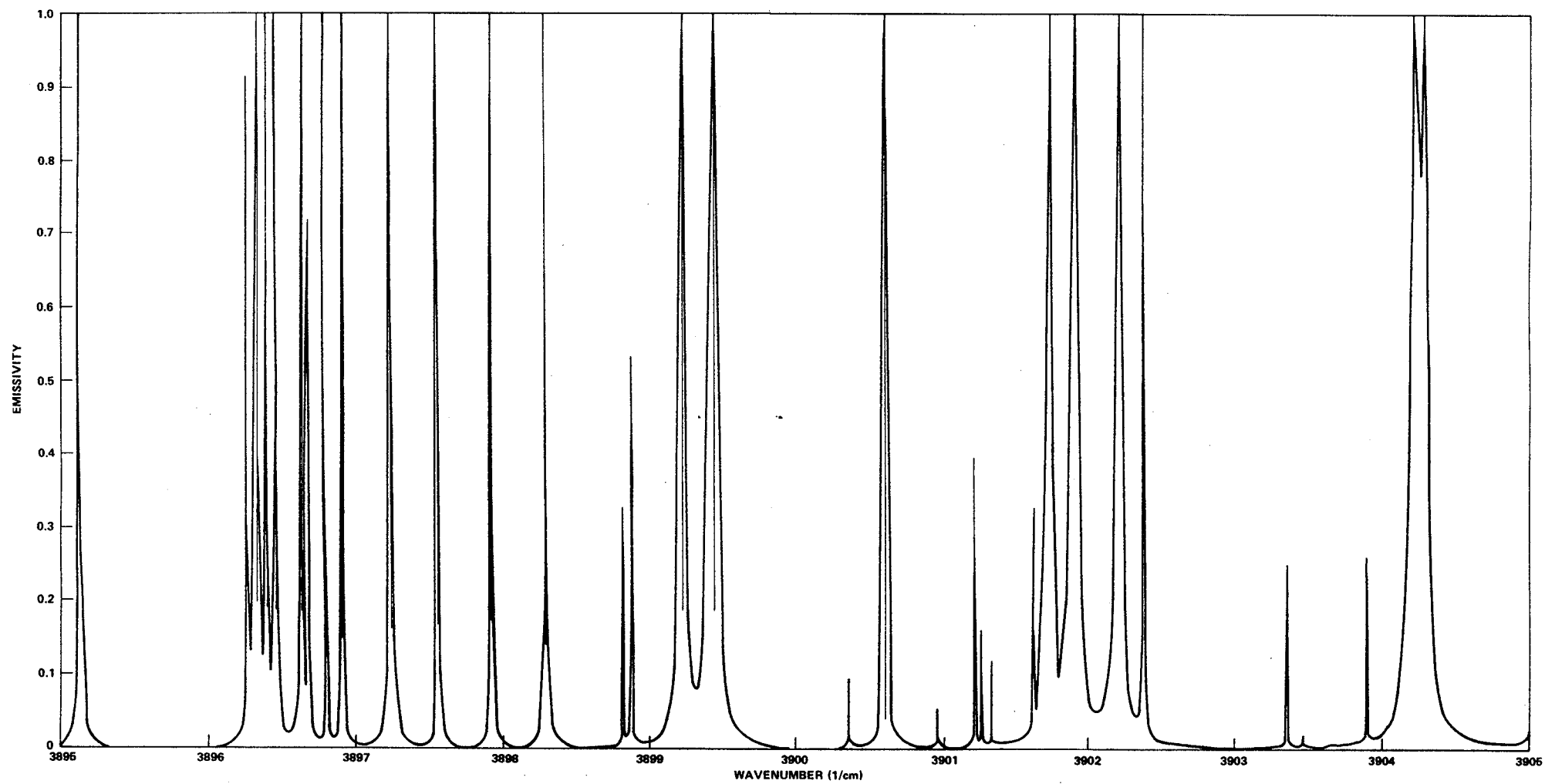


Figure 5-24. Monochromatic spectral emissivity for H<sub>2</sub>O.

where the optical depth  $X$  is the sum for all the (i) radiating species

$$X(\ell, \omega) = \sum_i X(\ell, \omega, i) \quad (5-22a)$$

Detailed procedures for evaluating optical depth vary depending upon the radiating species and the band model (MLG or SLG) considered. Recommended procedures for gases are described in this section while those for carbon particles (soot) are described in Section 5.4. In the following equations, notations for position,  $\ell$ , wavenumber,  $\omega$ , and species,  $i$ , will be omitted except where required for clarity.

The equations used with the MLG and SLG models are listed in Table 5-18 to show the similarities and differences in the two models. Some of the parameters used in the models are listed in Tables 5-18 and 5-19 while others are tabulated in the General Appendix.

The values of the band model parameters for  $H_2O$  were determined experimentally [5-11] by fitting the SLG model to experimental results from a hydrogen/oxygen burner to determine values for  $k$  and  $1/d$ . Values for  $1/d_0$  are determined from the experimental  $1/d$  values by inverting an approximation previously recommended [5-12] for obtaining  $1/d$  from  $1/d_0$ . Further theoretical studies [5-13] have indicated that the  $f_n$  and  $g_n$  values for  $H_2O$  increase with the line group index,  $n$ , but no revised expressions have been recommended.

The band model parameters for  $CO_2$  and the diatomic molecules were determined by fitting the models to theoretical calculations of Malkmus and Thomson [5-2, 5-14]. In the case of  $CO_2$ , all values ( $k$ ,  $1/d_0$ , and  $1/d$ ) are tabulated, while for the diatomic molecules only  $k$  and  $1/d$  are tabulated. The value of  $1/d_0$  may be determined from the value for  $1/d$  according to

$$\frac{1}{d} = \frac{1}{d_0} \frac{\left[ \sum_{n=0}^{\infty} f_n^{1/2} g_n^{1/2} e^{-n\theta/2T} \right]^2}{\sum_{n=0}^{\infty} f_n e^{-n\theta/T}} \quad (5-23)$$

However, because of the large values of  $\theta$ , it is unlikely that the MLG model would be required for diatomic molecules.

The method of temperature and pressure adjustments to the absorption coefficient ( $k$ ) and the optical thickness ( $u$ ) which are shown in Table 5-18 correspond to the method of presentation of data in the General Appendix. Values of absorption coefficient ( $k$ ) are tabulated as functions of temperature at standard temperature and pressure (STP). Therefore, the absorption coefficient must be multiplied by an optical thickness ( $u$ ) which has been corrected to the equivalent thickness at STP using equation (5-33) (see Table 5-18). This is equivalent to the actual pathlength times the ratio of actual to standard density.

The specification of the collision broadened half-width as a function of pressure and temperature is more complex than the method used for the absorption coefficient. The line width is expected to be proportional to the number of collisions experienced by a molecule per unit time. Since self broadening collisions are more effective than those with other species, it has been found [5-15] that good agreement with experimental data at room temperature has been obtained by assuming the line width is proportional to  $(\gamma_a p_a + \gamma_b p_b)$ , where the subscripts  $a$  and  $b$  designate self broadening and foreign gas broadening. In extending this proportionality to higher temperatures it is necessary to take into account the effect of variation in temperature dependency [5-16, 5-17] between resonating and nonresonating self-broadening collisions described in Section 2.4.3. This results in the formulation of equation (5-34) (see Table 5-18)

$$\gamma_{ci} = \left[ \sum_j (\gamma_{i,j})_{273} p_j (273/T)^{\eta_{i,j}} \right] + (\gamma_{i,i})_{273} p_i (273/T)^{\eta_{i,i}} .$$

In this expression, the self-broadening of the radiating species under consideration is included in two ways. First it is included as one of the  $j$  foreign gas broadeners to account for nonresonant collisions and, second, it is included in the separate term  $(\gamma_{i,i})$  to account for resonant collisions which have a different temperature dependency. The use of this formulation depends upon the assumption that the line widths, which are functions of frequency, can be approximated by a band averaged value so all frequency dependence in the fine structure parameter ( $a_c$ ) will appear through the mean line density (1/d).

Since the values listed for  $\gamma$  in Table 5-19 are per unit pressure at standard temperature rather than per unit length at standard density (as in the case of  $k$ ), the subscript 273 is used in preference to the STP used for the absorption coefficients. The factors for temperature correction of the half-width,  $\eta_{i,j}$  and  $\eta_{i,i}$ , have been assumed to be 0.5 and 1.0 as shown in Table 5-19. Although there is some evidence that other values may improve the representation (see Sections 2.4.3 and 5.2.2.2), the values given in Table 5-19 must be used to be consistent with the experimental data reduction of the line density ( $1/d$ ) for water vapor.

TABLE 5-18. EQUATIONS FOR RECOMMENDED MLG AND SLG MODELS

Parameter	MLG Model	SLG Model
Optical Depth of all Line Groups	$X = \sum_{n=0}^{\infty} X_n$	Not Applicable (5-24)
Optical Depth	$X_n = \sqrt{1 - Y_n^{-1/2}} X_n^*$	$X = \sqrt{1 - Y^{-1/2}} X^*$ (5-25)
Combined Collision and Doppler Optical Depths	$Y_n = \left[ 1 - \left( \frac{X_{cn}}{X_n^*} \right)^2 \right]^{-2} + \left[ 1 - \left( \frac{X_{Dn}}{X_n^*} \right)^2 \right]^{-2} - 1$	$Y = \left[ 1 - \left( \frac{X_c}{X^*} \right)^2 \right]^{-2} + \left[ 1 - \left( \frac{X_D}{X^*} \right)^2 \right]^{-2} - 1$ (5-26)
Optical Depth for the Weak Line Limit	$X_n^* = \int_0^u k_n du'$	$X^* = \int_0^u k(\omega, T) du'$ (5-27)
Optical Depth for a Pure Collision Curve of Growth	$X_{cn} = X_n^* \left[ 1 + X_n^*/4a_{cn} \right]^{-1/2}$	$X_c = X^* \left[ 1 + X^*/4a_c \right]^{-1/2}$ (5-28)
Optical Depth for a Pure Doppler Curve of Growth	$X_{Dn} = 1.7a_{Dn} \sqrt{\ln \left[ 1 + \left( \frac{X_n^*}{1.7a_{Dn}} \right)^2 \right]}$	$X_D = 1.7a_D \sqrt{\ln \left[ 1 + \left( \frac{X^*}{1.7a_D} \right)^2 \right]}$ (5-29)
Collision Broadened Fine Structure Parameter	$a_{cn} = \frac{1}{X_n^*} \int_0^u \frac{\gamma_c}{d_n} k_n du'$	$a_c = \frac{1}{X^*} \int_0^u \frac{\gamma_c}{d} k(\omega, T) du'$ (5-30)
Doppler Broadened Fine Structure Parameter	$a_{Dn} = \frac{1}{X_n^*} \int_0^u \frac{\gamma_D}{d_n} k_n du'$	$a_D = \frac{1}{X^*} \int_0^u \frac{\gamma_D}{d} k(\omega, T) du'$ (5-31)

TABLE 5-18. (Continued)

Parameter	MLG Model	SLG Model																											
Absorption Coefficient for the nth Line Group	$k_n = \bar{k}(\omega, T) \frac{f_n \exp(-\theta n/T)}{\sum_{n=0}^{\infty} f_n \exp(-\theta n/T)}$ <table border="0" style="margin-left: auto; margin-right: auto;"> <tr> <td></td> <td style="text-align: center;"><math>\frac{f_n}{n}</math></td> <td style="text-align: center;"><math>\theta (K)</math></td> </tr> <tr> <td>H<sub>2</sub>O</td> <td style="text-align: center;">1</td> <td style="text-align: center;">2300</td> </tr> <tr> <td>CO<sub>2</sub></td> <td style="text-align: center;">1</td> <td style="text-align: center;">960</td> </tr> <tr> <td>CO</td> <td style="text-align: center;">n+1</td> <td style="text-align: center;">3123</td> </tr> <tr> <td>NO</td> <td style="text-align: center;">n+1</td> <td style="text-align: center;">2740</td> </tr> <tr> <td>CN</td> <td style="text-align: center;">n+1</td> <td style="text-align: center;">2970</td> </tr> <tr> <td>OH</td> <td style="text-align: center;">n+1</td> <td style="text-align: center;">5350</td> </tr> <tr> <td>HCl</td> <td style="text-align: center;">n+1</td> <td style="text-align: center;">4170</td> </tr> <tr> <td>HF</td> <td style="text-align: center;">n+1</td> <td style="text-align: center;">5950</td> </tr> </table>		$\frac{f_n}{n}$	$\theta (K)$	H <sub>2</sub> O	1	2300	CO <sub>2</sub>	1	960	CO	n+1	3123	NO	n+1	2740	CN	n+1	2970	OH	n+1	5350	HCl	n+1	4170	HF	n+1	5950	Not Applicable (5-32)
	$\frac{f_n}{n}$	$\theta (K)$																											
H <sub>2</sub> O	1	2300																											
CO <sub>2</sub>	1	960																											
CO	n+1	3123																											
NO	n+1	2740																											
CN	n+1	2970																											
OH	n+1	5350																											
HCl	n+1	4170																											
HF	n+1	5950																											
Line Density (cm)	$1/d_n = g_n/d_0$ <table border="0" style="margin-left: auto; margin-right: auto;"> <tr> <td style="text-align: center;"><u>Species</u></td> <td style="text-align: center;"><math>\frac{g_n}{n}</math></td> <td style="text-align: center;"><math>\frac{1/d_0}{n}</math></td> </tr> <tr> <td>H<sub>2</sub>O</td> <td style="text-align: center;">1</td> <td style="text-align: center;">See Note Below</td> </tr> <tr> <td>CO<sub>2</sub></td> <td style="text-align: center;"><math>(1+\epsilon n)^2</math></td> <td style="text-align: center;">1/d<sub>0</sub> and <math>\epsilon</math> are tabulated as a function of <math>\omega</math> and T in the General Appendix</td> </tr> <tr> <td>Diatomics</td> <td style="text-align: center;">1</td> <td style="text-align: center;">equation (5-23)</td> </tr> </table> <p><u>For H<sub>2</sub>O</u></p> $1/d_0 = 1/d \frac{[1-\exp(-\theta/2T)]}{[1+\exp(-\theta/2T)]}$ <p>where 1/d is determined as in the SLG model</p>	<u>Species</u>	$\frac{g_n}{n}$	$\frac{1/d_0}{n}$	H <sub>2</sub> O	1	See Note Below	CO <sub>2</sub>	$(1+\epsilon n)^2$	1/d <sub>0</sub> and $\epsilon$ are tabulated as a function of $\omega$ and T in the General Appendix	Diatomics	1	equation (5-23)	<p><u>For H<sub>2</sub>O</u></p> <p>1/d is tabulated as a function of <math>\omega</math> and T, in the General Appendix, but an approximate mathematical expression is</p> $1/d = \exp[0.7941 \sin(0.0036\omega - 8.043) + D(T) - 2.294 + 0.3004 \times 10^{-2}T - 0.366 \times 10^{-6}T^2]$ <p><u>For CO<sub>2</sub> and Diatomic Species</u></p> <p>1/d is tabulated as a function of <math>\omega</math> and T in the General Appendix</p>															
<u>Species</u>	$\frac{g_n}{n}$	$\frac{1/d_0}{n}$																											
H <sub>2</sub> O	1	See Note Below																											
CO <sub>2</sub>	$(1+\epsilon n)^2$	1/d <sub>0</sub> and $\epsilon$ are tabulated as a function of $\omega$ and T in the General Appendix																											
Diatomics	1	equation (5-23)																											

TABLE 5-18. (Concluded)

Parameter	Both MLG and SLG Models
Band Averaged Absorption Coefficient ( $\text{cm}^{-1}$ ) For the $i$ th Species	The coefficient $k$ for standard density is tabulated as a function of wavenumber and temperature in the General Appendix
Optical Thickness for the $i$ th Species ( $\text{cm}_{\text{STP}}$ )	$u_i = p_i (273/T)\ell$ where $p_i$ is the partial pressure of the $i$ th species in atm, and $\ell$ is the physical pathlength in cm <span style="float: right;">(5-33)</span>
Collision Half-Width ( $\text{cm}^{-1}$ ) for the $i$ th Species. Broadening Species Denoted by $j$ . Partial Pressures $p_i$ And $p_j$ are in Atmospheres.	$\gamma_{c_i} = \left[ \sum_j (\gamma_{i,j})_{273} p_j (273/T)^{\eta_{i,j}} \right] + (\gamma_{i,i})_{273} p_i (273/T)^{\eta_{i,i}}$ <span style="float: right;">(5-34)</span> <p style="text-align: center;">See Table 5-19 for recommended values</p>
Doppler Half-Width ( $\text{cm}^{-1}$ )	$\gamma_{D_i} = (5.94 \cdot 10^{-6}) \frac{\omega}{m_i^{1/2}} (T/273)^{1/2}$ where $m_i$ = molecular wt of the $i$ th species <span style="float: right;">(5-35)</span>

TABLE 5-19. MODEL VALUES FOR THE COLLISION  
 LINE WIDTH PARAMETERS

Molecule (i)	Broadener (j)	$(\gamma_{i,j})_{273}$ $\text{cm}^{-1}\text{atm}^{-1}$	$\eta_{i,j}$	$(\gamma_{i,i})_{273}$ $\text{cm}^{-1}\text{atm}^{-1}$	$\eta_{i,i}$
H <sub>2</sub> O	H <sub>2</sub> O	(0.09)	0.5	0.44	1.0
	N <sub>2</sub>	0.09	0.5		
	O <sub>2</sub>	0.04	0.5		
	H <sub>2</sub>	(0.05)	0.5		
	CO <sub>2</sub>	0.12	0.5		
	CO	(0.10)	0.5		
CO <sub>2</sub>	CO <sub>2</sub>	0.09	0.5	0.01	1.0
	H <sub>2</sub> O	(0.07)	0.5		
	N <sub>2</sub>	0.07	0.5		
	O <sub>2</sub>	0.055	0.5		
	H <sub>2</sub>	0.08	0.5		
	CO	(0.06)	0.5		
CO	CO	0.06	0.5	0.0	1.0
	H <sub>2</sub> O	(0.06)	0.5		
	CO <sub>2</sub>	(0.07)	0.5		
	H <sub>2</sub>	0.06	0.5		
	N <sub>2</sub>	0.06	0.5		
	O <sub>2</sub>	0.05	0.5		
NO	NO	0.05	0.5	0.0	1.0
	N <sub>2</sub>	(0.05)	0.5		
	O <sub>2</sub>	(0.04)	0.5		
	Other	(0.05)	0.5		
CN	CN	(0.05)	0.5	0.0	1.0
	Other	(0.05)	0.5		
OH	OH	(0.05)	0.5	0.45	1.0
	Other	(0.05)	0.5		
HCl	HCl	(0.05)	0.5	0.15	1.0
	Other	(0.05)	0.5		
HF	HF	(0.05)	0.5	0.45	1.0
	Other	(0.05)	0.5		

NOTE: Values in parenthesis are estimated.

#### 5.4 CALCULATION PROCEDURE FOR CARBON PARTICLES

Although calculation of scattering phenomena normally associated with particle radiation is not completely treated in this handbook, a method developed [ 5-18] for predicting the radiation from soot particles in rocket exhaust plumes will be described. The theoretical calculations used in the development assumed the particles to be small in comparison with the wavelength range of interest ( $\lambda > 1.0\mu$ ) and the experimental measurements indicated the mean particle size was probably less than  $0.4\mu$ . As pointed out by Hottel [ 5-19], this particle size range is much less than particle sizes resulting from furnaces using powdered-coal or heavy residual oils, so the method to be presented should be applied only when the particle size range is applicable.

When the particle size is small, the monochromatic absorption coefficient is independent of the particle size, and may be expressed as [ 5-20]

$$k = 36 \pi \rho F(\lambda) / \rho_0 \lambda$$

where  $\rho$  is the particle mass density (gm/cm<sup>3</sup> of cloud),  $\rho_0$  is the bulk carbon density, and  $\lambda$  is the wavelength. The function  $F(\lambda)$  is related to the complex index of refraction. This was evaluated [ 5-18] using previous results of Stull and Plass [ 5-21], and the results of these calculations are presented in Figure 5-25.

Experimental measurements were made by Boynton et al. [ 5-18] near the exit of small rocket motors in an experiment similar to that used by Ferriso and Ludwig [ 5-15] to measure emissivities of hot H<sub>2</sub>O and CO<sub>2</sub>. Temperature was varied by changing the nozzle area ratio, and both temperature and particle mass density were varied by changing the mixture ratio of the rocket propellants (RP-1 and gaseous oxygen).

The experimental results generally agreed with the theoretical predictions with two exceptions. At low temperature (1045K) and short wavelength ( $\lambda < 2\mu$ ) there was evidence that scattered radiation from the rocket chamber was significant. In addition, at temperatures above 1700K, theoretical predictions of the spectral dependency of  $k$  were incorrect. In this temperature range,  $k$  becomes almost independent of wavelength but is strongly dependent on temperature. It is postulated that this difference between theoretical and experimental results could be caused by the high temperature properties of rocket motor soot being quite different from those of the bulk material used in the calculations.

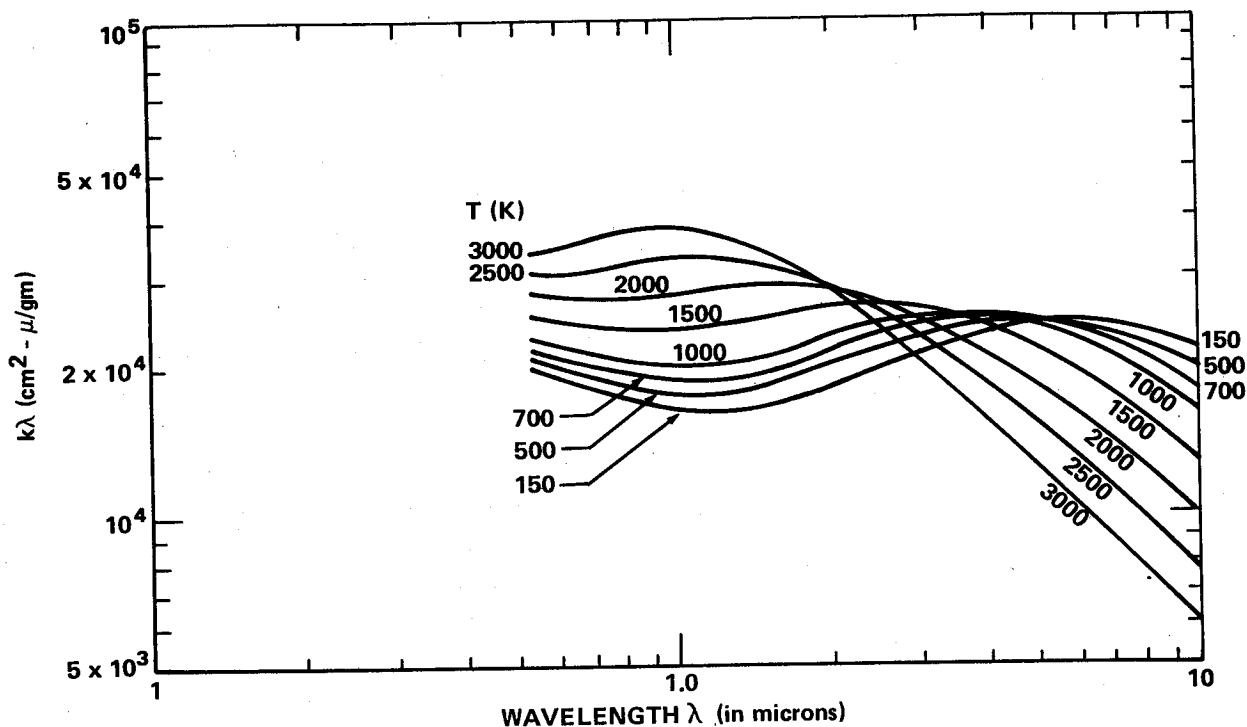


Figure 5-25. Linear absorption coefficient for clouds of very small carbon particles.

The observed and theoretical values of  $k$  are presented in Figure 5-26 showing the sharp change in trends at 1700K. The cross plot presented in Figure 5-27 is consistent with the experimental data as shown by the comparison in Figure 5-28. These data are recommended for radiant heat transfer calculations and are tabulated in the General Appendix.

The absorption coefficient developed for carbon particles should be treated as a linear absorption coefficient for a gas so that the optical depth is

$$X = k_c(\omega, T)u_c \quad (5-36)$$

where  $k_c$  is the absorption coefficient ( $\text{cm}^2/\text{gm}$ ). The pathlength ( $u_c$ ) is the product of the cloud density ( $\rho - \text{gm}/\text{cm}^3$ ) and the physical pathlength ( $l - \text{cm}$ ). This optical depth ( $X$ ) is combined with those of other species as described by equation (5-22a).

**CHAPTER 5 – REPRESENTATIONS  
FOR SPECIFIC MOLECULES**

In using the carbon particle data it should be noted that extrapolation of the results beyond  $4\mu$  will probably be necessary to achieve reasonable heat transfer results. Unfortunately strong molecular radiation bands mask the carbon continuum radiation beyond  $4\mu$ , so it was not possible to obtain experimental results.

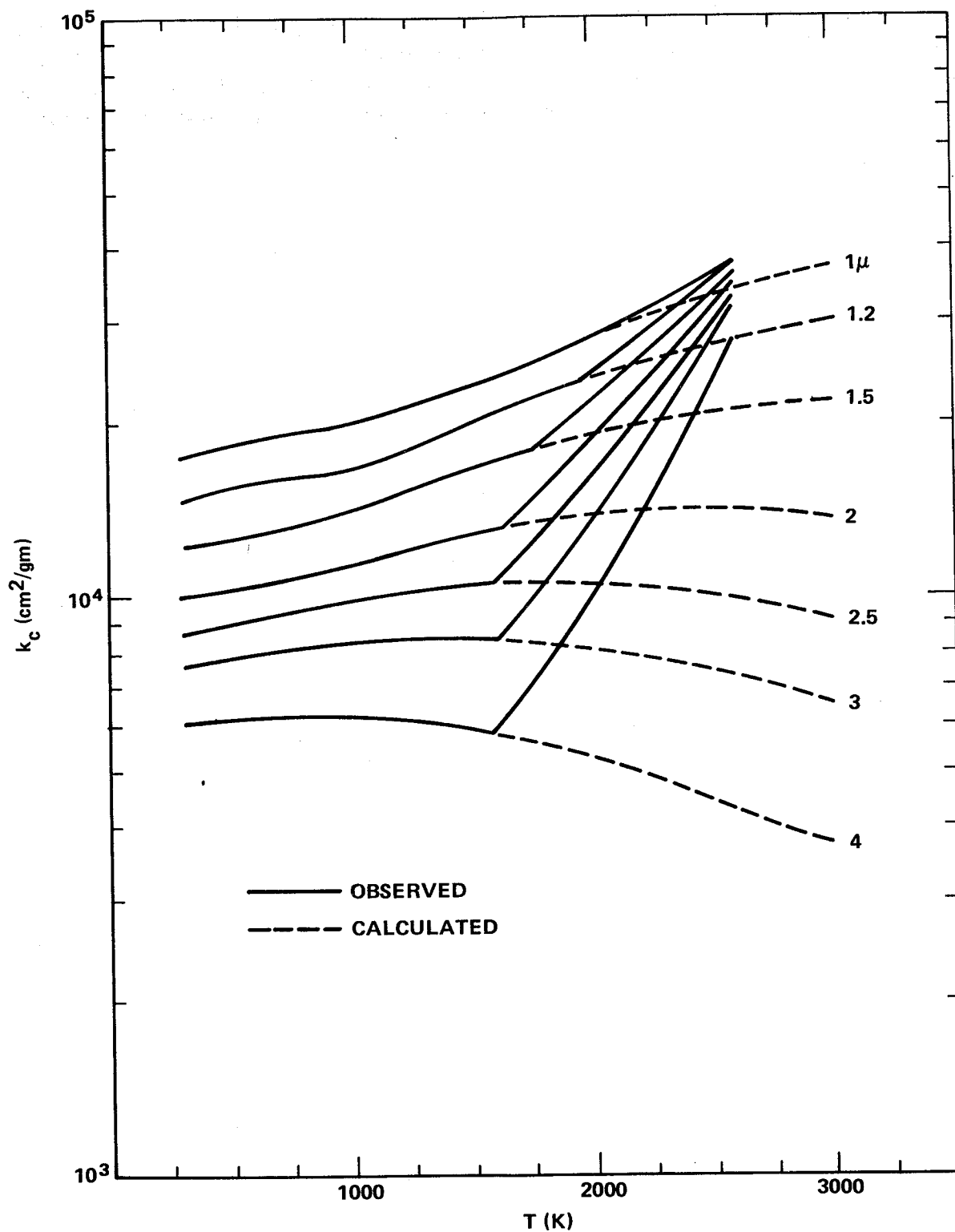


Figure 5-26. Comparison of theoretical and experimental values for the carbon particle absorption coefficient.

CHAPTER 5 – REPRESENTATIONS  
FOR SPECIFIC MOLECULES

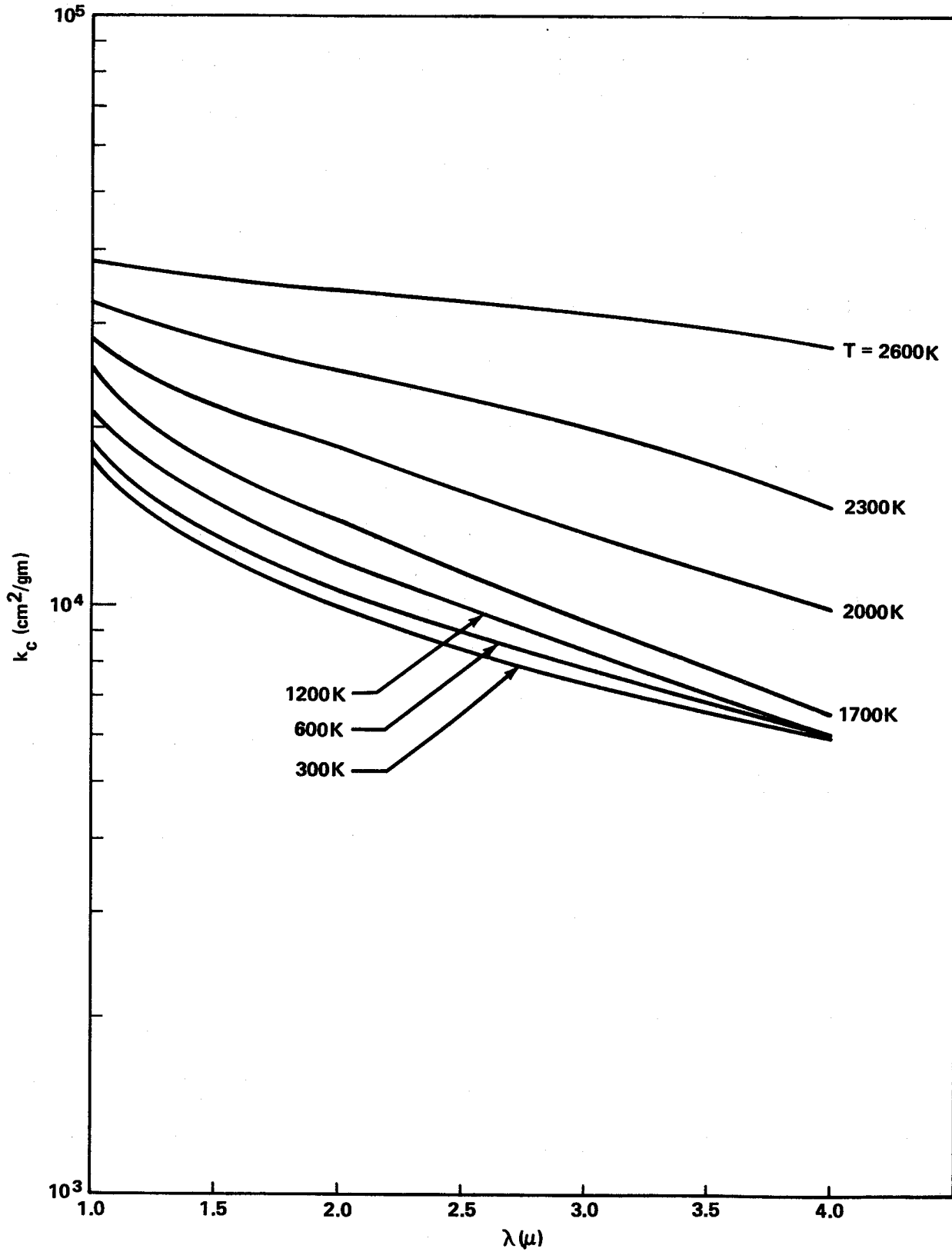


Figure 5-27. Results of the experimental determination of the carbon absorption coefficients. (This is a cross plot of Figure 5-26.)

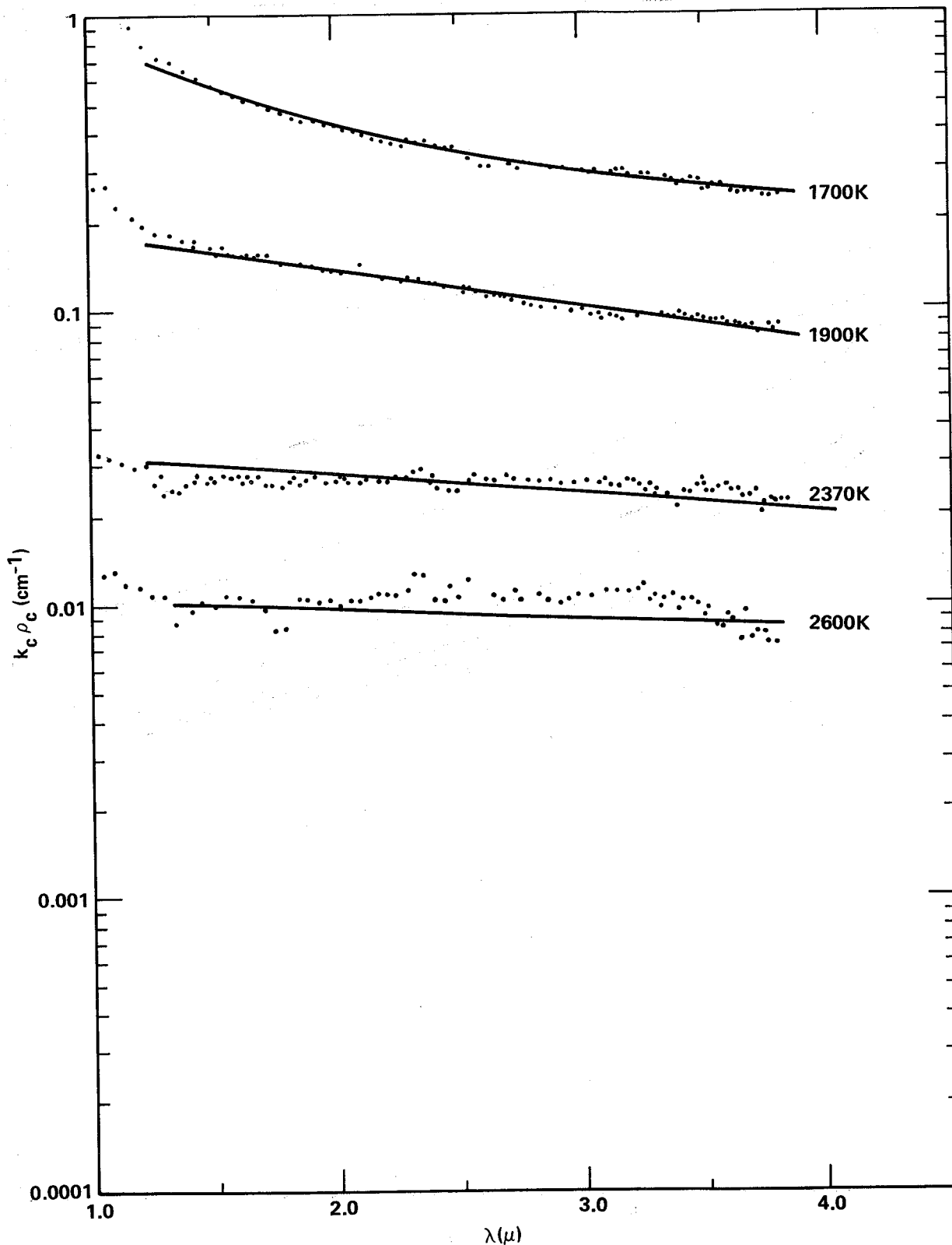


Figure 5-28. Comparison of experimental data with the set of absorption coefficients given in Figure 5-27 and tabulated in the General Appendix.

APPENDIX 5-A

CALCULATION OF DIATOMIC SPECTRA — THEORY

Because of the very limited calculational effort required to compute local line strengths and spacings for diatomic molecules, it may be more convenient to compute such band model parameters as needed within a program, rather than to store them in some tabular form and interpolate to the required wavenumber and temperature.

With such a use in view, the expressions for line strength and line spacing are presented here in equations (5-A-4) and (5-A-6), respectively.

The energy levels of an anharmonic oscillator, in the first approximation to the vibration-rotation interaction, are given by equation (2-45):

$$\begin{aligned} \frac{E(v,j)}{hc} = & \omega_e \left(v + \frac{1}{2}\right) - \omega_e x_e \left(v + \frac{1}{2}\right)^2 + \omega_e y_e \left(v + \frac{1}{2}\right)^3 + \omega_e z_e \left(v + \frac{1}{2}\right)^4 \\ & + B_e j(j+1) - \alpha_e \left(v + \frac{1}{2}\right) j(j+1) \end{aligned} \quad .$$

The frequency of a transition for  $|\Delta v| = 1$  is then given by

$$\begin{aligned} \omega = & [E(v+1, j') - E(v, j)] / hc \\ = & \omega_v + B_e [j'(j'+1) - j(j+1)] \\ & - \alpha_e \left[ \left(v + \frac{3}{2}\right) j'(j'+1) - \left(v + \frac{1}{2}\right) j(j+1) \right] \end{aligned} \quad , \quad (5-A-1)$$

where

$$\omega_v = \omega_e - 2(v+1)\omega_e x_e + \left[ 3(v+1)^2 + \frac{1}{4} \right] \omega_e y_e + [4(v+1)^3 + (v+1)] \omega_e z_e \quad .$$

In terms of  $m$  ( $m = j+1$  for the R-branch,  $m = -j$  for the P-branch),

$$\omega(m) = \omega_v + 2B_e m - \alpha_e \left[ m(m+1) + 2\left(v + \frac{1}{2}\right)m \right] \quad (5-A-2)$$

This equation expresses  $\omega$  as a quadratic function of  $m$ . On solving for  $m$ , this becomes

$$m(\omega) = \frac{B_e - \alpha_e (v+1) \mp \sqrt{[B_e - \alpha_e (v+1)]^2 - \alpha_e (\omega - \omega_v)}}{\alpha_e} \quad (5-A-3)$$

For the anharmonic vibrating rotator model, the average line strength  $S_v^{v+1}(\bar{\tau})(\omega)$  at frequency  $\omega$  for a  $|\Delta v| = 1$  transition is given in terms of the total band absorption  $\alpha_v^{v+1}$  by [5-2]:

$$\begin{aligned} S_v^{v+1}(\bar{\tau})(\omega) &= \frac{\alpha_v^{v+1} B_e hc}{\omega \bar{\omega}_v^{v+1} kT} \frac{B_e - \alpha_e (v+1) + \sqrt{[B_e - \alpha_e (v+1)]^2 - \alpha_e (\omega - \omega_v)}}{\alpha_e} \\ &\times \exp \left[ \frac{-hc [B_e - \alpha_e (v+1)]}{k \alpha_e^2 T} \right] \left\{ 2[B_e - \alpha_e (v+1)] [B_e - \alpha_e (v+1)] \right. \\ &\left. \mp \sqrt{[B_e - \alpha_e (v+1)]^2 - \alpha_e (\omega - \omega_v)} - \left[ 1 + \frac{\frac{1}{2} \alpha_e}{B_e - \alpha_e (v+1)} \right] \alpha_e (\omega - \omega_v) \right\} \\ &\times \left\{ 1 + \frac{C}{\alpha_e} [B_e - \alpha_e (v+1) \mp \sqrt{[B_e - \alpha_e (v+1)]^2 - \alpha_e (\omega - \omega_v)}] \right\} \\ &\times \left[ 1 - \exp \left( \frac{-hc\omega}{-kT} \right) \right] \quad (5-A-4) \end{aligned}$$

where the upper sign refers to the main portion of the band and the lower sign to the returning R-branch. The quantity  $\bar{\omega}_v^{v+1}$  is approximated by [5-2]:

$$\bar{\omega}_v^{v+1} = \omega_v \left[ 1 - \exp \left( - \frac{hc\omega_v}{kT} \right) \right] \quad (5-A-5)$$

The average line spacing at frequency  $\omega$  is given by:

$$|d\omega/dm| = |dm/d\omega|^{-1}$$

$$d_v(\omega) = 2\sqrt{[B_e - \alpha_e(v+1)]^2 - \alpha_e(\omega - \omega_v)} \quad (5-A-6)$$

The total band strength at any temperature,  $\alpha_v^{v+1}(T)$ , can be approximated from an experimental value of the strength at a reference temperature  $T_0$ . A convenient approximation is given by [5-2]

$$\frac{\alpha_v^{v+1}(T)}{\alpha_v^{v+1}(T_0)} = \frac{\bar{\omega}_0^1(T)\omega_v^{v+1}(T)}{\bar{\omega}_0^1(T_0)\bar{\omega}_v^{v+1}(T_0)} \exp \left\{ [E(v) - E(0,0)] \frac{hc}{k} \left( \frac{1}{T_0} - \frac{1}{T} \right) \right\} \quad (5-A-7)$$

where  $\alpha_v^{v+1}$  is given in STP units.

If data are not available for higher-order bands, the harmonic oscillator approximation yields the result

$$\frac{\alpha_v^{v'+1}(T)}{\alpha_v^{v+1}(T)} = \frac{v'+1}{v+1} \exp \left\{ - [E(v') - E(v)] \frac{hc}{kT} \right\} \quad (5-A-8)$$

APPENDIX 5-B

MOLECULAR CONSTANTS

Molecular constants for the gases considered in Chapter 5 are included in this appendix to facilitate computations. The constants for diatomic molecules are presented in Table 5-B-1 and those for water vapor and carbon monoxide are shown in Table 5-B-2.

TABLE 5-B-1. MOLECULAR CONSTANTS FOR DIATOMIC MOLECULES (EQUILIBRIUM VALUES)<sup>a</sup>

Molecule	$\omega_e$ ( $\text{cm}^{-1}$ )	$\omega_e x_e$ ( $\text{cm}^{-1}$ )	$\omega_e y_e$ ( $\text{cm}^{-1}$ )	$\omega_e z_e$ ( $\text{cm}^{-1}$ )	$B_e$ ( $\text{cm}^{-1}$ )	$\alpha_e$ ( $\text{cm}^{-1}$ )	$D_e$ ( $\text{cm}^{-1}$ )	$\beta_e$ ( $\text{cm}^{-1}$ )
$\text{C}^{12}\text{O}^{16}$	2170.21	13.461	0.0308		1.93139	0.017485	$6.43 \times 10^{-6}$	$4. \times 10^{-8}$
$\text{N}^{14}\text{O}^{16}$	1903.68 ( $^2\Pi_{3/2}$ )	13.97	-0.00120		1.70426	0.0178	$5. \times 10^{-6}$	
	1904.03 ( $^2\Pi_{1/2}$ )							
$\text{O}^{16}\text{H}^1$	3735.21	82.81			18.871	0.714	$18.8 \times 10^{-4}$	$0.3 \times 10^{-4}$
$\text{C}^{12}\text{N}^{14}$	2068.705	13.144			1.8996	0.01735		
$\text{H}^1\text{Cl}^{35}$	2989.74	52.05	0.056		10.5909	0.3019	0.000532	$-4. \times 10^{-6}$
$\text{H}^1\text{Cl}^{37}$	2987.47	51.97	0.056		10.5748	0.3012	0.000530	$-4. \times 10^{-6}$
$\text{H}^1\text{F}^{19}$	4137.253	88.726	0.5334	0.0211	20.9456	0.7888	0.002131	-0.000038

- a. G. Herzberg, Molecular Spectra and Molecular Structure, I. Spectra of Diatomic Molecules, D. Van Nostrand Company, Inc., Princeton, N.J., 1950.

TABLE 5-B-2. MOLECULAR CONSTANTS FOR CO<sub>2</sub> AND H<sub>2</sub>O  
 MOLECULES (EQUILIBRIUM VALUES)

Constant	Molecule		Constant	Molecule	
	C <sup>12</sup> O <sub>2</sub> <sup>16</sup> <sup>a</sup>	H <sub>2</sub> O <sup>16</sup> <sup>b</sup>		C <sup>12</sup> O <sub>2</sub> <sup>16</sup> <sup>a</sup>	H <sub>2</sub> O <sup>16</sup> <sup>b</sup>
$\omega_1$	1354.91	3285.3	$g_{22}$	0.775	
$\omega_2$	673.00	1653.9	A <sub>e</sub> B <sub>e</sub> C <sub>e</sub>	0.391635	27.33
$\omega_3$	2396.49	3935.6			14.575
$x_{11}$	- 3.75	- 43.89			9.499
$x_{22}$	- 0.63	- 19.5	$\alpha_1$ $\alpha_2$ $\alpha_3$	0.00120 -0.00072 0.0030875	
$x_{33}$	- 12.63	- 46.37			
$x_{12}$	3.65	- 20.02			
$x_{13}$	- 19.37	-155.06	A $\alpha_1$ B $\alpha_1$ C $\alpha_1$		0.495
$x_{23}$	- 12.53	- 19.81			0.224
$y_{111}$	0.13				0.145
$y_{222}$	0.01		A $\alpha_2$ B $\alpha_2$ C $\alpha_2$		-2.659
$y_{333}$	0.015				-0.202
$y_{112}$	- 0.08				0.105
$y_{122}$	- 0.07		A $\alpha_3$ B $\alpha_3$ C $\alpha_3$		1.234
$y_{133}$	0.015				0.112
$y_{113} = y_{223}$	0				0.169
$y_{233}$	0.01				
$y_{123}$	0.02				

a. C. P. Courtoy, Can. J. Phys., no. 35, 1957, p. 608.

b. G. Herzberg, Infrared and Raman Spectra, D. Van Nostrand Co., Inc., Princeton, N.J., 1945, p. 488.

REFERENCES

- 5-1. Penner, S. S.: Quantitative Molecular Spectroscopy and Gas Emissivities, Addison-Wesley Co., Reading, Mass., 1959.
- 5-2. Malkmus, W. and Thomson, A.: J. Quant. Spectry. Radiative Transfer, vol. 2, 1962, p. 17.
- 5-3. Plass, G. N.: J. Opt. Soc. Am., no. 48, 1958, p. 690.
- 5-4. Plass, G. N.: J. Opt. Soc. Am., no. 50, 1960, p. 868.
- 5-5. Ferriso, C. C. and Ludwig, C. B.: JOSA, no. 54, 1964, p. 657.
- 5-6. Breeze, J. C. and Ferriso, C. C.: JCP, no. 39, 1963, p. 2619.
- 5-7. Eggers, D. F. and Crawford, B. L.: JCP, no. 19, 1951, p. 1554.
- 5-8. Benedict, W. S. and Kaplan, L. D.: J. Chem. Phys., no. 30, 1959, p. 388.
- 5-9. Benedict, W. S. and Kaplan, L. D.: J. Quant. Spectry. Radiative Transfer, no. 4, 1964, p. 453.
- 5-10. Gates, D. M.; Calfee, R. F.; Hansen, D. W.; and Benedict, W. S.: Line Parameters and Computed Spectra for Water Vapor Bands at  $2.7\mu$ . NBS Monograph 71, 1964.
- 5-11. General Dynamics Corp.: Study of Exhaust Plume Radiation Predictions. Progress Report on Contract NAS8-21082, Convair Division, GDC-DBE-67-021, November 1967.
- 5-12. General Dynamics Corp.: Study of Exhaust Plume Radiation Predictions. Interim Progress Report on Contract NAS8-11363, Convair Division, GDC-DBE-66-001a, February 1966.
- 5-13. General Dynamics Corp.: Study of Exhaust Plume Radiation Predictions. Final Report on Contract NAS8-11363, Convair Division, GDC-DBE-66-017, December 1966.
- 5-14. Malkmus, W.: J. Opt. Soc. Am., vol. 53, 1963, p. 951.

REFERENCES (Concluded)

- 5-15. Burch, D. E.; Singleton, E. B.; and Williams, D.: Applied Optics, no. 1, 1962, p. 359.
- 5-16. Benedict, W. S. and Kaplan, L. D.: J. Chem. Phys., no. 30, 1959, p. 388.
- 5-17. Benedict, W.S. and Kaplan, L.D.: JQSRT, no. 4, 1964, p. 453.
- 5-18. Boynton, F. P.; Ludwig, C. B.; and Thomson, A.: AIAA J., no. 6, 1968, p. 865.
- 5-19. Hottel, H. C. and Sarofim, A. F.: Radiative Transfer. McGraw-Hill Book Co., 1967.
- 5-20. Millikan, R. C.: JOSA, no. 51, 1961, p. 535.
- 5-21. Stull, V. R. and Plass, G. N.: JOSA, no. 50, 1960, p. 121.



CHAPTER 6

COMPUTED RADIATION DATA

This chapter contains a range of computed radiation characteristics which may be used for calculations as well as familiarization with the spectral characteristics of gaseous radiation. The data are arranged in four sections: spectral characteristics of gaseous radiators, band absorptances for diatomic gases, total emissivities and band absorptances for carbon dioxide, and total emissivities for water vapor.

6.1 SPECTRAL CHARACTERISTICS OF GASEOUS RADIATORS

In this section, some typical spectra calculated using the SLG model will be presented for water vapor, carbon dioxide, carbon monoxide, and carbon particles. These examples will illustrate the characteristics of the particular gas as well as the relative effects of pressure, pathlength, and temperature on the spectra. For each gas, the absorptivity  $(1 - \tau_\omega)$  is presented over a range of  $p_i \ell$  from 1 to 1000 cm-atm. In each illustration a portion of the blackbody curves is presented to illustrate which portions of the spectra will be enhanced by the distribution of the blackbody radiance.

## 6.1.1 WATER VAPOR

The spectra presented in Figures 6-1a and b clearly illustrate the wide spectral region over which radiation from water vapor may be important. The relative strength of the spectra with increasing temperature, which is apparent in the illustration, is a result of many factors. First, the optical path,  $u$ , decreases because of the decreasing density, but this is offset in some spectral regions by an increase in absorption coefficient. The fine structure parameters  $a_C$  and  $a_D$  both tend to increase with increasing temperature, with  $a_D$  increasing more rapidly. The combination of these temperature trends appears to have relatively minor effects in the band centers compared with the effects in the wings. In the wings of the bands there is a significant increase in absorption with increasing temperature.

An important point to note in the water vapor spectra is the strong absorption at long wavelengths (small values of wavenumber). For example, with the conditions shown for 1200K and 200 cm in Figure 6-1a the 4- to 10- $\mu\text{m}$  region ( $1000$  to  $2500 \text{ cm}^{-1}$ ) will produce 51 percent of the total radiation for the spectral region shown. This compares with 35 percent for blackbody radiation in the 4- to 10- $\mu\text{m}$  region at the same temperature.

A comparison of the effects of the pressure and pathlength in Figures 6-1a and b shows the variation which is expected when collision broadening predominates. The absorption at low and moderate temperatures is more sensitive to pressure than pathlength. For example the absorption at  $p_T \ell = 2000 \text{ atm cm}$  is much greater for  $p_T = 10 \text{ atm}$  in Figure 6-1a than for  $\ell = 2000$ .

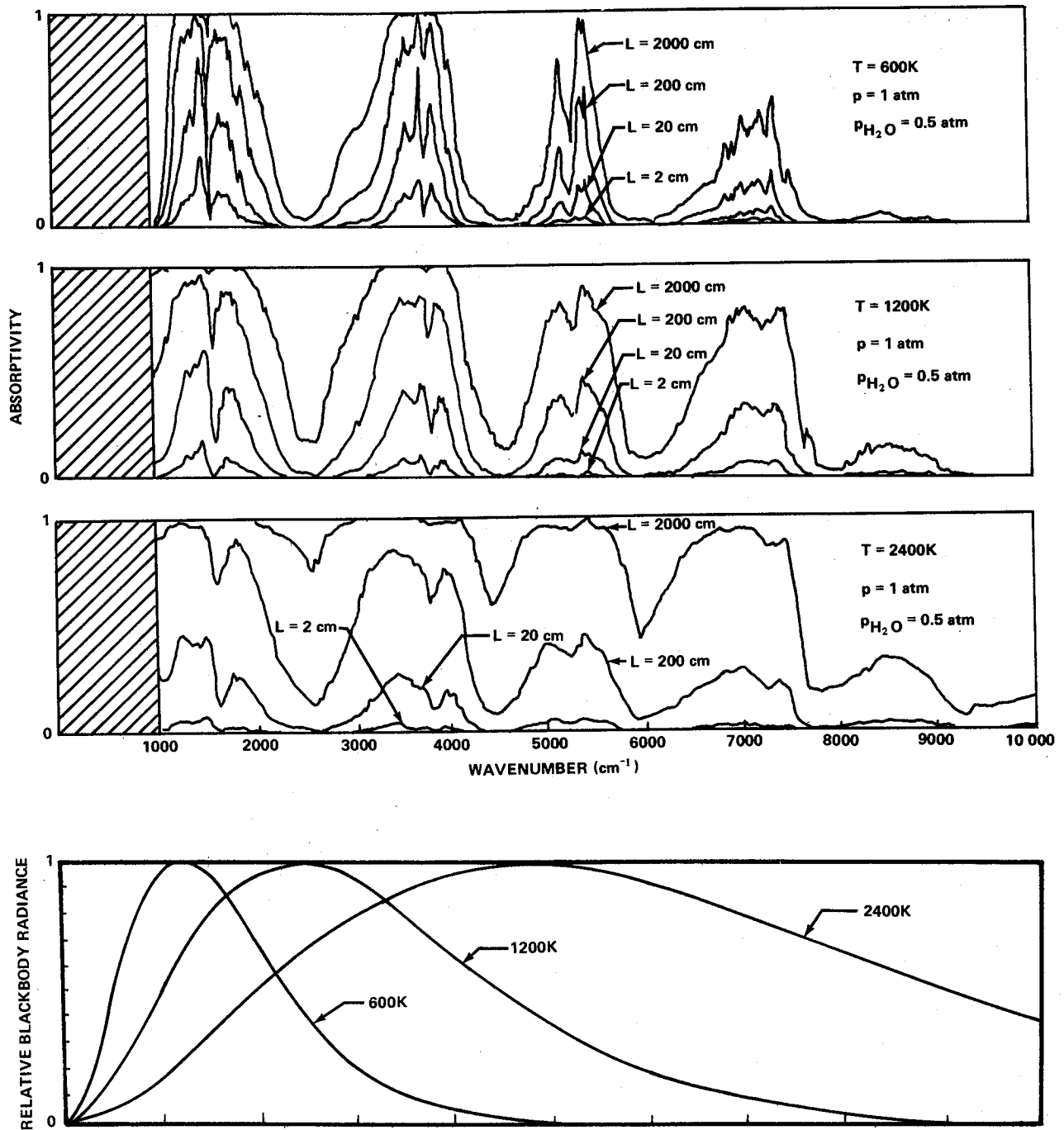


Figure 6-1a. Water vapor spectra — effect of pathlength.

CHAPTER 6 — COMPUTED RADIATION DATA

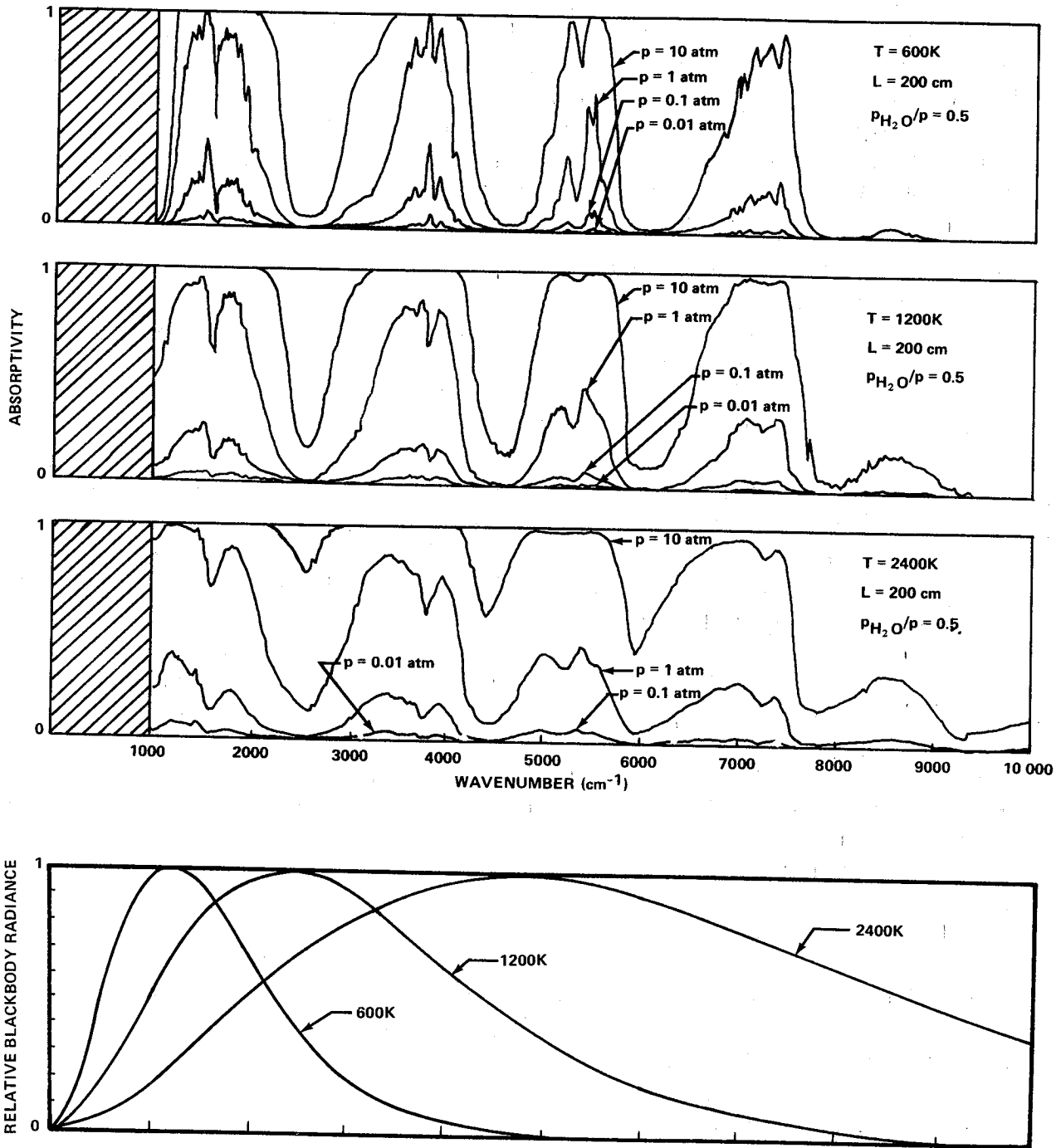


Figure 6-1b. Water vapor spectra — effect of pressure.

This behavior illustrates the effect of the curve of growth on the optical depth. In the square root limit ( $X = \sqrt{4\gamma k u / d}$ ) for conditions of constant temperature and mole fraction,  $X \propto p(\ell)^{1/2}$ , so there is a greater increase in optical depth with increasing pressure than with an increase in  $\ell$ . This behavior is illustrated in Figure 3-8. The effect is not as pronounced at the highest temperature in Figure 6-1 because of a combination of two factors. First, the line density,  $1/d$ , increases significantly at higher temperatures while the optical,  $u$ , decreases, so the optical depth moves toward the linear limit ( $X = k_{\omega} u$ ) where the optical depth is proportional to  $u$  with no differentiation between pressure and pathlength effects. Second, the increase in temperature causes a decrease in the collision-broadened line width while increasing the Doppler line width so the importance of Doppler broadening, which is not a function of pressure, increases.

### 6.1.2 CARBON DIOXIDE

In contrast to the wide spectral range of water vapor, the carbon dioxide spectrum is confined to several narrow bands. The bands of primary interest from a heat transfer standpoint are the two shown in Figures 6-2a and b. The predominant feature of the  $\text{CO}_2$  spectrum is the band at  $2300 \text{ cm}^{-1}$ . It is opaque at very short pathlengths at high pressure, and even at low pressure, the absorption is high. The same relative effects for pressure and pathlength noted for water vapor are also true for carbon dioxide, but the absorption is so high for the examples chosen that the effects are somewhat masked.

A more detailed illustration of the band structure in both the  $4.2\text{-}\mu$  band and the  $2.7\text{-}\mu$  band are presented in Figures 6-3 through 6-10. These figures illustrate the effects of the rapid increase of line density with temperature. For temperatures above  $1500\text{K}$ , the line density is so great that the Doppler component of the lines is sufficient by itself to smear out the spectral structure effectively.

There is another carbon dioxide band at  $670 \text{ cm}^{-1}$  which has not been included in Figure 6-2, but it may need to be considered in problems involving low temperatures.

### 6.1.3 CARBON MONOXIDE

The carbon monoxide spectra calculated using the SLG model described in Section 5.3 are illustrated in Figures 6-11a and b. They show single bands near  $2100 \text{ cm}^{-1}$ , but since carbon monoxide occurs with carbon dioxide in most applications, the carbon monoxide band is usually strongly overlapped by the carbon dioxide band.

CHAPTER 6 – COMPUTED RADIATION DATA

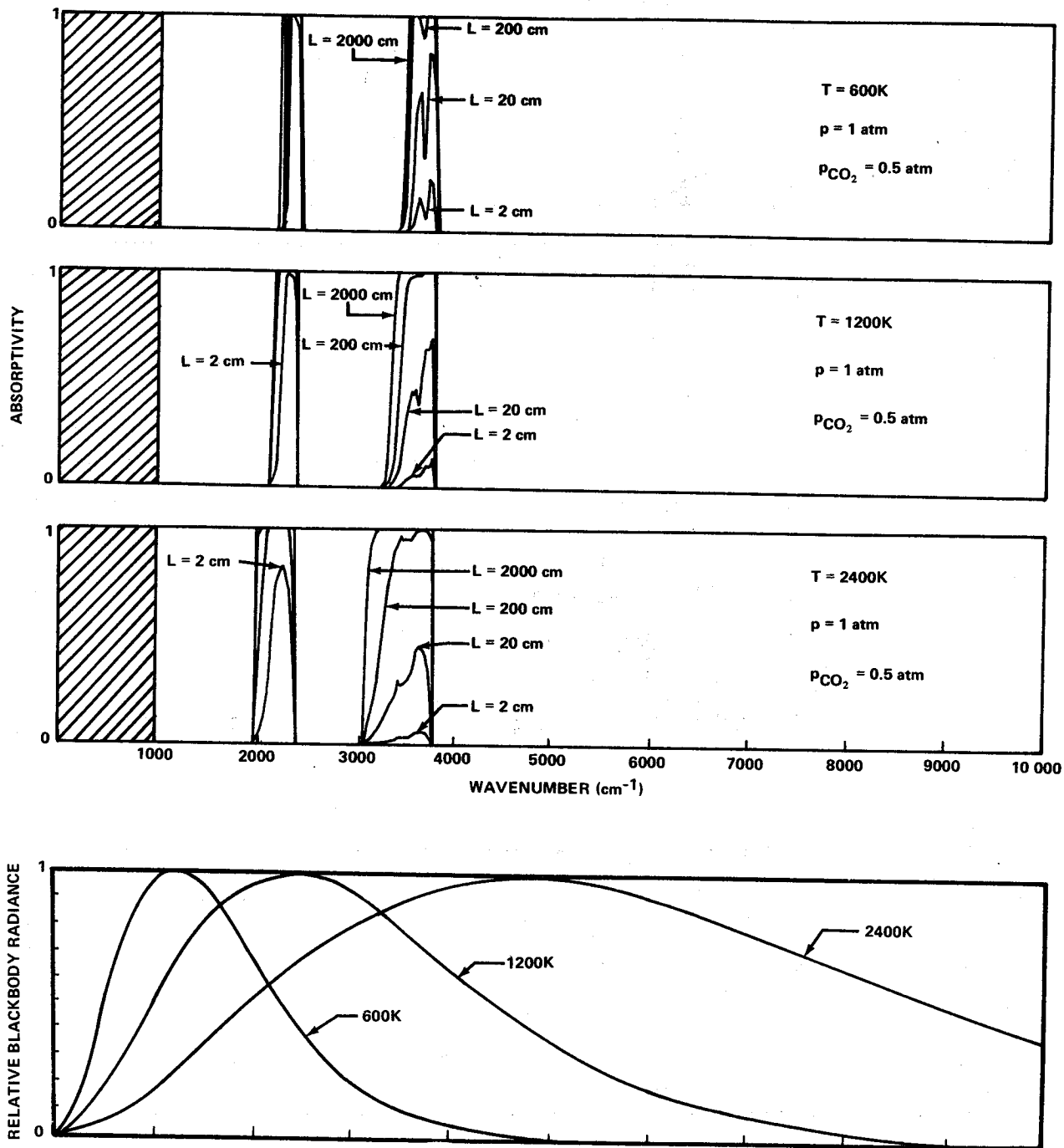


Figure 6-2a. Carbon dioxide spectra — effect of pathlength.

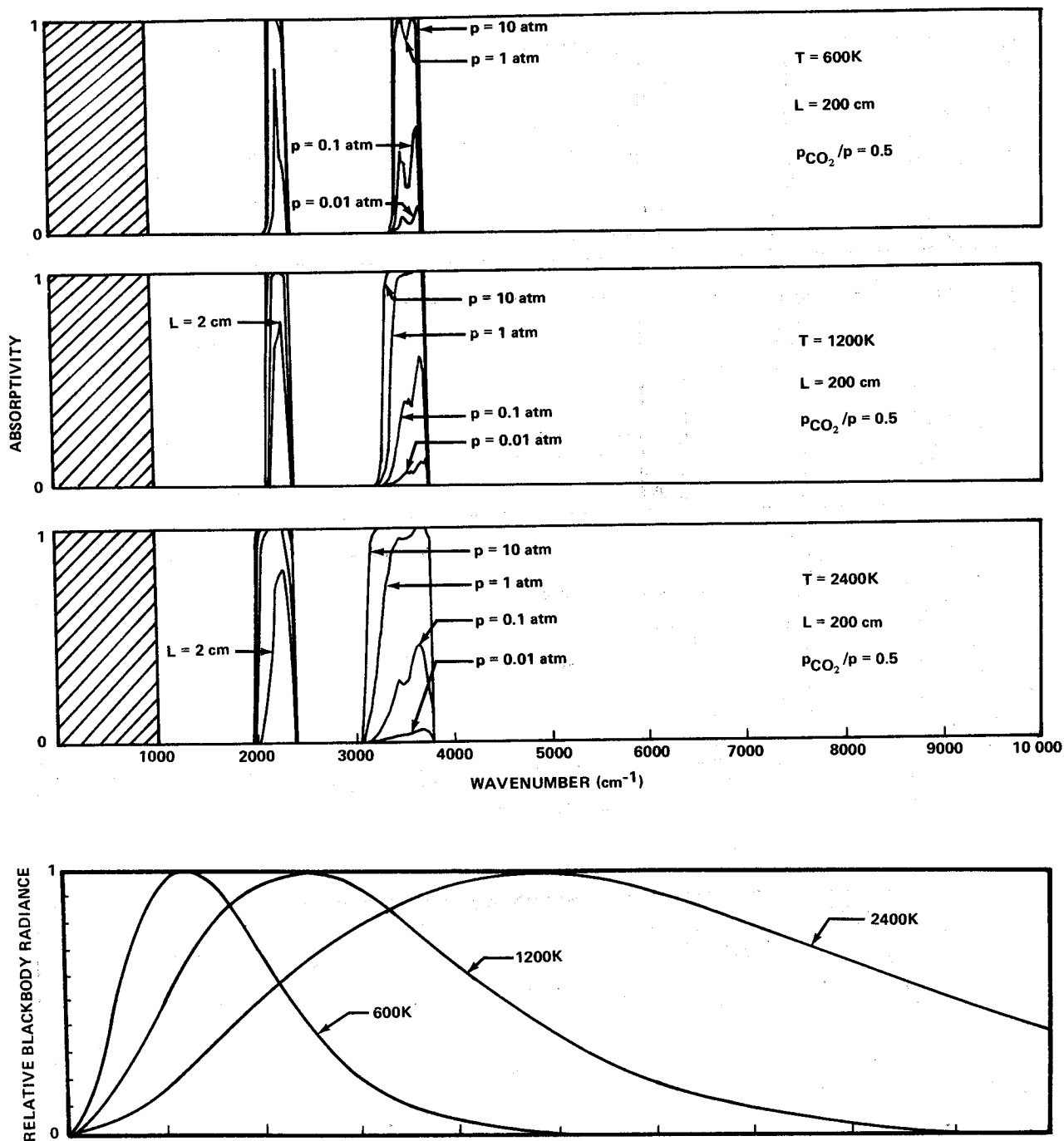


Figure 6-2b. Carbon dioxide spectra – effect of pressure.

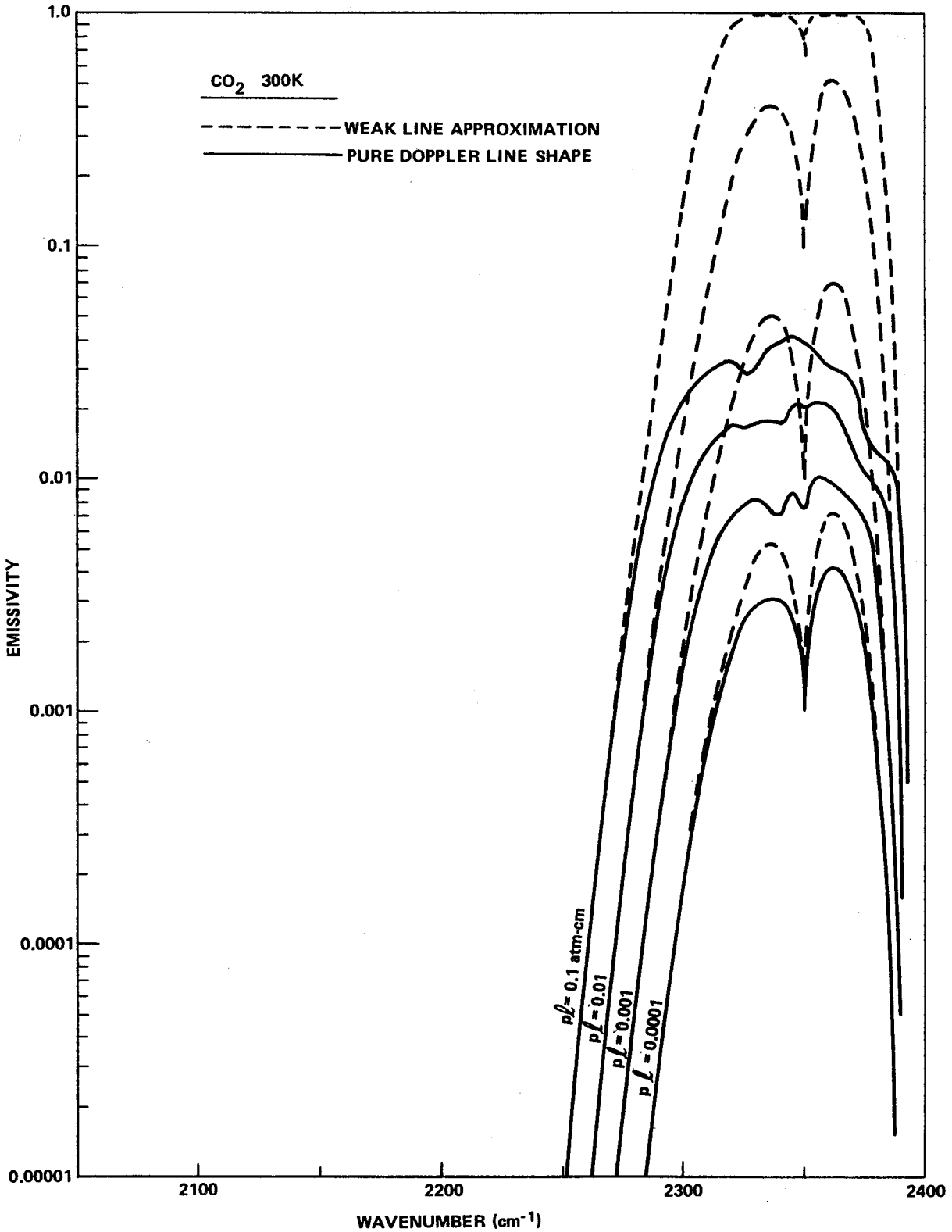


Figure 6-3. CO<sub>2</sub> 4.3- $\mu$  band emissivity versus wavenumber for pure Doppler line shape and weak line approximation for T = 300K.

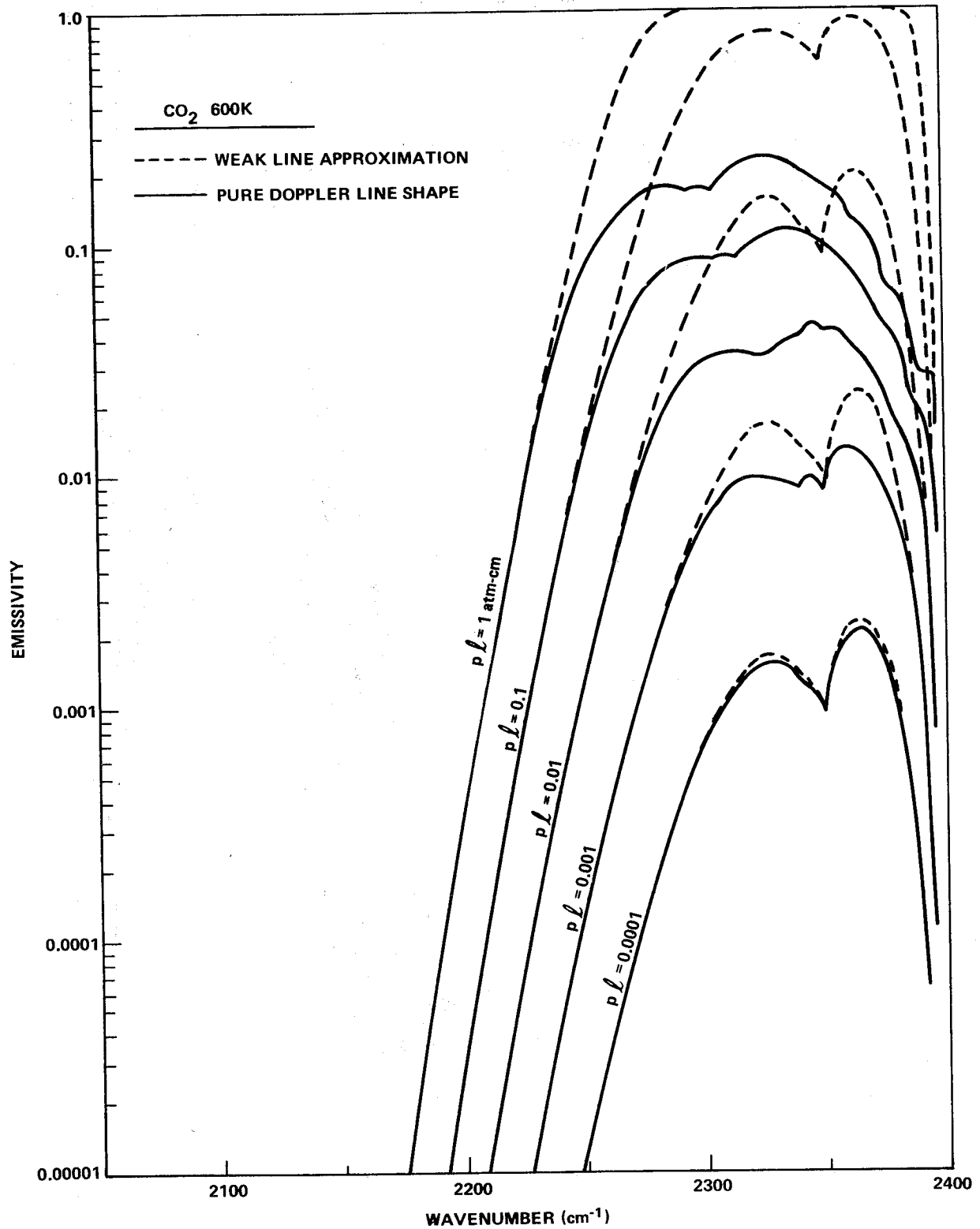


Figure 6-4. CO<sub>2</sub> 4.3-μ band emissivity versus wavenumber for pure Doppler line shape and weak line approximation for T = 600K.

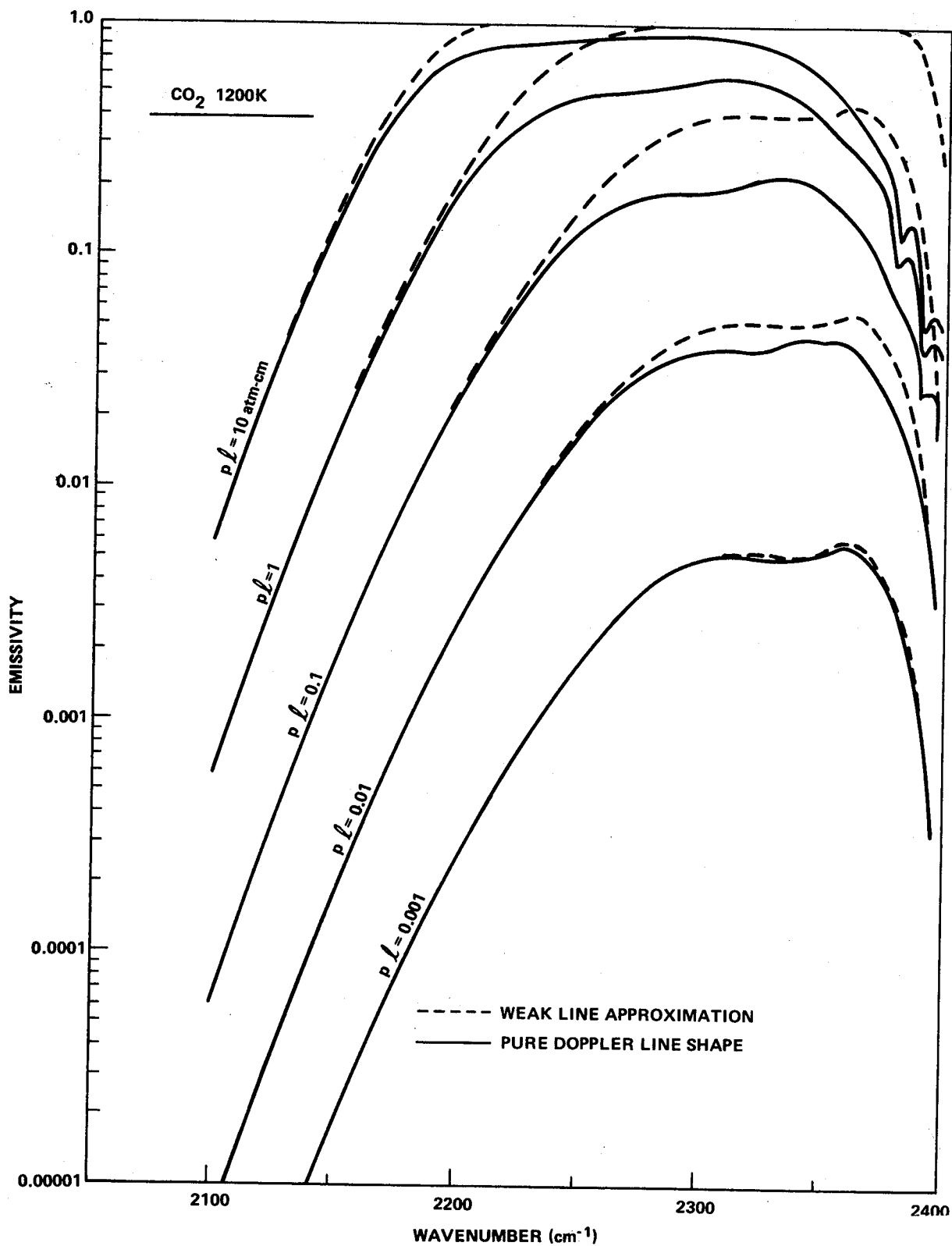


Figure 6-5. CO<sub>2</sub> 4.3- $\mu$  band emissivity versus wavenumber for pure Doppler line shape and weak line approximation for T = 1200K.

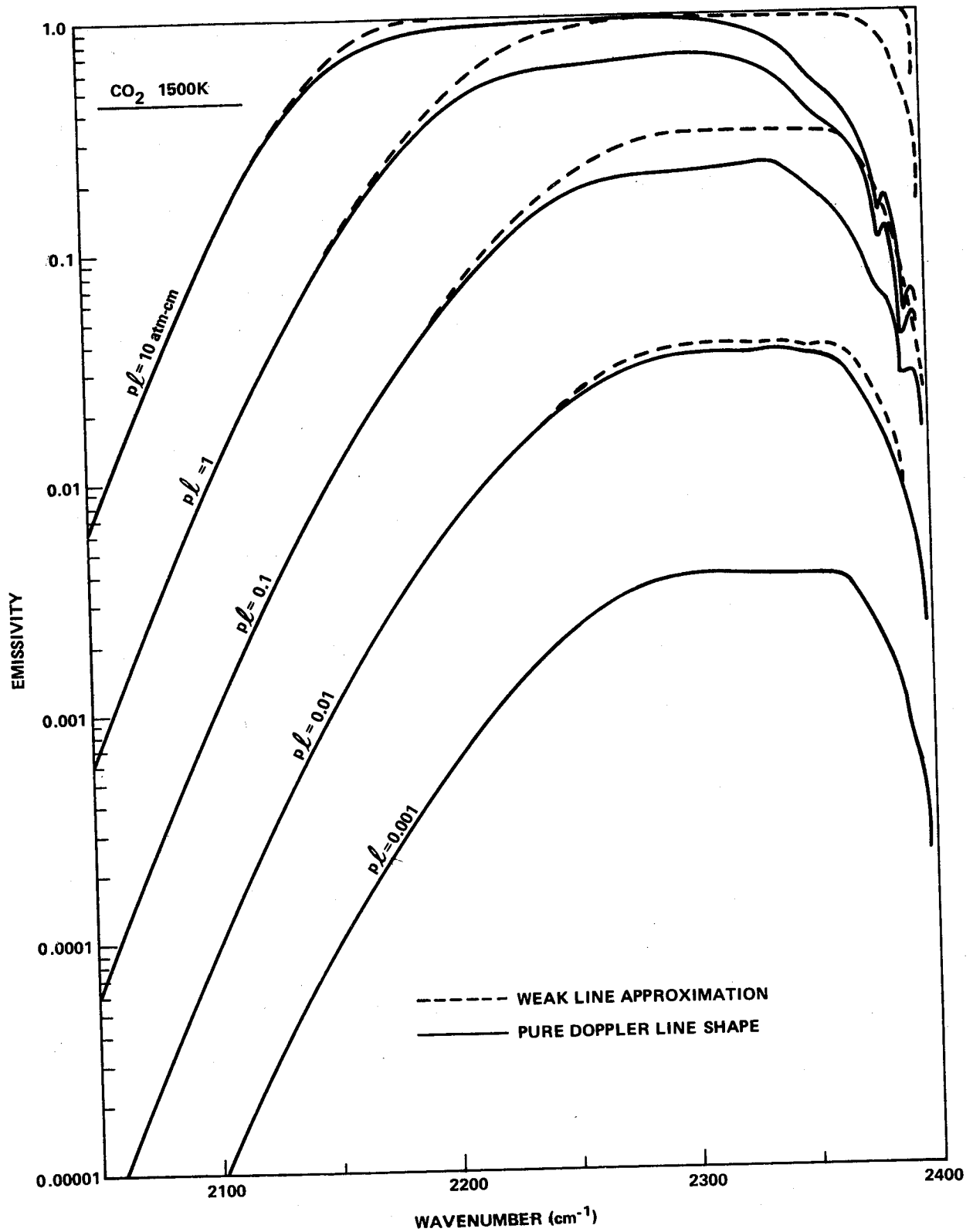


Figure 6-6. CO<sub>2</sub> 4.3- $\mu$  band emissivity versus wavenumber for pure Doppler line shape and weak line approximation for T = 1500K.

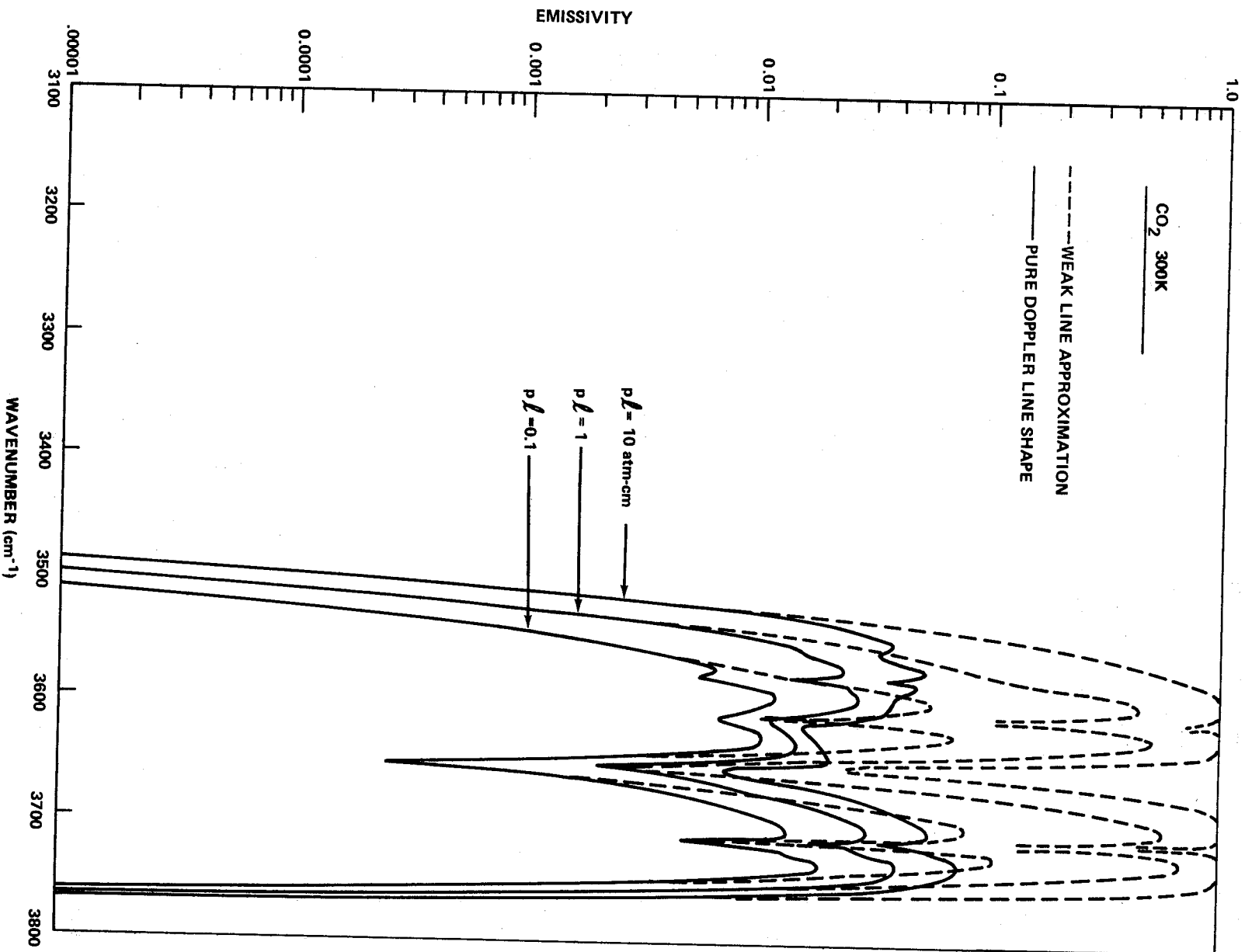


Figure 6-7. CO<sub>2</sub> 2.7- $\mu$  band emissivity versus wavenumber for pure Doppler line shape and weak line approximation for T = 300K.

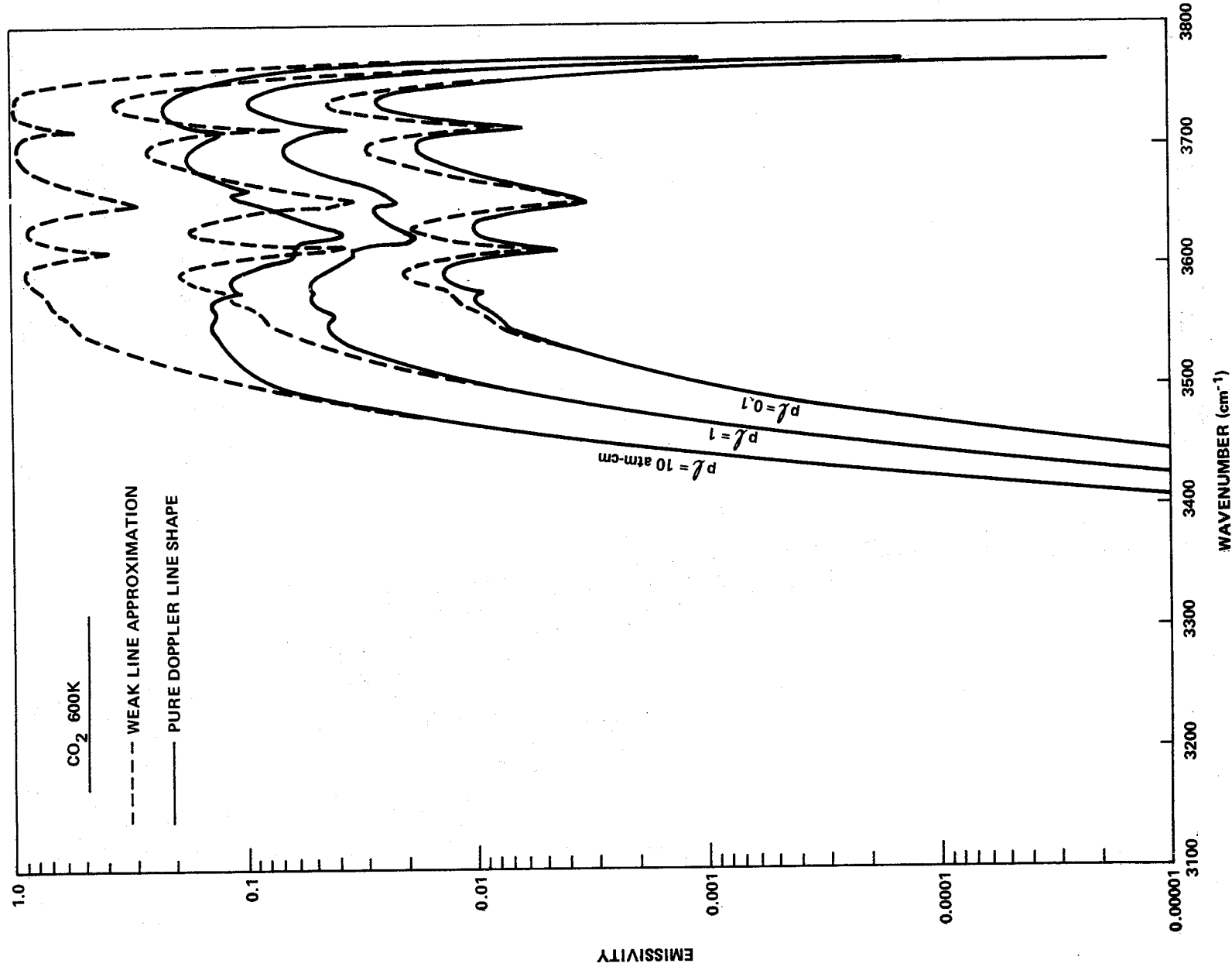


Figure 6-8.  $\text{CO}_2$   $2.7\text{-}\mu$  band emissivity versus wavenumber for pure Doppler line shape and weak line approximation for  $T = 600\text{K}$ .

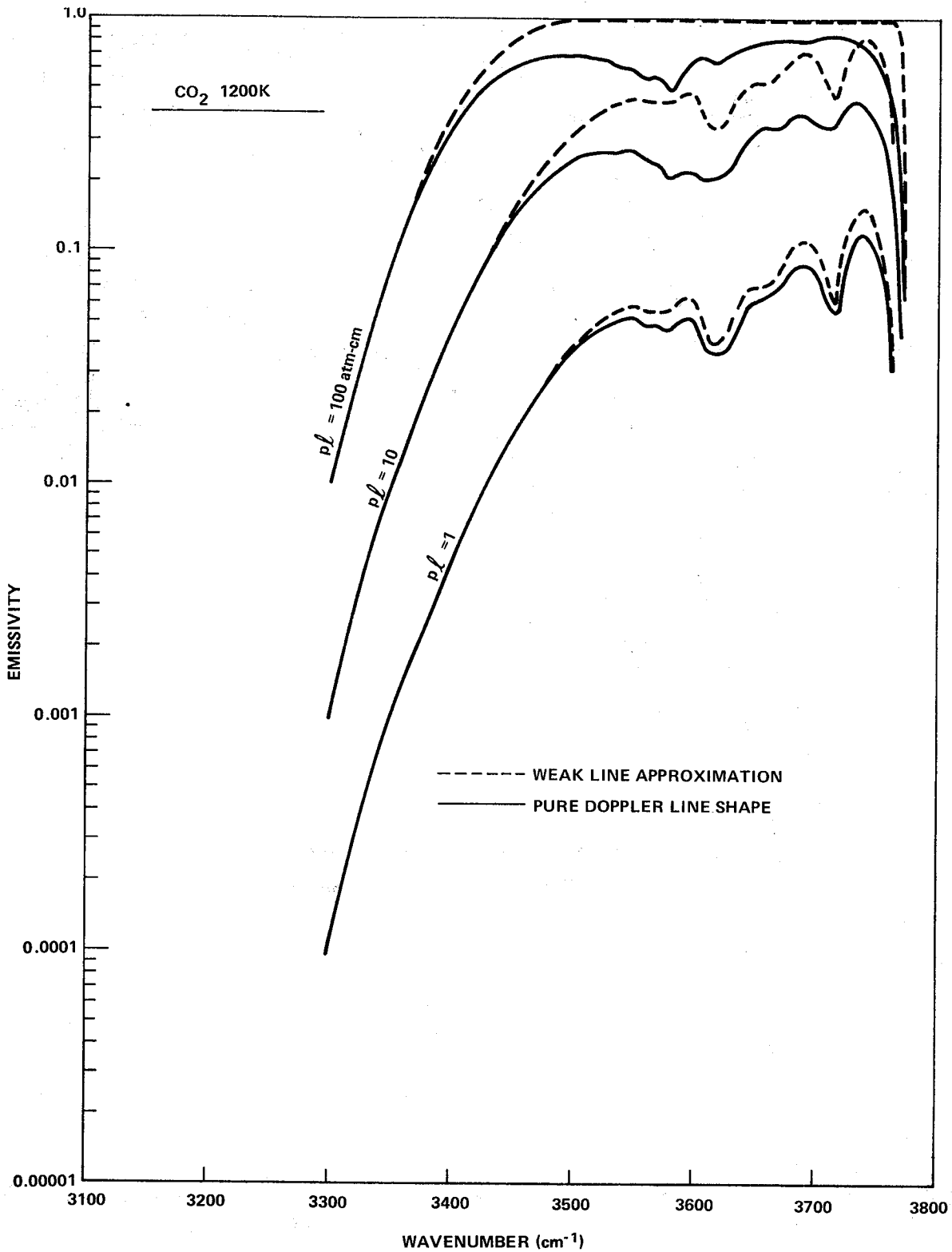


Figure 6-9. CO<sub>2</sub> 2.7- $\mu$  band emissivity versus wavenumber for pure Doppler line shape and weak line approximation for T = 1200K.

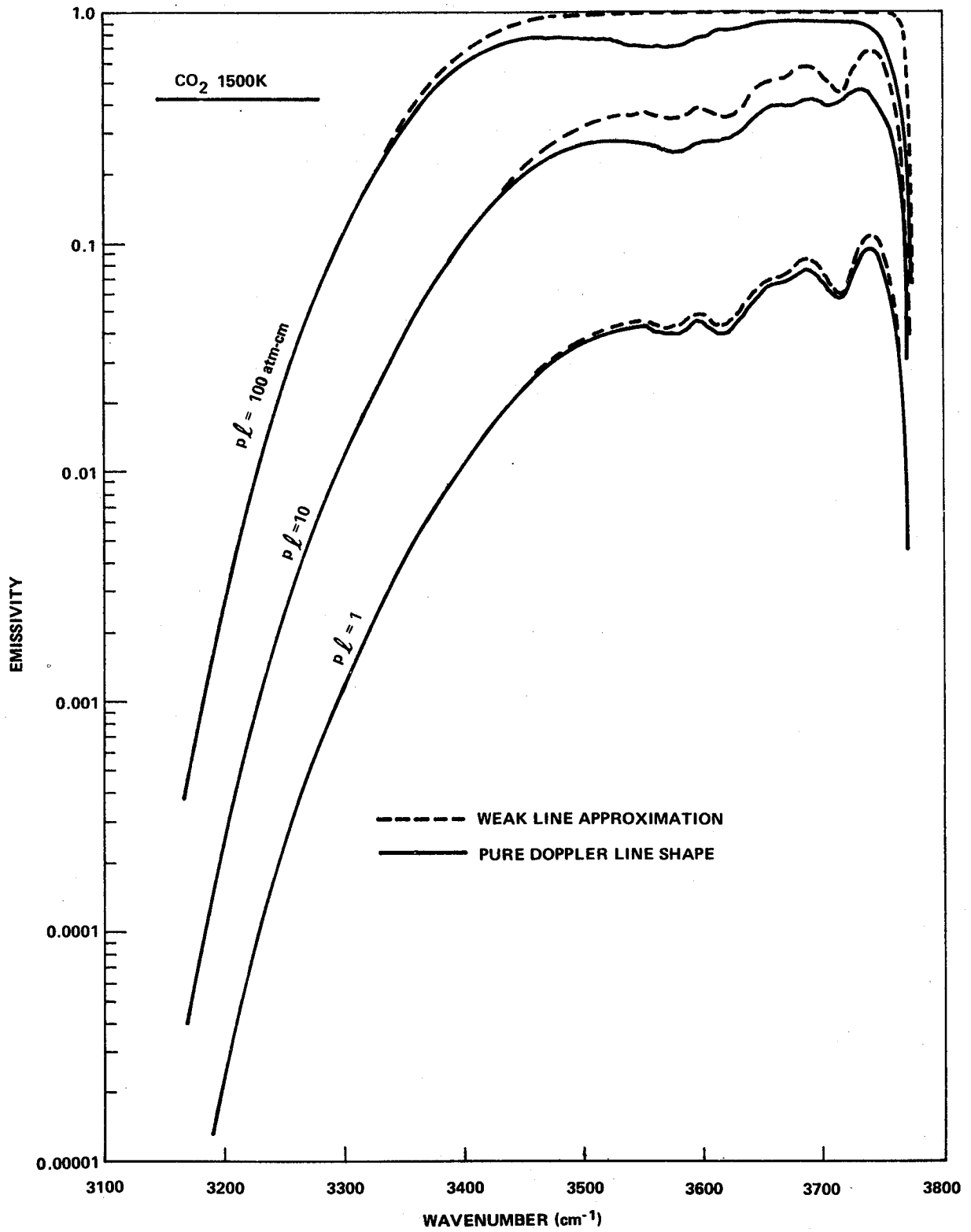


Figure 6-10. CO<sub>2</sub> 2.7- $\mu$  band emissivity versus wavenumber for pure Doppler line shape and weak line approximation for T = 1500K.

CHAPTER 6 – COMPUTED RADIATION DATA

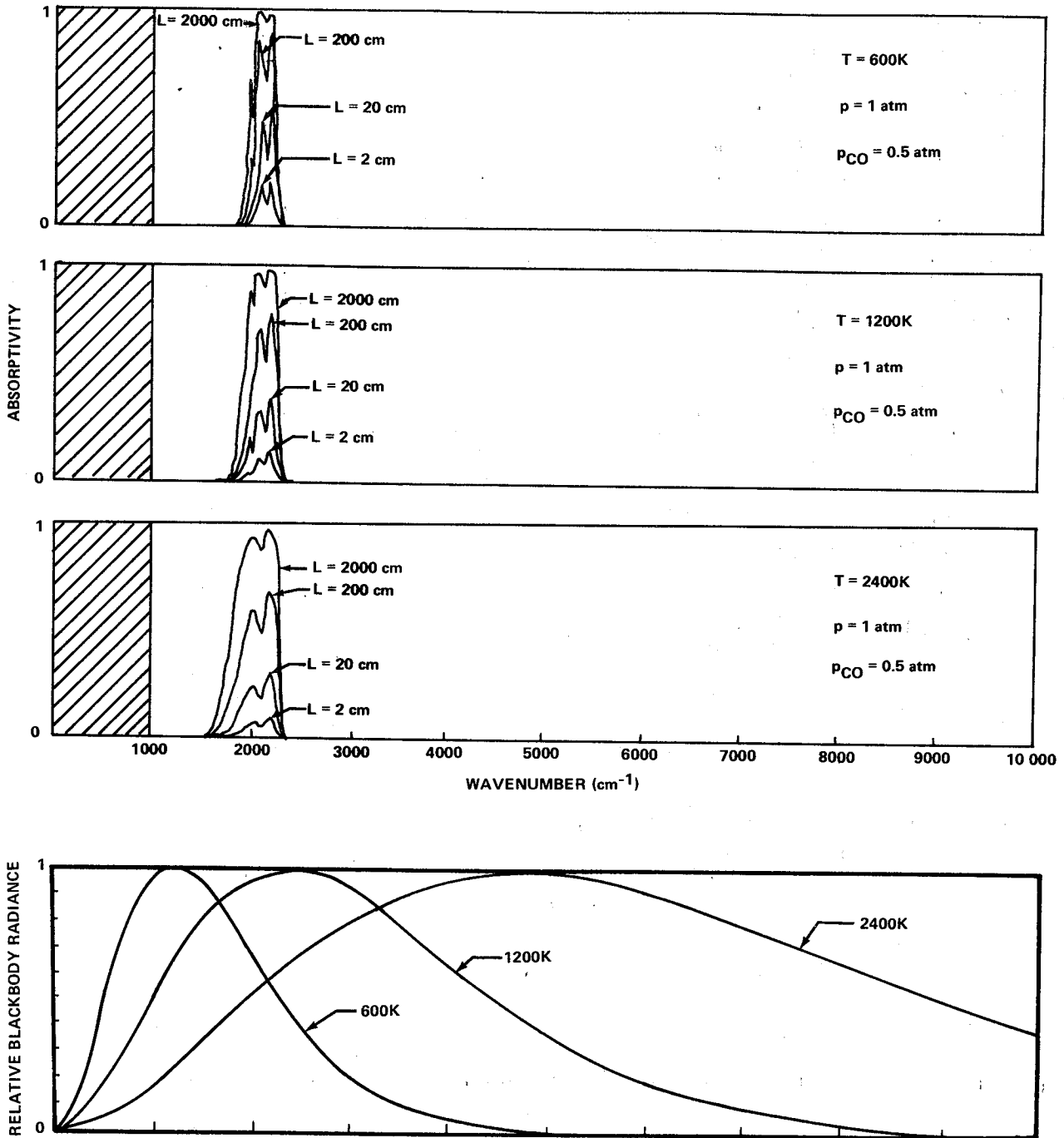


Figure 6-11a. Carbon monoxide spectra — effect of pathlength.

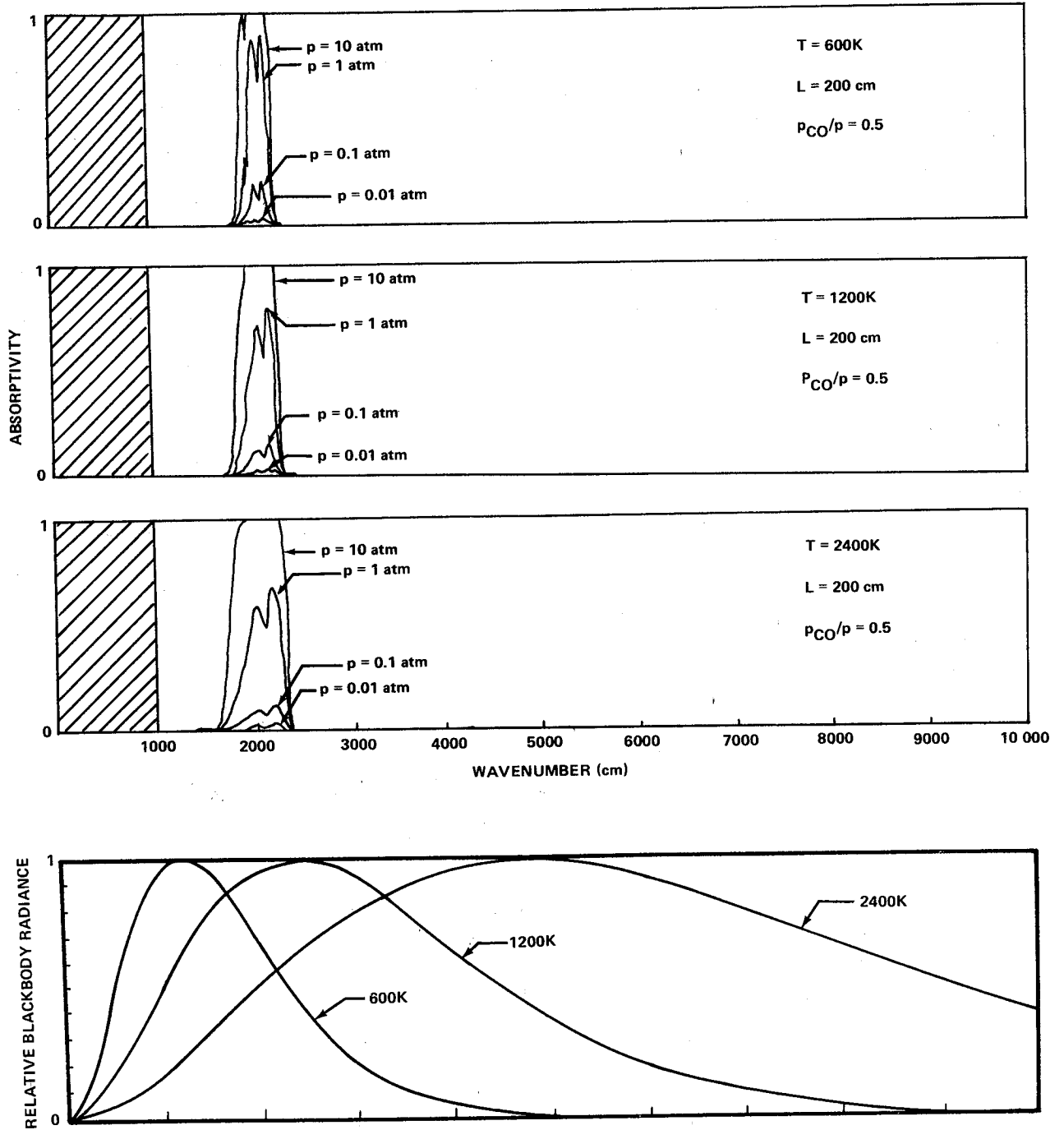


Figure 6-11b. Carbon monoxide spectra — effect of pressure.

## CHAPTER 6 – COMPUTED RADIATION DATA

### 6.1.4 CARBON PARTICLES

Since carbon particles are solid, they radiate in a continuum, and pressure effects are negligible. Spectral absorptivity calculated using the procedure described in Section 5.4 for finely divided soot is shown in Figure 6-12. The significant spectral characteristic is the continuous decrease in the absorption coefficient at short wavenumbers.

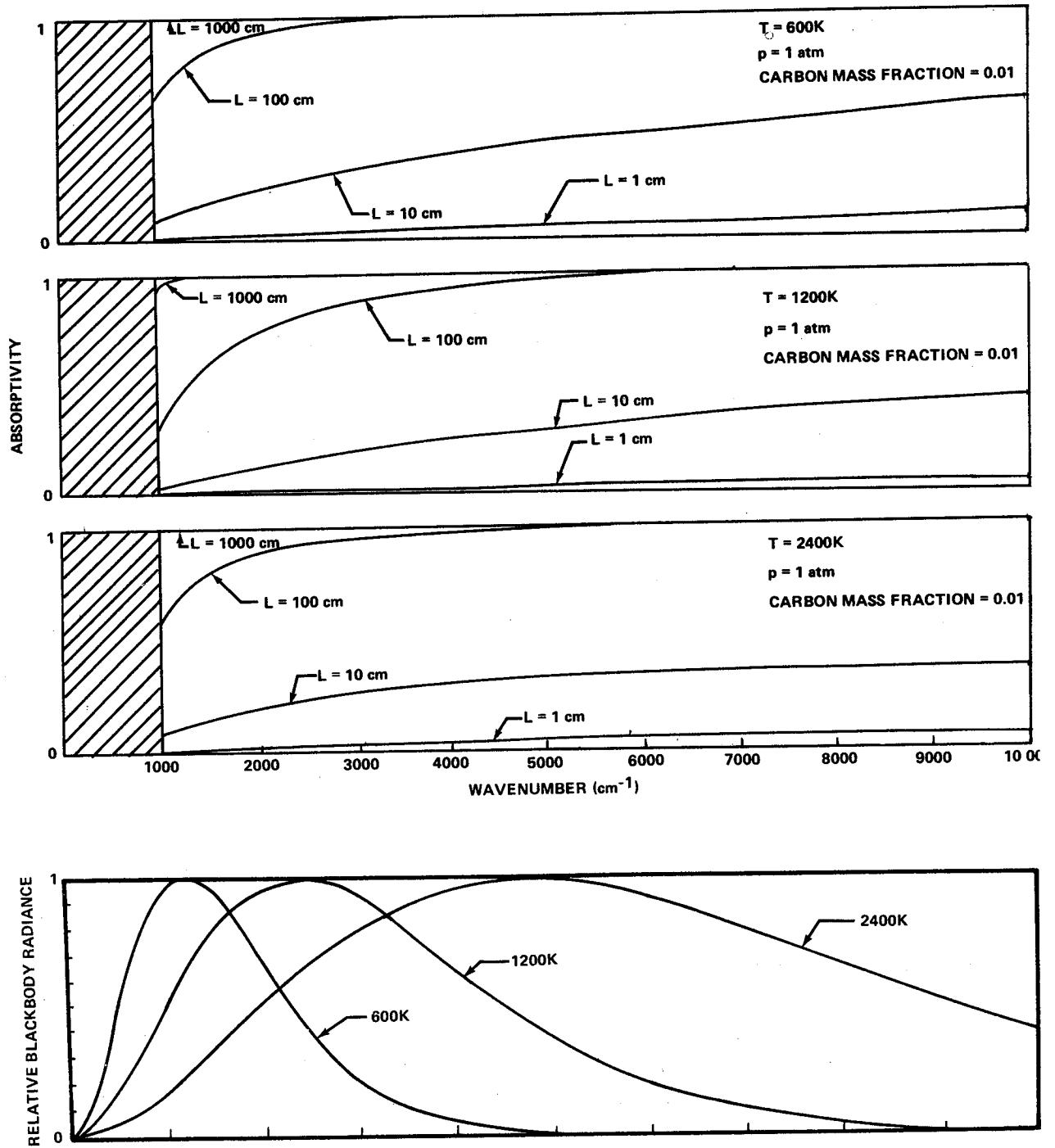


Figure 6-12. Absorptivity of finely divided soot particles.

6.2 INTEGRATED ABSORPTANCES FOR DIATOMIC GASES

Because of the narrow spectral width of the bands of diatomic gases, the integrated absorptance is often used in computing heat transfer. The integrated absorptance is defined as

$$\int_0^{\infty} \epsilon(\omega, T) d\omega = \int_0^{\infty} [1 - \tau(\omega, T)] d\omega \quad . \quad (6-1)$$

The radiance can be written in the approximate form

$$W(\tau) = W_{\omega}^0(\omega_0, T) \int_0^{\infty} \epsilon(\omega, T) d\omega \quad , \quad (6-2)$$

where  $W_{\omega}^0(\omega_0, T)$  is evaluated at the band center ( $\omega = \omega_0$ ).

Integrated absorptances of several diatomic gases are presented in Figures 6-13 through 6-30 as functions of total pressure, temperature, and pathlength. The order of presentation is tabulated below:

Figure Number for Pressure Indicated

<u>Gas</u>	<u>0.01 atm</u>	<u>0.1 atm</u>	<u>1.0 atm</u>
CO	6-13	6-14	6-15
NO	6-16	6-17	6-18
CN	6-19	6-20	6-21
OH	6-22	6-23	6-24
HCl	6-25	6-26	6-27
HF	6-28	6-29	6-30

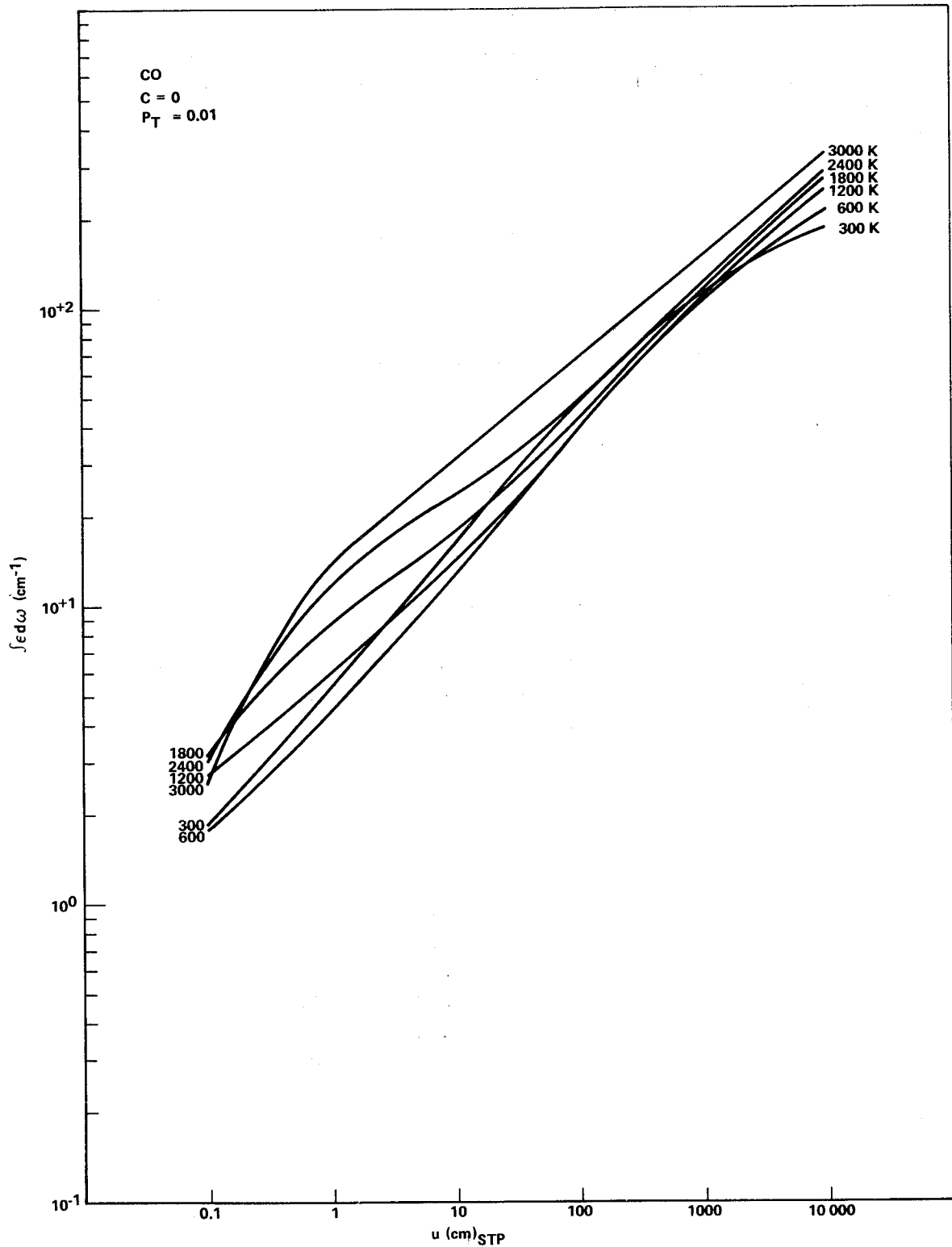


Figure 6-13. Integrated absorptance for the fundamental band of CO at 0.01 atm pressure.

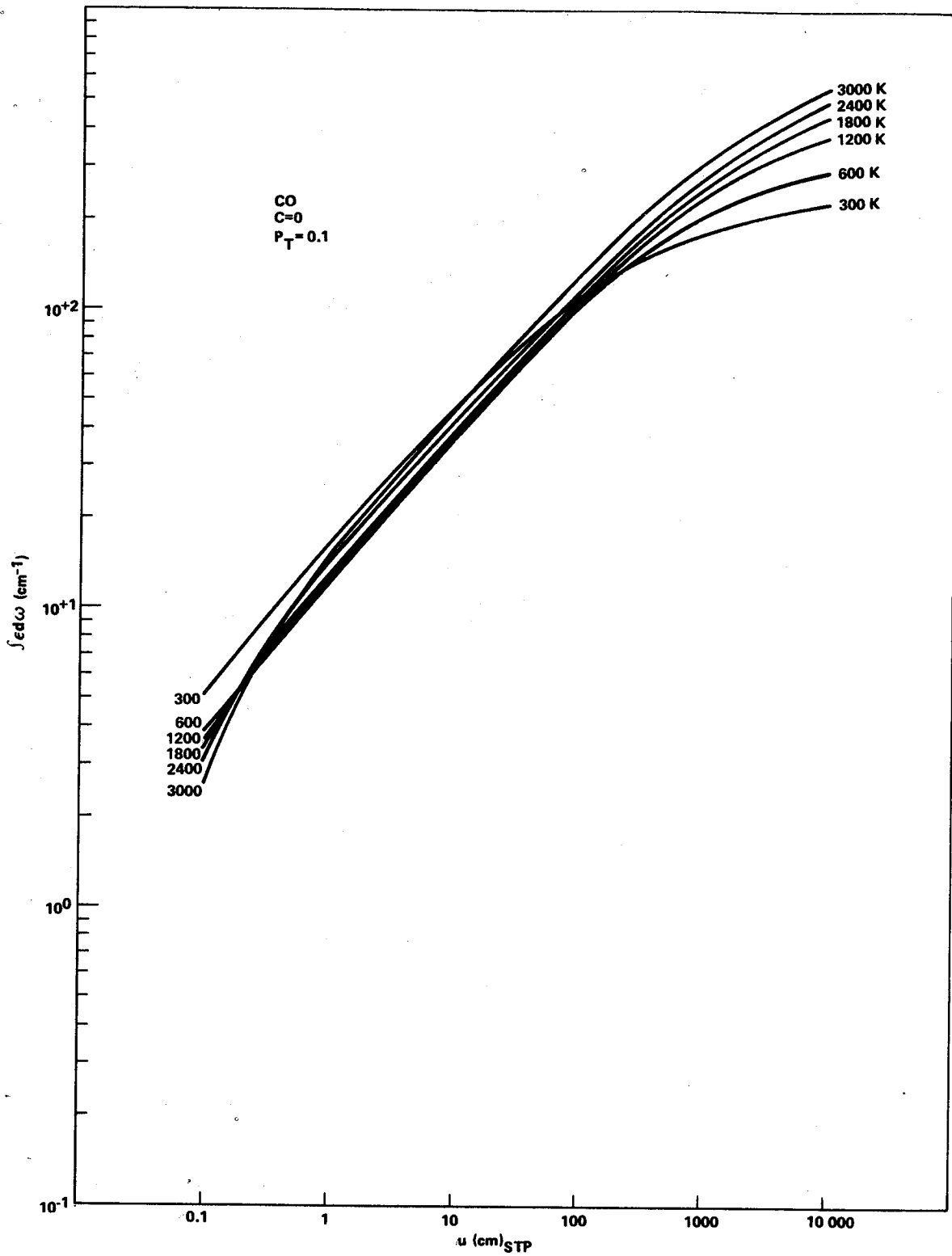
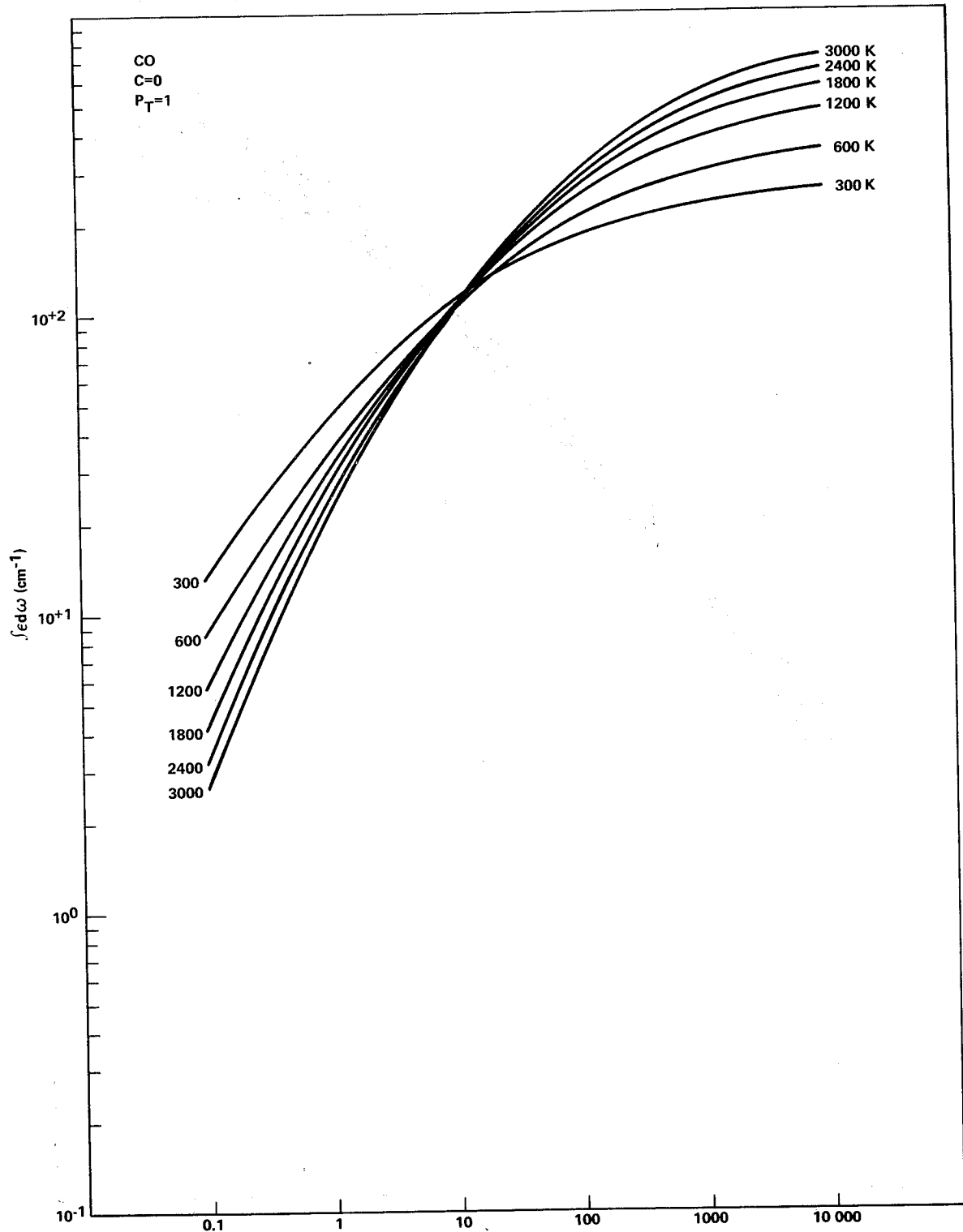


Figure 6-14. Integrated absorptance for the fundamental band of CO at 0.1 atm pressure.



at 1.0 atm pressure.

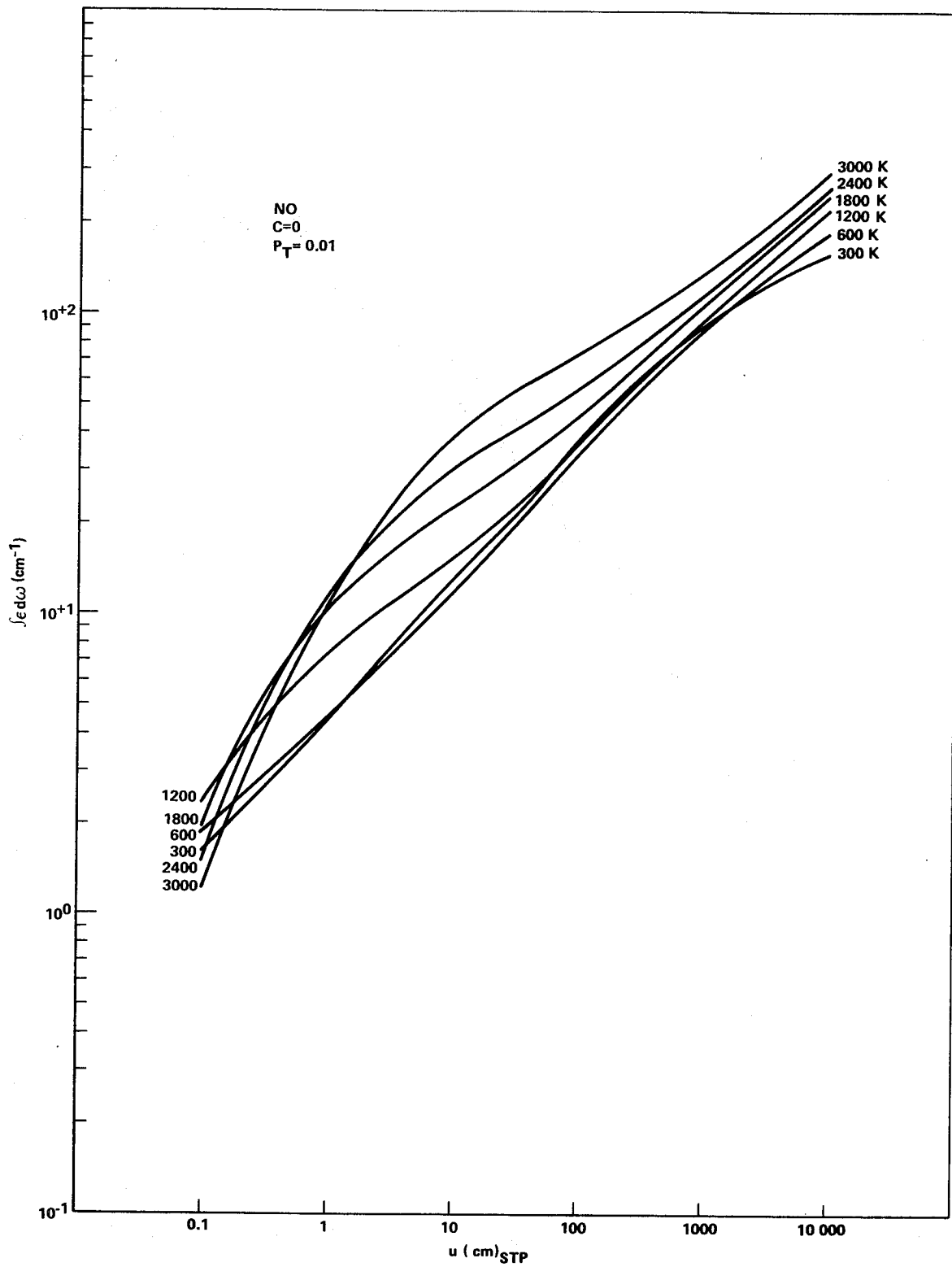


Figure 6-16. Integrated absorptance for the fundamental band of NO at 0.01 atm pressure.

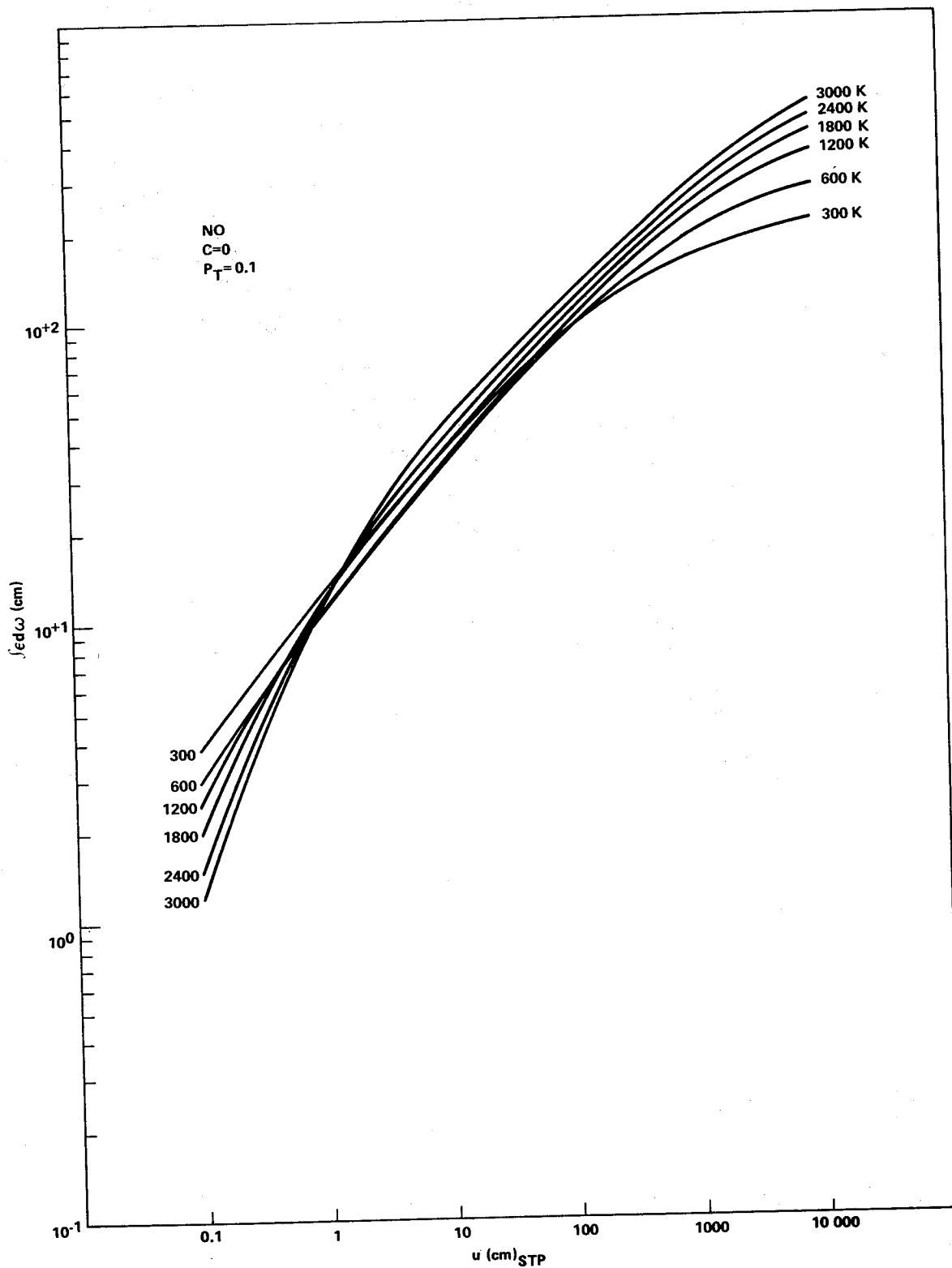


Figure 6-17. Integrated absorptance for the fundamental band of NO at 0.1 atm pressure.

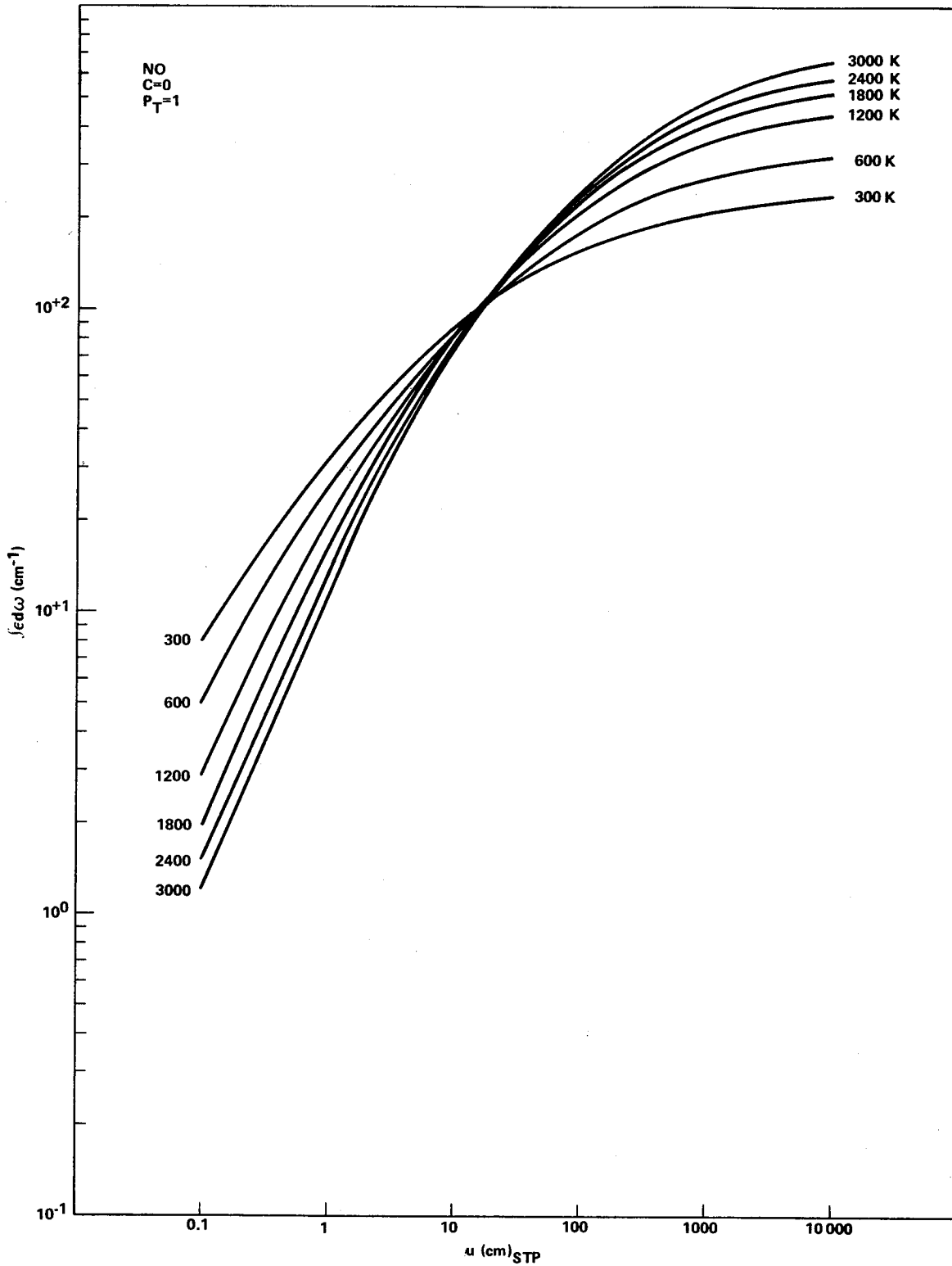


Figure 6-18. Integrated absorptance for the fundamental band of NO at 1.0 atm pressure.

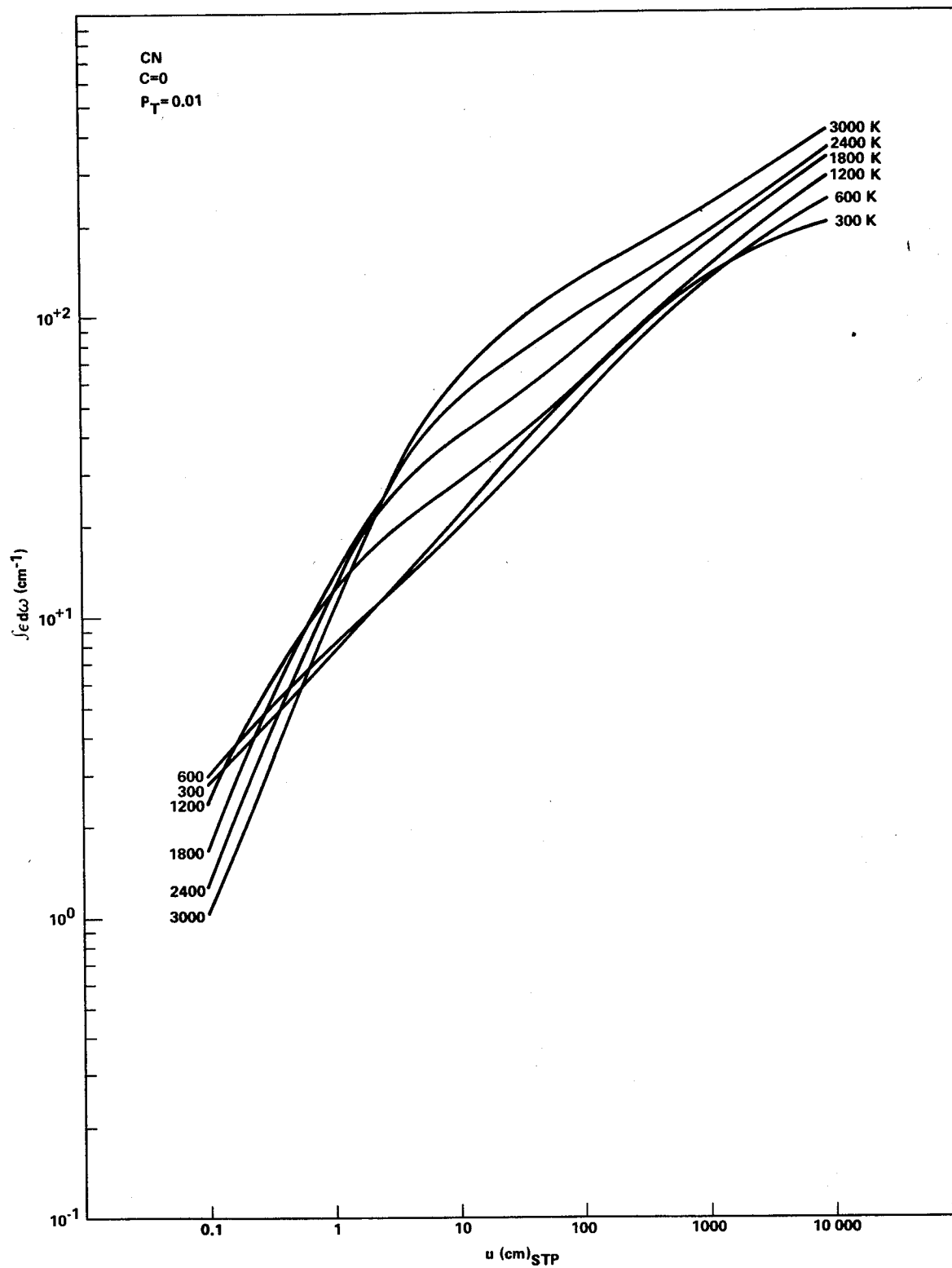


Figure 6-19. Integrated absorptance for the fundamental band of CN at 0.01 atm pressure.

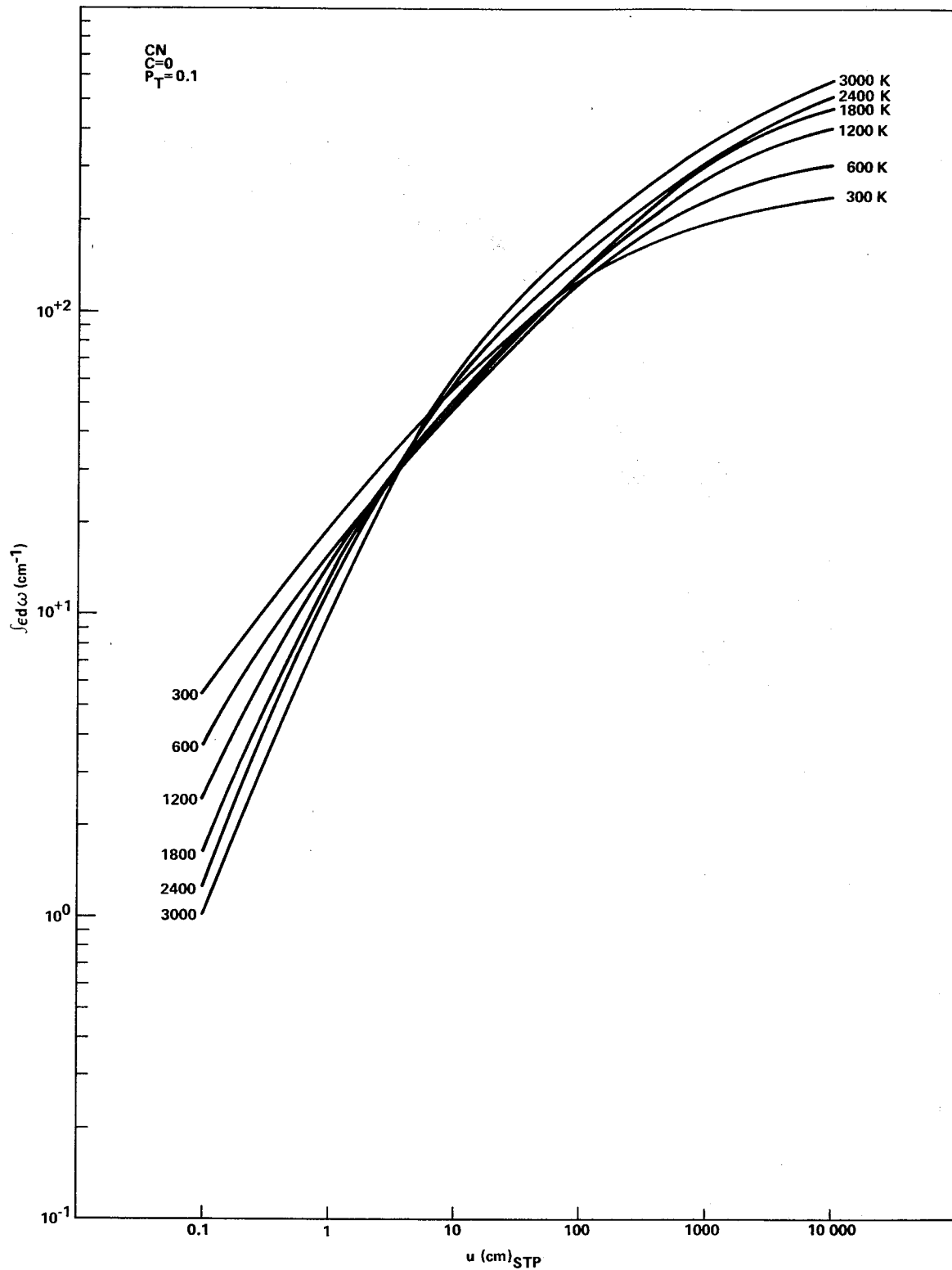


Figure 6-20. Integrated absorptance for the fundamental band of CN at 0.1 atm pressure.

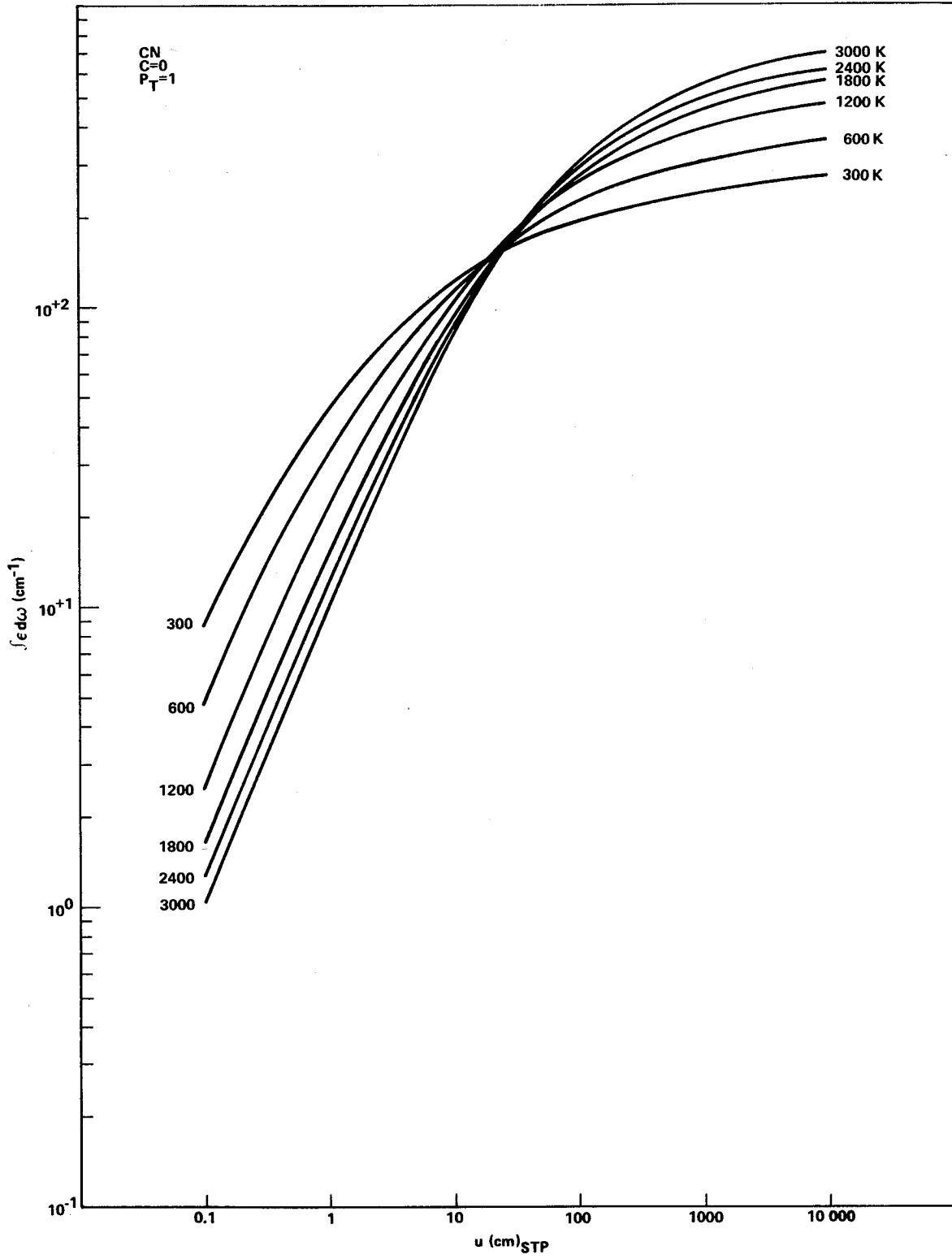


Figure 6-21. Integrated absorptance for the fundamental band of CN at 1.0 atm pressure.

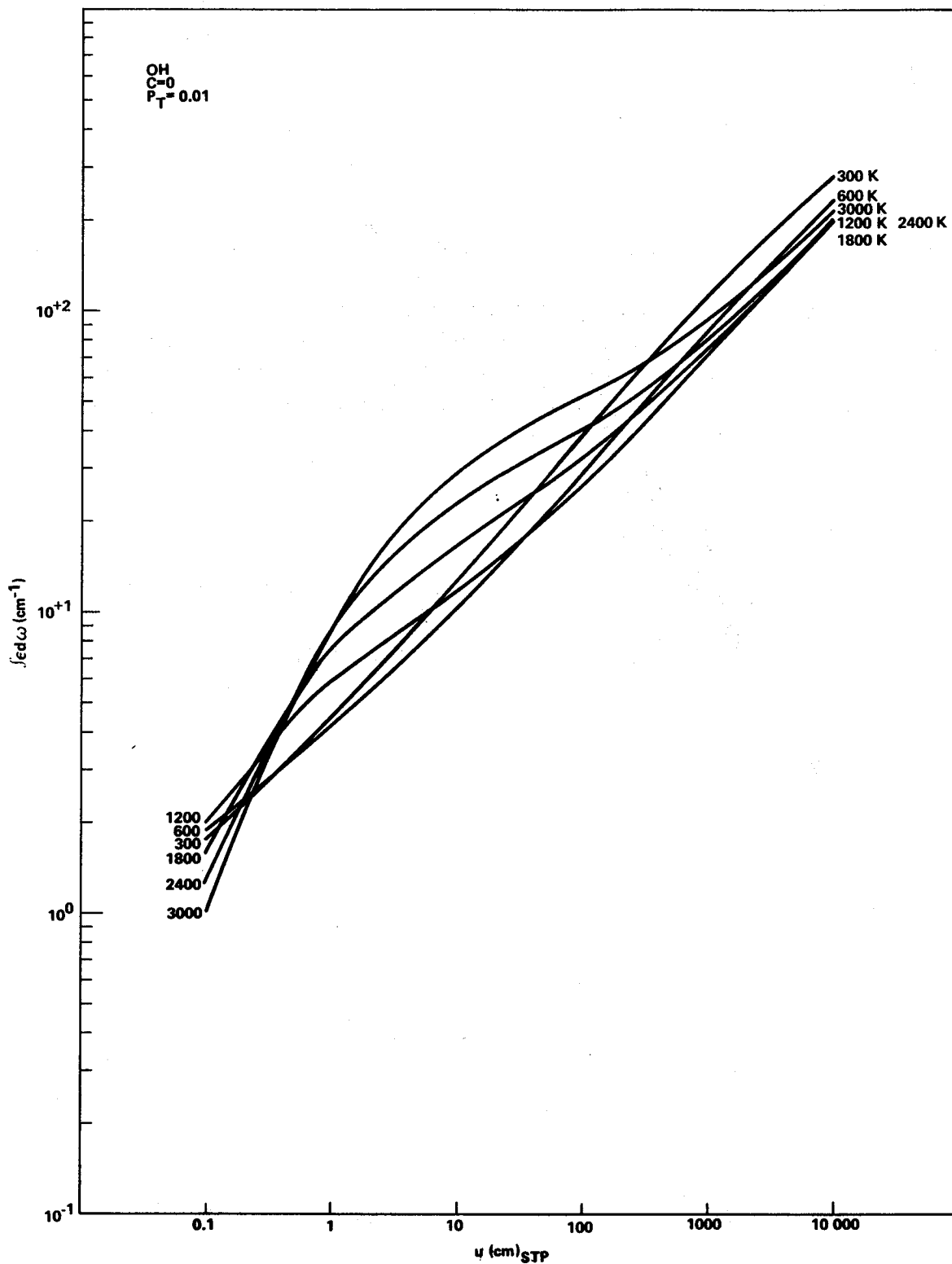


Figure 6-22. Integrated absorptance for the fundamental band of OH at 0.01 atm pressure.

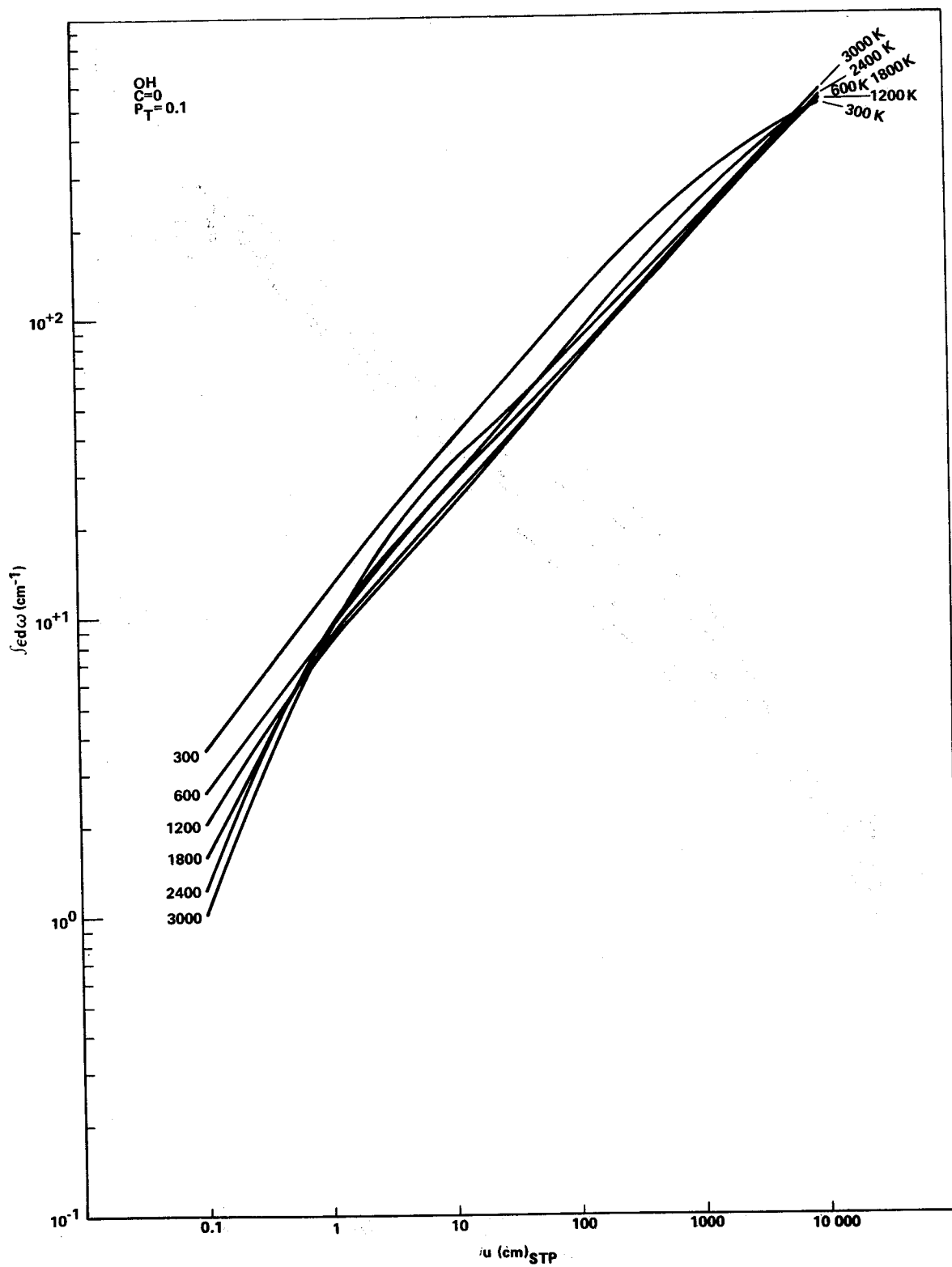


Figure 6-23. Integrated absorbance for the fundamental band of OH at 0.1 atm pressure.



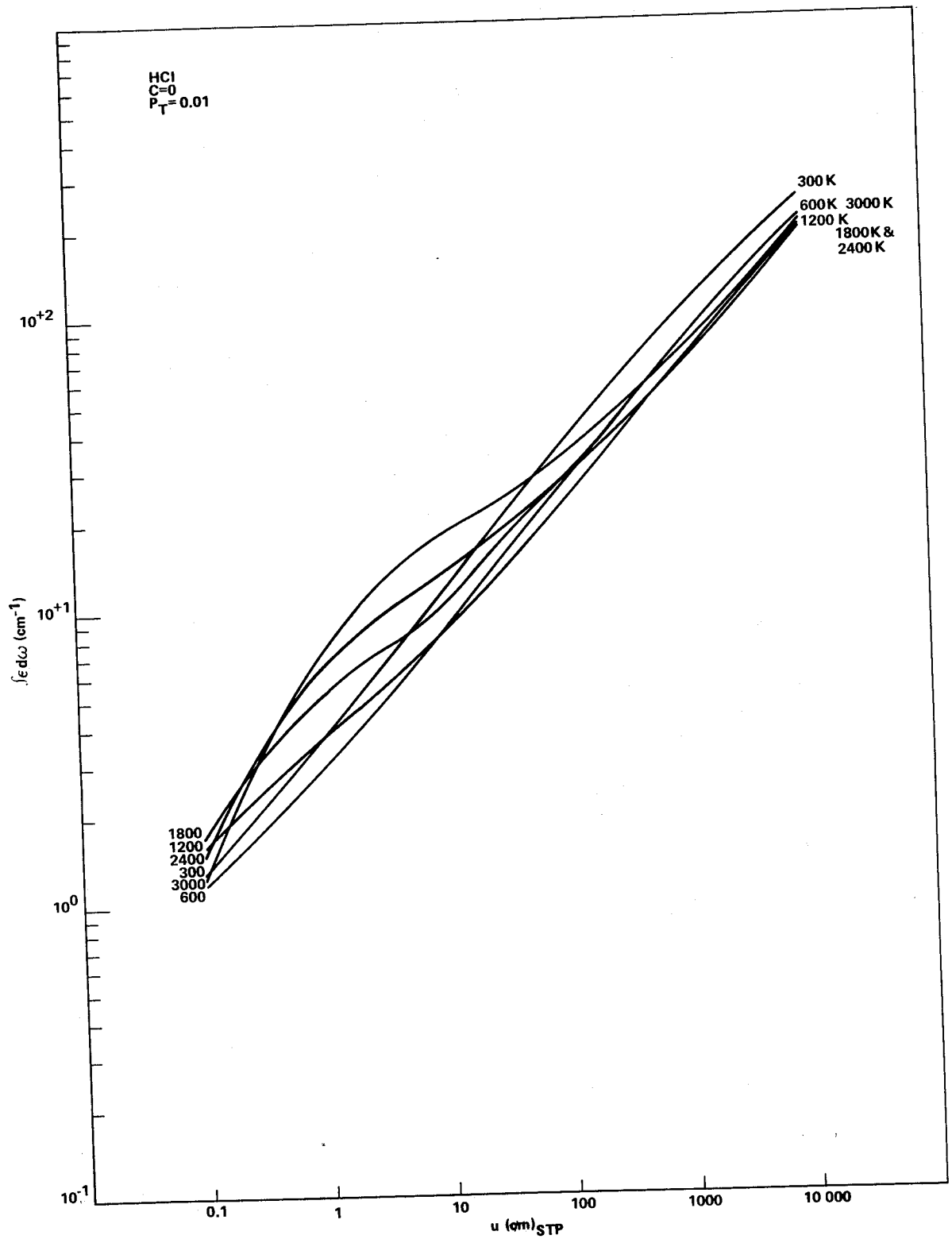


Figure 6-25. Integrated absorptance for the fundamental band of HCl at 0.01 atm pressure.

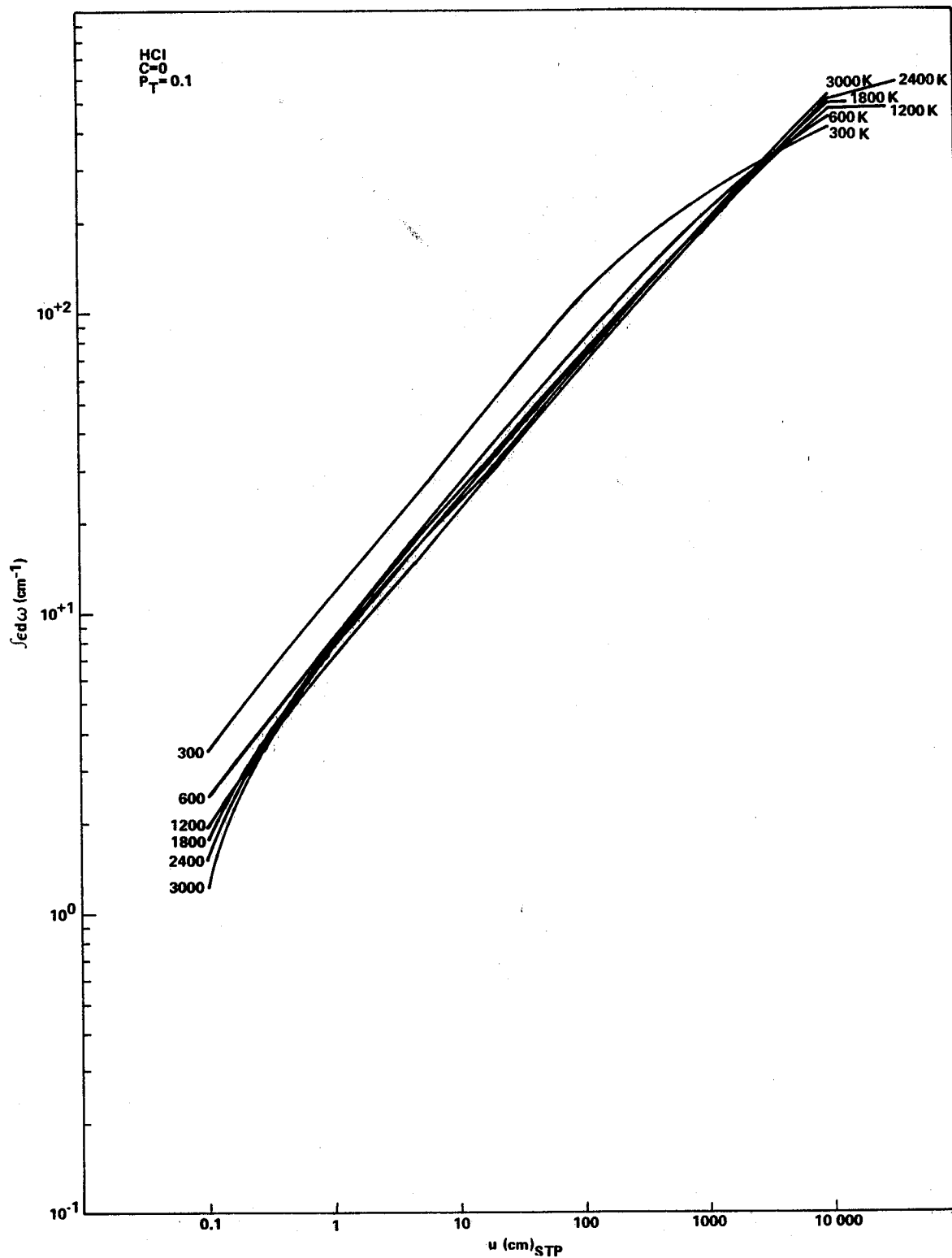


Figure 6-26. Integrated absorptance for the fundamental band of HCl at 0.1 atm pressure.

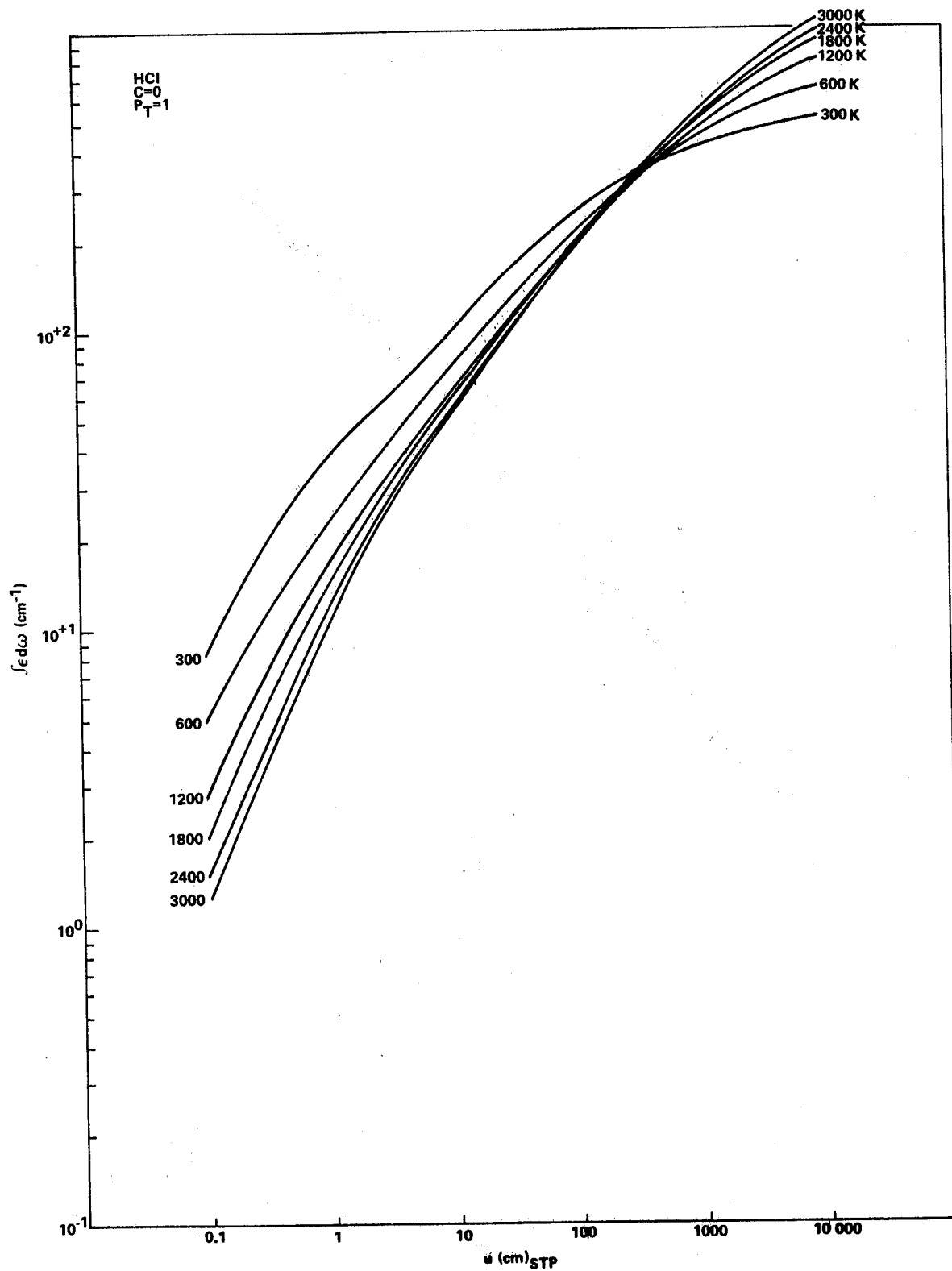


Figure 6-27. Integrated absorptance for the fundamental band of HCl at 1.0 atm pressure.

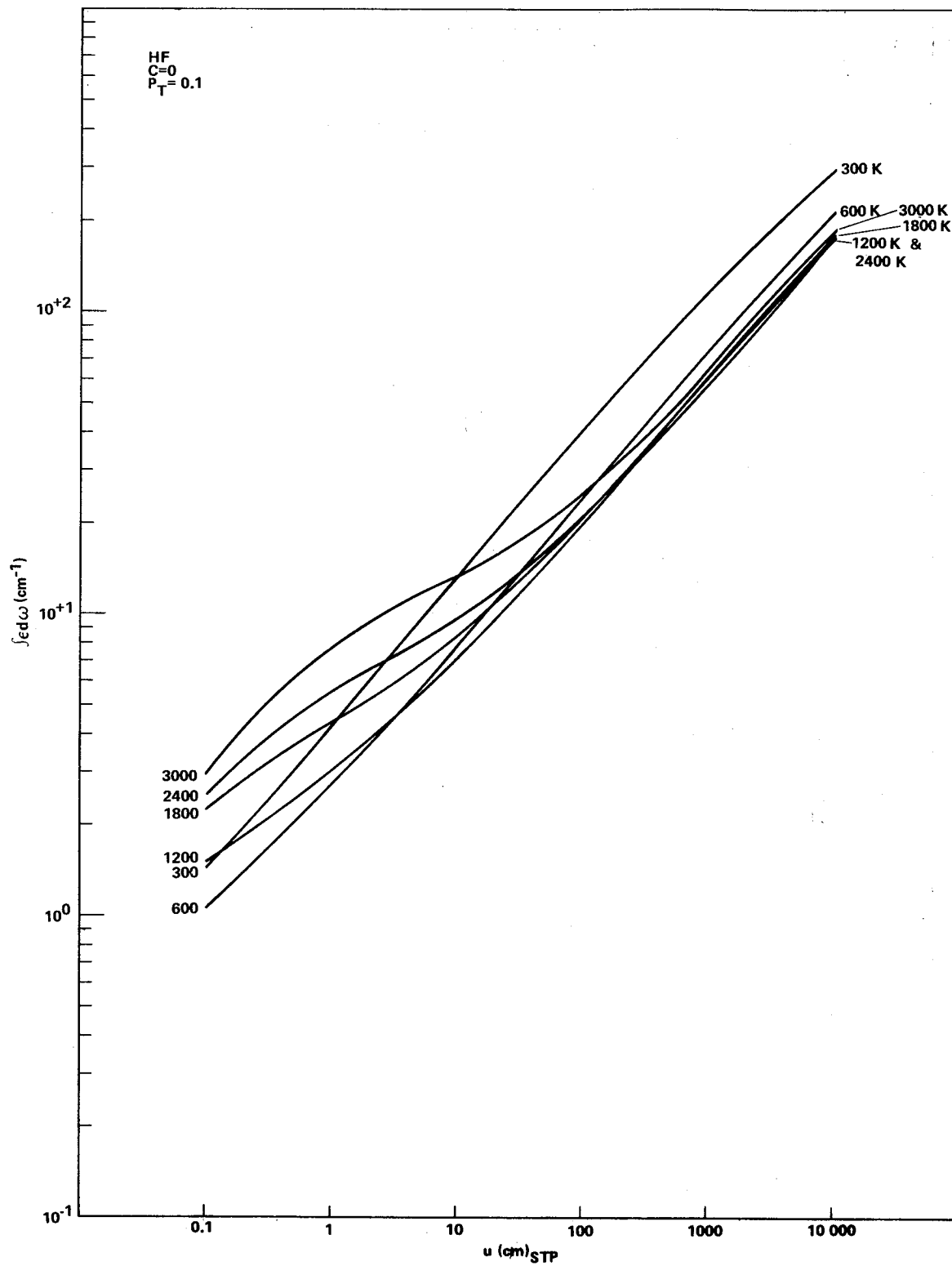


Figure 6-28. Integrated absorptance for the fundamental band of HF at 0.01 atm pressure.

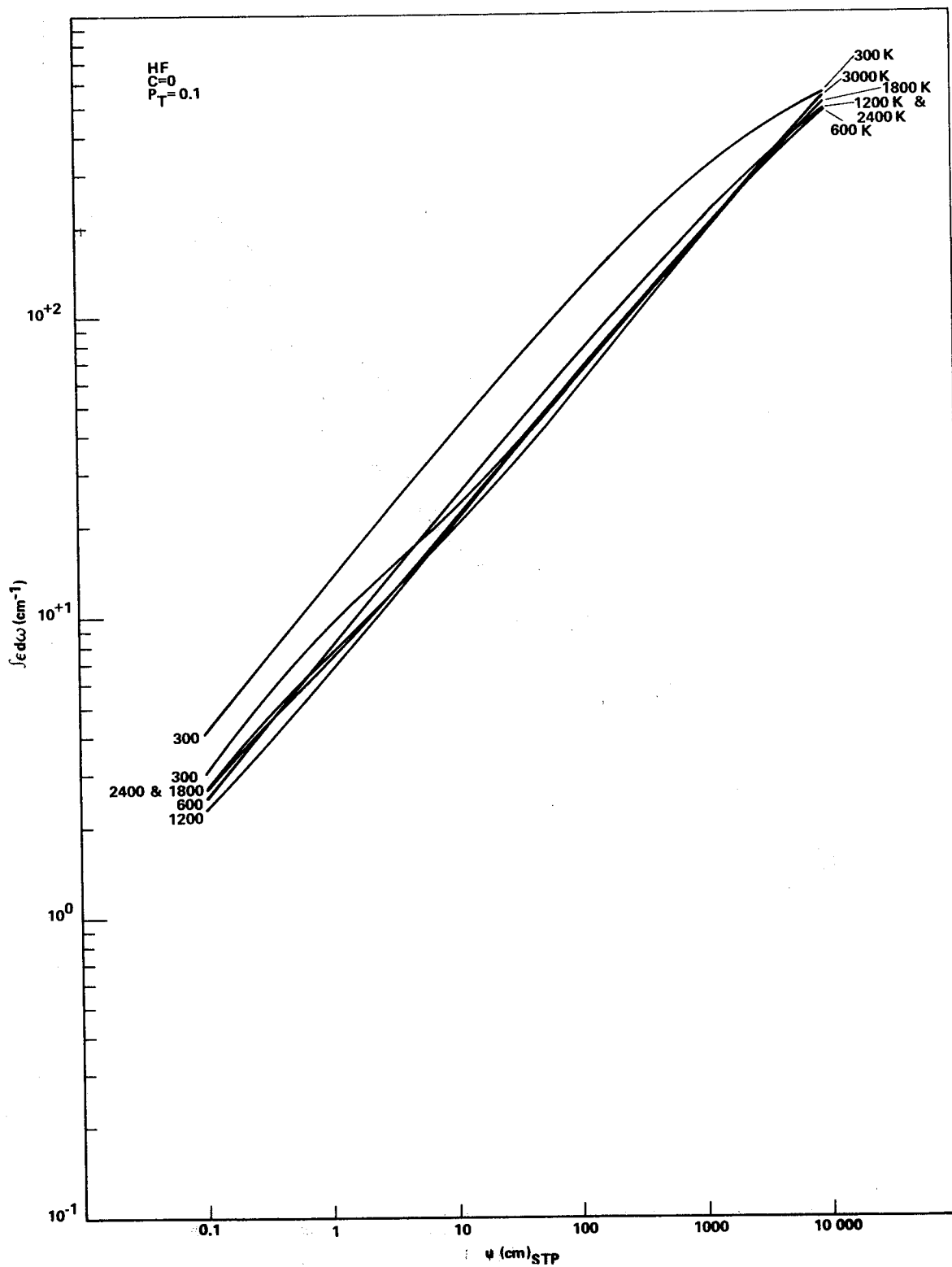


Figure 6-29. Integrated absorptance for the fundamental band of HF at 0.1 atm pressure.

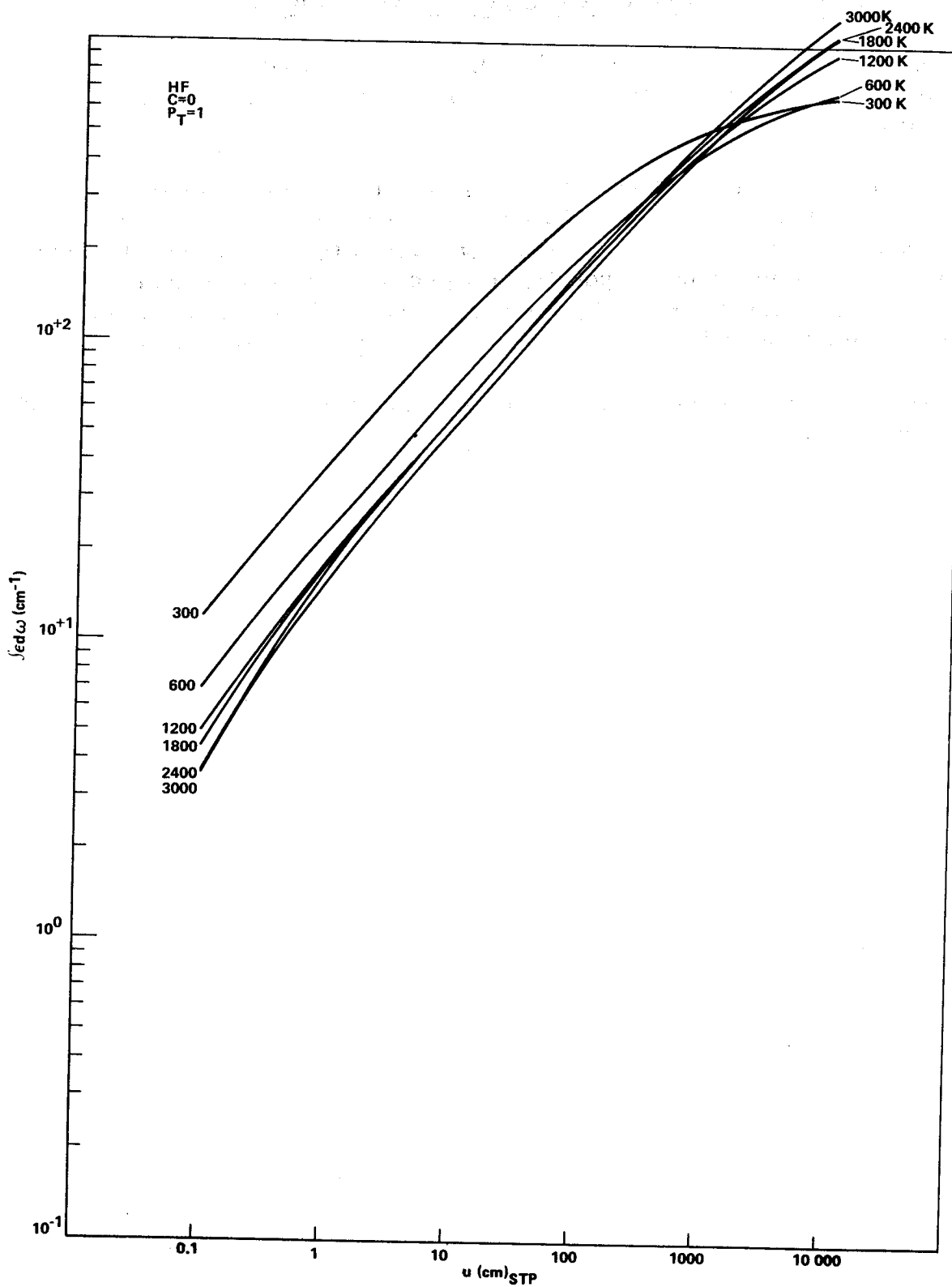


Figure 6-30. Integrated absorptance for the fundamental band of HF at 1.0 atm pressure.

### 6.3 INTEGRATED ABSORPTANCE FOR CARBON DIOXIDE

Because of the narrow spectral width of the CO<sub>2</sub> band systems, this molecule may be treated like the diatomic molecules, for which integrated band absorptances were presented.

Figures 6-31 and 6-32 show the integrated absorptances for the 4.3- and 2.7- $\mu$ m bands of CO<sub>2</sub> in the weak-line and Doppler-line limits, which provide upper and lower limits, respectively. These figures clearly show the severe restriction placed on the possible range of integrated absorptance by increasing temperatures. For all practical purposes, the weak-line limit may be used for temperatures of 1800K and above for any total pressure.

Data for integrated emissivity versus pathlength are found in Table A2-26 in the General Appendix.

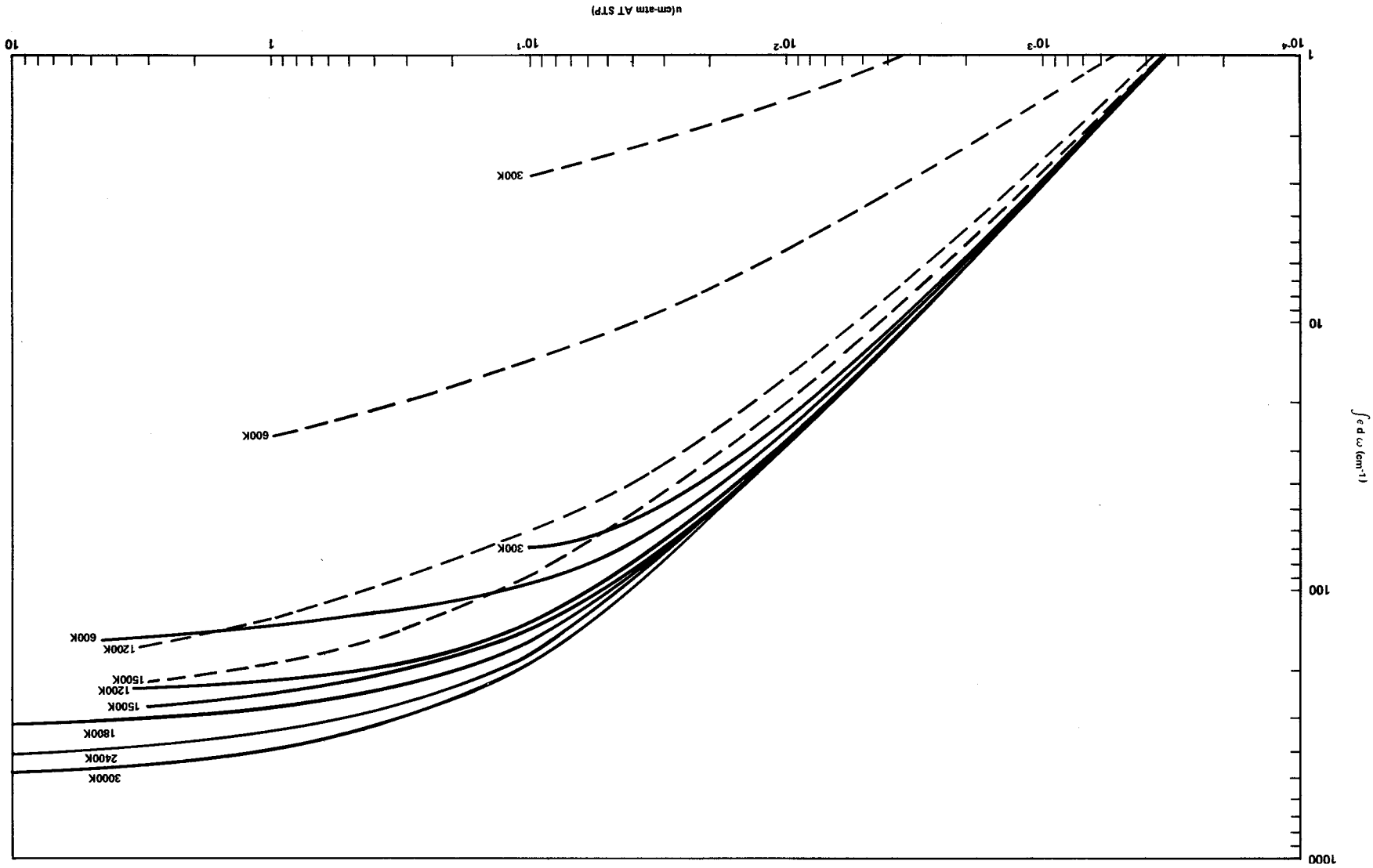


Figure 6-31. Integrated absorptivity for the CO<sub>2</sub> 4.3-μm band system from 300 to 3000K, in weak-line (solid) and Doppler-line (dashed) limits.

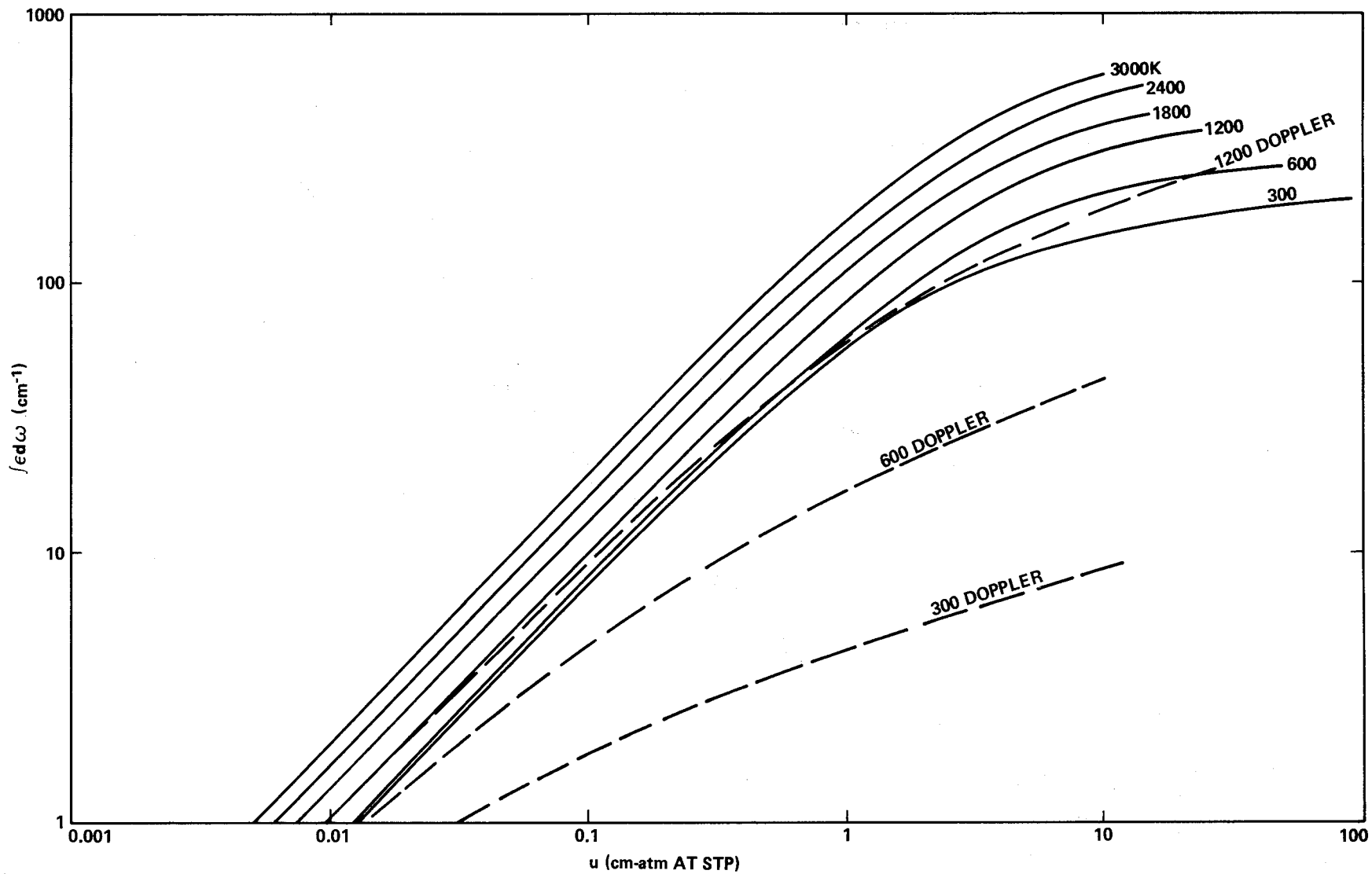


Figure 6-32. Integrated absorptivity for the CO<sub>2</sub> 2.7- $\mu$ m band system in weak-line limit (solid) from 300 to 3000K and Doppler-line limit (dashed) from 300 to 1200K.

6.4 TOTAL EMISSIVITY FOR WATER VAPOR

A considerable body of total emissivity data was assembled in the 1920's and 1930's. These data showed that the total emissivity depends upon temperature, composition, pressure, and optical pathlength. Hottel and his coworkers reduced and correlated their own and other people's measurements over many years; these studies culminated in the preparation of two charts [6-1] which can be used to obtain the total emissivity at a variety of conditions.

Hottel's charts are based upon a careful evaluation and correlation of experimental measurements. Total emissivities derived from these charts are entirely satisfactory for engineering predictions of heat transfer from homogeneous volumes of hot water vapor at conditions near those of the measurements. However, the charts also show estimates of the total emissivities based on extrapolation of the data to other conditions — primarily, long paths, high temperatures, and pressures other than atmospheric — and in these situations the values derived from the charts are less accurate. Some current applications, such as radiative heat transfer from rocket combustion gases, involve hot water vapor at conditions where the chart values are extrapolated over a considerable distance from the measured data. Based on the absorption coefficients and fine structure parameters presented in the General Appendix, the total emissivity (defined in Section 3.1.5) has been calculated at optical depths from 0.1 to 1000 cm-atm and at temperatures from 600 to 3000K. The results were presented in Reference 6-2 and are summarized here.

The charts are similar in concept to Hottel's, showing the total emissivity of hot water vapor at various conditions. In preparing these charts, an attempt was made to keep the number of independent variables as small as possible, as Hottel did in his presentation. However, the wide temperature range covered affects the pressure/composition dependence to a degree which should not be ignored. Like Hottel, the total emissivity is shown as a function of temperature for various optical paths  $p\ell$  for an infinitely dilute mixture of water vapor and other gases at a total pressure  $P_T = 1$  atm; a second chart is to be used to convert emissivities read from the first chart to other pressures and compositions.

The emissivity of hot water at  $p = 0$ , and  $P_T = 1$  atm is shown in Figure 6-33. In preparing this chart, it was assumed that  $\gamma_j = 0.09$ . Emissivities read from this chart are thus correct if  $N_2$  is the principal foreign gas. Inspection of the data shown in Table 5-19 indicates that for most practical applications, in which air or  $N_2$  are the predominant foreign gases, the values should be reasonably accurate.

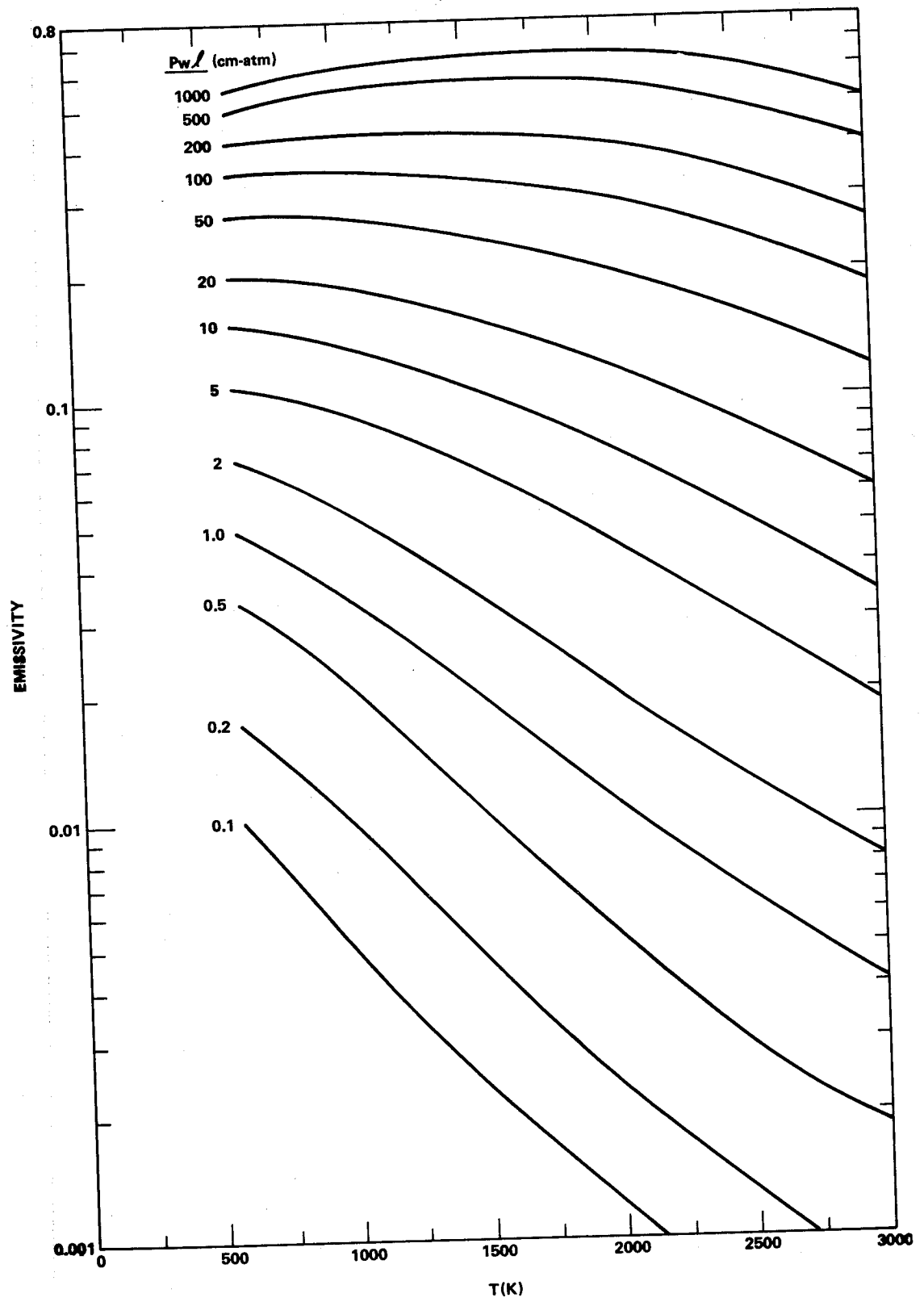


Figure 6-33. Total emissivity for water vapor.

The correction chart, giving the quantity  $C_w$  by which  $\epsilon(p=0, P_T=1)$  is multiplied to obtain  $\epsilon(p, P_T)$ , is presented as Figure 6-34. This chart is more complicated than Hottel's, since the temperature dependence of  $C_w$  has been retained. This temperature dependence is evident in the intermediate plots of Hottel and Egbert [6-1] but was omitted in their final chart in order to simplify the presentation. Since this work covers a smaller temperature range (the data considered were taken between 400 and 1000K), this omission was reasonable. In the present results, the temperature dependence is significant. The plotted curves are  $C_w$  at various pathlengths  $p\ell$  and temperatures as a function of pressure and water content, which according to the model for  $\gamma$  and the  $\gamma_j$  and  $\gamma_j^*$  values of Table 5-19 can be expressed in combined form as  $P_T [1 + 5\chi_{H_2O} (273/T)^{1/2}]$  where  $\chi_{H_2O}$  is the mole fraction of water vapor. The chart shows that the correction factor, which shows the effect of fine structure, is most variable at low temperatures and least variable at high temperatures. At high temperatures there are many more lines in the spectrum of hot water vapor than at low temperatures, so the fine structure is effectively crowded out or filled up. The upper limit of the total emissivities is given by the "high pressure limit" which is expressed using the linear limit of the optical depth as

$$\epsilon_T' = \int_0^{\infty} \{1 - \exp[-k(\omega)u]\} W^0(\omega, T) d\omega / \sigma T^4 \quad .$$

The results are given in Figure 6-35. The upper-limit calculations are potentially subject to error because of the effects of great broadening of strong lines near the band center. These lines then contribute more strongly to emission in the band wings than do the wing lines themselves, and so the spectral contour of the band changes such that the true upper-limit total emissivity becomes larger than the calculated values. We have estimated that this effect contributes, at the very most, 20 percent to the emission in that valley between bands to which the total emissivity is most sensitive. The analysis is somewhat similar to that of Penner [6-3]. The absorption coefficient in the wings at this pressure is assumed to be made up of wing line contributions and those of lines centered near the band center. The resulting expression for the limiting pressure (in atm) is

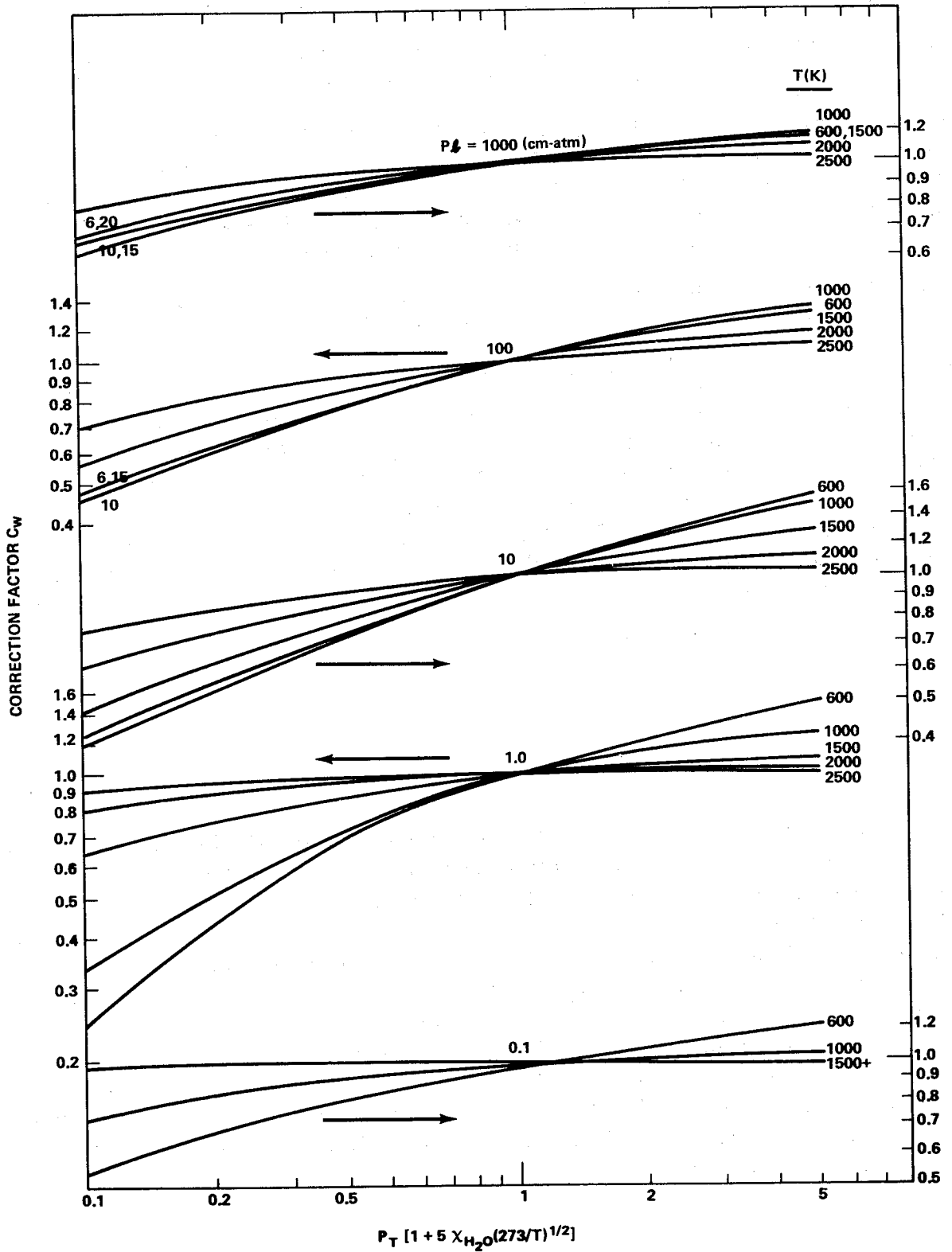


Figure 6-34. Pressure correction for water vapor total emissivity.

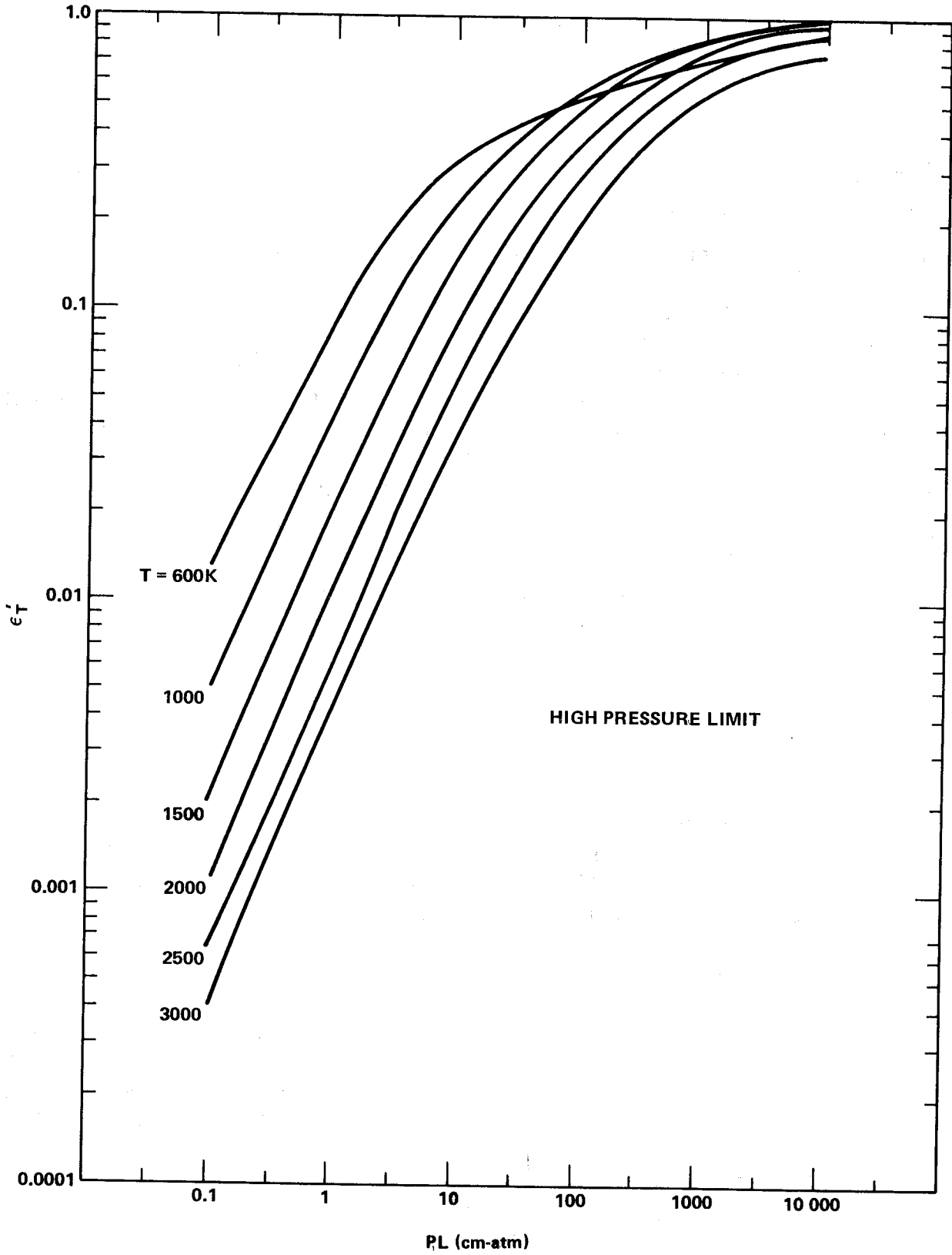


Figure 6-35. Total emissivity for water vapor at the high pressure limit.

$$P = \pi^2 k_w (T/300) / \sum_i [\alpha_i / (\omega_w - \omega_{c,i})^2] \quad , \quad (6-3)$$

where  $k_w$  is the mean absorption coefficient at a wavenumber  $\omega_w$  at the bottom of a valley between bands,  $T$  is the temperature in K, and  $\alpha_i$  the integrated intensity of the  $i$ th band centered at the wavenumber  $\omega_{c,i}$ .

Equation (6-3) can be evaluated numerically by use of the absorption coefficients given in the General Appendix. One considers that the valley region which has the greatest effect upon the total emissivity will be that lying nearest the spectral blackbody emission peak (that is, at temperatures between 1000 and 1500K, the valley between the 6.3- and 2.7- $\mu$  bands, and at temperatures between 1500 and 2000K, the valley between the 2.7- and 1.84- $\mu$  bands). One chooses  $k_w$  and  $\omega_w$  accordingly to obtain the values of the pressure at which the absorption coefficients are 20 percent in error in these valley regions. The results are tabulated in Table 6-1. The authors have not directly evaluated the effect of an error of this magnitude in  $k$  upon the total emissivity, since the effect depends upon both temperature and optical depth. However, one can say that the effect will always be less than 20 percent and much less at optical depths low enough that the wings contribute little to the total emission.

TABLE 6-1. VALUES OF PRESSURE ABOVE WHICH THE CALCULATED "UPPER LIMIT" EMISSIVITIES MAY NOT BE TRUE UPPER LIMITS

Temperature (K)	Pressure (atm)
1000	60
1500	180
2000	400

Our limiting pressure estimate assumes that  $H_2O$  is the principal broadening agent. Since  $H_2O$  is a more effective broadener of  $H_2O$  lines than other gases, systems dilute in  $H_2O$  will follow our upper-limit estimate to higher pressures better than will pure water. The reader should note that the pressures required to invalidate the upper-limit prediction are considerably higher at high temperature. This effect is primarily a consequence of the increase in  $\bar{k}_w$

caused by the overlapping of the band wings, which is apparent in all our experimental spectra above 1000K.

6.5 TOTAL EMISSIVITY FOR MIXTURES OF GASES

The total emissivity of a mixture of gases can be obtained by adding the total emissivities of the different species present, if the different vibration-rotation bands do not overlap significantly. One of the more common gas mixtures involves  $\text{H}_2\text{O}$  and  $\text{CO}_2$ . These two species overlap significantly in the  $2.7\text{-}\mu$  region, with the result that the total emissivity is less than the sum of the total emissivities of the two species calculated separately. Hottel [6-4] has given charts which give the amount by which the sum of  $\epsilon_T$  of  $\text{CO}_2$  and  $\text{H}_2\text{O}$  has to be reduced (each evaluated as if the other gas were transparent) to obtain  $\epsilon_T$  of the mixture. The charts are plotted up to a temperature of 1200K. For gas mixtures higher than 1200K, calculations may be performed according to

$$\epsilon_T = \frac{1}{\sigma T^4} \int_{\omega} (1 - \overline{\tau_1 \tau_2}) W_{\omega}^0(\omega, \tau) d\omega$$

where  $\overline{\tau_1 \tau_2}$  represents an appropriate band model value of the transmissivity of the gas mixture (see Chapter 5).

## REFERENCES

- 6-1. Hottel, H. C. and Egbert, R. B.: Am. Inst. Chem. Eng, no. 38, 1942, p. 531.
- 6-2. Boynton, F. P. and Ludwig, C. B.: Int. J. Heat & Mass Transfer, no. 14, 1971, p. 963.
- 6-3. Penner, S. S.: Quantitative Molecular Spectroscopy and Emissivities. Addison-Wesley, 1959.
- 6-4. Hottel, H. C. and Sarofim, A. F.: Radiative Transfer. McGraw-Hill, 1967.



CHAPTER 7

ACCURACY OF CALCULATIONAL MODELS

The ultimate test of the reasonableness of any model lies in the accuracy with which it predicts experimental measurements. This section is a survey of existing experimental data and comparisons of these with calculations using the band model parameters presented in Chapter 5.

During the last 20 years, experimental data have been obtained by several laboratories using many different experimental procedures. Numerous comparisons for diatomic molecules, water vapor, and carbon dioxide are presented here, both for homogeneous as well as nonhomogeneous optical paths. The experimental conditions were selected to be as wide and as representative as possible. As an example, the ranges of temperature and optical depth for which experimental data on water vapor are currently available are indicated on Figure 7-1. The accuracy and range of the experimental data available for the comparison with calculations presented in this chapter are insufficient in general to discriminate between the band models discussed in Chapter 3 on the basis of goodness of fit.

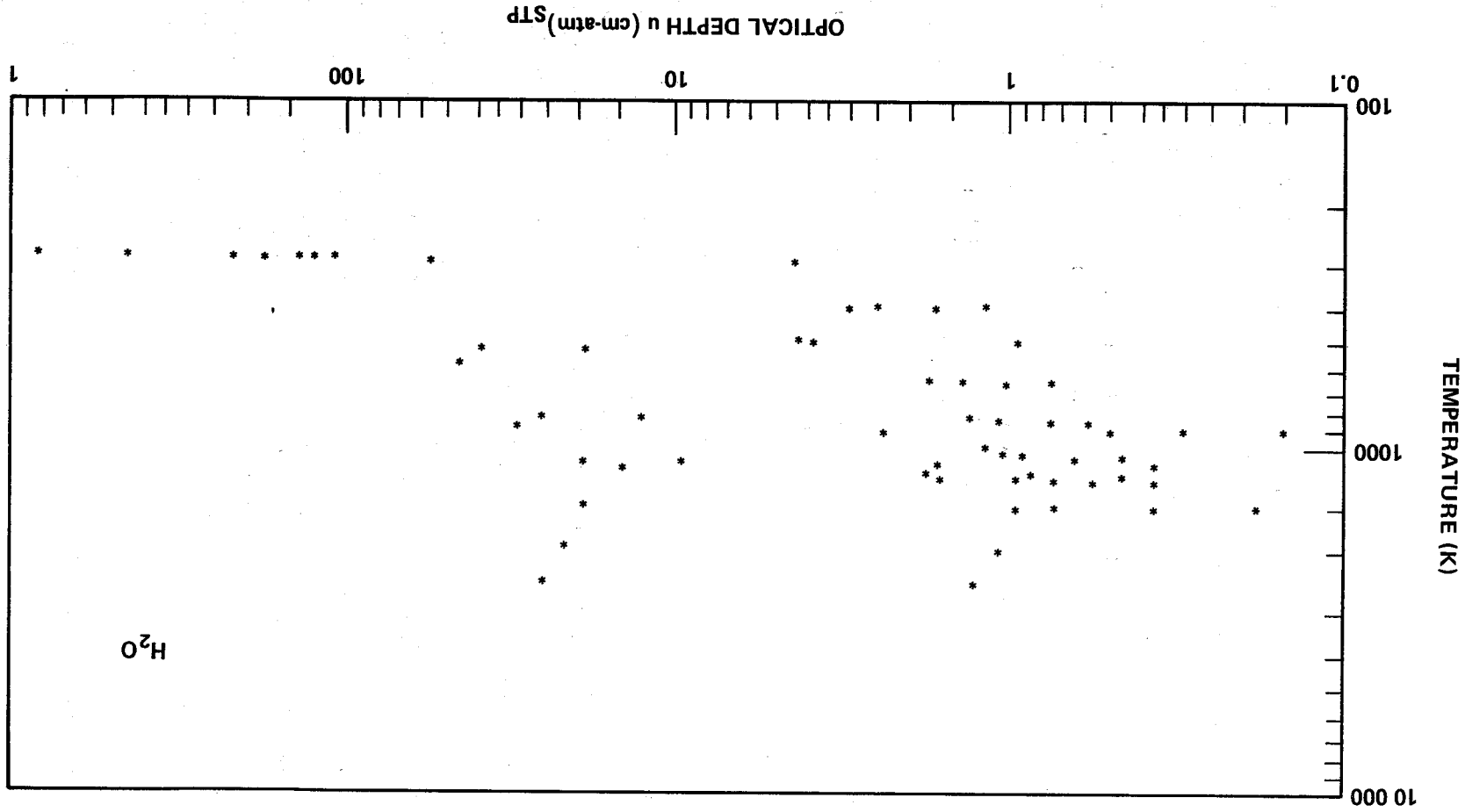


Figure 7-1. Temperatures and optical paths for which experimental data of water vapor exist. (All the data are at total pressures equal to or less than 2 atm.)

## 7.1 EXPERIMENTAL PROCEDURES

### 7.1.1 EQUIPMENT FOR HIGH-TEMPERATURE GAS SPECTROSCOPY

Quantitative spectroscopy requires the hot gas sample to be of uniform temperature, concentration, and total pressure. The following methods have been used: heated cell, subsonic burner, supersonic burner, and shock tube. All methods have particular advantages and disadvantages. Cell measurements are generally restricted to temperatures  $< 1500\text{K}$ , but the thermodynamic parameters can be chosen freely. Hot gases created in both sub- and supersonic burners can be at temperatures as high as  $3000\text{K}$ , but the mole fractions and the total pressure cannot be freely chosen because they are functions of the temperatures. The same is true to some degree for shock tubes, with the additional disadvantage of obtaining a limited amount of spectral data per test run.

The problem of thermal or concentration gradients at the interface of hot gas and the ambient atmosphere is common to all experimental methods. The problem is minimized in the case of large optical pathlengths. For heated cells, in which the windows are replaced by a flowing hot inert gas stream, the thermal gradient is replaced by a concentration gradient in the mixing zone.

Another problem is atmospheric absorption. In closed systems, the atmosphere is usually replaced by nitrogen gas. However, in the case of burner measurements, a certain amount of unflushed atmosphere exists between the hot gas and the flushed system.

A typical example of a heated cell is the arrangement of Goldman and Oppenheim [7-1] which is shown in Figure 7-2. The absorption cell is located in the center of a furnace which is much longer than the cell in order to avoid temperature gradients at the windows. The source and transfer optics as well as the spectrometer are all enclosed, evacuated, and then flushed with dry nitrogen to eliminate atmospheric absorption.

To overcome the limitation of a fixed cell length, Herget et al. [7-2] have used the arrangement shown in Figure 7-3, in which the light beam is passed four times through the cell. Thus, by using single, double, and quadruple passes, the determination of the curve of growth becomes possible.

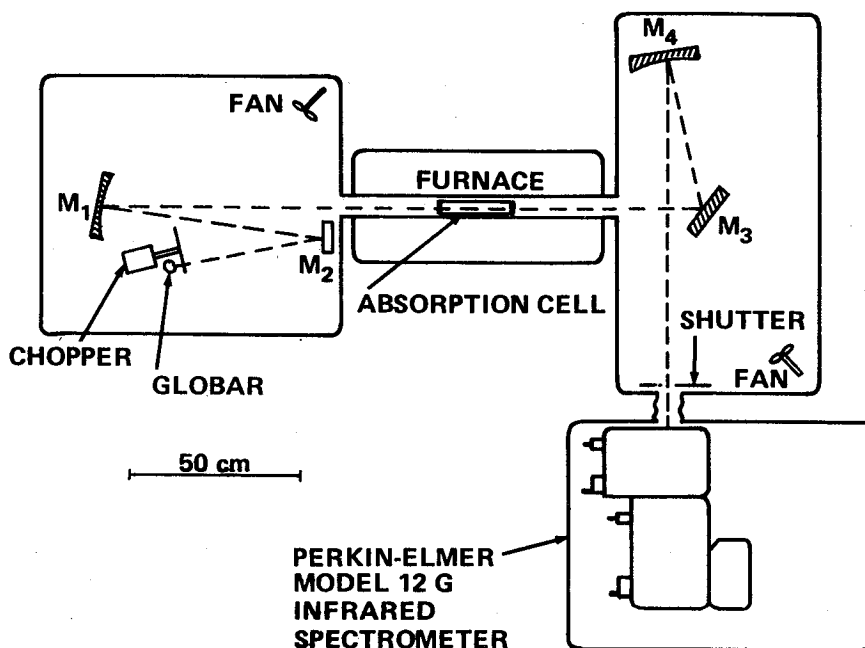


Figure 7-2. Schematic diagram of the enclosed optical system as used by Goldman and Oppenheim [7-1].

Burch et al. [7-3] have used the arrangement shown in Figure 7-4 to study the effect of the absorption by a cold atmosphere. Radiation from the light source is focused near the center of a sample cell which is located in the furnace. The sapphire windows shown are the windows of the sample cell, and the sample is confined to the region between them. Argon gas fills the two end sections of the furnace between the sapphire and calcium fluoride windows. The beam entering the "optical tank" is deflected toward a White-cell arrangement, in which the beam is reflected many times between two mirrors.

The arrangement by Simmons et al. [7-4], shown in Figure 7-5, permits measurements of hot gas samples that are not isothermal. The furnace is partitioned into sections which can be individually controlled from room temperature to 1200K. The actual gas temperature is measured by thermocouples in the cell.

The combination of cell and flowing gas system has the potential of attaining higher temperatures. The arrangement as used by Nelson [7-5] is shown in Figure 7-6.

The use of burners goes back to the last century when spectroscopy started. These burners (Bunsen, Meeker, etc.) are readily available as

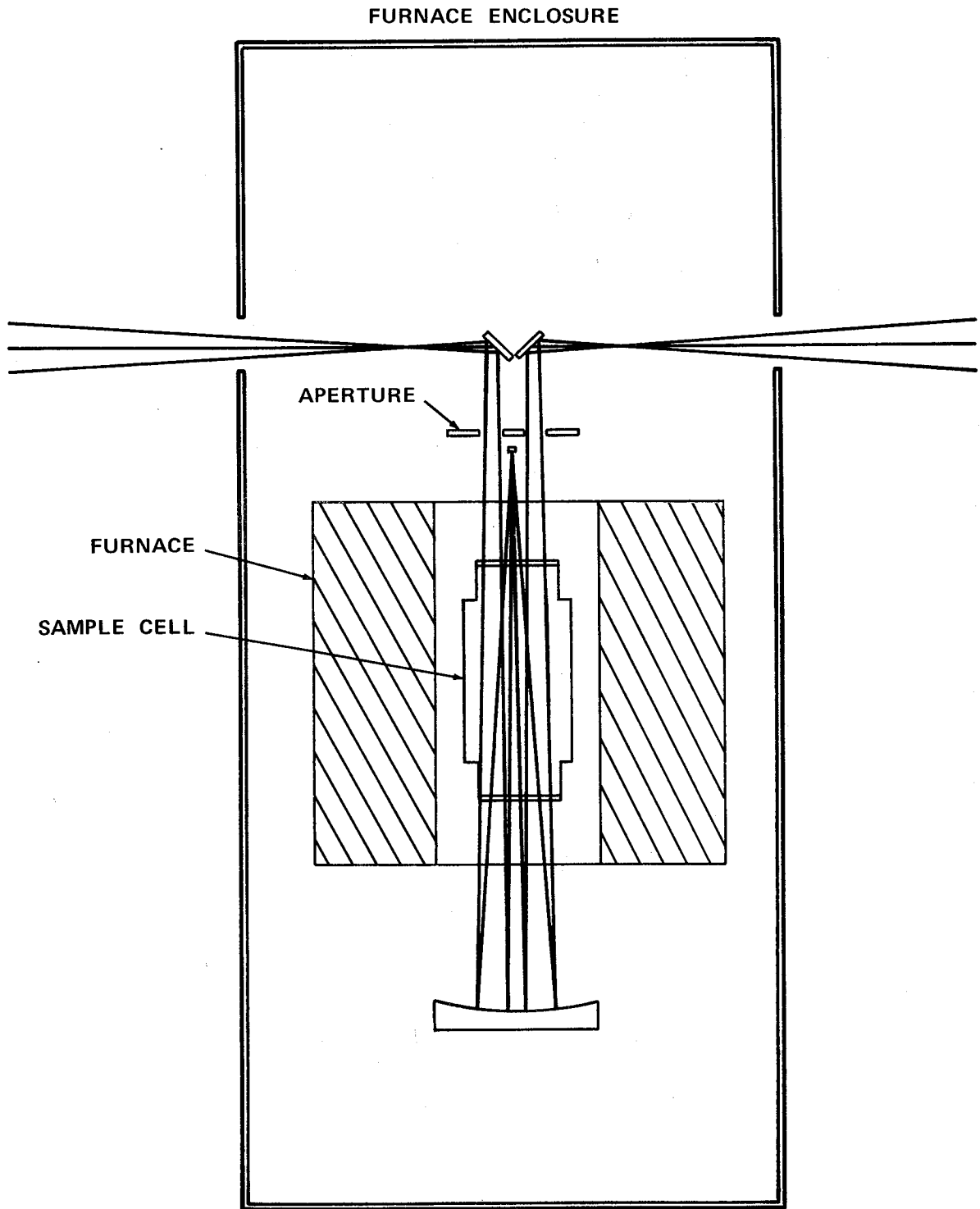


Figure 7-3. Multiple pass arrangement used by Herget et al. [7-2].

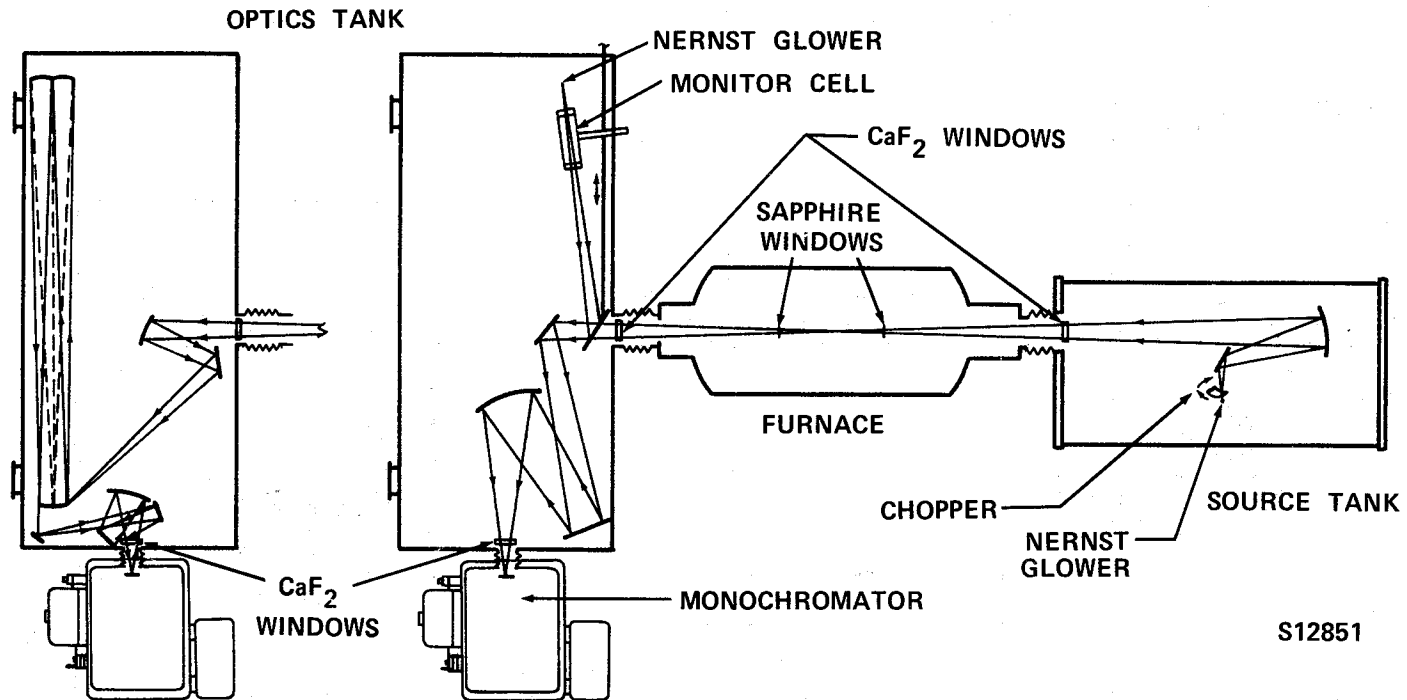


Figure 7-4. Arrangement as used by Burch et al. [7-3] with White-cell at the left-hand side.

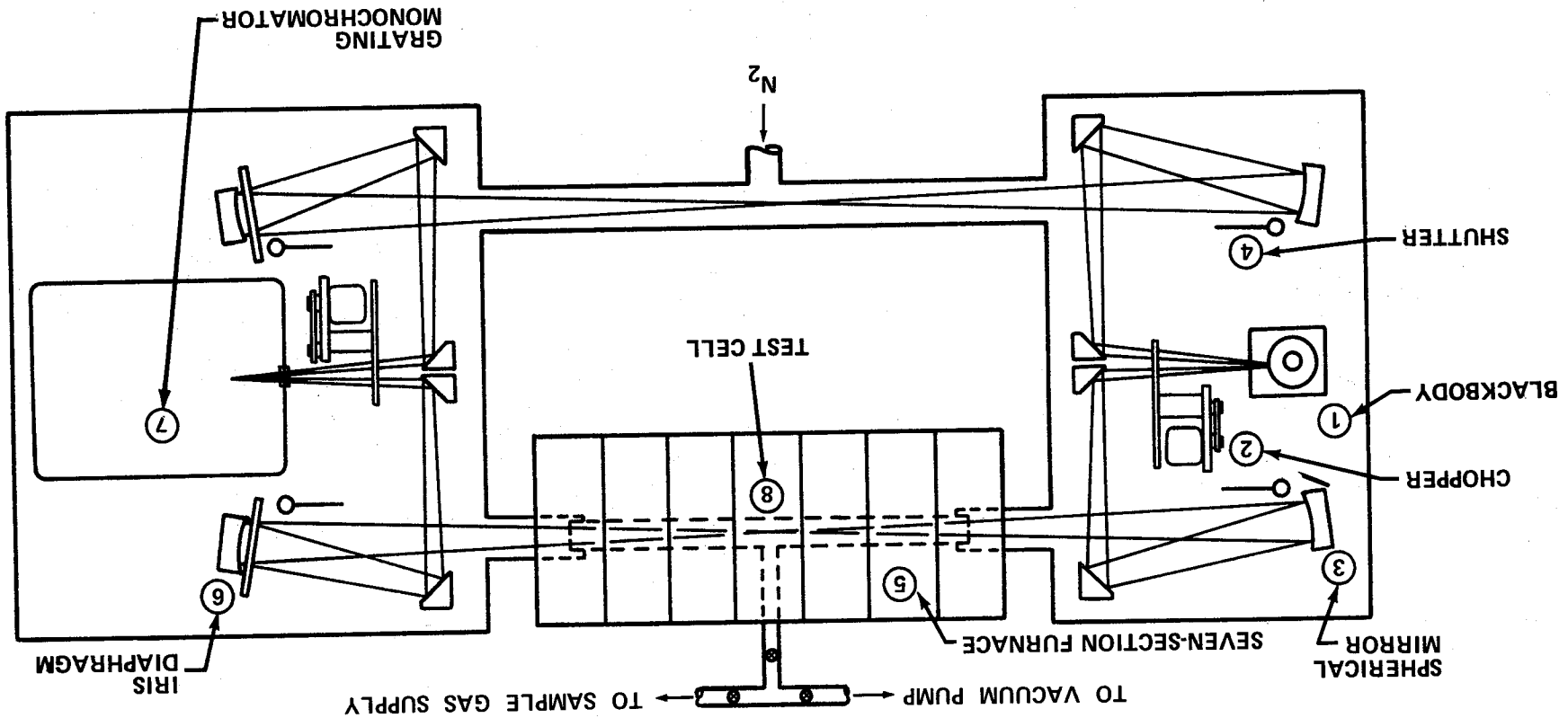


Figure 7-5. Arrangement for nonisothermal gas samples in cell [7-4].

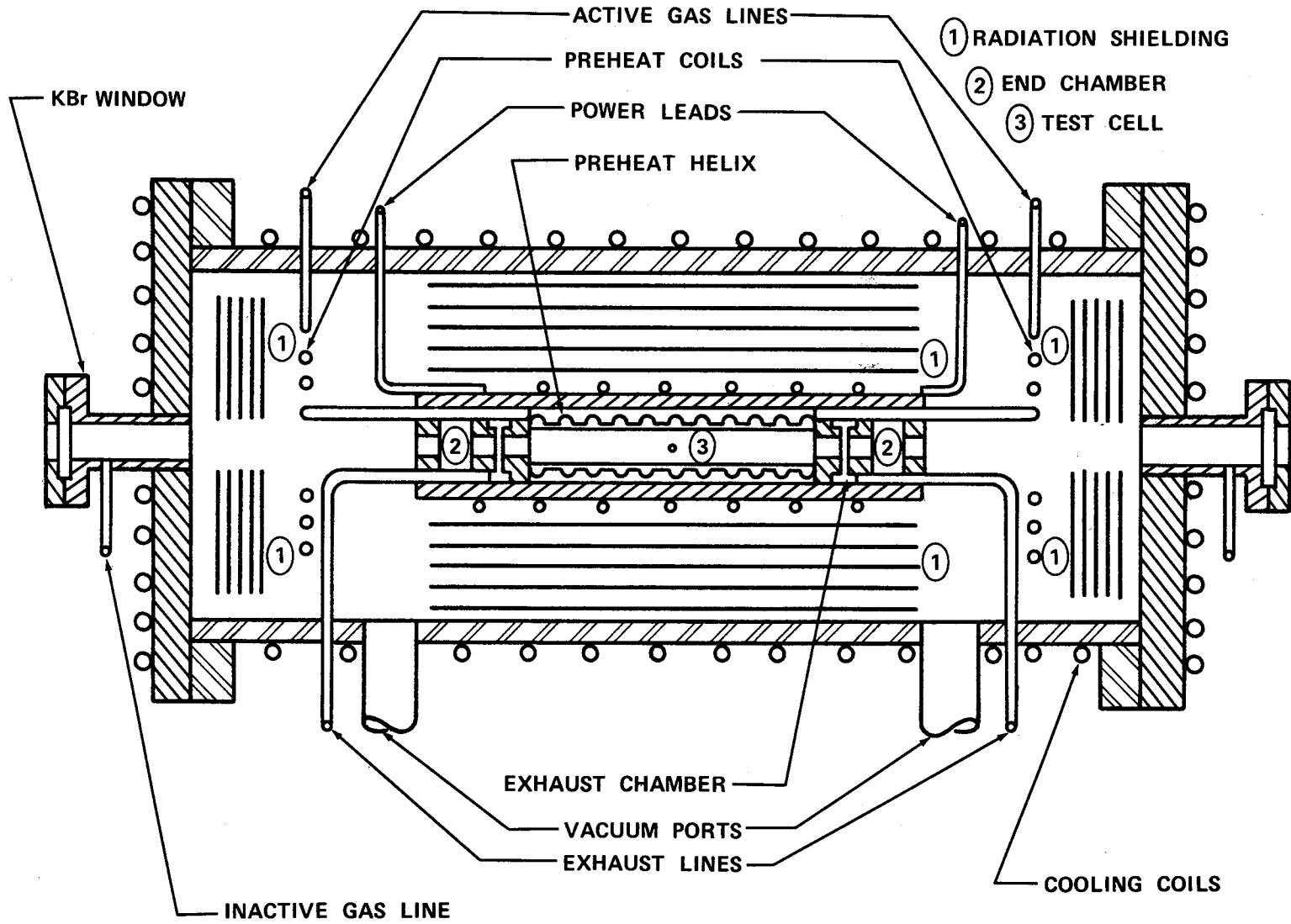


Figure 7-6. Schematic of gas containment system.

sources of hot gas. To overcome the large nonhomogeneities in flames, long narrow burners have been used. Mixing with the ambient atmosphere can be further suppressed by surrounding the burner with a stream of transparent hot gas.

A diagram of a section (2 ft) of the 20-ft long burner used by Ludwig [7-6] is shown in Figure 7-7. This apparatus was used to obtain curves of

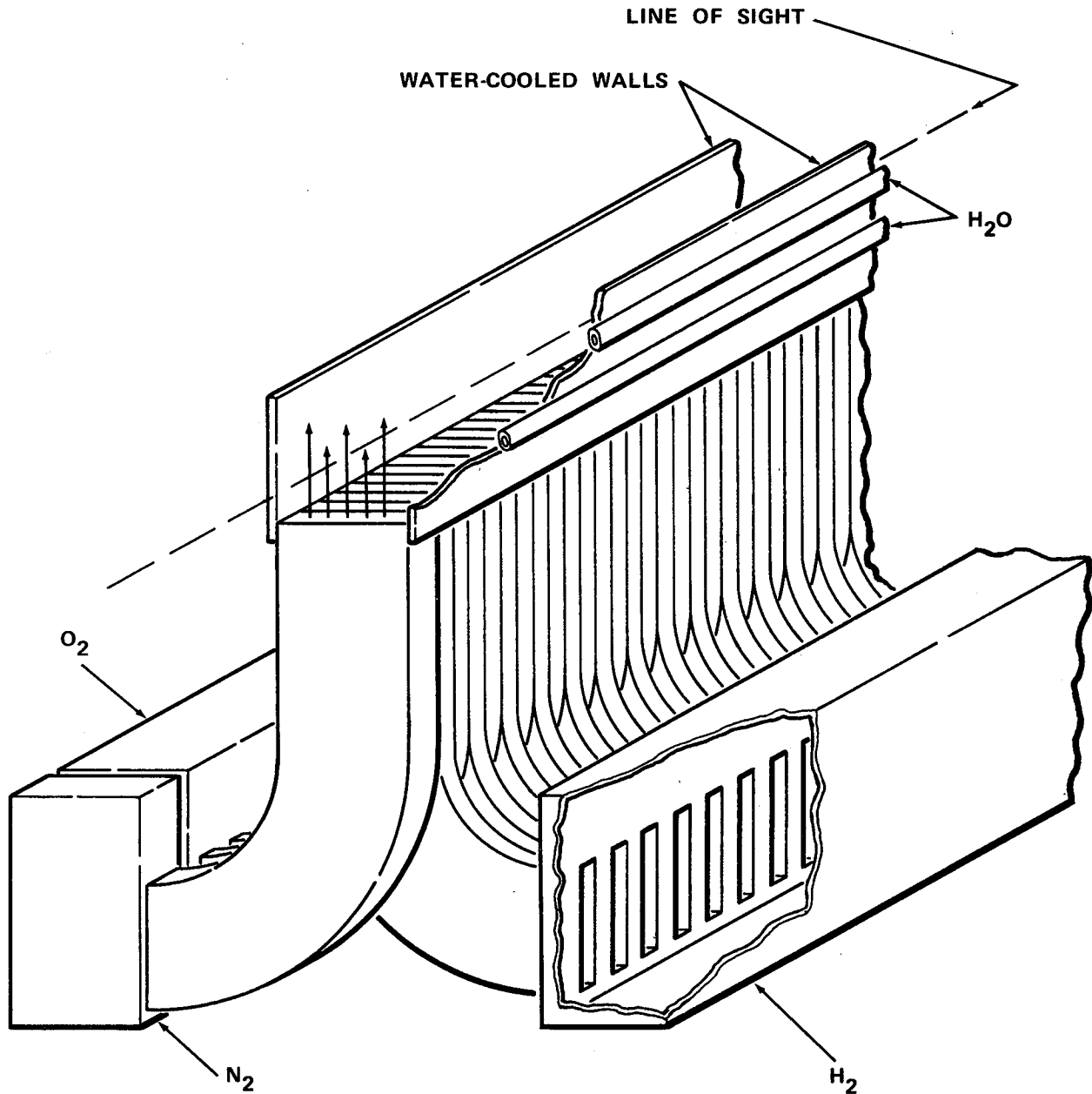


Figure 7-7. Schematics of one section of "long burner"  
(30 cm long) [7-6].

growth for hot water vapor. The burner had four sections which were individually controlled. Temperatures of up to 3000K were obtained. Gaseous oxygen and hydrogen were fed alternately through slots, as shown in the figure. At both ends, a dry hot nitrogen stream was used to minimize mixing with the ambient atmosphere.

A diagram of a supersonic burner (rocket) used by Ferriso [7-7] is shown in Figure 7-8. To avoid shock formation, which introduces large inhomogeneities, a Foelsch nozzle [7-8] which produces uniform conditions and parallel flow at the nozzle exit was used (with exit pressure equal to the ambient pressure). However, a small mixing boundary layer still exists for which compensation has to be made in the data reduction. Larger rockets were used by DeBell et al. [7-9]; however, these did not use Foelsch nozzles and shock structure is present at the measuring plane. All optical equipment and flushing tubes to minimize atmospheric absorption must be thermally protected.

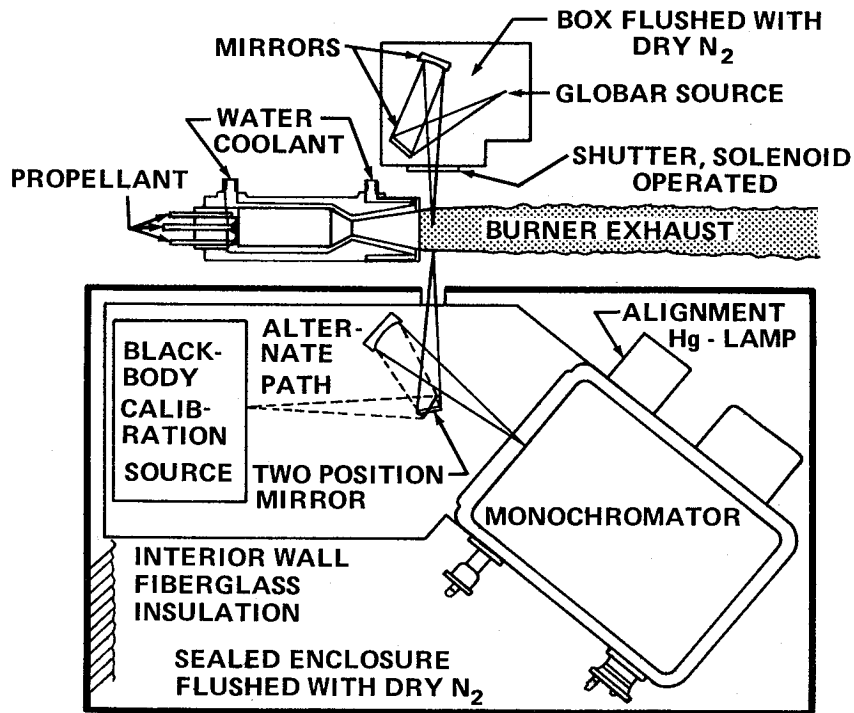


Figure 7-8. Schematics of supersonic burner [7-7].

Shock tubes have been used extensively for radiant intensity measurements, particularly when only low spectral resolution was required. Here (see Figure 7-9) a sample of the test gas is admitted to the low pressure section of the shock tube. A diaphragm separating the low and high pressure sections is then broken, allowing a strong shock wave to pass through and heat the test gas. The changes in absorption and/or emission are usually recorded photographically during this process.

The foregoing procedure was used by Patch [7-10] to obtain the water spectrum. However, for each spectral interval a new shock wave was needed, which has to be repeatable within error limits. Either multiple detector arrangements or very fast scanning spectrometers have been used to overcome this limitation.

Another approach, used by Breeze and Ferriso [7-11, 7-12], uses a reflected shock wave to heat the gas to the high temperature and views along the shock tube axis. The experimental arrangement is shown in Figure 7-10. By using wide entrance slits in the monochromator, the total integrated band emissivity as a function of pathlength is obtained. The oscillogram of the pressure and the emitted energy is shown in Figure 7-11.

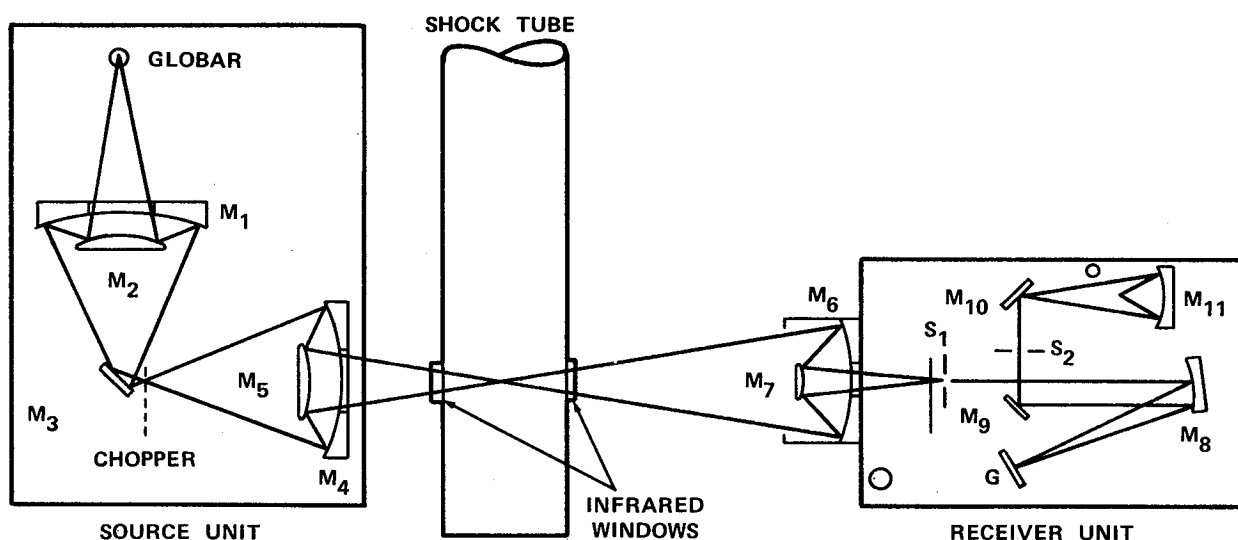


Figure 7-9. Schematic of shock tube for high temperature gas absorption studies [7-10].

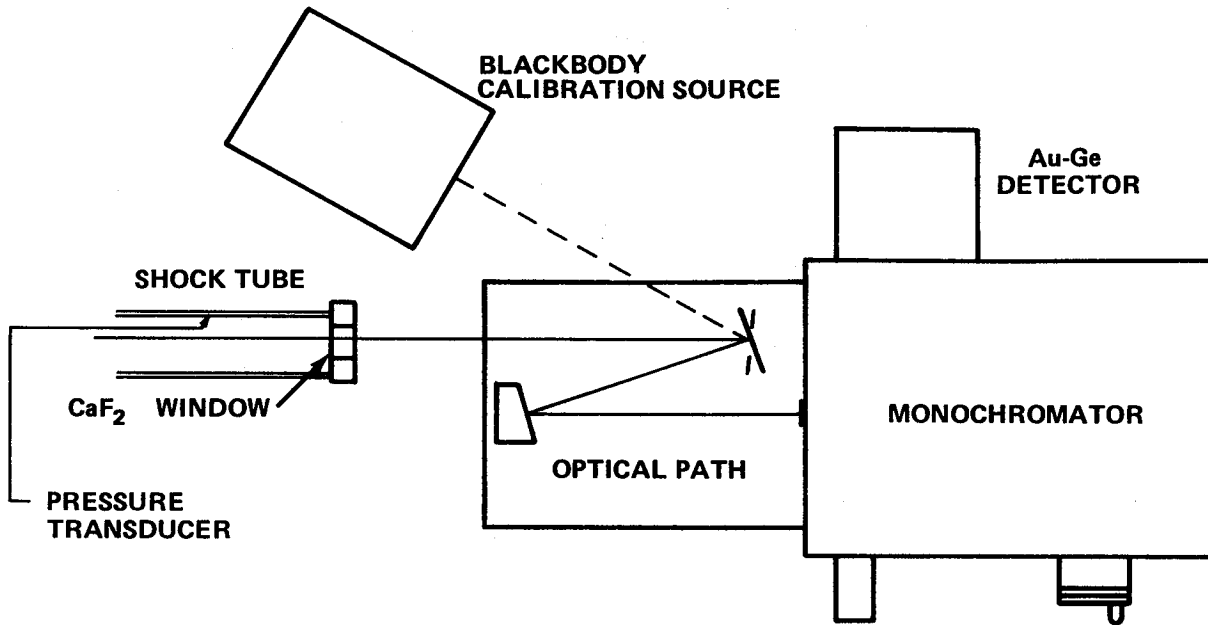


Figure 7-10. Schematic of reflective shock wave experiment to determine total integrated band emissivities [7-12].

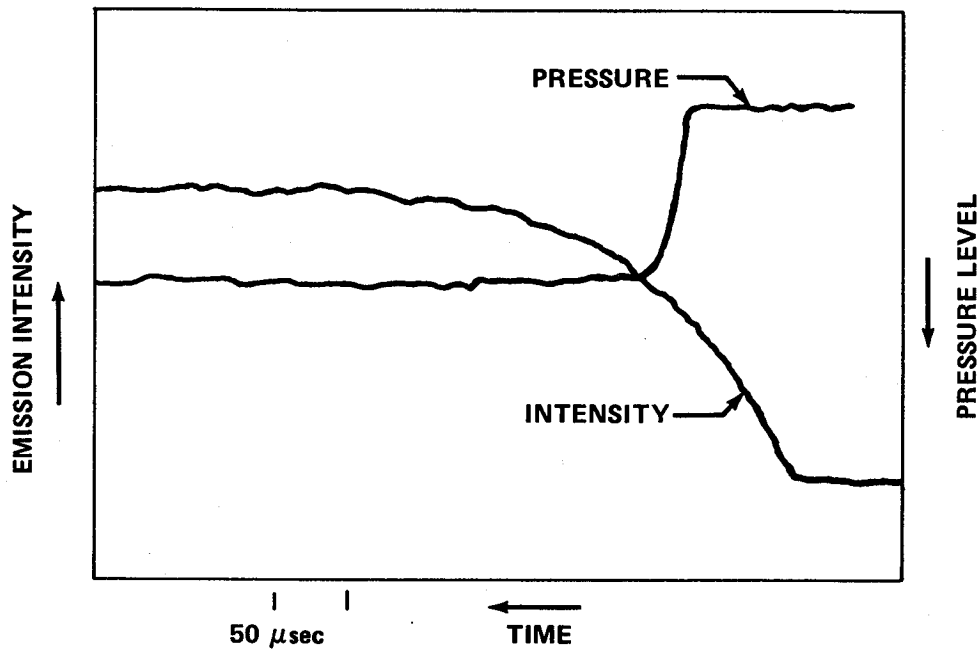


Figure 7-11. Oscillogram of pressure and emitted energy from reflected shock wave experiment [7-12].

## 7.1.2 OPTICAL DETERMINATION OF THE GAS TEMPERATURE

Because of its importance in quantitative spectroscopy, a brief review of the optical methods for the determination of the gas temperature is given in this section. In general, if it can be assumed that the gas is in complete thermal equilibrium, i. e., is isothermal, and the reflectivity of the gas is negligible, then Kirchhoff's law applies:  $\alpha(\omega) = \epsilon(\omega)$ .

7.1.2.1 Homogeneous Gases

There are two basic methods of optical temperature determination: One is the radiance method, which is based upon the variation of the Planck blackbody function with temperature. The other one is the intensity distribution method, which is based upon the Maxwell-Boltzmann population distribution function [7-13 and 7-14].

In the radiance method (Planck-Kirchhoff), the measurement of the emissivity and the radiated energy from the hot gas at a given wavelength is sufficient to determine the temperature using the relation

$$W^0(\omega, T) = W(\omega) / \epsilon(\omega) \quad .$$

The radiated energy  $W(\omega)$  is measured by calibrating the detector with a standard blackbody source, and the spectral emissivity  $\epsilon(\omega)$  is determined in an absorption experiment:

$$\epsilon(\omega) = 1 - I(\omega) / I_0(\omega) \quad ,$$

where  $I_0(\omega)$  and  $I(\omega)$  are the intensities of a hot source measured in the absence and presence of the hot gas, respectively. The results are independent of  $\omega$ . In practice, however, the measurement errors are much larger in the band wings, where the transmission becomes greater than 90 percent. An example of the temperature determination within the  $2.7\text{-}\mu$  band of  $\text{CO}_2$  is given in Figure 7-12, where the uncertainty increases from about 1 percent in the strongly absorbing regions to over 20 percent in the wings [7-4]. In using this method, it is assumed that the gas is in thermal equilibrium, that the nonequilibrium between the gas and its radiation is negligible, and that the reflectivity of the gas is insignificant. It should be noted that this last assumption is not valid when the gas contains large numbers of solid particles [7-15].

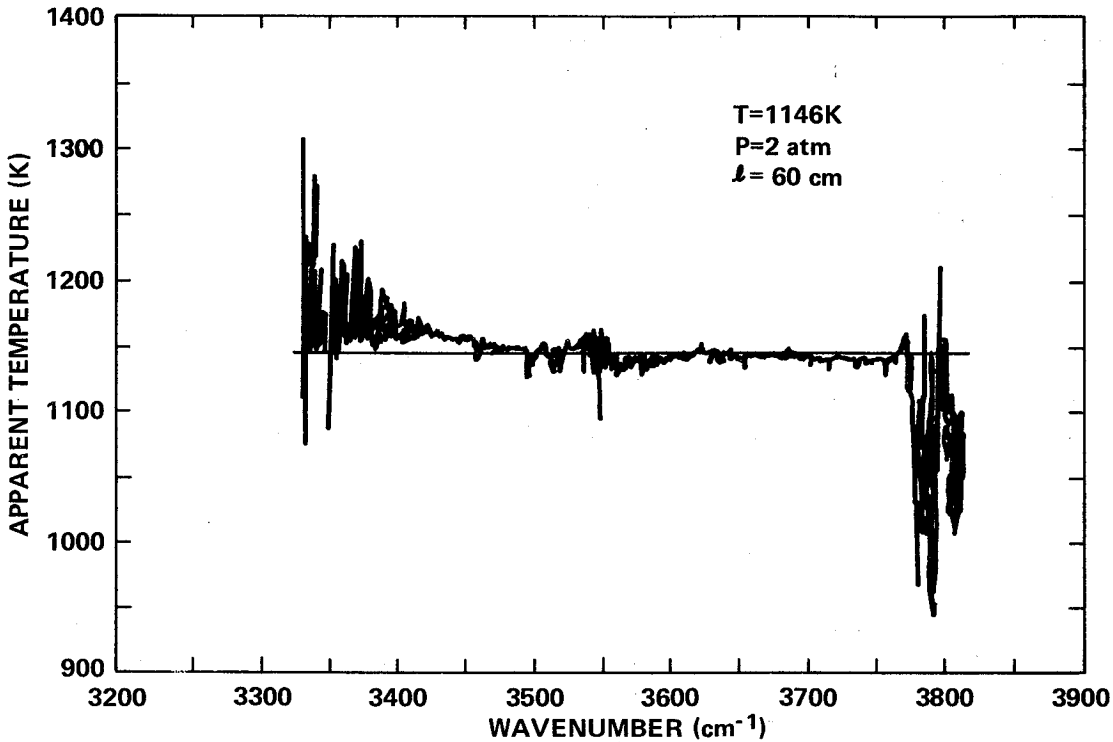


Figure 7-12. Temperature determination as a function of wavenumber [7-4].

A variation of the radiance method is the reversal method, in which a particular transition at a given  $\omega$  is selected for the absorption and emission measurement. The most frequently used method is to seed the gas with sodium and use the two yellow lines at 5890 and 5896 Å. This method can also be used to probe inhomogeneous gas samples by restricting the seeding to selected regions [7-16].

Another variation of the radiance method is the two-color method, in which the emitted radiant intensity is measured at two different wavelengths. If the emissivities at these two wavelengths are the same, the ratio of the emitted radiant intensity at the two wavelengths is the same as the ratio of the blackbody function evaluated at the gas temperature. If the emissivities are unknown, they have to be determined by the absorption method [7-17]. In general,

$$\frac{N^0(\lambda_1, T)}{N^0(\lambda_2, T)} = \frac{\epsilon_2}{\epsilon_1} \frac{N(\lambda_1)}{N(\lambda_2)}$$

Another application of the radiance method is the measurement of the width of a discrete spectral line [7-18] using a high resolution instrument.

If the gas is at low pressure, the broadening of lines is given by the transitional velocity distribution (and not by collisions), i. e.,

$$T = \left( \frac{\gamma_{D^c}}{\omega_0} \right)^2 \frac{m}{k \ln 2}$$

In the intensity distribution method, a number of nonblack lines are observed in high-resolution. The distribution of the intensity of these lines is related to the Maxwell-Boltzmann population distribution function. The temperature is obtained from the slope of the curve, which represents the natural logarithm of the ratio of the intensity of the lines to a frequency dependent factor versus the frequency of each line [7-19].

A variation of this method is the band-ratio-technique which is based upon the different temperature-dependencies of the strengths of combination, overtone, and fundamental bands, i. e., the intensity distributions of various vibrational bands in their ground electronic state [7-20].

#### 7.1.2.2 Inhomogeneous Gases

If nonisothermal gases are measured and in-situ temperature probes are not feasible, temperature inversion methods can be used to obtain the spatial variation of temperature. For axisymmetric inhomogeneous gases, the so-called "onion-peel" method has been used, in which the cross section of the plume is divided into concentric rings [7-21]. Optical measurements are made as indicated in Figure 7-13. Another method is the spectral

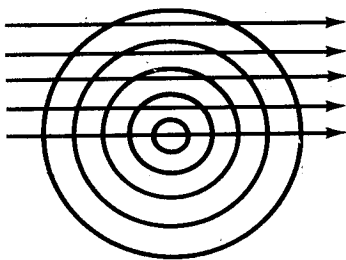


Figure 7-13. "Onion-peel" method.

temperature inversion method, in which the temperature is deduced from spectral measurements made at different wavelengths within a given rotation-vibration band. The method for sounding the atmospheric temperature was first suggested by King [7-22] and Kaplan [7-23]. The problem of mathematical inversion was treated by Twomey [7-24], and Wark et al. [7-25]. A review of the theory and applications of inversion techniques was given by Wang [7-26]. The application of these techniques for the determination of temperature profiles in hot gases has been discussed by Krakow [7-27].

7.2 DIATOMIC MOLECULES

A comparison between the band model parameters presented in this handbook and available experimental data for diatomic molecules is given. Oppenheim et al. [7-28] have made measurements of heated NO (fundamental band) between 300 and 800K and have compared their results with previously reported calculated values of Malkmus and Thomson [7-29]. In their comparison, Oppenheim et al. had to correct the absorption coefficients by the factor of (125/69), the ratio of the recently established integrated band intensity to the previous value. They also included the factor (T/273) to give the absorption coefficients in terms of standard temperature and pressure. Their comparison is shown in Figure 7-14 for T = 800K. The corrections made by Oppenheim are incorporated in the values given in the General Appendix. Oppenheim et al. have also determined the statistical band model parameter  $2\pi\gamma^0/d(\text{atm}^{-1})$  for the NO fundamental band at 300, 500, and 800K. A comparison of their values with the values given in the General Appendix is presented in Figure 7-15.

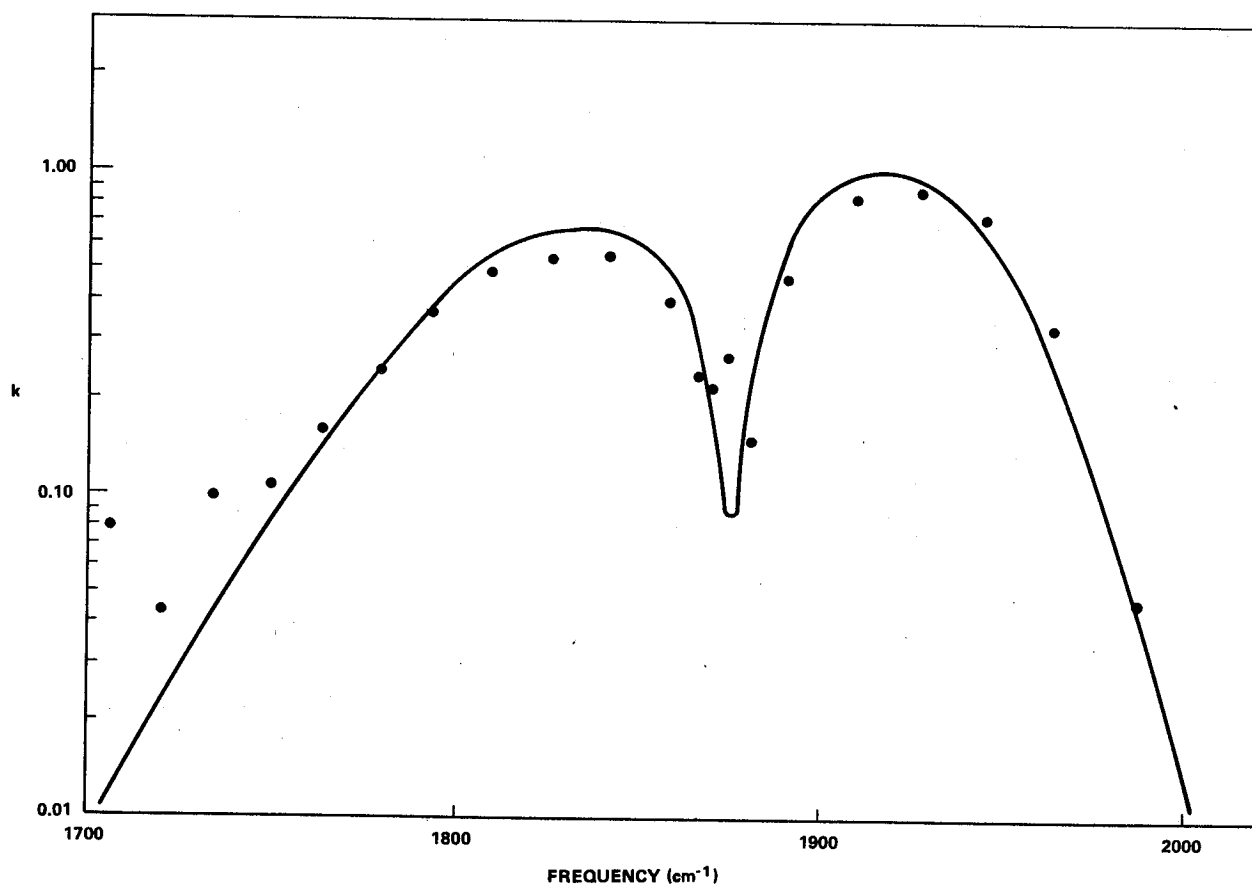


Figure 7-14. Comparison of measured [7-28] and calculated absorption coefficient  $k$  (in  $\text{cm}^{-1} \text{atm}^{-1}$  at 273K) for the NO fundamental band at 800K. Measured data given by points.

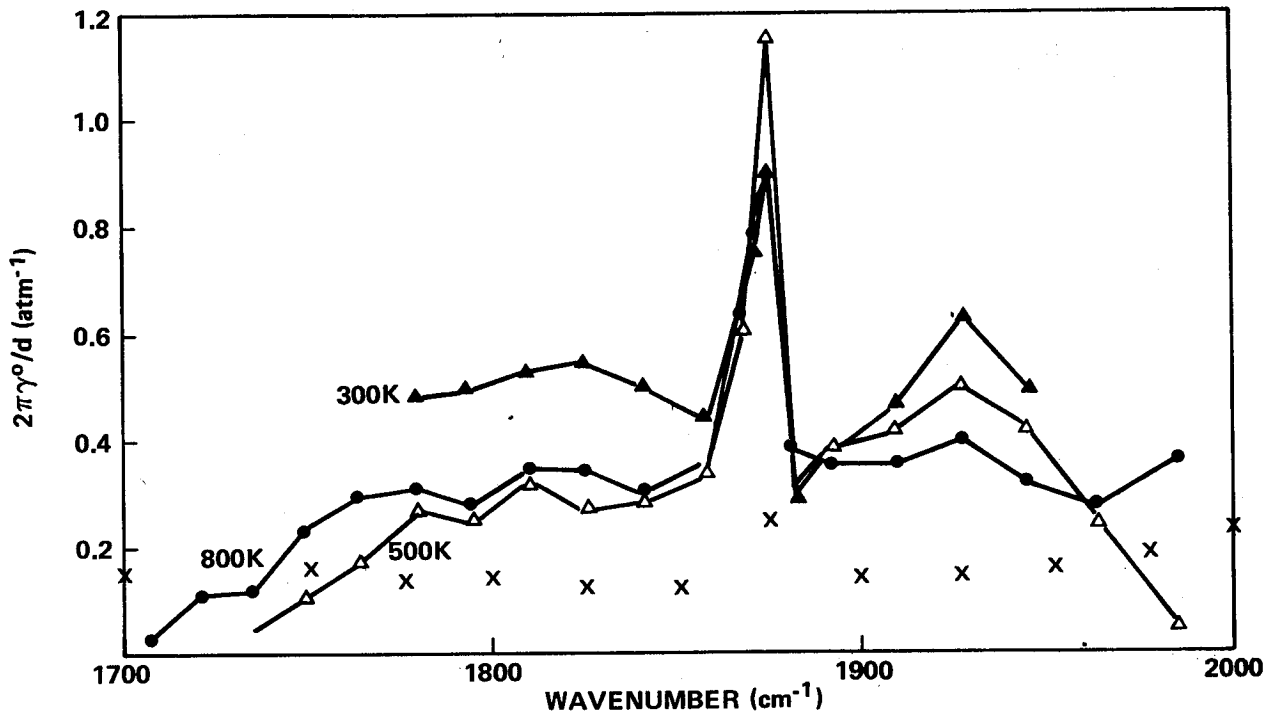


Figure 7-15. Values of the statistical band model parameter  $2\pi\gamma^0/d$  for NO as deduced by Oppenheim for 300, 500 and 800K. Theoretical values for 600K are indicated by (x).

In Reference 7-30, comparisons between experimental and theoretical data were made for the absorptance of HCl at temperatures up to 1200K. The theoretical predictions [7-31] were based upon the random Elsasser model. These theoretical results were substantially the same as quoted in Reference 7-29, using the statistical model. Thus, the comparison shown in Figure 7-16 for HCl at 1200K is indicative of the agreement between experiment and theoretical predictions based upon data presented in the General Appendix. A direct comparison between the random Elsasser and statistical model calculations and experimental data at room temperature is shown in Figure 7-17 [7-32]. Comparisons for heated CO gas at 1200K are shown in Figure 7-18, using the results of Abu-Romia and Tien [7-33].

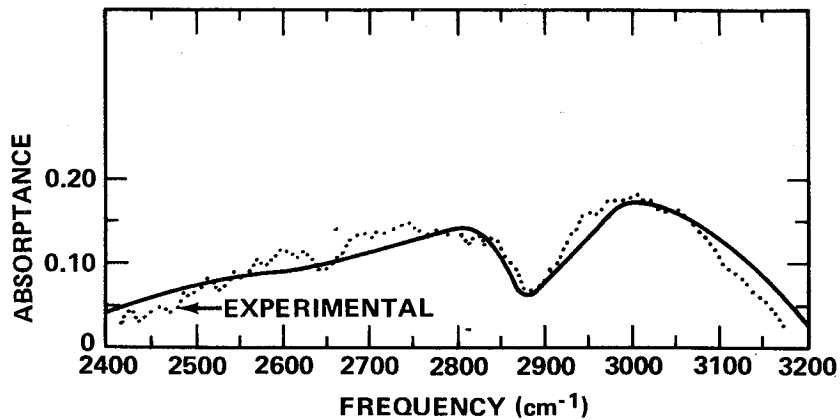


Figure 7-16. Experimental and predicted spectral absorbance of HCl at 1200K and  $P^2l = 10 \text{ atm}^2 \text{ cm}$ .

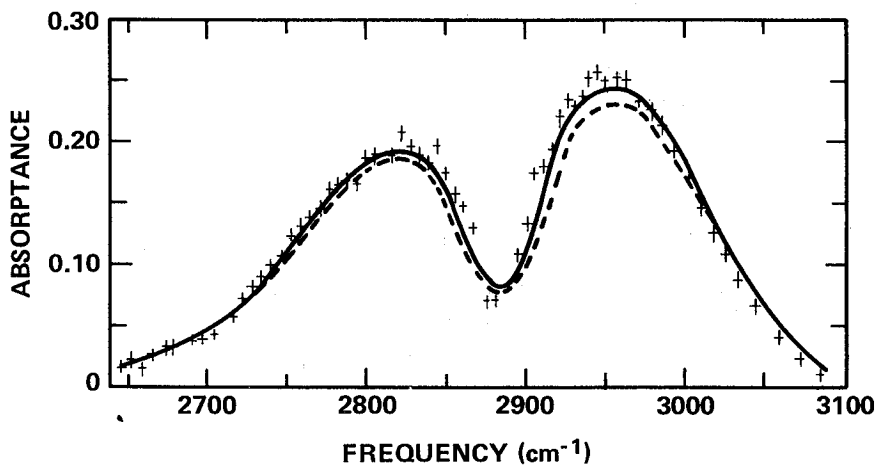


Figure 7-17. Spectral absorbance of HCl at room temperature, showing experimental points, random Elsasser model calculation (solid curve), and statistical model calculation (dashed curve).  $P^2l = 1 \text{ atm}^2 \text{ cm}$ .

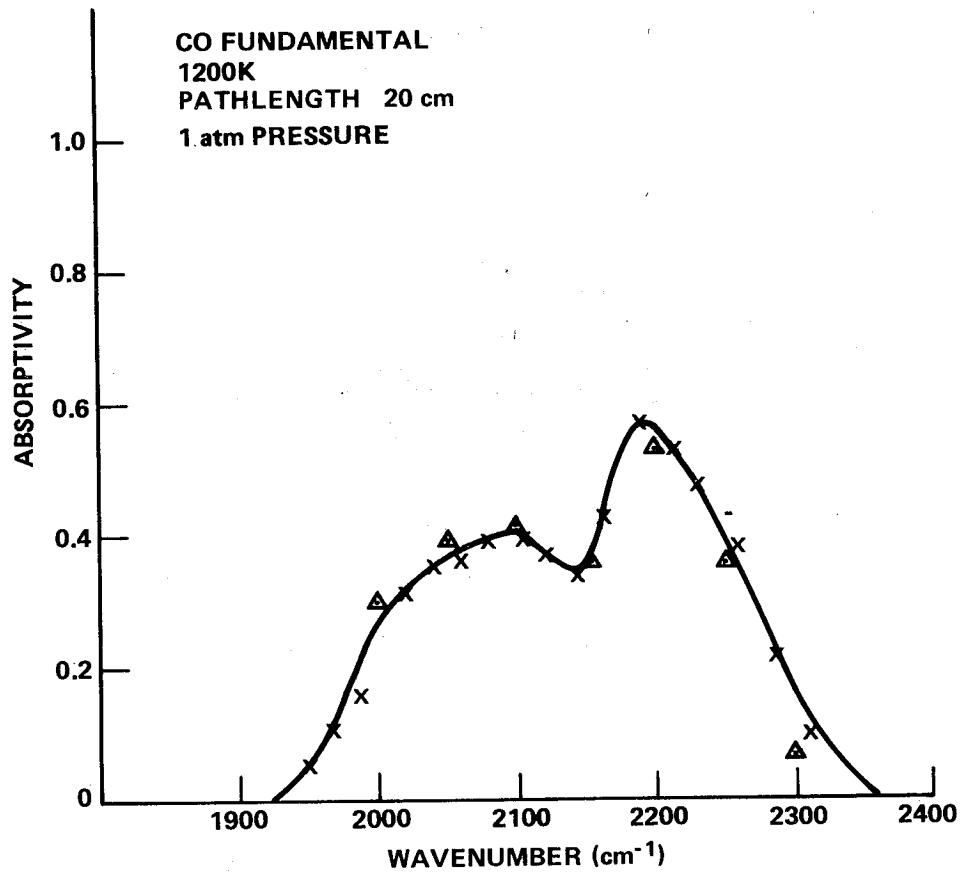


Figure 7-18. Solid line is a smooth curve through the experimental values (x). Values calculated using the SLG Model (Section 5.3) are given by Δ.

### 7.3 CARBON DIOXIDE

#### 7.3.1 HOMOGENEOUS

Comparisons of experiment with theory for the absorption coefficient and emissivities for the CO<sub>2</sub> bands at 2.7 μ and 4.3 μ are made in this section.

##### 7.3.1.1 The 2.7-μ Band

For the comparison with experimental results at 1200K, one of several experimental runs reported by Burch and Gryvnak [7-34], by Tourin [7-35] and by Ferriso et al. [7-36] were selected. The results of Burch and Gryvnak, as well as of Tourin and Ferriso, showed that the spectral emissivities were independent of partial and total pressure, within the experimental uncertainties. Thus the band acted as if it were smeared and the various measured emissivities  $\epsilon'$  at optical paths  $u'$  could be scaled to a common optical path  $u$  according to

$$\epsilon(v, T) = 1 - \exp\left(-\frac{u}{u'} \ln \frac{1}{1 - \epsilon'}\right)$$

The comparison of the experimental results with theoretical calculations [7-29] at 1200K as given in Figure 7-19 shows good overall agreement. The difference of the two maxima near the band head between the four results has several explanations. The spectral slitwidths in the experiments (Ferriso's, Tourin's, Burch, and Gryvnak's) were 20, 10, and 6 cm<sup>-1</sup>, respectively. This probably accounts for the differences in the experimental results in the band head region. The large differences between the experimental curves and the theoretical results in the band region are probably due to three effects [7-36]. First, the accuracy of the theoretical calculations in the spectral region from 3600 to 3800 cm<sup>-1</sup> is lower than in the rest of the spectrum; second, the calculations do not refer to a particular slitwidth as do the experiments, but rather refer to a limiting case of a slitwidth which becomes small compared with the widths of the entire band, but still sufficiently large not to resolve the individual line structure; and, third, the weak line approximation is an upper limit and the deviations from this approximation will show up more in the region near the band head because of the smaller line density.

Finally, Figure 7-20 illustrates the radiance of the same 2.7-μ band at T = 1146K. For this sample, most of the band was black [7-4].

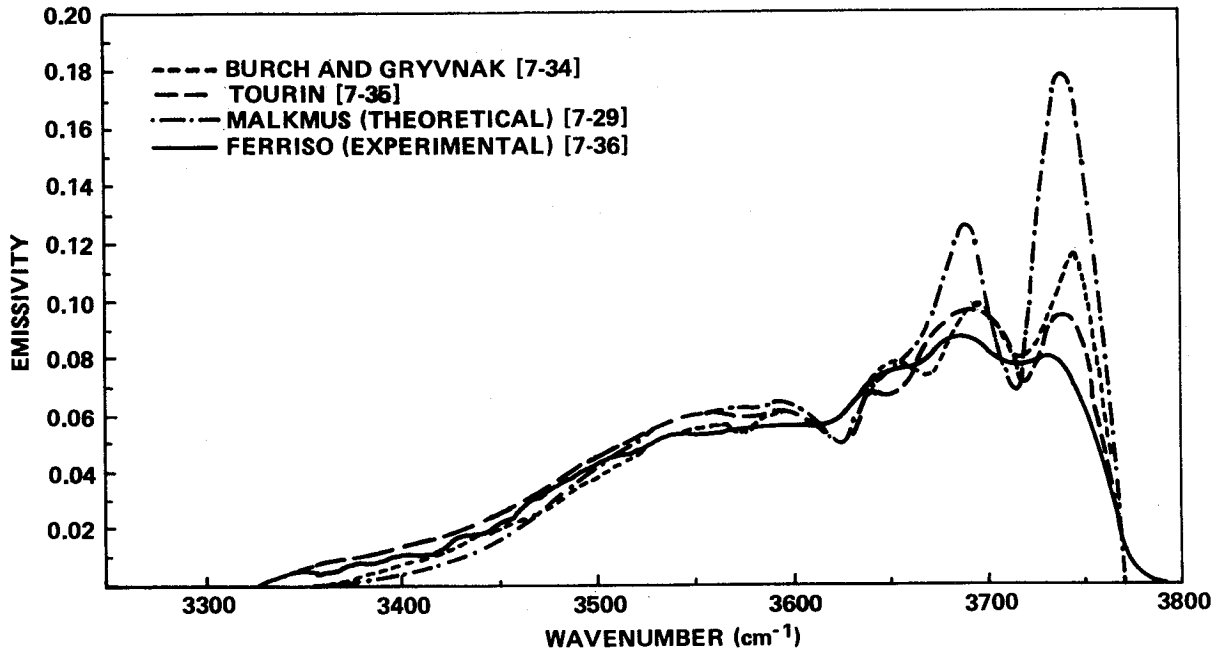


Figure 7-19. Comparison of experimental spectral emissivities of the  $2.7\text{-}\mu\text{ CO}_2$  band at 1200K [total pressure = 1 atm; pathlength  $3.12\text{ cm} \pm 5\%$ ;  $p\ell = 1.03\text{ (cm-atm)}$ ; normalized optical path,  $u = 0.245\text{ (cm-atm)}_{\text{STP}} \pm 5\%$ ].

#### 7.3.1.2 The 4.3- $\mu$ Band

A comparison of experimental measurements made with a supersonic burner [7-37] and theory is shown in Figure 7-21. A shock tube measurement [7-38] at one particular wavenumber ( $2355\text{ cm}^{-1}$ ) is also shown. Within experimental uncertainties good agreement exists in this band head region. The experimental data are lower by approximately 25 percent than the calculated values near the maximum of the band, but higher by approximately 25 percent in the long wavelength wing of the band. This difference is about twice as large as the estimated uncertainty for the present measurements. It does appear that the effect of anharmonicity on the Boltzmann factor for the population of the higher vibrational levels becomes significant and may account for the differences between the present experimental results and theoretical calculations at the low wavenumber wing of the band. (The effects due to  $\text{C}^{13}\text{O}_2$  isotopes which would show up in the low wavenumber wing of the band are less than two percent at temperatures around 3000K.)

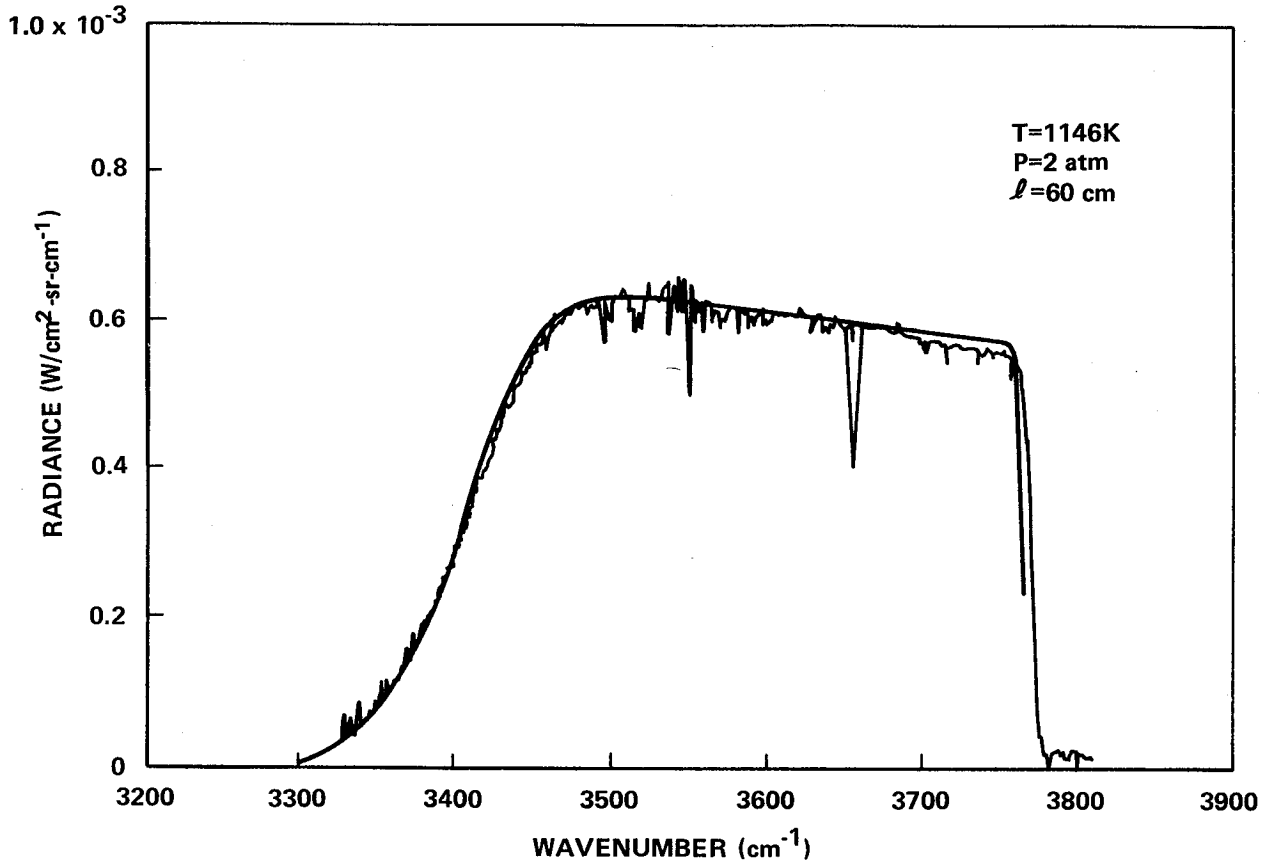


Figure 7-20. Comparison of isothermal CO<sub>2</sub> spectra with band model calculations by Simmons et al. [7-4].

### 7.3.2 INHOMOGENEOUS GAS

As an example of the radiation from an inhomogeneous slab of CO<sub>2</sub>, the results of Simmons et al. [7-4] for the 2.7- $\mu$  band of CO<sub>2</sub> are shown in Figure 7-22. The experimental conditions were: The sample cell (with a total length of 60 cm) contained pure CO<sub>2</sub> at 1 atm total pressure. The temperature profile was 386, 528, 719, 953, 1130, 1160, 979, 737, 541, and 387K for each section with a nominal length of 6 cm. The comparison with the theoretical predictions was made by Simmons et al. [7-4], in a similar fashion to that outlined in Chapter 5, using the band model parameters listed in the General Appendix.

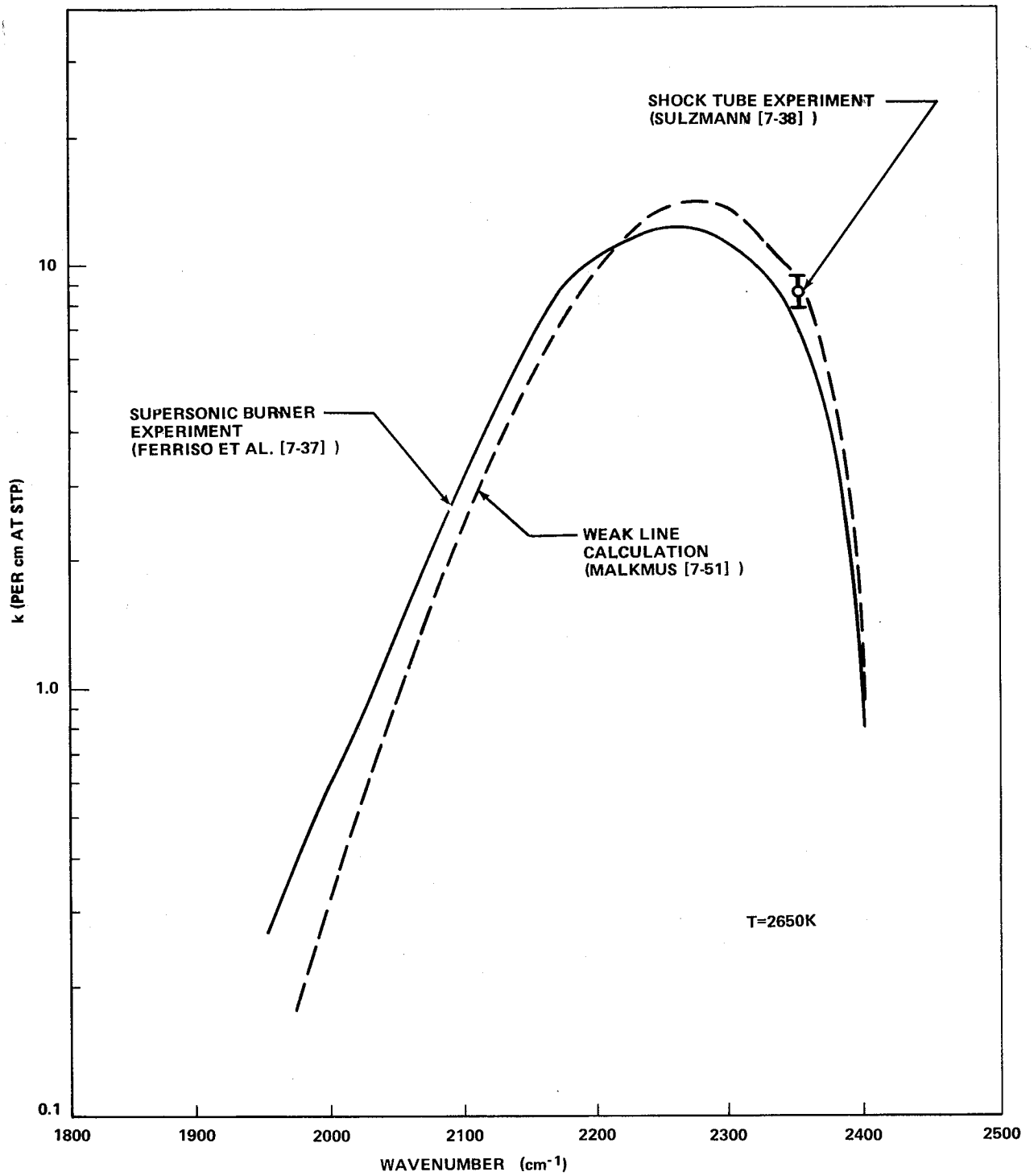


Figure 7-21. Average absorption coefficient of  $\text{CO}_2$  at 2650K.

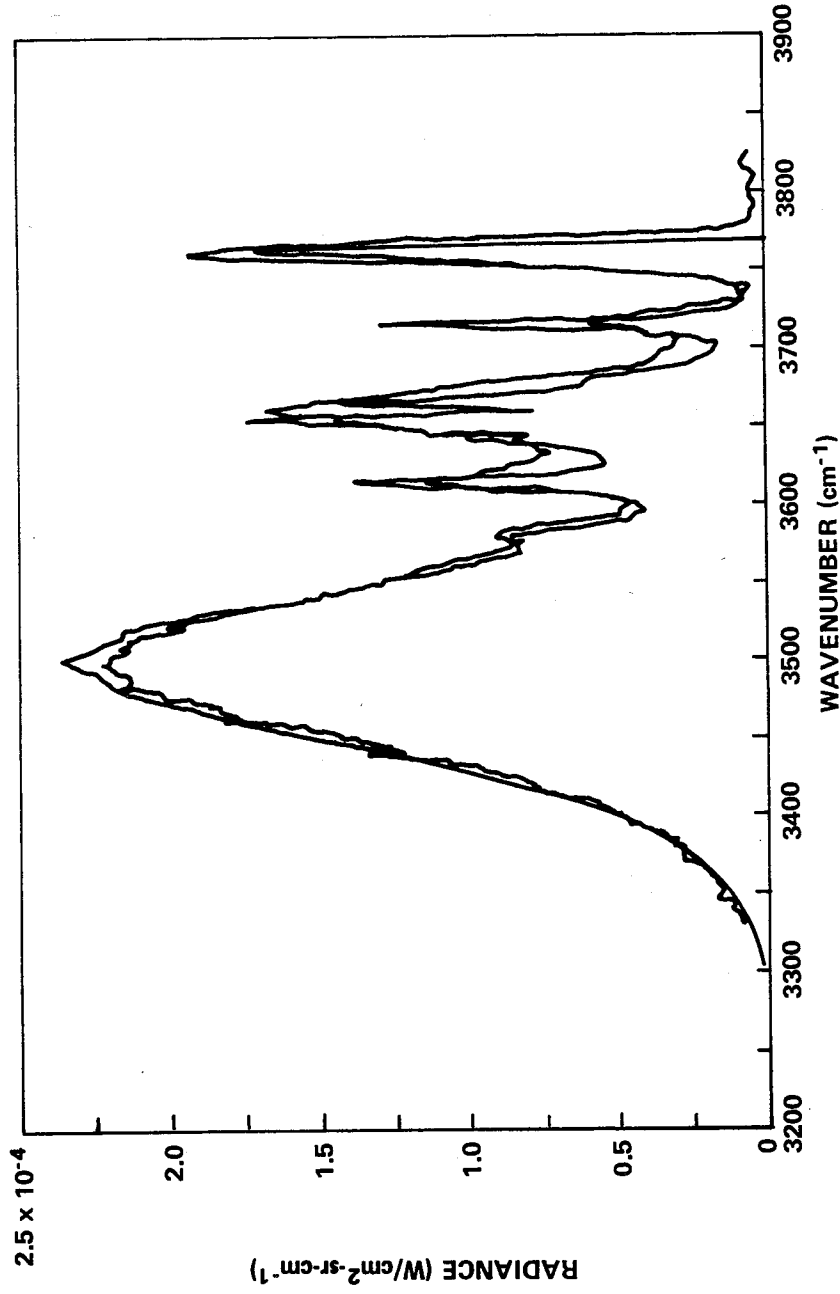


Figure 7-22. Comparison of nonisothermal CO<sub>2</sub> spectra with band-model calculations by Simmons et al. [7-4]. Test conditions are defined in the text.

## 7.4 WATER VAPOR

### 7.4.1 HOMOGENEOUS GAS

#### 7.4.1.1 Absorption Coefficient Data

The band model data presented in this handbook for water vapor have been derived from experimental data, notably from the long burner measurements of Ludwig [7-6]. A comparison between the absorption coefficients recommended in this handbook and other independent experimental evidence is possible for some selected temperatures. Theoretical line strengths for individual lines in the  $6.3\text{-}\mu$  band at  $\approx 300\text{K}$  and  $\approx 600\text{K}$ , and in the  $1.87\text{-}\mu$  and  $2.7\text{-}\mu$  bands at  $300\text{K}$  are listed in References 7-39 and 7-40. These high resolution data are averaged over  $25\text{ cm}^{-1}$  intervals and an example is given in Figure 7-23. Detailed measurements of the absorption coefficients in the  $2.7\text{-}\mu$  band  $1200\text{K}$  by Oppenheim and Goldman [7-41] are compared in Figure 7-24. Goldstein's [7-42] determinations of the absorption coefficients of the  $1.38\text{-}$ ,  $1.87\text{-}$ ,  $2.7\text{-}$ , and  $6.3\text{-}\mu$  bands at  $500$  and  $1200\text{K}$  have been compared with the theoretical models and a typical result is shown in Figure 7-25.

#### 7.4.1.2 Spectral Emissivities

For the comparison of measured and computed high-temperature water vapor spectra, a few examples for widely varying conditions were selected. The computations are based on the procedure outlined in section 5.3, using the SLG model with the band model parameters given in the General Appendix. Of all the existing experimental data, the highest temperatures at the longest pathlengths were obtained using a long burner [7-6]. Results of this experiment for a homogeneous slab of water vapor with a pathlength of 20 feet at  $2500\text{K}$  are compared with computed values in Figure 7-26 for the five major water bands at  $6.3$ ,  $2.7$ ,  $1.8$ ,  $1.4$ , and  $1.1\text{ }\mu$ . Since the band model parameters were derived exclusively from the long burner measurements at these high temperatures, this comparison is primarily a consistency check. At the lower temperature of  $1500\text{K}$ , where a number of spectra from other investigators were included in determining the absorption coefficient (especially for the  $2.7\text{-}\mu$  band), some differences between the long burner experimental data and the computed results are noted (see Figure 7-27). At both temperatures there is a difference between the experimental and computed spectra in the  $2200$  to  $2400\text{ cm}^{-1}$  range. This is a result of the experimental data being shown with no compensation for  $\text{CO}_2$  absorption at the ends of the long burner, while the absorption coefficient data were derived from compensated experimental results.

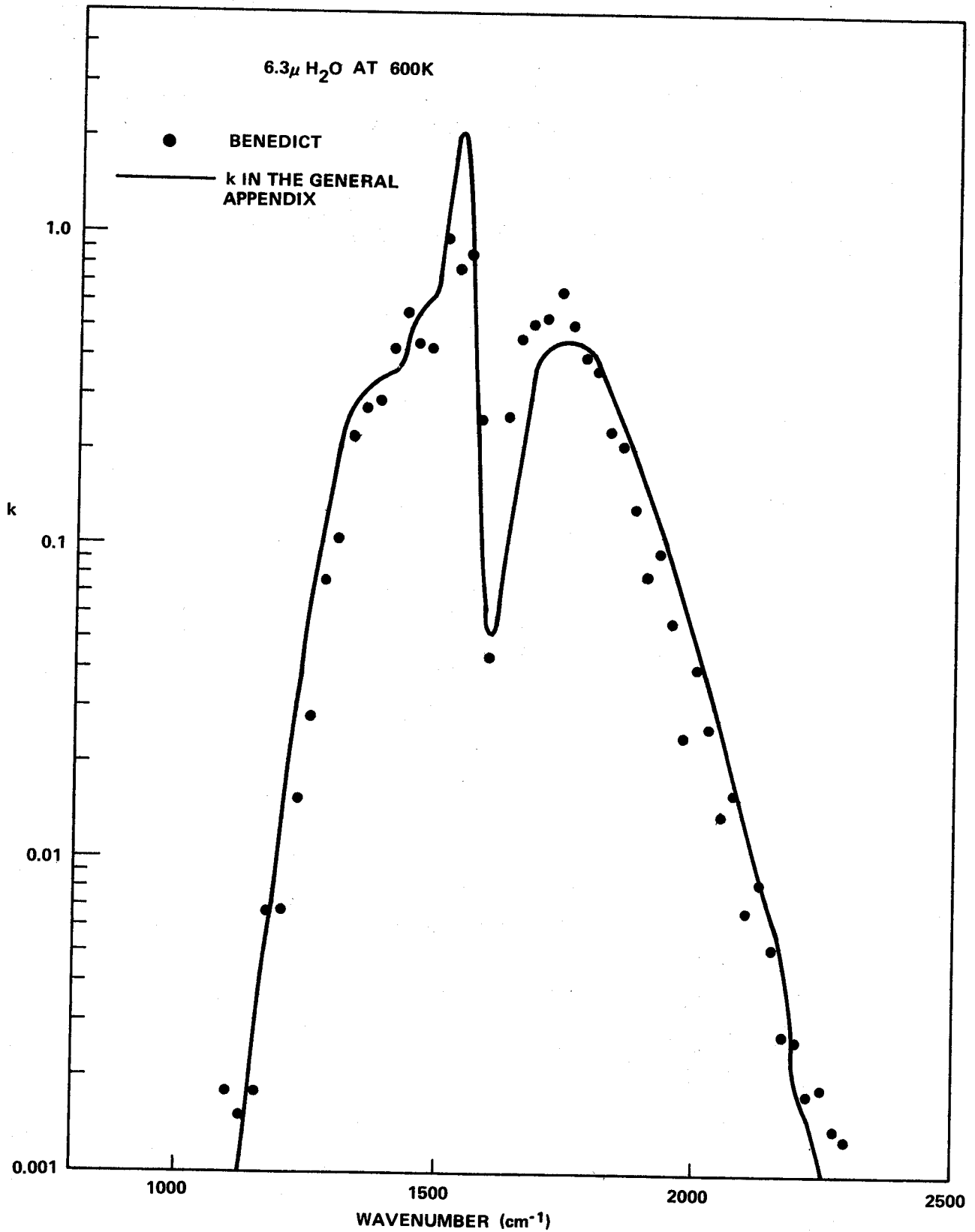


Figure 7-23. Comparison of absorption coefficients obtained by Benedict and Calfee [7-40] at 600K (averaged over 25 cm<sup>-1</sup>) with values of k presented in General Appendix.

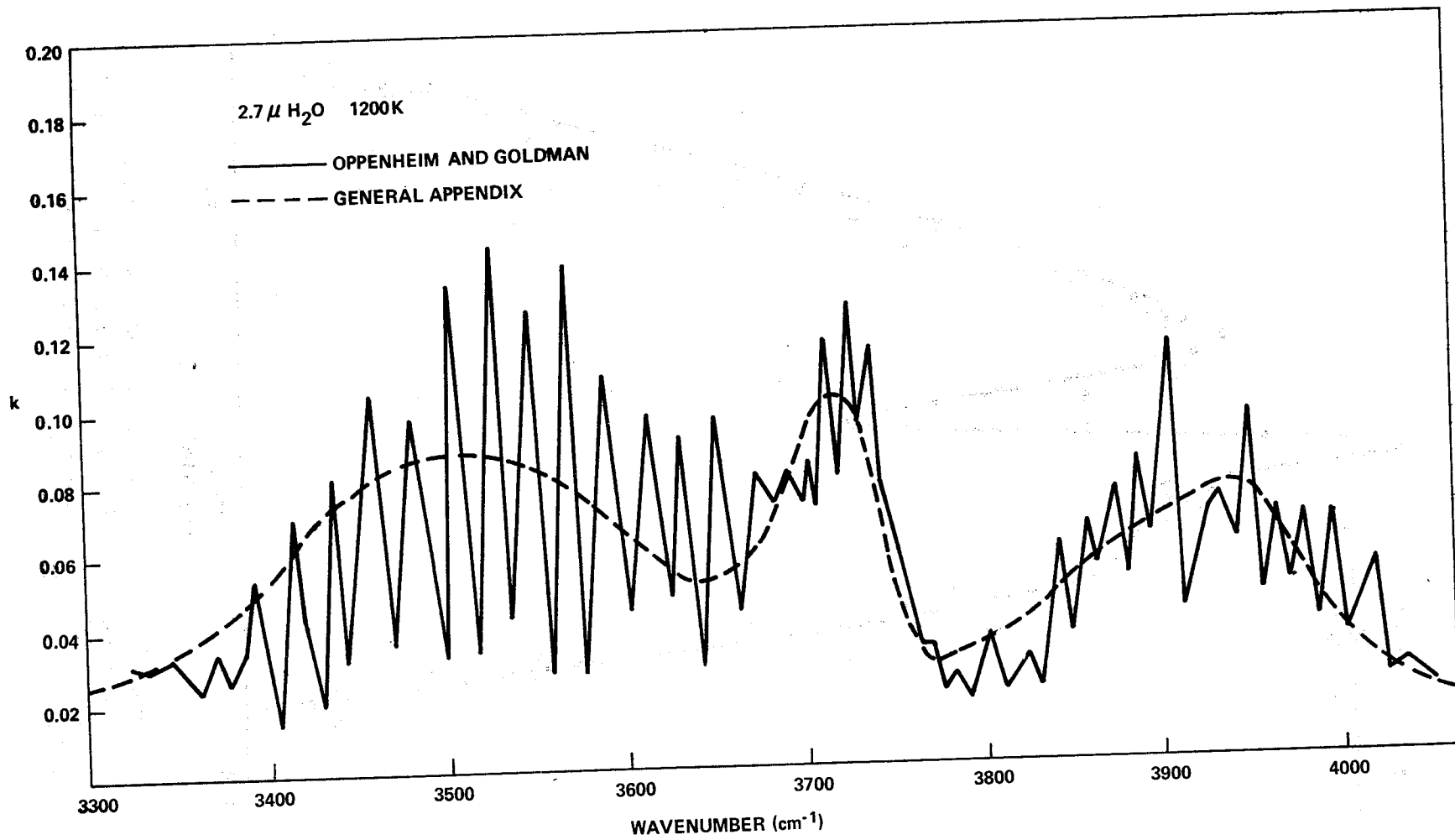


Figure 7-24. Comparison of absorption coefficients obtained by Oppenheim [7-41] (slit width  $\sim 8$  cm<sup>-1</sup>) with values of  $k$  presented in General Appendix.

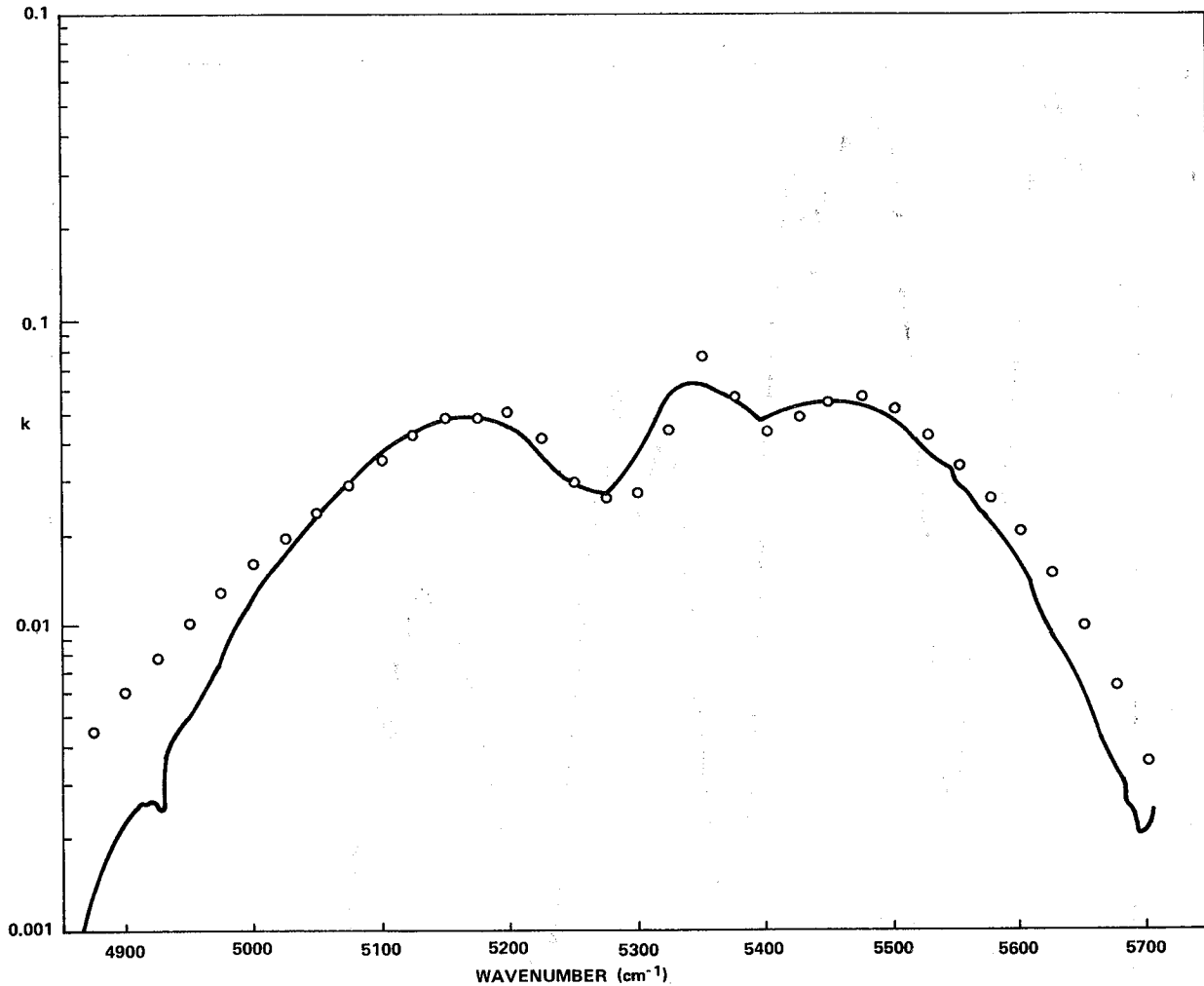


Figure 7-25. Comparison of absorption coefficients, obtained by Goldstein [7-42], of the 1.9- $\mu$  band of H<sub>2</sub>O at 873K (solid line) (Points represent data from the General Appendix).

It has been estimated that the calculation of integrated radiances (or total engineering emissivities) based on the data presented here are within  $\pm 5$  percent for  $pL \leq 20$  ft-atm. For greater pathlengths, the uncertainty is surely greater because it depends more on the individual foreign gas broadener parameters, which are uncertain and, in some cases, are only rough estimates. For the calculation of spectral radiances (or spectral emissivities), the estimated overall error is within  $\pm 20$  percent. There are several exceptions to this value. The center of the 2.7- $\mu$  band at the higher temperatures is known better than  $\pm 10$  percent, while all the trough regions and bands at the lower temperatures are probably known with less certainty than  $\pm 20$  percent.

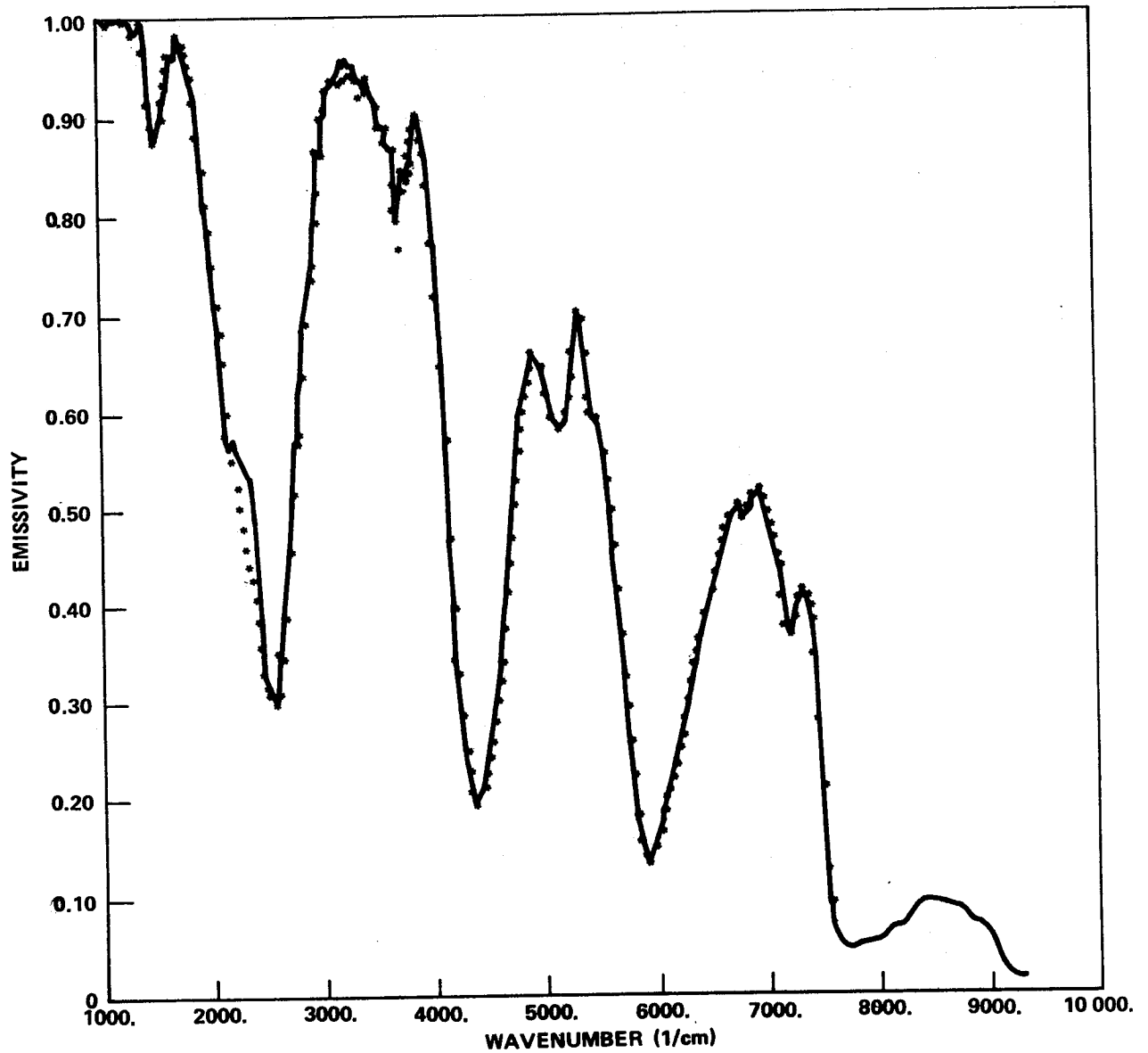


Figure 7-26. Comparison between experimental (solid line) and computed spectra (\*) at 2500K and 20-ft pathlength.

Representative comparisons with other independent experimental data are shown in the Figures 7-28 through 7-37. In general, the agreement is very good. Differences between experimental and computed spectral emissivities are mostly within  $\pm 10$  percent. In some cases, larger differences are observed, especially in the comparison with the spectra obtained by Nelson [7-5]. The authors believe that the experimental difficulties in a flow

system as used by Nelson are somewhat greater than in heated cell systems and, thus, account for the discrepancies. Except for the comparison with the spectrum obtained by Tourin and Henry [7-43], the water vapor concentrations were 100 percent in all of the comparisons by Burch and Gryvnak [7-34], Simmons et al. [7-44], and Nelson [7-5].

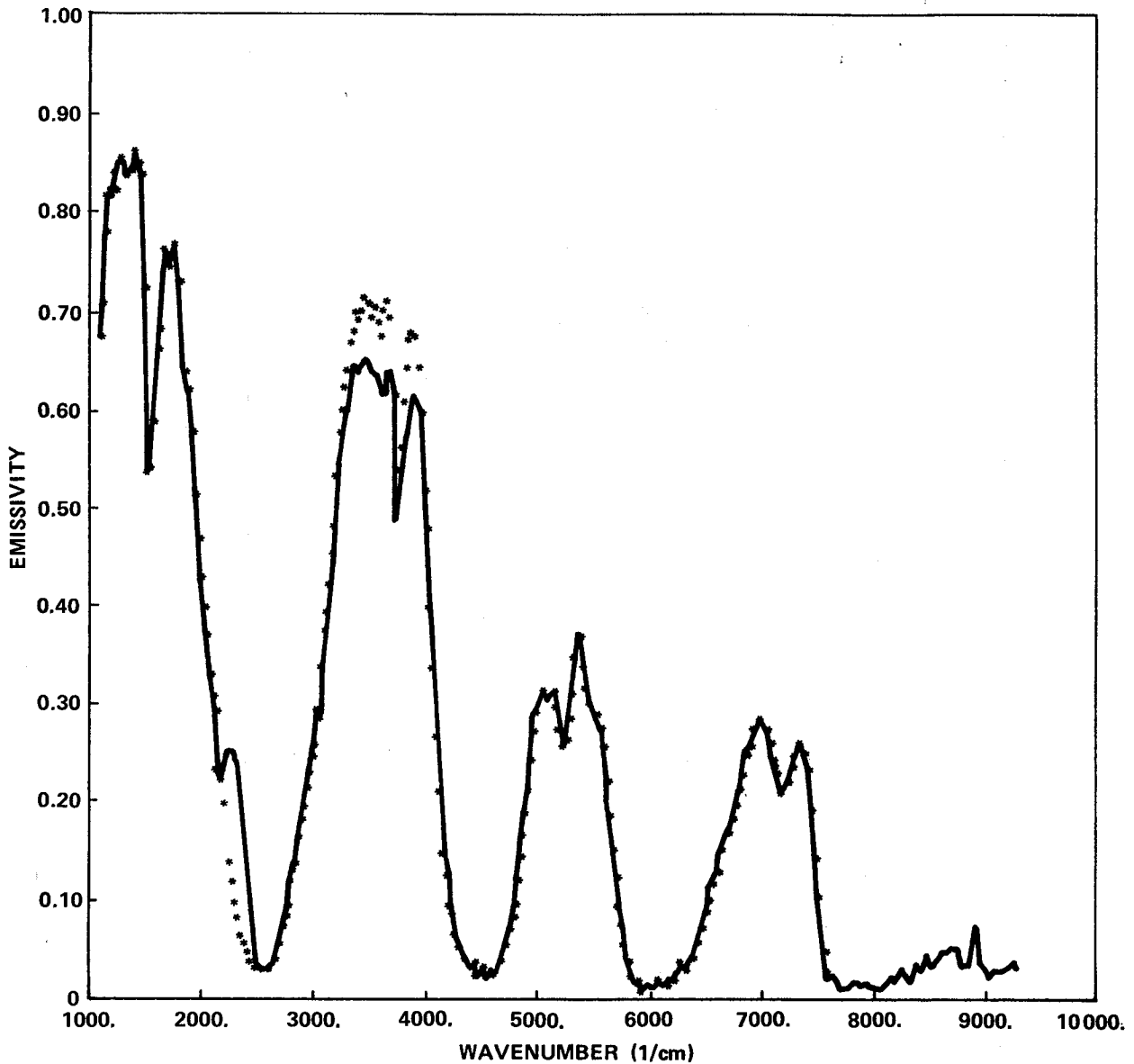


Figure 7-27. Comparison between experimental (solid line) and computed spectra (\*) at 1500K and 20-ft pathlength.

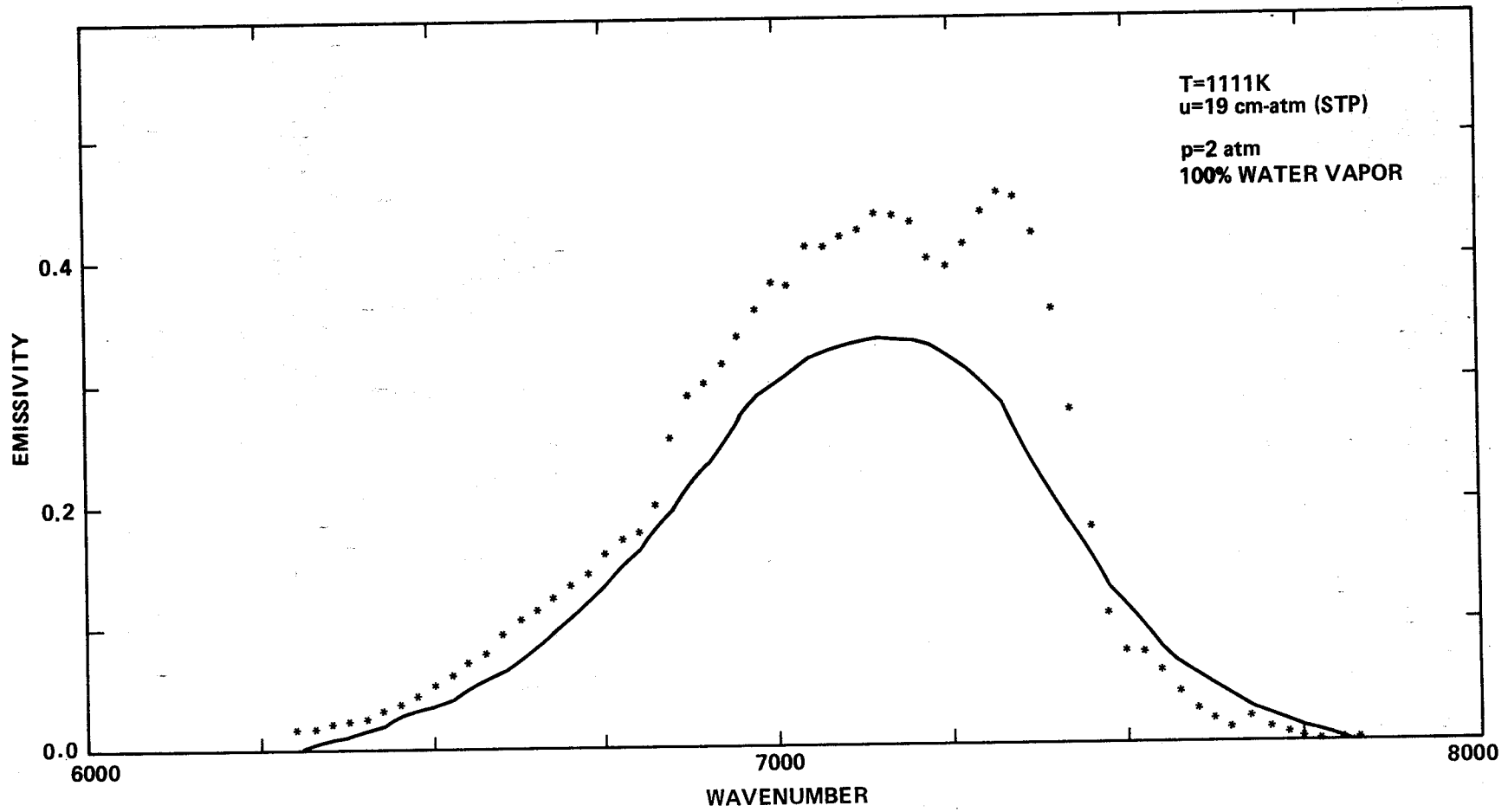


Figure 7-28. Comparison of computed results (\*) with experimental values by Nelson [7-5].

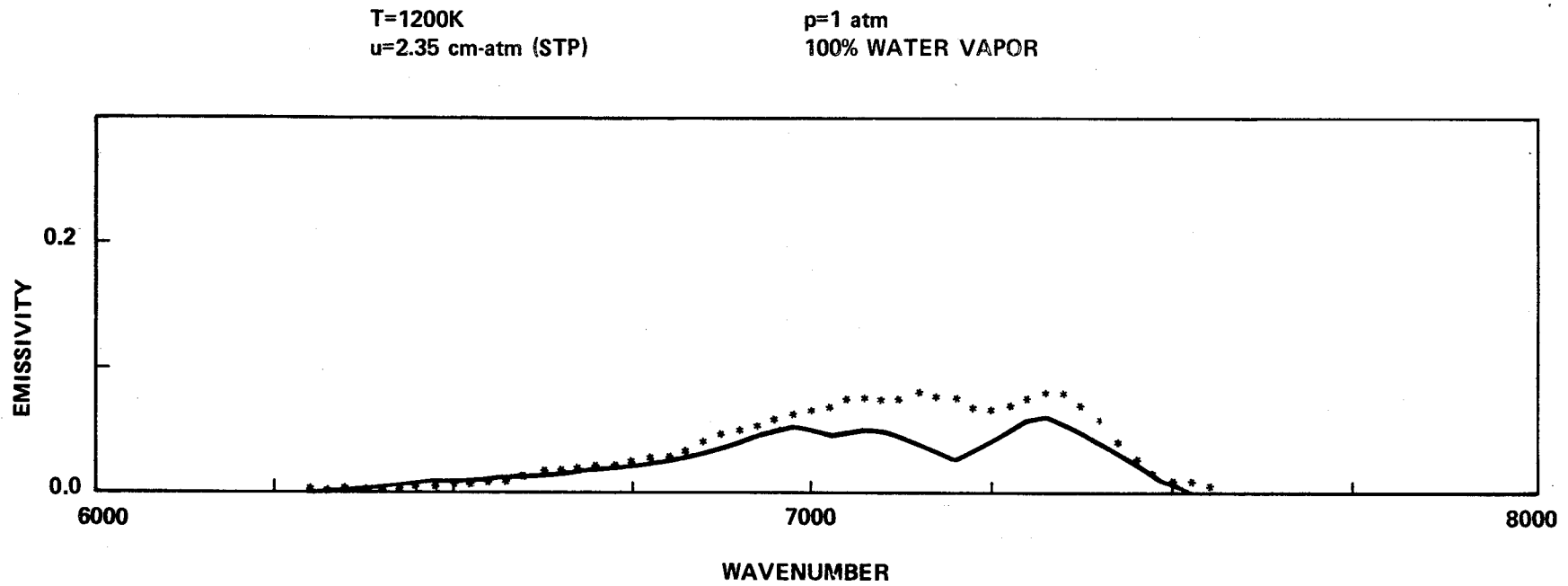


Figure 7-29. Comparison of calculated (\*) and experimental spectra at  $1.38\mu$  (Burch and Gryvnak [7-34]).

T = 832K  
u = 12.7 cm-atm (STP)

p = 1 atm  
100% WATER VAPOR

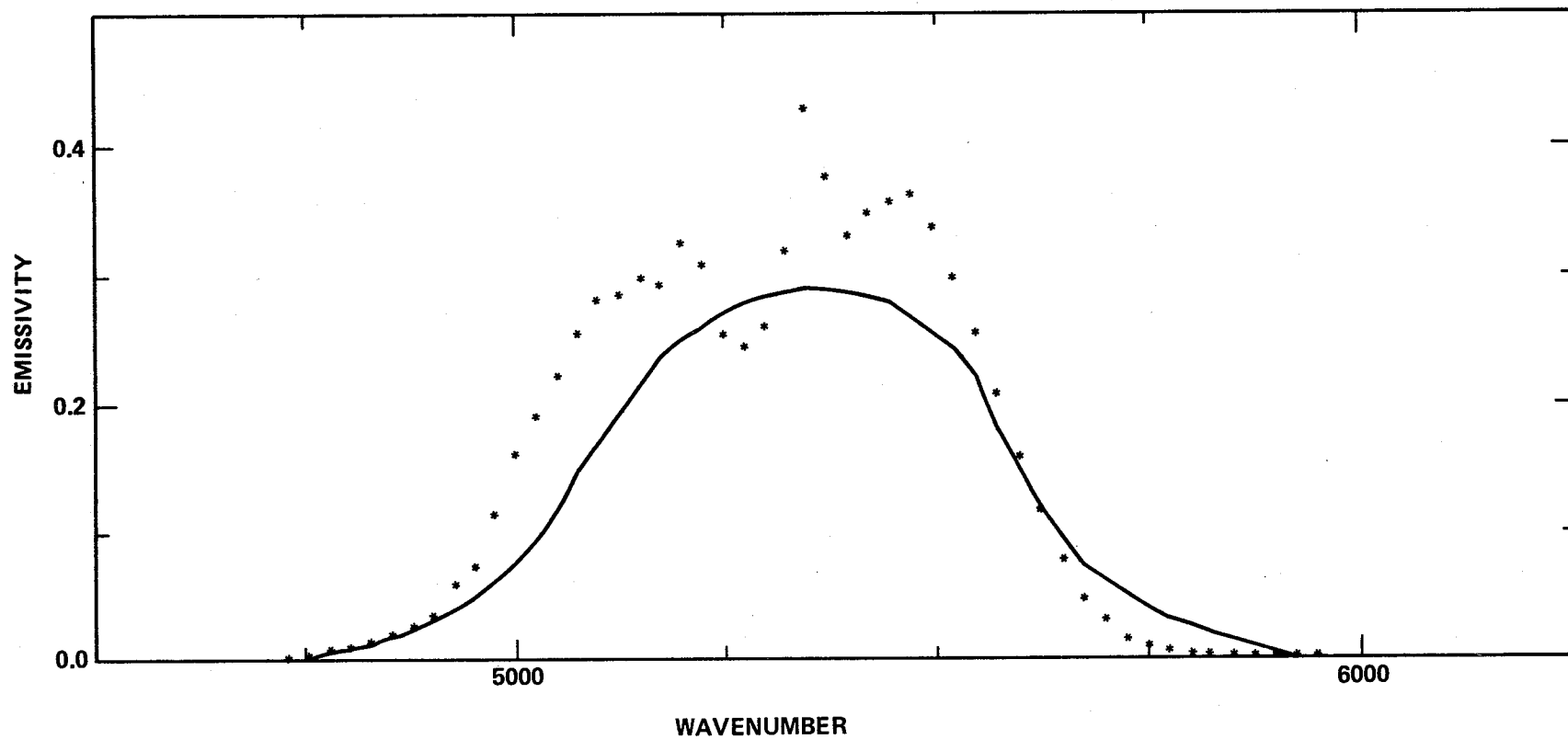


Figure 7-30. Comparison of calculated (\*) and experimental spectra (Nelson [7-5]).

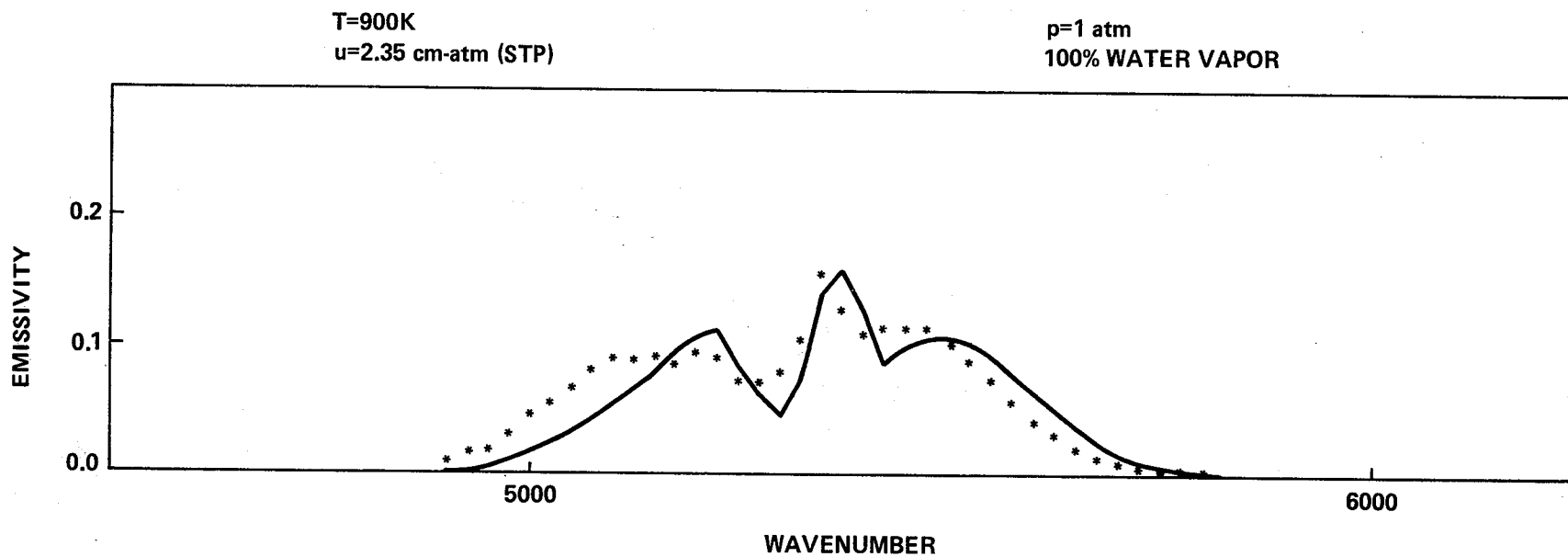


Figure 7-31. Comparison of calculated (\*) and experimental spectra at  $1.9\mu$  (Burch and Gryvnak [7-34]).

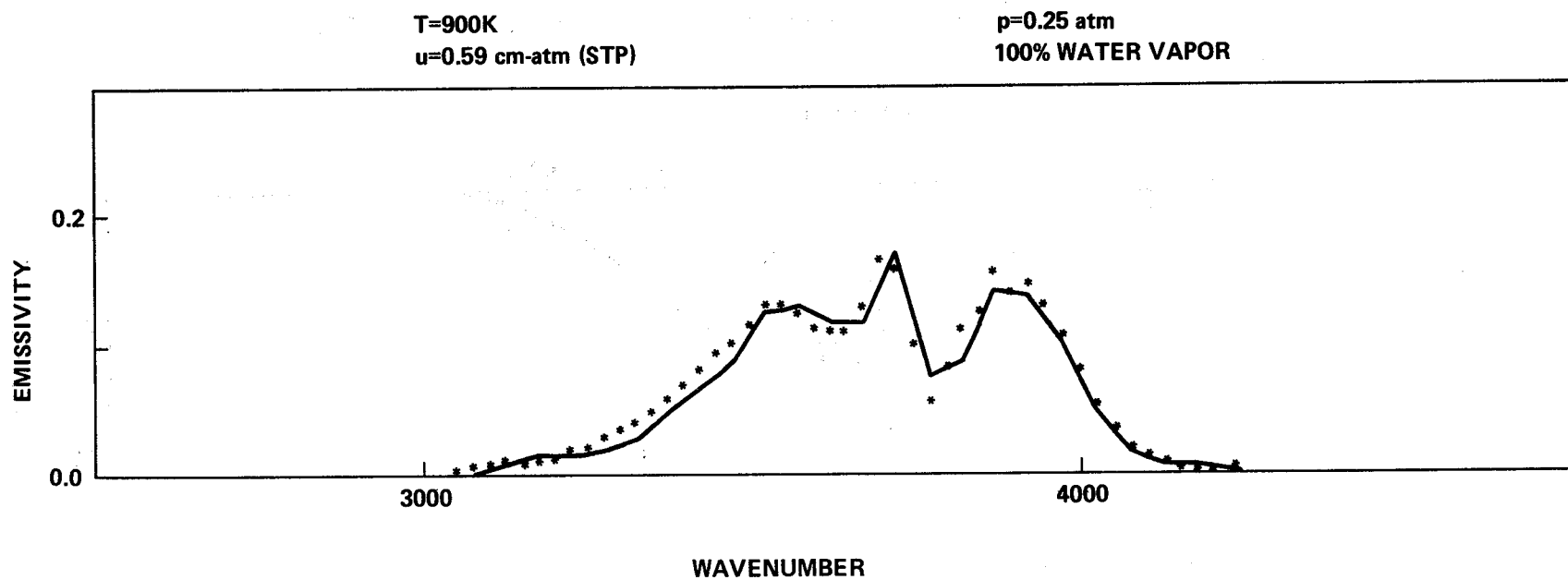


Figure 7-32. Comparison of calculated (\*) and experimental spectra at  $2.7\mu$  (Burch and Gryvnak [7-34]).

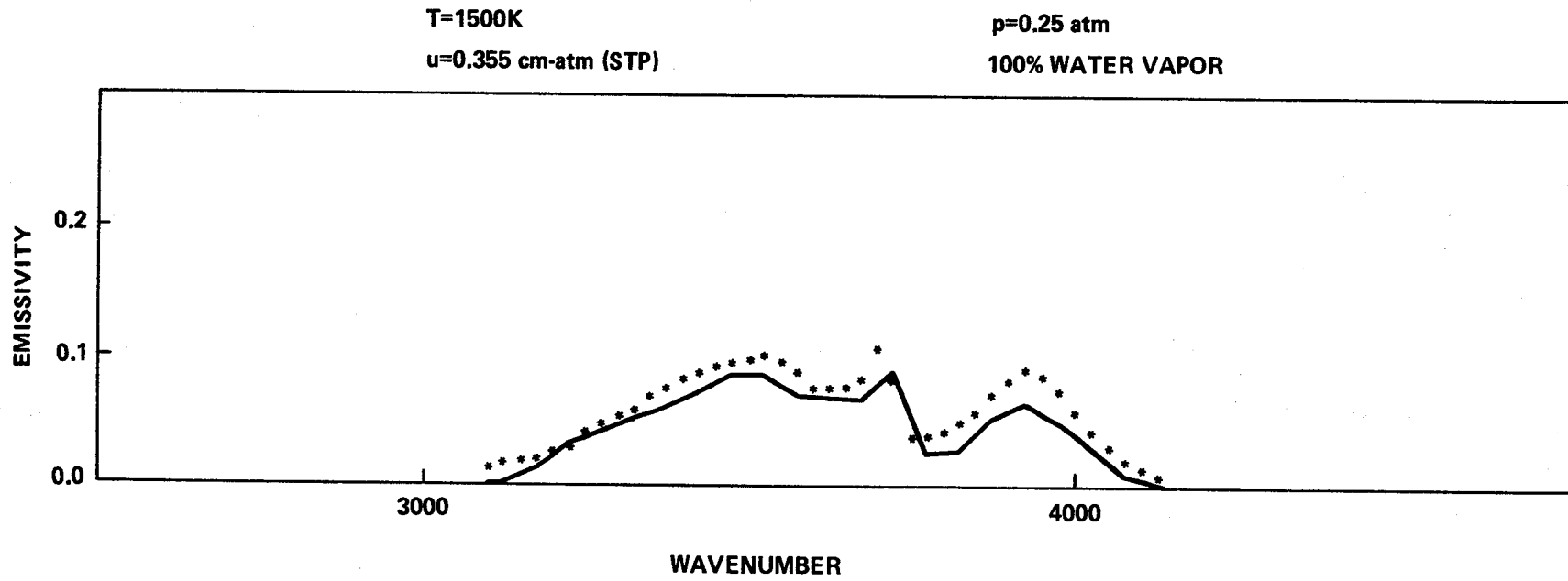


Figure 7-33. Comparison of calculated (\*) and experimental spectra at  $2.7\mu$   
(Burch and Gryvna [7-34]).

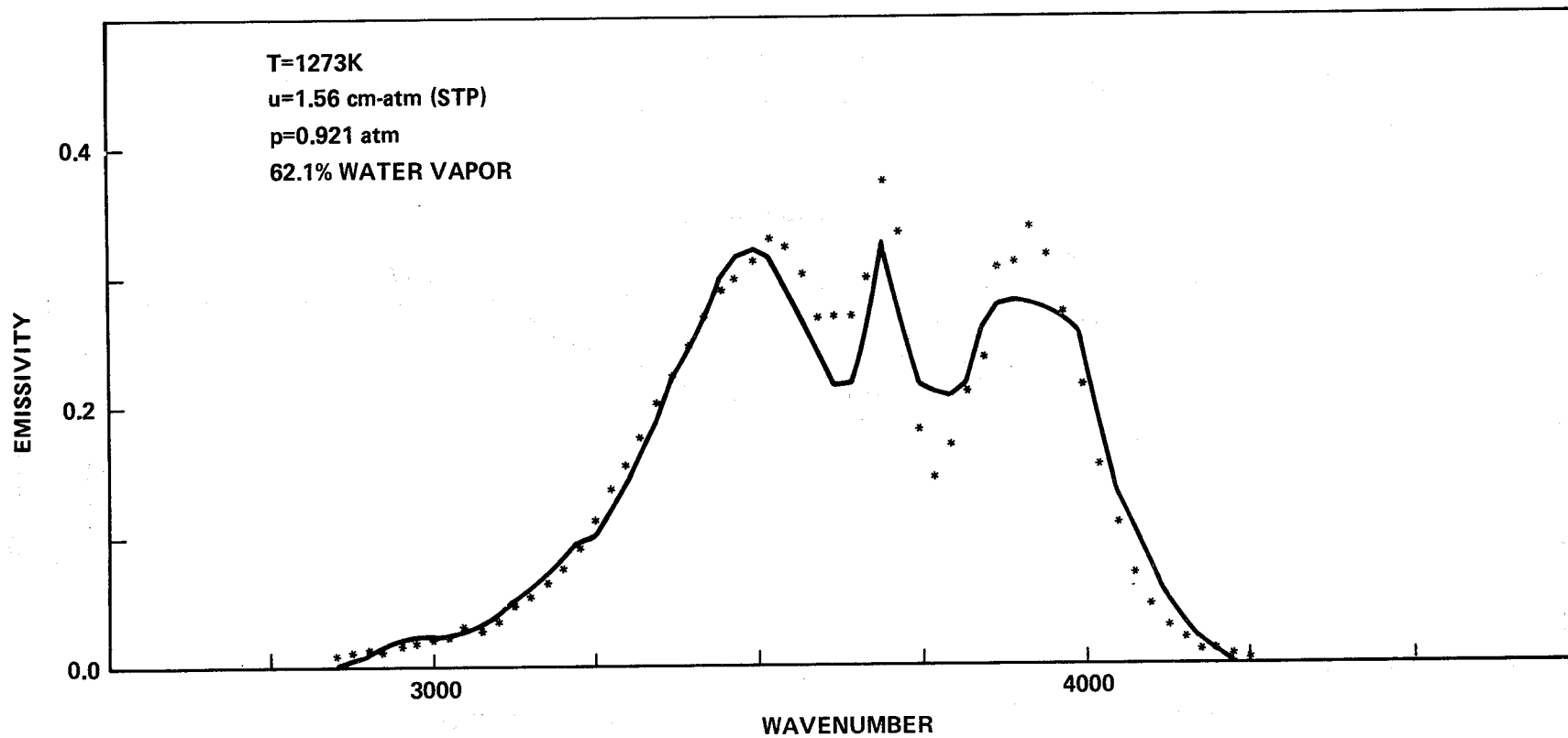


Figure 7-34. Comparison of calculated (\*) and experimental spectra at  $2.7\mu$  (Tourin and Henry [7-43]).

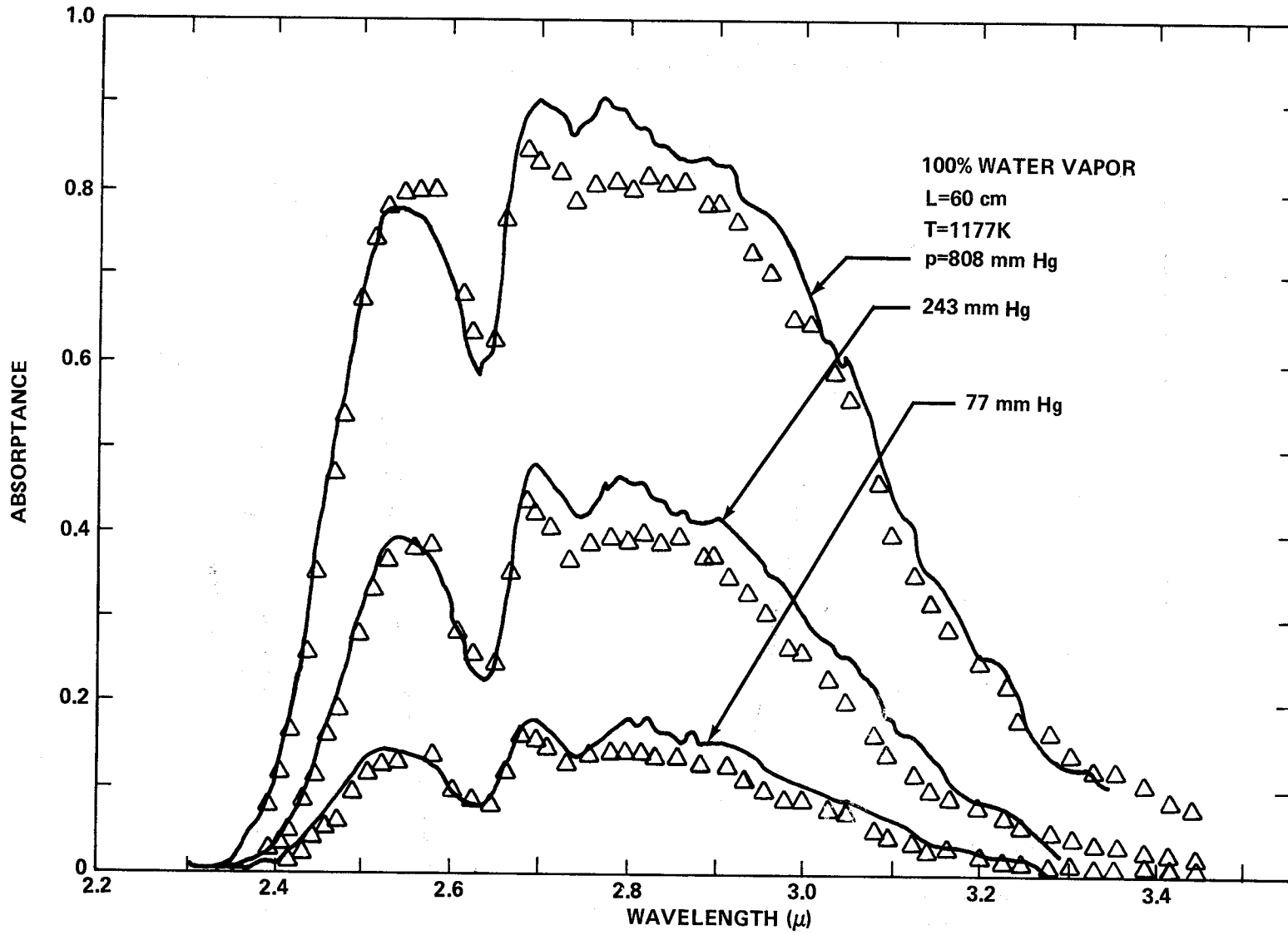


Figure 7-35. Comparisons of computed ( $\Delta$ ) and experimental spectra (Simmons et al. [7-44]).

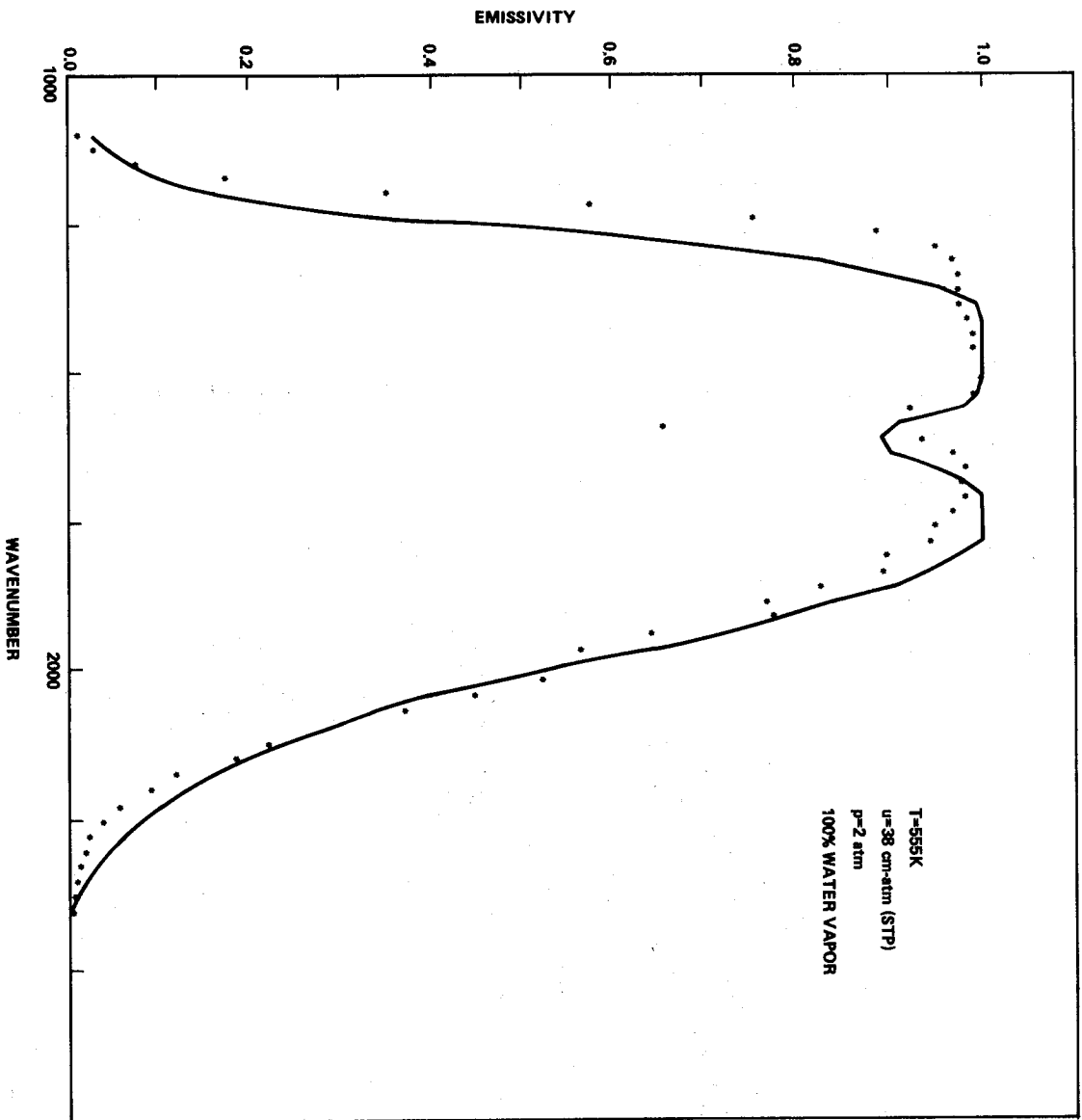


Figure 7-36. Comparison of calculated (\*) and experimental spectra at  $6.3 \mu$  (Nelson [7-5]).

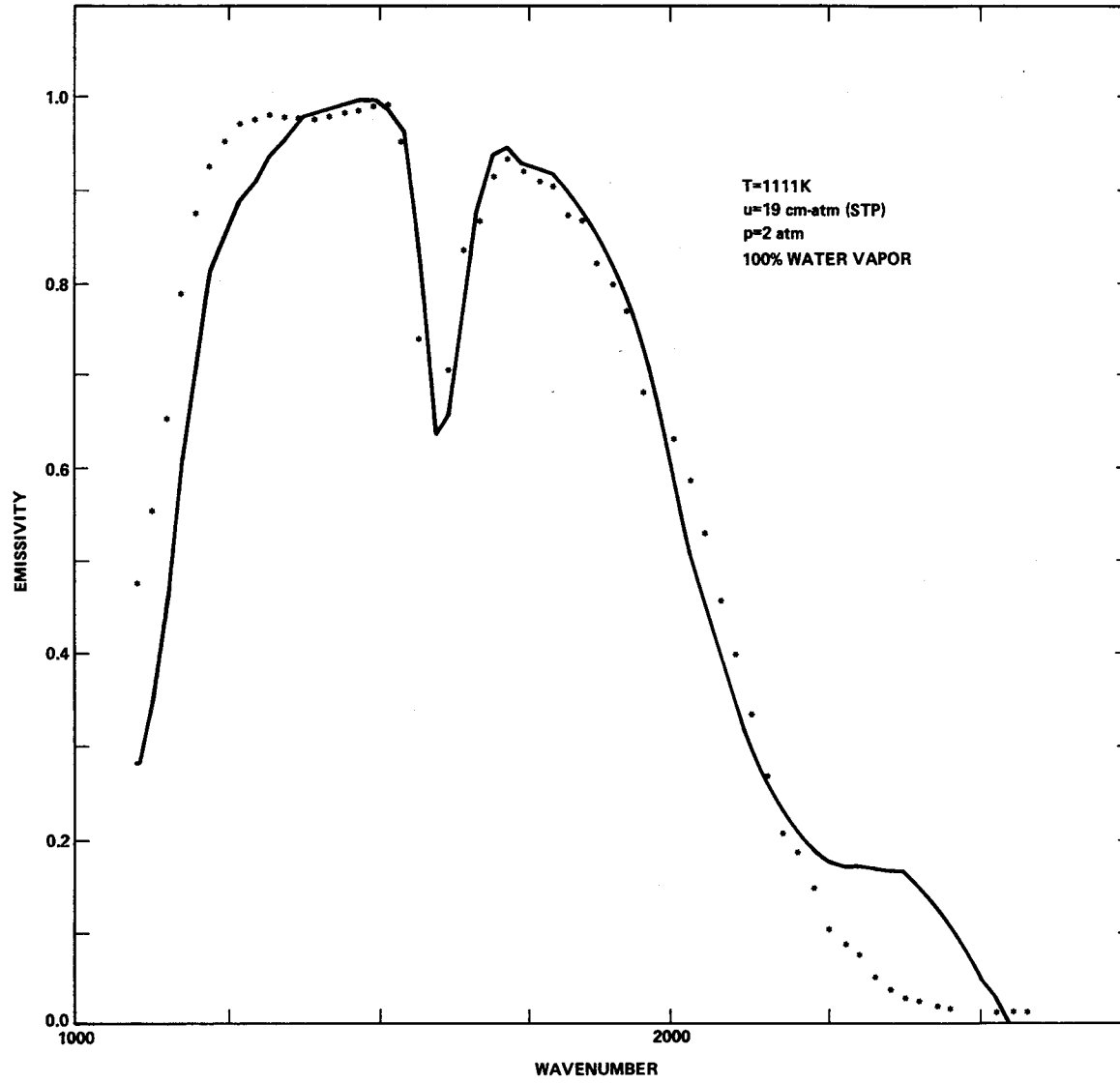


Figure 7-37. Comparison of calculated (\*) and experimental spectra at  $6.3 \mu$  (Nelson [7-5]).

7.4.2 INHOMOGENEOUS GAS

Radiance measurements of controlled inhomogeneous gas samples have been carried out by Ludwig et al. and by Simmons. The experimental results of Ludwig et al. [7-45] are compared to model calculations in Figures 7-38 through 7-40 for the conditions shown in Table 7-1.

TABLE 7-1. PROPERTIES OF INHOMOGENEOUS  
GAS SAMPLES

Section	Temp (K) Conc (H <sub>2</sub> O)	Fig. 7-38	Fig. 7-39	Fig. 7-40
A	T	2480	1210	1210
	c	0.37	0.14	0.14
B	T	1220	1520	1210
	c	0.14	0.18	0.14
C	T	1180	2000	1180
	c	0.13	0.26	0.13
D	T	2480	2480	2480
	c	0.37	0.37	0.37

The theoretical data were calculated using the Curtis-Godson approximation with the MLG and SLG band models described in section 5.3. The agreement of the theoretical and experimental values is within the uncertainty of the temperature measurement. The comparisons are made at 1 atm and the difference between the theoretical values determined by the two models is at most 12 percent. In addition to the calculations at 1 atm, calculations were performed at 0.1 atm, where no experimental data exist. In that case, the largest difference of the theoretical values amounted to 50 percent between the two models, the SLG model always being higher.

The experimental results of Simmons [7-4] are compared with model calculations in Figure 7-41. The experimental conditions were as follows: The sample cell (total length was 60 cm) was filled with pure water vapor at a total pressure of 670 mm Hg. The temperature profile was 382, 537, 723, 953, 1128, 1160, 990, 751, 558, and 389K for each section with a nominal

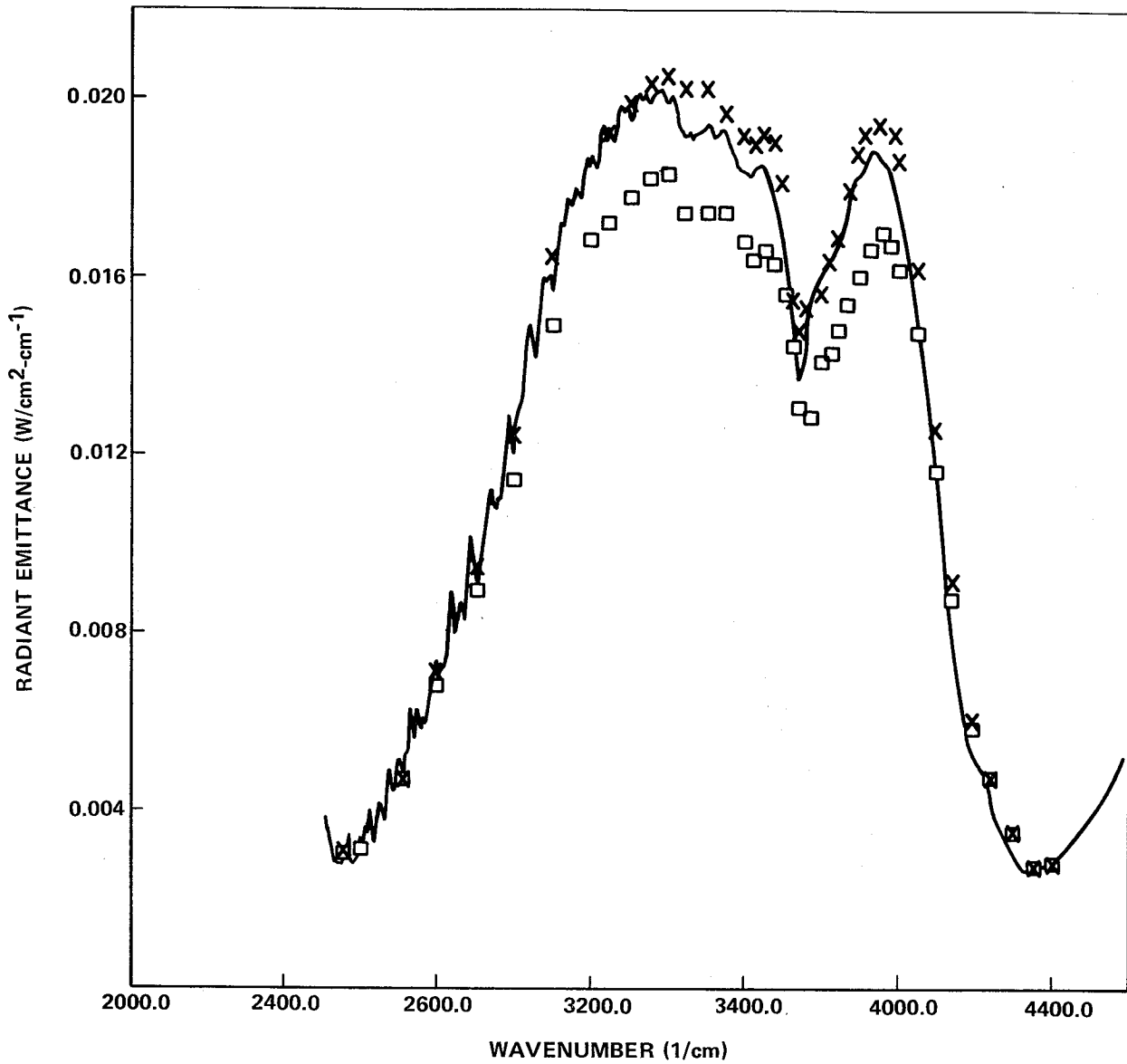


Figure 7-38. Radiance from four slabs ( $l = 150$  cm each). (Solid line is the experimental curve. Calculated values from MLG model are given by ( $\square$ ), from SLG model are given by (X). Conditions for T and c are given in Table 7-1.)

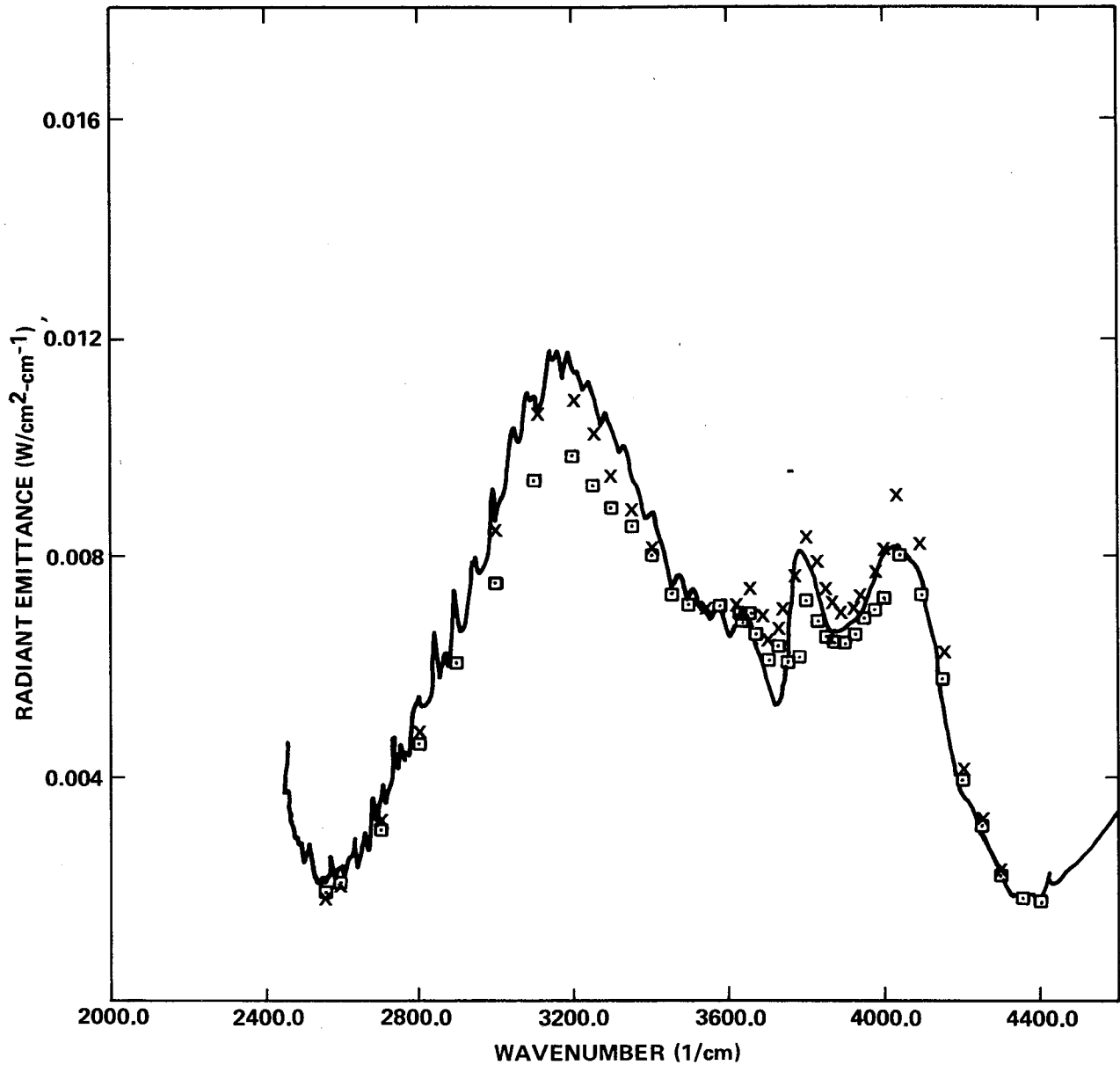


Figure 7-39. Radiance from four slabs ( $l = 150$  cm each).  
 (Solid line is the experimental curve. Calculated  
 values from the MLG model are given by (□),  
 from the SLG model are given by (X).  
 Conditions for  $T$  and  $c$  are given  
 in Table 7-1.)

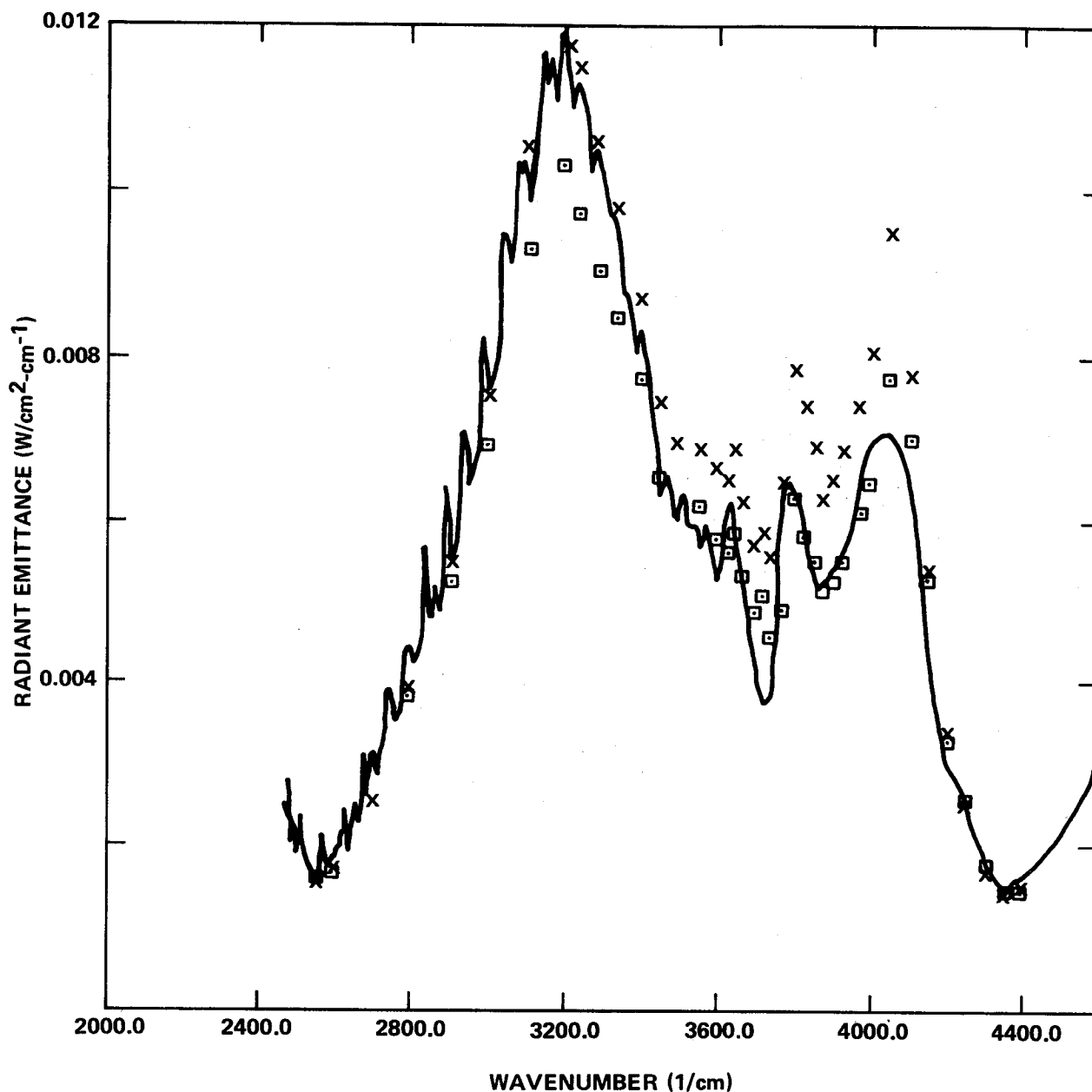


Figure 7-40. Radiance from four slabs ( $l = 150$  cm each).  
(Solid line is the experimental curve. Calculated  
values from the MLG model are given by (□),  
from the SLG model are given by (X).  
Conditions for T and c are given  
in Table 7-1.)

length of 6 cm. The comparison with the theoretical predictions were made by Simmons et al. in a similar fashion as outlined in Chapter 5, using the band model parameters listed in the General Appendix.

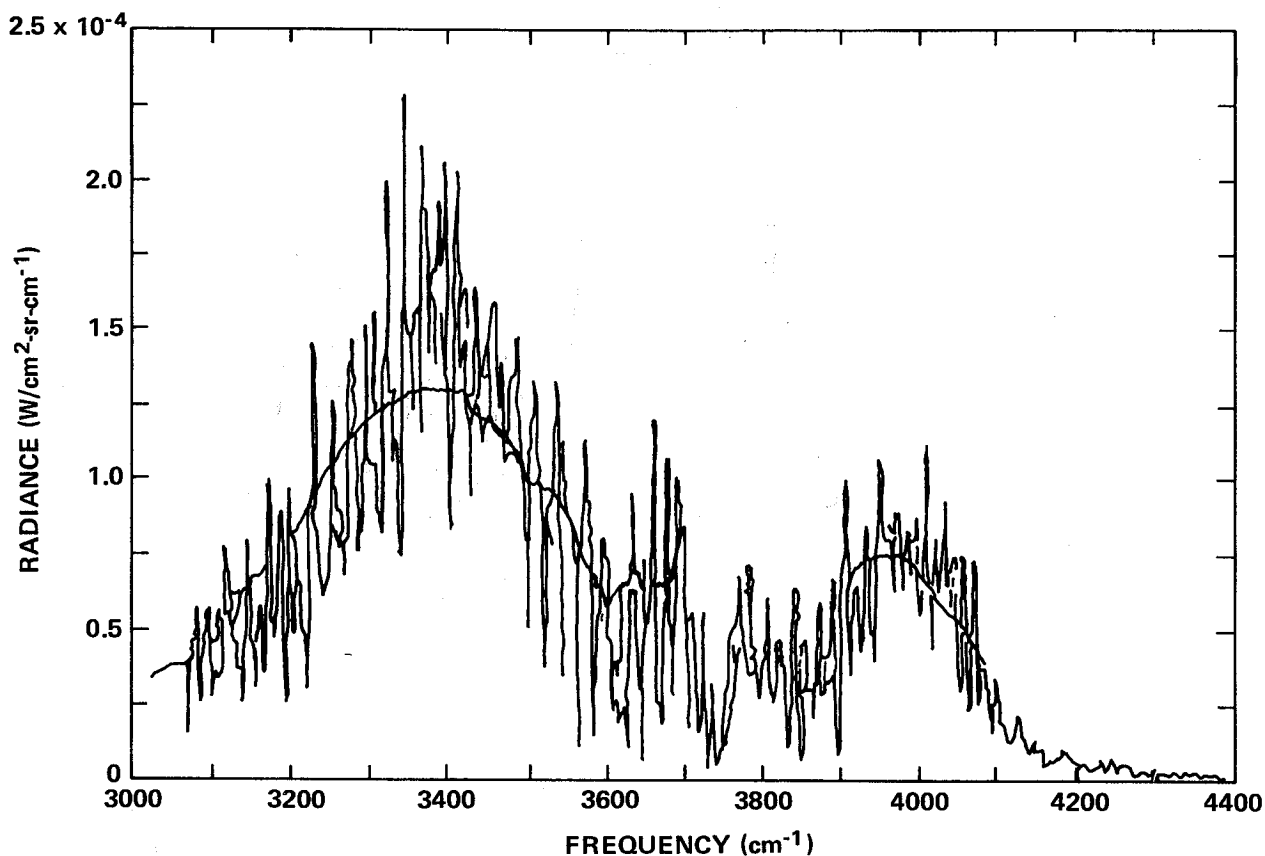


Figure 7-41. Comparison of nonisothermal H<sub>2</sub>O spectra with band-model calculations.

#### 7.4.3 BAND ABSORPTION

Over the years many measurements of the band emissivities up to 1200K were made by different workers. Edwards et al. [7-46] have summarized these measurements and presented correlations in terms of wideband adaptation of the Mayer-Goody statistical band model using a mean line width to line spacing ratio and spectral band contours calculated in the just-overlapping line model by Gray [7-47]. They then compared the measured band absorptances with their calculated values and gave the RMS value of the deviations for each individual band. A similar comparison was made by Ludwig and Ferriso [7-48], using band model parameters as given in Reference 7-49. A comparison of the RMS deviation of the different bands is given in Table 7-2.

TABLE 7-2. RMS DEVIATIONS OF MEASURED BAND  
ABSORPTANCES FROM BAND MODEL PREDICTIONS  
FOR FOUR WATER VAPOR BAND SYSTEMS

	6.3 $\mu$	2.7 $\mu$	1.87 $\mu$	1.38 $\mu$
Edwards	$\pm 11\%$	$\pm 13\%$	$\pm 23\%$	$\pm 34\%$
Ludwig	$\pm 15\%$	$\pm 16\%$	$\pm 21\%$	$\pm 21\%$

## 7.5

MIXTURE OF CARBON DIOXIDE AND WATER VAPOR

Isothermal mixtures of  $\text{CO}_2$  and  $\text{H}_2\text{O}$  gases at elevated temperatures were measured by Ferriso et al. [7-50]. However, since both gases were optically thin, the spectral emissivities added directly.

Simmons et al. [7-4] measured the radiance of a mixture of 28 torr  $\text{CO}_2$  + 54 torr  $\text{H}_2\text{O}$  + 675 torr  $\text{N}_2$  in a sample cell of 60 cm length, using the temperature profile 378, 537, 723, 958, 1127, 1158, 990, 752, 555, and 383K for each section of 6 cm nominal length, and compared the results with theoretical predictions (see Figure 7-42).

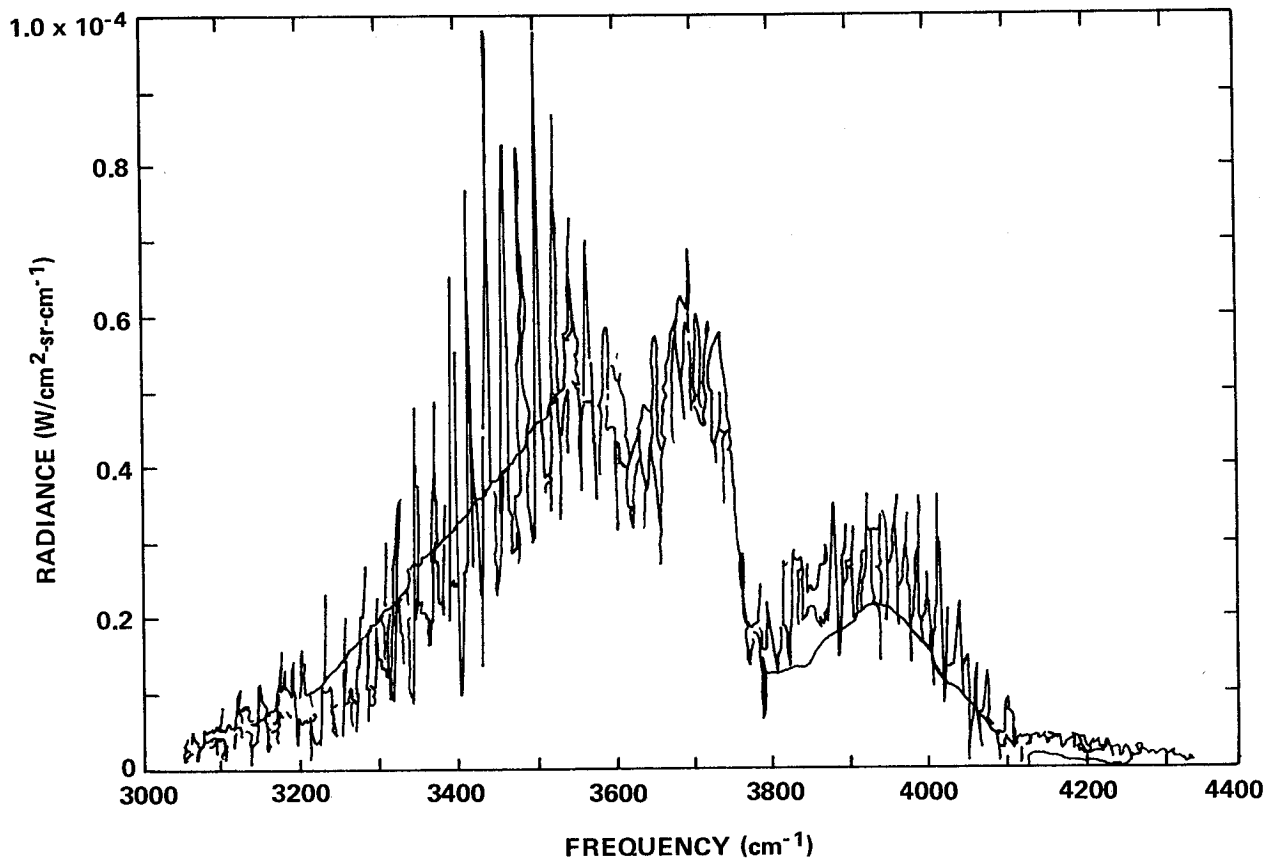


Figure 7-42. Comparison of nonisothermal  $\text{H}_2\text{O}/\text{CO}_2/\text{N}_2$  spectra with band-model calculations.

REFERENCES

- 7-1. Goldman, A. and Oppenheim, U. P.: JOSA, no. 55, 1965, p. 794.
- 7-2. Herget, W. F.; Muirhead, J. S.; and Golden, S. A.: Band Model Parameters for H<sub>2</sub>O. R-6916, Rocketdyne, Jan. 27, 1967.
- 7-3. Burch et al.: JOSA, no. 57, 1967, p. 885.
- 7-4. Simmons, F. S.; Yamada, H. Y.; and Arnold, C. B.: NASA CR-72491, April 1969.
- 7-5. Nelson, K. E.: Experimental Determination of the Band Absorptivities of Water Vapor at Elevated Pressures and Temperatures. M. S. Thesis, University of California, 1959.
- 7-6. Ludwig, C. B.: Applied Optics, no. 10, 1971, p. 1057.
- 7-7. Ferriso, C. C.: JCP, no. 37, 1962, p. 1955.
- 7-8. Foelsch, K.: J. Aeronaut. Sci., no. 16, 1949, p. 161.
- 7-9. DeBell, A. G.; Simmons, F. S.; and Levine, B. P.: Spectral Radiance and Emissivities of Rocket Exhaust Plumes. R-3216, Rocketdyne, December 1961 (Secret).
- 7-10. Patch, R. W.: JQRST, no. 5, 1965, p. 137.
- 7-11. Breeze, J. C. and Ferriso, C. C.: JCP, no. 39, 1963, p. 2619.
- 7-12. Breeze, J. C. and Ferriso, C. C.: JCP, no. 40, 1964, p. 1276.
- 7-13. Penner, S. S.: Quantitative Molecular Spectroscopy and Gas Emissivities. Addison-Wesley, 1959.
- 7-14. Hornbeck, G. A.: Appl. Optics, no. 5, 1966, p. 179.
- 7-15. Tourin, R. H.: Temperature, Its Measurement and Control in Science and Industry. Vol. III, Reinhold, New York, 1962, p. 455.
- 7-16. Gaydon, A. G. and Wolfhard, W. G.: Flames, Their Structure, Radiation, and Temperature. Chapman & Hall, London, 1953.

REFERENCES (Continued)

- 7-17. Uyehara, O. A.; Myers, P. S.; Watson, K. M.; and Wilson, L. A.: Trans. ASME 68, 1946, p. 17.
- 7-18. Gaydon, A. G. and Wolfhard, H. G.: Proc. Roy. Soc. London, B199, 1949, p. 89.
- 7-19. Broida, H. P.: Temperature, Its Measurement and Control in Science and Industry. Vol. II, Reinhold, New York, 1955, p. 265.
- 7-20. Ferriso, C. C.; Ludwig, C. B.; and Boynton, F. P.: International Symposium on Combustion. Combustion Institute, 1965, p. 161.
- 7-21. Herget, W.: Proceedings of the NASA-MSFC Conference on Molecular Radiation. ed. R. Goulard, NASA TMX-53711, 1968, p. 359.
- 7-22. King, J. I. F.: J. Atmos. Sciences, no. 21, 1964, p. 324.
- 7-23. Kaplan, L. D.: JOSA, no. 49, 1959, p. 1004.
- 7-24. Twomey, S.: Monthly Weather Review, no. 94, 1966, p. 363.
- 7-25. Wark, D. Q. and Fleming, H. E.: Monthly Weather Review, no. 94, 1966, p. 351.
- 7-26. Wang, J. Y.: Theory and Applications of Inversion Techniques: A Review. Purdue University, AA&ES 70-6, September 1970.
- 7-27. Krakow, B.: Appl. Optics, no. 5, 1966, p. 201.
- 7-28. Oppenheim, U. P.; Goldman, A.; and Aviv, Y.: JOSA, no. 59, 1969, p. 734.
- 7-29. Malkmus, W. and Thomson, A.: JQRST, no. 2, 1961, p. 17.
- 7-30. Babrov, H. J.: JOSA, no. 53, 1963, p. 945.
- 7-31. Stull, V. R. and Plass, G. N.: JOSA, no. 50, 1960, p. 1279.
- 7-32. Malkmus, W.; Maclay, G. J.; and Barbrov, H. J.: JOSA, no. 54, 1964, p. 422.

REFERENCES (Continued)

- 7-33. Abu-Romia, M. M. and Tien, C. L.: JQSRT, no. 6, 1966, p. 143.
- 7-34. Burch, D. E. and Gryvnak, D. A.: Report No. V-1929, Ford Motor Company, Aeronutronic Division, Newport Beach, California, October 1962.
- 7-35. Tourin, R. H.: Infrared Physics, no. 1, 1961, p. 105.
- 7-36. Ferriso, C. C. and Ludwig, C. B.: JOSA, no. 54, 1964, p. 657.
- 7-37. Ferriso, C. C., et al.: JOSA, no. 56, 1966, p. 171.
- 7-38. Sulzmann, K. G. P.: JQSRT, no. 4, 1964, p. 375.
- 7-39. Gates, D. M.; Calfee, R. F.; Hansen, D. W.; and Benedict, W. S.: NBS Monograph 71, 1964.
- 7-40. Benedict, W. S. and Calfee, R. F.: ESSA Professional Paper 2, June 1967.
- 7-41. Oppenheim, U. P. and Goldman, A.: JOSA, no. 55, 1965, p. 794.
- 7-42. Goldstein, R.: JQSRT, no. 3, 1963, p. 91, and JQSRT, no. 4, 1964, p. 343.
- 7-43. Tourin, R. H. and Henry, P. M.: Infrared Spectral Emissivities and Internal Energy Distributions of Carbon Dioxide and Water Vapor at High Temperatures. AFCRC-TR-60-203, The Warner and Swasey Co., 1959.
- 7-44. Simmons, F. S.; Arnold, C. B.; and Smith, D. H.: Studies of Infrared Radiative Transfer in Hot Gases, 1. Spectral Absorptance Measurements in the 2.7- $\mu$  H<sub>2</sub>O Bands. BAMIRAC Report 4613-91-T, Infrared Physics Laboratory, 1965.
- 7-45. Ludwig, C. B., et al.: Study on Exhaust Plume Radiation Predictions. NASA CR 61233, July 1968.

REFERENCES (Concluded)

- 7-46. Edwards, D. K.; Flornes, B. J.; Glassen, L. K.; and Sun, W.: Appl. Opt., no. 4, 1965, p. 715.
- 7-47. Gray, L. D.: Ph.D. Thesis, California Institute of Technology, Pasadena, California, 1963.
- 7-48. Ludwig, C. B. and Ferriso, C. C.: JQSRT, no. 7, 1966, p. 7.
- 7-49. Ferriso, C. C.; Ludwig, C. B.; and Thomson, A. L.: JQSRT, no. 6, 1966, p. 241.
- 7-50. Ferriso, C. C. and Ludwig, C. B.: Appl. Optics, no. 3, 1964, p. 1435.



## CHAPTER 8

## PREDICTIVE TECHNIQUES

The transfer equation defined in Chapter 2 [equation (2-22)] is integrated over the spectral range  $\omega_i$  to  $\omega_f$  and the solid angle which includes the gas to give the radiant flux per unit area to a surface at  $l = 0$ .

$$\dot{q}/A = - \int_{\theta_i}^{\theta_f} \int_{\phi_i}^{\phi_f} \int_{\omega_i}^{\omega_f} \int_0^L N_{\omega}^0 \frac{\partial \tau}{\partial l} dl d\omega d\phi \cos\theta \sin\theta d\theta \quad . \quad (8-1)$$

The spherical coordinate system used is shown in Figure 8-1.

Since for the general case, equation (8-1) cannot be evaluated analytically, a finite difference approximation must be introduced. For the present discussion, consider the form

$$\dot{q}/A = - \sum_{\theta_i}^{\theta_f} \sum_{\phi_i}^{\phi_f} \sum_{\omega_i}^{\omega_f} \sum_0^L N_{\omega}^0 [\bar{\tau}(l, \omega) - \bar{\tau}(l - \Delta l, \omega)] \cos\theta \sin\theta \Delta\theta \Delta\phi \Delta\omega \quad , \quad (8-2)$$

where  $N_{\omega}^0$  is a mean value over the interval  $l - \Delta l$  to  $l$  and  $\tau(l, \omega)$  is the average transmission over the (small) spectral interval  $\Delta\omega$  :

$$\tau(l, \omega) = \exp [-X(l, \omega)] \quad , \quad (8-3)$$

where the optical depth is summed over  $i$  radiating species

$$X(l, \omega) = \sum_i X(l, \omega, i) \quad .$$

The optical depth for gaseous species will vary depending upon the particular representation chosen. The two methods to be described here are the SLG and the MLG models which were presented in section 5.3. The more

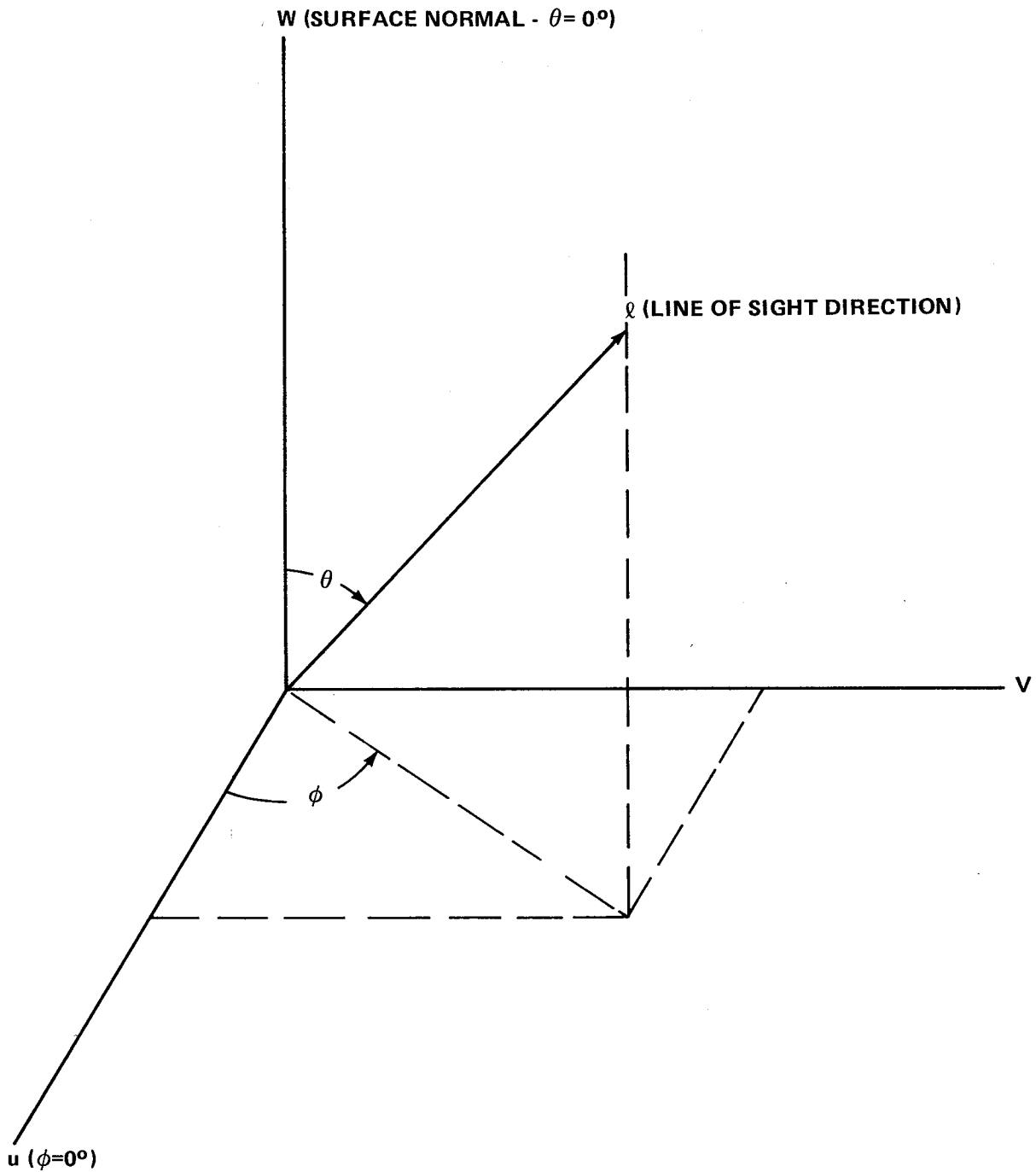


Figure 8-1. Coordinate system used in integrating radiation heat transfer.

detailed method (MLG) uses a number of line groups for each species to account for 'hot lines' from high temperature regions which are not significantly attenuated when passing through lower temperature regions. The

simpler SLG model is derived from the MLG model by grouping all the lines for each species. Although the MLG model is shown analytically as an infinite sum of line groups, only four or five groups need be considered in most applications.

Experimental evidence for the validity and accuracy of these models was presented in Chapter 7, and theoretical analysis of the regions of validity were evaluated in Chapter 4. This chapter will review integration interval considerations, comparisons between the SLG and MLG models, comparison with experiments, and behavior of rocket plume radiation with changes in scale.

## 8.1 INTEGRATION INTERVAL CONSIDERATIONS

A computer program [ 8-1] has been prepared using both SLG and MLG models for the prediction of radiation from rocket exhaust plumes. This program has been used to evaluate the effect on accuracy and computation time of increasing either spatial or spectral integration intervals. Results of these analyses are presented to give guidelines for choosing the integration cell size, but the user must be aware that the errors involved depend on the particular characteristics of the flow field, and trial calculations for each new flow configuration considered are recommended.

If radiation heat transfer calculations are made using geometric integration intervals small enough to define the temperature and density variations with high accuracy, the computation time for many applications would be excessive. A study has been made of averaging methods which may be used to obtain larger spectral and spatial intervals ( $\Delta\omega$ ,  $\Delta\ell$ ,  $\Delta\phi$ ). Unfortunately, there is no quantitative guide that can be used in applying the larger integration intervals, so each problem must be evaluated based on past experience and the characteristics of the problem.

### 8.1.1 LINE OF SIGHT INTERVAL – $\Delta\ell$

This interval can be controlled by a temperature step,  $\Delta T$ , so that an integration step in equation (8-2) is taken only when a specified value of temperature difference has been reached. This allows a small value of  $\Delta\ell$  to be used in searching the gas properties to define accurately the regions of strong gradients, without wasting computation time in regions of relatively uniform temperature. When an integration step is computed, the simple arithmetic averages of the property values in each spatial interval ( $\Delta\ell$ ) can be used to define the mean property of the larger interval.

Experience with calculations of large rocket plumes indicates that less than one percent error is incurred by using temperature intervals of 50 to 100 K, compared to  $\Delta\ell$  intervals of 5 to 10 cm with no temperature limitations. The best procedure for a particular problem is to select a typical line of sight with severe property variations and to evaluate the precision obtained with various values at  $\Delta T$  and  $\Delta\ell$ .

### 8.1.2 SPECTRAL INTERVAL – $\Delta\omega$

Various methods of averaging the absorption coefficients over larger spectral intervals were examined in an attempt to find a method for using a

larger spectral integration interval,  $\Delta\omega$ . The experience which has been gained with averaging should be used only as a guide, and a typical line of sight for a particular problem should be tested before an averaging method is selected for integration.

In general, the carbon oxides, because of their narrow spectral range, are most sensitive to increasing spectral intervals. Water vapor radiation can usually be integrated with wavenumber intervals up to  $100\text{ cm}^{-1}$  using a simple arithmetic average of  $k$  and  $1/d$ . In the case of carbon particles, large spectral intervals may be used since the absorption coefficient varies slowly with wavenumber and it can be approximated as a grey body over large intervals. In one example of a low altitude exhaust plume with a moderate carbon concentration (1 percent mass fraction) and high temperatures near the outer boundary due to afterburning, integration with a spectral interval of  $8000\text{ cm}^{-1}$  (using an integrated arithmetic average of  $k$ ) was only 2.23 percent greater than the result using a  $25\text{ cm}^{-1}$  integration interval.

To obtain a more representative value for  $1/d$  to use with larger spectral intervals, it was assumed that the case to be considered was in the square-root limit, so the desired result was the proper value for  $\sqrt{k(1/d)}$ . The equations for this averaging method were applied to data for the SLG model. For the spectral interval  $\omega_1$  and  $\omega_2$  this gives

$$\bar{k} = \left( \frac{\sum_{\omega_2}^{\omega_1} \sqrt{k_{\omega}} N_{\omega}^0 \Delta\omega}{\sum_{\omega_2}^{\omega_1} N_{\omega}^0 \Delta\omega} \right)^2 \tag{8.4a}$$

and

$$1/\bar{d} = \left[ \frac{\sum_{\omega_2}^{\omega_1} \sqrt{k_{\omega} (1/d)_{\omega}} N_{\omega}^0 \Delta\omega}{\sum_{\omega_2}^{\omega_1} \sqrt{k_{\omega}} N_{\omega}^0 \Delta\omega} \right]^2 \tag{8.4b}$$

Results of this averaging method are compared with the normal  $25\text{ cm}^{-1}$  spectral interval in Table 8-1. In all cases except the hydrocarbon plume without carbon particles, results with intervals of  $400$  to  $800\text{ cm}^{-1}$  were accurate enough to be used for many applications.

Even though the estimated error may be larger than desired for a final result, the use of large spectral intervals can be extremely helpful in making parametric studies, such as determining which location receives peak heating or what incremental solid angle is best to use.

TABLE 8-1. RESULTS OF EXPERIMENTS WITH LARGE SPECTRAL INTEGRATION INTERVALS

Line of Sight (Engine type or stage)	Gas		$\Delta\omega$ $\text{cm}^{-1}$	Predicted Radiance watts/ $\text{cm}^2\text{-sr}$	Percent Change from $\Delta\omega = 25 \text{ cm}^{-1}$
	Constituent	Mole Fract.			
Rocketdyne H-1 (No carbon)	H <sub>2</sub> O	0.359	25	4.978	0.6 16 20 12 5
	CO <sub>2</sub>	0.167	100	5.008	
	CO	0.335	400	5.760	
	H <sub>2</sub>	0.139	800	5.970	
			1600	5.926	
			8000	5.232	
(With 1 per- cent mass fraction of carbon)	H <sub>2</sub> O	0.359	25	18.612	0.1 1 2 3 3
	CO <sub>2</sub>	0.167	100	18.599	
	CO	0.335	400	18.837	
	Carbon	0.020	800	19.013	
	H <sub>2</sub>	0.119	1600	19.227	
			8000	19.172	
Saturn S-II Stage	H <sub>2</sub> O	0.693	25	1.407	0.3 3 7 6 49
	H <sub>2</sub>	0.307	100	1.411	
			400	1.449	
			800	1.512	
			1600	1.495	
			8000	2.096	
Rocketdyne J-2	H <sub>2</sub> O	0.693	25	0.1511	0.1 2 4 7 13
	H <sub>2</sub>	0.307	100	0.1513	
			400	0.1536	
			800	0.1569	
			1600	0.1622	
			8000	0.1701	

Note: All cases integrated from 1000 to 9000  $\text{cm}^{-1}$ .

a. Carbon is treated as a gas with a molecular weight of 12.

## 8.2 COMPARISON OF VARIOUS BAND MODELS IN ROCKET EXHAUST CALCULATIONS

When applying radiation prediction techniques, it is difficult to determine the degree of complexity that is required to produce results with satisfactory accuracy. In this section an effort is made to provide some basis for judgment by comparing results that were obtained with several prediction techniques on certain applied problems which are representative of radiation predictions for rocket exhaust plumes.

The four cases chosen for examples are four individual lines of sight through rocket exhaust plumes. Calculations were made to predict the radiation in each of the four examples using (1) the weak line limit (Beer's law), (2) the single line group band model (SLG), and (3) the multiple line group band model (MLG). Figure references for gas property data and spectral results on each case are listed in Table 8-2 along with the integrated results for radiance and absorption. The absorption for the various cases ranges from nearly opaque ( $\alpha = 0.97$ ) for Case 1 to very low absorption ( $\alpha = 0.05$ ) for Case 3. Results for the sample cases illustrate the usual results that (1) serious errors are caused by using Beer's law when gaseous radiation predominates over the continuum carbon particle radiation and (2) the simplified SLG calculation method predicts slightly higher radiation than the more complex MLG model.

Case 1 (Figs. 8-2 through 8-4) is representative of a hydrocarbon/oxygen plume at low altitude. Fuel-rich exhaust gases mix with the airstream and continue to burn in a hot "after-burning" layer around the jet. Property data in Figure 8-2 show the variation of temperature and constituent fractions in the annulus around a core of uniform properties. Spectral radiance results in Figure 8-3 show the continuum carbon particle radiation from the core of the plume with some absorption from the cooler gases surrounding the core. The most significant characteristic of the radiation in demonstrating the effects of the different calculation models is the radiance in the  $\text{CO}_2$  band at  $4.3 \mu$ . In this case the spectral radiance of the MLG model is higher than either of the other two. This is contrary to the general trend of results mentioned previously, but this is the type of behavior which is to be expected if a significant cool gas layer is present between the observer and the hotter gas. In spite of this effect, integrated radiance is so dominated by the carbon radiation that there is no difference noted within the precision of the calculation.

TABLE 8-2. CHARACTERISTICS AND RESULTS OF COMPARATIVE CALCULATIONS

Case	General Description	Property Data	Spectral Radiance	Spectral Absorption	Radiance watts/cm <sup>2</sup> -sr			Average Absorption $\int \alpha d\omega / \int d\omega$		
					Beer's law	SLG	MLG	Beer's law	SLG	MLG
1	Hydrocarbon/oxygen with afterburning — H-1 engine	Fig. 8-2	Fig. 8-3	Fig. 8-4	47.67	47.32	47.62	0.971	0.967	0.965
2	Hydrocarbon/oxygen with no afterburning — H-1 engine	Fig. 8-5	Fig. 8-6	Fig. 8-7	2.805	2.332	2.305	0.650	0.591	0.586
3	Hydrogen/oxygen — J-2 engine	Fig. 8-8	Fig. 8-9	Fig. 8-10	0.558	0.162	0.153	0.196	0.052	0.048
4	Hydrogen/oxygen with multiple plume impingement — J-2 engines on S-II stage	Fig. 8-11	Fig. 8-12	Fig. 8-13	2.010	1.342	1.129	0.304	0.131	0.116

- NOTES: (1) PRESSURE IS CONSTANT AT 0.88 ATM.  
 (2) CARBON "MOLE FRACTION" SHOWN CORRESPONDS TO A MASS FRACTION OF 1 PERCENT IN THE CENTER OF THE PLUME.

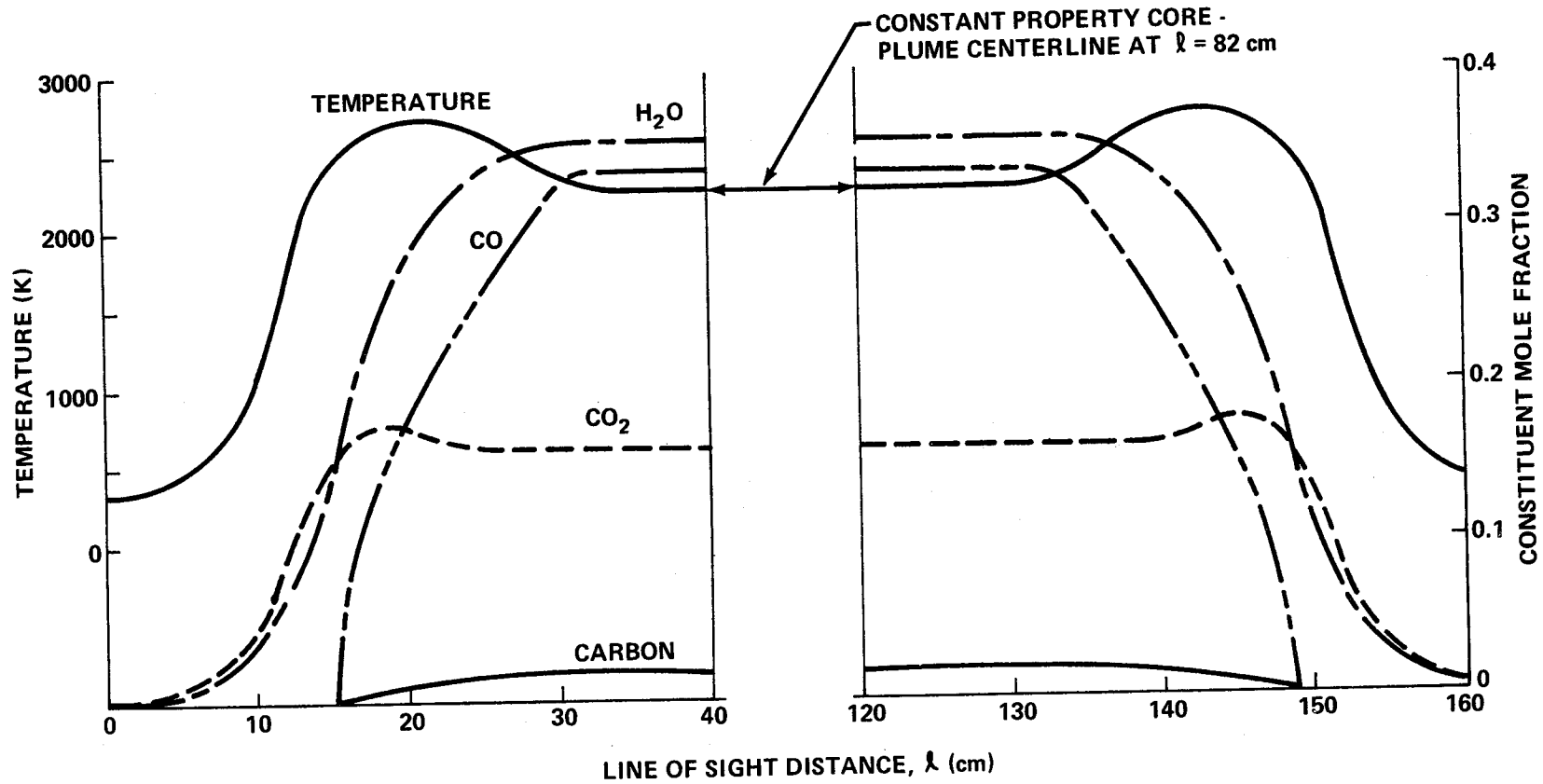


Figure 8-2. Property predictions for an afterburning plume from an H-1 engine. (Line of sight normal to plume centerline 1.27 meters from the engine exit plane.)

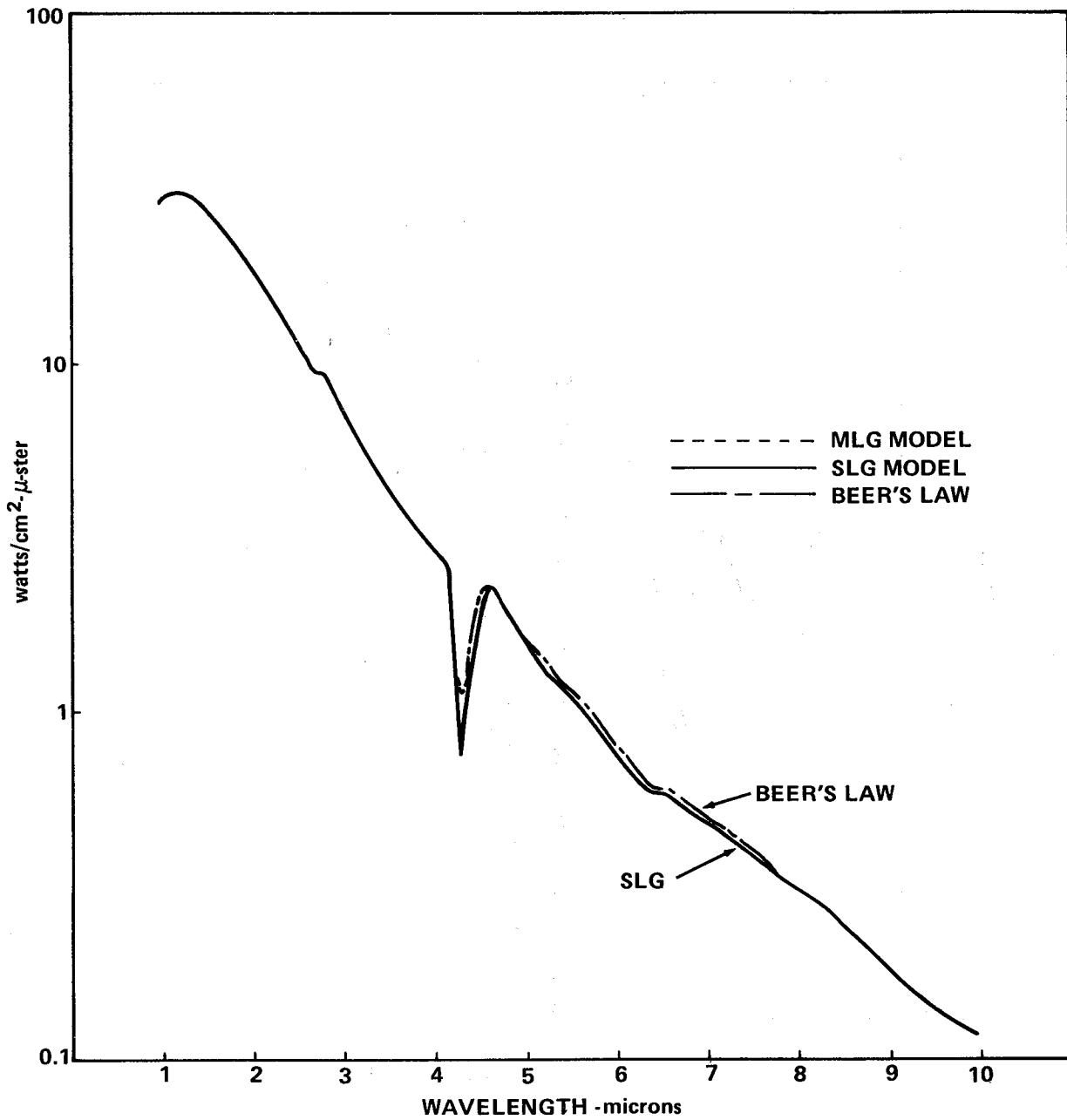


Figure 8-3. Spectral radiance comparisons for Case 1.

Case 2 (Figs. 8-5 through 8-7) is a hydrocarbon/oxygen exhaust plume at high altitude where the surrounding air is not dense enough to support further combustion. The property data in Figure 8-5 shows the plume boundaries expanded to very low temperature and pressure with the center of the plume still relatively hot. Spectral radiance results in

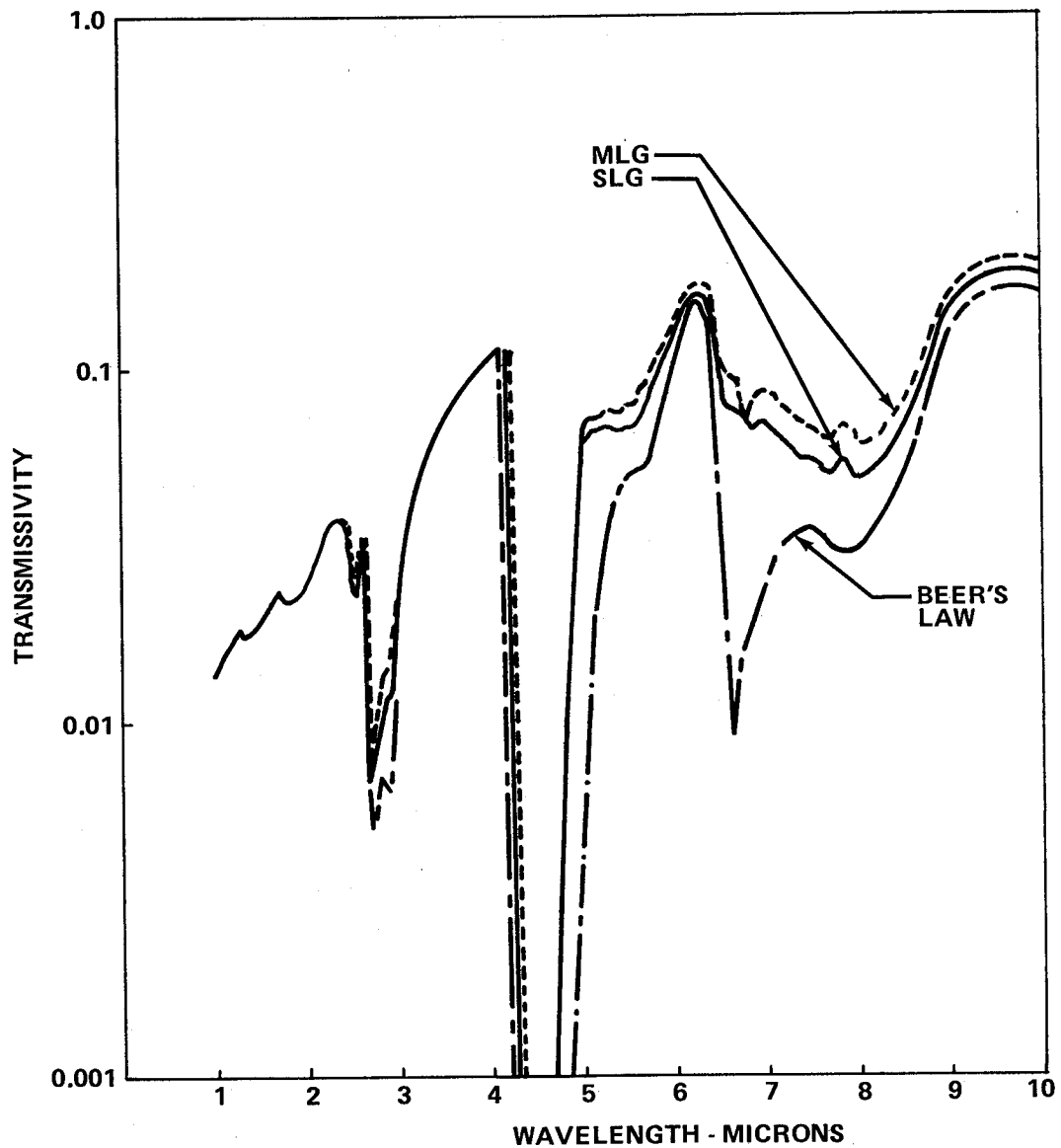


Figure 8-4. Comparative transmissivities for Case 1.

Figure 8-6 show significant gaseous radiation superimposed on the continuum carbon radiation. In this case the gaseous radiation is important enough to cause an over-prediction of approximately 20 percent using Beer's law, so use of the SLG model is advantageous in this case.

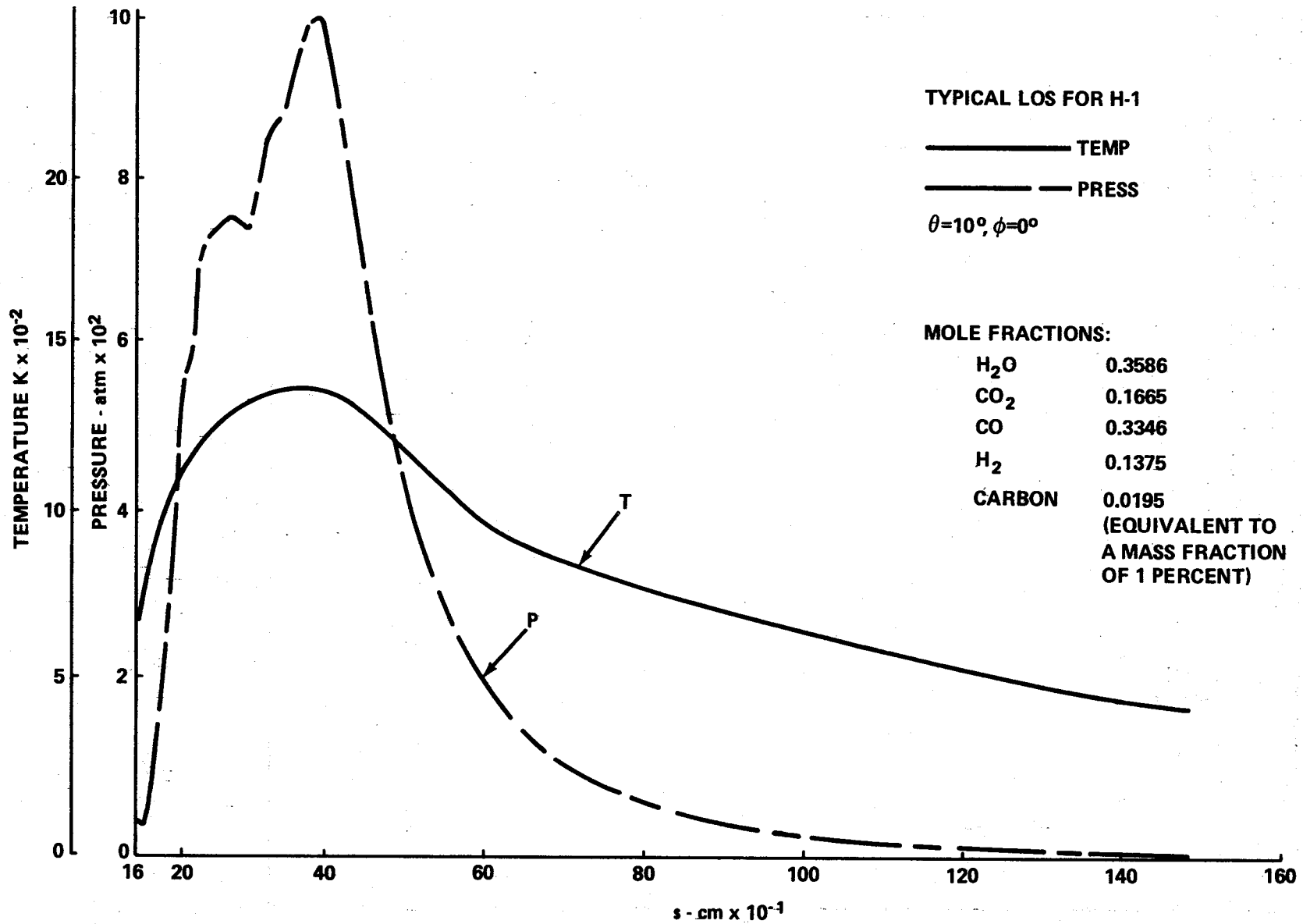


Figure 8-5. Property predictions for Case 2.

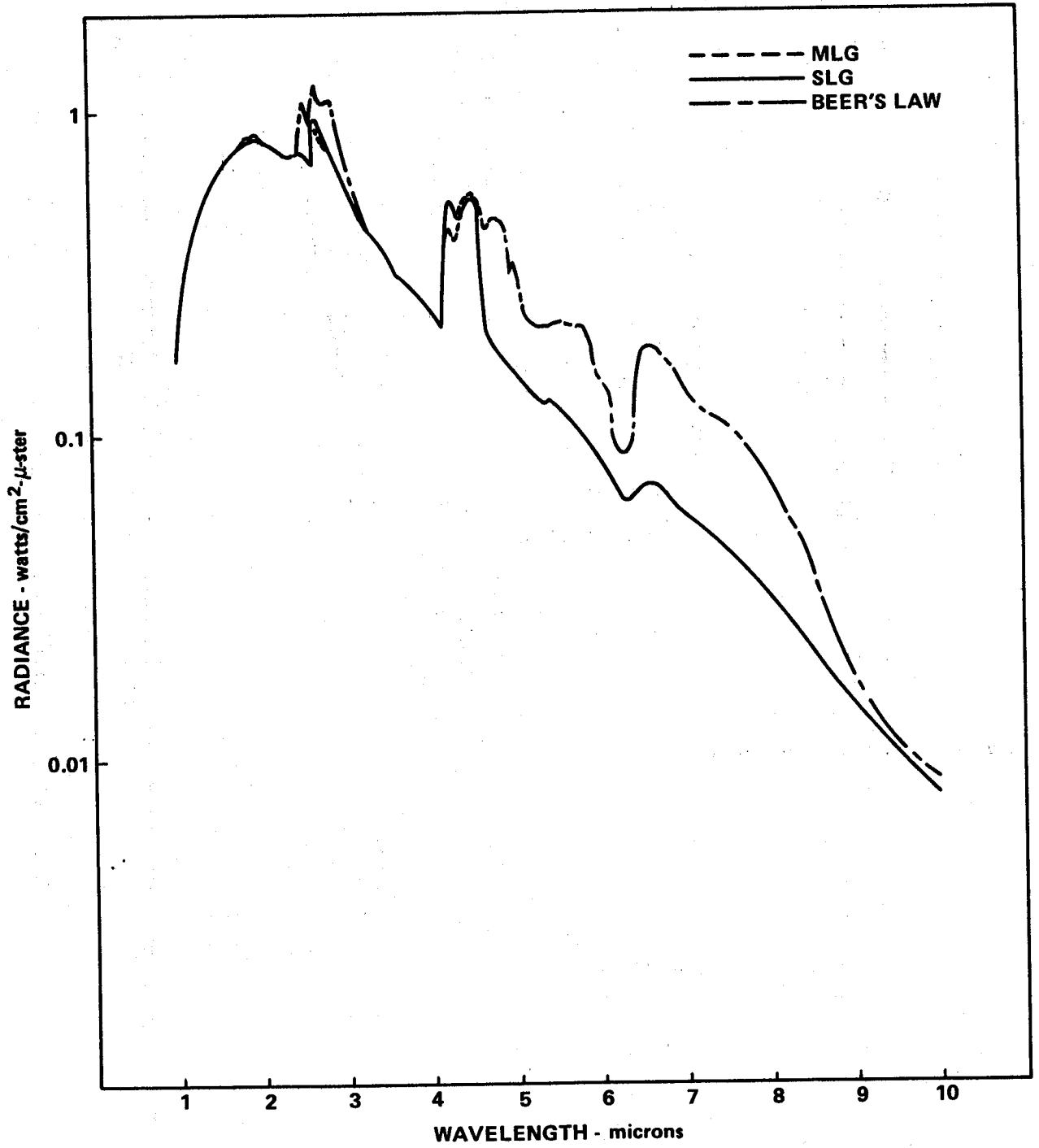


Figure 8-6. Comparative spectral radiance for Case 2.

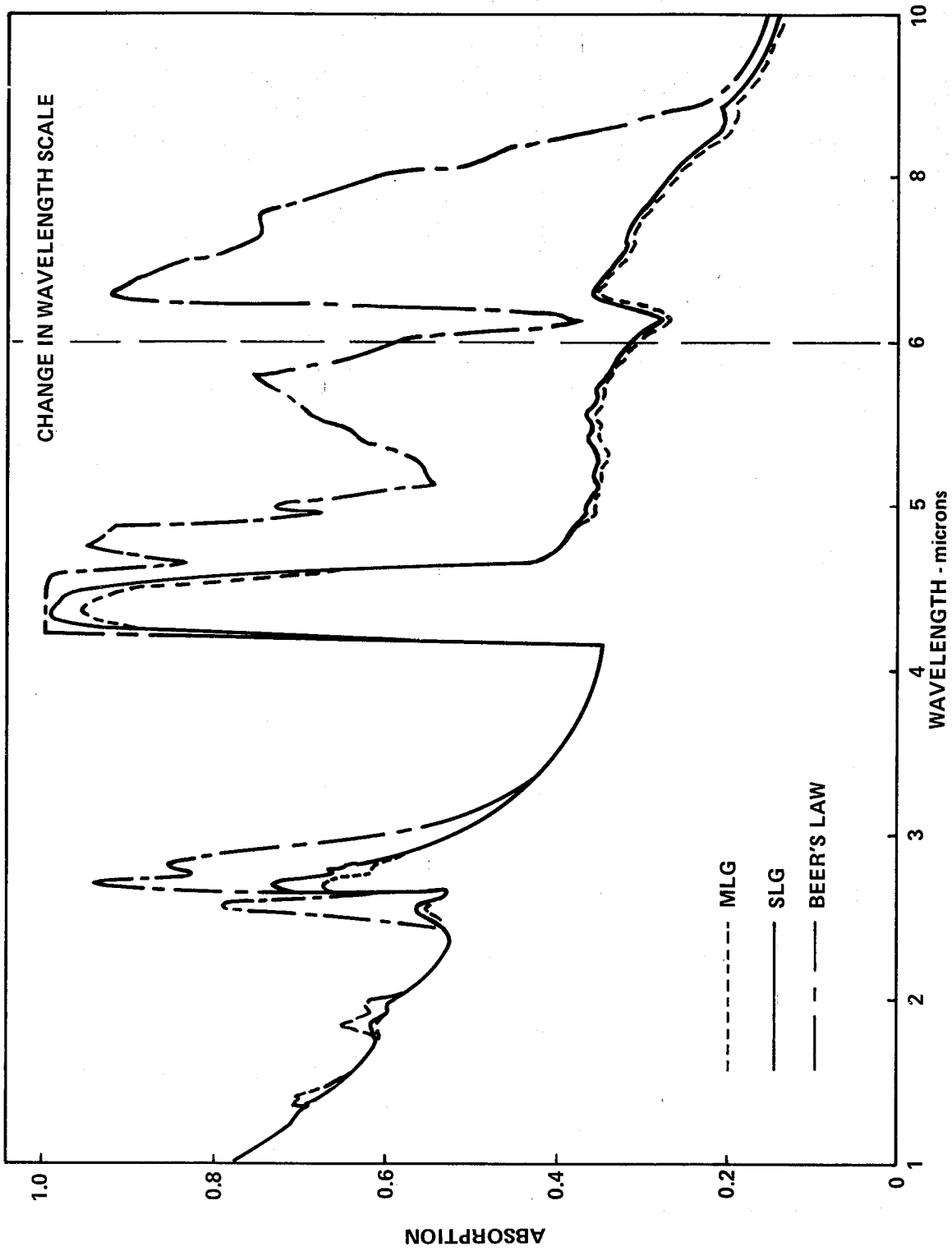


Figure 8-7. Comparative absorption for Case 2.

Case 3 (Figs. 8-8 through 8-10) is a high altitude hydrogen/oxygen exhaust plume. Property data in Figure 8-8 show the cool expanded gas surrounding a hotter core. The core has a significant variation in properties as a result of the nozzle shape which produces a nonuniform exit plane profile with higher velocities in the center. Spectral radiance results in Figure 8-4 show a typical water vapor spectrum. The feature of this spectrum which is often overlooked is the significant radiation at long wavelengths. This could be important in material selection, particularly in selecting windows for instruments designed to measure the integrated radiance.

Case 4 (Figs. 8-11 through 8-13) illustrates a line of sight through impingement regions between plumes of a multi-engine cluster. Property data in Figure 8-11 indicate the sharp rise in temperature at the center of the impingement region (about  $l = 375$  cm). The pressure does not rise in proportion because of the loss in stagnation pressure through the shocks surrounding the impingement region. It is in cases such as this with significant sharp variations in properties with high peak temperatures that the

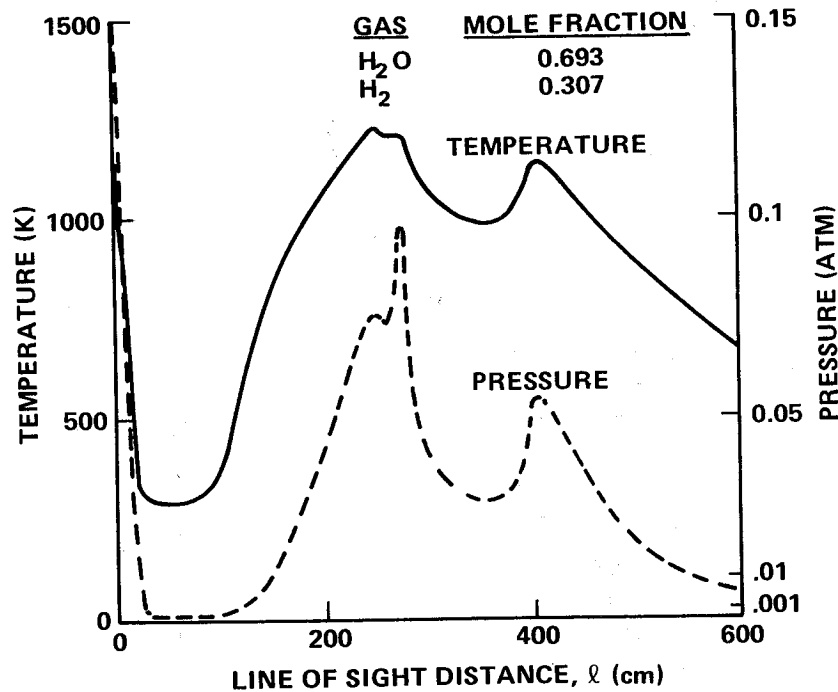


Figure 8-8. Predicted property variations for Case 3.

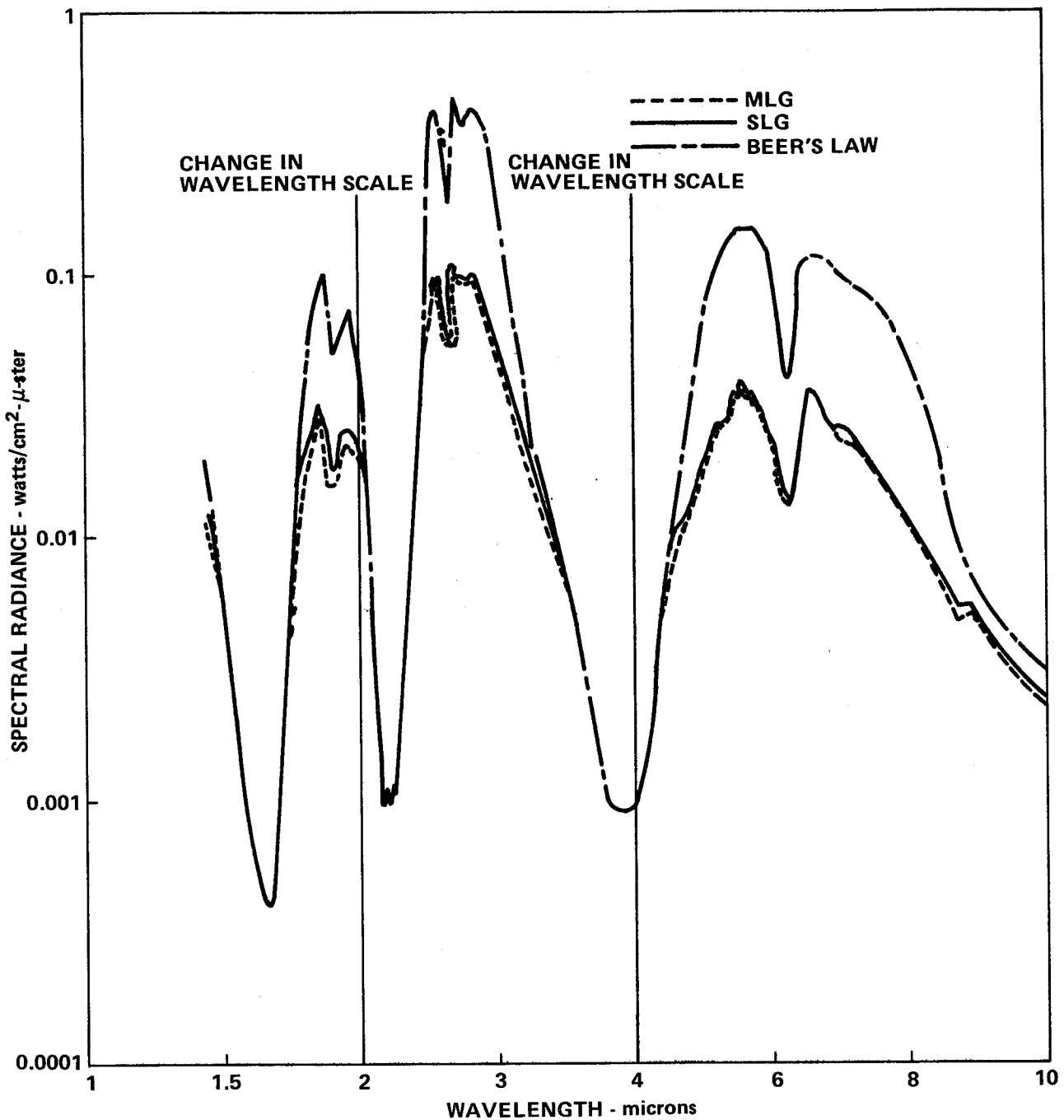


Figure 8-9. Comparative spectral radiance for Case 3.

differences in the calculation models are most apparent. At the point of peak radiation (which occurs at approximately  $1.85 \mu$  because of the high temperature) the level predicted by Beer's law is lower than the SLG and MLG models. The results are listed as follows:

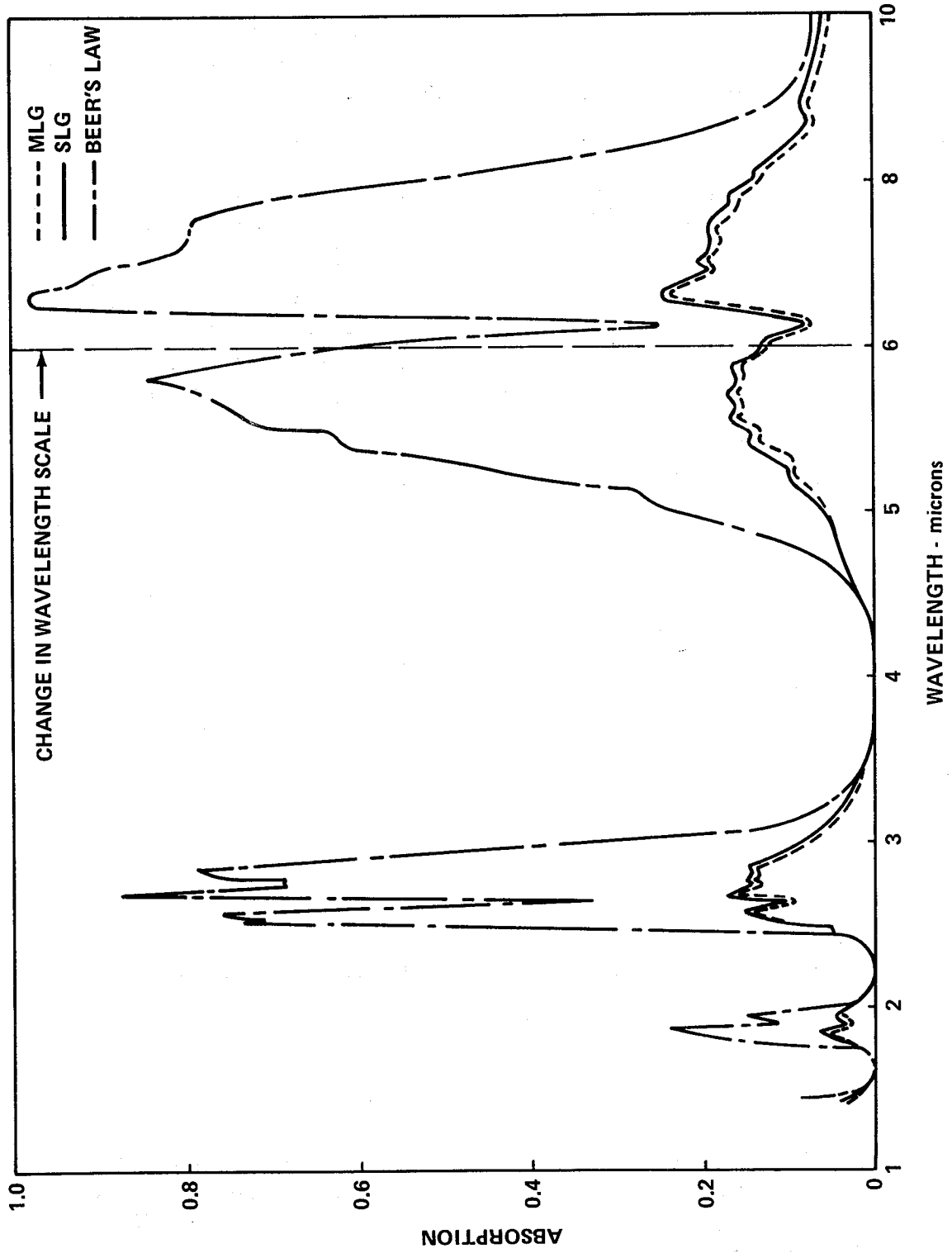


Figure 8-10. Comparative absorption for Case 3.

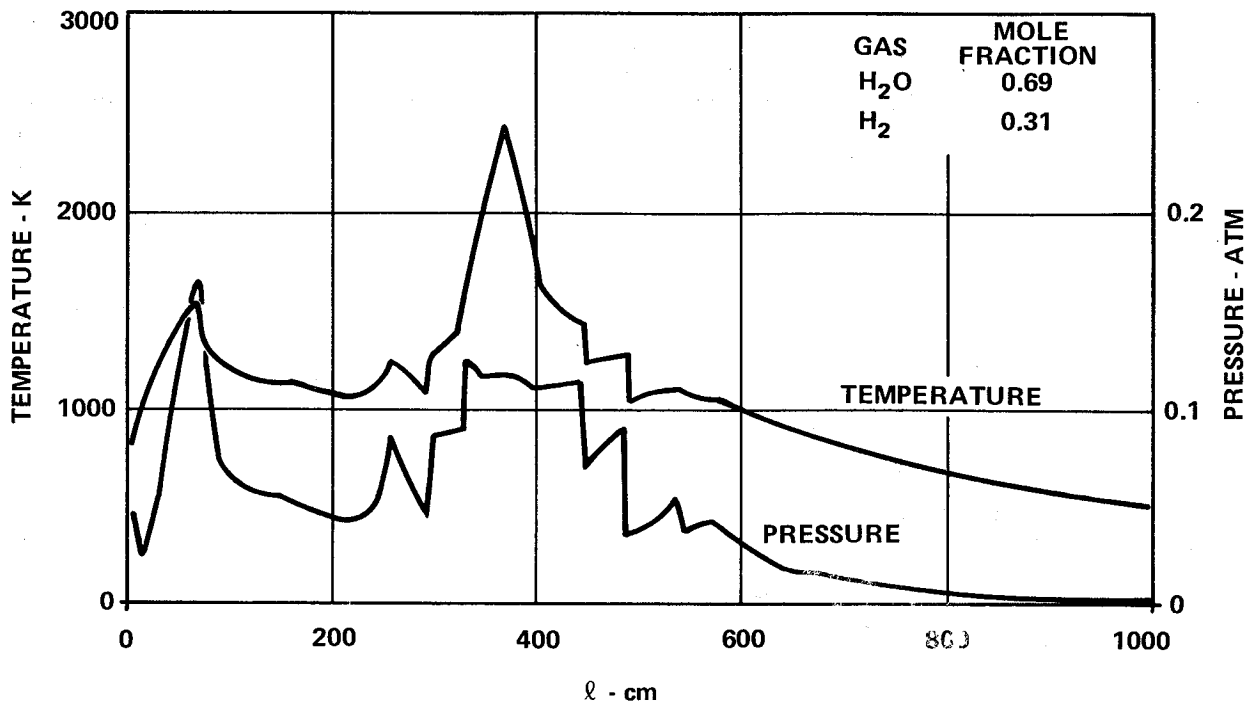


Figure 8-11. Property predictions for Case 4.

<u>Model</u>	<u>Spectral Radiance watts/cm<sup>2</sup>-μ-sr</u>
Beer's law	0.820
SLG	1.642
MLG	1.084

Here the higher absorption of Beer's law in the relatively cool gas reduces the radiance which can be transmitted from the high temperature spike. Although in this problem, this effect is limited to the very high absorbing regions, it illustrates the type of behavior which should be evaluated when a hot gas is viewed through a cooler one. At longer wavelengths the higher absorption in the cool gas does not produce a reversal in the expected radiance behavior because of the reduction in the relative increase in black-body radiance with increasing temperature.

In summary, the results of the comparative studies indicate that the SLG model is the most satisfactory, considering accuracy and calculation time. For some problems, such as Case 1, the contribution of gases to

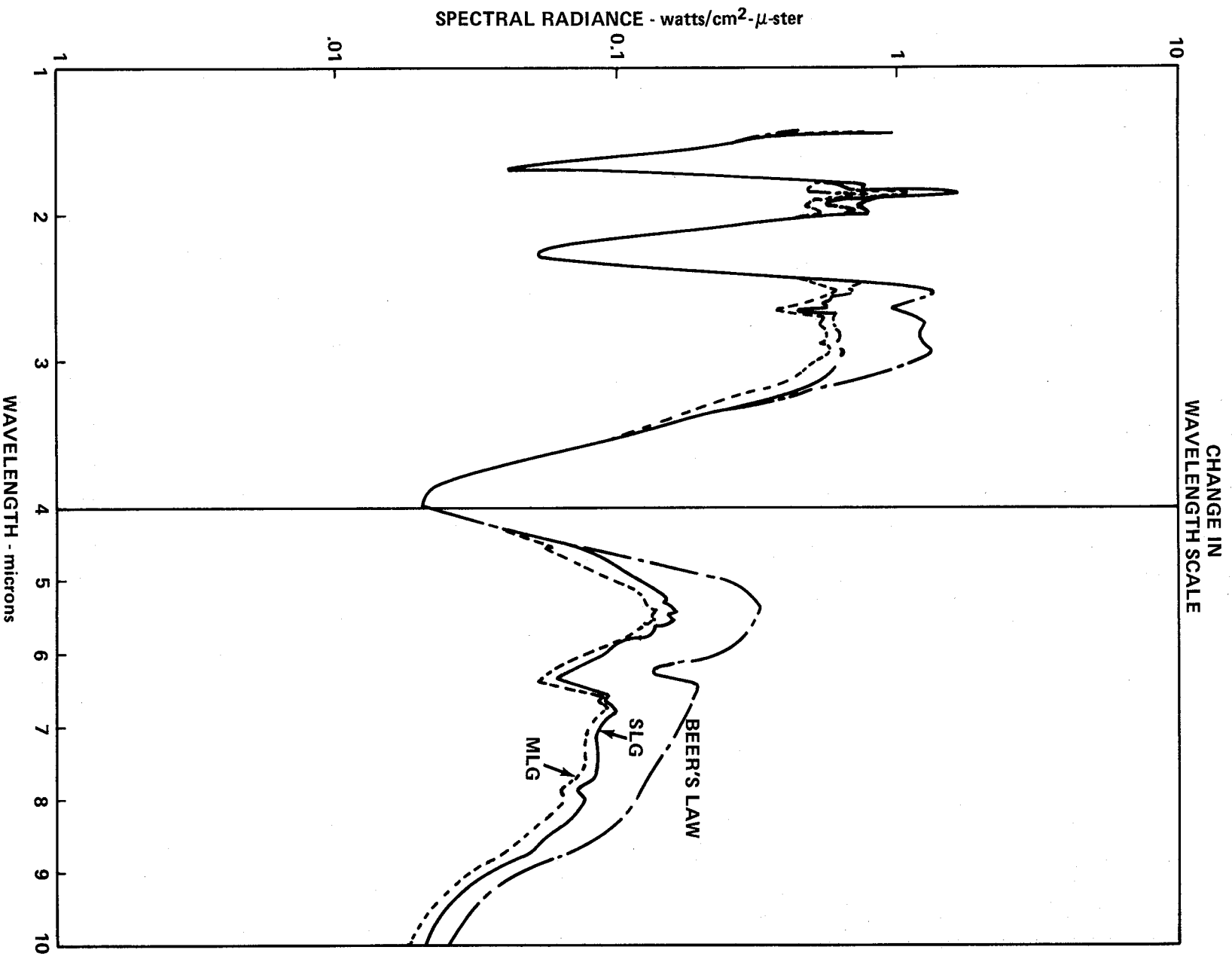


Figure 8-12. Comparative spectral radiance for Case 4.

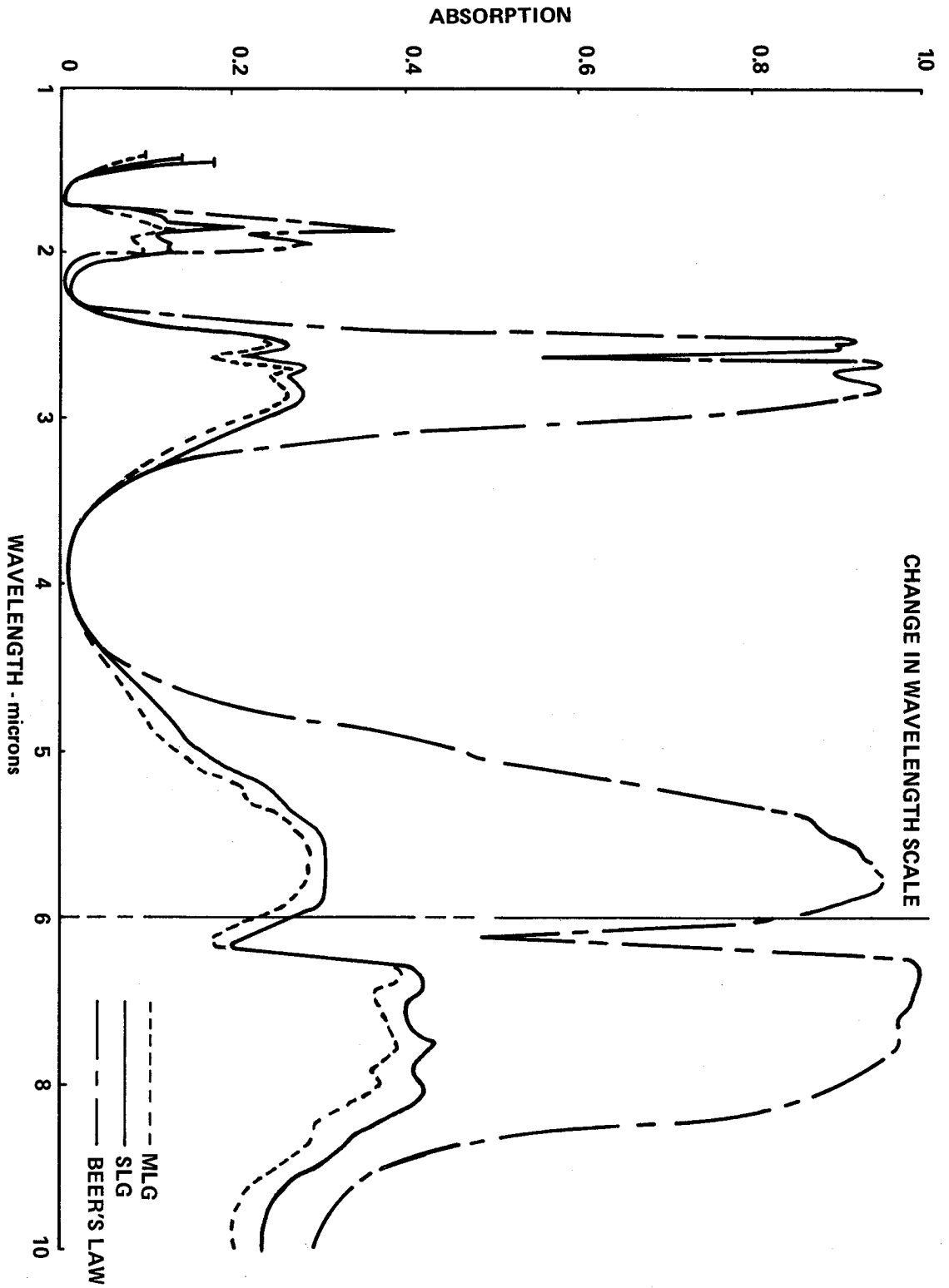


Figure 8-13. Comparative absorption for Case 4.

radiation can be neglected entirely compared to that of carbon particles. Also, in cases where a very hot gas is viewed through a cool gas, a careful evaluation of the validity of the results of any of the calculation models should be made.

### 8.3 COMPARISON OF PREDICTIONS WITH MEASUREMENTS FOR ROCKET EXHAUSTS

A radiation measurement program has been conducted to obtain verification of the analytical methods discussed in this handbook for the prediction of exhaust plume gas properties and radiation. Unfortunately, the uncertainties associated with radiation measurements (in particular spectrometer measurements) on engine static test stands or during inflight tests have hindered proper evaluation of the analytical methods. In particular, reliable determination of gas temperatures by independent methods has generally been unavailable. To illustrate the degree of agreement which has been obtained, several examples of test results will be presented. These include a laboratory spectral measurement of a model F-1 engine and a spectral measurement of a J-2 engine during a sea level static firing.

#### 8.3.1 MODEL F-1 MEASUREMENT

Tests of 1/45 scale model of a Rocketdyne F-1 engine were conducted at Cornell Aeronautical Laboratory. A short-duration technique that produces a steady gas flow out of the engines for approximately 5 msec was used. The propellants were gaseous ethylene and oxygen, and the nozzle stagnation pressure was approximately 68.1 atm. Simulated altitude during the short test period was approximately 36.58 km. No carbon particles were apparent in the free plume; however, carbon particles were apparently formed in the impingement region between plumes when two engines were fired.

Radiation measurements were made using a Warner and Swasey fast scanning spectrometer [8-3] which was set up to scan from 1.6 to 5  $\mu$  in 1 msec with a 0.25-msec interval between scans. With this timing, 4 scans could be completed during the 5-msec test event. Because of timing difficulties, only one or two scans were usually made when the rocket operation and altitude simulation were both satisfactory.

The results of these tests have been reported in References 8-2, 8-3, and 8-4, but no comparisons have been made for the impingement region between plumes. Gas property predictions for two locations on the nozzle axis 1.52 and 25.25 cm downstream of the exit are shown in Figures 8-14 and 8-15, and the corresponding radiation prediction is compared with measured values in Figures 8-16 and 8-17. The levels of the measurements agree with the predictions, but there appears to be a slight discrepancy in the wavelength. This discrepancy is attributed to uncertainties in the data reduction. It was necessary to assign a wavelength to some spectral feature in the data to obtain absolute wavelength values, and the radiation predictions were not available at the time the data were reduced.

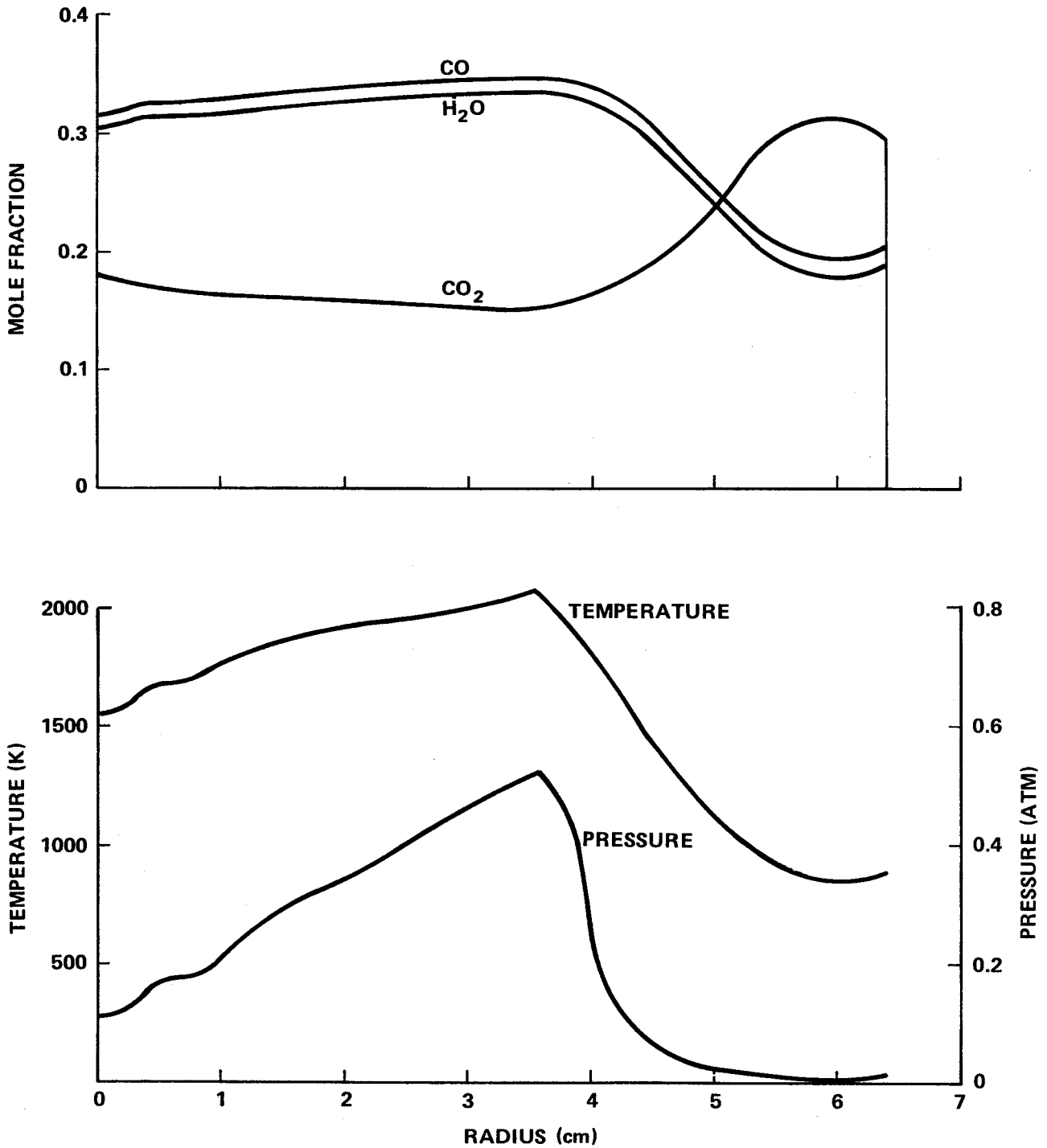


Figure 8-14. Predicted property variations 1.52 cm downstream of a 1/45 scale F-1 engine exit.

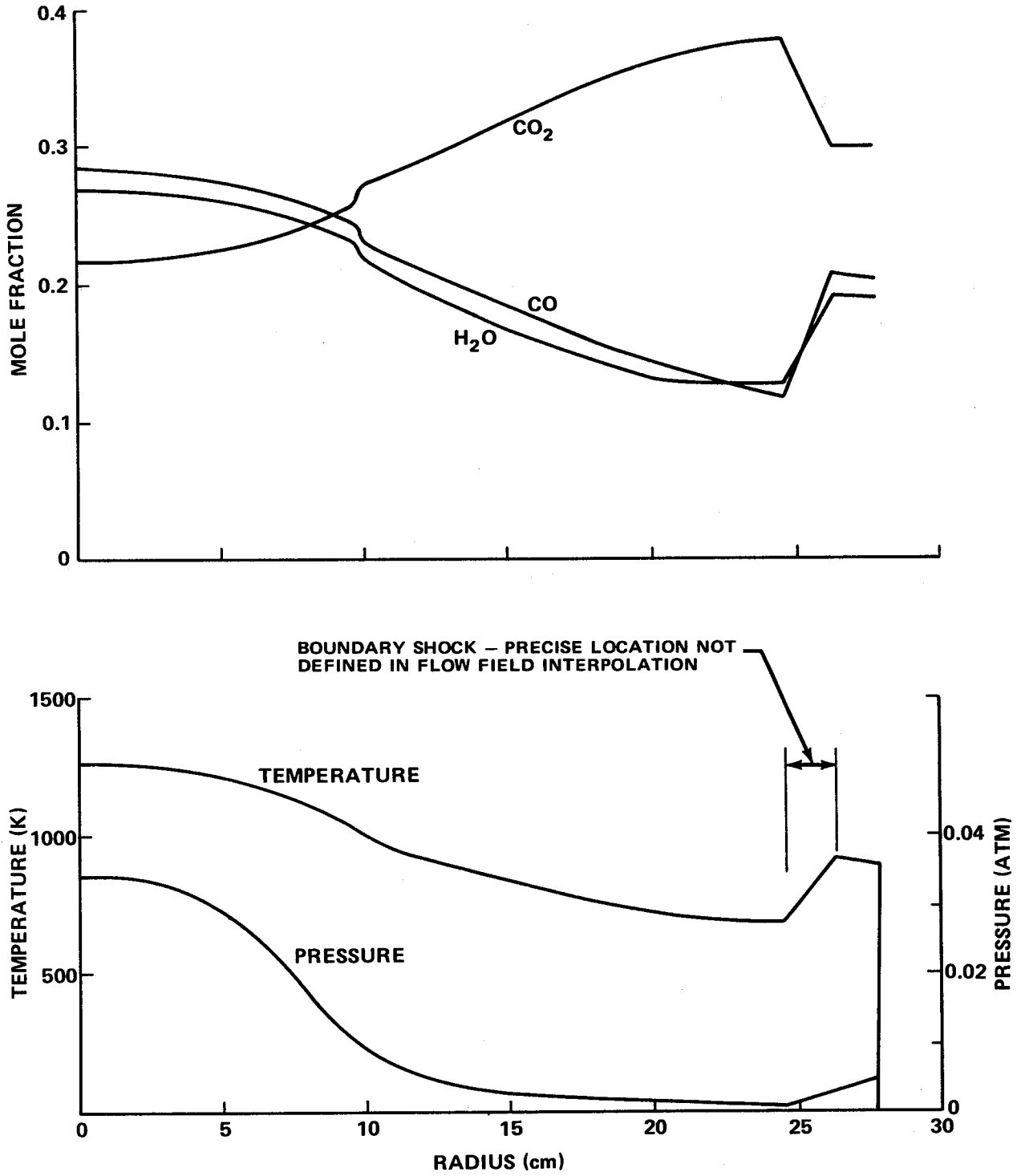


Figure 8-15. Predicted property variations 25.25 cm downstream of a 1/45 scale F-1 engine exit.

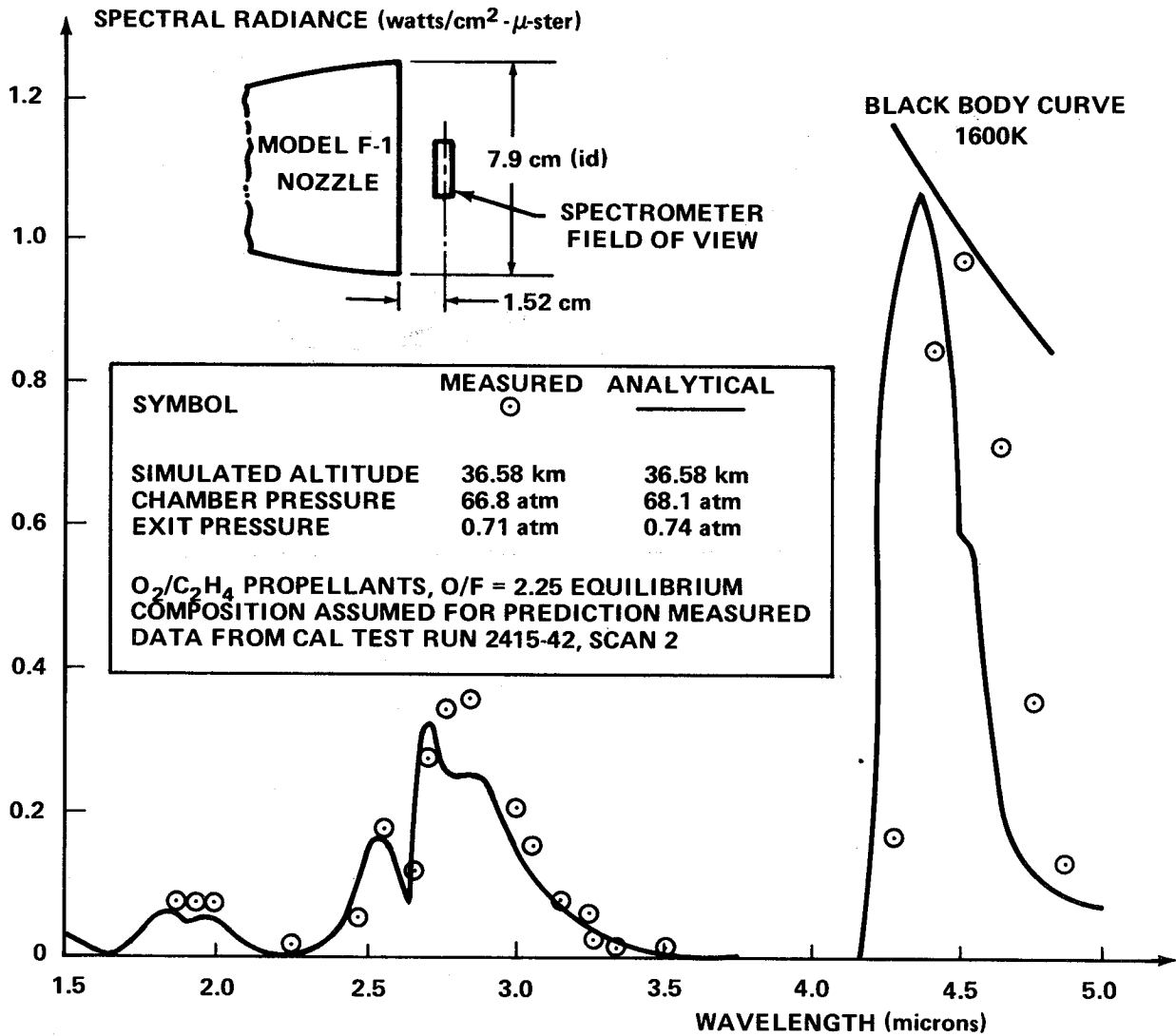


Figure 8-16. Comparison of measured and predicted radiation near the exit of a 1/45 scale F-1 engine.

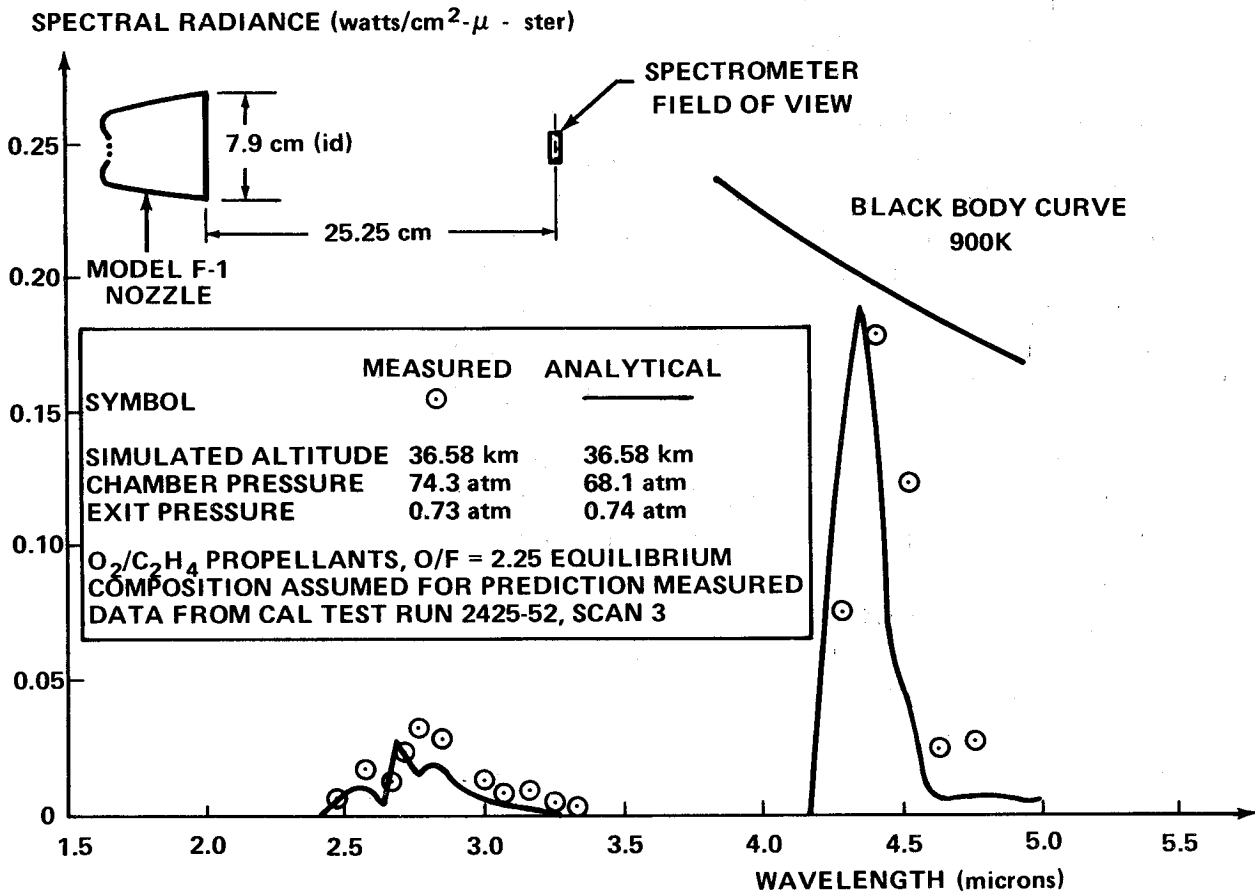


Figure 8-17. Comparison of measured and predicted radiation 2.25 cm aft of the exit of a 1/45 scale F-1 engine.

### 8.3.2 J-2 SEA LEVEL MEASUREMENT

The spectral radiance of a Rocketdyne J-2 engine was measured during sea level static firings at Marshall Space Flight Center. The measurements were made with a Block Engineering Company BD-1A spectrometer mounted 3.49 m from the engine centerline and aligned to view normal to the centerline 19.1 cm downstream from the exit.

For sea level tests, it was necessary to install a short conical diffuser on the J-2 engine to prevent possible flow disturbances in the nozzle. With the diffuser installed, the predicted plume properties along the spectrometer line of sight contain a strong discontinuity because of an oblique shock wave, as shown in Figure 8-18. In making the gas property predictions, the nozzle boundary layer was neglected since it would be difficult to obtain a reasonable boundary layer prediction for this case due to possible flow separation caused by the rapid pressure rise of the shock.

A comparison of measured and predicted radiation (Fig. 8-19) shows that the predicted radiance is somewhat lower than the measured values. However, the agreement is considered to be reasonable when possible gas property and measurement errors are considered. It was predicted that most of the radiation is emitted by the relatively narrow high temperature region outside the oblique shocks. On the line of sight of the spectrometer, 55 percent of the radiance originated from the near side region and 29 percent from the far side region. Because of this intense radiation, small errors in predicting the shock position could lead to appreciable errors in the predicted flux.

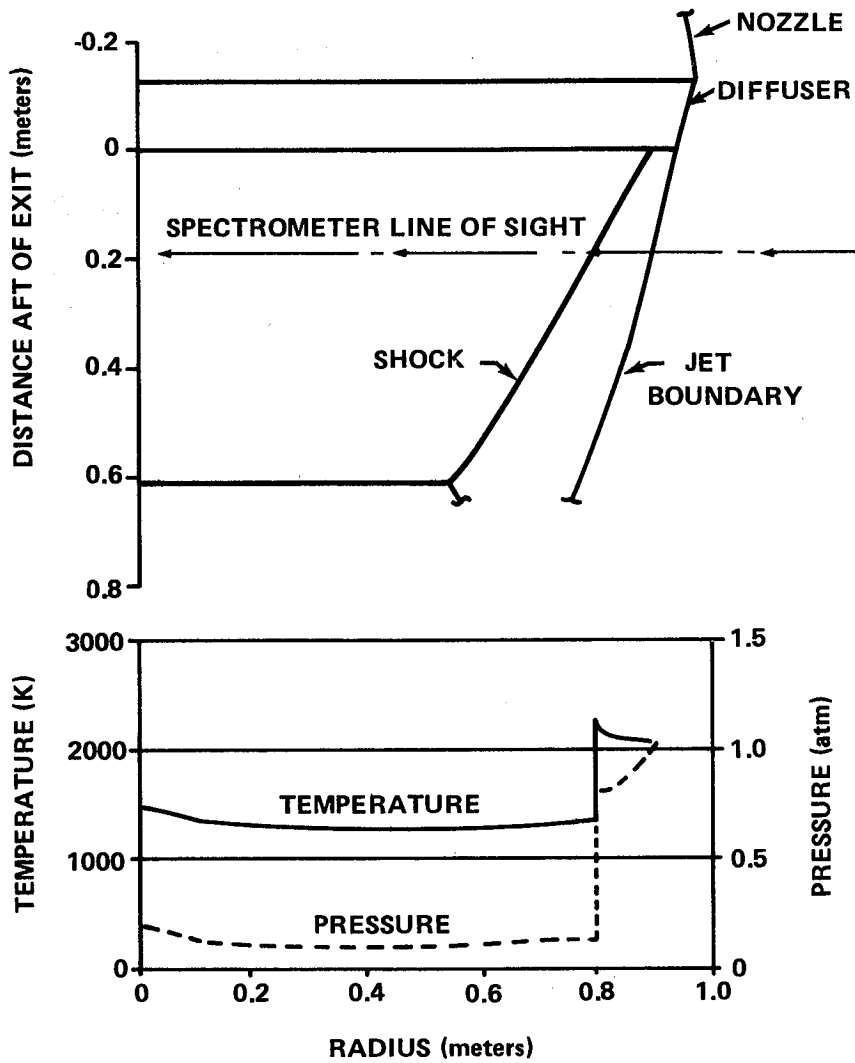


Figure 8-18. Flow field predictions for the J-2 sea level static tests.

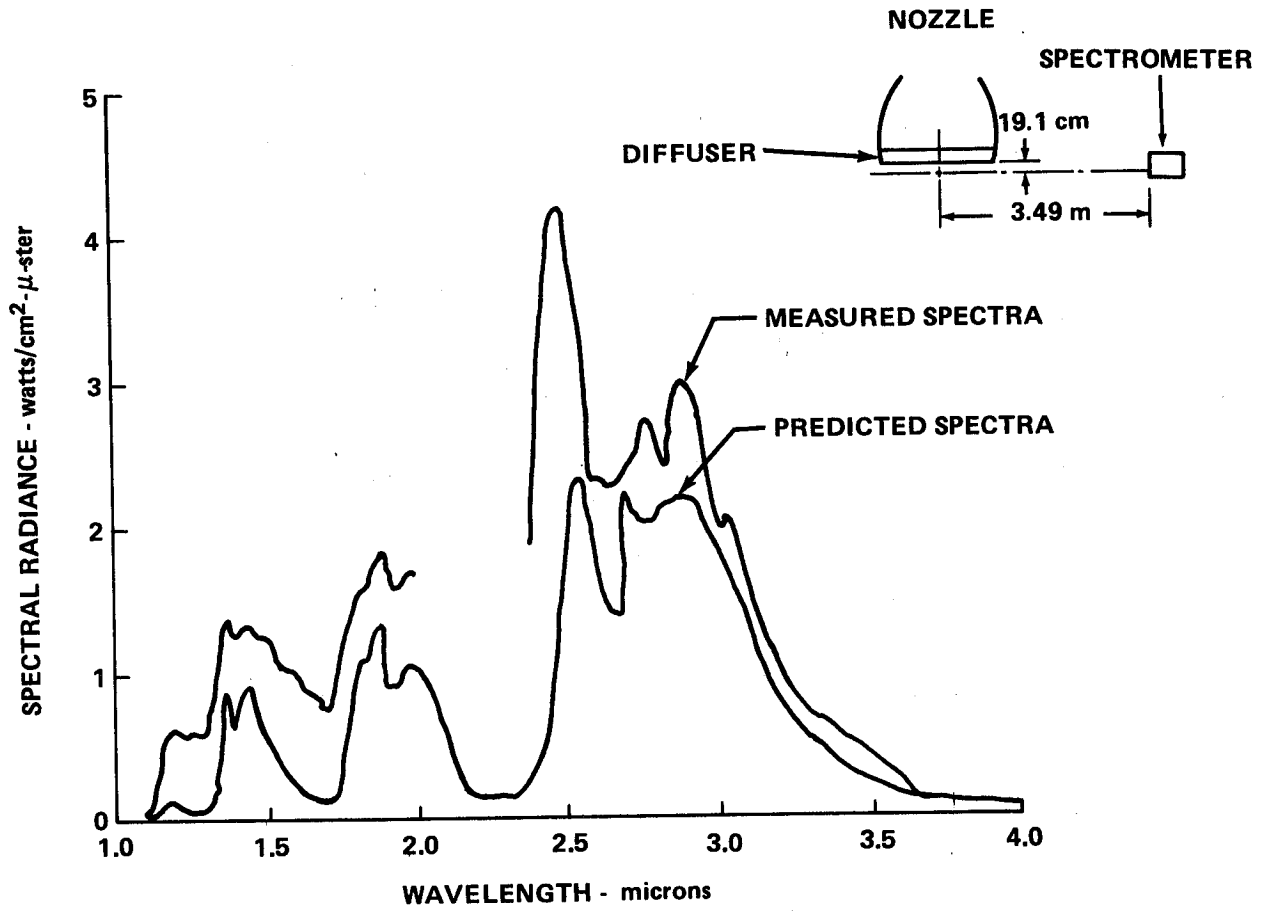


Figure 8-19. Comparison of measured and predicted radiation on a J-2 engine sea level static firing.

8. 4 EFFECT OF SCALE ON GASEOUS RADIATION

An evaluation of the effect of spatial scale on gaseous radiation is helpful in understanding the radiation characteristics of typical problems and is desirable when there is not sufficient information about the gas properties to accurately predict radiation analytically. Even if no scaling laws can be developed, the knowledge of the sensitivity of gaseous radiation to scale can be a great help in making an engineering evaluation of the radiation heat transfer.

Geometric scaling of rocket exhaust plumes is illustrated in Figure 8-20. It is necessary that the spatial distribution of gas properties as well as the location and orientation of the observer be geometrically similar. In the figure and in the subsequent discussion for a single line of sight, the characteristic length is taken as the distance along a line of sight from the observer to the farthest gas boundary, but in an integrated heat transfer calculation any characteristic dimension, such as the engine exit diameter, could be used.

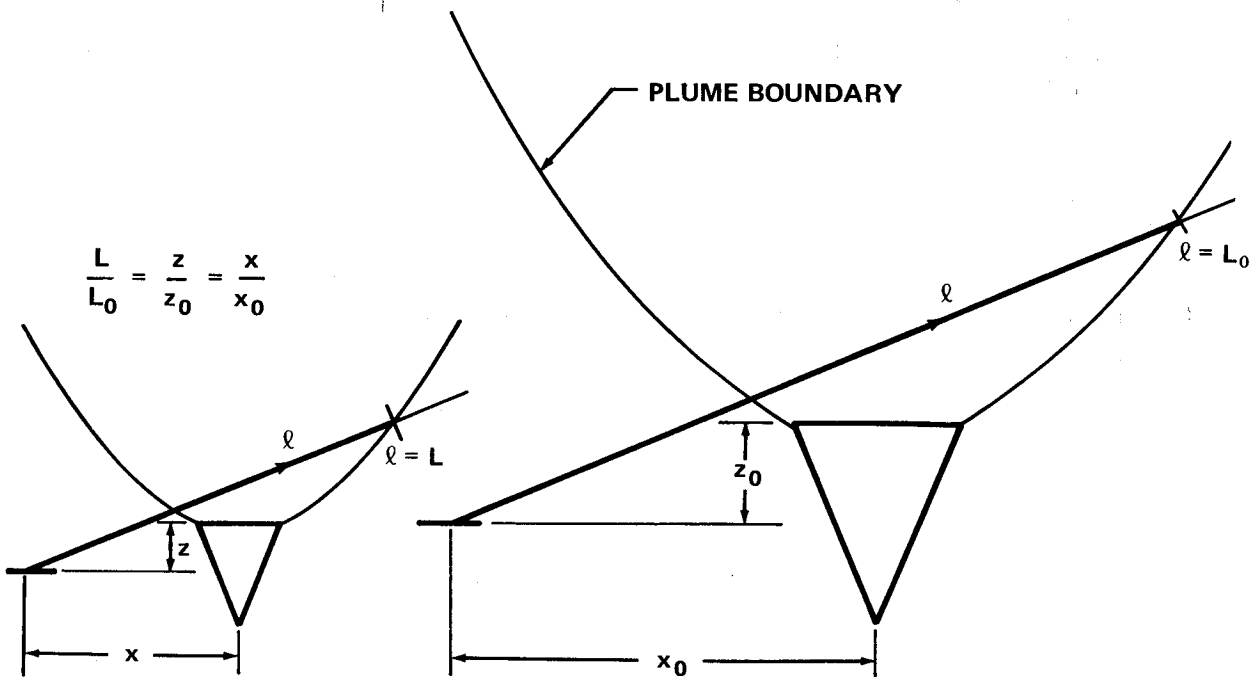


Figure 8-20. Geometric similarities.

In examining the scaling properties, two cases are to be considered: first, a transparent gas in both the linear and square root limits and, second, an opaque gas.

In the transparent isothermal gas case, a direct relation for scaling can be obtained since the optical depth [  $X(\omega, L)$  ] is small compared to unity. For this case, equation (8-3) becomes

$$\tau(\omega, L) \approx 1 - X(\omega, L) \quad (8-5)$$

and the optical depth is equal to the spectral emissivity. The spectral radiance then reduces to

$$N_{\omega} = N_{\omega}^0 X(\omega, L) \quad (8-6)$$

If the entire spectral region of interest is in the linear limit ( $X = ku$ ), the radiance may be scaled to some reference condition (subscript 0) and integrated to yield

$$N/N_0 = L/L_0 \quad (8-7)$$

A similar approach for radiation in the square-root region ( $X = \sqrt{4a ku}$ ) yields

$$N/N_0 = (L/L_0)^{1/2} \quad (8-8)$$

When the radiance varies with the scale length according to

$$N \propto L^n,$$

then the logarithmic derivative  $(L/N) (dN/dL)$  is equal to the exponent  $n$ . Thus a slow variation of this quantity with scale length implies the existence of an approximate scaling law.

CHAPTER 8 – PREDICTIVE TECHNIQUES

Scaling properties for these rocket engines, including those using both oxygen/kerosene and oxygen/hydrogen propellants, were evaluated. The cases of oxygen/kerosene propellants included both low altitude (after-burning) and high altitude conditions. For the oxygen/hydrogen cases, the Rocketdyne J-2 engine plume (76.8-in. exit diameter) was used. In one of these cases the line of sight was through an impingement zone between plumes on the S-II stage, while two others were chosen through the undisturbed high altitude plume. In each case, the ratio of the integrated radiances,  $N/N_0$  (where  $N = \int_0^\infty N_\omega d\omega$ ) and its logarithmic derivative,  $d[\ln(N/N_0)]/d[\ln(L/L_0)]$ , were computed over a wide range of characteristic scales.

Typical results are presented in Figures 8-21 and 8-22. Only one case is presented for oxygen/kerosene plumes since it presents the typical condition that scale effects are strongly dependent on the carbon concentration, and one of the J-2 lines of sight was also omitted since the radiance was so low it did not appear to be significant.

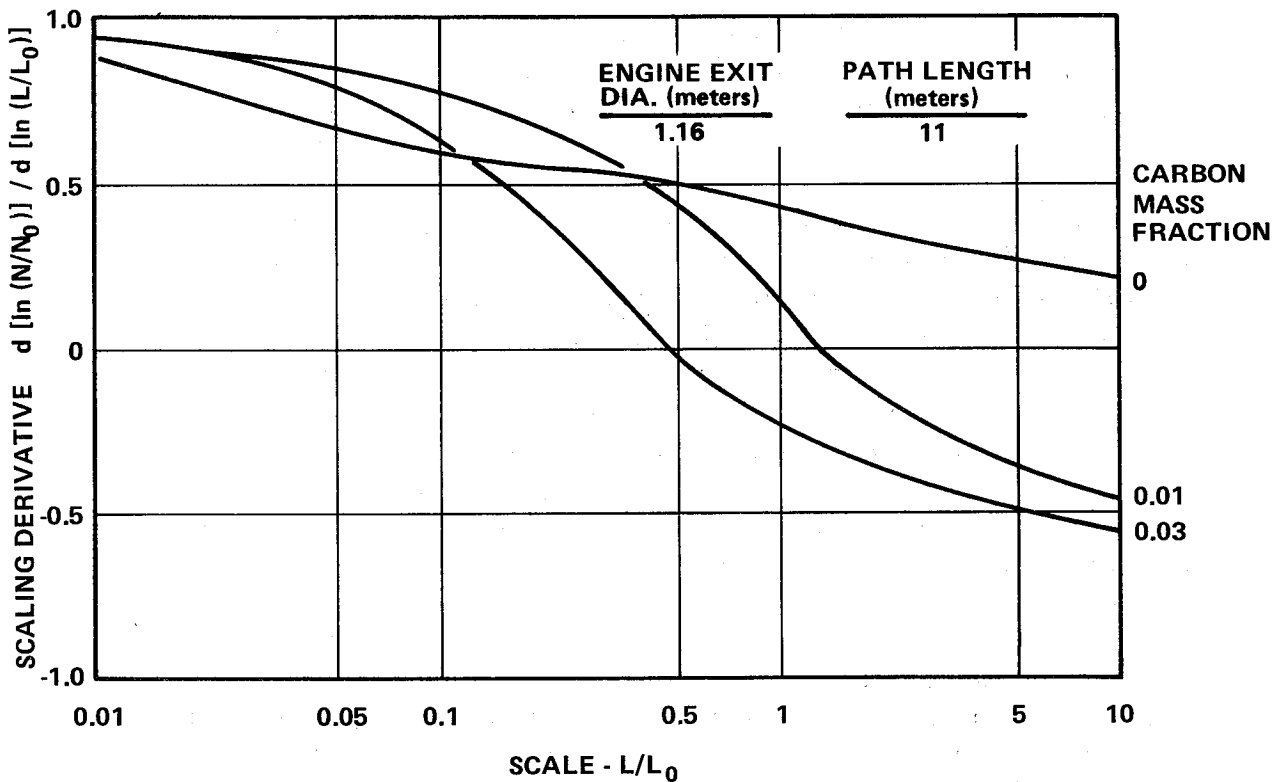


Figure 8-21. Scaling derivative variation for the oxygen/kerosene (H-1) exhaust plume.

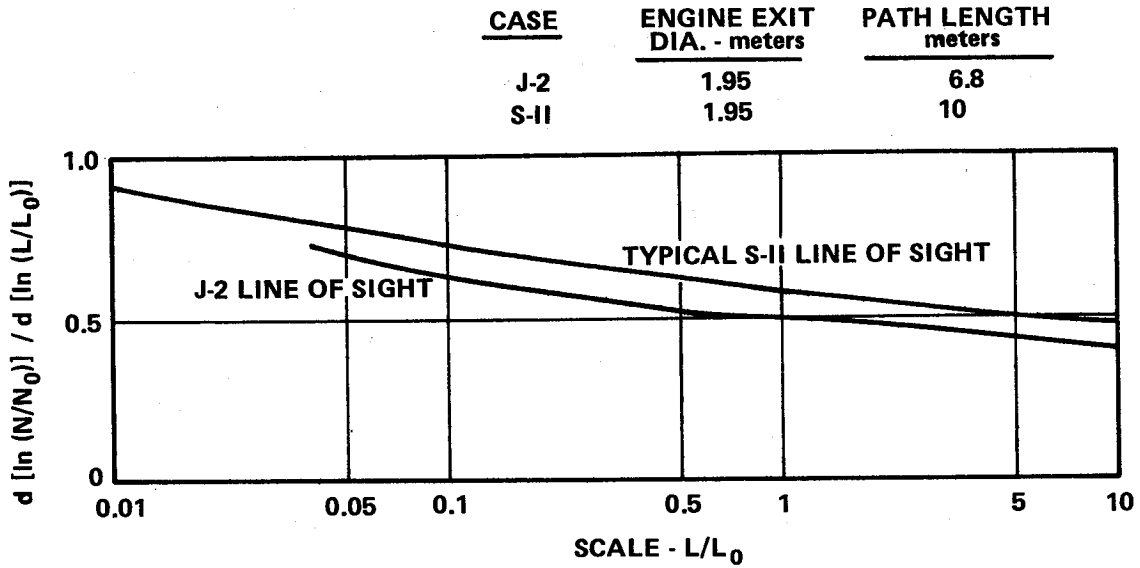


Figure 8-22. Scaling derivative variation for the oxygen/hydrogen exhaust plumes.

The behavior of the hydrocarbon plume without carbon is influenced by strong carbon dioxide and water vapor emission. The scaling exponent decreases smoothly from the linear value (1.0) at small scales to roughly the square root value (0.5) at the nominal scale to about 0.2 at 10 times the nominal scale. With finite concentrations of carbon, the scaling properties change drastically. At large scale the scaling exponent is negative, implying that the radiation decreases with increasing scale. Here, the hotter regions are effectively masked by absorption in the outer portions of the plume, and this masking becomes more and more effective at larger scales.

In the case of the typical S-II line of sight (Fig. 8-22), the radiance gradually approaches the linear limit at very small scales and is very close to a square-root variation at scales greater than 1. On the J-2 line of sight in Figure 8-22, the region from which most of the radiation is emitted is at a lower pressure than for the S-II, so the approach to the linear limit is not as rapid.

The radiance derivatives presented in Figure 8-21 for hydrocarbon fuel indicate the rather uniform behavior of gaseous plumes compared with those containing carbon particles. With the drastic effect carbon particles have on scaling it would be improbable that scaling would be successful over a very large range. However it is interesting to note that engines larger than those presently used may actually show a reduction in radiation.

The more uniform behavior of scaling derivatives for oxygen/hydrogen exhaust plumes (Fig. 8-22) appears to hold more promise for achieving a suitable scaling procedure. The problem still remains that values of the scaling derivatives cannot be assessed precisely without gas property data, but the relatively small difference in scaling derivatives indicates that it may not be too sensitive to property variations. Therefore, useful scaling estimates may be possible over moderate ranges in scale using derivatives calculated from approximate gas property data.

## REFERENCES

- 8-1. Application of Moderate Resolution Band Models in the Prediction of Heat Transfer from Rocket Exhaust Plumes. Hayes International Corp. , ER1677, April 1970.
- 8-2. Study of the Radiation and Convection Environment of the Saturn V Summary Report on Contract NAS8-11350, Hayes International Corp. , ER1333, October 1966.
- 8-3. Klein, L. and Penzias, G. J. : AIAA Journal, vol. 5, 1967, p. 9.
- 8-4. Huffaker, R. M. : Inhomogeneous Radiant Heat Transfer from Saturn Rocket Exhaust Plumes. NASA TM X-53630, June 1967.



## GENERAL APPENDIX

A1 INTRODUCTION TO THE USE OF THE TABLES

Several radiation calculation methods have been discussed in the handbook. Some were very crude such as the thin gas or box models discussed in Section 3.1 and some were accurate but lengthy such as line by line calculations.

The main purpose of the handbook, however, is to provide a reasonably accurate representation of radiation fluxes without producing a computer overload. The two procedures outlined in Section 5.3 constitute, from the experience of the authors, an effective compromise. The multiple line group model (MLG) provides the possibility to consider  $n$  possible line groups, reflecting better the dependence of the band parameters on temperature. The single line group model (SLG) is usually satisfactory for relatively low temperature flames.

The calculation procedures for MLG and SLG (Section 5.3) make use of a number of properties and refer to this General Appendix for the corresponding tables. These tables are given in Section A2. The rest of Section A1 will be devoted to a typical illustration of the procedures recommended in Section 5.3.

## A1.1 TYPICAL CALCULATION

Nonhomogeneous gases typical of flames have been studied experimentally by Simmons and discussed earlier in the handbook (see Reference 7-4). The example calculation will estimate the radiative flux emerging in the frequency range of the  $2.7\text{-}\mu$  band from the left side of an inhomogeneous  $\text{CO}_2$  gas sample at standard pressure conditions ( $p = 760$  mm Hg) (see Fig. 7-22). The temperature distribution across the 60 cm path is given at 10 equidistant points (including both extremities) as (see Reference 7-4):

368, 528, 719, 953, 1130, 1160, 979, 737, 541, 387 in K

A1.1.1 Calculation Procedure

The emerging radiance for a particular wavenumber  $\omega$  can be written in general [equation (5-21)]:

$$N_{\omega} = - \int_0^L N_{\omega}^0(T) \frac{d}{dl} (\tau_{\omega}) dl \quad (\text{A-1})$$

GENERAL APPENDIX

where the transmittance  $\tau_\omega$  is given by

$$\tau_\omega \equiv \exp \left( - \sum_i X_{\omega,i} \right) \quad (A-2)$$

where  $i$  indicates the number of chemical components contributing to the flame radiation. Equation (A-1) is usually transformed into a numerical summation form such that

$$N_\omega = - \sum_{m=1}^{m=M} N_\omega(T_m) (\tau_{\omega,m} - \tau_{\omega,m-1}) \quad (A-3)$$

where the index  $m$  refers to the sections across the flame. If all sections are of equal width,  $\Delta\ell$ , then the total width  $L = M(\Delta\ell)$ .

Whether one uses equation (A-3) or a more sophisticated integration procedure for equation (A-1), the two key parameters of the calculation are the Planck function  $N_\omega^0(T)$  and the transmittance  $\tau_\omega$ . The Planck function is tabulated in Section A2.1 and the transmittance is given by equation (A-2).

The case under consideration involves a single chemical component ( $\text{CO}_2$ ) so  $i = 1$ . Also, the temperature ratio across the flame is relatively low, so the single line group (SLG) model will be used. For the SLG model, the optical depth through each position extending from the observation side ( $u = 0, m = 1$ ) to a given pathlength  $u$  (or section  $M$ ) inside the flame<sup>1</sup> is

$$X = f(X^*, \bar{a}_c, \bar{a}_D) \quad , \quad (A-4)$$

where

$$X^* = \int_0^u k \, du' \quad \text{or} \quad X^* = \sum_{m'=1}^{m'=m} k_{m'} \Delta u_{m'} \quad (A-5)$$

1. The absorption coefficient tabulated in Table A-2 corresponds to standard density conditions. Therefore, the equivalent pathlength ( $\Delta u$ ) over an assumed isothermal interval is obtained by multiplying the physical pathlength  $\Delta\ell$  by  $\left(\frac{273}{T, K}\right) \left(\frac{P}{1 \text{ atm}}\right)$ .

$$\bar{a}_c = \frac{1}{X^*} \int_0^u \frac{\gamma_c}{d} k \, du' \quad \text{or} \quad \bar{a}_c = \frac{1}{X^*} \sum_{m'=1}^{m'=m} \left( \frac{\gamma_c}{d} k \right)_{m'} \Delta u_{m'} \quad (\text{A-6})$$

$$\bar{a}_D = \frac{1}{X^*} \int_0^u \frac{\gamma_D}{d} k \, du' \quad \text{or} \quad \bar{a}_D = \frac{1}{X^*} \sum_{m'=1}^{m'=m} \left( \frac{\gamma_D}{d} k \right)_{m'} \Delta u_{m'} \quad (\text{A-7})$$

The values of  $X^*$ ,  $\bar{a}_c$  and  $\bar{a}_D$  will be necessary at each position ( $0 < u' < u$ ;  $1 < m < M$ ) in order to calculate  $N_\omega$  [equations (A-1) or (A-3)]. The functional form of  $f$ , the "curve of growth," is given by equation (5-25):

$$f(X^*, a_c, a_D) = X^* (1 - y^{-1/2})^{1/2}, \quad (\text{A-8})$$

where

$$y = \left[ 1 - \left( \frac{X_c}{X^*} \right)^2 \right]^{-2} + \left[ 1 - \left( \frac{X_D}{X^*} \right)^2 \right]^{-2} - 1. \quad (\text{A-9})$$

Finally, the values of  $X_c$  and  $X_D$  are given by:

$$X_c = X \left( 1 + \frac{X^*}{4\bar{a}_c} \right)^{-1/2} \quad (\text{A-10})$$

$$X_D = 1.7 a_D \left\{ \ln \left[ 1 + \left( 0.589 \frac{X^*}{\bar{a}_D} \right)^2 \right] \right\}^{1/2}. \quad (\text{A-11})$$

The information needed for the solution of equations (A-4) through (A-11) includes the temperatures, pressures, and the mole fractions of the radiating

## GENERAL APPENDIX

species in addition to the four band model parameters:

absorption coefficient,  $k$ ,

line density,  $1/d$ ,

collision half-width,  $\gamma_c$ ,

Doppler half-width,  $\gamma_D$ .

The absorption coefficient  $k$  and the line density  $1/d$  can be found in tables of Section A2. A short index, at the beginning of the tables, points out the appropriate page numbers for each substance. The collision and Doppler half-widths vary with ambient conditions as expressed by equations (5-34) and (5-35):

$$\gamma_{c_i} = \left[ \sum_j (\gamma_{ij})_{273} P_j \left( \frac{273}{T} \right)^{\eta_{ij}} \right] + (\gamma_{ii}^*)_{273} P_i \left( \frac{273}{T} \right)^{\eta_{ii}^*} \quad (\text{A-12})$$

and

$$\gamma_D = (5.94 \times 10^{-6}) \frac{\omega}{M^{1/2}} \left( \frac{T}{273} \right)^{1/2} \quad (\text{A-13})$$

where  $i$  refers to the radiating component under study and  $j$  to the other components of the sample;  $p$  is the partial pressure;  $M$  is the molecular weight; and the values of  $(\gamma_{ij}^*)_{273}$ ,  $(\gamma_{ii}^*)_{273}$ ,  $\eta_{ij}$  and  $\eta_{ii}^*$  are given in Table 5-19.

### A1.1.2 Example Calculation

The formulas listed in equations (A-1) through (A-13) can now be applied to the inhomogeneous gas sample described at the beginning of this section (A1.1). For purposes of illustration, the sample calculation will be made using 10 equal increments of 6 cm along the path through the gas. A linear temperature variation will be assumed between the measured

temperature points, and the temperature for each 6 cm section will be taken as the temperature at the center of the section. The resulting pathlength increment adjusted to STP conditions is

$$\Delta u = 6 \text{ cm} \left( \frac{273}{T} \right) (1 \text{ atm}) .$$

Temperatures and  $\Delta u$  increments are listed in Table A1-1 along with radiation calculations for 4 wavenumbers: 3400, 3450, 3500, and 3600  $\text{cm}^{-1}$ . Values of  $k$  (STP) and  $1/d$  were obtained from the tables of Section A2 using linear interpolation on temperature.

Since the gas sample is pure  $\text{CO}_2$ , the collision broadened half-width is evaluated using coefficients from Table 5-19 for  $\text{CO}_2$  self broadening only:  $\gamma_{ij} = 0.09$ ,  $\eta_{ij} = 0.5$ ,  $\gamma_{ii}^* = 0.1$ , and  $\eta_{ii}^* = 1.0$ . Using these coefficients and one atmosphere partial pressure, equation (A-12) reduces to

$$\gamma_c = 0.09 (273/T)^{1/2} + 0.01 (273/T) .$$

The Doppler half-width for  $\text{CO}_2$  is obtained from equation (A-13) using the molecular weight of 44

$$\gamma_D = 0.895(10^{-6}) \omega (T/273)^{1/2} .$$

Values of  $\gamma_c$  and  $\gamma_D$  for each section of the gas are given in Table A1-1.

The fine structure parameters are averaged using equations (A-6) and (A-7) to give effective values of  $a_c$  and  $a_D$  from the edge of the gas through each successive increment. These averaged values are then used in equations (A-10) and (A-11) to estimate the optical depth at the end of each increment in the gas. These results are presented in Table A1-1.

Examination of the values of  $\bar{a}_c$  and  $\bar{a}_D$  indicates that  $\bar{a}_c$  is generally an order of magnitude larger than  $\bar{a}_D$ . As a result, when the optical depths

## GENERAL APPENDIX

become less than the linear limit ( $X^*$ ), the optical depth due to Doppler broadening becomes much less than that for collision broadening. In cases such as this, Doppler broadening can be neglected and the calculation procedure significantly shortened. However, to illustrate the procedure equations (A-8) and (A-9) were used in the sample problem to compute the combined optical depth,  $X$ . Using this combined optical depth, the transmissivity was computed using equation (A-2) ( $i = 1$ ) and the radiance was calculated by equation (A-3) for  $m = 1$  to 10. The results are listed in Table A1-1 and the overall radiance ( $m = 10$ ) agrees very well with the measured and computed values in Figure 7-22.

The excellent agreement between the measured data and the sample problem is better than should be expected considering the simplifications made in the solution. In a high pressure gas such as the example, the transmissivity changes too much in some of the 6 cm ( $\Delta u$ ) increments, so a smaller increment should be used if the summations are to be a reasonable representation of the integrals. In addition, the interpolation of  $k$  and  $1/d$  would probably be better represented by a curve fit or interpolation based on the logarithm of  $k$  or  $1/d$ .

TABLE A1-1. RESULTS OF EXAMPLE CALCULATION

Increment	$\omega$ ( $\text{cm}^{-1}$ )	T (K)	$\Delta u(\text{STP})$ ( $\text{cm-atm}$ )	$k(\text{STP})$ ( $\text{cm}^{-1}\text{-atm}^{-1}$ )	1/d (cm)	$\gamma_c$ ( $\text{cm}^{-1}$ )	$\gamma_D$ ( $\text{cm}^{-1}$ )	$X^*$	$\bar{a}_c$	$\bar{a}_D$	$X_c$	$X_D$	X	$\tau$	$-\Delta\tau$	$N_\omega^0 \times 10^6$ (watts/cm-st)	$\sum N_\omega^0 (-\Delta\tau)$ (watts/cm-st)	
1	3400	440	3.723	4.305E-7	5.81	0.0771	0.00386	1.603E-6	0.4479	0.02243	1.603E-6	1.603E-6	1.603E-6	1.0000	0	-	0.00	
	3450			1.695E-4	7.76		0.00392	6.310E-4	0.5983	0.008171	6.310E-4	6.310E-4	6.310E-4	6.310E-4	0.9994	0.0006	0.64	0.00
	3500			0.008402	9.38		0.00398	0.03128	0.7231	0.01003	0.03111	0.0207	0.03111	0.9694	0.0306	0.0306	0.55	0.02
	3600			0.5368	2.27		0.00409	1.999	0.1750	0.002911	1.018	0.0172	1.018	0.2765	0.7235	0.43	0.31	
2	3400	595	2.753	9.071E-7	10.5	0.0656	0.00449	4.100E-6	0.5946	0.03749	4.100E-6	4.100E-6	4.100E-6	1.0000	0	-	0.00	
	3450			3.571E-4	14.3		0.00456	0.001614	0.8055	0.4004	0.001614	0.001614	0.001614	0.9984	0.0016	0.0016	11.65	0.01
	3500			0.1769	17.1		0.00462	0.07998	0.9659	0.05203	0.07916	0.06834	0.07916	0.9249	0.0445	0.0445	10.78	0.50
	3600			0.4985	3.61		0.00476	3.371	0.2002	0.008493	1.477	0.04204	1.481	0.2270	0.0495	0.0495	9.21	0.77
3	3400	777	2.108	0.006207	72.1	0.0569	0.00513	0.01308	4.102	0.3699	0.01307	0.01307	0.01307	0.9870	0.0130	86.45	-1.12	
	3450			0.02216	51.0		0.00521	0.04832	2.831	0.2703	0.04822	0.04819	0.04824	0.9529	0.0455	0.0455	82.32	3.76
	3500			0.06746	33.0		0.00528	0.2222	1.550	0.1302	0.2183	0.1849	0.2183	0.8075	0.1174	0.1174	78.34	9.69
	3600			0.3832	15.3		0.00543	4.179	0.3297	0.02291	2.047	0.1034	2.048	0.1285	0.0985	0.0985	70.82	7.74
4	3400	979	1.673	0.01329	142.0	0.0503	0.00576	0.03531	6.018	0.6519	0.03528	0.03531	0.03531	0.9653	0.0217	318.48	8.04	
	3450			0.04703	92.7		0.00584	0.1270	3.966	0.4382	0.1265	0.1261	0.1266	0.8810	0.0719	0.0719	309.02	25.98
	3500			0.1239	50.8		0.00593	0.4295	2.035	0.2128	0.4186	0.3391	0.4187	0.6580	0.1495	0.1495	299.65	54.49
	3600			0.3349	28.7		0.00610	4.739	0.4615	0.04092	2.509	0.2022	2.512	0.0812	0.0473	0.0473	281.29	21.05
5	3400	1131	1.448	0.1862	195.	0.0466	0.00619	0.06227	7.347	0.8922	0.06220	0.06226	0.06226	0.9396	0.0257	627.42	24.16	
	3450			0.06574	124.		0.00628	0.2222	4.743	0.5842	0.2209	0.2198	0.2211	0.8017	0.0793	0.0793	614.62	74.72
	3500			0.1664	64.2		0.00637	0.6704	2.379	0.2833	0.6480	0.5000	0.6482	0.5235	0.1345	0.1345	601.71	135.42
	3600			0.2986	38.7		0.00656	5.172	0.5737	0.05872	2.867	0.2806	2.872	0.0568	0.0244	0.0244	575.74	35.10
6	3400	1159	1.413	0.01960	205.	0.0460	0.00627	0.08996	7.988	1.013	0.08983	0.08996	0.08996	0.9139	0.0257	697.57	42.08	
	3450			0.06919	130.		0.00636	0.3200	5.119	0.6581	0.3175	0.3137	0.3177	0.7280	0.0737	0.0737	684.32	125.15
	3500			0.1742	66.7		0.00645	0.9165	2.564	0.3226	0.8781	0.6330	0.8784	0.4160	0.1075	0.1075	670.95	207.55
	3600			0.2919	40.6		0.00664	5.584	0.6692	0.07430	3.179	0.3478	3.185	0.0412	0.0156	0.0156	634.87	45.00
7	3400	1006	1.628	0.01424	152.	0.0496	0.00584	0.1131	7.899	0.9876	0.1129	0.1131	0.1131	0.8930	0.0209	364.53	49.70	
	3450			0.05035	98.3		0.00593	0.4019	5.071	0.6429	0.3980	0.3894	0.3982	0.6715	0.0565	0.0565	354.38	145.17
	3500			0.1315	53.2		0.00601	1.131	2.577	0.3219	1.074	0.7053	1.074	0.3415	0.0745	0.0745	344.31	233.20
	3600			0.3285	30.5		0.00618	6.119	0.7429	0.08428	3.499	0.3926	3.506	0.0300	0.0112	0.0112	334.22	48.74
8	3400	798	2.053	0.006944	79.4	0.0561	0.00520	0.1274	7.511	0.9231	0.1271	0.1271	0.1272	0.8808	0.0122	102.07	50.95	
	3450			0.02474	55.3		0.00528	0.4527	4.850	0.6035	0.4475	0.4320	0.4477	0.6390	0.0325	0.0325	97.42	148.34
	3500			0.07333	34.8		0.00536	1.281	2.504	0.3062	1.206	0.7270	1.207	0.3000	0.0415	0.0415	92.93	237.06
	3600			0.3782	16.7		0.00551	6.895	0.7649	0.08515	3.823	0.4052	3.830	0.0216	0.0084	0.0084	84.42	49.45
9	3400	610	2.685	3.516E-4	14.2	0.0647	0.00455	0.1283	7.465	0.9213	0.1280	0.1281	0.1281	0.8797	0.0011	15.40	50.97	
	3450			0.001594	16.6		0.00461	0.4570	4.814	0.5987	0.4517	0.4361	0.4519	0.6360	0.0030	0.0030	13.74	148.38
	3500			0.02079	18.2		0.00468	1.337	2.449	0.2969	1.254	0.7280	1.255	0.2850	0.0150	0.0150	13.27	237.26
	3600			0.4231	4.31		0.00481	8.031	0.6962	0.07603	4.075	0.3715	4.082	0.0170	0.0046	0.0046	11.41	49.50
10	3400	456	3.592	4.797E-7	6.30	0.0756	0.00393	0.1283	7.465	0.9213	0.1280	0.1281	0.1281	0.8797	0	-	50.97	
	3450			1.889E-4	8.43		0.00399	0.4575	4.811	0.5980	0.4522	0.4372	0.4523	0.6359	0.0001	0.0001	0.93	148.38
	3500			0.009361	10.2		0.00405	1.362	2.419	0.2922	1.275	0.7271	1.276	0.2795	0.0055	0.0055	0.82	237.26
	3600			0.5257	2.41		0.00416	9.443	0.6193	0.06617	4.305	0.3348	4.311	0.0134	0.0036	0.0036	0.65	49.51

GENERAL APPENDIX

A2 RADIATION DATA TABLES

This section contains tables and graphs to be used in conjunction with the calculation procedures given in the text of this handbook. The following is a guide for the reader to locate by page number the specific table and/or graph needed.

A 2.1 BLACKBODY RADIATION FUNCTIONS 386

A 2.2 DIATOMIC MOLECULES

	<u>Absorption Coefficient</u>	<u>Line Spacing</u>	<u>Integrated Emissivity</u>	<u>Total Emissivity</u>
CO	390	392	394	396
NO	398	400	402	404
CN	406	408	410	412
OH	414	416	418	420
HCl	422	424	426	428
HF	430	432	434	436

A 2.3 CO<sub>2</sub>

Integrated Emissivity	4.3 $\mu$	438
	2.7 $\mu$	440
Absorption Coefficient	15 $\mu$	442
	4.3 $\mu$	445
	2.7 $\mu$	448
Fine Structure Parameter		
MLG Model	4.3 $\mu$	452
	2.7 $\mu$	454
SLG Model	4.3 $\mu$	457
	2.7 $\mu$	459

## A2.4 WATER VAPOR

Absorption Coefficients (50 to 9300 $\text{cm}^{-1}$ )	462
Line Density Parameter (1150 to 7500 $\text{cm}^{-1}$ )	476

## A2.5 CARBON

Absorption Coefficient	486
------------------------	-----

TABLE A2-1. BLACKBODY RADIATION FUNCTIONS

$\omega/T$	$\frac{W_{\omega}^0 \times 10^{11}}{T^3}$	$\frac{N_{\omega}^0 \times 10^{11}}{T^3}$	$\frac{\int_0^{\omega} W_{\omega}^0 d\omega}{\sigma T^4}$	$\omega/T$	$\frac{W_{\omega}^0 \times 10^{11}}{T^3}$	$\frac{N_{\omega}^0 \times 10^{11}}{T^3}$	$\frac{\int_0^{\omega} W_{\omega}^0 d\omega}{\sigma T^4}$
.05	.000627	.000200	.000019	.61	.060417	.019231	.024605
.06	.000896	.000285	.000032	.62	.061902	.019704	.025684
.07	.001211	.000385	.000050	.63	.063389	.020177	.026789
.08	.001570	.000500	.000075	.64	.064879	.020651	.027921
.09	.001972	.000628	.000106	.65	.066369	.021126	.029079
.10	.002417	.000769	.000145	.66	.067861	.021601	.030263
.11	.002903	.000924	.000192	.67	.069353	.022076	.031473
.12	.003430	.001092	.000247	.68	.070846	.022551	.032710
.13	.003995	.001272	.000313	.69	.072338	.023026	.033973
.14	.004600	.001464	.000389	.70	.073829	.023500	.035262
.15	.005241	.001668	.000475	.71	.075319	.023975	.036578
.16	.005919	.001884	.000574	.72	.076807	.024448	.037920
.17	.006632	.002111	.000684	.73	.078293	.024921	.039288
.18	.007380	.002349	.000808	.74	.079777	.025394	.040682
.19	.008161	.002598	.000945	.75	.081257	.025865	.042103
.20	.008974	.002857	.001096	.76	.082735	.026335	.043549
.21	.009820	.003126	.001262	.77	.084209	.026804	.045022
.22	.010696	.003405	.001443	.78	.085678	.027272	.046520
.23	.011602	.003693	.001639	.79	.087144	.027739	.048045
.24	.012538	.003991	.001852	.80	.088604	.028204	.049595
.25	.013501	.004298	.002082	.81	.090059	.028667	.051171
.26	.014492	.004613	.002329	.82	.091509	.029128	.052773
.27	.015509	.004937	.002594	.83	.092954	.029588	.054400
.28	.016551	.005268	.002876	.84	.094392	.030046	.056053
.29	.017619	.005608	.003178	.85	.095823	.030501	.057731
.30	.018710	.005956	.003498	.86	.097248	.030955	.059434
.31	.019825	.006310	.003838	.87	.098665	.031406	.061162
.32	.020962	.006672	.004198	.88	.100076	.031855	.062915
.33	.022120	.007041	.004578	.89	.101478	.032302	.064693
.34	.023299	.007416	.004978	.90	.102873	.032746	.066496
.35	.024498	.007798	.005400	.91	.104259	.033187	.068323
.36	.025717	.008186	.005843	.92	.105637	.033625	.070174
.37	.026954	.008580	.006307	.93	.107006	.034061	.072050
.38	.028209	.008979	.006794	.94	.108367	.034494	.073950
.39	.029480	.009384	.007303	.95	.109717	.034924	.075874
.40	.030768	.009794	.007834	.96	.111059	.035351	.077821
.41	.032072	.010209	.008389	.97	.112390	.035775	.079792
.42	.033390	.010629	.008966	.98	.113712	.036196	.081787
.43	.034723	.011053	.009567	.99	.115023	.036613	.083804
.44	.036070	.011481	.010191	1.00	.116324	.037027	.085845
.45	.037429	.011914	.010840	1.01	.117614	.037438	.087909
.46	.038800	.012350	.011512	1.02	.118893	.037845	.089995
.47	.040183	.012791	.012209	1.03	.120162	.038249	.092104
.48	.041577	.013234	.012930	1.04	.121419	.038649	.094235
.49	.042981	.013681	.013676	1.05	.122664	.039045	.096388
.50	.044395	.014131	.014447	1.06	.123898	.039438	.098563
.51	.045818	.014584	.015242	1.07	.125121	.039827	.100759
.52	.047249	.015040	.016063	1.08	.126331	.040212	.102978
.53	.048688	.015498	.016910	1.09	.127529	.040594	.105217
.54	.050135	.015958	.017781	1.10	.128715	.040971	.107477
.55	.051588	.016421	.018679	1.11	.129888	.041345	.109758
.56	.053047	.016885	.019602	1.12	.131049	.041714	.112060
.57	.054512	.017352	.020550	1.13	.132197	.042080	.114382
.58	.055982	.017820	.021525	1.14	.133333	.042441	.116725
.59	.057457	.018289	.022526	1.15	.134455	.042798	.119087
.60	.058935	.018760	.023552	1.16	.135564	.043151	.121469

Notes: (1) Units of the tabulated functions are as follows:

$$\omega/T - \text{cm}^{-1} \text{K}^{-1}; W_{\omega}^0/T^3 - \text{watts cm}^{-1} \text{K}^{-3}$$

$$N_{\omega}^0/T^3 - \text{watts cm}^{-1} \text{st}^{-1} \text{K}^{-3}; \int_0^{\omega} W_{\omega}^0 d\omega / \sigma T^4 - \text{dimensionless}$$

(2) Tabulated values based on the following constants from Table 2.2:  $c_1 = 3.7405 \times 10^{-12}$  watts  $\text{cm}^2$ ;  $c_2 = 1.43879$  cm K;  $\sigma = 5.6697 \times 10^{-12}$  watts  $\text{cm}^{-2} \text{K}^{-4}$ .

TABLE A2-1. (Continued)

$\omega/T$	$\frac{W_{\omega}^0 \times 10^{11}}{T^3}$	$\frac{N_{\omega}^0 \times 10^{11}}{T^3}$	$\frac{\int_0^{\omega} W_{\omega}^0 d\omega}{\sigma T^4}$	$\omega/T$	$\frac{W_{\omega}^0 \times 10^{11}}{T^3}$	$\frac{N_{\omega}^0 \times 10^{11}}{T^3}$	$\frac{\int_0^{\omega} W_{\omega}^0 d\omega}{\sigma T^4}$
1.17	.136660	.043500	.123870	1.73	.175261	.055787	.281656
1.18	.137743	.043845	.126291	1.74	.175544	.055877	.284748
1.19	.138812	.044185	.128730	1.75	.175813	.055963	.287845
1.20	.139868	.044521	.131188	1.76	.176069	.056045	.290946
1.21	.140910	.044853	.133665	1.77	.176311	.056122	.294051
1.22	.141938	.045180	.136160	1.78	.176541	.056195	.297161
1.23	.142952	.045503	.138673	1.79	.176757	.056264	.300274
1.24	.143953	.045822	.141204	1.80	.176960	.056328	.303391
1.25	.144939	.046136	.143752	1.81	.177150	.056389	.306511
1.26	.145912	.046445	.146318	1.82	.177328	.056445	.309634
1.27	.146870	.046750	.148900	1.83	.177492	.056498	.312759
1.28	.147814	.047051	.151500	1.84	.177644	.056546	.315888
1.29	.148744	.047347	.154116	1.85	.177784	.056590	.319018
1.30	.149659	.047638	.156748	1.86	.177910	.056631	.322151
1.31	.150560	.047925	.159396	1.87	.178025	.056667	.325285
1.32	.151447	.048207	.162060	1.88	.178127	.056700	.328421
1.33	.152319	.048485	.164740	1.89	.178217	.056728	.331558
1.34	.153176	.048758	.167434	1.90	.178294	.056753	.334696
1.35	.154020	.049026	.170144	1.91	.178360	.056774	.337835
1.36	.154848	.049290	.172868	1.92	.178414	.056791	.340975
1.37	.155662	.049549	.175607	1.93	.178455	.056804	.344115
1.38	.156461	.049803	.178361	1.94	.178485	.056814	.347256
1.39	.157246	.050053	.181128	1.95	.178504	.056820	.350396
1.40	.158015	.050298	.183908	1.96	.178511	.056822	.353535
1.41	.158771	.050538	.186703	1.97	.178506	.056820	.356675
1.42	.159511	.050774	.189510	1.98	.178490	.056815	.359813
1.43	.160237	.051005	.192330	1.99	.178463	.056807	.362951
1.44	.160948	.051231	.195163	2.00	.178425	.056794	.366087
1.45	.161644	.051453	.198009	2.02	.178315	.056760	.372355
1.46	.162326	.051670	.200866	2.04	.178162	.056711	.378614
1.47	.162993	.051882	.203736	2.06	.177967	.056649	.384865
1.48	.163645	.052090	.206617	2.08	.177730	.056573	.391103
1.49	.164282	.052293	.209509	2.10	.177452	.056485	.397328
1.50	.164905	.052491	.212412	2.12	.177134	.056384	.403538
1.51	.165514	.052685	.215327	2.14	.176778	.056270	.409731
1.52	.166107	.052874	.218251	2.16	.176383	.056144	.415904
1.53	.166686	.053058	.221187	2.18	.175951	.056007	.422056
1.54	.167251	.053238	.224132	2.20	.175483	.055858	.42832
1.55	.167800	.053413	.227087	2.22	.174979	.055698	.435015
1.56	.168336	.053583	.230051	2.24	.174440	.055526	.441180
1.57	.168857	.053749	.233025	2.26	.173868	.055344	.447325
1.58	.169363	.053910	.236008	2.28	.173263	.055151	.453449
1.59	.169855	.054067	.238999	2.30	.172626	.054949	.459551
1.60	.170333	.054219	.241999	2.32	.171958	.054736	.465631
1.61	.170796	.054366	.245007	2.34	.171260	.054514	.471686
1.62	.171245	.054509	.248023	2.36	.170533	.054282	.477716
1.63	.171680	.054648	.251047	2.38	.169777	.054042	.483720
1.64	.172101	.054782	.254079	2.40	.168993	.053792	.489697
1.65	.172508	.054911	.257117	2.42	.168183	.053534	.495645
1.66	.172901	.055036	.260163	2.44	.167347	.053268	.501565
1.67	.173279	.055157	.263215	2.46	.166486	.052994	.507454
1.68	.173644	.055273	.266274	2.48	.165600	.052712	.513313
1.69	.173995	.055384	.269339	2.50	.164692	.052423	.519140
1.70	.174332	.055492	.272410	2.52	.163761	.052127	.524935
1.71	.174655	.055595	.275486	2.54	.162808	.051823	.530697
1.72	.174965	.055693	.278568	2.56	.161834	.051513	.536424

Notes: (1) Units of the tabulated functions are as follows:  
 $\omega/T$  -  $\text{cm}^{-1} \text{K}^{-1}$ ;  $W_{\omega}^0/T^3$  -  $\text{watts cm}^{-1} \text{K}^{-3}$   
 $N_{\omega}^0/T^3$  -  $\text{watts cm}^{-1} \text{st}^{-1} \text{K}^{-3}$ ;  $\int_0^{\omega} W_{\omega}^0 d\omega/\sigma T^4$  - dimensionless

(2) Tabulated values based on the following constants from Table 2.2:  $c_1 = 3.7405 \times 10^{-12}$  watts  $\text{cm}^2$ ;  $c_2 = 1.43879$  cm K;  $\sigma = 5.6697 \times 10^{-12}$  watts  $\text{cm}^{-2} \text{K}^{-4}$ .

TABLE A2-1. (Continued)

$\omega/T$	$\frac{W_{\omega}^0 \times 10^{11}}{T^3}$	$\frac{N_{\omega}^0 \times 10^{11}}{T^3}$	$\frac{\int_0^{\omega} W_{\omega}^0 d\omega}{\sigma T^4}$	$\omega/T$	$\frac{W_{\omega}^0 \times 10^{11}}{T^3}$	$\frac{N_{\omega}^0 \times 10^{11}}{T^3}$	$\frac{\int_0^{\omega} W_{\omega}^0 d\omega}{\sigma T^4}$
2.58	.160840	.051197	.542117	3.70	.092828	.029548	.794042
2.60	.159827	.050874	.547774	3.72	.091653	.029174	.797297
2.62	.158795	.050546	.553395	3.74	.090485	.028802	.800510
2.64	.157745	.050212	.558980	3.76	.089325	.028433	.803682
2.66	.156679	.049872	.564527	3.78	.088172	.028066	.806813
2.68	.155596	.049528	.570036	3.80	.087027	.027702	.809904
2.70	.154498	.049178	.575507	3.82	.085891	.027340	.812955
2.72	.153385	.048824	.580939	3.84	.084762	.026981	.815966
2.74	.152258	.048465	.586331	3.86	.083642	.026624	.818937
2.76	.151117	.048102	.591683	3.88	.082530	.026270	.821868
2.78	.149964	.047735	.596995	3.90	.081427	.025919	.824761
2.80	.148799	.047364	.602266	3.92	.080332	.025570	.827615
2.82	.147622	.046990	.607496	3.94	.079246	.025225	.830430
2.84	.146435	.046612	.612683	3.96	.078169	.024882	.833207
2.86	.145238	.046231	.617829	3.98	.077101	.024542	.835946
2.88	.144032	.045847	.622933	4.00	.076042	.024205	.838648
2.90	.142817	.045460	.627993	4.02	.074992	.023871	.841312
2.92	.141594	.045071	.633011	4.04	.073951	.023539	.843940
2.94	.140363	.044679	.637985	4.06	.072920	.023211	.846531
2.96	.139126	.044285	.642916	4.08	.071898	.022886	.849086
2.98	.137882	.043889	.647803	4.10	.070885	.022563	.851605
3.00	.136632	.043491	.652646	4.12	.069882	.022244	.854089
3.02	.135378	.043092	.657445	4.14	.068888	.021928	.856537
3.04	.134118	.042691	.662200	4.16	.067903	.021614	.858950
3.06	.132855	.042289	.666910	4.18	.066929	.021304	.861329
3.08	.131588	.041886	.671575	4.20	.065964	.020997	.863673
3.10	.130317	.041481	.676196	4.22	.065008	.020693	.865984
3.12	.129045	.041076	.680771	4.24	.064062	.020392	.868261
3.14	.127770	.040670	.685302	4.26	.063126	.020094	.870505
3.16	.126493	.040264	.689788	4.28	.062199	.019799	.872716
3.18	.125216	.039857	.694229	4.30	.061283	.019507	.874894
3.20	.123937	.039450	.698624	4.32	.060375	.019218	.877040
3.22	.122658	.039043	.702975	4.34	.059478	.018932	.879155
3.24	.121380	.038636	.707280	4.36	.058590	.018650	.881238
3.26	.120102	.038230	.711540	4.38	.057712	.018370	.883290
3.28	.118825	.037823	.715756	4.40	.056844	.018094	.885311
3.30	.117549	.037417	.719926	4.42	.055985	.017821	.887301
3.32	.116275	.037012	.724051	4.44	.055136	.017550	.889262
3.34	.115003	.036607	.728131	4.46	.054297	.017283	.891192
3.36	.113734	.036203	.732167	4.48	.053467	.017019	.893093
3.38	.112467	.035799	.736157	4.50	.052647	.016758	.894965
3.40	.111204	.035397	.740103	4.52	.051836	.016500	.896809
3.42	.109944	.034996	.744005	4.54	.051035	.016245	.898624
3.44	.108688	.034596	.747862	4.56	.050244	.015993	.900410
3.46	.107436	.034198	.751675	4.58	.049462	.015744	.902169
3.48	.106188	.033801	.755444	4.60	.048689	.015498	.903901
3.50	.104945	.033405	.759168	4.62	.047926	.015255	.905605
3.52	.103707	.033011	.762850	4.64	.047172	.015015	.907283
3.54	.102474	.032619	.766487	4.66	.046428	.014778	.908934
3.56	.101247	.032228	.770081	4.68	.045693	.014544	.910560
3.58	.100025	.031839	.773632	4.70	.044967	.014313	.912159
3.60	.098809	.031452	.777140	4.72	.044250	.014085	.913733
3.62	.097600	.031067	.780605	4.74	.043542	.013860	.915282
3.64	.096397	.030684	.784027	4.76	.042843	.013638	.916806
3.66	.095201	.030303	.787408	4.78	.042154	.013418	.918305
3.68	.094011	.029925	.790746	4.80	.041473	.013201	.919781

Notes: (1) Units of the tabulated functions are as follows:  
 $\omega/T$  -  $\text{cm}^{-1} \text{K}^{-1}$ ;  $W_{\omega}^0/T^3$  -  $\text{watts cm}^{-1} \text{K}^{-3}$   
 $N_{\omega}^0/T^3$  -  $\text{watts cm}^{-1} \text{st}^{-1} \text{K}^{-3}$ ;  $\int_0^{\omega} W_{\omega}^0 d\omega / \sigma T^4$  - dimensionless

(2) Tabulated values based on the following constants from Table 2.2:  $c_1 = 3.7405 \times 10^{-12}$  watts  $\text{cm}^2$ ;  $c_2 = 1.43879$  cm K;  $\sigma = 5.6697 \times 10^{-12}$  watts  $\text{cm}^{-2} \text{K}^{-4}$ .

TABLE A2-1. (Concluded)

$\omega/T$	$\frac{W_{\omega}^0 \times 10^{11}}{T^3}$	$\frac{N_{\omega}^0 \times 10^{11}}{T^3}$	$\frac{\int_0^{\omega} W_{\omega}^0 d\omega}{\sigma T^4}$	$\omega/T$	$\frac{W_{\omega}^0 \times 10^{11}}{T^3}$	$\frac{N_{\omega}^0 \times 10^{11}}{T^3}$	$\frac{\int_0^{\omega} W_{\omega}^0 d\omega}{\sigma T^4}$
4.82	.040801	.012988	.921232	7.35	.003794	.001208	.993755
4.84	.040139	.012776	.922660	7.40	.003603	.001147	.994081
4.86	.039484	.012568	.924065	7.45	.003421	.001089	.994391
4.88	.038839	.012363	.925447	7.50	.003249	.001034	.994685
4.90	.038202	.012160	.926806	7.55	.003084	.000982	.994964
4.92	.037574	.011960	.928142	7.60	.002927	.000932	.995229
4.94	.036954	.011763	.929457	7.65	.002778	.000884	.995481
4.96	.036343	.011568	.930750	7.70	.002636	.000839	.995720
4.98	.035740	.011376	.932022	7.75	.002501	.000796	.995946
5.00	.035146	.011187	.933273	7.80	.002373	.000755	.996161
5.05	.033695	.010726	.936309	7.85	.002251	.000717	.996365
5.10	.032296	.010280	.939219	7.90	.002135	.000680	.996559
5.15	.030945	.009850	.942008	7.95	.002025	.000645	.996742
5.20	.029643	.009436	.944680	8.00	.001920	.000611	.996916
5.25	.028388	.009036	.947239	8.05	.001821	.000580	.997081
5.30	.027178	.008651	.949689	8.10	.001726	.000549	.997237
5.35	.026013	.008280	.952035	8.15	.001636	.000521	.997386
5.40	.024892	.007923	.954280	8.20	.001551	.000494	.997526
5.45	.023813	.007580	.956428	8.25	.001470	.000468	.997659
5.50	.022775	.007249	.958482	8.30	.001393	.000443	.997786
5.55	.021777	.006932	.960447	8.35	.001320	.000420	.997905
5.60	.020817	.006626	.962325	8.40	.001250	.000398	.998018
5.65	.019895	.006333	.964120	8.45	.001184	.000377	.998126
5.70	.019010	.006051	.965836	8.50	.001122	.000357	.998227
5.75	.018160	.005780	.967475	8.55	.001062	.000338	.998324
5.80	.017344	.005521	.969041	8.60	.001006	.000320	.998415
5.85	.016560	.005271	.970536	8.65	.000953	.000303	.998501
5.90	.015809	.005032	.971963	8.70	.000902	.000287	.998583
5.95	.015089	.004803	.973326	8.75	.000854	.000272	.998661
6.00	.014398	.004583	.974626	8.80	.000808	.000257	.998734
6.05	.013736	.004372	.975867	8.85	.000765	.000244	.998803
6.10	.013102	.004171	.977051	8.90	.000724	.000231	.998869
6.15	.012495	.003977	.978179	8.95	.000685	.000218	.998931
6.20	.011914	.003792	.979256	9.00	.000649	.000206	.998990
6.25	.011357	.003615	.980282	9.05	.000614	.000195	.999046
6.30	.010824	.003445	.981260	9.10	.000581	.000185	.999098
6.35	.010314	.003283	.982192	9.15	.000549	.000175	.999148
6.40	.009827	.003128	.983080	9.20	.000520	.000165	.999195
6.45	.009361	.002980	.983927	9.25	.000491	.000156	.999240
6.50	.008915	.002838	.984732	9.30	.000465	.000148	.999282
6.55	.008489	.002702	.985500	9.35	.000439	.000140	.999322
6.60	.008082	.002573	.986231	9.40	.000416	.000132	.999359
6.65	.007693	.002449	.986926	9.45	.000393	.000125	.999395
6.70	.007322	.002331	.987588	9.50	.000371	.000118	.999429
6.75	.006967	.002218	.988219	9.55	.000351	.000112	.999461
6.80	.006629	.002110	.988818	9.60	.000332	.000106	.999491
6.85	.006306	.002007	.989389	9.65	.000314	.000100	.999519
6.90	.005998	.001909	.989931	9.70	.000297	.000094	.999546
6.95	.005703	.001815	.990447	9.75	.000280	.000089	.999572
7.00	.005423	.001726	.990938	9.80	.000265	.000084	.999596
7.05	.005155	.001641	.991404	9.85	.000250	.000080	.999618
7.10	.004900	.001560	.991848	9.90	.000236	.000075	.999640
7.15	.004657	.001482	.992269	9.95	.000223	.000071	.999660
7.20	.004425	.001409	.992670	10.00	.000211	.000067	.999679
7.25	.004205	.001338	.993050				
7.30	.003994	.001271	.993412				

Notes: (1) Units of the tabulated functions are as follows:

$$\omega/T - \text{cm}^{-1} \text{K}^{-1}; W_{\omega}^0/T^3 - \text{watts cm}^{-1} \text{K}^{-3}$$

$$N_{\omega}^0/T^3 - \text{watts cm}^{-1} \text{st}^{-1} \text{K}^{-3}; \int_0^{\omega} W_{\omega}^0 d\omega/\sigma T^4 - \text{dimensionless}$$

(2) Tabulated values based on the following constants from Table 2.2:  $c_1 = 3.7405 \times 10^{-12}$  watts  $\text{cm}^2$ ;  $c_2 = 1.43879$  cm K;  $\sigma = 5.6697 \times 10^{-12}$  watts  $\text{cm}^{-2} \text{K}^{-4}$ .

TABLE A2-2. ABSORPTION COEFFICIENTS FOR CO  
k (per cm at STP)

1/cm	300K	600K	1200K	1800K	2400K	3000K
1100				3.934E-16	4.727E-12	1.708E-09
1200				5.866E-14	2.028E-10	3.210E-08
1300				7.815E-12	7.571E-09	5.416E-07
1400			5.874E-15	7.612E-10	2.412E-07	8.071E-06
1500			4.834E-12	6.254E-08	6.395E-06	1.040E-04
1550				5.134E-07	3.041E-05	3.501E-04
1600		6.555E-19	2.679E-09	3.909E-06	1.361E-04	1.123E-03
1650				2.739E-05	5.700E-04	3.410E-03
1700		9.802E-14	9.157E-07	1.747E-04	2.214E-03	9.736E-03
1750				1.003E-03	7.899E-03	2.590E-02
1800	2.607E-18	4.540E-09	1.702E-04	5.096E-03	2.555E-02	6.343E-02
1850	4.534E-14			2.248E-02	7.365E-02	1.408E-01
1900	3.317E-10	4.550E-05	1.414E-02	8.377E-02	1.849E-01	2.773E-01
1950	8.733E-07	2.158E-03		2.537E-01	3.906E-01	4.691E-01
2000	6.674E-04	5.370E-02	3.686E-01	5.871E-01	6.567E-01	6.474E-01
2025				7.825E-01	7.592E-01	6.873E-01
2050	1.076E-01	5.810E-01	9.703E-01	9.272E-01	7.929E-01	6.701E-01
2075				9.401E-01	7.286E-01	5.950E-01
2100	2.054E+00	1.847E+00	1.152E+00	7.690E-01	5.813E-01	4.972E-01
2125	2.413E+00	1.098E+00	6.969E-01	5.050E-01	4.592E-01	4.639E-01
2150	1.207E+00	6.295E-01	4.884E-01	5.346E-01	5.819E-01	6.169E-01
2175	3.581E+00	2.423E+00	1.481E+00	1.178E+00	1.041E+00	9.627E-01
2200	1.470E+00	2.198E+00	1.846E+00	1.506E+00	1.297E+00	1.161E+00
2225	1.395E-01	8.704E-01	1.428E+00	1.379E+00	1.258E+00	1.148E+00

TABLE A2-2. (Concluded)

1/cm	300K	600K	1200K	1800K	2400K	3000K
2250	2.337E-03	1.398E-01	6.883E-01	9.146E-01	9.539E-01	9.311E-01
2275	3.789E-06	6.931E-03	1.849E-01	4.122E-01	5.413E-01	5.980E-01
2300	1.783E-10	5.948E-05	2.123E-02	1.078E-01	2.061E-01	2.794E-01
2325	1.214E-17	2.070E-08	5.281E-04	1.091E-02	4.008E-02	7.619E-02
2350		9.665E-17	7.579E-08	4.912E-05	1.013E-03	5.444E-03

TABLE A2-3. LINE SPACING FOR CO  
1/d (cm)

1/cm	300K	600K	1200K	1800K	2400K	3000K
1100				1.112E+00	1.118E+00	1.964E+00
1200				1.141E+00	1.168E+00	2.018E+00
1300				1.094E+00	1.215E+00	2.051E+00
1400			7.739E-01	1.169E+00	1.258E+00	2.058E+00
1500			7.649E-01	1.164E+00	1.295E+00	2.031E+00
1550				1.156E+00	1.309E+00	2.003E+00
1600		3.675E-01	7.475E-01	1.152E+00	1.319E+00	1.962E+00
1650				1.127E+00	1.324E+00	1.906E+00
1700		3.513E-01	7.201E-01	1.105E+00	1.322E+00	1.833E+00
1750				1.076E+00	1.311E+00	1.740E+00
1800	1.977E-01	3.343E-01	6.822E-01	1.040E+00	1.288E+00	1.657E+00
1850	1.998E-01			9.965E-01	1.246E+00	1.573E+00
1900	2.033E-01	3.181E-01	6.309E-01	9.397E-01	1.174E+00	1.477E+00
1950	2.085E-01	3.105E-01		8.743E-01	1.093E+00	1.387E+00
2000	2.161E-01	3.034E-01	5.562E-01	8.051E-01	1.032E+00	1.351E+00
2025				7.705E-01	1.015E+00	1.357E+00
2050	2.271E-01	2.960E-01	5.059E-01	7.414E-01	1.024E+00	1.415E+00
2075				7.380E-01	1.090E+00	1.563E+00
2100	2.422E-01	2.845E-01	4.779E-01	8.102E-01	1.279E+00	1.828E+00
2125	2.540E-01	3.717E-01	5.871E-01	1.089E+00	1.600E+00	2.043E+00
2150	2.735E-01	3.914E-01	8.267E-01	1.222E+00	1.561E+00	1.879E+00
2175	2.867E-01	3.449E-01	6.472E-01	1.024E+00	1.375E+00	1.697E+00
2200	3.074E-01	3.471E-01	5.892E-01	9.183E-01	1.251E+00	1.613E+00
2225	3.353E-01	3.611E-01	5.586E-01	8.474E-01	1.147E+00	1.465E+00

TABLE A2-3. (Concluded)

1/cm	300K	600K	1200K	1800K	2400K	300K
2250	3.732E-01	3.879E-01	5.423E-01	7.935E-01	1.468E+00	1.341E+00
2275	4.288E-01	4.343E-01	5.423E-01	7.521E-01	9.808E-01	1.210E+00
2300	5.205E-01	5.206E-01	5.746E-01	7.264E-01	8.906E-01	1.036E+00
2325	7.170E-01	7.157E-01	7.156E-01	7.222E-01	7.156E-01	7.175E-01
2350		2.238E-00	2.247E+00	2.329E+00	2.442E+00	2.627E+00

GENERAL APPENDIX

TABLE A2-4. INTEGRATED ABSORPTANCE OF CO FUNDAMENTAL BAND SYSTEM ( $\text{cm}^{-1}$ )

T = 300K, C = 0 P <sub>T</sub> (atm) =			
u(cm) <sub>STP</sub>	.01	.1	1
.1	1.81 E+0	5.06 E+0	1.30 E+1
1.	5.37 E+0	1.60 E+1	4.38 E+1
10.	1.62 E+1	4.56 E+1	1.07 E+2
100.	4.61 E+1	1.09 E+2	1.78 E+2
1000.	1.09 E+2	1.79 E+2	2.23 E+2
10000.	1.80 E+2	2.24 E+2	2.51 E+2
T = 600K, C = 0 P <sub>T</sub> (atm) =			
u(cm) <sub>STP</sub>	.01	.1	1
.1	1.77 E+0	3.82 E+0	8.44 E+0
1.	4.50 E+0	1.24 E+1	3.43 E+1
10.	1.30 E+1	3.75 E+1	9.80 E+1
100.	3.79 E+1	1.00 E+2	2.03 E+2
1000.	1.01 E+2	2.05 E+2	2.86 E+2
10000.	2.05 E+2	2.88 E+2	3.40 E+2
T = 1200K, C = 0 P <sub>T</sub> (atm) =			
u(cm) <sub>STP</sub>	.01	.1	1
.1	2.70 E+0	3.58 E+0	5.60 E+0
1.	5.97 E+0	1.22 E+1	3.00 E+1
10.	1.40 E+1	3.67 E+1	9.82 E+1
100.	3.81 E+1	1.03 E+2	2.34 E+2
1000.	1.04 E+2	2.37 E+2	3.73 E+2
10000.	2.38 E+2	3.77 E+2	4.58 E+2

TABLE A2-4. (Concluded)

T = 1800K, C = 0 P <sub>T</sub> (atm) =			
u(cm) <sub>STP</sub>	.01	.1	1
.1	3.17 E+0	3.36 E+0	4.04 E+0
1.	8.71 E+0	1.30 E+1	2.65 E+1
10.	1.76 E+1	3.82 E+1	9.85 E+1
100.	4.15 E+1	1.07 E+2	2.51 E+2
1000.	1.10 E+2	2.58 E+2	4.33 E+2
10000.	2.60 E+2	4.39 E+2	5.47 E+2
T = 2400K, C = 0 P <sub>T</sub> (atm) =			
u(cm) <sub>STP</sub>	.01	.1	1
.1	3.00 E+0	3.02 E+0	3.16 E+0
1.	1.16 E+1	1.43 E+1	2.37 E+1
10.	2.31 E+1	4.12 E+1	9.91 E+1
100.	4.74 E+1	1.13 E+2	2.65 E+2
1000.	1.17 E+2	2.74 E+2	4.78 E+2
10000.	2.79 E+2	4.87 E+2	6.18 E+2
T = 3000K, C = 0 P <sub>T</sub> (atm) =			
u(cm) <sub>STP</sub>	.01	.1	1
.1	2.57 E+0	2.57 E+0	2.59 E+0
1.	1.37 E+1	1.51 E+1	2.09 E+1
10.	3.04 E+1	4.54 E+1	9.82 E+1
100.	6.62 E+1	1.28 E+2	2.83 E+2
1000.	1.46 E+2	3.08 E+2	5.33 E+2
10000.	3.16 E+2	5.45 E+2	6.92 E+2

TABLE A2-5. TOTAL EMISSIVITY OF CO

T = 300K, C = 0 P <sub>T</sub> (atm) =			
u(cm) <sub>STP</sub>	.01	.1	1
.1	5.12 E-5	1.43 E-4	3.65 E-4
1.	1.52 E-4	4.51 E-4	1.24 E-3
10.	4.59 E-4	1.30 E-3	3.04 E-3
100.	1.30 E-3	3.09 E-3	5.13 E-3
1000.	3.10 E-3	5.18 E-3	6.56 E-3
10000.	5.19 E-3	6.59 E-3	7.60 E-3
T = 600K, C = 0 P <sub>T</sub> (atm) =			
u(cm) <sub>STP</sub>	.01	.1	1
.1	5.36 E-4	1.16 E-3	2.55 E-3
1.	1.36 E-3	3.78 E-3	1.04 E-2
10.	3.94 E-3	1.14 E-2	2.98 E-2
100.	1.15 E-2	3.06 E-2	6.20 E-2
1000.	3.07 E-2	6.26 E-2	8.83 E-2
10000.	6.27 E-2	8.90 E-2	1.05 E-1
T = 1200K, C = 0 P <sub>T</sub> (atm) =			
u(cm) <sub>STP</sub>	.01	.1	1
.1	7.69 E-4	9.58 E-4	1.47 E-3
1.	1.72 E-3	3.28 E-3	7.88 E-3
10.	4.00 E-3	1.00 E-2	2.61 E-2
100.	1.07 E-2	2.84 E-2	6.43 E-2
1000.	2.90 E-2	6.64 E-2	1.10 E-1
10000.	6.69 E-2	1.12 E-1	1.52 E-1

TABLE A2-5. (Concluded)

T = 1800K, C = 0 P <sub>T</sub> (atm) =			
u(cm) <sub>STP</sub>	.01	.1	1
.1	4.72 E-4	4.76 E-4	5.56 E-4
1.	1.32 E-3	1.87 E-3	3.65 E-3
10.	2.90 E-3	5.71 E-3	1.39 E-2
100.	7.03 E-3	1.66 E-2	3.80 E-2
1000.	1.78 E-2	4.10 E-2	7.41 E-2
10000.	4.22 E-2	7.69 E-2	1.15 E-1
T = 2400K, C = 0 P <sub>T</sub> (atm) =			
u(cm) <sub>STP</sub>	.01	.1	1
.1	2.40 E-4	2.34 E-4	2.39 E-4
1.	9.45 E-4	1.13 E-3	1.80 E-3
10.	2.14 E-3	3.49 E-3	7.78 E-3
100.	5.06 E-3	1.02 E-2	2.29 E-2
1000.	1.19 E-2	2.60 E-2	4.84 E-2
10000.	2.78 E-2	5.17 E-2	8.10 E-2
T = 3000K, C = 0 P <sub>T</sub> (atm) =			
u(cm) <sub>STP</sub>	.01	.1	1
.1	1.16 E-4	1.15 E-4	1.17 E-4
1.	6.27 E-4	6.85 E-4	9.46 E-4
10.	1.65 E-3	2.30 E-3	4.59 E-3
100.	4.35 E-3	7.19 E-3	1.46 E-2
1000.	9.86 E-3	1.84 E-2	3.38 E-2
10000.	2.18 E-2	3.80 E-2	5.83 E-2

TABLE A2-6. ABSORPTION COEFFICIENTS FOR NO  
k (per cm at STP)

1/cm	300K	600K	1200K	1800K	2400K	3000K
800				3.956E-16	3.480E-12	
900				4.133E-14	1.194E-10	
1000			1.753E-18	3.724E-12	3.616E-09	
1050				3.329E-11	1.892E-08	
1100			1.328E-15	2.850E-10	9.548E-08	4.982E-06
1150				2.329E-09	4.634E-07	1.608E-05
1200			7.735E-13	1.810E-08	2.156E-06	5.028E-05
1250				1.332E-07	9.578E-06	1.520E-04
1300		1.169E-20	3.302E-10	9.231E-07	4.045E-05	4.428E-04
1350				5.988E-06	1.615E-04	1.239E-03
1400		1.378E-15	9.659E-08	3.608E-05	6.055E-04	3.318E-03
1450		3.412E-13		1.999E-04	2.114E-03	8.471E-03
1500	7.940E-22	6.536E-11	1.754E-05	1.007E-03	6.803E-03	2.032E-02
1525						3.060E-02
1550	1.882E-17	9.306E-09		4.537E-03	1.990E-02	4.516E-02
1575						6.509E-02
1600	2.250E-13	9.365E-07	1.692E-03	1.790E-02	5.201E-02	9.152E-02
1625	1.832E-11					1.247E-01
1650	1.194E-09	6.228E-05	1.212E-02	6.002E-02	1.185E-01	1.646E-01
1675	6.092E-08			1.021E-01	1.682E-01	2.094E-01
1700	2.364E-06	2.492E-03	6.567E-02	1.635E-01	2.269E-01	2.548E-01
1725	6.743E-05			2.441E-01	2.887E-01	2.946E-01
1750	1.355E-03	5.210E-02	2.462E-01	3.349E-01	3.418E-01	3.213E-01
1775	1.813E-02	1.744E-01		4.250E-01		3.270E-01
1800	1.497E-01	4.462E-01	5.370E-01	4.460E-01	3.622E-01	3.100E-01
1825	6.764E-01	8.014E-01	5.739E-01	4.012E-01		2.793E-01

TABLE A2-6. (Concluded)

1/cm	300K	600K	1200K	1800K	2400K	3000K
1850	1.304E+00	8.246E-01	4.140E-01	2.896E-01	2.617E-01	2.620E-01
1875	1.026E-01	7.629E-02	1.650E-01	2.420E-01	2.888E-01	3.173E-01
1900	1.764E+00	1.070E+00	6.622E-01	5.538E-01	5.048E-01	4.743E-01
1925	9.247E-01	1.182E+00	9.180E-01	7.366E-01	6.317E-01	5.621E-01
1950	7.783E-02	4.629E-01	7.173E-01	6.696E-01	5.986E-01	5.347E-01
1975	6.066E-04	5.362E-02	3.048E-01	4.070E-01	4.168E-01	3.910E-01
2000	9.184E-12	8.886E-04	5.179E-02	1.391E-01	1.935E-01	2.213E-01
2025	8.428E-16	1.367E-07	1.033E-03	1.382E-02	4.061E-02	6.730E-02

TABLE A2-7. LINE SPACING FOR NO  
1/d (cm)

1/cm	300K	600K	1200K	1800K	2400K	3000K
800				2.205E+00	2.209E+00	
900				2.396E+00	2.382E+00	
1000			1.775E+00	2.590E+00	2.569E+00	
1050				2.685E+00	2.667E+00	
1100			1.886E+00	2.778E+00	2.769E+00	5.503E+00
1150				2.865E+00	2.872E+00	5.683E+00
1200			1.979E+00	2.944E+00	2.978E+00	5.817E+00
1250				3.014E+00	3.083E+00	5.886E+00
1300		1.071E+00	2.041E+00	3.068E+00	3.187E+00	5.863E+00
1350				3.103E+00	3.285E+00	5.713E+00
1400		1.052E+00	2.058E+00	3.113E+00	3.370E+00	5.304E+00
1450		1.034E+00		3.092E+00	3.581E+00	5.174E+00
1500	5.133E-01	1.010E+00	2.011E+00	3.030E+00	3.464E+00	5.096E+00
1525						4.813E+00
1550	5.110E-01	9.808E-01		2.919E+00	3.432E+00	4.610E+00
1575						4.407E+00
1600	5.098E-01	9.463E-01	1.878E+00	2.742E+00	3.288E+00	5.024E+00
1625	5.100E-01					4.171E+00
1650	5.108E-01	9.076E-01	1.772E+00	2.508E+00	3.032E+00	4.013E+00
1675	5.128E-01			2.418E+00	2.987E+00	3.897E+00
1700	5.160E-01	8.648E-01	1.627E+00	2.327E+00	2.962E+00	3.799E+00
1725	5.209E-01			2.238E+00	2.955E+00	3.725E+00
1750	5.278E-01	8.184E-01	1.470E+00	2.153E+00	2.989E+00	4.073E+00
1775	5.371E-01	7.919E-01		2.334E+00		4.104E+00
1800	5.500E-01	7.623E-01	1.317E+00	2.081E+00	3.116E+00	4.264E+00
1825	5.662E-01	7.275E-01	1.023E+00	1.995E+00		4.460E+00

TABLE A2-7. (Concluded)

1/cm	300K	600K	1200K	1800K	2400K	3000K
1850	5.837E-01	6.731E-01	1.330E+00	2.553E+00	3.679E+00	4.350E+00
1875	7.071E-01	1.419E+00	2.226E+00	3.044E+00	3.963E+00	4.959E+00
1900	6.891E-01	9.146E-01	1.815E+00	2.787E+00	3.686E+00	4.457E+00
1925	7.522E-01	8.895E-01	1.579E+00	2.420E+00	3.189E+00	3.782E+00
1950	8.497E-01	9.261E-01	1.453E+00	2.141E+00	2.720E+00	3.108E+00
1975	1.007E+00	1.035E+00	1.381E+00	1.843E+00	2.155E+00	2.327E+00
2000	1.311E+00	1.312E+00	1.440E+00	1.955E+00	2.793E+00	3.747E+00
2025	2.377E+00	2.377E+00	2.377E+00	2.391E+00	2.439E+00	2.524E+00

TABLE A2-8. INTEGRATED ABSORPTANCE OF NO FUNDAMENTAL BAND SYSTEM ( $\text{cm}^{-1}$ )

T = 300K, C = 0 P <sub>T</sub> (atm) =			
u(cm) <sub>STP</sub>	.01	.1	1
.1	1.60 E+0	3.72 E+0	7.84 E+0
1.	4.43 E+0	1.25 E+1	3.23 E+1
10.	1.30 E+1	3.66 E+1	8.66 E+1
100.	3.70 E+1	8.94 E+1	1.55 E+2
1000.	8.97 E+1	1.57 E+2	2.04 E+2
10000.	1.57 E+2	2.05 E+2	2.36 E+2
T = 600K, C = 0 P <sub>T</sub> (atm) =			
u(cm) <sub>STP</sub>	.01	.1	1
.1	1.84 E+0	2.94 E+0	4.93 E+0
1.	4.56 E+0	1.05 E+1	2.58 E+1
10.	1.18 E+1	3.23 E+1	8.27 E+1
100.	3.33 E+1	8.76 E+1	1.80 E+2
1000.	8.84 E+1	1.84 E+2	2.64 E+2
10000.	1.84 E+2	2.67 E+2	3.15 E+2
T = 1200K, C = 0 P <sub>T</sub> (atm) =			
u(cm) <sub>STP</sub>	.01	.1	1
.1	2.34 E+0	2.45 E+0	2.83 E+0
1.	7.26 E+0	1.07 E+1	2.03 E+1
10.	1.53 E+1	3.29 E+1	8.16 E+1
100.	3.64 E+1	9.21 E+1	2.07 E+2
1000.	9.45 E+1	2.15 E+2	3.46 E+2
10000.	2.17 E+2	3.51 E+2	4.29 E+2

TABLE A2-8. (Concluded)

T = 1800K, C = 0 P <sub>T</sub> (atm) =			
u(cm) <sub>STP</sub>	.01	.1	1
.1	1.92 E+0	1.93 E+0	1.95 E+0
1.	1.02 E+1	1.16 E+1	1.63 E+1
10.	2.25 E+1	3.64 E+1	8.04 E+1
100.	4.47 E+1	9.88 E+1	2.24 E+2
1000.	1.05 E+2	2.37 E+2	3.99 E+2
10000.	2.42 E+2	4.10 E+2	5.07 E+2
T = 2400K, C = 0 P <sub>T</sub> (atm) =			
u(cm) <sub>STP</sub>	.01	.1	1
.1	1.50 E+0	1.50 E+0	1.50 E+0
1.	1.12 E+1	1.15 E+1	1.34 E+1
10.	3.04 E+1	4.05 E+1	7.70 E+1
100.	5.60 E+1	1.05 E+2	2.34 E+2
1000.	1.16 E+2	2.53 E+2	4.40 E+2
10000.	2.61 E+2	4.54 E+2	5.73 E+2
T = 3000K, C = 0 P <sub>T</sub> (atm) =			
u(cm) <sub>STP</sub>	.01	.1	1
.1	1.22 E+0	1.22 E+0	1.22 E+0
1.	1.07 E+1	1.08 E+1	1.13 E+1
10.	3.82 E+1	4.51 E+1	7.30 E+1
100.	7.23 E+1	1.16 E+2	2.43 E+2
1000.	1.37 E+2	2.73 E+2	2.82 E+2
10000.	2.90 E+2	5.06 E+2	6.48 E+2

TABLE A2-9. TOTAL EMISSIVITY OF NO

T = 300K, C = 0 P <sub>T</sub> (atm) =			
u(cm) <sub>STP</sub>	.01	.1	1
.1	1.08 E-4	2.50 E-4	5.24 E-4
1.	2.99 E-4	8.41 E-4	2.18 E-3
10.	8.78 E-4	2.48 E-3	5.88 E-3
100.	2.51 E-3	6.09 E-3	1.07 E-2
1000.	6.12 E-3	1.09 E-2	1.43 E-2
10000.	1.09 E-2	1.45 E-2	1.70 E-2
T = 600K, C = 0 P <sub>T</sub> (atm) =			
u(cm) <sub>STP</sub>	.01	.1	1
.1	7.15 E-4	1.14 E-3	1.90 E-3
1.	1.77 E-3	4.09 E-3	1.00 E-2
10.	4.59 E-3	1.25 E-2	3.21 E-2
100.	1.29 E-2	3.40 E-2	7.03 E-2
1000.	3.43 E-2	7.18 E-2	1.04 E-1
10000.	7.22 E-2	1.05 E-1	1.25 E-1
T = 1200K, C = 0 P <sub>T</sub> (atm) =			
u(cm) <sub>STP</sub>	.01	.1	1
.1	6.19 E-4	9.18 E-4	7.10 E-4
1.	1.95 E-3	2.75 E-3	5.12 E-3
10.	4.43 E-3	8.89 E-3	2.11 E-2
100.	1.08 E-2	2.55 E-2	5.69 E-2
1000.	2.71 E-2	6.16 E-2	1.06 E-1
10000.	6.30 E-2	1.10 E-1	1.54 E-1

TABLE A2-9. (Concluded)

T = 1800K, C = 0 P <sub>T</sub> (atm) =			
u(cm) <sub>STP</sub>	.01	.1	1
.1	2.30 E-4	2.35 E-4	2.44 E-4
1.	1.26 E-3	1.44 E-3	2.04 E-3
10.	3.37 E-3	5.01 E-3	1.06 E-2
100.	7.67 E-3	1.48 E-2	3.24 E-2
1000.	1.78 E-2	3.76 E-3	6.83 E-2
10000.	4.05 E-2	7.40 E-2	1.12 E-1
T = 2400K, C = 0 P <sub>T</sub> (atm) =			
u(cm) <sub>STP</sub>	.01	.1	1
.1	9.43 E-5	9.65 E-5	9.90 E-5
1.	7.24 E-4	7.57 E-4	8.86 E-4
10.	2.40 E-3	3.01 E-3	5.24 E-3
100.	5.76 E-3	9.15 E-3	1.83 E-2
1000.	1.28 E-2	2.40 E-2	4.33 E-2
10000.	2.77 E-2	4.99 E-2	7.84 E-2
T = 3000K, C = 0 P <sub>T</sub> (atm) =			
u(cm) <sub>STP</sub>	.01	.1	1
.1	4.57 E-5	4.59 E-5	4.70 E-5
1.	4.13 E-4	4.16 E-4	4.40 E-4
10.	1.78 E-3	1.95 E-3	2.93 E-3
100.	4.47 E-3	6.25 E-3	1.13 E-2
1000.	1.01 E-2	1.57 E-2	2.95 E-2
10000.	2.13 E-2	3.59 E-2	5.61 E-2

TABLE A2-10. ABSORPTION COEFFICIENTS FOR CN  
k (per cm at STP)

1/cm	300K	600K	1200K	1800K	2400K	3000K
1400					2.885E-06	4.629E-05
1425					6.283E-06	8.496E-05
1450					1.349E-05	1.541E-04
1475					2.853E-05	2.760E-04
1500				1.587E-06	5.941E-05	4.880E-04
1525				4.243E-06	1.217E-04	8.508E-04
1550				1.110E-05	2.449E-04	1.462E-03
1575				2.836E-05	4.837E-04	2.473E-03
1600			3.908E-07	7.071E-05	9.369E-04	4.116E-03
1625			1.532E-06	1.717E-04	1.777E-03	6.729E-03
1650			5.768E-06	4.052E-04	3.294E-03	1.079E-02
1675			2.079E-05	9.279E-04	5.962E-03	1.696E-02
1700		2.448E-09	7.157E-05	2.056E-03	1.051E-02	2.606E-02
1725		2.808E-08	2.343E-04	4.397E-03	1.800E-02	3.910E-02
1750		2.901E-07	7.265E-04	9.046E-03	2.990E-02	5.711E-02
1775		2.679E-06	2.124E-03	1.784E-02	4.797E-02	8.100E-02
1800	8.237E-10	2.191E-05	5.825E-03	3.357E-02	7.408E-02	1.111E-01
1825	3.662E-08	1.571E-04	1.487E-02	5.997E-02	1.096E-01	1.468E-01
1850	1.203E-06	9.752E-04	3.510E-02	1.010E-02	1.545E-01	1.857E-01
1875	2.870E-05	5.160E-03	7.575E-02	1.590E-01	2.056E-01	2.235E-01
1900	4.918E-04	2.283E-02	1.476E-01	2.312E-01	2.558E-01	2.532E-01
1925	5.986E-03	8.242E-02	2.549E-01	3.052E-01	2.933E-01	2.676E-01
1950	5.030E-02	2.342E-01	3.800E-01	3.572E-01	3.038E-01	2.599E-01
1975	2.710E-01	4.961E-01	4.672E-01	3.575E-01	2.778E-01	2.317E-01
2000	8.028E-01	7.055E-01	4.348E-01	2.902E-01	2.240E-01	1.972E-01
2025	9.181E-01	5.122E-01	2.662E-01	2.001E-01	1.876E-01	1.923E-01

TABLE A2-10. (Concluded)

1/cm	300K	600K	1200K	1800K	2400K	3000K
2050	5.480E-01	2.946E-01	2.244E-01	2.352E-01	2.485E-01	2.608E-01
2075	1.359E+00	9.486E-01	5.944E-01	4.748E-01	4.180E-01	3.891E-01
2100	5.082E-01	8.119E-01	7.081E-01	5.830E-01	5.033E-01	4.554E-01
2125	4.204E-02	2.997E-01	5.245E-01	5.152E-01	4.730E-01	4.382E-01
2150	5.619E-04	4.312E-02	2.387E-01	3.271E-01	3.459E-01	3.441E-01
2175	6.103E-07	1.760E-03	5.839E-02	1.382E-01	1.864E-01	2.111E-01
2200	1.284E-10	1.023E-05	5.592E-03	3.221E-02	6.506E-02	9.164E-02
2225		1.252E-09	8.577E-05	2.435E-03	1.045E-02	2.186E-02

TABLE A2-11. LINE DENSITY FOR CN  
1/d (cm)

1/cm	300K	600K	1200K	1800K	2400K	3000K
1400					8.060E+00	1.008E+01
1425					8.138E+00	1.017E+01
1450					8.216E+00	1.026E+01
1475					8.275E+00	1.032E+01
1500				6.599E+00	8.329E+00	1.036E+01
1525				6.604E+00	8.371E+00	1.039E+01
1550				6.594E+00	8.395E+00	1.039E+01
1575				6.578E+00	8.407E+00	1.036E+01
1600			4.831E+00	6.547E+00	8.395E+00	1.030E+01
1625			4.805E+00	6.500E+00	8.365E+00	1.019E+01
1650			4.771E+00	6.438E+00	8.305E+00	1.005E+01
1675			4.725E+00	6.359E+00	8.216E+00	9.826E+00
1700		3.087E+00	4.665E+00	6.266E+00	8.096E+00	9.530E+00
1725		3.051E+00	4.593E+00	6.146E+00	7.928E+00	9.289E+00
1750		3.002E+00	4.503E+00	6.010E+00	7.713E+00	9.054E+00
1775		2.940E+00	4.394E+00	5.844E+00	7.414E+00	8.812E+00
1800	1.795E+00	2.861E+00	4.267E+00	5.646E+00	7.132E+00	8.557E+00
1825	1.934E+00	2.765E+00	4.119E+00	5.401E+00	6.856E+00	8.295E+00
1850	2.080E+00	2.648E+00	3.945E+00	5.153E+00	6.551E+00	8.034E+00
1875	2.208E+00	2.510E+00	3.741E+00	4.900E+00	6.281E+00	7.805E+00
1900	2.265E+00	2.350E+00	3.491E+00	4.643E+00	6.012E+00	7.638E+00
1925	2.189E+00	2.168E+00	3.206E+00	4.339E+00	5.862E+00	7.691E+00
1950	1.953E+00	1.958E+00	2.896E+00	4.048E+00	5.840E+00	8.000E+00
1975	1.607E+00	1.694E+00	2.604E+00	3.961E+00	6.275E+00	9.268E+00
2000	1.131E+00	1.367E+00	2.487E+00	4.431E+00	7.497E+00	1.068E+01
2025	1.468E+00	1.838E+00	3.828E+00	6.740E+00	9.844E+00	1.222E+01

TABLE A2-11. (Concluded)

1/cm	300K	600K	1200K	1800K	2400K	3000K
2050	1.633E+00	2.610E+00	4.356E+00	7.297E+00	9.341E+00	1.109E+01
2075	1.307E+00	1.817E+00	3.628E+00	5.719E+00	7.743E+00	9.510E+00
2100	1.301E+00	1.638E+00	3.049E+00	4.857E+00	6.623E+00	8.188E+00
2125	1.389E+00	1.592E+00	2.695E+00	4.240E+00	5.907E+00	7.792E+00
2150	1.546E+00	1.648E+00	2.460E+00	3.745E+00	5.180E+00	6.732E+00
2175	1.793E+00	1.830E+00	2.342E+00	3.347E+00	4.529E+00	5.775E+00
2200	2.222E+00	2.231E+00	2.431E+00	3.075E+00	3.881E+00	4.674E+00
2225		3.273E+00	3.265E+00	3.275E+00	3.263E+00	3.278E+00

TABLE A2-12. INTEGRATED ABSORPTANCE OF CN FUNDAMENTAL BAND SYSTEM ( $\text{cm}^{-1}$ )

T = 300K, C = 0 P <sub>T</sub> (atm) =			
u(cm) <sub>STP</sub>	.01	.1	1
.1	2.76 E+0	5.32 E+0	8.68 E+0
1.	7.46 E+0	1.93 E+1	4.47 E+1
10.	2.10 E+1	5.60 E+1	1.19 E+2
100.	5.75 E+1	1.27 E+2	1.89 E+2
1000.	1.28 E+2	1.96 E+2	2.32 E+2
10000.	1.97 E+2	2.38 E+2	2.66 E+2
T = 600K, C = 0 P <sub>T</sub> (atm) =			
u(cm) <sub>STP</sub>	.01	.1	1
.1	2.94 E+0	3.65 E+0	4.72 E+0
1.	7.95 E+0	1.55 E+1	3.18 E+1
10.	1.91 E+1	4.78 E+1	1.11 E+2
100.	5.06 E+1	1.23 E+2	2.22 E+2
1000.	1.26 E+2	2.31 E+2	2.97 E+2
10000.	2.34 E+2	3.05 E+2	3.47 E+2
T = 1200K, C = 0 P <sub>T</sub> (atm) =			
u(cm) <sub>STP</sub>	.01	.1	1
.1	2.41 E+0	2.42 E+0	2.48 E+0
1.	1.20 E+1	1.46 E+1	2.10 E+1
10.	2.75 E+1	4.85 E+1	1.03 E+2
100.	5.83 E+1	1.30 E+2	2.57 E+2
1000.	1.37 E+2	2.74 E+2	3.86 E+2
10000.	2.80 E+2	4.00 E+2	4.63 E+2

TABLE A2-12. (Concluded)

T = 1800K, C = 0 P <sub>T</sub> (atm) =			
u(cm) <sub>STP</sub>	.01	.1	1
.1	1.64 E+0	1.64 E+0	1.64 E+0
1.	1.30 E+1	1.33 E+1	1.51 E+1
10.	3.85 E+1	5.16 E+1	9.19 E+1
100.	7.64 E+1	1.37 E+2	2.67 E+2
1000.	1.63 E+2	3.05 E+2	4.43 E+2
10000.	3.22 E+2	4.69 E+2	5.46 E+2
T = 2400K, C = 0 P <sub>T</sub> (atm) =			
u(cm) <sub>STP</sub>	.01	.1	1
.1	1.26 E+0	1.26 E+0	1.26 E+0
1.	1.17 E+1	1.18 E+1	1.20 E+1
10.	5.07 E+1	5.79 E+1	8.49 E+1
100.	9.88 E+1	1.51 E+2	2.82 E+2
1000.	1.80 E+2	3.23 E+2	4.81 E+2
10000.	3.44 E+2	5.11 E+2	6.02 E+2
T = 3000K, C = 0 P <sub>T</sub> (atm) =			
u(cm) <sub>STP</sub>	.01	.1	1
.1	1.03 E+0	1.03 E+0	1.03 E+0
1.	1.00 E+1	1.00 E+1	1.00 E+1
10.	5.94 E+1	6.25 E+1	7.77 E+1
100.	1.30 E+2	1.71 E+2	2.96 E+2
1000.	2.20 E+2	3.59 E+2	5.37 E+2
10000.	3.92 E+2	5.77 E+2	6.78 E+2

TABLE A2-13. TOTAL EMISSIVITY OF CN

T = 300K, C = 0 P <sub>T</sub> (atm) =			
u(cm) <sub>STP</sub>	.01	.1	1
.1	1.09 E-4	2.09 E-4	3.38 E-4
1.	2.98 E-4	7.64 E-4	1.76 E-3
10.	8.42 E-4	2.23 E-3	4.74 E-3
100.	2.31 E-3	5.12 E-3	7.72 E-3
1000.	5.19 E-3	8.07 E-3	9.68 E-3
10000.	8.13 E-3	1.00 E-2	1.14 E-2
T = 600K, C = 0 P <sub>T</sub> (atm) =			
u(cm) <sub>STP</sub>	.01	.1	1
.1	9.83 E-4	1.22 E-3	1.57 E-3
1.	2.67 E-3	5.18 E-3	1.06 E-2
10.	6.42 E-3	1.60 E-2	3.73 E-2
100.	1.70 E-2	4.15 E-2	7.51 E-2
1000.	4.24 E-2	7.83 E-2	1.01 E-2
10000.	7.92 E-2	1.04 E-1	1.19 E-1
T = 1200K, C = 0 P <sub>T</sub> (atm) =			
u(cm) <sub>STP</sub>	.01	.1	1
.1	6.33 E-4	6.40 E-4	6.46 E-4
1.	3.19 E-3	3.85 E-3	5.47 E-3
10.	7.80 E-3	1.32 E-2	2.74 E-2
100.	1.77 E-2	3.70 E-2	7.21 E-2
1000.	4.11 E-2	8.21 E-2	1.24 E-1
10000.	8.56 E-2	1.31 E-1	1.70 E-1

TABLE A2-13. (Concluded)

T = 1800K, C = 0 P <sub>T</sub> (atm) =			
u(cm) <sub>STP</sub>	.01	.1	1
.1	2.24 E-4	2.13 E-4	2.21 E-4
1.	1.77 E-3	1.72 E-3	2.03 E-3
10.	5.67 E-3	7.44 E-3	1.26 E-2
100.	1.38 E-2	2.22 E-2	4.04 E-2
1000.	3.01 E-2	5.31 E-2	8.43 E-2
10000.	6.21 E-2	9.67 E-2	1.33 E-1
T = 2400K, C = 0 P <sub>T</sub> (atm) =			
u(cm) <sub>STP</sub>	.01	.1	1
.1	9.46 E-5	9.43 E-5	9.36 E-5
1.	8.74 E-4	8.75 E-4	8.93 E-4
10.	4.05 E-3	4.54 E-3	6.44 E-3
100.	1.05 E-2	1.42 E-2	2.40 E-2
1000.	2.20 E-2	3.55 E-2	5.52 E-2
10000.	4.33 E-2	6.58 E-2	9.29 E-2
T = 3000K, C = 0 P <sub>T</sub> (atm) =			
u(cm) <sub>STP</sub>	.01	.1	1
.1	4.59 E-5	4.23 E-5	4.58 E-5
1.	4.48 E-4	4.12 E-4	4.48 E-4
10.	2.78 E-3	2.93 E-3	3.54 E-3
100.	8.40 E-3	9.92 E-3	1.53 E-2
1000.	1.84 E-2	2.58 E-2	3.91 E-2
10000.	3.65 E-2	5.22 E-2	7.24 E-2

TABLE A2-14. ABSORPTION COEFFICIENTS FOR OH  
k (per cm at STP)

1/cm	300K	600K	1200K	1800K	2400K	3000K
1400					1.639E-06	2.685E-05
1600					9.042E-06	1.004E-04
1800				1.479E-06	4.608E-05	3.507E-04
2000				1.249E-05	2.158E-04	1.141E-03
2200			8.759E-07	9.365E-05	9.191E-04	3.440E-03
2300					1.821E-03	5.771E-03
2400			1.634E-05	6.107E-04	3.501E-03	9.446E-03
2500				1.468E-03	6.514E-03	1.501E-02
2600		6.823E-08	2.420E-04	3.368E-03	1.166E-02	2.311E-02
2700				7.333E-03	2.000E-02	3.419E-02
2800		1.090E-05	2.689E-03	1.505E-02	3.267E-02	4.859E-02
2900	1.193E-08			2.882E-02	5.027E-02	6.520E-02
2950						7.429E-02
3000	9.094E-07	8.828E-04	2.057E-02	5.089E-02	7.240E-02	8.302E-02
3050					8.404E-02	9.031E-02
3100	4.524E-05	5.739E-03	4.728E-02	8.141E-02	9.564E-02	9.728E-02
3150				9.849E-02	1.060E-01	1.025E-01
3200	1.355E-03	2.831E-02	9.294E-02	1.148E-01	1.134E-01	1.039E-01
3250			1.208E-01		1.170E-01	1.017E-01
3300	2.177E-02	9.867E-02	1.478E-01	1.377E-01	1.179E-01	9.999E-02
3325					1.155E-01	9.683E-02
3350		1.560E-01	1.675E-01	1.378E-01	1.110E-01	9.194E-02
3375					1.041E-01	8.521E-02
3400	1.555E-01	2.134E-01	1.717E-01	1.254E-01	9.480E-02	7.660E-02
3425			1.678E-01	1.199E-01	9.104E-02	7.491E-02
3450		2.410E-01	1.575E-01	1.118E-01	8.630E-02	7.118E-02

TABLE A2-14. (Concluded)

1/cm	300K	600K	1200K	1800K	2400K	3000K
3475			1.397E-01	9.988E-02	7.969E-02	6.825E-02
3500	3.170E-01	2.001E-01	1.141E-01	8.394E-02	7.057E-02	6.356E-02
3525		1.459E-01	8.097E-02	6.408E-02	5.891E-02	5.698E-02
3550	1.358E-01	7.050E-02	4.119E-02	4.064E-02	4.479E-02	4.849E-02
3575	4.133E-02	2.066E-02	1.638E-02	2.636E-02	3.641E-02	4.361E-02
3600	2.356E-01	1.173E-01	6.294E-02	4.185E-02	5.581E-02	5.749E-02
3625			1.083E-01	8.404E-03	7.448E-02	7.129E-02
3650		2.781E-01	1.494E-01	1.020E-01	9.100E-02	7.940E-02
3675				1.296E-01	1.066E-01	9.124E-02
3700	3.946E-01	3.259E-01	2.063E-01	1.485E-01	1.191E-01	1.008E-01
3725					1.280E-01	1.077E-01
3750			2.158E-01	1.658E-01	1.329E-01	1.117E-01
3775					1.337E-01	1.125E-01
3800	2.999E-02	1.258E-01	1.777E-01	1.571E-01	1.303E-01	1.102E-01
3825					1.234E-01	1.067E-01
3850			1.122E-01	1.253E-01	1.120E-01	9.313E-02
3875					1.005E-01	8.778E-02
3900	3.780E-05	5.845E-03	5.016E-02	8.018E-02	8.587E-02	7.957E-02
3925					6.907E-02	6.886E-02
3950			1.317E-02	3.647E-02	5.144E-02	5.624E-02
3975					3.443E-02	4.250E-02
4000	9.619E-13	1.388E-06	1.153E-03	8.478E-03	1.951E-02	2.866E-02

TABLE A2-15. LINE SPACING FOR OH  
1/d (cm)

1/cm	300K	600K	1200K	1800K	2400K	3000K
1400					4.085E-01	5.480E-01
1600					4.083E-01	5.482E-01
1800				2.783E-01	4.022E-01	5.354E-01
2000				2.721E-01	3.898E-01	5.035E-01
2200			1.668E-01	2.634E-01	3.696E-01	4.808E-01
2300					3.554E-01	4.351E-01
2400			1.618E-01	2.518E-01	3.354E-01	4.277E-01
2500				2.445E-01	3.285E-01	3.937E-01
2600		8.286E-02	1.600E-01	2.361E-01	3.178E-01	3.920E-01
2700				2.258E-01	2.952E-01	3.527E-01
2800		8.442E-02	1.490E-01	2.176E-01	2.905E-01	3.628E-01
2900	7.033E-02			2.058E-01	2.598E-01	3.079E-01
2950						3.246E-01
3000	7.367E-02	8.688E-02	1.400E-01	2.008E-01	2.657E-01	3.394E-01
3050					2.386E-01	2.816E-01
3100	7.752E-02	8.859E-02	1.353E-01	1.881E-01	2.402E-01	2.908E-01
3150				1.874E-01	2.475E-01	3.126E-01
3200	8.206E-02	9.077E-02	1.301E-01	1.808E-01	2.457E-01	3.295E-01
3250			1.032E-01		2.118E-01	2.537E-01
3300	8.748E-02	9.342E-02	1.298E-01	1.792E-01	2.402E-01	3.025E-01
3325					2.487E-01	3.208E-01
3350		9.481E-02	1.248E-01	1.792E-01	2.537E-01	3.369E-01
3375					2.530E-01	3.492E-01
3400	9.415E-02	9.526E-02	1.105E-01	1.538E-01	2.328E-01	3.437E-01
3425			1.233E-01	1.841E-01	3.077E-01	5.213E-01
3450		1.019E-01	1.356E-01	1.967E-01	2.620E-01	3.130E-01

TABLE A2-15. (Concluded)

1/cm	300K	600K	1200K	1800K	2400K	3000K
3475			1.478E-01	2.220E-01	2.975E-01	3.528E-01
3500	1.026E-01	1.085E-01	1.616E-01	2.497E-01	3.336E-01	3.907E-01
3525		1.124E-01	1.804E-01	2.834E-01	3.716E-01	4.270E-01
3550	1.078E-01	1.183E-01	2.161E-01	3.277E-01	4.056E-01	4.534E-01
3575	1.107E-01	1.293E-01	2.688E-01	3.393E-01	3.982E-01	4.508E-01
3600	1.139E-01	1.209E-01	2.023E-01	4.125E-01	4.215E-01	5.240E-01
3625			1.828E-01	2.906E-01	4.782E-01	7.525E-01
3650		1.243E-01	1.725E-01	2.550E-01	2.780E-01	2.930E-01
3675				2.364E-01	2.800E-01	3.027E-01
3700	1.300E-01	1.314E-01	1.656E-01	2.298E-01	2.822E-01	3.130E-01
3725					2.847E-01	3.244E-01
3750			1.641E-01	2.230E-01	2.874E-01	3.380E-01
3775					2.906E-01	3.566E-01
3800	1.556E-01	1.556E-01	1.671E-01	2.165E-01	2.980E-01	3.914E-01
3825					3.813E-01	6.391E-01
3850			1.758E-01	1.760E-01	1.758E-01	1.757E-01
3875					1.894E-01	1.894E-01
3900	2.065E-01	2.064E-01	2.066E-01	2.069E-01	2.067E-01	2.069E-01
3925					2.300E-01	2.307E-01
3950			2.626E-01	2.630E-01	2.636E-01	2.655E-01
3975					3.190E-01	3.245E-01
4000	4.228E-01	4.226E-01	4.236E-01	4.288E-01	4.409E-01	4.595E-01

GENERAL APPENDIX

TABLE A2-16. INTEGRATED ABSORPTANCE OF OH FUNDAMENTAL BAND SYSTEM ( $\text{cm}^{-1}$ )

T = 300K, C = 0 P <sub>T</sub> (atm) =			
u(cm) <sub>STP</sub>	.01	.1	1
.1	1.73 E+0	3.58 E+0	7.20 E+0
1.	4.44 E+0	1.22 E+1	3.35 E+1
10.	1.27 E+1	3.81 E+1	1.08 E+2
100.	3.86 E+1	1.11 E+2	2.76 E+2
1000.	1.12 E+2	2.78 E+2	5.00 E+2
10000.	2.78 E+2	5.03 E+2	6.49 E+2
T = 600K, C = 0 P <sub>T</sub> (atm) =			
u(cm) <sub>STP</sub>	.01	.1	1
.1	1.86 E+0	2.59 E+0	4.22 E+0
1.	4.21 E+0	8.89 E+0	2.27 E+1
10.	1.02 E+1	2.77 E+1	7.98 E+1
100.	2.85 E+1	8.36 E+1	2.30 E+2
1000.	8.41 E+1	2.33 E+2	5.20 E+2
10000.	2.33 E+2	5.21 E+2	8.09 E+2
T = 1200K, C = 0 P <sub>T</sub> (atm) =			
u(cm) <sub>STP</sub>	.01	.1	1
.1	1.97 E+0	2.03 E+0	2.32 E+0
1.	5.92 E+0	8.04 E+0	1.56 E+1
10.	1.17 E+1	2.33 E+1	6.27 E+1
100.	2.60 E+1	6.88 E+1	1.96 E+2
1000.	7.07 E+1	2.00 E+2	5.11 E+2
10000.	2.02 E+2	5.14 E+2	9.71 E+2

TABLE A2-16. (Concluded)

T = 1800K, C = 0 P <sub>T</sub> (atm) =			
u(cm) <sub>STP</sub>	.01	.1	1
.1	1.56 E+0	1.56 E+0	1.58 E+0
1.	7.63 E+0	8.46 E+0	1.22 E+1
10.	1.66 E+1	2.45 E+1	5.62 E+1
100.	3.23 E+1	6.83 E+1	1.86 E+2
1000.	7.45 E+1	1.96 E+2	5.15 E+2
10000.	2.00 E+2	5.22 E+2	1.08 E+3
T = 2400K, C = 0 P <sub>T</sub> (atm) =			
u(cm) <sub>STP</sub>	.01	.1	1
.1	1.24 E+0	1.24 E+0	1.24 E+0
1.	8.82 E+0	9.04 E+0	1.05 E+1
10.	2.27 E+1	2.83 E+1	5.48 E+1
100.	4.00 E+1	7.15 E+1	1.86 E+2
1000.	8.02 E+1	1.98 E+2	5.27 E+2
10000.	2.04 E+2	5.37 E+2	1.16 E+3
T = 3000K, C = 0 P <sub>T</sub> (atm) =			
u(cm) <sub>STP</sub>	.01	.1	1
.1	1.00 E+0	1.00 E+0	1.00 E+0
1.	8.62 E+0	8.66 E+0	9.07 E+0
10.	2.87 E+1	3.26 E+1	5.30 E+1
100.	5.18 E+1	7.88 E+1	1.89 E+2
1000.	9.36 E+1	2.07 E+2	5.45 E+2
10000.	2.16 E+2	5.58 E+2	1.52 E+3

TABLE A2-17. TOTAL EMISSIVITY OF OH

T = 300K, C = 0 P <sub>T</sub> (atm) =			
u(cm) <sub>STP</sub>	.01	.1	1
.1	2.84 E-7	5.73 E-7	1.12 E-6
1.	7.51 E-7	2.01 E-6	5.39 E-6
10.	2.17 E-6	6.37 E-6	1.80 E-5
100.	6.54 E-6	1.89 E-5	4.82 E-5
1000.	1.91 E-5	4.92 E-5	9.58 E-5
10000.	4.93 E-5	9.68 E-5	1.43 E-4
T = 600K, C = 0 P <sub>T</sub> (atm) =			
u(cm) <sub>STP</sub>	.01	.1	1
.1	9.06 E-5	1.24 E-4	2.01 E-4
1.	2.08 E-4	4.33 E-4	1.09 E-3
10.	5.07 E-4	1.36 E-3	3.90 E-3
100.	1.41 E-3	4.13 E-3	1.15 E-2
1000.	4.18 E-3	1.16 E-2	2.68 E-2
10000.	1.17 E-2	2.70 E-2	4.44 E-2
T = 1200K, C = 0 P <sub>T</sub> (atm) =			
u(cm) <sub>STP</sub>	.01	.1	1
.1	4.18 E-4	4.27 E-4	4.86 E-4
1.	1.27 E-3	1.71 E-3	3.27 E-3
10.	2.56 E-3	5.02 E-3	1.33 E-2
100.	5.72 E-3	1.48 E-2	4.19 E-2
1000.	1.54 E-2	4.33 E-2	1.11 E-1
10000.	4.36 E-2	1.12 E-1	2.17 E-1

TABLE A2-17. (Concluded)

T = 1800K, C = 0 P <sub>T</sub> (atm) =			
u(cm) <sub>STP</sub>	.01	.1	1
.1	2.82 E-4	2.82 E-4	2.81 E-4
1.	1.38 E-3	1.53 E-3	2.17 E-3
10.	3.21 E-3	4.61 E-3	1.02 E-2
100.	6.52 E-3	1.31 E-2	3.43 E-2
1000.	1.47 E-2	3.74 E-2	9.81 E-2
10000.	3.85 E-2	1.00 E-1	2.12 E-1
T = 2400K, C = 0 P <sub>T</sub> (atm) =			
u(cm) <sub>STP</sub>	.01	.1	1
.1	1.53 E-4	1.50 E-4	1.50 E-4
1.	1.09 E-3	1.11 E-3	1.28 E-3
10.	3.07 E-3	3.75 E-3	6.85 E-3
100.	6.15 E-3	9.98 E-3	2.46 E-2
1000.	1.20 E-2	2.73 E-2	7.15 E-2
10000.	2.86 E-2	7.39 E-2	1.65 E-1
T = 3000K, C = 0 P <sub>T</sub> (atm) =			
u(cm) <sub>STP</sub>	.01	.1	1
.1	1.37 E-4	8.05 E-5	8.05 E-5
1.	7.02 E-4	7.04 E-4	7.34 E-4
10.	2.59 E-3	2.90 E-3	4.45 E-3
100.	5.69 E-3	7.86 E-3	1.70 E-2
1000.	1.03 E-2	2.03 E-2	5.13 E-2
10000.	2.19 E-2	5.39 E-2	1.24 E-1

TABLE A2-18. ABSORPTION COEFFICIENTS FOR HCl  
k (per cm at STP)

1/cm	300K	600K	1200K	1800K	2400K	3000K
1000					1.113E-07	3.398E-06
1200				1.028E-08	1.302E-06	
1400				2.394E-07	1.329E-05	1.446E-04
1600				4.692E-06	1.177E-04	
1700			6.097E-08		3.303E-04	
1800			4.950E-07	7.566E-05	8.879E-04	3.682E-03
1900			3.713E-06	2.790E-04	2.275E-03	
2000			2.547E-05	9.638E-04	5.525E-03	1.470E-02
2100			1.580E-04	3.090E-03	1.262E-02	
2200		5.625E-07	8.723E-04	9.090E-03	2.689E-02	4.782E-02
2300		1.555E-05	4.204E-03	2.416E-02	5.273E-02	7.769E-02
2350						9.587E-02
2400	7.222E-08	3.203E-04	1.721E-02	5.679E-02	9.321E-02	1.152E-01
2450						1.346E-01
2500	1.785E-05	4.617E-03	5.764E-02	1.144E-01	1.445E-01	1.525E-01
2550	2.076E-04					1.652E-01
2600	1.909E-03	4.246E-02	1.486E-01	1.877E-01	1.874E-01	1.722E-01
2625						1.739E-01
2650	1.342E-02		2.098E-01	2.164E-01	1.945E-01	1.687E-01
2675						1.609E-01
2700	6.884E-02	2.133E-01	2.648E-01	2.282E-01	1.884E-01	1.571E-01
2725						1.496E-01
2750	2.408E-01	3.481E-01	2.863E-01	2.118E-01	1.648E-01	1.349E-01
2775						1.170E-01
2800	5.094E-01	4.118E-01	2.522E-01	1.719E-01	1.338E-01	1.143E-01
2825	5.662E-01	3.703E-01	2.129E-01	1.531E-01		1.146E-01

TABLE A2-18. (Concluded)

1/cm	300K	600K	1200K	1800K	2400K	3000K
2850	4.651E-01	2.608E-01	1.503E-01	1.227E-01		1.094E-01
2875	1.679E-01	8.672E-02	6.656E-02	8.095E-02	9.264E-02	9.618E-02
2900	2.583E-01	1.295E-01	8.810E-02	9.833E-02	1.085E-01	1.109E-01
2925	6.440E-01	3.389E-01	1.898E-01	1.596E-01	1.500E-01	1.411E-01
2950	8.147E-01	4.934E-01	2.784E-01	2.133E-01		1.656E-01
2975	7.203E-01	5.548E-01	3.419E-01	2.544E-01		1.826E-01
3000	4.688E-01	5.147E-01	3.712E-01	2.790E-01	2.276E-01	1.896E-01
3025			3.627E-01	2.843E-01		1.959E-01
3050	7.561E-02	2.571E-01	3.196E-01	2.697E-01		1.914E-01
3075			2.520E-01			1.761E-01
3100	2.401E-03	5.468E-02	1.749E-01	1.933E-01	1.747E-01	1.518E-01
3125			1.037E-01			1.214E-01
3150	5.964E-06	3.200E-03	4.983E-02	9.271E-02	1.054E-01	1.001E-01
3175						7.342E-02
3200	6.931E-11	1.294E-05	3.790E-03	1.880E-02	3.496E-02	4.458E-02
3225			2.374E-04	3.273E-03	1.016E-02	1.763E-02

TABLE A2-19. LINE SPACING FOR HCl  
1/d (cm)

1/cm	300K	600K	1200K	1800K	2400K	3000K
1000					3.192E-01	4.161E-01
1200				2.387E-01	3.339E-01	
1400				2.455E-01	3.456E-01	4.581E-01
1600				2.498E-01	3.528E-01	
1700			1.818E-01		3.539E-01	
1800			1.794E-01	2.510E-01	3.528E-01	4.603E-01
1900			1.765E-01	2.500E-01	3.488E-01	
2000			1.730E-01	2.476E-01	3.405E-01	4.226E-01
2100			1.690E-01	2.433E-01	3.260E-01	
2200		8.423E-02	1.642E-01	2.363E-01	3.082E-01	3.842E-01
2300		8.386E-02	1.585E-01	2.254E-01	2.967E-01	3.539E-01
2350						3.547E-01
2400	6.255E-02	8.363E-02	1.514E-01	2.120E-01	2.748E-01	3.262E-01
2450						3.301E-01
2500	6.547E-02	8.361E-02	1.410E-01	2.011E-01	2.751E-01	3.656E-01
2550	6.725E-02					3.114E-01
2600	6.930E-02	8.382E-02	1.346E-01	1.908E-01	2.574E-01	3.337E-01
2625						3.275E-01
2650	7.170E-02		1.295E-01	1.836E-01	2.446E-01	3.042E-01
2675						2.924E-01
2700	7.448E-02	8.423E-02	1.259E-01	1.841E-01	2.598E-01	3.421E-01
2725						3.863E-01
2750	7.771E-02	8.403E-02	1.229E-01	1.869E-01	2.591E-01	3.193E-01
2775						3.195E-01
2800	8.167E-02	8.690E-02	1.277E-01	2.074E-01	3.036E-01	3.831E-01
2825	8.402E-02	9.270E-02	1.518E-01	2.493E-01		4.421E-01

TABLE A2-19. (Concluded)

1/cm	300K	600K	1200K	1800K	2400K	3000K
2850	8.641E-02	9.909E-02	1.799E-01	2.872E-01		4.886E-01
2875	8.772E-02	1.116E-01	2.276E-01	2.922E-01	3.185E-01	3.271E-01
2900	9.448E-02	1.141E-01	2.248E-01	2.978E-01	3.342E-01	3.499E-01
2925	9.687E-02	1.078E-01	1.892E-01	2.778E-01	3.404E-01	2.768E-01
2950	1.005E-01	1.080E-01	1.731E-01	2.582E-01		3.895E-01
2975	1.048E-01	1.102E-01	1.636E-01	2.417E-01		4.042E-01
3000	1.098E-01	1.137E-01	1.573E-01	2.128E-01	2.470E-01	2.621E-01
3025			1.547E-01	2.118E-01		2.782E-01
3050	1.228E-01	1.247E-01	1.531E-01	2.095E-01		2.963E-01
3075			1.526E-01			3.170E-01
3100	1.420E-01	1.439E-01	1.542E-01	1.966E-01	2.686E-01	3.484E-01
3125			1.599E-01			1.608E-01
3150	1.748E-01	1.792E-01	1.812E-01	1.817E-01	1.825E-01	1.826E-01
3175						2.166E-01
3200	2.542E-01	2.699E-01	2.773E-01	2.793E-01	2.812E-01	2.817E-01
3225			4.916E-01	5.021E-01	5.090E-01	5.120E-01

GENERAL APPENDIX

TABLE A2-20. INTEGRATED ABSORPTANCE OF HCl FUNDAMENTAL BAND SYSTEM ( $\text{cm}^{-1}$ )

T = 300K, C = 0 P <sub>T</sub> (atm) =			
u(cm) <sub>STP</sub>	.01	.1	1
.1	1.28 E+0	3.45 E+0	8.23 E+0
1.	3.79 E+0	1.14 E+1	3.27 E+1
10.	1.16 E+1	3.52 E+1	9.90 E+1
100.	3.54 E+1	1.01 E+2	2.39 E+2
1000.	1.01 E+2	2.41 E+2	4.03 E+2
10000.	2.41 E+2	4.04 E+2	5.05 E+2
T = 600K, C = 0 P <sub>T</sub> (atm) =			
u(cm) <sub>STP</sub>	.01	.1	1
.1	1.19 E+0	2.38 E+0	4.86 E+0
1.	2.98 E+0	8.04 E+0	2.24 E+1
10.	8.48 E+0	2.53 E+1	7.41 E+1
100.	2.56 E+1	7.63 E+1	2.06 E+2
1000.	7.65 E+1	2.07 E+2	4.37 E+2
10000.	2.08 E+2	4.38 E+2	6.36 E+2
T = 1200K, C = 0 P <sub>T</sub> (atm) =			
u(cm) <sub>STP</sub>	.01	.1	1
.1	1.58 E+0	1.95 E+0	2.83 E+0
1.	3.70 E+0	6.96 E+0	1.67 E+1
10.	8.31 E+0	2.15 E+1	6.19 E+1
100.	2.26 E+1	6.57 E+1	1.87 E+2
1000.	6.65 E+1	1.90 E+2	4.61 E+2
10000.	1.90 E+2	4.64 E+2	8.02 E+2

TABLE A2-20. (Concluded)

T = 1800K, C = 0 P <sub>T</sub> (atm) =			
u(cm) <sub>STP</sub>	.01	.1	1
.1	1.71 E+0	1.76 E+0	2.00 E+0
1.	5.18 E+0	7.23 E+0	1.40 E+1
10.	1.03 E+1	2.14 E+1	5.79 E+1
100.	2.37 E+1	6.40 E+1	1.83 E+2
1000.	6.56 E+1	1.87 E+2	4.78 E+2
10000.	1.88 E+2	4.82 E+2	9.12 E+2
T = 2400K, C = 0 P <sub>T</sub> (atm) =			
u(cm) <sub>STP</sub>	.01	.1	1
.1	1.48 E+0	1.49 E+0	1.52 E+0
1.	6.47 E+0	7.58 E+0	1.19 E+1
10.	1.32 E+1	2.22 E+1	5.46 E+1
100.	2.64 E+1	6.35 E+1	1.79 E+2
1000.	6.66 E+1	1.86 E+2	4.88 E+2
10000.	1.88 E+2	4.93 E+2	9.95 E+2
T = 3000K, C = 0 P <sub>T</sub> (atm) =			
u(cm) <sub>STP</sub>	.01	.1	1
.1	1.25 E+0	1.25 E+0	1.26 E+0
1.	7.34 E+0	7.89 E+0	1.04 E+1
10.	1.70 E+1	2.43 E+1	5.32 E+1
100.	3.20 E+1	6.71 E+1	1.82 E+2
1000.	7.25 E+1	1.93 E+2	5.10 E+2
10000.	1.96 E+2	5.17 E+2	1.08 E+3

TABLE A2-21. TOTAL EMISSIVITY OF HCl

T = 300K, C = 0 P <sub>T</sub> (atm) =			
u(cm) <sub>STP</sub>	.01	.1	1
.1	2.69 E-6	7.11 E-6	1.67 E-5
1.	7.99 E-6	2.38 E-5	6.78 E-5
10.	2.46 E-5	7.42 E-5	2.10 E-4
100.	7.51 E-5	2.16 E-4	5.23 E-4
1000.	2.16 E-4	5.29 E-4	9.42 E-4
10000.	5.30 E-4	9.47 E-4	1.30 E-3
T = 600K, C = 0 P <sub>T</sub> (atm) =			
u(cm) <sub>STP</sub>	.01	.1	1
.1	1.53 E-4	3.04 E-4	6.16 E-4
1.	3.84 E-4	1.03 E-3	2.85 E-3
10.	1.09 E-3	3.26 E-3	9.53 E-3
100.	3.31 E-3	9.85 E-3	2.68 E-2
1000.	9.90 E-3	2.69 E-2	5.80 E-2
10000.	2.71 E-2	5.81 E-2	8.77 E-2
T = 1200K, C = 0 P <sub>T</sub> (atm) =			
u(cm) <sub>STP</sub>	.01	.1	1
.1	4.18 E-4	4.98 E-4	7.13 E-4
1.	9.82 E-4	1.79 E-3	4.21 E-3
10.	2.22 E-3	5.60 E-3	1.59 E-2
100.	5.96 E-3	1.71 E-2	4.85 E-2
1000.	1.74 E-2	4.94 E-2	1.22 E-1
10000.	4.99 E-2	1.23 E-1	2.20 E-1

TABLE A2-21. (Concluded)

T = 1800K, C = 0 P <sub>T</sub> (atm) =			
u(cm) <sub>STP</sub>	.01	.1	1
.1	3.00 E-4	3.02 E-4	3.37 E-4
1.	9.31 E-4	1.25 E-3	2.36 E-3
10.	2.02 E-3	3.89 E-3	1.00 E-2
100.	4.62 E-3	1.17 E-2	3.28 E-2
1000.	1.24 E-2	3.43 E-2	8.85 E-2
10000.	3.49 E-2	8.83 E-2	1.80 E-1
T = 2400K, C = 0 P <sub>T</sub> (atm) =			
u(cm) <sub>STP</sub>	.01	.1	1
.1	1.53 E-4	1.51 E-4	1.57 E-4
1.	6.86 E-4	7.91 E-4	1.22 E-3
10.	1.65 E-3	2.58 E-3	5.77 E-3
100.	3.53 E-3	7.50 E-3	2.02 E-2
1000.	8.30 E-3	2.18 E-2	5.75 E-2
10000.	2.23 E-2	5.87 E-2	1.27 E-1
T = 3000K, C = 0 P <sub>T</sub> (atm) =			
u(cm) <sub>STP</sub>	.01	.1	1
.1	7.96 E-5	7.94 E-5	8.11 E-5
1.	4.78 E-4	5.11 E-4	6.72 E-4
10.	1.32 E-3	1.80 E-3	3.52 E-3
100.	2.96 E-3	5.21 E-3	1.31 E-2
1000.	6.18 E-3	1.48 E-2	3.87 E-2
10000.	1.55 E-2	4.04 E-2	8.96 E-2

TABLE A2-22. ABSORPTION COEFFICIENTS FOR HF  
k (per cm at STP)

1/cm	300K	600K	1200K	1800K	2400K	3000K
1400						5.171E-06
1600						2.218E-05
1800				7.676E-08	6.388E-06	8.974E-05
2000				7.733E-07	3.525E-05	3.423E-04
2200				7.090E-06	1.805E-04	1.226E-03
2400				5.854E-05	8.496E-04	4.088E-03
2500			1.204E-06	1.610E-04		
2600			5.416E-06	4.286E-04	3.632E-03	1.258E-02
2700			2.320E-05	1.102E-03	7.207E-03	
2800			9.424E-05	2.728E-03	1.386E-02	3.511E-02
2900		4.902E-08	3.611E-04	6.470E-03	2.576E-02	
3000	1.126E-13	6.837E-07	1.297E-03	1.464E-02	4.606E-02	8.685E-02
3100		8.343E-06	4.332E-03	3.144E-02	7.881E-02	1.291E-01
3200	2.130E-09	8.765E-05	1.334E-02	6.355E-02	1.283E-01	1.839E-01
3300	1.838E-07	7.769E-04	3.740E-02	1.198E-01	1.973E-01	2.482E-01
3400	1.097E-05	5.665E-03	9.402E-02	2.081E-01	2.819E-01	3.150E-01
3500	4.277E-04	3.285E-02	2.075E-01	3.273E-01	3.708E-01	3.708E-01
3600	1.006E-02	1.445E-01	3.895E-01	4.530E-01	4.349E-01	3.917E-01
3650			4.949E-01	5.030E-01		3.894E-01
3700	1.278E-01	4.491E-01	5.908E-01	5.306E-01	4.466E-01	3.745E-01
3750			6.524E-01	5.224E-01		3.359E-01
3800	7.264E-01	8.633E-01	6.530E-01	4.816E-01	3.596E-01	2.865E-01
3850	1.142E+00	9.114E-01	5.716E-01	4.077E-01	3.166E-01	2.623E-01
3900	1.149E+00	6.878E-01	3.815E-01	2.817E-01	2.389E-01	2.171E-01
3925	8.395E-01		2.471E-01			
3950		1.544E-01	9.152E-02	1.030E-01	1.281E-01	1.452E-01

TABLE A2-22. (Concluded)

1/cm	300K	600K	1200K	1800K	2400K	3000K
3975	3.870E-01		1.084E-01	1.152E-01	1.398E-01	
4000	1.090E+00	5.451E-01	2.812E-01	2.233E-01	2.111E-01	2.072E-01
4050	1.904E+00		5.944E-01	4.231E-01	3.463E-01	2.992E-01
4100	1.524E+00	1.253E+00	7.938E-01	5.701E-01	4.501E-01	3.756E-01
4150	6.569E-01		8.222E-01	6.334E-01	5.018E-01	4.132E-01
4200	1.452E-01	5.194E-01	6.829E-01	5.997E-01	4.929E-01	4.060E-01
4250			4.468E-01	4.811E-01		3.568E-01
4300	4.768E-04	3.595E-02	2.170E-01	3.148E-01	3.243E-01	2.949E-01
4350				1.529E-01		2.015E-01
4400	1.633E-09	7.193E-05	1.050E-02	4.412E-02	7.748E-02	9.706E-02
4450			1.685E-04	2.228E-03	6.945E-03	1.228E-02

TABLE A2-23. LINE SPACING FOR HF  
1/d (cm)

1/cm	300K	600K	1200K	1800K	2400K	3000K
1400						1.132E-01
1600					8.320E-02	1.125E-01
1800				5.638E-02	8.175E-02	1.105E-01
2000				5.513E-02	7.975E-02	1.073E-01
2200				5.371E-02	7.725E-02	1.026E-01
2400				5.213E-02	7.410E-02	9.536E-02
2500			3.200E-02	5.125E-02		
2600			3.165E-02	5.038E-02	7.020E-02	8.966E-02
2700			3.129E-02	4.938E-02	6.775E-02	
2800			3.094E-02	4.829E-02	6.520E-02	8.285E-02
2900		1.743E-02	3.057E-02	4.713E-02	6.335E-02	
3000	1.462E-02	1.764E-02	3.019E-02	4.575E-02	6.160E-02	7.654E-02
3100		1.790E-02	2.980E-02	4.413E-02	5.780E-02	7.547E-02
3200	1.575E-02	1.821E-02	2.937E-02	4.296E-02	5.675E-02	7.050E-02
3300	1.640E-02	1.857E-02	2.888E-02	4.132E-02	5.295E-02	6.408E-02
3400	1.714E-02	1.901E-02	3.259E-02	3.986E-02	5.180E-02	6.475E-02
3500	1.800E-02	1.954E-02	2.777E-02	3.837E-02	4.938E-02	6.061E-02
3600	1.901E-02	2.018E-02	2.686E-02	3.572E-02	4.636E-02	5.938E-02
3650			2.683E-02	3.578E-02		6.117E-02
3700	2.019E-02	2.095E-02	2.672E-02	3.648E-02	4.878E-02	6.218E-02
3750			2.588E-02	3.523E-02		6.475E-02
3800	2.163E-02	2.190E-02	2.514E-02	3.420E-02	4.738E-02	6.525E-02
3850	2.277E-02	2.310E-02	2.964E-02	4.225E-02	5.655E-02	6.860E-02
3900	2.343E-02	2.432E-02	3.456E-02	5.258E-02	7.050E-02	8.352E-02
3925	2.396E-02		3.537E-02			
3950		2.645E-02	4.877E-02	7.075E-02	8.220E-02	9.106E-02

TABLE A2-23. (Concluded)

1/cm	300K	600K	1200K	1800K	2400K	3000K
3975	2.512E-02		4.770E-02	6.979E-02	8.170E-02	
4000	2.577E-02	2.665E-02	3.977E-02	6.050E-02	7.850E-02	9.279E-02
4050	2.724E-02		3.576E-02	4.925E-02	5.865E-02	6.324E-02
4100	2.894E-02	2.919E-02	3.492E-02	4.683E-02	5.770E-02	6.486E-02
4150	3.113E-02		3.498E-02	4.504E-02	5.650E-02	6.598E-02
4200	3.383E-02	3.385E-02	3.583E-02	4.325E-02	5.395E-02	6.508E-02
4250			3.770E-02	3.979E-02		5.021E-02
4300	4.234E-02	4.233E-02	4.236E-02	4.242E-02	4.236E-02	4.230E-02
4350				5.013E-02		4.996E-02
4400	6.429E-02	6.429E-02	6.434E-02	6.442E-02	6.430E-02	6.425E-02
4450			1.092E-01	1.094E-01	1.092E-01	1.090E-01

TABLE A2-24. INTEGRATED ABSORPTANCE OF HF FUNDAMENTAL BAND SYSTEM ( $\text{cm}^{-1}$ )

T = 300K, C = 0 P <sub>T</sub> (atm) =			
u(cm) <sub>STP</sub>	.01	.1	1
.1	1.43 E+0	4.13 E+0	1.21 E+1
1.	4.25 E+0	1.30 E+1	3.96 E+1
10.	1.32 E+1	4.03 E+1	1.17 E+2
100.	4.04 E+1	1.18 E+2	2.94 E+2
1000.	1.18 E+2	2.94 E+2	5.27 E+2
10000.	2.94 E+2	5.28 E+2	6.74 E+2
T = 600K, C = 0 P <sub>T</sub> (atm) =			
u(cm) <sub>STP</sub>	.01	.1	1
.1	1.06 E+0	2.48 E+0	6.89 E+0
1.	2.70 E+0	7.77 E+0	2.35 E+1
10.	7.93 E+0	2.42 E+1	7.27 E+1
100.	2.44 E+1	7.33 E+1	2.03 E+2
1000.	7.46 E+1	2.05 E+2	4.51 E+2
10000.	2.16 E+2	4.63 E+2	6.83 E+2
T = 1200K, C = 0 P <sub>T</sub> (atm) =			
u(cm) <sub>STP</sub>	.01	.1	1
.1	1.50 E+0	2.24 E+0	4.95 E+0
1.	2.99 E+0	6.54 E+0	1.86 E+1
10.	7.11 E+0	1.98 E+1	5.99 E+1
100.	2.02 E+1	6.08 E+1	1.80 E+2
1000.	6.11 E+1	1.80 E+2	4.73 E+2
10000.	1.80 E+2	4.73 E+2	9.31 E+2

TABLE A2-24. (Concluded)

T = 1800K, C = 0 P <sub>T</sub> (atm) =			
u(cm) <sub>STP</sub>	.01	.1	1
.1	2.24 E+0	2.63 E+0	4.39 E+0
1.	4.35 E+0	7.16 E+0	1.81 E+1
10.	8.46 E+0	2.03 E+1	5.95 E+1
100.	2.12 E+1	6.11 E+1	1.82 E+2
1000.	6.18 E+1	1.83 E+2	4.99 E+2
10000.	1.84 E+2	5.00 E+2	1.07 E+3
T = 2400K, C = 0 P <sub>T</sub> (atm) =			
u(cm) <sub>STP</sub>	.01	.1	1
.1	2.48 E+0	2.64 E+0	3.51 E+0
1.	5.50 E+0	7.39 E+0	1.60 E+1
10.	9.73 E+0	1.93 E+1	5.38 E+1
100.	2.10 E+1	5.62 E+1	1.66 E+2
1000.	5.74 E+1	1.68 E+2	4.70 E+2
10000.	1.69 E+2	4.71 E+2	1.08 E+3
T = 3000K, C = 0 P <sub>T</sub> (atm) =			
u(cm) <sub>STP</sub>	.01	.1	1
.1	2.96 E+0	3.01 E+0	3.41 E+0
1.	7.70 E+0	9.24 E+0	1.72 E+1
10.	1.33 E+1	2.25 E+1	5.89 E+1
100.	2.56 E+1	6.27 E+1	1.83 E+2
1000.	6.50 E+1	1.86 E+2	5.22 E+2
10000.	1.87 E+2	5.24 E+2	1.22 E+3

TABLE A2-25. TOTAL EMISSIVITY OF HF

T = 300K, C = 0 P <sub>T</sub> (atm) =			
u(cm) <sub>STP</sub>	.01	.1	1
.1	5.88 E-8	1.63 E-7	4.62 E-7
1.	1.72 E-7	5.21 E-7	1.56 E-6
10.	5.30 E-7	1.62 E-6	4.74 E-6
100.	1.64 E-6	4.79 E-6	1.23 E-5
1000.	4.81 E-6	1.24 E-5	2.41 E-5
10000.	1.24 E-5	2.42 E-5	3.61 E-5
T = 600K, C = 0 P <sub>T</sub> (atm) =			
u(cm) <sub>STP</sub>	.01	.1	1
.1	2.63 E-5	6.10 E-5	1.68 E-4
1.	6.82 E-5	1.93 E-4	5.79 E-4
10.	2.00 E-4	6.03 E-4	1.81 E-3
100.	6.15 E-4	1.84 E-3	5.10 E-3
1000.	1.90 E-3	5.18 E-3	1.15 E-2
10000.	5.68 E-3	1.21 E-2	1.86 E-2
T = 1200K, C = 0 P <sub>T</sub> (atm) =			
u(cm) <sub>STP</sub>	.01	.1	1
.1	2.81 E-4	4.11 E-4	8.90 E-4
1.	5.61 E-4	1.20 E-3	3.37 E-3
10.	1.33 E-3	3.65 E-3	1.10 E-2
100.	3.74 E-3	1.12 E-2	3.31 E-2
1000.	1.13 E-3	3.32 E-2	8.78 E-2
10000.	3.33 E-2	8.80 E-2	1.77 E-1

TABLE A2-25. (Concluded)

T = 1800K, C = 0 P <sub>T</sub> (atm) =			
u(cm) <sub>STP</sub>	.01	.1	1
.1	4.23 E-4	4.83 E-4	7.70 E-4
1.	8.30 E-4	1.36 E-3	3.20 E-3
10.	1.63 E-3	3.71 E-3	1.07 E-2
100.	3.95 E-3	1.11 E-2	3.29 E-2
1000.	1.13 E-2	3.33 E-2	9.12 E-2
10000.	3.33 E-2	9.15 E-2	2.00 E-1
T = 2400K, C = 0 P <sub>T</sub> (atm) =			
u(cm) <sub>STP</sub>	.01	.1	1
.1	3.51 E-4	3.61 E-4	4.45 E-4
1.	7.85 E-4	1.01 E-3	2.05 E-3
10.	1.46 E-3	2.67 E-3	7.13 E-3
100.	3.07 E-3	7.70 E-3	2.24 E-2
1000.	7.95 E-3	2.27 E-2	6.38 E-2
10000.	2.30 E-2	6.44 E-2	1.50 E-1
T = 3000K, C = 0 P <sub>T</sub> (atm) =			
u(cm) <sub>STP</sub>	.01	.1	1
.1	2.93 E-4	2.89 E-4	2.94 E-4
1.	7.74 E-4	8.96 E-4	1.52 E-3
10.	1.49 E-3	2.28 E-3	5.57 E-3
100.	2.88 E-3	6.27 E-3	1.77 E-2
1000.	6.65 E-3	1.82 E-2	5.10 E-2
10000.	1.84 E-2	5.16 E-2	1.23 E-1

TABLE A2-26. INTEGRATED ABSORPTANCE OF CO<sub>2</sub>  
4.3- $\mu$  BAND SYSTEM (cm<sup>-1</sup>)

T = 300K		
PL (atm-cm STP)	Weak Line Limit	Doppler Limit
.0001	.295	.195
.001	2.90	.62
.01	23.4	1.47
.1	69.	2.9
1.	94.	
T = 600K		
PL (atm-cm STP)	Weak Line Limit	Doppler Limit
.0001	.297	
.001	2.95	1.49
.01	25.0	5.45
.1	96.	13.9
1.	137.	27.0
10.	165.	
T = 1200K		
PL (atm-cm STP)	Weak Line Limit	Doppler Limit
.001	2.95	2.45
.01	27.0	15.8
.1	130.	60.
1.	210.	135.
10.	250.	

TABLE A2-26. (Concluded)

T = 1800K	
PL (atm-cm STP)	Weak Line Limit
.0001	.297
.001	2.95
.01	27.8
.1	201.
1.	267.
10.	325.
T = 2400K	
PL (atm-cm STP)	Weak Line Limit
.0001	.297
.001	2.95
.01	27.8
.1	235.
1.	330.
10.	415.
T = 3000K	
PL (atm-cm STP)	Weak Line Limit
.0001	.297
.001	2.95
.01	27.8
.1	263.
1.	390.
10.	480.

GENERAL APPENDIX

TABLE A2-27. INTEGRATED ABSORPTANCE OF CO<sub>2</sub>  
2.7- $\mu$  BAND SYSTEM (cm<sup>-1</sup>)

T = 300K		
PL (atm-cm STP)	Weak Line Limit	Doppler Limit
.001	.078	
.01	.78	
.1	7.6	1.78
1.	57.	4.4
10.	153.	8.7
T = 600K		
PL (atm-cm STP)	Weak Line Limit	Doppler Limit
.001	.081	
.01	.81	
.1	8.1	4.5
1.	55.	17.
10.	212.	44.
T = 1200K		
PL (atm-cm STP)	Weak Line Limit	Doppler Limit
.001	.103	
.01	1.03	
.1	10.1	9.1
1.	84.	61.
10.	305.	185.

TABLE A2-27. (Concluded)

T = 1800K	
PL (atm-cm STP)	Weak Line Limit
.0001	.013
.001	.132
.01	1.32
.1	13.0
1.	110.
10.	370.
T = 2400K	
PL (atm-cm STP)	Weak Line Limit
.0001	.017
.001	.165
.01	1.65
.1	16.2
1.	139.
10.	445.
T = 3000K	
PL (atm-cm STP)	Weak Line Limit
.0001	.020
.001	.199
.01	1.99
.1	19.7
1.	169.
10.	585.

TABLE A2-28. ABSORPTION COEFFICIENTS FOR CO<sub>2</sub>, 15- $\mu$   
 FUNDAMENTAL BAND k (per cm at STP)

1/cm	300K	600K	1200K	1500K	1800K	2400K
500	.0000E+00	.0000E+00	.0000E+00	.1050E-01	.3000E-01	.8800E-01
505	.0000E+00	.0000E+00	.0000E+00	.1800E-01	.4900E-01	.8000E-01
510	.0000E+00	.0000E+00	.0000E+00	.3000E-01	.5400E-01	.7400E-01
515	.0000E+00	.0000E+00	.0000E+00	.3000E-01	.5600E-01	.8900E-01
520	.0000E+00	.0000E+00	.0000E+00	.3300E-01	.6900E-01	.9900E-01
525	.0000E+00	.0000E+00	.8800E-02	.3800E-01	.7200E-01	.9700E-01
530	.0000E+00	.0000E+00	.1100E-01	.5300E-01	.9500E-01	.1240E+00
535	.0000E+00	.0000E+00	.2850E-01	.6300E-01	.9900E-01	.1400E+00
540	.0000E+00	.0000E+00	.3300E-01	.6800E-01	.1030E+00	.1340E+00
545	.0000E+00	.0000E+00	.4500E-01	.9200E-01	.1380E+00	.1760E+00
550	.0000E+00	.0000E+00	.4900E-01	.9700E-01	.1480E+00	.1910E+00
555	.0000E+00	.0000E+00	.4900E-01	.1200E+00	.1880E+00	.2470E+00
560	.0000E+00	.0000E+00	.4800E-01	.1260E+00	.2010E+00	.2410E+00
565	.0000E+00	.0000E+00	.8200E-01	.1980E+00	.2700E+00	.2650E+00
570	.0000E+00	.7500E-02	.6900E-01	.1400E+00	.2250E+00	.3400E+00
575	.0000E+00	.2050E-01	.8200E-01	.1450E+00	.2360E+00	.5300E+00
580	.0000E+00	.3550E-01	.1170E+00	.1930E+00	.2950E+00	.5500E+00
585	.1570E-01	.5200E-01	.1700E+00	.2350E+00	.3050E+00	.4100E+00
590	.1500E-01	.8800E-01	.2700E+00	.3300E+00	.4400E+00	.5200E+00
595	.5100E-01	.1300E+00	.4000E+00	.5300E+00	.5600E+00	.5400E+00
600	.1200E+00	.1650E+00	.2750E+00	.3200E+00	.4200E+00	.5600E+00
605	.8800E-01	.1900E+00	.4300E+00	.5400E+00	.6200E+00	.6800E+00
610	.1100E+00	.3500E+00	.7100E+00	.7600E+00	.7600E+00	.6900E+00
615	.1800E+00	.4700E+00	.9200E+00	.9700E+00	.9100E+00	.6700E+00
620	.9700E-01	.2650E+00	.6100E+00	.7200E+00	.7800E+00	.7300E+00

TABLE A2-28. (Continued)

1/cm	300K	600K	1200K	1500K	1800K	2400K
625	.1750E+00	.3800E+00	.7200E+00	.7900E+00	.8300E+00	.8400E+00
630	.3700E+00	.6400E+00	.9200E+00	.9600E+00	.9800E+00	.9400E+00
635	.5900E+00	.8400E+00	.1070E+01	.1100E+01	.1110E+01	.1060E+01
640	.9400E+00	.1030E+01	.1150E+01	.1150E+01	.1150E+01	.1180E+01
645	.1960E+01	.1770E+01	.1460E+01	.1360E+01	.1320E+01	.1390E+01
650	.3450E+01	.2820E+01	.1980E+01	.1720E+01	.1560E+01	.1480E+01
655	.2820E+01	.2480E+01	.2000E+01	.1900E+01	.1860E+01	.2050E+01
660	.2540E+01	.2340E+01	.1840E+01	.1760E+01	.1740E+01	.2030E+01
665	.1420E+02	.8600E+01	.3700E+01	.2600E+01	.1960E+01	.1420E+01
670	.4500E+01	.5700E+01	.5800E+01	.5200E+01	.3500E+01	.4200E+01
675	.3600E+01	.3100E+01	.3300E+01	.2900E+01	.2050E+01	.2000E+01
680	.3100E+01	.2600E+01	.2000E+01	.1960E+01	.1800E+01	.2100E+01
685	.2400E+01	.2500E+01	.2300E+01	.2200E+01	.1700E+01	.1940E+01
690	.1820E+01	.2000E+01	.2180E+01	.2050E+01	.1840E+01	.1300E+01
695	.1040E+01	.1350E+01	.1720E+01	.1720E+01	.1650E+01	.1300E+01
700	.5500E+00	.1200E+01	.1430E+01	.1470E+01	.1480E+01	.1250E+01
705	.1360E+01	.1280E+01	.1280E+01	.1350E+01	.1380E+01	.1340E+01
710	.2100E+00	.7800E+00	.1270E+01	.1330E+01	.1370E+01	.1320E+01
715	.1900E+00	.7800E+00	.1400E+01	.1460E+01	.1470E+01	.1420E+01
720	.9000E+00	.1060E+01	.1400E+01	.1500E+01	.1550E+01	.1340E+01
725	.7200E-01	.3000E+00	.8000E+00	.1000E+01	.1150E+01	.1260E+01
730	.6400E-01	.2100E+00	.5600E+00	.7200E+00	.8600E+00	.1020E+01
735	.6800E-01	.2100E+00	.5300E+00	.6700E+00	.7900E+00	.1010E+01
740	.6900E-01	.2100E+00	.5400E+00	.6900E+00	.8200E+00	.9100E+00
745	.3300E-01	.1400E+00	.3900E+00	.5300E+00	.1650E+04	.7700E+00
750	.2300E-01	.7800E-01	.2700E+00	.4100E+00	.5600E+00	.8900E+00

1/cm	300K	600K	1200K	1500K	1800K	2400K
755	.3000E-01	.8600E-01	.2800E+00	.4000E+00	.5200E+00	.7100E+00
760	.1750E-01	.6200E-01	.2250E+00	.3350E+00	.4500E+00	.6600E+00
765	.1050E-01	.4500E-01	.1800E+00	.2800E+00	.3800E+00	.6000E+00
770	.4500E-02	.3000E-01	.1480E+00	.2400E+00	.3450E+00	.5700E+00
775	.0000E+00	.1400E-01	.1240E+00	.2050E+00	.2850E+00	.4300E+00
780	.0000E+00	.1150E-01	.1100E+00	.1850E+00	.2600E+00	.3750E+00
785	.0000E+00	.1350E-01	.8400E-01	.1400E+00	.2050E+00	.3350E+00
790	.0000E+00	.4300E-02	.6500E-01	.1200E+00	.1850E+00	.3250E+00
795	.0000E+00	.0000E+00	.5400E-01	.1150E+00	.1800E+00	.3150E+00
800	.0000E+00	.0000E+00	.4400E-01	.9500E-01	.1500E+00	.2700E+00
805	.0000E+00	.0000E+00	.3600E-01	.7900E-01	.1250E+00	.2050E+00
810	.0000E+00	.0000E+00	.2500E-01	.6500E-01	.1100E+00	.1780E+00
815	.0000E+00	.0000E+00	.1800E-01	.6200E-01	.1030E+00	.1530E+00
820	.0000E+00	.0000E+00	.3200E-01	.5800E-01	.8600E-01	.1470E+00
825	.0000E+00	.0000E+00	.8000E-02	.5100E-01	.8700E-01	.1340E+00
830	.0000E+00	.0000E+00	.6000E-02	.4800E-01	.8300E-01	.1330E+00
835	.0000E+00	.0000E+00	.0000E+00	.4300E-01	.7800E-01	.1180E+00
840	.0000E+00	.0000E+00	.0000E+00	.4200E-01	.7000E-01	.1080E+00
845	.0000E+00	.0000E+00	.0000E+00	.3600E-01	.6400E-01	.9800E-01
850	.0000E+00	.0000E+00	.0000E+00	.3500E-01	.6100E-01	.8700E-01
855	.0000E+00	.0000E+00	.0000E+00	.3200E-01	.5800E-01	.8600E-01
860	.0000E+00	.0000E+00	.0000E+00	.3300E-01	.5600E-01	.7500E-01
865	.0000E+00	.0000E+00	.0000E+00	.3000E-01	.5300E-01	.7500E-01
870	.0000E+00	.0000E+00	.0000E+00	.2900E-01	.5300E-01	.8500E-01
875	.0000E+00	.0000E+00	.0000E+00	.2400E-01	.4700E-01	.9000E-01
880	.0000E+00	.0000E+00	.0000E+00	.2200E-01	.4500E-01	.8600E-01

TABLE A2-28. (Concluded)

TABLE A2-29. ABSORPTION COEFFICIENTS FOR CO<sub>2</sub>, 4.3- $\mu$  FUNDAMENTAL BAND k (per cm at STP)

1/cm	300K	600K	1200K	1500K	1800K	2400K	3000K
1900	-0.	-0.	-0.	-0.	-0.	-0.	6.923E-02
1910	-0.	-0.	-0.	-0.	-0.	-0.	8.943E-02
1920	-0.	-0.	-0.	-0.	-0.	-0.	1.144E-01
1930	-0.	-0.	-0.	-0.	-0.	-0.	1.447E-01
1940	-0.	-0.	-0.	-0.	-0.	-0.	1.812E-01
1950	-0.	-0.	-0.	-0.	-0.	-0.	2.259E-01
1960	-0.	-0.	-0.	-0.	-0.	-0.	2.815E-01
1970	-0.	-0.	-0.	-0.	-0.	-0.	3.504E-01
1980	-0.	-0.	-0.	-0.	-0.	-0.	4.352E-01
1990	-0.	-0.	-0.	6.525E-05	-0.	6.443E-02	5.372E-01
2000	-0.	-0.	-0.	1.305E-04	-0.	1.289E-01	6.558E-01
2010	-0.	-0.	-0.	3.076E-04	-0.	1.727E-01	8.004E-01
2020	-0.	-0.	-0.	4.848E-04	-0.	2.284E-01	9.665E-01
2030	-0.	-0.	-0.	1.098E-03		2.985E-01	1.159E+00
2040	-0.	-0.	-0.	1.712E-03	-0.	3.883E-01	1.427E+00
2050	-0.	-0.	-0.	3.710E-03	-0.	5.030E-01	1.662E+00
2060	-0.	-0.	-0.	5.708E-03	-0.	6.488E-01	1.958E+00
2070	-0.	-0.	-0.	1.178E-02	-0.	8.320E-01	2.299E+00
2080	-0.	-0.	-0.	1.785E-02	-0.	1.059E+00	2.802E+00
2090	-0.	-0.	-0.	3.491E-02	1.461E-01	1.331E+00	3.171E+00
2100	-0.	-0.	-0.	5.196E-02	2.923E-01	1.663E+00	3.651E+00
2110	-0.	-0.	-0.	8.608E-02	4.157E-01	2.058E+00	4.180E+00
2120	-0.	-0.	-0.	1.396E-01	5.813E-01	2.539E+00	4.881E+00
2130	-0.	-0.	3.746E-02	2.216E-01	8.043E-01	3.083E+00	5.474E+00
2140	-0.	-0.	7.491E-02	3.437E-01	1.104E+00	3.717E+00	6.125E+00
2150				5.212E-01	1.501E+00	4.521E+00	7.315E+00

TABLE A2-29. (Continued)

1/cm	300K	600K	1200K	1500K	1800K	2400K	3000K
2155	-0.	-0.	1.012E-01	6.468E-01	1.758E+00	4.898E+00	7.494E+00
2160	-0.	-0.	1.357E-01	7.724E-01	2.016E+00	5.276E+00	7.673E+00
2165	-0.	-0.	1.807E-01	9.488E-01	2.340E+00	5.722E+00	8.006E+00
2170	-0.	-0.	2.388E-01	1.125E+00	2.664E+00	6.169E+00	8.339E+00
2175	-0.	-0.	3.134E-01	1.372E+00	3.066E+00	6.652E+00	8.670E+00
2180	-0.	-0.	4.081E-01	1.618E+00	3.467E+00	7.136E+00	9.000E+00
2185	-0.	-0.	5.274E-01	1.954E+00	3.960E+00	7.724E+00	9.742E+00
2190	-0.	-0.	6.765E-01	2.289E+00	4.453E+00	8.313E+00	1.048E+01
2195	-0.	3.728E-04	8.611E-01	2.734E+00	5.037E+00	8.829E+00	1.057E+01
2200	-0.	7.456E-04	1.088E+00	3.180E+00	5.621E+00	9.344E+00	1.066E+01
2205	-0.	1.444E-03	1.364E+00	3.753E+00	6.284E+00	9.870E+00	1.088E+01
2210	-0.	2.760E-03	1.702E+00	4.326E+00	6.975E+00	1.040E+01	1.110E+01
2215	-0.	5.202E-03	2.110E+00	5.042E+00	7.706E+00	1.090E+01	1.127E+01
2220	-0.	9.661E-03	2.606E+00	5.758E+00	8.493E+00	1.140E+01	1.145E+01
2225	-0.	1.767E-02	3.191E+00	6.629E+00	9.294E+00	1.200E+01	1.201E+01
2230	-0.	3.183E-02	3.883E+00	7.500E+00	1.016E+01	1.261E+01	1.257E+01
2235	-0.	5.641E-02	4.690E+00	8.494E+00	1.098E+01	1.298E+01	1.252E+01
2240	-0.	9.829E-02	5.614E+00	9.489E+00	1.185E+01	1.336E+01	1.247E+01
2245	3.878E-05	1.683E-01	6.679E+00	1.059E+01	1.276E+01	1.366E+01	1.241E+01
2250	7.757E-05	2.829E-01	7.846E+00	1.168E+01	1.351E+01	1.396E+01	1.236E+01
2255	2.543E-04	4.667E-01	9.179E+00	1.288E+01	1.439E+01	1.479E+01	1.390E+01
2260	8.058E-04	7.550E-01	1.058E+01	1.398E+01	1.521E+01	1.562E+01	1.544E+01
2265	2.464E-03	1.197E+00	1.213E+01	1.517E+01	1.585E+01	1.525E+01	1.398E+01
2270	7.260E-03	1.856E+00	1.368E+01	1.620E+01	1.640E+01	1.489E+01	1.252E+01
2275	2.056E-02	2.816E+00	1.533E+01	1.726E+01	1.697E+01	1.483E+01	1.216E+01

TABLE A2-29. (Concluded)

1/cm	300K	600K	1200K	1500K	1800K	2400K	3000K
2280	5.587E-02	4.174E+00	1.689E+01	1.812E+01	1.734E+01	1.477E+01	1.181E+01
2285	1.452E-01	6.032E+00	1.842E+01	1.907E+01	1.789E+01	1.462E+01	1.143E+01
2290	3.602E-01	8.490E+00	1.985E+01	1.960E+01	1.793E+01	1.447E+01	1.105E+01
2295	8.492E-01	1.162E+01	2.092E+01	2.000E+01	1.817E+01	1.510E+01	1.211E+01
2300	1.896E+00	1.550E+01	2.209E+01	2.042E+01	1.858E+01	1.574E+01	1.317E+01
2305	3.985E+00	1.989E+01	2.241E+01	2.038E+01	1.809E+01	1.434E+01	1.223E+01
2310	7.844E+00	2.482E+01	2.329E+01	2.092E+01	1.849E+01	1.474E+01	1.129E+01
2315	1.434E+01	2.934E+01	2.300E+01	2.048E+01	1.849E+01	1.594E+01	1.064E+01
2320	2.407E+01	3.349E+01	2.327E+01	2.072E+01	1.815E+01	1.384E+01	9.987E+00
2325	3.660E+01	3.552E+01	2.263E+01	2.034E+01	1.775E+01	1.328E+01	9.291E+00
2330	4.955E+01	3.616E+01	2.262E+01	2.039E+01	1.766E+01	1.271E+01	8.595E+00
2335	5.733E+01	3.401E+01	2.275E+01	2.053E+01	1.745E+01	1.202E+01	8.926E+00
2340	5.428E+01	2.931E+01	2.238E+01	2.116E+01	1.785E+01	1.308E+01	9.257E+00
2345	3.709E+01	2.640E+01	2.308E+01	2.033E+01	1.654E+01	1.039E+01	8.216E+00
2350	1.138E+01	2.082E+01	2.282E+01	2.028E+01	1.680E+01	1.113E+01	7.175E+00
2355	5.283E+01	3.627E+01	2.523E+01	1.989E+01	1.706E+01	1.177E+01	6.247E+00
2360	7.796E+01	4.701E+01	2.620E+01	2.047E+01	1.556E+01	9.080E+00	5.319E+00
2365	7.550E+01	5.033E+01	2.546E+01	1.939E+01	1.464E+01	8.851E+00	4.436E+00
2370	5.149E+01	4.548E+01	2.319E+01	1.699E+01	1.223E+01	6.507E+00	3.553E+00
2375	2.410E+01	3.436E+01	1.960E+01	1.446E+01	1.066E+01	6.027E+00	2.653E+00
2380	7.111E+00	2.096E+01	1.508E+01	1.089E+01	8.982E+00	3.566E+00	1.753E+00
2385	1.123E+00	9.634E+00	1.063E+01	8.434E+00	6.427E+00	3.568E+00	1.263E+00
2390	6.789E-02	2.886E+00	5.809E+00	4.217E+00	3.314E+00	1.585E+00	7.741E-01
2395	6.472E-04	3.776E-01	2.817E+00	-0.	2.496E+00	1.502E+00	-0.

TABLE A2-30. ABSORPTION COEFFICIENTS FOR CO<sub>2</sub>, 2.7- $\mu$   
COMBINATION BAND k (per cm at STP)

1/cm	300K	600K	1200K	1500K	1800K	2400K	3000K
3000	-0.	-0.	-0.	-0.	-0.	-0.	1.166E-02
3010	-0.	-0.	-0.	-0.	-0.	-0.	1.270E-02
3020	-0.	-0.	-0.	-0.	-0.	-0.	1.373E-02
3030	-0.	-0.	-0.	-0.	-0.	-0.	1.567E-02
3040	-0.	-0.	-0.	-0.	-0.	-0.	1.761E-02
3050	-0.	-0.	-0.	-0.	-0.	-0.	2.032E-02
3060	-0.	-0.	-0.	-0.	-0.	-0.	2.303E-02
3070	-0.	-0.	-0.	-0.	-0.	-0.	2.489E-02
3080	-0.	-0.	-0.	-0.	-0.	-0.	2.675E-02
3090	-0.	-0.	-0.	-0.	-0.	3.399E-03	3.016E-02
3100	-0.	-0.	-0.	-0.	-0.	6.798E-03	3.356E-02
3110	-0.	-0.	2.145E-10	-0.	-0.	8.290E-03	3.803E-02
3120	-0.	-0.	4.290E-10	-0.	-0.	9.782E-03	4.250E-02
3130	-0.	-0.	1.516E-09	-0.	-0.	1.131E-02	4.590E-02
3140	-0.	-0.	2.602E-09	-0.	-0.	1.324E-02	4.929E-02
3150	-0.	-0.	8.828E-09	-0.	-0.	1.565E-02	5.510E-02
3160	-0.	-0.	1.505E-08	1.361E-05	5.917E-04	1.806E-02	6.091E-02
3170	-0.	-0.	4.883E-08	2.723E-05	1.183E-03	2.132E-02	6.984E-02
3180	-0.	-0.	8.260E-08	4.842E-05	1.661E-03	2.459E-02	7.878E-02
3190	-0.	-0.	2.548E-07	8.452E-05	2.267E-03	2.755E-02	8.107E-02
3200	-0.	-0.	4.271E-07	1.446E-04	3.003E-03	3.052E-02	8.336E-02
3210	-0.	3.505E-20	1.246E-06	2.419E-04	3.853E-03	3.505E-02	9.171E-02
3220	-0.	7.010E-20	2.064E-06	3.953E-04	4.785E-03	3.958E-02	1.001E-01
3230	-0.	1.554E-18	4.412E-06	6.295E-04	6.050E-03	4.569E-02	1.124E-01

TABLE A2-30. (Continued)

1/cm	300K	600K	1200K	1500K	1800K	2400K	3000K
3240	-0.	3.038E-18	9.237E-06	9.745E-04	7.677E-03	5.179E-02	1.248E-01
3250	-0.	6.243E-17	1.891E-05	1.463E-03	9.785E-03	5.728E-02	1.276E-01
3260	-0.	1.218E-16	3.780E-05	2.125E-03	1.225E-02	6.296E-02	1.304E-01
3270	-0.	2.302E-15	7.361E-05	2.981E-03	1.519E-02	7.520E-02	1.414E-01
3280	-0.	4.483E-15	1.394E-04	4.030E-03	1.821E-02	7.927E-02	1.524E-01
3290	1.100E-32	7.724E-14	2.558E-04	5.252E-03	2.185E-02	8.682E-02	1.667E-01
3300	2.200E-32	1.500E-13	4.542E-04	6.917E-03	2.639E-02	9.940E-02	1.811E-01
3310	8.768E-31	2.331E-12	7.774E-04	9.072E-03	3.111E-02	1.071E-01	1.860E-01
3320	3.397E-29	4.512E-12	1.279E-03	1.195E-02	3.726E-02	1.179E-01	1.908E-01
3330	1.243E-27	2.368E-11	2.017E-03	1.532E-02	4.405E-02	1.334E-01	2.041E-01
3340	4.340E-26	1.204E-10	3.041E-03	1.942E-02	5.182E-02	1.425E-01	2.174E-01
3350	1.442E-24	5.914E-10	4.378E-03	2.412E-02	5.986E-02	1.495E-01	2.468E-01
3360	4.549E-23	2.802E-09	6.029E-03	2.986E-02	7.100E-02	1.785E-01	2.761E-01
3370	1.358E-21	1.276E-08	8.331E-03	3.688E-02	8.066E-02	1.763E-01	2.380E-01
3380	3.819E-20	5.572E-08	1.155E-02	4.486E-02	9.186E-02	1.851E-01	2.397E-01
3390	1.009E-18	2.324E-07	1.586E-02	5.462E-02	1.064E-01	2.063E-01	2.705E-01
3400	2.493E-17	9.225E-07	2.104E-02	6.493E-02	1.185E-01	2.116E-01	2.637E-01
3410	5.730E-16	3.470E-06	2.806E-02	7.862E-02	1.354E-01	2.256E-01	2.718E-01
3420	1.219E-14	1.230E-05	3.617E-02	9.178E-02	1.511E-01	2.471E-01	3.126E-01
3430	2.385E-13	4.091E-05	4.683E-02	1.090E-01	1.681E-01	2.516E-01	2.996E-01
3440	4.262E-12	1.267E-04	5.915E-02	1.254E-01	1.812E-01	2.463E-01	2.801E-01
3450	6.900E-11	3.632E-04	7.424E-02	1.433E-01	2.052E-01	3.020E-01	3.865E-01
3460	1.003E-09	9.565E-04	9.206E-02	1.640E-01	2.143E-01	2.694E-01	3.053E-01
3470	1.295E-08	2.299E-03	1.112E-01	1.816E-01	2.242E-01	2.682E-01	3.027E-01
3480	1.467E-07	5.017E-03	1.351E-01	2.038E-01	2.442E-01	2.928E-01	3.389E-01

TABLE A2-30. (Continued)

1/cm	300K	600K	1200K	1500K	1800K	2400K	3000K
3490	5.300E-04	9.936E-03	1.548E-01	2.169E-01	2.469E-01	2.819E-01	3.314E-01
3500	1.198E-05	1.799E-02	1.857E-01	2.422E-01	2.664E-01	2.988E-01	3.501E-01
3510	8.339E-05	3.103E-02	2.054E-01	2.477E-01	2.698E-01	3.137E-01	3.913E-01
3520	4.747E-04	5.290E-02	2.310E-01	2.652E-01	2.772E-01	3.192E-01	3.899E-01
3530	2.162E-03	8.412E-02	2.483E-01	2.685E-01	2.693E-01	3.006E-01	3.694E-01
3540	4.889E-02	1.228E-01	2.656E-01	2.692E-01	3.033E-01	4.050E-01	5.155E-01
3550	2.125E-02	1.684E-01	2.763E-01	2.818E-01	2.837E-01	3.358E-01	4.173E-01
3560	4.482E-02	1.912E-01	2.544E-01	2.566E-01	2.643E-01	3.353E-01	4.292E-01
3565	6.359E-02	2.163E-01	2.611E-01	2.622E-01	2.740E-01	3.508E-01	4.436E-01
3570	8.610E-02	2.537E-01	2.679E-01	2.677E-01	2.836E-01	3.662E-01	4.580E-01
3575	1.106E-01	2.716E-01	2.631E-01	2.632E-01	2.809E-01	3.684E-01	4.608E-01
3580	1.465E-01	2.648E-01	2.583E-01	2.587E-01	2.782E-01	3.705E-01	4.636E-01
3585	2.826E-01	3.578E-01	2.784E-01	2.774E-01	3.004E-01	3.965E-01	4.822E-01
3590	4.404E-01	4.281E-01	2.986E-01	2.961E-01	3.226E-01	4.225E-01	5.008E-01
3595	5.782E-01	4.560E-01	2.903E-01	2.956E-01	3.264E-01	4.277E-01	5.029E-01
3600	6.342E-01	4.255E-01	2.821E-01	2.952E-01	3.301E-01	4.330E-01	5.050E-01
3605	5.391E-01	3.292E-01	2.413E-01	2.798E-01	3.345E-01	4.521E-01	5.216E-01
3610	2.525E-01	1.740E-01	2.004E-01	2.643E-01	3.390E-01	4.712E-01	5.383E-01
3615	1.824E-01	1.063E-01	1.958E-01	2.641E-01	3.383E-01	4.662E-01	5.337E-01
3620	6.008E-01	2.321E-01	1.911E-01	2.638E-01	3.377E-01	4.613E-01	5.290E-01
3625	8.115E-01	3.494E-01	2.163E-01	2.797E-01	3.706E-01	4.948E-01	5.549E-01
3630	7.264E-01	4.134E-01	2.415E-01	2.957E-01	4.035E-01	5.283E-01	5.807E-01
3635	4.525E-01	3.977E-01	2.752E-01	3.366E-01	4.180E-01	5.218E-01	5.683E-01
3640	1.890E-01	3.130E-01	3.089E-01	3.776E-01	4.325E-01	5.154E-01	5.558E-01
3645	4.820E-02	2.013E-01	3.248E-01	4.019E-01	4.536E-01	5.254E-01	5.600E-01

TABLE A2-30. (Concluded)

1/cm	300K	600K	1200K	1500K	1800K	2400K	3000K
3650	7.095E-03	1.127E-01	3.407E-01	4.261E-01	4.746E-01	5.354E-01	5.642E-01
3655	3.107E-03	7.624E-02	1.877E-01	4.323E-01	4.803E-01	5.375E-01	5.646E-01
3660	7.331E-03	8.834E-02	3.471E-02	4.385E-01	4.859E-01	5.397E-01	5.651E-01
3665	1.776E-02	1.290E-01	2.197E-01	4.495E-01	4.841E-01	5.302E-01	5.555E-01
3670	4.043E-02	1.881E-01	4.046E-01	4.605E-01	4.822E-01	5.207E-01	5.459E-01
3675	8.591E-02	2.671E-01	4.544E-01	4.921E-01	5.005E-01	5.277E-01	5.468E-01
3680	1.691E-01	3.634E-01	5.042E-01	5.238E-01	5.187E-01	5.346E-01	5.477E-01
3685	3.051E-01	4.691E-01	5.254E-01	5.303E-01	5.214E-01	5.388E-01	5.485E-01
3690	4.982E-01	5.696E-01	5.465E-01	5.368E-01	5.241E-01	5.429E-01	5.493E-01
3695	7.218E-01	6.423E-01	5.125E-01	5.045E-01	5.032E-01	5.340E-01	5.376E-01
3700	8.999E-01	6.584E-01	4.786E-01	4.722E-01	4.822E-01	5.252E-01	5.259E-01
3705	9.102E-01	5.888E-01	4.041E-01	4.234E-01	4.554E-01	5.101E-01	5.038E-01
3710	6.358E-01	4.169E-01	3.296E-01	3.746E-01	4.286E-01	4.950E-01	4.817E-01
3715	6.328E-02	1.545E-01	3.313E-01	3.832E-01	4.337E-01	4.800E-01	4.497E-01
3720	6.949E-01	3.365E-01	3.330E-01	3.918E-01	4.388E-01	4.649E-01	4.177E-01
3725	1.159E+00	5.998E-01	4.776E-01	4.953E-01	4.942E-01	4.603E-01	3.845E-01
3730	1.256E+00	8.751E-01	6.222E-01	5.988E-01	5.496E-01	4.557E-01	3.513E-01
3735	9.516E-01	9.845E-01	6.958E-01	6.468E-01	5.735E-01	4.482E-01	3.315E-01
3740	5.092E-01	9.013E-01	7.695E-01	6.947E-01	5.973E-01	4.407E-01	3.118E-01
3745	1.869E-01	6.716E-01	6.933E-01	6.351E-01	5.457E-01	3.929E-01	2.709E-01
3750	4.535E-02	3.965E-01	6.171E-01	5.755E-01	4.942E-01	3.450E-01	2.300E-01
3755	7.247E-03	1.762E-01	4.440E-01	4.339E-01	3.840E-01	2.709E-01	1.793E-01
3760	7.296E-04	5.455E-02	2.708E-01	2.923E-01	2.738E-01	1.967E-01	1.285E-01
3765	2.915E-05	1.048E-02	1.505E-01	1.667E-01	1.594E-01	1.168E-01	7.680E-02
3770	1.079E-07	6.896E-04	3.010E-02	4.100E-02	4.508E-02	3.681E-02	2.507E-02

TABLE A2-31. FINE STRUCTURE PARAMETERS FOR CO<sub>2</sub>  
(MLG MODEL), 4.3- $\mu$  BAND, 1/d<sub>0</sub> (cm)

1/cm	300K	600K	1200K	1500K	1800K	2400K	3000K	epsilon
2000	1.50	3.80	16.00	23.00	35.00	62.00	94.00	.25
2010	1.50	3.80	16.00	23.00	35.00	61.80	92.00	.25
2020	1.50	3.80	16.00	23.00	35.00	61.50	87.00	.25
2030	1.50	3.80	16.00	23.00	35.00	61.00	82.00	.25
2040	1.50	3.80	16.00	23.00	35.00	60.70	77.00	.25
2050	1.50	3.80	16.00	23.00	35.00	60.50	72.00	.25
2060	1.50	3.80	16.00	23.00	35.00	59.70	67.00	.25
2070	1.50	3.80	16.00	23.00	35.00	59.00	61.00	.25
2080	1.50	3.80	16.00	23.00	35.00	58.00	57.00	.25
2090	1.50	3.80	16.00	23.00	35.00	56.40	52.00	.25
2100	1.50	3.80	16.00	23.00	34.50	55.00	48.00	.25
2110	1.50	3.80	16.00	23.00	34.20	51.50	44.00	.25
2120	1.50	3.80	16.00	23.00	33.50	48.50	41.00	.25
2130	1.50	3.80	16.00	23.00	32.50	45.00	37.50	.25
2140	1.50	3.80	16.00	23.00	31.20	41.00	34.00	.25
2150	1.50	3.80	16.00	23.00	30.00	37.50	31.00	.25
2160	1.50	3.80	15.70	22.80	28.30	34.80	27.50	.25
2170	1.50	3.80	15.30	22.50	26.80	30.50	24.50	.25
2180	1.50	3.80	15.00	22.20	25.30	27.00	21.60	.25
2190	1.50	3.80	14.60	21.50	23.80	24.00	19.20	.25
2200	1.50	3.80	14.00	20.30	22.00	21.00	17.00	.25
2210	1.50	3.75	13.20	18.70	20.00	18.80	14.80	.25
2220	1.50	3.73	12.30	16.00	17.30	17.00	13.00	.25
2230	1.50	3.70	11.30	13.50	15.00	14.90	11.20	.25

TABLE A2-31. (Concluded)

1/cm	300K	600K	1200K	1500K	1800K	2400K	3000K	epsilon
2240	1.50	3.65	10.10	11.30	13.00	12.10	9.80	.25
2250	1.50	3.60	9.10	10.00	11.20	10.00	8.50	.25
2260	1.50	3.48	8.00	9.00	10.00	9.60	7.40	.25
2270	1.50	3.25	7.00	8.40	8.90	9.00	6.20	.25
2280	1.45	2.90	6.00	7.70	7.40	7.30	4.90	.25
2290	1.40	2.35	5.10	6.70	5.80	5.10	3.50	.25
2300	1.20	1.50	4.10	3.20	4.20	3.20	2.20	.50
2310	1.00	1.25	3.15	2.75	2.50	2.10	1.30	.50
2320	.80	1.10	2.25	2.40	1.70	1.20	.80	.50
2330	.63	1.10	1.80	1.90	1.30	.83	.57	.50
2340	.61	1.40	1.70	1.50	1.20	.85	.56	.50
2350	1.80	2.60	3.20	3.40	2.80	2.30	1.80	.10
2360	.83	1.50	2.20	2.00	1.70	1.50	1.10	.10
2370	.71	.86	1.30	1.50	1.10	.70	.50	.04
2380	.73	.67	.67	.57	.44	.39	.25	.00
2390	.97	.56	.29	.23	.20	.19	.14	.00

TABLE A2-32. FINE STRUCTURE PARAMETERS FOR CO<sub>2</sub>  
(MLG MODEL), 2.7- $\mu$  BAND, 1/d<sub>0</sub> (cm)

1/cm	300K	600K	1200K	1500K	1800K	2400K	3000K	epsilon
3080	.72	1.90	8.00	14.00	25.00			.25
3090	.72	1.90	8.00	14.00	25.00			.25
3100	.72	1.90	8.00	14.00	25.00			.25
3110	.72	1.90	8.00	14.00	25.00			.25
3120	.72	1.90	8.00	14.00	25.00			.25
3130	.72	1.90	8.00	14.00	25.00			.25
3140	.72	1.90	8.00	14.00	25.00			.25
3150	.72	1.90	8.00	14.00	25.00			.25
3160	.72	1.91	8.10	14.00	25.00			.25
3170	.72	1.91	8.15	14.10	25.00			.25
3180	.72	1.92	8.20	14.20	25.00			.25
3190	.72	1.92	8.30	14.50	25.20			.25
3200	.72	1.93	8.50	14.70	25.80			.25
3210	.72	1.93	8.70	15.00	26.40			.25
3220	.72	1.94	8.90	15.30	27.20			.25
3230	.72	1.95	9.30	15.80	28.50			.25
3240	.72	1.96	9.70	16.60	30.00			.25
3250	.72	1.97	10.20	17.60	32.00			.25
3260	.72	1.99	10.70	18.60	34.50			.25
3270	.73	2.01	11.20	20.00	37.50			.25
3280	.73	2.02	11.80	21.20	41.00			.25
3290	.73	2.05	12.60	22.80	45.00			.25
3300	.74	2.08	13.30	24.50	53.00			.25
3310	.75	2.12	14.30	26.70	71.00			.25

TABLE A2-32. (Continued)

1/cm	300K	600K	1200K	1500K	1800K	2400K	3000K	epsilon
3320	.76	2.15	15.30	29.20	90.00			.25
3330	.77	2.20	16.40	32.00	95.00			.25
3340	.79	2.24	17.10	34.80	98.00			.25
3350	.81	2.30	18.00	38.00	100.00			.25
3360	.83	2.37	18.30	41.50	104.00			.25
3370	.85	2.47	18.80	45.00	107.00			.25
3380	.87	2.57	19.10	45.50	113.00			.25
3390	.89	2.68	19.20	43.50	118.00			.25
3400	.92	2.80	19.00	40.00	120.00			.25
3410	.95	2.96	18.10	35.00	110.00			.25
3420	.98	3.13	17.00	30.00	70.00			.25
3430	1.02	3.32	15.40	25.00	44.00			.25
3440	1.06	3.55	13.70	20.00	31.50			.25
3450	1.10	3.80	12.00	16.30	23.50			.25
3460	1.15	4.05	10.50	13.30	17.40			.25
3470	1.20	4.37	9.30	11.00	13.30			.25
3480	1.26	4.65	8.10	9.10	10.50			.25
3490	1.33	4.68	7.00	7.60	8.50			.25
3500	1.41	4.55	6.10	6.60	7.20			.25
3510	1.50	4.30	5.40	5.70	6.40			.25
3520	1.62	4.00	4.70	5.10	5.50			.25
3530	1.80	3.60	4.20	4.50	4.70			.25
3540	1.86	3.15	3.80	4.10	4.30			.25
3550	1.70	2.70	3.50	3.70	3.90			.25
3560	1.48	2.25	3.30	3.50	3.65			.25

TABLE A2-32. (Concluded)

1/cm	300K	600K	1200K	1500K	1800K	2400K	3000K	epsilon
3570	1.24	1.84	3.55	3.35	3.65			.25
3580	1.00	1.27	3.45	3.30	3.85			.25
3590	.76	.91	2.45	3.25	4.50			.50
3600	.56	.70	2.10	3.20	5.70			.50
3610	.44	.54	2.50	3.35	7.50			.50
3620	.40	.35	3.20	4.30	10.50			.50
3630	.39	.27	3.65	6.50	14.80			.50
3640	.80	.40	3.95	8.10	19.80			.50
3650	.89	1.10	4.20	8.40	21.00			.50
3660	.81	1.40	4.70	8.30	19.80			.50
3670	.43	1.31	3.90	8.10	17.40			.50
3680	.44	1.20	3.75	7.70	15.20			.50
3690	.50	1.15	4.05	7.20	13.00			.50
3700	.58	1.20	4.30	6.70	11.20			.50
3710	.69	1.30	4.10	6.10	9.70			.50
3720	.83	1.45	3.80	5.60	8.40			.50
3730	1.09	1.60	3.50	5.10	7.30			.50
3740	1.55	1.72	3.30	4.60	6.30			.50
3750	2.30	1.80	3.10	4.10	5.40			.10
3760	2.40	1.67	2.40	3.70	4.70			.10
3770	1.80	1.50	1.45	3.25	4.00			.10

TABLE A2-33. FINE STRUCTURE PARAMETERS FOR CO<sub>2</sub> (SLG MODEL),  
4.3- $\mu$  BAND, 1/d (cm)

1/cm	300K	600K	1200K	1500K	1800K	2400K	3000K
2000	.2553E+01	.1449E+02	.1844E+03	.4008E+03	.8727E+03	.2820E+04	.7015E+04
2010	.2553E+01	.1449E+02	.1844E+03	.4008E+03	.8727E+03	.2810E+04	.6865E+04
2020	.2553E+01	.1449E+02	.1844E+03	.4008E+03	.8727E+03	.2797E+04	.6492E+04
2030	.2553E+01	.1449E+02	.1844E+03	.4008E+03	.8727E+03	.2774E+04	.6119E+04
2040	.2553E+01	.1449E+02	.1844E+03	.4008E+03	.8727E+03	.2760E+04	.5746E+04
2050	.2553E+01	.1449E+02	.1844E+03	.4008E+03	.8727E+03	.2751E+04	.5373E+04
2060	.2553E+01	.1449E+02	.1844E+03	.4008E+03	.8727E+03	.2715E+04	.5000E+04
2070	.2553E+01	.1449E+02	.1844E+03	.4008E+03	.8727E+03	.2683E+04	.4552E+04
2080	.2553E+01	.1449E+02	.1844E+03	.4008E+03	.8727E+03	.2638E+04	.4253E+04
2090	.2553E+01	.1449E+02	.1844E+03	.4008E+03	.8727E+03	.2565E104	.3880E+04
2100	.2553E+01	.1449E+02	.1844E+03	.4008E+03	.8603E+03	.2501E+04	.3582E+04
2110	.2553E+01	.1449E+02	.1844E+03	.4008E+03	.8528E+03	.2342E+04	.3283E+04
2120	.2553E+01	.1449E+02	.1844E+03	.4008E+03	.8353E+03	.2205E+04	.3059E+04
2130	.2553E+01	.1449E+02	.1844E+03	.4008E+03	.8104E+03	.2046E+04	.2798E+04
2140	.2553F+01	.1449E+02	.1844E+03	.4008E+03	.7780E+03	.1864E+04	.2537E+04
2150	.2553E+01	.1449E+02	.1844E+03	.4008E+03	.7480E+03	.1705E+04	.2313E+04
2160	.2553E+01	.1449E+02	.1809E+03	.3974E+03	.7057E+03	.1852E+04	.2052E+04
2170	.2553E+01	.1449E+02	.1763E+03	.3921E+03	.6682E+03	.1387E+04	.1828E+04
2180	.2553E+01	.1449E+02	.1728E+03	.3869E+03	.6308E+03	.1228E+04	.1611E+04
2190	.2553E+01	.1449E+02	.1682E+03	.3747E+03	.5934E+03	.1091E+04	.1432E+04
2200	.2553E+01	.1449E+02	.1613E+03	.3538E+03	.5486E+03	.9551E+03	.1268E+04
2210	.2553E+01	.1430E+02	.1521E+03	.3259E+03	.4987E+03	.8551E+03	.1104E+04
2220	.2553E+01	.1423E+02	.1417E+03	.2788E+03	.4314E+03	.7732E+03	.9701E+03
2230	.2553E+01	.1411E+02	.1302E+03	.2353E+03	.3740E+03	.6777E+03	.8358E+03
2240	.2553E+01	.1392E+02	.1164E+03	.1969E+03	.3241E+03	.5503E+03	.7313E+03

TABLE A2-33. (Continued)

1/cm	300K	600K	1200K	1500K	1800K	2400K	3000K
2250	.2553E+01	.1373E+02	.1048E+03	.1743E+03	.2792E+03	.4548E+03	.6343E+03
2260	.2553E+01	.1327E+02	.9221E+02	.1568E+03	.2493E+03	.4366E+03	.5522E+03
2270	.2553E+01	.1239E+02	.8068E+02	.1464E+03	.2219E+03	.4093E+03	.4627E+03
2280	.2468E+01	.1106E+02	.6915E+02	.1342E+03	.1845E+03	.3320E+03	.3656E+03
2290	.2383E+01	.8965E+01	.5878E+02	.1167E+03	.1446E+03	.2319E+03	.2612E+03
2300	.2293E+01	.7826E+01	.8447E+02	.1091E+03	.2201E+03	.3408E+03	.4152E+03
2310	.1910E+01	.6521E+01	.6490E+02	.9376E+02	.1310E+03	.2236E+03	.2453E+03
2320	.1528E+01	.5739E+01	.4635E+02	.8183E+02	.8912E+02	.1278E+03	.1509E+03
2330	.1203E+01	.5739E+01	.3708E+02	.6478E+02	.6815E+02	.8841E+02	.1075E+03
2340	.1165E+01	.7304E+01	.3502E+02	.5114E+02	.6291E+02	.9054E+02	.1056E+03
2350	.2849E+01	.8005E+01	.2347E+02	.3430E+02	.3721E+02	.4863E+02	.5602E+02
2360	.1313E+01	.4618E+01	.1613E+02	.2017E+02	.2259E+02	.3171E+02	.3423E+02
2370	.1090E+01	.2413E+01	.7701E+01	.1156E+02	.1061E+02	.9790E+01	.9484E+01
2380	.1099E+01	.1763E+01	.3394E+01	.3380E+01	.3319E+01	.3912E+01	.3131E+01
2390	.1460E+01	.1473E+01	.1469E+01	.1470E+01	.1508E+01	.1906E+01	.1753E+01

TABLE A2-34. FINE STRUCTURE PARAMETERS FOR CO<sub>2</sub> (SLG MODEL),  
2.7- $\mu$  BAND, 1/d (cm)

1/cm	300K	600K	1200K	1500K	1800K	2400K	3000K
3080	.1225E+01	.7248E+01	.9221E+02	.2440E+03	.6234E+03		
3090	.1225E+01	.7248E+01	.9221E+02	.2440E+03	.6234E+03		
3100	.1225E+01	.7248E+01	.9221E+02	.2440E+03	.6234E+03		
3110	.1225E+01	.7248E+01	.9221E+02	.2440E+03	.6234E+03		
3120	.1225E+01	.7248E+01	.9221E+02	.2440E+03	.6234E+03		
3130	.1225E+01	.7248E+01	.9221E+02	.2440E+03	.6234E+03		
3140	.1225E+01	.7248E+01	.9221E+02	.2440E+03	.6234E+03		
3150	.1225E+01	.7248E+01	.9221E+02	.2440E+03	.6234E+03		
3160	.1225E+01	.7287E+01	.9336E+02	.2440E+03	.6234E+03		
3170	.1225E+01	.7287E+01	.9393E+02	.2457E+03	.6234E+03		
3180	.1225E+01	.7325E+01	.9451E+02	.2475E+03	.6234E+03		
3190	.1225E+01	.7325E+01	.9566E+02	.2527E+03	.6283E+03		
3200	.1225E+01	.7363E+01	.9797E+02	.2562E+03	.6433E+03		
3210	.1225E+01	.7363E+01	.1002E+03	.2614E+03	.6583E+03		
3220	.1225E+01	.7401E+01	.1025E+03	.2666E+03	.6782E+03		
3230	.1225E+01	.7439E+01	.1071E+03	.2753E+03	.7106E+03		
3240	.1225E+01	.7477E+01	.1118E+03	.2893E+03	.7480E+03		
3250	.1225E+01	.7516E+01	.1175E+03	.3067E+03	.7979E+03		
3260	.1225E+01	.7592E+01	.1233E+03	.3241E+03	.8603E+03		
3270	.1234E+01	.7668E+01	.1290E+03	.3486E+03	.9351E+03		
3280	.1237E+01	.7706E+01	.1360E+03	.3695E+03	.1022E+04		
3290	.1242E+01	.7821E+01	.1452E+03	.3974E+03	.1122E+04		
3300	.1254E+01	.7935E+01	.1532E+03	.4270E+03	.1321E+04		
3310	.1270E+01	.8088E+01	.1648E+03	.4653E+03	.1770E+04		
3320	.1285E+01	.8202E+01	.1763E+03	.5089E+03	.2244E+04		

TABLE A2-34. (Continued)

1/cm	300K	600K	1200K	1500K	1800K	2400K	3000K
3330	.1310E+01	.8393E+01	.1890E+03	.5577E+03	.2368E+04		
3340	.1344E+01	.8546E+01	.1970E+03	.6065E+03	.2443E+04		
3350	.1370E+01	.8775E+01	.2074E+03	.6623E+03	.2493E+04		
3360	.1404E+01	.9042E+01	.2109E+03	.7233E+03	.2593E+04		
3370	.1438E+01	.9423E+01	.2166E+03	.7843E+03	.2668E+04		
3380	.1472E+01	.9805E+01	.2201E+03	.7930E+03	.2817E+04		
3390	.1506E+01	.1022E+02	.2213E+03	.7582E+03	.2942E+04		
3400	.1557E+01	.1068E+02	.2189E+03	.6972E+03	.2992E+04		
3410	.1608E+01	.1129E+02	.2086E+03	.6100E+03	.2743E+04		
3420	.1663E+01	.1194E+02	.1959E+03	.5229E+03	.1745E+04		
3430	.1736E+01	.1266E+02	.1775E+03	.4357E+03	.1097E+04		
3440	.1804E+01	.1354E+02	.1579E+03	.3486E+03	.7854E+03		
3450	.1872E+01	.1449E+02	.1383E+03	.2841E+03	.5860E+03		
3460	.1957E+01	.1545E+02	.1210E+03	.2318E+03	.4338E+03		
3470	.2042E+01	.1667E+02	.1071E+03	.1917E+03	.3316E+03		
3480	.2145E+01	.1774E+02	.9336E+02	.1586E+03	.2618E+03		
3490	.2264E+01	.1785E+02	.8068E+02	.1324E+03	.2119E+03		
3500	.2400E+01	.1735E+02	.7031E+02	.1150E+03	.1795E+03		
3510	.2553E+01	.1640E+02	.6224E+02	.9936E+02	.1595E+03		
3520	.2757E+01	.1526E+02	.5417E+02	.8889E+02	.1371E+03		
3530	.3064E+01	.1373E+02	.4841E+02	.7843E+02	.1172E+03		
3540	.3166E+01	.1201E+02	.4379E+02	.7146E+02	.1072E+03		
3550	.2894E+01	.1030E+02	.4034E+02	.6449E+02	.9725E+02		
3560	.2519E+01	.8584E+01	.3803E+02	.6100E+02	.9101E+02		
3570	.2111E+01	.7020E+01	.4091E+02	.5839E+02	.9101E+02		
3580	.1702E+01	.4845E+01	.3976E+02	.5751E+02	.9600E+02		

TABLE A2-34. (Concluded)

1/cm	300K	600K	1200K	1500K	1800K	2400K	3000K
3590	.1452E+01	.4748E+01	.5048E+02	.1108E+03	.2359E+03		
3600	.1070E+01	.3652E+01	.4326E+02	.1091E+03	.2988E+03		
3610	.8408E+00	.2817E+01	.5151E+02	.1142E+03	.3931E+03		
3620	.7643E+00	.1826E+01	.6593E+02	.1466E+03	.5504E+03		
3630	.7452E+00	.1408E+01	.7520E+02	.2216E+03	.7759E+03		
3640	.1528E+01	.2087E+01	.8138E+02	.2761E+03	.1038E+04		
3650	.1700E+01	.5739E+01	.8653E+02	.2864E+03	.1100E+04		
3660	.1547E+01	.7304E+01	.9683E+02	.2830E+03	.1038E+04		
3670	.8121E+00	.6835E+01	.8035E+02	.2761E+03	.9122E+03		
3680	.8312E+00	.6261E+01	.7726E+02	.2625E+03	.7968E+03		
3690	.9459E+00	.6000E+01	.8344E+02	.2454E+03	.6815E+03		
3700	.1108E+01	.6261E+01	.8859E+02	.2284E+03	.5871E+03		
3710	.1318E+01	.6782E+01	.8447E+02	.2079E+03	.5085E+03		
3720	.1576E+01	.7565E+01	.7829E+02	.1909E+03	.4403E+03		
3730	.2082E+01	.8348E+01	.7211E+02	.1738E+03	.3827E+03		
3740	.2962E+01	.8974E+01	.6799E+02	.1568E+03	.3302E+03		
3750	.3641E+01	.5542E+01	.2274E+02	.4136E+02	.7176E+02		
3760	.3799E+01	.5141E+01	.1760E+02	.3733E+02	.6246E+02		
3770	.2849E+01	.4618E+01	.1063E+02	.3278E+02	.5315E+02		

TABLE A2-35. ABSORPTION COEFFICIENTS OF H<sub>2</sub>O  
k (per cm at STP)

1/cm	300K	600K	1000K	1500K	2000K	2500K	3000K
50	.950E+00	.103E+00	.420E-01	.114E-01	.450E-02	.300E-02	.190E-02
75	.208E+01	.365E+00	.113E+00	.375E-01	.195E-01	.134E-01	.670E-02
100	.386E+01	.990E+00	.300E+00	.104E+00	.577E-01	.365E-01	.211E-01
125	.650E+01	.201E+01	.650E+00	.214E+00	.128E+00	.845E-01	.529E-01
150	.825E+01	.325E+01	.121E+01	.415E+00	.260E+00	.168E+00	.109E+00
175	.870E+01	.452E+01	.189E+01	.765E+00	.450E+00	.289E+00	.193E+00
200	.810E+01	.540E+01	.261E+01	.126E+01	.695E+00	.460E+00	.309E+00
225	.682E+01	.600E+01	.337E+01	.179E+01	.101E+01	.679E+00	.454E+00
250	.493E+01	.622E+01	.407E+01	.230E+01	.135E+01	.935E+00	.620E+00
275	.316E+01	.592E+01	.456E+01	.281E+01	.172E+01	.122E+01	.822E+00
300	.199E+01	.528E+01	.479E+01	.328E+01	.213E+01	.149E+01	.104E+01
325	.113E+01	.450E+01	.484E+01	.361E+01	.249E+01	.179E+01	.128E+01
350	.585E+00	.370E+01	.471E+01	.383E+01	.284E+01	.208E+01	.154E+01
375	.293E+00	.289E+01	.443E+01	.394E+01	.312E+01	.237E+01	.182E+01
400	.138E+00	.205E+01	.400E+01	.396E+01	.330E+01	.260E+01	.207E+01
425	.620E-01	.143E+01	.347E+01	.388E+01	.341E+01	.280E+01	.229E+01
450	.255E-01	.950E+00	.292E+01	.370E+01	.345E+01	.295E+01	.248E+01
475	.940E-02	.610E+00	.236E+01	.343E+01	.342E+01	.304E+01	.262E+01
500	.340E-02	.386E+00	.188E+01	.310E+01	.334E+01	.309E+01	.273E+01
525	.105E-02	.236E+00	.145E+01	.274E+01	.319E+01	.307E+01	.280E+01
550	.350E-03	.144E+00	.110E+01	.238E+01	.300E+01	.301E+01	.283E+01
575	.126E-03	.820E-01	.818E+00	.204E+01	.276E+01	.289E+01	.282E+01
600	.430E-04	.445E-01	.598E+00	.174E+01	.248E+01	.275E+01	.277E+01
625	.150E-04	.242E-01	.427E+00	.145E+01	.222E+01	.260E+01	.269E+01
650	.510E-05	.127E-01	.294E+00	.118E+01	.195E+01	.241E+01	.258E+01
675	.170E-05	.630E-02	.200E+00	.950E+00	.169E+01	.221E+01	.245E+01

TABLE A2-35. (Continued)

1/cm	300K	600K	1000K	1500K	2000K	2500K	3000K
700	.570E-06	.300E-02	.134E+00	.748E+00	.146E+01	.200E+01	.229E+01
725	.195E-06	.140E-02	.902E-01	.580E+00	.124E+01	.178E+01	.213E+01
750	.680E-07	.620E-03	.590E-01	.443E+00	.103E+01	.156E+01	.196E+01
775	.385E-07	.275E-03	.450E-01	.330E+00	.845E+00	.136E+01	.177E+01
800	.670E-07	.113E-03	.355E-01	.242E+00	.695E+00	.117E+01	.159E+01
825	.113E-06	.500E-04	.289E-01	.174E+00	.560E+00	.100E+01	.143E+01
850	.195E-06	.230E-04	.245E-01	.123E+00	.450E+00	.855E+00	.126E+01
875	.328E-06	.103E-04	.214E-01	.100E+00	.357E+00	.718E+00	.111E+01
900	.560E-06	.460E-05	.189E-01	.830E-01	.278E+00	.595E+00	.955E+00
925	.950E-06	.205E-05	.174E-01	.730E-01	.239E+00	.492E+00	.825E+00
950	.160E-05	.140E-05	.166E-01	.665E-01	.211E+00	.405E+00	.705E+00
975	.275E-05	.350E-05	.165E-01	.630E-01	.195E+00	.352E+00	.600E+00
1000	.470E-05	.850E-05	.167E-01	.620E-01	.190E+00	.312E+00	.510E+00
1025	.810E-05	.215E-04	.175E-01	.630E-01	.191E+00	.289E+00	.425E+00
1050	.136E-04	.570E-04	.188E-01	.675E-01	.194E+00	.281E+00	.358E+00
1075	.235E-04	.150E-03	.208E-01	.745E-01	.202E+00	.283E+00	.329E+00
1100	.400E-04	.380E-03	.233E-01	.865E-01	.223E+00	.314E+00	.357E+00
1125	.680E-04	.950E-03	.268E-01	.122E+00	.260E+00	.380E+00	.449E+00
1150	.120E-03	.245E-02	.343E-01	.176E+00	.328E+00	.461E+00	.507E+00
1175	.200E-03	.620E-02	.638E-01	.251E+00	.411E+00	.511E+00	.568E+00
1200	.365E-03	.140E-01	.107E+00	.330E+00	.458E+00	.542E+00	.604E+00
1225	.680E-03	.330E-01	.166E+00	.405E+00	.487E+00	.571E+00	.632E+00
1250	.130E-02	.635E-01	.244E+00	.459E+00	.535E+00	.557E+00	.637E+00
1275	.250E-02	.123E+00	.341E+00	.477E+00	.502E+00	.562E+00	.608E+00
1300	.500E-02	.212E+00	.407E+00	.547E+00	.531E+00	.514E+00	.578E+00
1325	.103E-01	.285E+00	.489E+00	.592E+00	.497E+00	.486E+00	.554E+00
1350	.219E-01	.328E+00	.491E+00	.558E+00	.489E+00	.485E+00	.537E+00

TABLE A2-35. (Continued)

1/cm	300K	600K	1000K	1500K	2000K	2500K	300K
1375	.485E-01	.345E+00	.505E+00	.521E+00	.477E+00	.484E+00	.520E+00
1400	.114E+00	.361E+00	.538E+00	.563E+00	.503E+00	.502E+00	.516E+00
1425	.249E+00	.460E+00	.621E+00	.624E+00	.538E+00	.538E+00	.514E+00
1450	.397E+00	.569E+00	.749E+00	.768E+00	.581E+00	.565E+00	.518E+00
1475	.418E+00	.627E+00	.824E+00	.849E+00	.640E+00	.594E+00	.530E+00
1500	.108E+01	.125E+01	.113E+01	.940E+00	.807E+00	.663E+00	.525E+00
1525	.165E+01	.155E+01	.118E+01	.670E+00	.562E+00	.483E+00	.430E+00
1550	.142E+01	.675E+00	.557E+00	.349E+00	.276E+00	.263E+00	.277E+00
1575	.451E+00	.202E+00	.132E+00	.118E+00	.134E+00	.156E+00	.173E+00
1600	.603E-01	.538E-01	.863E-01	.112E+00	.120E+00	.125E+00	.125E+00
1625	.501E+00	.252E+00	.118E+00	.112E+00	.131E+00	.140E+00	.140E+00
1650	.730E+00	.430E+00	.237E+00	.191E+00	.171E+00	.170E+00	.170E+00
1675	.149E+01	.506E+00	.294E+00	.238E+00	.210E+00	.201E+00	.202E+00
1700	.100E+01	.553E+00	.434E+00	.340E+00	.260E+00	.220E+00	.173E+00
1725	.802E+00	.658E+00	.528E+00	.411E+00	.300E+00	.240E+00	.191E+00
1750	.580E+00	.527E+00	.460E+00	.378E+00	.322E+00	.283E+00	.240E+00
1775	.330E+00	.403E+00	.430E+00	.356E+00	.318E+00	.270E+00	.226E+00
1800	.250E+00	.393E+00	.405E+00	.342E+00	.301E+00	.275E+00	.242E+00
1825	.147E+00	.249E+00	.313E+00	.318E+00	.291E+00	.268E+00	.250E+00
1850	.910E-01	.252E+00	.298E+00	.295E+00	.269E+00	.253E+00	.247E+00
1875	.580E-01	.158E+00	.214E+00	.244E+00	.244E+00	.245E+00	.238E+00
1900	.370E-01	.113E+00	.184E+00	.218E+00	.214E+00	.218E+00	.222E+00
1925	.244E-01	.118E+00	.156E+00	.188E+00	.195E+00	.200E+00	.206E+00
1950	.162E-01	.606E-01	.976E-01	.141E+00	.166E+00	.179E+00	.185E+00
1975	.112E-01	.425E-01	.903E-01	.133E+00	.148E+00	.156E+00	.166E+00
2000	.780E-02	.400E-01	.765E-01	.112E+00	.129E+00	.137E+00	.147E+00
2025	.540E-02	.352E-01	.647E-01	.876E-01	.110E+00	.118E+00	.129E+00

TABLE A2-35. (Continued)

1/cm	300K	600K	1000K	1500K	2000K	2500K	3000K
2050	.380E-02	.252E-01	.507E-01	.705E-01	.888E-01	.100E+00	.111E+00
2075	.260E-02	.179E-01	.377E-01	.546E-01	.724E-01	.828E-01	.960E-01
2100	.180E-02	.123E-01	.294E-01	.443E-01	.608E-01	.686E-01	.840E-01
2125	.127E-02	.850E-02	.212E-01	.378E-01	.579E-01	.640E-01	.725E-01
2150	.880E-03	.680E-02	.152E-01	.275E-01	.449E-01	.521E-01	.628E-01
2175	.620E-02	.400E-02	.107E-01	.214E-01	.374E-01	.453E-01	.530E-01
2200	.480E-03	.298E-02	.931E-02	.189E-01	.329E-01	.403E-01	.455E-01
2225	.405E-03	.175E-02	.696E-02	.152E-01	.295E-01	.365E-01	.398E-01
2250	.321E-03	.120E-02	.452E-02	.101E-01	.252E-01	.331E-01	.350E-01
2275	.229E-03	.721E-03	.364E-02	.930E-02	.225E-01	.305E-01	.312E-01
2300	.195E-03	.544E-03	.318E-02	.750E-02	.202E-01	.284E-01	.290E-01
2325	.154E-03	.375E-03	.185E-02	.603E-02	.175E-01	.269E-01	.275E-01
2350	.101E-03	.263E-03	.119E-02	.480E-02	.156E-01	.253E-01	.267E-01
2375	.852E-04	.185E-03	.909E-03	.360E-02	.133E-01	.241E-01	.259E-01
2400	.763E-04	.137E-03	.711E-03	.316E-02	.122E-01	.237E-01	.252E-01
2425	.615E-04	.126E-03	.610E-03	.257E-02	.101E-01	.218E-01	.251E-01
2450	.480E-04	.113E-03	.518E-03	.201E-02	.920E-02	.200E-01	.249E-01
2475	.372E-04	.106E-03	.435E-03	.168E-02	.785E-02	.183E-01	.247E-01
2500	.355E-04	.101E-03	.376E-03	.168E-02	.669E-02	.166E-01	.248E-01
2525	.358E-04	.990E-04	.366E-03	.167E-02	.651E-02	.156E-01	.249E-01
2550	.389E-04	.102E-03	.376E-03	.167E-02	.641E-02	.152E-01	.251E-01
2575	.422E-04	.106E-03	.373E-03	.168E-02	.656E-02	.150E-01	.253E-01
2600	.521E-04	.111E-03	.371E-03	.170E-02	.673E-02	.152E-01	.258E-01
2625	.646E-04	.121E-03	.384E-03	.179E-02	.798E-02	.179E-01	.263E-01
2650	.742E-04	.129E-03	.479E-03	.201E-02	.788E-02	.175E-01	.270E-01
2675	.953E-04	.165E-03	.544E-03	.249E-02	.945E-02	.204E-01	.280E-01
2700	.101E-03	.190E-03	.761E-03	.324E-02	.106E-01	.231E-01	.295E-01

TABLE A2-35. (Continued)

1/cm	300K	600K	1000K	1500K	2000K	2500K	3000K
2725	.147E-03	.272E-03	.892E-03	.441E-02	.125E-01	.257E-01	.318E-01
2750	.195E-03	.326E-03	.100E-02	.499E-02	.147E-01	.295E-01	.343E-01
2775	.261E-03	.421E-03	.145E-02	.568E-02	.161E-01	.306E-01	.378E-01
2800	.305E-03	.515E-03	.195E-02	.754E-02	.185E-01	.363E-01	.417E-01
2825	.362E-03	.645E-03	.237E-02	.830E-02	.205E-01	.373E-01	.459E-01
2850	.507E-03	.850E-03	.274E-02	.888E-02	.234E-01	.431E-01	.500E-01
2875	.799E-03	.118E-02	.322E-02	.110E-01	.262E-01	.451E-01	.550E-01
2900	.935E-03	.160E-02	.386E-02	.126E-01	.292E-01	.530E-01	.602E-01
2925	.108E-02	.231E-02	.451E-02	.140E-01	.306E-01	.536E-01	.665E-01
2950	.192E-02	.271E-02	.563E-02	.159E-01	.357E-01	.629E-01	.735E-01
2975	.263E-02	.300E-02	.625E-02	.179E-01	.385E-01	.666E-01	.801E-01
3000	.295E-02	.330E-02	.701E-02	.203E-01	.460E-01	.782E-01	.885E-01
3025	.310E-02	.370E-02	.846E-02	.220E-01	.519E-01	.889E-01	.970E-01
3050	.340E-02	.400E-02	.969E-02	.279E-01	.662E-01	.109E+00	.106E+00
3075	.730E-02	.450E-02	.111E-01	.272E-01	.676E-01	.109E+00	.117E+00
3100	.900E-02	.480E-02	.137E-01	.372E-01	.864E-01	.133E+00	.129E+00
3125	.100E-02	.510E-02	.162E-01	.471E-01	.100E+00	.142E+00	.142E+00
3150	.640E-03	.550E-02	.205E-01	.530E-01	.122E+00	.168E+00	.155E+00
3175	.160E-02	.600E-02	.247E-01	.633E-01	.135E+00	.177E+00	.170E+00
3200	.330E-02	.700E-02	.283E-01	.770E-01	.153E+00	.185E+00	.187E+00
3225	.410E-02	.860E-02	.376E-01	.914E-01	.166E+00	.206E+00	.202E+00
3250	.410E-02	.103E-01	.514E-01	.117E+00	.194E+00	.228E+00	.220E+00
3275	.290E-02	.129E-01	.664E-01	.147E+00	.220E+00	.254E+00	.241E+00
3300	.220E-02	.161E-01	.834E-01	.171E+00	.237E+00	.263E+00	.262E+00
3325	.220E-02	.212E-01	.103E+00	.201E+00	.268E+00	.283E+00	.280E+00
3350	.250E-02	.285E-01	.135E+00	.240E+00	.295E+00	.295E+00	.293E+00
3375	.310E-02	.385E-01	.169E+00	.272E+00	.312E+00	.301E+00	.302E+00

TABLE A2-35. (Continued)

1/cm	300K	600K	1000K	1500K	2000K	2500K	3000K
3400	.420E-02	.540E-01	.214E+00	.309E+00	.329E+00	.307E+00	.308E+00
3425	.600E-02	.770E-01	.267E+00	.343E+00	.332E+00	.314E+00	.300E+00
3450	.940E-02	.117E+00	.333E+00	.372E+00	.344E+00	.303E+00	.290E+00
3475	.165E-01	.173E+00	.365E+00	.385E+00	.353E+00	.300E+00	.272E+00
3500	.360E-01	.258E+00	.438E+00	.393E+00	.315E+00	.288E+00	.265E+00
3525	.720E-01	.375E+00	.510E+00	.409E+00	.294E+00	.271E+00	.241E+00
3550	.133E+00	.401E+00	.499E+00	.390E+00	.281E+00	.257E+00	.222E+00
3575	.215E+00	.500E+00	.443E+00	.341E+00	.254E+00	.230E+00	.208E+00
3600	.318E+00	.450E+00	.346E+00	.286E+00	.245E+00	.219E+00	.201E+00
3625	.442E+00	.400E+00	.354E+00	.279E+00	.233E+00	.216E+00	.210E+00
3650	.473E+00	.405E+00	.347E+00	.281E+00	.238E+00	.219E+00	.213E+00
3675	.568E+00	.501E+00	.423E+00	.315E+00	.243E+00	.218E+00	.200E+00
3700	.690E+00	.708E+00	.673E+00	.432E+00	.268E+00	.189E+00	.150E+00
3725	.617E+00	.831E+00	.566E+00	.320E+00	.194E+00	.123E+00	.113E+00
3750	.181E+01	.520E+00	.200E+00	.131E+00	.124E+00	.107E+00	.108E+00
3775	.136E+00	.124E+00	.120E+00	.119E+00	.115E+00	.115E+00	.109E+00
3800	.455E+00	.298E+00	.167E+00	.129E+00	.123E+00	.112E+00	.122E+00
3825	.760E+00	.503E+00	.242E+00	.154E+00	.129E+00	.127E+00	.136E+00
3850	.836E+00	.584E+00	.277E+00	.184E+00	.161E+00	.145E+00	.154E+00
3875	.840E+00	.728E+00	.422E+00	.236E+00	.197E+00	.167E+00	.177E+00
3900	.505E+00	.500E+00	.379E+00	.276E+00	.227E+00	.192E+00	.197E+00
3925	.117E+00	.400E+00	.423E+00	.315E+00	.243E+00	.202E+00	.209E+00
3950	.460E-01	.300E+00	.358E+00	.290E+00	.230E+00	.202E+00	.207E+00
3975	.183E-01	.205E+00	.269E+00	.235E+00	.195E+00	.192E+00	.190E+00
4000	.730E-02	.135E+00	.186E+00	.179E+00	.159E+00	.168E+00	.161E+00
4025	.557E-02	.790E-01	.113E+00	.124E+00	.124E+00	.134E+00	.132E+00
4050	.283E-02	.415E-01	.662E-01	.886E-01	.103E+00	.106E+00	.104E+00

TABLE A2-35. (Continued)

1/cm	300K	600K	1000K	1500K	2000K	2500K	3000K
4075	.226E-02	.197E-01	.367E-01	.594E-01	.801E-01	.879E-01	.860E-01
4100	.155E-02	.860E-02	.211E-01	.395E-01	.503E-01	.610E-01	.710E-01
4125	.103E-02	.521E-02	.119E-01	.246E-01	.354E-01	.480E-01	.598E-01
4150	.821E-03	.365E-02	.759E-02	.166E-01	.258E-01	.370E-01	.499E-01
4175	.752E-03	.183E-02	.445E-02	.100E-01	.179E-01	.268E-01	.418E-01
4200	.429E-03	.141E-02	.354E-02	.821E-02	.142E-01	.212E-01	.348E-01
4225	.327E-03	.902E-03	.209E-02	.588E-02	.112E-01	.172E-01	.287E-01
4250	.225E-03	.685E-03	.189E-02	.512E-02	.101E-01	.164E-01	.236E-01
4275	.186E-03	.551E-03	.156E-02	.366E-02	.812E-02	.136E-01	.189E-01
4300	.173E-03	.472E-03	.139E-02	.306E-02	.661E-02	.115E-01	.150E-01
4325	.138E-03	.395E-03	.110E-02	.272E-02	.587E-02	.104E-01	.126E-01
4350	.900E-04	.270E-03	.968E-03	.222E-02	.497E-02	.921E-02	.119E-01
4375	.752E-04	.233E-03	.744E-03	.208E-02	.466E-02	.876E-02	.119E-01
4400	.618E-04	.175E-03	.638E-03	.185E-02	.465E-02	.914E-02	.123E-01
4425	.504E-04	.134E-03	.499E-03	.174E-02	.455E-02	.935E-02	.128E-01
4450	.375E-04	.123E-03	.485E-03	.182E-02	.456E-02	.971E-02	.134E-01
4475	.305E-04	.892E-04	.338E-03	.134E-02	.460E-02	.104E-01	.142E-01
4500	.257E-04	.790E-04	.329E-03	.154E-02	.477E-02	.112E-01	.151E-01
4525	.242E-04	.740E-04	.308E-03	.135E-02	.497E-02	.122E-01	.162E-01
4550	.215E-04	.653E-04	.282E-03	.131E-02	.521E-02	.133E-01	.173E-01
4575	.218E-04	.660E-04	.272E-03	.152E-02	.573E-02	.148E-01	.187E-01
4600	.215E-04	.671E-04	.268E-03	.134E-02	.607E-02	.159E-01	.202E-01
4625	.217E-04	.695E-04	.285E-03	.161E-02	.677E-02	.173E-01	.223E-01
4650	.219E-04	.722E-04	.297E-03	.169E-02	.783E-02	.197E-01	.246E-01
4675	.226E-04	.771E-04	.341E-03	.236E-02	.925E-02	.226E-01	.270E-01
4700	.250E-04	.815E-04	.387E-03	.286E-02	.106E-01	.250E-01	.300E-01
4725	.280E-04	.845E-04	.420E-03	.357E-02	.124E-01	.276E-01	.338E-01

TABLE A2-35. (Continued)

1/cm	300K	600K	1000K	1500K	2000K	2500K	3000K
4750	.351E-04	.192E-03	.470E-03	.467E-02	.166E-01	.313E-01	.370E-01
4775	.435E-04	.200E-03	.105E-02	.566E-02	.185E-01	.341E-01	.399E-01
4800	.522E-04	.233E-03	.129E-02	.736E-02	.229E-01	.378E-01	.422E-01
4825	.673E-04	.306E-03	.183E-02	.982E-02	.258E-01	.404E-01	.440E-01
4850	.886E-04	.399E-03	.246E-02	.128E-01	.302E-01	.430E-01	.458E-01
4875	.113E-03	.618E-03	.346E-02	.161E-01	.358E-01	.459E-01	.465E-01
4900	.174E-03	.825E-03	.441E-02	.200E-01	.417E-01	.493E-01	.473E-01
4925	.265E-03	.163E-02	.777E-02	.245E-01	.450E-01	.507E-01	.478E-01
4950	.355E-03	.200E-02	.978E-02	.317E-01	.492E-01	.527E-01	.478E-01
4975	.538E-03	.271E-02	.167E-01	.401E-01	.503E-01	.523E-01	.473E-01
5000	.651E-03	.301E-02	.264E-01	.467E-01	.520E-01	.526E-01	.460E-01
5025	.987E-03	.530E-02	.321E-01	.499E-01	.523E-01	.510E-01	.447E-01
5050	.135E-02	.860E-02	.389E-01	.528E-01	.513E-01	.492E-01	.430E-01
5075	.226E-02	.130E-01	.472E-01	.559E-01	.500E-01	.469E-01	.415E-01
5100	.431E-02	.198E-01	.526E-01	.557E-01	.480E-01	.452E-01	.400E-01
5125	.628E-02	.282E-01	.488E-01	.495E-01	.451E-01	.430E-01	.390E-01
5150	.900E-02	.390E-01	.471E-01	.449E-01	.430E-01	.423E-01	.385E-01
5175	.180E-01	.462E-01	.412E-01	.391E-01	.403E-01	.415E-01	.393E-01
5200	.348E-01	.710E-01	.402E-01	.360E-01	.384E-01	.414E-01	.405E-01
5225	.718E-01	.590E-01	.399E-01	.360E-01	.376E-01	.420E-01	.418E-01
5250	.111E+00	.368E-01	.340E-01	.369E-01	.409E-01	.454E-01	.434E-01
5275	.329E-01	.285E-01	.365E-01	.423E-01	.461E-01	.482E-01	.450E-01
5300	.281E-01	.270E-01	.432E-01	.505E-01	.529E-01	.511E-01	.462E-01
5325	.121E+00	.422E-01	.589E-01	.598E-01	.572E-01	.544E-01	.470E-01
5350	.139E+00	.105E+00	.844E-01	.687E-01	.593E-01	.560E-01	.480E-01
5375	.774E-01	.710E-01	.683E-01	.618E-01	.556E-01	.534E-01	.478E-01
5400	.858E-01	.483E-01	.579E-01	.547E-01	.503E-01	.495E-01	.460E-01

TABLE A2-35. (Continued)

1/cm	300K	600K	1000K	1500K	2000K	2500K	3000K
5425	.985E-01	.575E-01	.589E-01	.510E-01	.451E-01	.449E-01	.425E-01
5450	.996E-01	.682E-01	.539E-01	.489E-01	.454E-01	.446E-01	.400E-01
5475	.680E-01	.680E-01	.548E-01	.495E-01	.460E-01	.458E-01	.405E-01
5500	.325E-01	.520E-01	.515E-01	.483E-01	.449E-01	.454E-01	.418E-01
5525	.150E-01	.350E-01	.451E-01	.464E-01	.452E-01	.449E-01	.438E-01
5550	.620E-02	.238E-01	.369E-01	.408E-01	.414E-01	.417E-01	.420E-01
5575	.270E-02	.158E-01	.282E-01	.339E-01	.366E-01	.384E-01	.400E-01
5600	.113E-02	.101E-01	.203E-01	.263E-01	.303E-01	.333E-01	.360E-01
5625	.829E-03	.590E-02	.148E-01	.206E-01	.247E-01	.295E-01	.320E-01
5650	.365E-03	.310E-02	.969E-02	.154E-01	.203E-01	.258E-01	.280E-01
5675	.240E-03	.130E-02	.589E-02	.112E-01	.164E-01	.222E-01	.250E-01
5700	.158E-03	.400E-03	.417E-02	.850E-02	.134E-01	.190E-01	.220E-01
5725	.103E-03	.262E-03	.208E-02	.594E-02	.109E-01	.162E-01	.190E-01
5750	.741E-04	.181E-03	.142E-02	.455E-02	.907E-02	.141E-01	.170E-01
5775	.625E-04	.135E-03	.816E-03	.316E-02	.698E-02	.121E-01	.150E-01
5800	.499E-04	.111E-03	.624E-03	.230E-02	.551E-02	.102E-01	.130E-01
5825	.325E-04	.677E-04	.425E-03	.124E-02	.385E-02	.818E-02	.120E-01
5850	.231E-04	.563E-04	.278E-03	.986E-03	.290E-02	.672E-02	.105E-01
5875	.165E-04	.481E-04	.247E-03	.944E-03	.253E-02	.612E-02	.980E-02
5900	.126E-04	.432E-04	.241E-03	.886E-03	.220E-02	.582E-02	.940E-02
5925	.118E-04	.420E-04	.235E-03	.847E-03	.209E-02	.571E-02	.930E-02
5950	.110E-04	.408E-04	.226E-03	.812E-03	.221E-02	.604E-02	.925E-02
5975	.101E-04	.400E-04	.213E-03	.805E-03	.239E-02	.641E-02	.930E-02
6000	.983E-05	.395E-04	.186E-03	.801E-03	.247E-02	.691E-02	.950E-02
6025	.979E-05	.401E-04	.193E-03	.805E-03	.260E-02	.732E-02	.970E-02
6050	.976E-05	.410E-04	.201E-03	.814E-03	.285E-02	.776E-02	.100E-01
6075	.988E-05	.420E-04	.210E-03	.832E-03	.317E-02	.842E-02	.103E-01

TABLE A2-35. (Continued)

1/cm	300K	600K	1000K	1500K	2000K	2500K	3000K
6100	.991E-05	.425E-04	.219E-03	.877E-03	.340E-02	.888E-02	.105E-01
6125	.102E-04	.435E-04	.231E-03	.937E-03	.361E-02	.929E-02	.110E-01
6150	.110E-04	.486E-04	.244E-03	.971E-03	.402E-02	.994E-02	.113E-01
6175	.127E-04	.579E-04	.257E-03	.111E-02	.437E-02	.104E-01	.119E-01
6200	.131E-04	.612E-04	.277E-03	.113E-02	.465E-02	.110E-01	.125E-01
6225	.150E-04	.783E-04	.353E-03	.116E-02	.510E-02	.116E-01	.130E-01
6250	.178E-04	.922E-04	.394E-03	.157E-02	.555E-02	.123E-01	.135E-01
6275	.203E-04	.115E-03	.481E-03	.188E-02	.601E-02	.131E-01	.143E-01
6300	.230E-04	.145E-03	.617E-03	.183E-02	.644E-02	.139E-01	.150E-01
6325	.280E-04	.187E-03	.723E-03	.202E-02	.686E-02	.146E-01	.157E-01
6350	.305E-04	.209E-03	.811E-03	.243E-02	.779E-02	.157E-01	.164E-01
6375	.455E-04	.244E-03	.935E-03	.243E-02	.844E-02	.166E-01	.172E-01
6400	.661E-04	.320E-03	.989E-03	.288E-02	.902E-02	.173E-01	.180E-01
6425	.723E-04	.397E-03	.122E-02	.359E-02	.100E-01	.184E-01	.191E-01
6450	.847E-04	.481E-03	.143E-02	.429E-02	.108E-01	.192E-01	.200E-01
6475	.103E-03	.591E-03	.174E-02	.488E-02	.116E-01	.200E-01	.211E-01
6500	.131E-03	.703E-03	.217E-02	.549E-02	.124E-01	.205E-01	.222E-01
6525	.165E-03	.872E-03	.265E-02	.641E-02	.131E-01	.211E-01	.233E-01
6550	.205E-03	.110E-02	.298E-02	.749E-02	.140E-01	.218E-01	.244E-01
6575	.253E-03	.130E-02	.346E-02	.811E-02	.150E-01	.230E-01	.255E-01
6600	.338E-03	.150E-02	.445E-02	.890E-02	.159E-01	.237E-01	.267E-01
6625	.437E-03	.170E-02	.491E-02	.107E-01	.170E-01	.245E-01	.276E-01
6650	.581E-03	.190E-02	.537E-02	.116E-01	.179E-01	.254E-01	.287E-01
6675	.685E-03	.220E-02	.578E-02	.128E-01	.189E-01	.263E-01	.296E-01
6700	.900E-03	.250E-02	.649E-02	.134E-01	.195E-01	.275E-01	.305E-01
6725	.121E-02	.280E-02	.722E-02	.142E-01	.202E-01	.281E-01	.313E-01
6750	.152E-02	.330E-02	.813E-02	.161E-01	.212E-01	.288E-01	.320E-01

TABLE A2-35. (Continued)

1/cm	300K	600K	1000K	1500K	2000K	2500K	3000K
6775	.185E-02	.370E-02	.907E-02	.168E-01	.222E-01	.292E-01	.329E-01
6800	.220E-02	.430E-02	.929E-02	.183E-01	.233E-01	.294E-01	.335E-01
6825	.255E-02	.500E-02	.114E-01	.195E-01	.245E-01	.289E-01	.339E-01
6850	.290E-02	.580E-02	.167E-01	.215E-01	.260E-01	.291E-01	.343E-01
6875	.320E-02	.670E-02	.208E-01	.237E-01	.274E-01	.293E-01	.345E-01
6900	.360E-02	.880E-02	.220E-01	.253E-01	.282E-01	.300E-01	.343E-01
6925	.400E-02	.920E-02	.238E-01	.273E-01	.290E-01	.304E-01	.341E-01
6950	.460E-02	.108E-01	.272E-01	.279E-01	.298E-01	.310E-01	.339E-01
6975	.530E-02	.128E-01	.304E-01	.292E-01	.297E-01	.312E-01	.333E-01
7000	.620E-02	.152E-01	.344E-01	.303E-01	.293E-01	.310E-01	.325E-01
7025	.760E-02	.182E-01	.341E-01	.297E-01	.290E-01	.300E-01	.313E-01
7050	.980E-02	.222E-01	.398E-01	.318E-01	.291E-01	.294E-01	.299E-01
7075	.132E-01	.271E-01	.402E-01	.294E-01	.274E-01	.282E-01	.283E-01
7100	.190E-01	.335E-01	.421E-01	.286E-01	.262E-01	.269E-01	.263E-01
7125	.240E-01	.432E-01	.431E-01	.276E-01	.245E-01	.257E-01	.243E-01
7150	.288E-01	.570E-01	.458E-01	.270E-01	.228E-01	.243E-01	.223E-01
7175	.323E-01	.740E-01	.449E-01	.261E-01	.214E-01	.221E-01	.208E-01
7200	.570E-01	.890E-01	.435E-01	.255E-01	.199E-01	.196E-01	.199E-01
7225	.216E-01	.680E-01	.378E-01	.239E-01	.195E-01	.192E-01	.190E-01
7250	.126E-01	.475E-01	.364E-01	.238E-01	.197E-01	.192E-01	.187E-01
7275	.117E-01	.369E-01	.385E-01	.249E-01	.212E-01	.204E-01	.200E-01
7300	.140E-01	.370E-01	.419E-01	.272E-01	.228E-01	.213E-01	.224E-01
7325	.425E-01	.418E-01	.440E-01	.280E-01	.248E-01	.229E-01	.243E-01
7350	.640E-01	.460E-01	.427E-01	.290E-01	.263E-01	.238E-01	.260E-01
7375	.385E-01	.385E-01	.374E-01	.259E-01	.235E-01	.224E-01	.260E-01
7400	.182E-01	.179E-01	.282E-01	.231E-01	.211E-01	.214E-01	.240E-01
7425	.170E-01	.810E-02	.191E-01	.175E-01	.181E-01	.194E-01	.210E-01

TABLE A2-35. (Continued)

1/cm	300K	600K	1000K	1500K	2000K	2500K	3000K
7450	.161E-01	.370E-02	.105E-01	.127E-01	.152E-01	.171E-01	.180E-01
7475	.145E-01	.170E-02	.554E-02	.855E-02	.113E-01	.131E-01	.150E-01
7500	.175E-02	.140E-02	.385E-02	.595E-02	.803E-02	.945E-02	.120E-01
7525	.772E-03	.751E-03	.384E-02	.575E-02	.537E-02	.594E-02	.800E-02
7550	.491E-03	.600E-03	.301E-02	.453E-02	.380E-02	.434E-02	.600E-02
7575	.275E-03	.410E-03	.193E-02	.366E-02	.319E-02	.332E-02	.500E-02
7600	.185E-03	.280E-03	.131E-02	.232E-02	.247E-02	.256E-02	.420E-02
7625	.101E-03	.160E-03	.915E-03	.150E-02	.186E-02	.197E-02	.370E-02
7650	.691E-04	.110E-03	.565E-03	.114E-02	.205E-02	.192E-02	.340E-02
7675	.476E-04	.750E-04	.114E-02	.124E-02	.175E-02	.187E-02	.320E-02
7700	.305E-04	.590E-04	.529E-03	.114E-02	.160E-02	.185E-02	.300E-02
7725	.240E-04	.480E-04	.293E-03	.842E-03	.141E-02	.184E-02	.290E-02
7750	.170E-04	.360E-04	.122E-03	.435E-03	.124E-02	.182E-02	.290E-02
7775	.120E-04	.240E-04	.121E-03	.435E-03	.118E-02	.187E-02	.291E-02
7800	.810E-05	.170E-04	.103E-03	.439E-03	.126E-02	.192E-02	.295E-02
7825	.550E-05	.120E-04	.866E-04	.367E-03	.119E-02	.193E-02	.300E-02
7850	.390E-05	.900E-05	.716E-04	.351E-03	.116E-02	.194E-02	.303E-02
7875	.295E-05	.830E-05	.373E-04	.254E-03	.114E-02	.196E-02	.310E-02
7900	.230E-05	.800E-05	.465E-04	.298E-03	.117E-02	.201E-02	.320E-02
7925	.225E-05	.820E-05	.367E-04	.252E-03	.116E-02	.205E-02	.330E-02
7950	.220E-05	.840E-05	.371E-04	.268E-03	.127E-02	.211E-02	.340E-02
7975	.223E-05	.920E-05	.396E-04	.273E-03	.128E-02	.216E-02	.355E-02
8000	.235E-05	.103E-04	.415E-04	.263E-03	.121E-02	.221E-02	.365E-02
8025	.280E-05	.125E-04	.633E-04	.363E-03	.136E-02	.231E-02	.380E-02
8050	.310E-05	.150E-04	.979E-04	.492E-03	.150E-02	.241E-02	.400E-02
8075	.370E-05	.180E-04	.120E-03	.580E-03	.167E-02	.251E-02	.410E-02
8100	.420E-05	.200E-04	.987E-04	.509E-03	.171E-02	.257E-02	.420E-02

TABLE A2-35. (Continued)

1/cm	300K	600K	1000K	1500K	2000K	2500K	3000K
8125	.510E-05	.240E-04	.134E-03	.547E-03	.173E-02	.267E-02	.440E-02
8150	.600E-05	.270E-04	.121E-03	.534E-03	.172E-02	.274E-02	.457E-02
8175	.720E-05	.300E-04	.204E-03	.684E-03	.184E-02	.285E-02	.468E-02
8200	.820E-05	.330E-04	.276E-03	.819E-03	.199E-02	.297E-02	.479E-02
8225	.100E-04	.380E-04	.317E-03	.859E-03	.214E-02	.308E-02	.485E-02
8250	.125E-04	.420E-04	.240E-03	.818E-03	.220E-02	.317E-02	.490E-02
8275	.145E-04	.500E-04	.452E-03	.109E-02	.238E-02	.293E-02	.499E-02
8300	.175E-04	.560E-04	.301E-03	.941E-03	.243E-02	.342E-02	.500E-02
8325	.198E-04	.630E-04	.280E-03	.107E-02	.260E-02	.353E-02	.501E-02
8350	.230E-04	.710E-04	.276E-03	.109E-02	.272E-02	.365E-02	.502E-02
8375	.280E-04	.830E-04	.369E-03	.127E-02	.295E-02	.377E-02	.501E-02
8400	.330E-04	.890E-04	.430E-03	.139E-02	.306E-02	.385E-02	.500E-02
8425	.360E-04	.950E-04	.371E-03	.135E-02	.306E-02	.384E-02	.499E-02
8450	.390E-04	.980E-04	.434E-03	.147E-02	.316E-02	.385E-02	.495E-02
8475	.400E-04	.990E-04	.397E-03	.143E-02	.318E-02	.384E-02	.490E-02
8500	.400E-04	.980E-04	.364E-03	.141E-02	.317E-02	.381E-02	.480E-02
8525	.390E-04	.940E-04	.390E-03	.142E-02	.314E-02	.376E-02	.475E-02
8550	.380E-04	.900E-04	.380E-03	.145E-02	.318E-02	.375E-02	.463E-02
8575	.330E-04	.750E-04	.358E-03	.138E-02	.310E-02	.372E-02	.455E-02
8600	.300E-04	.680E-04	.343E-03	.136E-02	.309E-02	.369E-02	.443E-02
8625	.270E-04	.580E-04	.382E-03	.143E-02	.315E-02	.369E-02	.433E-02
8650	.240E-04	.500E-04	.343E-03	.136E-02	.306E-02	.363E-02	.420E-02
8675	.200E-04	.450E-04	.309E-03	.134E-02	.306E-02	.359E-02	.408E-02
8700	.180E-04	.400E-04	.281E-03	.127E-02	.294E-02	.341E-02	.395E-02
8725	.170E-04	.360E-04	.276E-03	.124E-02	.290E-02	.336E-02	.380E-02
8750	.160E-04	.310E-04	.272E-03	.122E-02	.283E-02	.323E-02	.367E-02
8775	.140E-04	.280E-04	.241E-03	.117E-02	.273E-02	.309E-02	.351E-02

TABLE A2-35. (Concluded)

1/cm	300K	600K	1000K	1500K	2000K	2500K	3000K
8800	.120E-04	.250E-04	.237E-03	.115E-02	.269E-02	.297E-02	.338E-02
8825	.100E-04	.220E-04	.218E-03	.111E-02	.259E-02	.284E-02	.323E-02
8850	.920E-05	.198E-04	.206E-03	.105E-02	.246E-02	.269E-02	.310E-02
8875	.810E-05	.170E-04	.205E-03	.100E-02	.235E-02	.257E-02	.295E-02
8900	.720E-05	.160E-04	.177E-03	.921E-03	.220E-02	.245E-02	.280E-02
8925	.650E-05	.150E-04	.172E-03	.834E-03	.205E-02	.232E-02	.268E-02
8950	.590E-05	.130E-04	.147E-03	.735E-03	.194E-02	.218E-02	.253E-02
8975	.510E-05	.110E-04	.120E-03	.629E-03	.177E-02	.203E-02	.240E-02
9000	.460E-05	.950E-05	.960E-04	.513E-03	.154E-02	.180E-02	.238E-02
9025	.420E-05	.800E-05	.578E-04	.314E-03	.123E-02	.154E-02	.218E-02
9050	.380E-05	.720E-05	.529E-04	.292E-03	.114E-02	.137E-02	.207E-02
9075	.330E-05	.660E-05	.485E-04	.269E-03	.102E-02	.122E-02	.197E-02
9100	.290E-05	.580E-05	.430E-04	.239E-03	.896E-03	.107E-02	.187E-02
9125	.270E-05	.520E-05	.259E-04	.193E-03	.784E-03	.944E-03	.179E-02
9150	.240E-05	.450E-05	.316E-04	.207E-03	.671E-02	.848E-03	.171E-02
9175	.220E-05	.400E-05	.444E-05	.602E-04	.516E-03	.750E-03	.163E-02
9200	.190E-05	.360E-05	.324E-05	.460E-04	.439E-03	.688E-03	.156E-02
9225	.170E-05	.320E-05	.180E-05	.321E-04	.384E-03	.653E-03	.149E-02
9250	.140E-05	.280E-05	.171E-05	.344E-04	.340E-03	.616E-03	.143E-02
9275	.130E-05	.250E-05	.299E-05	.600E-04	.343E-03	.619E-03	.138E-02
9300	.120E-05	.220E-05	.299E-05	.600E-04	.343E-03	.619E-03	.133E-02

TABLE A2-36. LINE DENSITY PARAMETER FOR H<sub>2</sub>O (SLG MODEL)  
1/d (cm)

1/cm	600K	1000K	1500K	2000K	2500K	3000K
1150	.439E+00	.983E+00	.293E+01	.110E+02	.442E+02	.205E+03
1175	.327E+00	.767E+00	.238E+01	.936E+01	.384E+02	.178E+03
1200	.434E+00	.951E+00	.267E+01	.106E+02	.423E+02	.203E+03
1225	.440E+00	.969E+00	.270E+01	.107E+02	.431E+02	.203E+03
1250	.328E+00	.784E+00	.238E+01	.964E+01	.394E+02	.183E+03
1275	.497E+00	.939E+00	.234E+01	.758E+01	.286E+02	.125E+03
1300	.296E+00	.717E+00	.226E+01	.909E+01	.378E+02	.176E+03
1325	.361E+00	.800E+00	.229E+01	.889E+01	.355E+02	.164E+03
1350	.486E+00	.949E+00	.245E+01	.801E+01	.310E+02	.137E+03
1375	.403E+00	.869E+00	.239E+01	.730E+01	.239E+02	.854E+02
1400	.474E+00	.957E+00	.229E+01	.607E+01	.161E+02	.434E+02
1425	.507E+00	.966E+00	.209E+01	.496E+01	.110E+02	.247E+02
1450	.260E+00	.642E+00	.165E+01	.459E+01	.101E+02	.195E+02
1475	.552E+00	.898E+00	.175E+01	.444E+01	.121E+02	.350E+02
1500	.653E+00	.871E+00	.139E+01	.248E+01	.500E+01	.116E+02
1525	.377E+00	.773E+00	.182E+01	.354E+01	.758E+01	.126E+02
1550	.388E+00	.787E+00	.177E+01	.368E+01	.718E+01	.123E+02
1575	.277E+00	.695E+00	.208E+01	.472E+01	.104E+02	.193E+02
1600	.341E+00	.781E+00	.227E+01	.657E+01	.209E+02	.631E+02
1625	.394E+00	.100E+01	.308E+01	.635E+01	.136E+02	.237E+02
1650	.295E+00	.817E+00	.244E+01	.592E+01	.115E+02	.186E+02
1675	.258E+00	.712E+00	.216E+01	.534E+01	.108E+02	.188E+02
1700	.357E+00	.812E+00	.208E+01	.527E+01	.112E+02	.248E+02
1725	.222E+00	.581E+00	.169E+01	.474E+01	.125E+02	.262E+02
1750	.340E+00	.794E+00	.213E+01	.534E+01	.129E+02	.276E+02
1775	.385E+00	.775E+00	.194E+01	.481E+01	.138E+02	.368E+02

TABLE A2-36. (Continued)

1/cm	600K	1000K	1500K	2000K	2500K	3000K
1800	.444E+00	.917E+00	.239E+01	.645E+01	.194E+02	.583E+02
1825	.358E+00	.758E+00	.200E+01	.550E+01	.165E+02	.492E+02
1850	.432E+00	.878E+00	.224E+01	.598E+01	.203E+02	.563E+02
1875	.204E+00	.540E+00	.171E+01	.494E+01	.149E+02	.359E+02
1900	.228E+00	.587E+00	.181E+01	.537E+01	.160E+02	.409E+02
1925	.306E+00	.693E+00	.196E+01	.541E+01	.143E+02	.415E+02
1950	.353E+00	.779E+00	.209E+01	.521E+01	.135E+02	.330E+02
1975	.153E+00	.442E+00	.150E+01	.435E+01	.111E+02	.257E+02
2000	.170E+00	.446E+00	.141E+01	.389E+01	.981E+01	.244E+02
2025	.213E+00	.496E+00	.146E+01	.360E+01	.913E+01	.233E+02
2050	.192E+00	.484E+00	.152E+01	.403E+01	.101E+02	.261E+02
2075	.217E+00	.551E+00	.175E+01	.447E+01	.115E+02	.281E+02
2100	.261E+00	.574E+00	.166E+01	.413E+01	.124E+02	.348E+02
2125	.389E+00	.683E+00	.170E+01	.364E+01	.110E+02	.358E+02
2150	.421E+00	.128E+01	.273E+01	.495E+01	.168E+02	.654E+02
2175	.433E+00	.101E+01	.208E+01	.401E+01	.144E+02	.890E+02
2200	.449E+00	.109E+01	.247E+01	.488E+01	.190E+02	.117E+03
2225	.462E+00	.113E+01	.267E+01	.532E+01	.209E+02	.125E+03
2250	.480E+00	.116E+01	.289E+01	.581E+01	.230E+02	.133E+03
2275	.496E+00	.120E+01	.313E+01	.634E+01	.254E+02	.141E+03
2300	.522E+00	.124E+01	.338E+01	.691E+01	.279E+02	.151E+03
2325	.530E+00	.128E+01	.366E+01	.755E+01	.308E+02	.161E+03
2350	.548E+00	.132E+01	.396E+01	.823E+01	.339E+02	.171E+03
2375	.565E+00	.137E+01	.428E+01	.898E+01	.374E+02	.182E+03
2400	.585E+00	.141E+01	.463E+01	.980E+01	.412E+02	.194E+03
2425	.602E+00	.146E+01	.501E+01	.106E+02	.454E+02	.207E+03
2450	.625E+00	.151E+01	.542E+01	.116E+02	.500E+02	.221E+03

TABLE A2-36. (Continued)

1/cm	600K	1000K	1500K	2000K	2500K	3000K
2475	.646E+00	.156E+01	.587E+01	.127E+02	.550E+02	.235E+03
2500	.668E+00	.161E+01	.635E+01	.138E+02	.607E+02	.251E+03
2525	.690E+00	.166E+01	.686E+01	.151E+02	.668E+02	.267E+03
2550	.718E+00	.171E+01	.743E+01	.165E+02	.736E+02	.284E+03
2575	.674E+00	.163E+01	.707E+01	.158E+02	.694E+02	.260E+03
2600	.632E+00	.156E+01	.673E+01	.152E+02	.654E+02	.237E+03
2625	.592E+00	.148E+01	.641E+01	.146E+02	.616E+02	.217E+03
2650	.556E+00	.141E+01	.610E+01	.140E+02	.581E+02	.198E+03
2675	.522E+00	.135E+01	.580E+01	.135E+02	.547E+02	.181E+03
2700	.489E+00	.128E+01	.553E+01	.129E+02	.516E+02	.165E+03
2725	.471E+00	.122E+01	.526E+01	.124E+02	.486E+02	.151E+03
2750	.454E+00	.117E+01	.501E+01	.119E+02	.458E+02	.137E+03
2775	.438E+00	.113E+01	.477E+01	.114E+02	.432E+02	.125E+03
2800	.422E+00	.109E+01	.454E+01	.110E+02	.407E+02	.115E+03
2825	.409E+00	.104E+01	.432E+01	.105E+02	.383E+02	.105E+03
2850	.393E+00	.100E+01	.411E+01	.101E+02	.361E+02	.960E+02
2875	.380E+00	.969E+00	.391E+01	.977E+01	.341E+02	.876E+02
2900	.368E+00	.930E+00	.372E+01	.938E+01	.321E+02	.800E+02
2925	.355E+00	.895E+00	.354E+01	.901E+01	.302E+02	.730E+02
2950	.342E+00	.864E+00	.337E+01	.865E+01	.285E+02	.667E+02
2975	.332E+00	.836E+00	.321E+01	.831E+01	.268E+02	.609E+02
3000	.320E+00	.805E+00	.306E+01	.798E+01	.253E+02	.556E+02
3025	.311E+00	.786E+00	.291E+01	.766E+01	.239E+02	.508E+02
3050	.303E+00	.759E+00	.277E+01	.736E+01	.225E+02	.464E+02
3075	.294E+00	.736E+00	.264E+01	.707E+01	.212E+02	.424E+02
3100	.284E+00	.710E+00	.251E+01	.679E+01	.200E+02	.387E+02
3125	.278E+00	.688E+00	.239E+01	.652E+01	.188E+02	.353E+02

TABLE A2-36. (Continued)

1/cm	600K	1000K	1500K	2000K	2500K	3000K
3150	.270E+00	.675E+00	.227E+01	.626E+01	.177E+02	.323E+02
3175	.262E+00	.659E+00	.217E+01	.601E+01	.167E+02	.295E+02
3200	.255E+00	.640E+00	.206E+01	.577E+01	.157E+02	.269E+02
3225	.249E+00	.625E+00	.196E+01	.554E+01	.148E+02	.246E+02
3250	.243E+00	.609E+00	.203E+01	.469E+01	.109E+02	.266E+02
3275	.238E+00	.592E+00	.202E+01	.449E+01	.958E+01	.229E+02
3300	.232E+00	.580E+00	.191E+01	.462E+01	.966E+01	.173E+02
3325	.228E+00	.567E+00	.184E+01	.413E+01	.879E+01	.170E+02
3350	.222E+00	.554E+00	.167E+01	.400E+01	.859E+01	.137E+02
3375	.217E+00	.542E+00	.172E+01	.396E+01	.841E+01	.136E+02
3400	.214E+00	.533E+00	.159E+01	.384E+01	.817E+01	.124E+02
3425	.208E+00	.525E+00	.159E+01	.397E+01	.761E+01	.107E+02
3450	.205E+00	.516E+00	.141E+01	.320E+01	.629E+01	.958E+01
3475	.201E+00	.509E+00	.141E+01	.318E+01	.643E+01	.101E+02
3500	.199E+00	.500E+00	.148E+01	.372E+01	.685E+01	.103E+02
3525	.195E+00	.498E+00	.140E+01	.405E+01	.779E+01	.132E+02
3550	.178E+00	.491E+00	.145E+01	.406E+01	.809E+01	.159E+02
3575	.211E+00	.548E+00	.156E+01	.424E+01	.894E+01	.185E+02
3600	.347E+00	.802E+00	.200E+01	.440E+01	.842E+01	.140E+02
3625	.256E+00	.695E+00	.189E+01	.421E+01	.717E+01	.941E+01
3650	.233E+00	.624E+00	.171E+01	.392E+01	.709E+01	.100E+02
3675	.227E+00	.635E+00	.176E+01	.403E+01	.669E+01	.877E+01
3700	.162E+00	.448E+00	.133E+01	.342E+01	.742E+01	.129E+02
3725	.366E+00	.687E+00	.166E+01	.413E+01	.157E+02	.447E+02
3750	.155E+01	.193E+01	.326E+01	.434E+01	.987E+01	.201E+02
3775	.843E+00	.112E+01	.179E+01	.337E+01	.652E+01	.158E+02
3800	.282E+00	.662E+00	.185E+01	.435E+01	.122E+02	.245E+02

TABLE A2-36. (Continued)

1/cm	600K	1000K	1500K	2000K	2500K	3000K
3825	.165E+00	.520E+00	.173E+01	.448E+01	.902E+01	.136E+02
3850	.340E+00	.700E+00	.188E+01	.387E+01	.824E+01	.126E+02
3875	.354E+00	.745E+00	.173E+01	.347E+01	.730E+01	.116E+02
3900	.263E+00	.665E+00	.173E+01	.360E+01	.679E+01	.889E+01
3925	.184E+00	.530E+00	.154E+01	.360E+01	.710E+01	.930E+01
3950	.191E+00	.559E+00	.165E+01	.403E+01	.791E+01	.108E+02
3975	.177E+00	.565E+00	.175E+01	.451E+01	.763E+01	.994E+01
4000	.169E+00	.552E+00	.179E+01	.484E+01	.804E+01	.116E+02
4025	.786E-01	.363E+00	.171E+01	.569E+01	.118E+02	.179E+02
4050	.170E+00	.550E+00	.205E+01	.585E+01	.144E+02	.295E+02
4075	.191E+00	.556E+00	.198E+01	.516E+01	.122E+02	.277E+02
4100	.155E+00	.482E+00	.220E+01	.885E+01	.228E+02	.404E+02
4125	.144E+00	.288E+00	.247E+01	.132E+02	.249E+02	.286E+02
4150	.126E+00	.379E+00	.275E+01	.162E+02	.328E+02	.691E+02
4175	.121E+00	.432E+00	.306E+01	.179E+02	.376E+02	.794E+02
4200	.119E+00	.491E+00	.340E+01	.198E+02	.430E+02	.912E+02
4225	.121E+00	.559E+00	.378E+01	.219E+02	.492E+02	.104E+03
4250	.124E+00	.635E+00	.421E+01	.242E+02	.563E+02	.120E+03
4275	.127E+00	.723E+00	.468E+01	.267E+02	.644E+02	.138E+03
4300	.136E+00	.823E+00	.521E+01	.295E+02	.737E+02	.159E+03
4325	.158E+00	.936E+00	.580E+01	.326E+02	.843E+02	.182E+03
4350	.185E+00	.106E+01	.645E+01	.360E+02	.964E+02	.209E+03
4375	.218E+00	.218E+01	.717E+01	.399E+02	.110E+03	.241E+03
4400	.256E+00	.137E+01	.798E+01	.440E+02	.126E+03	.277E+03
4425	.228E+00	.122E+01	.693E+01	.394E+02	.112E+03	.251E+03
4450	.202E+00	.108E+01	.601E+01	.352E+02	.994E+02	.228E+03
4475	.180E+00	.957E+00	.522E+01	.314E+02	.882E+02	.207E+03

TABLE A2-36. (Continued)

1/cm	600K	1000K	1500K	2000K	2500K	3000K
4500	.160E+00	.847E+00	.452E+01	.281E+02	.783E+02	.189E+03
4525	.142E+00	.750E+00	.393E+01	.251E+02	.694E+02	.171E+03
4550	.126E+00	.664E+00	.341E+01	.225E+02	.616E+02	.156E+03
4575	.112E+00	.588E+00	.296E+01	.201E+02	.547E+02	.141E+03
4600	.100E+00	.521E+00	.257E+01	.179E+02	.485E+02	.128E+03
4625	.893E-01	.461E+00	.223E+01	.160E+02	.430E+02	.117E+03
4650	.792E-01	.408E+00	.193E+01	.143E+02	.382E+02	.106E+03
4675	.705E-01	.362E+00	.168E+01	.128E+02	.339E+02	.967E+02
4700	.628E-01	.320E+00	.145E+01	.114E+02	.301E+02	.879E+02
4725	.558E-01	.284E+00	.126E+01	.102E+02	.267E+02	.799E+02
4750	.173E+00	.428E+00	.123E+01	.442E+01	.220E+02	.817E+02
4775	.156E+00	.396E+00	.121E+01	.510E+01	.206E+02	.871E+02
4800	.244E+00	.461E+00	.119E+01	.407E+01	.193E+02	.103E+03
4825	.175E+00	.396E+00	.118E+01	.465E+01	.202E+02	.100E+03
4850	.151E+00	.368E+00	.117E+01	.462E+01	.193E+02	.894E+02
4875	.134E+00	.337E+00	.115E+01	.401E+01	.174E+02	.770E+02
4900	.148E+00	.349E+00	.114E+01	.369E+01	.153E+02	.706E+02
4925	.962E-01	.286E+00	.112E+01	.394E+01	.166E+02	.628E+02
4950	.782E-01	.258E+00	.111E+01	.412E+01	.169E+02	.612E+02
4975	.616E-01	.230E+00	.110E+01	.474E+01	.187E+02	.691E+02
5000	.465E-01	.205E+00	.107E+01	.464E+01	.165E+02	.466E+02
5025	.462E-01	.202E+00	.106E+01	.464E+01	.170E+02	.507E+02
5050	.726E-01	.258E+00	.110E+01	.460E+01	.169E+02	.541E+02
5075	.601E-01	.228E+00	.102E+01	.443E+01	.163E+02	.499E+02
5100	.786E-01	.261E+00	.104E+01	.431E+01	.156E+02	.507E+02
5125	.978E-01	.302E+00	.117E+01	.452E+01	.173E+02	.581E+02
5150	.140E+00	.382E+00	.135E+01	.465E+01	.176E+02	.596E+02

TABLE A2-36. (Continued)

1/cm	600K	1000K	1500K	2000K	2500K	3000K
5175	.144E+00	.399E+00	.149E+01	.492E+01	.187E+02	.641E+02
5200	.735E-01	.260E+00	.127E+01	.464E+01	.190E+02	.615E+02
5225	.316E-01	.162E+00	.108E+01	.480E+01	.183E+02	.534E+02
5250	.336E-01	.159E+00	.100E+01	.422E+01	.140E+02	.455E+02
5275	.280E-01	.138E+00	.907E+00	.383E+01	.135E+02	.423E+02
5300	.436E-01	.170E+00	.913E+00	.365E+01	.146E+02	.531E+02
5325	.483E-01	.184E+00	.955E+00	.394E+01	.153E+02	.583E+02
5350	.749E-01	.241E+00	.111E+01	.471E+01	.197E+02	.947E+02
5375	.341E+00	.510E+00	.151E+01	.668E+01	.438E+02	.716E+03
5400	.673E+00	.702E+00	.180E+01	.881E+01	.110E+03	.333E+04
5425	.343E+00	.465E+00	.148E+01	.807E+01	.888E+02	.242E+04
5450	.592E+00	.569E+00	.128E+01	.519E+01	.201E+02	.727E+03
5475	.175E+00	.346E+00	.110E+01	.408E+01	.129E+02	.108E+03
5500	.134E+00	.313E+00	.109E+01	.421E+01	.134E+02	.873E+02
5525	.931E-01	.275E+00	.109E+01	.400E+01	.132E+02	.519E+02
5550	.104E+00	.310E+00	.122E+01	.450E+01	.157E+02	.610E+02
5575	.963E-01	.340E+00	.146E+01	.528E+01	.168E+02	.463E+02
5600	.744E-01	.331E+00	.174E+01	.707E+01	.246E+02	.611E+02
5625	.683E-01	.334E+00	.191E+01	.981E+01	.315E+02	.955E+02
5650	.604E-01	.316E+00	.195E+01	.112E+02	.420E+02	.129E+03
5675	.646E-01	.345E+00	.216E+01	.132E+02	.496E+02	.158E+03
5700	.691E-01	.377E+00	.240E+01	.155E+02	.584E+02	.194E+03
5725	.742E-01	.413E+00	.266E+01	.182E+02	.689E+02	.238E+03
5750	.793E-01	.451E+00	.294E+01	.215E+02	.812E+02	.292E+03
5775	.850E-01	.493E+00	.326E+01	.253E+02	.958E+02	.358E+03
5800	.912E-01	.539E+00	.362E+01	.298E+02	.112E+03	.440E+03
5825	.976E-01	.589E+00	.401E+01	.351E+02	.133E+03	.539E+03

TABLE A2-36. (Continued)

1/cm	600K	1000K	1500K	2000K	2500K	3000K
5850	.104E+00	.644E+00	.445E+01	.413E+02	.156E+03	.661E+03
5875	.112E+00	.704E+00	.493E+01	.487E+02	.184E+03	.811E+03
5900	.119E+00	.770E+00	.547E+01	.573E+02	.218E+03	.994E+03
5925	.128E+00	.841E+00	.606E+01	.675E+02	.257E+03	.121E+04
5950	.137E+00	.919E+00	.672E+01	.794E+02	.302E+03	.149E+04
5975	.147E+00	.100E+01	.745E+01	.936E+02	.357E+03	.183E+04
6000	.157E+00	.109E+01	.826E+01	.110E+03	.420E+03	.224E+04
6025	.152E+00	.105E+01	.783E+01	.104E+03	.398E+03	.213E+04
6050	.146E+00	.100E+01	.743E+01	.988E+02	.376E+03	.201E+04
6075	.141E+00	.963E+00	.704E+01	.936E+02	.356E+03	.191E+04
6100	.136E+00	.922E+00	.668E+01	.887E+02	.336E+03	.181E+04
6125	.132E+00	.882E+00	.634E+01	.840E+02	.318E+03	.171E+04
6150	.127E+00	.844E+00	.601E+01	.795E+02	.301E+03	.162E+04
6175	.123E+00	.808E+00	.570E+01	.753E+02	.284E+03	.154E+04
6200	.119E+00	.774E+00	.541E+01	.713E+02	.269E+03	.146E+04
6225	.114E+00	.740E+00	.513E+01	.676E+02	.254E+03	.138E+04
6250	.110E+00	.708E+00	.487E+01	.640E+02	.240E+03	.131E+04
6275	.107E+00	.678E+00	.462E+01	.606E+02	.227E+03	.124E+04
6300	.103E+00	.648E+00	.438E+01	.574E+02	.215E+03	.117E+04
6325	.997E-01	.621E+00	.415E+01	.544E+02	.203E+03	.111E+04
6350	.963E-01	.594E+00	.394E+01	.515E+02	.192E+03	.105E+04
6375	.929E-01	.568E+00	.374E+01	.488E+02	.182E+03	.100E+04
6400	.898E-01	.544E+00	.354E+01	.462E+02	.172E+03	.949E+03
6425	.867E-01	.520E+00	.336E+01	.438E+02	.163E+03	.900E+03
6450	.836E-01	.498E+00	.319E+01	.414E+02	.154E+03	.852E+03
6475	.808E-01	.477E+00	.302E+01	.393E+02	.145E+03	.808E+03
6500	.780E-01	.456E+00	.287E+01	.372E+02	.137E+03	.765E+03

TABLE A2-36. (Continued)

1/cm	600K	1000K	1500K	2000K	2500K	3000K
6525	.752E-01	.436E+00	.272E+01	.352E+02	.130E+03	.725E+03
6550	.726E-01	.418E+00	.258E+01	.333E+02	.123E+03	.687E+03
6575	.702E-01	.400E+00	.245E+01	.316E+02	.116E+03	.651E+03
6600	.677E-01	.382E+00	.232E+01	.299E+02	.110E+03	.617E+03
6625	.654E-01	.366E+00	.220E+01	.283E+02	.104E+03	.584E+03
6650	.631E-01	.350E+00	.209E+01	.269E+02	.986E+02	.553E+03
6675	.609E-01	.335E+00	.198E+01	.254E+02	.933E+02	.524E+03
6700	.588E-01	.321E+00	.188E+01	.241E+02	.882E+02	.497E+03
6725	.568E-01	.307E+00	.178E+01	.228E+02	.834E+02	.471E+03
6750	.548E-01	.294E+00	.169E+01	.216E+02	.789E+02	.446E+03
6775	.422E-01	.277E+00	.197E+01	.175E+02	.657E+02	.220E+03
6800	.476E-01	.276E+00	.170E+01	.130E+02	.552E+02	.180E+03
6825	.538E-01	.286E+00	.179E+01	.101E+02	.447E+02	.143E+03
6850	.741E-01	.322E+00	.187E+01	.798E+01	.394E+02	.130E+03
6875	.103E+00	.395E+00	.211E+01	.834E+01	.381E+02	.138E+03
6900	.757E-01	.338E+00	.199E+01	.884E+01	.371E+02	.130E+03
6925	.453E-01	.245E+00	.172E+01	.922E+01	.434E+02	.164E+03
6950	.670E-01	.325E+00	.208E+01	.954E+01	.431E+02	.150E+03
6975	.398E-01	.244E+00	.190E+01	.105E+02	.447E+02	.151E+03
7000	.408E-01	.244E+00	.183E+01	.108E+02	.476E+02	.173E+03
7025	.635E-01	.311E+00	.202E+01	.105E+02	.505E+02	.200E+03
7050	.694E-01	.296E+00	.163E+01	.732E+01	.328E+02	.126E+03
7075	.437E-01	.224E+00	.154E+01	.745E+01	.318E+02	.113E+03
7100	.258E-01	.160E+00	.132E+01	.705E+01	.321E+02	.111E+03
7125	.258E-01	.162E+00	.132E+01	.746E+01	.323E+02	.111E+03
7150	.208E-01	.143E+00	.127E+01	.835E+01	.381E+02	.140E+03
7175	.183E-01	.130E+00	.117E+01	.788E+01	.342E+02	.122E+03

TABLE A2-36. (Concluded)

1/cm	600K	1000K	1500K	2000K	2500K	3000K
7200	.154E-01	.107E+00	.101E+01	.752E+01	.434E+02	.204E+03
7225	.253E-01	.152E+00	.123E+01	.845E+01	.460E+02	.218E+03
7250	.320E-01	.181E+00	.139E+01	.908E+01	.502E+02	.236E+03
7275	.274E-01	.175E+00	.141E+01	.798E+01	.328E+02	.106E+03
7300	.230E-01	.151E+00	.129E+01	.723E+01	.334E+02	.120E+03
7325	.314E-01	.193E+00	.146E+01	.592E+01	.189E+02	.421E+02
7350	.563E-01	.265E+00	.158E+01	.534E+01	.160E+02	.356E+02
7375	.567E-01	.286E+00	.188E+01	.794E+01	.302E+02	.872E+02
7400	.710E-01	.367E+00	.234E+01	.151E+02	.763E+02	.340E+03
7425	.804E-01	.490E+00	.370E+01	.253E+02	.135E+03	.612E+03
7450	.909E-01	.654E+00	.585E+01	.423E+02	.241E+03	.110E+04
7475	.102E+00	.872E+00	.924E+01	.708E+02	.428E+03	.197E+04
7500	.116E+00	.116E+01	.145E+02	.118E+03	.763E+03	.355E+04

TABLE A2-37. ABSORPTION COEFFICIENTS FOR CARBON (cm<sup>2</sup>/gm)

1/cm	300K	600K	1200K	1700K	2000K	2300K	2600K
2500.0	.610E+04	.615E+04	.611E+04	.669E+04	.100E+05	.151E+05	.282E+05
2750.0	.655E+04	.678E+04	.690E+04	.765E+04	.113E+05	.171E+05	.298E+05
3000.0	.700E+04	.730E+04	.760E+04	.850E+04	.122E+05	.187E+05	.308E+05
3333.3	.763E+04	.800E+04	.851E+04	.955E+04	.135E+05	.204E+05	.320E+05
3636.4	.810E+04	.850E+04	.932E+04	.105E+05	.145E+05	.218E+05	.328E+05
4000.0	.860E+04	.920E+04	.103E+05	.116E+05	.157E+05	.230E+05	.330E+05
4444.4	.925E+04	.983E+04	.111E+05	.127E+05	.172E+05	.240E+05	.340E+05
5000.0	.100E+05	.107E+05	.119E+05	.141E+05	.186E+05	.215E+05	.348E+05
5714.3	.110E+05	.118E+05	.133E+05	.155E+05	.200E+05	.267E+05	.352E+05
6666.7	.123E+05	.131E+05	.151E+05	.173E+05	.218E+05	.280E+05	.360E+05
8333.3	.146E+05	.157E+05	.182E+05	.210E+05	.250E+05	.305E+05	.374E+05
10000.0	.175E+05	.188E+05	.211E+05	.251E+05	.281E+05	.325E+05	.380E+05